University of Pretoria
Faculty of Engineering, Built Environment and Information Technology
Civil Engineering

DEVELOPMENT OF A WAKE AND BACKWATER PREDICTION APPROACH FOR HYDROKINETIC TURBINES

Chantel Monica NIEBUHR

Dissertation submitted for the degree of Doctor of Philosophy
July 2023

"For a successful technology, reality must take precedence over public relations, for nature cannot be fooled."

Richard P. Feynman

SUMMARY

DEVELOPMENT OF A WAKE AND BACKWATER PREDICTION APPROACH FOR HYDROKINETIC TURBINES

CHANTEL MONICA NIEBUHR

Supervisor:	Dr Marco van Dijk
Co-supervisor:	Dr Lelanie Smith
Department:	Civil Engineering
University:	University of Pretoria
Degree:	PhD (Civil Engineering)

Hydrokinetic turbine deployment in inland water reticulation systems holds untapped potential for future development in renewable energy. However, prior to implementation, it is crucial to understand the hydrodynamic effects associated with these devices. In particular, the flow fields effects prevalent in bounded subcritical flow regimes such as wake propagation and possible backwater effects. While a few analytical approximations for wake determination have been developed, most of them do not account for operational conditions in confined flow. Moreover, there is a lack of usable approaches for backwater determination in the existing literature. This limitation complicates the design and deployment process, leading to problematic installations and issues with regulatory procedures due to the numerous unknowns surrounding turbine deployment.

This study focuses on developing a new semi-empirical model for the prediction of the wake generation and flow recovery which includes a study on metrics found to affect wake generation. Once the flow behaviour is well understood a generic and simplified method for calculating the backwater effect of HK turbines is tested. In this dissertation, data obtained from experimentally validated computational fluid dynamics (CFD) simulations provides a basis for the new simplified wake and backwater prediction approach. Among the available commercial software capabilities, Reynolds-averaged Navier-Stokes (RANS) models showed a strong correlation with turbine performance. A virtual disk model utilising the blade element momentum theory and employing Reynolds's stress closure models was found to give the best representation of the wake and surrounding flow behaviour.

The developed semi-empirical wake model performed well across various performance conditions (linked to the specific turbine thrust), ambient turbulence conditions, and blockage ratios. This model facilitates a reasonably accurate estimation of wake behaviour, enabling effective planning of turbine placement and spatial requirements for inland hydrokinetic schemes. The analytical backwater model developed in this study also demonstrated good correlation with experimental results. Its energy-based approach offers a simplified tool that can be easily incorporated into backwater approximations, also allowing for the inclusion of retaining structures as additional blockages. All models utilise only the flow characteristics and the turbine thrust coefficient, making them valuable tools for the initial analysis of wake and backwater effects resulting from the deployment of inland turbine systems.

JOURNAL AND CONFERENCE PAPERS

The peer-reviewed conference papers and journal articles below were prepared and produced as progress was made in the preparation and completion of this PhD.

Articles

Niebuhr, CM., Van Dijk, M. and Bhagwan, JN., Development of a design and implementation process for the integration of hydrokinetic devices into existing infrastructure in South Africa. *Water SA*, 45(3):434-446, 2019.

Niebuhr, CM., Schmidt, S., van Dijk, M., Smith, L. and Neary, VS., "A review of commercial numerical modelling approaches for axial hydrokinetic turbine wake analysis in channel flow", *Renewable and Sustainable Energy Reviews*, 158(112151), 2022.

Niebuhr CM., Hill, C., van Dijk, M. and Smith, L., "Development of a Hydrokinetic Turbine Backwater Prediction Model for Inland Flow through Validated CFD Models", *Processes*, 10(1310), 2022.

Niebuhr CM., van Dijk, M., and Smith, L., "Development of a semi-empirical wake formation and dissipation prediction model for HAHT placed in channel flow", *Ocean Engineering,* 285(115249), 2023.

Peer-reviewed conference papers presented

Niebuhr, CM. and van Dijk, M. Monitoring operation and maintenance of hydrokinetic schemes through pilot installations in South Africa. *HYDRO 2021*, Strasbourg, France. 25-27 April 2022.

Niebuhr, CM; van Dijk, M. and de Wet, C. Investigating the Hydrokinetic Turbine wake effects as a result of operational parameter variations through validated CFD models. *7th Oxford Tidal Energy Workshop*, Oxford, UK. 8-9 April 2019.

DECLARATION

I, the undersigned hereby declare that:

- I understand what plagiarism is and I am aware of the University's policy in this regard;
- The work contained in this research project is my own original work;
- I did not refer to the work of current or previous students, lecture notes, handbooks or any other study material without proper referencing;
- Where other people's work has been used, this has been properly acknowledged and referenced;
- I have not allowed anyone to copy any part of my dissertation;
- I have not previously submitted this dissertation in its entirety or in part to any university for purposes of a degree.

DISCLAIMER:

The work presented in this report is that of the student alone. Students were encouraged to take ownership of their projects and to develop and execute their experiments with limited guidance and assistance. The content of the research does not necessarily represent the views of the supervisor or any staff member of the University of Pretoria, Department of Civil Engineering. The supervisor did not read or edit the final report and is not responsible for any technical inaccuracies, statements or errors. The conclusions and recommendations given in the report are also not necessarily those of the supervisor, sponsors or companies involved in the research.

Signature of student: _____

Date: 24/07/2023_____

ACKNOWLEDGEMENTS

TABLE OF CONTENTS

LIST OF FIGURES

LIST OF TABLES

LIST OF ACRONYMS, ABBREVIATIONS AND SYMBOLSU

A	-	Area
a	-	Axial induction factor
AD	-	Actuator disk
ADCP	-	Acoustic doppler current profiler
ADV	-	Acoustic Doppler velocimetry
b	-	Channel width
BBMC	-	Hydrokinetic turbine designed at the Southampton Solent University
BEMT	-	Blade element momentum Theory
c	-	Chord length
C	-	Chezy coefficient
CA	-	Channel aspect ratio
C_D	-	Drag coefficient
CFD	-	Computational fluid dynamics
C_L	-	Lift coefficient
C_P	-	Power coefficient
CPU	-	Central processing unit
C_T	-	Thrust coefficient
D	-	Turbine diameter
DES	-	Detached Eddy Simulation
Dg	-	Drag
DNS	-	Direct numerical simulation
dt	-	Rotor diameters
E	-	Energy term
EXP	-	Experimental
F	-	Force
Fr	-	Froude number
Fr_D	-	Froude number based on turbine diameter
FRG	-	Full turbine geometry
g	-	Gravitational acceleration
GCI	-	Grid convergence index
GVF	-	Gradually varied flow

H	-	Water depth
h	-	Channel height
HAHT	-	Horizontal axis hydrokinetic turbine
HK	-	Hydrokinetic
hp	-	Total power dissipated
I	-	Hydraulic loss
IDDES	-	Improved delayed detached eddy simulation
IFREMER	-	French Research Institute for exploration of the Sea
K	-	Kinetic energy component
L	-	Lift
L	-	Rotor diameter used for clearance coefficient
LDV	-	Laser Doppler Velocimeter
LES	-	Large eddy simulations
LPS2	-	Linear pressure strain 2-layer turbulence model
LR	-	Left rotor
LRR	-	Launder, Reece and Rodi model
MAE	-	Absolute error
MRF	-	Moving reference frame
N	-	Number of blades
n	-	Rotational speed
n	-	Manning n value
NACA	-	National advisory committee for Aeronautics airfoil profile
NS	-	Navier stokes
P	-	Wetted perimeter
$P_{position}$	-	Pressure
PMSG	-	Permanent Magnet Synchronous Generator
Q	-	Volumetric flow rate
RANS	-	Reynolds averaged Navier Stokes
Re	-	Reynolds number
R	-	Rotor radius
RM1	-	Reference model 1
$rmse$	-	Root mean square error
RR	-	Right rotor
RSM	-	Reynolds stress model
SST	-	Shear stress transport
T	-	Thrust coefficient
t	-	Time
T	-	Thrust
TI	-	Turbulence intensity
TKE	-	Turbulent kinetic energy
TSR	-	Tip speed ratio
U	-	Velocity
URANS	-	Unsteady Reynolds averaged Navier Stokes
$\bar{u}$	-	Averaged velocity
u'	-	Fluctuating energy term
VC	-	Volumetric control

VD	-	Virtual disk
VOF	-	Volume of fluid
V_x	-	Velocity deficit
WSP	-	Water surface profile
x	-	Position
y	-	Water depth
y+	-	Wall treatment factor
y_n	-	Normal flow depth
Yr	-	Turbine swept area
z	-	Depth relative to a datum
α	-	Energy coefficient
α	-	Coriolis coefficient
β	-	Blockage ratio
λ	-	Tip speed ratio
ρ	-	Density
σ	-	Turbine solidity
τ	-	Shear stress
ω	-	Angular velocity
φ	-	Flow angle
$\bar{u}$	-	Averaged velocity
u'	-	Fluctuating energy term

Subscripts

∞	-	Freestream
W	-	Wake
T	-	Thrust
P	-	Power
O	-	Available
P,opt	-	Optimum power
L	-	Lift
D	-	Drag
C	-	Cross sectional
1,2,3..	-	Positional
X	-	Positioned at point x
H	-	Height
eff	-	Effective
exp	-	Experimental
OD	-	Over the diameter

1. INTRODUCTION

1.1 Background

Considering the climate change crisis and increasing global electricity demand, there is a pressing need to rapidly accelerate the trend and transition to a renewable energy dominant portfolio. This can be achieved largely through the rapid expansion of utility-scale renewable energy projects and markets using mature and cost-effective renewable energy conversion technologies, e.g., solar, hydro and wind turbines. Efforts are also needed to accelerate the development of new renewable energy industries and markets using next generation energy conversion technologies that can extract untapped renewable energy reserves. This includes hydrokinetic (HK) power in water currents and waves. Studies on energy development such as those in water conduits create a forefront to accelerate development by allowing insights into available opportunities.

Ideally a renewable energy conversion technology should have minimum cost per annual average energy production. As well as minimal and mitigatable environmental impacts with maximum power output. Hydropower generation from water conveyance systems can be a valuable global renewable energy asset, but relatively little of this potential has been accurately assessed or developed. This potential renewable energy resource can be harvested from existing water-infrastructure without the need to construct new dams or diversions. This significantly reduces infrastructure costs and the need to develop additional capital-intensive centralised generation systems. By avoiding water impoundment, environmental impacts are minimised, further reducing the short- and long-term economic impact of environmental externalities. At the same time, innovative technologies have been developed, including low-head hydro technologies that efficiently generate at low and near-zero head with no local potential energy head requirement.

The basic working procedure of a kinetic hydropower or HK system is defined as a rotor that converts the kinetic energy in flowing water into rotational energy. This energy is then converted by a generator, typically a Permanent Magnet Synchronous Generator (PMSG), into mechanical energy, which can be either connected to the grid or stored in a battery system.

Multiple turbine designs and geometries exist. A primary characteristic that can be used to identify the turbine operational principle is the horizontal or vertical axis operation. These variations are based on different dependences on combinations of lift of drag forces driving the turbine rotor. Horizontal axis hydrokinetic turbines (HAHT) have a central axis aligned with the flow direction, with the blades orientated perpendicular to the flow. Vertical axis turbines (VAHT) are orientated with the axis perpendicular to the incoming flow. Although VAHT blade designs are less complicated in design and easier to implement, they have lower efficiencies due to their dependence on drag forces (Riglin, 2016).

The HK industry has advanced beyond its initial testing phase with full-scale projects being introduced, constructed, and tested globally. However primary hurdles such as reducing the cost of these systems, optimizing individual systems and arrays and balancing energy extraction with environmental impact still requires attention prior to achieving commercial success. In 2015 it was reported that around 300 initiatives for HK energy technology were

underway, with around 60% focussed on horizontal axis concepts (Yuce and Muratoglu, 2015).

Research in recent years has led to a deeper understanding into HK energy. As this development reaches a commercial stage it is important to have detailed information on the hydrodynamics of these systems, for not only turbine design but resource assessment too (Guerra and Thomson, 2019). Although substantial research on HAHTs has been published in recent years (specifically in tidal energy applications) solutions on hydraulic design, deployment and implementations are still lagging. Streamlined and simplified installation procedures are necessary to reduce the costs and provide more knowns than unknowns around the installations.

When considering HAHT installations in inland channels the size of a single device depends on the area of flow available as well as the orientation of the turbine itself. HAHT have a circular swept area due to the blade orientation, and therefore the size depends on the smallest spatial limitation as well as the commercial availability of turbines. Due to the spatial limitation's turbines are often placed in arrays, producing a higher overall power output over a larger section on the river/channel. The wake generated behind the turbine is therefore of specific importance as its features may have an impact on the distribution of further turbines downstream, their efficiencies (Myers and Bahaj, 2012; Neary *et al.*, 2013) as well as the combined large scale effect of the arrays scheme on the environment (De Dominicis, O'Hara Murray and Wolf, 2017; Goward Brown, Neill and Lewis, 2017). Much work has been done in the analysis of wind turbine wakes, however few focussed on HK wakes, especially in river sections where depth and width are limiting parameters (Silva *et al.*, 2016).

Additional to wake considerations, a HAHT device placed in a canal system may have significant water level and hydrodynamic energy loss effects. This is generally undesirable for water infrastructure operators, owners and waterboards, especially for irrigation water management (Gunawan, Roberts and Neary, 2015). Previous studies (both experimental (Gunawan, Roberts and Neary, 2015) and computational (Turnock *et al.*, 2011; Kartezhnikova and Ravens, 2014)) on the hydrodynamic effects in terms of velocity deficit downstream and damming levels upstream have been investigated. However, most of the studies are site specific and a simplified approach to determining the backwater effect from a HAHT is still lacking.

Providing clear and simple predictions of the hydrodynamic impacts in terms of upstream damming resulting from deployment as well as wake length and dissipation downstream would significantly simplify the preliminary design phase and provide a clear picture of the extractable potential. Previous work on wake models based on actuator disk theory (Lam, Chen and Hashim, 2015; Pyakurel *et al*., 2017) have proven to be impractical for inland installation conditions. This is primarily due to the lack of understanding of the impact of operational conditions on wall bounded HAHT installations.

A similar problem was identified in backwater models, this is primarily due to the lack of research in inland HAHT applications where backwater effects are more critical compared to unbounded tidal applications. Attempts at providing a methodology for determining backwater have been undertaken (Lalander and Leijon, 2011; Kartezhnikova and Ravens,

2014), however existing models have too many unknowns, making them difficult to use and multiple possible user errors.

A limit in development of simplified models for prediction of the hydrodynamic effects of HAHTs is difficulties in data collection. For adequate model validation detailed datasets of HK flow fields over a range of operational conditions are necessary. Limited laboratory test results are available in literature. Due to the constraints in HAHT laboratory testing, typically a single turbine geometry is tested over a limited set of operational conditions (Mycek *et al.*, 2014; Hill *et al.*, 2020). This may be attributed to cost and facility constraints.

The current advancements in computational efficiency and capacity allows the use of complex computational fluid dynamics (CFD) models for inland HK turbines modelling to expand on the existing knowledge base. Computational investigations on both performance and wake effects provide insight to the flow-structure interaction and power output of HK installations. The impact of environmental effects such as blockage (Consul, Willden and McIntosh, 2013), flow speed (Riglin *et al.*, 2016) and yawed flow (Bahaj, Molland, *et al.*, 2007) on turbine performance have be analysed and better understood through computational modelling. Additionally the primary wake recovery mechanisms (Salunkhe *et al.*, 2019) and wake interactions (Olivieri and Ingram, 2013) have also been analysed. A more informed understanding of these complex flow effects enables an improvement of the design and installation of HK devices. This also provides more clarity on site selection (Hill *et al.*, 2020), proper array spacing (Kolekar and Banerjee, 2015), and other challenges surrounding operations and maintenance.

1.2   Importance of the work

The ability to predict the hydrodynamic effects on the flow surrounding a HAHT have been highlighted. A new methodology and set of simplified equations that eliminate user subjectivity and provide a prediction of hydrodynamic effects to an acceptable degree of accuracy would make large strides in inland HAHT development. A major limitation of previous developments of such a methodology is the lack of experimental results. With most studies using a single turbine and calibrating the model to suit the specific turbines operational conditions and behaviour. This is due to the complexities around turbine design as well as the costs of large-scale laboratory testing.

The HAHT surrounding flow is a turbulent flow field, turbulence in flow in notoriously complex and due to this often treated using empirical or semi-empirical relationships and assumptions which hold for limited cases. As computational resources become ever more available a CFD approach is often used instead of laboratory testing. This is mainly due to the lower cost and broader range of control of specific variables which are difficult to ascertain in physical tests. However, in literature it was found that a broad range of approaches are often used without proper validation. Specifically in the selected turbulence models and combination with simplified rotor modelling techniques. This creates distrust in the use of simplified CFD approaches. To correct this, a rigorous process of validation of a CFD approach for not only performance tests but wake dissipation prediction is necessary. As the study utilises CFD for experimental test results, a correct approach was imperative and therefore this important work was undertaken as a primary objective.

Proper validation of the CFD models, justifies their use in hydrodynamic effect prediction. This allows generation of a larger dataset over a range of operational conditions, also allowing an in-depth view into the driving factors of wake dissipation and backwater effects.

1.3 Research objectives of the study

Ultimately the main objectives of the study may be simplified to the following points:

1. To determine a numerical CFD based modelling procedure which correctly depicts the behaviour in terms of wake formation and dissipation behind a HAHT.
2. Conduct CFD model benchmark validation with experimental results.
3. To observe, fundamentally the aspects of flow around a HAHT and investigate the driving factors behind wake formation and dissipation.
4. To derive a useful semi-empirical wake model allowing determination of the dissipation rate in the near and far wake behind a HAHT over typical channel flow conditions.
5. To establish a useful and correct method for determining the backwater expected from a HAHT in channel flow conditions.
6. To test the new models with experimentally and numerically generated results to ascertain the validity and accuracy of the models over a range of turbine geometries and operational conditions.

1.4 Structure of the dissertation

The dissertation is structured into three parts, preceded with a literature study. The three parts fit together as shown in Figure 1-1. These three parts summarise the critical research questions from the study. The parts also describe the three journal articles published as part of the study.
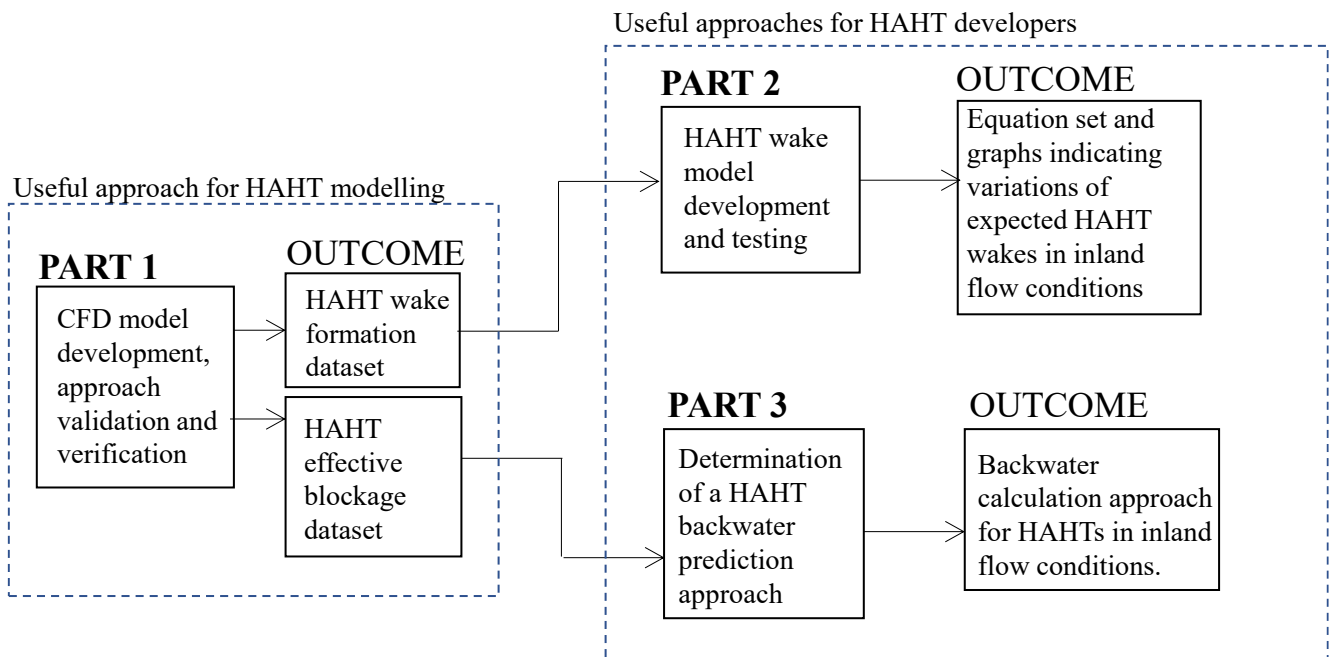
Figure 1-1: Compilation of the dissertation

Each chapter is summarised below:

Chapter 2 serves as a summary of important findings in literature. A short overview of HAHT generation is included. Thereafter the study focuses on the primary hydrodynamic effects, namely wake formation and backwater effects are explained. The fundamental driving factors previously identified, as well as existing analytical and empirical approaches are summarised. As CFD modelling is used as a tool for data collection, a literature study on previous approaches used in HAHT modelling as well as a comparison of approaches is included.

Chapter 3 covers *Part 1* of the study, following the development of a validated HAHT CFD modelling approach. Details of the benchmark validation, mesh and physics verification as well as a decision on the final modelling approach used in the study is included here.

Chapter 4 follows *Part 2* of the study, namely the development of a simplified wake prediction approach. Analysis of the driving factors affecting wake formation are investigated. Thereafter a semi-empirical wake model is derived and validated. Its accuracy and effectiveness over a range of data and operational scenarios is analysed.

Chapter 5 describes *Part 3* of the study, which follows the development of a backwater prediction approach. The derivation of the backwater prediction method through an energy approach is described together with testing and calibration of the equations and coefficients prescribed as part of the approach. The effectiveness of the approach is tested over a range of operational conditions.

Chapter 6 summarises the research and provides a final conclusion and summation of the results. Recommendations for future work and investigations for further improvements are suggested.

2. LITERATURE REVIEW

A concise review of relevant literature is summarised to give the necessary background knowledge on concepts applicable to the study as well as providing an overview of previous studies and approaches relevant to the study objectives.

2.1 Introduction

Horizontal axis hydrokinetic turbines (HAHT) may be identified as propeller-like turbines placed in flowing water to extract kinetic energy. Design and installation of HAHTs is fairly complex due to the intricate blade design, mooring, fastening and consideration of the variability of environmental conditions (Riglin, 2016).

HAHTs consist of around five components (as seen in Figure 2-1), with the turbine blades serving as the energy conversion mechanism. The kinetic energy of flowing water is converted to mechanical power in the form of torque. A gear box then converts the torque and angular velocity (through the blade rotation) to a value more advantageous to the mechanical-to-electrical conversion efficiency. Thereafter a generator converts the mechanical power to electrical power. As a HAHT is usually fully submerged, a nacelle is designed to hold the gearbox, generator and necessary electrical power transmission wiring.

1. Rotor
2. Gearbox
3. Generator
4. Converter/Inverter
5. Transformer
6. Grid connection
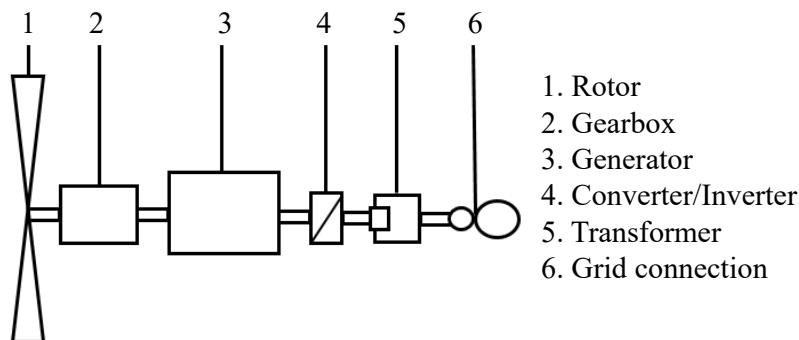
Figure 2-1: Grid connected HK turbine system components (Behrouzi *et al.*, 2016)

The changes in the surrounding water flow resulting from the deployment of a HAHT system is this study's focus. When these systems are placed in confined water conveyances systems such as river and channels, a number of changes to the flow behaviour may occur. The primary effects of consideration can be seen in Figure 2-2. These being the turbulent, slowed flow in the wake of the device, as well as the potential backwater effect caused through the blockage imposed on the flow area.
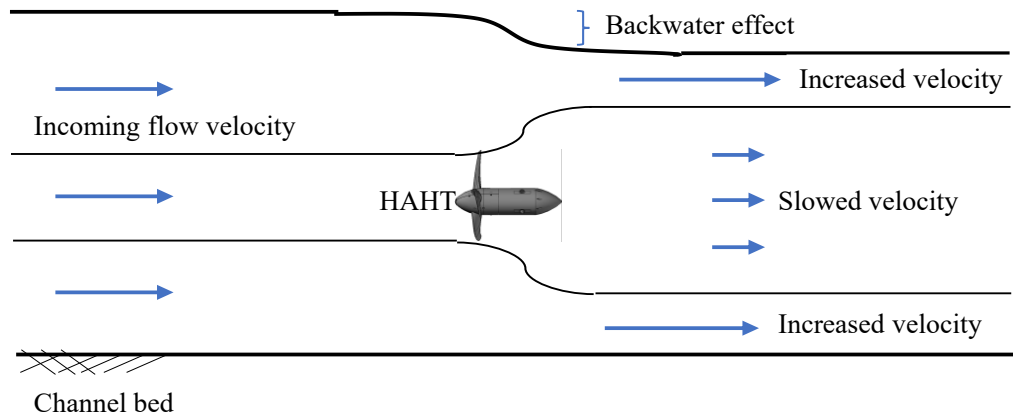
Figure 2-2: Schematic of basic flow effects of a HAHT in a channel (side view)

The following literature review aims to provide an overview of the primary driving factors behind these effects. Three focus points are highlighted namely:

1. The presence of the turbine (power extraction etc.) and quantification of these effects.
2. The subsequent wake formed due to the presence of the turbine, previous theoretical approaches to the analysis of the wake, and driving factors behind wake formation.
3. The subsequent free surface effects as a result of HAHTs placed in bounded inland flow.

2.2 HAHT power definition

The degree of flow disturbance is primarily linked to the turbine performance and overall drag. Derived theoretical concepts on turbine performance are most often used in efficiency analysis. The use of the actuator disk theory (momentum theory) is well established in wind turbine analysis and design. Aside from the fluid density change and the presence of the free-surface and wall boundaries, the energy capture and the conversion of fluid energy to electrical power is similar (Bahaj, Batten and McCann, 2007). Performance metrics often used in HAHT design are the power coefficient (C_P) and thrust coefficient (C_T) which are derived through simplified theoretical concepts included in the actuator disk theory.

HAHTs extract energy from moving water. The energy is harnessed by the rotor through lift and drag forces induced by the oncoming flow. Since energy is extracted from the water one may assume the fluid element passing through the rotor loses kinetic energy. An approach often used in turbine analysis is to simplify the rotor to an actuator disk (AD). By utilising the AD concept, the behaviour of the HAHT (and subsequent flow effects) may be simulated without explicitly modelling the individual rotor blades.

2.2.1 Actuator disk theory

Applying Froude's momentum theory over the AD results is a 1-dimensional approach where the rotor is modelled as a discontinuity moving through the fluid. The thin disk (replacing the rotor) has a uniform thrust loading and velocity over its area with negligible frictional resistance, only considering momentum flux and pressure changes (Eggleston and Stoddard, 1987).

The power extraction is approached as an energy transfer from the fluid to the rotor and manifested as a pressure drop. As the flow approaches the disc, its velocity decreases as the

pressure reaches its peak. It then drops immediately downstream of the rotor as seen in Figure 2-3. The velocity continues to decrease downstream, and due to mass continuity (assuming incompressible flow) the flow area expands. As the flow moves downstream the pressure gradually recovers (Sanderse, 2009).
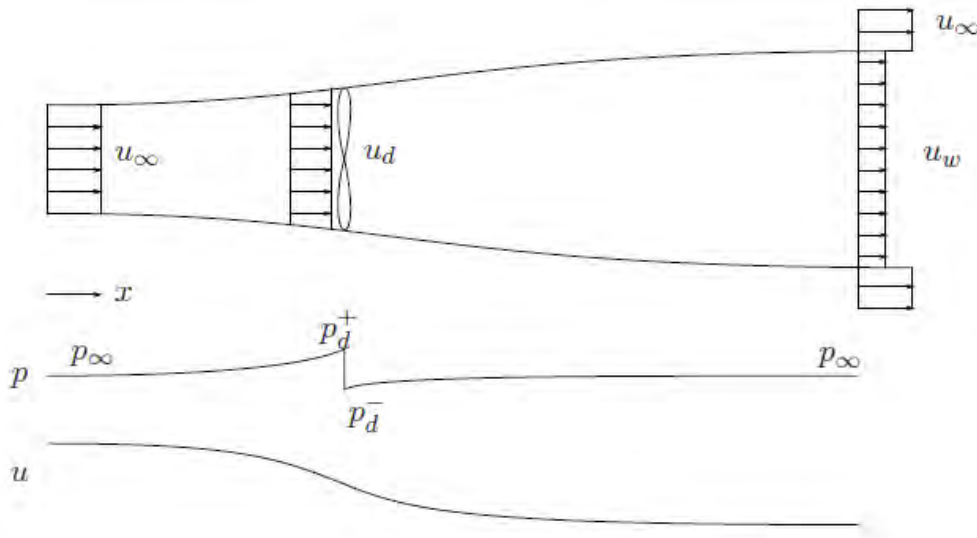
Figure 2-3: 1D flow through an actuator disk (Sanderse, 2009)

The pressure drop over the disk is associated with an axial force acting downstream. Assuming the disk is stationary, the force on the disk is equal in magnitude and opposite in direction to the rotor drag or thrust. This thrust (T) can be non-dimensionalised into a thrust coefficient (C_T) (Hansen, 2008):

$$C_T = \frac{T}{\frac{1}{2}\rho U_\infty^2 A} \tag{1}$$

Where U_∞ is the freestream velocity in (m/s), ρ the fluid density (kg/m³) and A the turbine swept area (m²).

Defining an axial induction factor (a) as the fractional decrease in fluid velocity, the flow velocity at the rotor (U_d) can be defined as:

$$U_d = (1 - a)U_\infty \tag{2}$$

And the velocity downstream (U_w) as:

$$U_w = (1 - 2a)U_\infty \tag{3}$$

A definition for C_T based on a may be determined through the freestream velocity and wake velocity:

$$C_T = 1 - \left(\frac{U_w}{U_\infty}\right)^2 = 4a(1 - a) \tag{4}$$

Power output is often expressed as a non-dimensional parameter referred to as the power coefficient (C_P), which is the power output of the turbine (P) relative to the available power (P_o) in the flow area over the turbine swept area (A):

$$C_P = \frac{P}{P_0} = \frac{P}{\frac{1}{2}\rho U_\infty^{\;3} A} \qquad (5)$$

Additionally, the axial induction factor may be related to power output. The energy removed by the rotor per unit time may be defined as:

$$P = \frac{1}{2}\rho U_\infty^{\;2} A U_t - \frac{1}{2}\rho U_w^{\;2} A U_t \qquad (6)$$

Substituting the expression for U_t defined in equation (3) it is found that:

$$P = \frac{1}{2}\rho A U_\infty^{\;3} 4a(1-a)^2 \qquad (7)$$

where power is defined in terms of a. Through this relationship it can be seen that if $a = 0$, there is no effect of the turbine presence on the flow, and therefore no power abstraction. Additionally, for $a = 1$ the fluid is slowed to zero velocity downstream of the rotor and therefore without the presence of flow, no power is generated (Eggleston and Stoddard, 1987). For a channel with an infinitely large domain an optimum C_P exists at $a = 1/3$, or $C_{P,opt} = 16/27 = 0.59259$, referred to as the Betz limit (Sanderse, 2009). However the effect of confinement on this efficiency has not been thoroughly investigated, but has in some cases shown to overcome this limit (Cardona-Mancilla *et al.*, 2018).

A similar definition for optimum conditions may be found for C_T within the assumptions of the actuator disk method as seen in equation 4 where $C_T = 8/9$.

These approximations and equations for C_T and C_P are often used in wind and tidal turbine analysis and design. The assumption within the derivations should be mentioned, and are as follows (Eggleston and Stoddard, 1987):

- Steady, homogeneous flow is assumed.
- No obstructions to fluid flow upstream or downstream are included.
- Uniform flow velocity is assumed over the disk.
- A well-defined streamtube separates the flow through the disk from the surrounding flow.
- Fluid flow is incompressible.
- No rotation is produced.

2.2.2 Typical HAHT performance and operation

Optimum performance of a HAHT is a crucial criterion for obtaining a visible installation As seen in equations (5) and (6) the available energy and therefore extractable power output is primarily a function of flow velocity. Although turbine swept area has an effect, it is usually governed by spatial constraints, and therefore this remains the primary parameter of interest. Due to this the turbine should be designed to operate optimally at each site-specific flow velocity.

The forces driving the rotor can be primarily defined as lift (L) and drag (Dg) components. To quantify these components the coefficient of lift (C_L) and drag (C_D) are useful definitions (Ferraiuolo *et al.*, 2022):

$$C_L = \frac{L}{\frac{1}{2}\rho U_\infty{}^2 c} \tag{8}$$

$$C_D = \frac{Dg}{\frac{1}{2}\rho U_\infty{}^2 c} \tag{9}$$

where c is the chord length of the airfoil.

These coefficients are functions of the flow angle of attack and Reynolds number. Turbine geometry design is governed by these metrics. As the Reynolds number is responsible for the boundary layer transition to turbulent flow which provokes the airfoil stall conditions. The relationship between C_L and C_D based on angle of attack represent the turbine performance and are primarily used for design. HAHTs are typically more efficient than drag devices with a vertical axis of rotation (e.g. Darrieus turbine) because they harness the lift force (Castelli and Benini, 2011).

When the force acting on the rotor (thrust force) as well as mechanical power produced is known for a given tip speed ratio (λ) the hydrodynamic performance is known. The power output is usually reported as a function of λ, defined as the blade tip speed relative to the flow velocity. It is simply calculated through rotor angular velocity (ω) turbine rotor radius (R) and freestream velocity (U_∞):

$$\lambda = \frac{\omega R}{U_\infty} \tag{10}$$

Final rotor design is a combination of blade design (airfoil properties), blade radius and the number of blades (N).

It is important that the defined operational velocity range is compatible with the specific design. Turbine solidity (σ) is often used to define this combination. Defined as:

$$\sigma = \frac{cN}{2\pi R} \tag{11}$$

The classical Glauert blade element momentum theories (BEMT) (Glauert, 1983) are often used to optimise the blade geometry. More recent improvements, specifically on the complex physical flow features (tip 3D effects, cavitation etc.) for HK turbines have been explored in literature (e.g. (Batten *et al.*, 2007; Li *et al.*, 2016)). These have also been combined with advanced fluid mechanics methodologies such as computational fluid dynamics (CFD) and vortex methods (Brasil Junior *et al.*, 2019).

2.3   HAHT wake formation

Placing a turbine in a moving flow field causes a disturbance in the downstream region. The subsequent wake is characterised by intense turbulent mixing, helical movements, and a complex eddy system. This may be attributed to two phenomena, the instability of boundary layers on the blades due to the adverse pressure gradient along the rotor plane. A spiral vortex structure which is shed outwards from the blade tip and rotor root is also found, resulting in large eddies formed in the flow which last a long time in the downstream flow field (Silva *et al.*, 2016) (depicted in Figure 2-4). A major difference between AD theory and reality is the rotation imposed by the rotor.
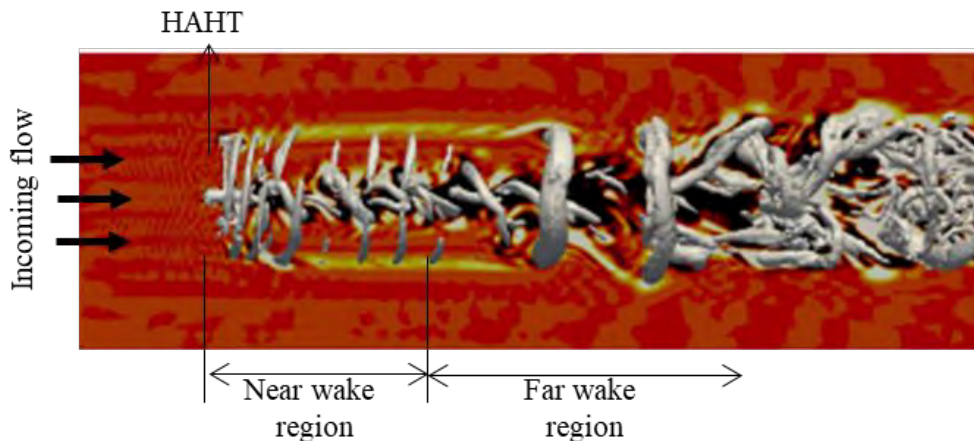
Figure 2-4: HAHT wake (adapted from (Lloyd, Turnock and Humphrey, 2014))

Understanding wake formation and development is critical in HAHT array optimisation. Similar to wind turbines, water turbine wake dynamics and structures exhibit the following behaviour (Chamorro *et al.*, 2013; Fontaine *et al.*, 2020):
- Wake rotation,
- wake meandering,
- the evolution of the shear layer,
- significant momentum transport across this shear layer and
- dynamic interaction and breakdown of hub, tip and stanchion vortices within and at the interface of the coherent wake structure.

There are clear differences for water turbine wake structures operating in depth-limited boundary layer flows, including changes in fluids interacting with the bounding surfaces/free surface (Bahaj, Myers, *et al.*, 2007). Additionally, far wake velocity deficits do not have the symmetric Gaussian profiles typically found downstream of wind turbines in unconfined atmospheric boundary layer flows, and these constraints can affect flow recovery, as proven in previous studies (Bahaj *et al.*, 2011; Aghsaee and Markfort, 2018).

Considering a simplified disk representation of a HK device, see Figure 2-5, may be used to describe a turbine wake and propagation thereof. Consider a turbine of area A in channel cross sectional area A_c Consider cross section A_o as the streamtube area in upstream undisturbed flow with the pressure p_o and flow speed u_o. The streamtube pressure is p_1 just upstream of

the turbine and p_2 just downstream (assumed uniform as in the Lanchester-Betz formulation (Garrett and Cummins, 2007)). The streamtube expands downstream of the turbine and continues to do so before settling to a constant area A_3 with speed u_3. The speed of flow outside the wake is u_4 and pressure p_4.

As indicated on the sketch, as A_c approaches infinity, $p_4 = p_0$ and $u_4 = u_o$. The flow further downstream allows lateral mixing which results in a change of pressure to p_5, which varies from p_0.

Figure 2-5: Definition for single turbine in a channel (Garrett and Cummins, 2007) (top view)

Immediately downstream of the turbine the wake physics is complex, and is influenced by the bypass flow, induced flow rotor and specific tip vortex interaction with the supporting structure (Olczak *et al.*, 2016). Further downstream the wake starts mixing with the bypass flow and causes wake expansion and velocity recovery over a long distance. This defines the two predominant behaviours which are more generally referred to as Mode-1 and Mode-2 (Johansson, 2002) or more specific to HK turbine theory the near wake and far wake (shown previously in Figure 2-4).

Mode-1 or the near wake may be characterised as a connected structure associated with vortex shedding behaviour. Mode-2 which may be related to the far wake is then associated with global instabilities and inhibits a slow movement of the whole mean velocity field. The near wake is specifically characterised and affected by the turbine geometry, whilst the far wake is not (Lam and Chen, 2014). The presence of tip vortices is clearly seen in this region. The tip and root vortices result in sharp velocity gradients and peaks in turbulence intensity. For extremely high tip speed ratios a vortex sheet may form downstream as the tip vortices join forming a shear layer (Sanderse *et al.*, 2011) and slower rotations being more similar to the Karman vortex street behaviour (Tian, Mao and Ding, 2018).

In the far-wake the turbulence and integration of the bypass-flow and wake flow regions mix and become more stochastic. Two primary features exist in the wake, low water speed and high turbulence intensity (Ge *et al.*, 2019), the former of which reduces the power output of any subsequent turbine placed in its wake.

2.3.1 HAHT wake studies in the context of inland flow

Inland HK schemes may be installed in river systems with varying flow depths and geometries, or canal systems. Most of the limited research on HK wakes has been carried out numerically (Blackmore *et al.*, 2014; Boudreau and Dumas, 2017; Chawdhary *et al.*, 2017) or at laboratory scale (Myers and Bahaj, 2007, 2012; Chamorro *et al.*, 2013; Chen, *et al.*, 2017) under controlled and simplified conditions, there are only a few field scale measurements and results available (Rowell, 2013; Gunawan, Roberts and Neary, 2015; Guerra and Thomson, 2019). This may be due to the difficulty in obtaining accurate field measurements on site.

For numerical analysis, the performance of the models analysed should be in context of practical installations and thus kept consistent with typical flow conditions experienced at deployment sites. This is specifically important for ambient flow conditions such as turbulence, which is known to have a large effect on wake formation and dissipation rate.

Sanderse *et al.* (2011) first identified turbulence as a dominating factor to physical processes, specifically in the far wake. Three sources of turbulence can be identified, namely atmospheric turbulence (turbulence present in the domain) mechanical turbulences (from the blades and tower) and wake turbulence (from tip vortex breakdown). Therefore, to allow accurate capture of the wake formation and dissipation it is imperative that the turbulence present in the flow is represented correctly (Sanderse *et al.*, 2011).

Neary *et al.* (2013) studied the typical turbulent inflow characteristics for HK systems in rivers (Neary *et al.*, 2013). The typical profile of the velocity and turbulence intensity is indicated in Figure 2-6. The distributions emphasise the importance of defining the effect of wall boundary layer formation in these confined scenarios where wall effects change the turbulence and velocity in the approach flow.

The typical profile adheres to the original log-law which has been used since Keulegan (1938) for open channel flow and should hold true for its entire flow depth. Correct capture of the boundary layer is imperative for inland installations due to the possibility of a close proximity of the turbine to the wall. For channel flow two flow regions can be distinguished, the inner flow region (near wall) and outer region (near free surface). The logarithmic law holds for the inner region and deviates slightly for the outer region. In the inner region flow it is dominated by the wall variables such as kinematic viscosity, roughness and friction velocity (Kironoto and Graf, 1995). The outer region is controlled by the maximum flow velocity and flow depth (Keulegan, 1938).
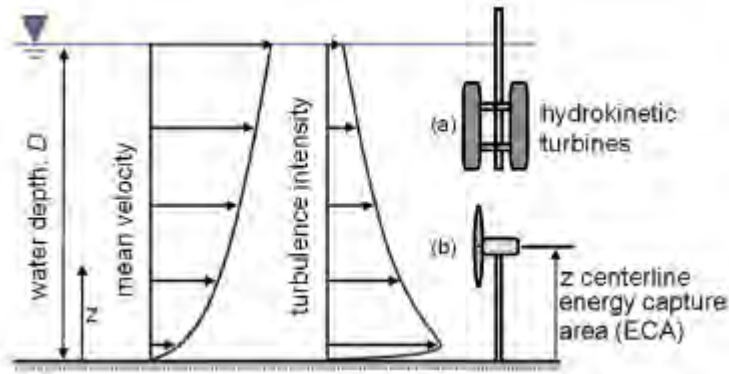
Figure 2-6: Typical profiles of velocity and turbulence intensity in open channel flow (Neary *et al.*, 2013)

Multiple studies have analysed the typical turbulent flow conditions in open channel flow, most being on smooth channel beds (Raichlen, 1967; McQuivery and Richardson, 1969; Nezu and Rodi, 1986) and some with a focus on rough beds (Kironoto and Graf, 1995; Bigillon et al., 2006). Usually turbulence characteristics vary between around 8-12% turbulence intensity (Neary *et al.,* 2013). Flow velocity and turbulence distribution along a channel cross section (whether for rough or smooth walls) is primarily governed by its aspect ratio. Even for rough beds, velocity profiles indicate roughness only has an effect in the near wall region (Bigillon *et al*., 2006). For large aspect ratios (*b/D* >5) which are most common, the maximum velocity zone is found at the free surface, and therefore it is favourable to place the turbine in this region. For smaller aspect ratios this rule may not hold true and the high velocity zone may be below the free surface, governed by the inner region.

Where flow velocity and roughness values are known, local velocities may be calculated due to the near wall region log law approximation as well as manning's equation and the power law exponent (Neary *et al*., 2013). Additionally, turbulence intensities may be approximated using Reynolds decomposition from fluctuating velocity measurements. As this method has been validated with experimental results over a large range of Reynolds numbers (Kironoto and Graf, 1995; Bigillon, Niño and Garcia, 2006), especially those experienced in subcritical open channel flow.

Flows in channels are mostly subcritical with low Reynolds numbers ranging from 0.2 $\times 10^6$ to 1 $\times 10^6$ (Neary *et al.*, 2013). Inflow velocities are typically around 1 m/s (Niebuhr *et al.*, 2019), however for optimal HK generation, velocities should be closer to 2 m/s.

2.3.2 Velocity deficit

Velocity deficit is used in wake analysis to quantify the extent of wake recovery. This is used to remove the dependence on onset velocity as well as turbine diameter size. The velocity deficit (*Vx*) for a downstream distance (*x*) is defined as follows:

$$V_x = \frac{U_\infty - U_x}{U_\infty} \tag{12}$$

2.3.3 Typical wake lengths

HK wakes have shown downstream velocity deficits between 10-20 rotor diameters (d_t) downstream (Maganga *et al.*, 2010; Mycek *et al.*, 2014). Chamorro *et al.* (2013) observed a wake propagating further than 15 d_t downstream with a 10% velocity deficit at 15 d_t with a slightly higher deficit at higher tip speed ratios. This was for a 3-bladed turbine at a chord length based Reynolds number (Re_c) of 1.5 x10^4. Bahaj *et al.* (2007) showed wake centreline measurements with velocity deficit existing for distances exceeding 20 d_t downstream. An experimental and numerical study by Edmunds *et al.* (2017) of a HAHT at a TSR of 3.67 recorded higher wake recovery rates. Here a 22% deficit measured at 1.2 d_t dissipated to a 12% deficit after only 10 d_t.

In one of the few documented far field experimental studies completed on a three-bladed HAHT, the far field wake dissipation rate was shown to be further than 35 d_t downstream (Neary *et al.*, 2013). Wake measurements indicated an 80% velocity recovery by around 10 d_t downstream. The velocity deficit in their study decays exponentially starting at 3 d_t downstream and reaching approximately 80% recovery between 9 - 10 d_t before maintaining an almost constant value to 35 d_t downstream (Figure 2-7).
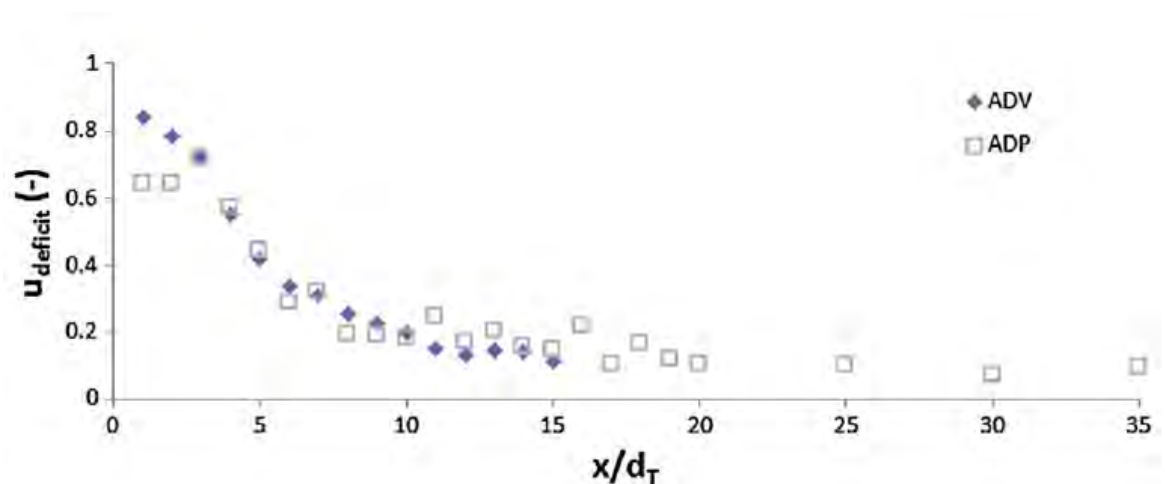
Figure 2-7: Velocity deficit in the wake of a 3 bladed hydrokinetic turbine (Neary *et al.*, 2013)

In summary wake dissipation length is strongly governed by operational conditions with variable results shown in literature. Additionally, the long wake length, and lack of experimental data past 10 d_t downstream, limits the ability to draw conclusions on wake recovery lengths.

2.4 Factors affecting wake formation

Following the previous section, wake formation and structure varies with different turbine application, geometries and operational conditions. Multiple physical processes exist in the flow affecting the performance and wake formation downstream of a HK device. These include the onset shear and turbulence, retaining structure interaction, tip vortices and wake rotation, as summarised in Figure 2-8. A limited number of studies have thoroughly investigated these effects on the far wake (discussed in the subsequent sections).
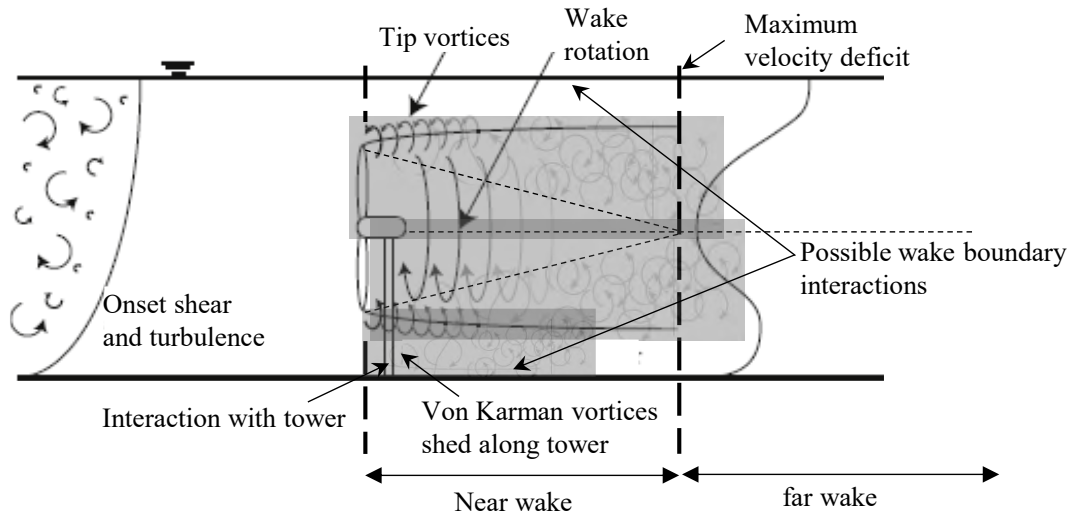
Figure 2-8: Schematic of flow affecting the loading and wake of a HK device (Olczak *et al.*, 2016)

Turbines are often placed in arrays to achieve a higher overall power output as single devices with smaller diameters alone may not supply the necessary electricity need. Turbine devices are usually staggered. This ensures wake recovery before the downstream turbine due to the potential performance reduction effects. Therefore, the placement limitations are usually governed by performance requirements.

As mentioned previously, the presence of the turbine results in extraction of momentum and energy from the flow resulting in a pressure drop and consequently an axial pressure gradient and formation of the wake (Sanderse *et al.,* 2011). The biggest contribution may be attributed to inlet turbulence as turbulence in the wake acts as an effective mixer leading to wake recovery of the velocity deficit and thus a decrease in overall turbulence intensity. This is the primary driver to wake dissipation or recovery. Some important factors found to affect the wake are summarised in the next sections.

2.4.1   Effect of onset turbulence

As discussed in section 2.3.1 onset flow turbulence intensity (TI) may vary due to environmental conditions (channel geometries, structure e.g. grids etc.) which is most often quantified through the flow characteristic namely, Reynolds number (R_e) and the flow regime defining Froude number (F_r). Maganga *et al.* (2010) tested the effect of ambient turbulence on the wake and found for a three-bladed HAHT at as tip speed ratio of 9 placed at higher turbulence rates (TI = 25%) the wake had recovered to 60% velocity deficit within 1.4 d_t downstream where lower levels (TI = 8%) only reached this recovery rate at 4.4 d_t.

Additionally, an interesting finding noted the high disturbance in the near wake of a HAHT due to the turbine hub, body and support structure at low TI (TI = 8%) which was not noticeable at high TI (TI = 25 %) due to the quick velocity deficit decrease and non-development of a wake caused by the hub. The vertical structure of the wake is also more prevalent at lower TI's (Maganga *et al.*, 2010). Similarly a 80% decay in streamwise velocity was found at 9 d_t downstream for TI = 8% and 3 d_t downstream for 25% (Maganga *et al.*, 2010). A contour plot of these comparisons can be seen in Figure 2-9.
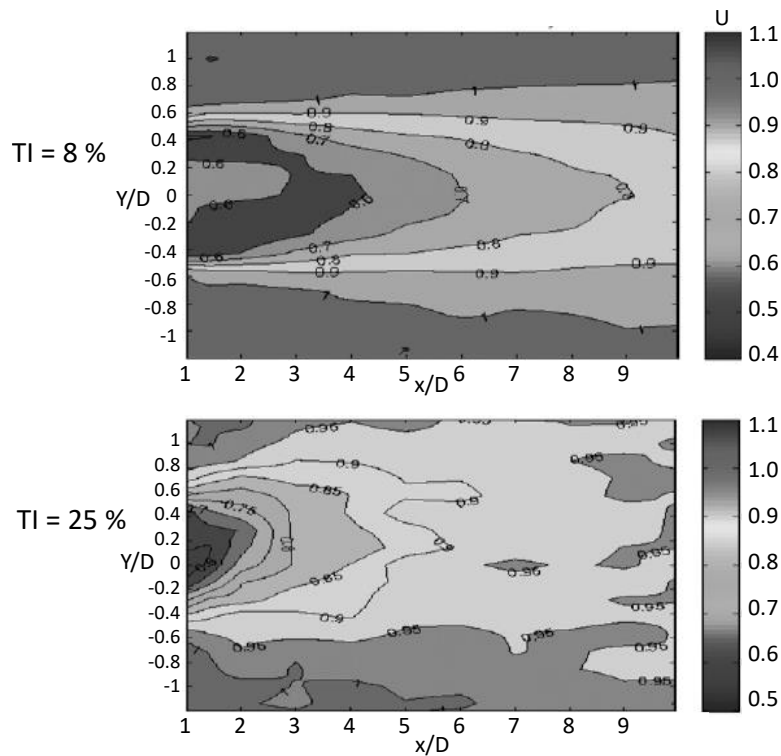
Figure 2-9: Velocity contours for varying turbulence intensities 8% and 25% (Maganga *et al.*, 2010)

MacLoed *et al*. (2002) numerically modelled a HAHT at three ambient turbulence levels, namely 3.65 %, 7 % and 14 % the increased levels of turbulence led to a faster wake recovery. Ahmadi (2019) found using large eddy simulations (LES) that the maximum velocity deficit in the wake reduces with an increase in upstream turbulence and its location shifts towards the turbine plane. The tip vortex breakdown is highly sensitive to upstream/ambient turbulence intensity.

Blackmore, Batten and Bahaj (2014) used an LES study to determine the effect of turbulence by varying grid inlet sizes of an upstream grid. Although the results were not validated experimentally and simply modelled using an actuator disk, the study concluded the following behaviour:

- By increasing the ambient turbulence, the velocity deficit is reduced and therefore the location of maximum velocity deficit shifts closer to the disk and essentially speeds up wake recovery.
- TI has a limited effect on wake width.
- Results in field may not replicate the laboratory tests performed in low turbulence environments.

The ambient turbulence has also been shown to have a significant impact on the power production and loading on a turbine. Although the time averaged power and axial loading values do not change significantly, the standard deviations increase (by about a factor of 4 with a TI change from 5% to 20 %) (Pyakurel, Vanzwieten, Dhanak, *et al.*, 2017). Mycek *et al.* (2014) performed an experimental analysis on a three-bladed 0.7 m diameter HAHT which

did not indicate significant changes in turbine performance when comparing 3% TI to 15% TI.

All studies involved a similar trend, namely, as turbulence levels were increased the wake behind the turbine dissipated at a significantly faster rate, reaching lower velocity deficits closer to the turbine. Increased wake expansion closer to the turbine at higher turbulence levels was also observed (Lo Brutto *et al.*, 2015; Pyakurel, Tian, *et al.*, 2017). This would indicate higher onset TI's could allow closer array spacing and thus reduction in costs with greater power outputs (Blackmore, Batten and Bahaj, 2014), although high onset TI may reduce turbine performance, although results on this were contradictory and require further investigation. Observations of experimental studies have also shown that in array schemes turbulence from an upstream device may aid the wake recovery of the downstream device (Bahaj and Myers, 2013).

Only a few experimental results or validated numerical results clearly ascertain the relationship between turbulence and wake behaviour, however it is clear that a common similarity in trends exists.

2.4.2 Effect of operational parameters

The turbine geometry, blade profile as well as solidity govern the optimal operational point of the turbine (the point of highest power output for the system). The optimal power output is calculated as the product of the angular velocity and turbine torque. These operational parameters govern the thrust experienced in the flow field surrounding the turbine. Ultimately according to the momentum theory, the disturbance caused by the turbine, and therefore initial point of lowest velocity in the wake is primarily dependant on the thrust. Studies on wind turbines and isolated stream turbines have shown that the wake of a single device is a function of the rotor operating state and specifically of the thrust (Stallard *et al.*, 2013).

Existing analytical wake models are typically a function of the thrust coefficient (C_T) (Lam and Chen, 2014; Pyakurel, Vanzwieten, Dhanak, *et al.*, 2017), which is determined as a function of thrust, density, rotational speed and turbine diameter. However, Wang *et al.* (2018) found the tip speed ratio (λ) plays a larger role in the efflux velocity than prior analytical equations allowed and proposed an added coefficient in these equations to change these values.

For better understanding of the flow characteristic differences in the vortex structures can be observed at rotational speed variations (Figure 2-10). The flow separation at the blade tips, and strong vortex shedding from this point is evident. As the λ increases, the pitch of the spiral vortices decreases, eventually merging into a cylindrical surface (as indicated by the $\lambda = 7$ case). This cylindrical surface dissipated quickly downstream of the rotor (Tian, Mao and Ding, 2018).
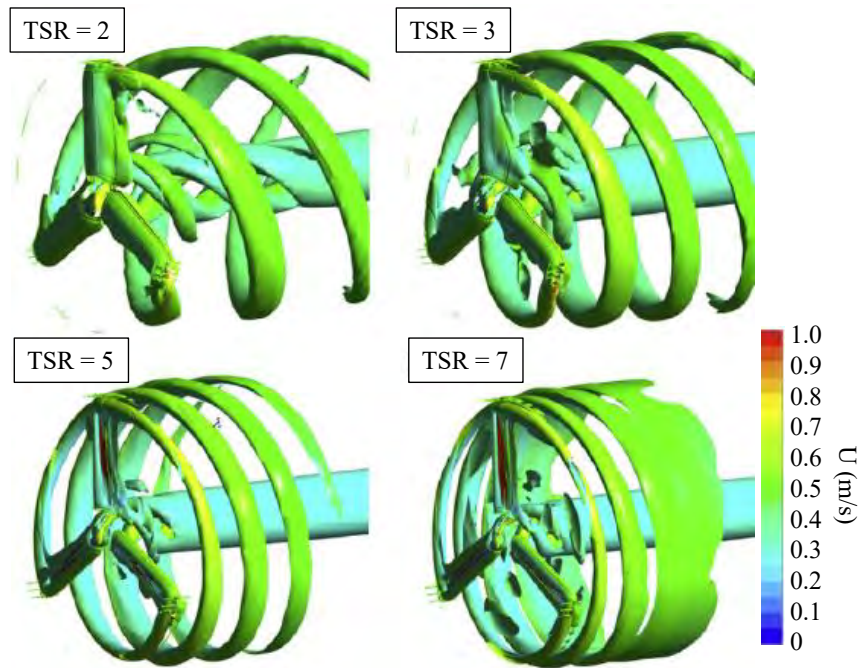
Figure 2-10: Vortical structure using iso-surfaces for varying tip speed rations (Tian, Mao and Ding, 2018)

Previously studies have been performed on the effects of rotational speed on the wake of wind turbines. Although the length of the wake and extremities of effects differ when comparing wind and water characteristics, the behavioural characteristics could be similar. A study by Siddiqui *et al.* (2017) using RANS simulations with moving reference frames concluded that larger vortices were generated at higher λ's, and smaller vortices present at high rotational rates.

Harrison *et al.* (2010) found a trend through CFD and experimental result comparisons, as the thrust coefficient increased the velocity in the near wake decreased. A similar result was found by MacLeod *et al.* (2002).who altered the thrust coefficient of a turbine and observed the differences in wake velocity deficit for a horizontal axis turbine. The velocity deficit increases as the thrust coefficient increased and this difference is visible up to 20 d_t downstream shown on Figure 2-11. This result agrees with the fundamental principle of most analytical wake models. Which show a thrust increase results in a higher velocity deficit in the wake (Lam, Chen and Hashim, 2015; Pyakurel, Vanzwieten, Wenlong, *et al.*, 2017).
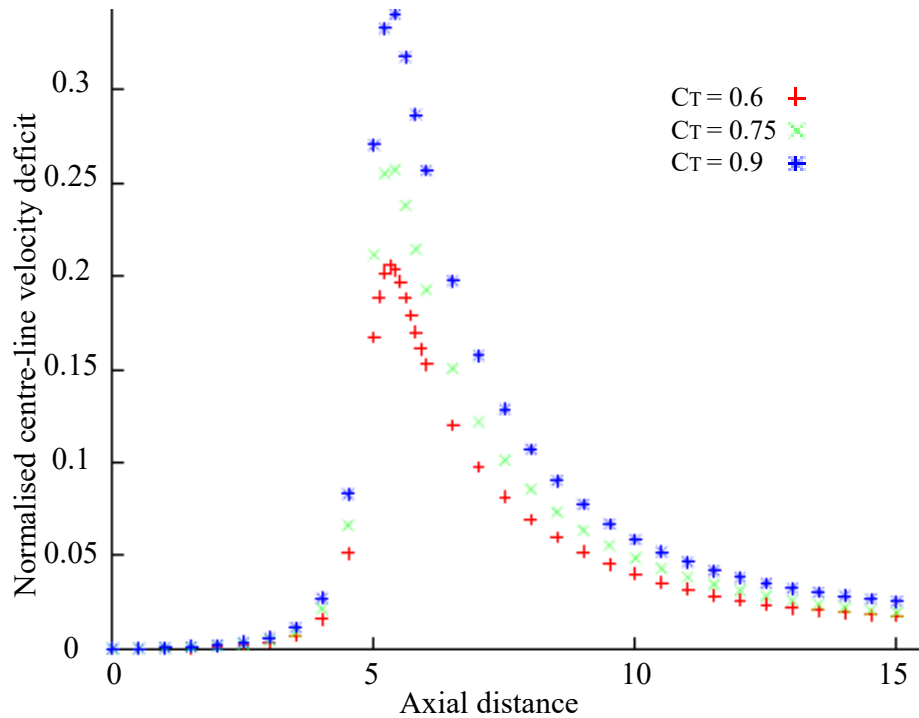
Figure 2-11: Centreline velocity deficit for various turbine thrust coefficients (Macleod et al., 2002)

2.4.3 Effect of blockage ratio

Blockage ratio (β) defined as the percentage cross sectional area taken up by the turbine swept area, has been proven to significantly alter turbine performance at ratios exceeding 5-10% (Kolekar and Banerjee, 2015). Generally for turbines operating at a given λ, higher β results in an increased stream-wise flow speed through and around the rotor which in turn increases the turbine performance (Ross and Polagye, 2020). Multiple studies have found significant increases is C_P and C_T attributed to the acceleration of the bypass flow (Nishino and Willden, 2012).

In HK energy β is usually of interest for two reasons. The first is for correction of scaled laboratory test results representing full-scale unconfined installations to remove the performance effects due to the confined flow (usually for tidal application). This correction is referred to as blockage correction (Whelan et al., 2009). The second being the interest in using the blockage induced increased performance to optimise schemes (Ross and Polagye, 2020) which is also useful for channel or riverine applications. However, past studies have also reported the insensitivity of C_p to β at low λ's (Kolekar et al., 2013; Kinsey and Dumas, 2017).

In terms of wake recovery, the bypass flow around a wall bounded turbine is faster due to the spatial restrictions of the channel bed and walls, as well as the free surface. This change results in a change in velocity deficit comparing to the same case of a turbine placed in unbounded flow. This effect results in changes in the rate of mixing between the wake and the bypass flow (which is the driving force for flow recovery) and thus affecting the wake recovery length scale (Stallard et al., 2013).

As the turbine is installed close to a boundary, wall bounded flow behaviour is exhibited. This increased blockage effect accelerates the flow between the turbine and boundary, improving wake recovery. Experimental results by Bahaj *et al.* (2011) indicated wake recovery is fastest when the wall is 4 d_t from the turbine edge, as this distance is reduced, flow is choked on the boundary side and wake recovery is altered, additional boundary roughness accelerates this effect.

The effect of the depth the HK device is placed below the free surface (usually defined as a H/D ratio with H = the depth of flow) may influence turbine performance as well as wake recovery. Complexities arise when turbines are placed near the free-surface, as the boundary may modify the turbine flow-field and affect device performance. Generally, this causes significant flow acceleration, its magnitude depending on the β extent. Kolekar and Banerjee (2015) found there exists an optimal clearance depth (depth from blade tip to free surface) resulting in improved turbine performance.

Tidal turbines have a minimum H/D of 1.5 usually specified, however this may not be applied to canal/river systems where cross-sectional limitations govern the ratio. Aghsaee and Markfort (2018) investigated the free surface effect experimentally with a scaled model placed in a 30 m long flume section at H/D = 1.25, 1.4 and 1.6. Results indicated the effects in terms of velocity deficit are not seen after 3 d_t downstream where deficit curves were almost equal for the 3 depths. The effects of the mounting rod (only experienced at lower depths) are also diffused by 3 d_t (Aghsaee and Markfort, 2018). The velocity deficit curves for the depths analysed can be seen in Figure 2-12.
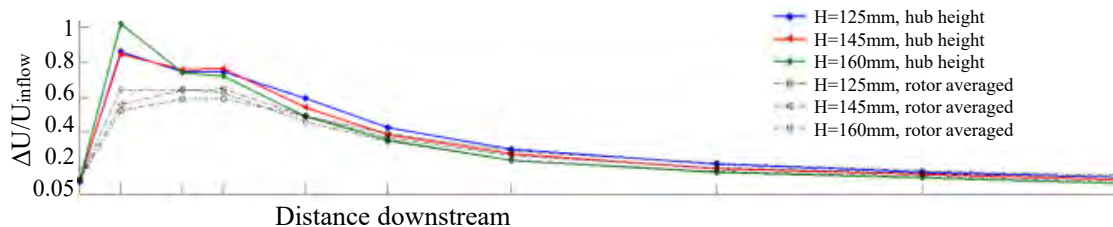
Figure 2-12: Velocity deficit to d_t = 25 downstream for varying turbine depths (Aghsaee and Markfort, 2018)

Stallard *et al.* (2013) also found that although the typical horizontal plane in the wake of a HK turbine follows a symmetrical pattern the vertical profile indicates asymmetry (different flow velocities above and below the wake) due to the presence of the free surface and rigid bed.

2.4.4 Effect of turbine retaining structure and multiple turbine wake interactions

The shape and size of the retaining structure as well as a grid or any other element placed into the flow field, may affect the wake propagation downstream as the blockage is increased/decreased. Even more so in inland HK applications where *β*'s are high. Many studies have stated the turbine geometry may affect the shape of the near wake but have negligible effect in the far wake (Lam and Chen, 2014).

Mason-jones (2010) investigated the HAHT performance effects of a stanchion structure and found the presence of a stanchion significantly increased the amplitude of the cyclic torque,

power and axial thrust during rotation. In terms of wake analysis Siddiqui *et al.* (2017) indicated a faster dissipation rate from the presence of a turbine tower on a HAHT CFD study. Another study found this effect to propagate until 3 d_t downstream (Zhang *et al.*, 2020) supporting the theory of negligible effect in the far wake (Lam and Chen, 2014).

El Fajri *et al.* (2020) investigated the effects of shallow water on the near wake recovery through a benchmark validated CFD model with a tip clearance of H/D of 0.35. The stanchion holding the turbine in place (as seen in Figure 2-13) initiated the free-surface wake interaction. A significant wake deformation can be seen at 7 d_t which affected the wake expansion. The results found suggest the free-surface blockage enhances wake dissipation in the near or intermediate wake by accelerating the flow in the upper bypass region. However, the wake recovery rate (specifically in the intermediate-far wake) was not significantly affected.

(a)   (b)
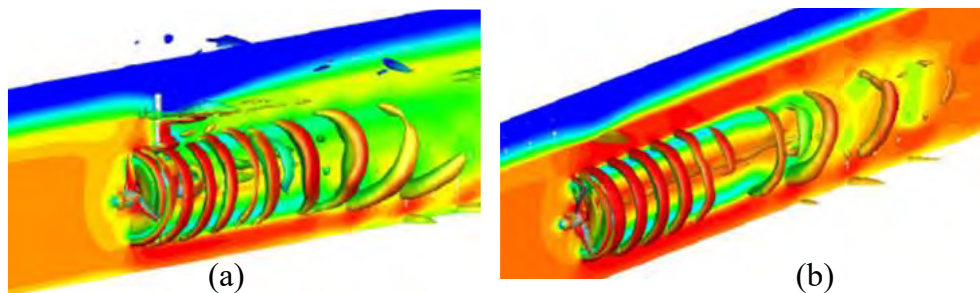
Figure 2-13: Velocity contours for two-phase flow (a) with stanchion and (b) without stanchion (El Fajri *et al.*, 2020)

Stallard *et al.* (2013) performed experimental measurements on the velocity field downstream of several line arrays of three-bladed HAHTs. The tests staggered and aligned configurations of devices and proved wake recovery is faster where the wakes interact. Stallard *et al.* (2013) also investigated lateral effects of turbine wakes when placed next to each other at various distances. Results showed the merging of lateral wakes where at approximately 6 d_t downstream the individual wakes are still apparent. At 8 d_t the lateral wakes seem to merge into 1 wake, accelerating dissipation.

Most studies focus on performance evaluation in arrays (Ahmadian and Falconer, 2012; Jeffcoate *et al.*, 2016) which is usually a direct result of upstream turbine wake recovery. Highlighting once again the importance of correct wake dissipation rates .

2.4.5   Summary of effects

Section 2.4.1 to 2.4.4 cover the most prominent factors affecting HAHT wake formation and dissipation previously investigated in literature. However, other specific factors have been thought to affect the wake such as grids placed upstream of HK devices, specific flow properties such as the freestream velocity, and flow regime, where the magnitude of the effect is still unknown.

A summary of known parameters affecting wake formation is listed in Table 2-1, with reference to the study and findings. This summarises the most researched aspects and highlights where contradictions and discrepancies exist in findings.

Table 2-1: Factors investigated for wake effects

Parameter	Quantified significant effect on the far wake	Quantified insignificant effect on the far wake	Investigation and unquantified effect on the wake
Free stream turbulence	(Lo Brutto *et al.*, 2015) (Pyakurel, Vanzwieten, Dhanak, *et al.*, 2017)(Birjandi, Woods and Bibeau, 2012)(Mycek *et al.*, 2014) (Pyakurel, Tian, *et al.*, 2017) (Blackmore, Batten and Bahaj, 2014)		(Maganga *et al.*, 2010)
Depth below free surface	(Silva *et al.*, 2016)	(El Fajri *et al.*, 2020) (Myers and Bahaj, 2007) 13] (Aghsaee and Markfort, 2018)	(Stallard *et al.*, 2013)
Blockage ratio	(Stallard *et al.*, 2013) (Kolekar and Banerjee, 2015) (Whelan *et al.*, 2009)	(Kolekar *et al.*, 2013; Kinsey and Dumas, 2017)	(Nishino and Willden, 2012) (Ross and Polagye, 2020)
Turbine geometry/retaining structure		(Aghsaee and Markfort, 2018) (Lam and Chen, 2014) (Zhang *et al.*, 2020)(El Fajri *et al.*, 2020)	(Mason-jones, 2010)
Turbine operational conditions (thrust/TSR)	(Wang *et al.*, 2018) (Tian, Mao and Ding, 2018) (Harrison *et al.*, 2010)		
Turbine array effect	(Stallard *et al.*, 2013) (Macleod *et al.*, 2002)		(Churchfield, Li and Moriarty, 2013) (Gotelli *et al.*, 2019)
Reynolds number			(Bachant and Wosnik, 2016)
Debris protection grids	None		
Freestream velocity			

2.5   Review of previously developed wake models

In recent years several analytical approaches have been developed to allow simple, fast and semi-accurate prediction of the wake behind a HK device. Most of these were developed specifically for tidal applications and unbounded flow conditions. Analytical wake models are based on analytical equations such as axial momentum theory, multiple stream tube theory and lifting line theory. In the past these were mainly used for simplified performance analysis and have only recently been employed for wake characterization (Lam and Chen, 2014).

Several analytical wake models have been previously used to model the wake behind a wind turbine, these are commonly referred to as the *Jensen* (Jensen, 1983) *Larsen* (Larsen, 1988), *Ainslie* (Ainslie, 1988) and *Frandsen* (Frandsen *et al.*, 2006) models. These initial wind turbine models differ in fundamental principles to water models, but provide an overview of possible approaches. Pyakurel *et al.* (2017) investigated and adapted three of these models for HK wake modelling (specifically for tidal applications).

Jensen (1983) first made the comparison to the far wake behind a turbine to a negative jet or turbulent wake and representing the wake as a "top-hat" distribution rather than the realistic Gaussian or bell-shaped profile. For wake approximations the maximum deficit in the wake is of importance, and not the average. Therefore, the models (using the top-hat assumption/constant velocity at a lateral distance) determine the worst deficit at a zone downstream of the turbine. This analytical approximation provides the necessary detail of what can be expected in the wake without the requirement of complex solutions.

Ainslie (1988) utilised the theoretical Navier-Stokes (NS) equation, and focused on the far wake, assuming the gradients of mean quantities in the radial direction are much greater than those in the axial direction. The momentum equation is then solved along with the NS equation for radial velocity resulting in a tri-diagonal matrix which can be quickly solved.

The *Larson* model was originally estimated based on Prantl's turbulent boundary equations and a similarity assumption is used to obtain a mean wake profile. The derived equations (containing constants) were then calibrated with wind turbine wakes (Larsen, 1988).

Pyakurel *et al*. (2017) used the basic theory of these models creating two combinations for tidal turbines referred to as the Jensen/Ainslie and Larsen/Ainslie approaches. Coefficients α (Jensen model) and c_1 (Larsen model) were calibrated for a HAHT using CFD generated data. The study concluded the Jensen/Ainslie approaches better suit ocean current turbines with the velocity deficit (U_c^*) calculated as a function of C_T, empirical coefficient *(α)*, radial location from the turbine centreline (r_o) and centreline location (*x*) by utilizing the relationship between axial induction factor and thrust coefficient (Hansen, 2008).

$$U_c^* = 1 - \frac{V_x}{U_o} = \frac{1 - \sqrt{1 - C_T}}{(1 + \frac{\alpha x}{r_0})^2} \tag{13}$$

As experimental results had indicated the strong dependence of wake recovery on turbulence intensity (Mycek *et al.*, 2014). Pyakural *et al.* (2017) provided an empirical coefficients (α for the model shown in equation (9)) accounting for three turbulence intensities (3%, 6 % and 9%).

Lam and Chen (2014) proposed a set of equations (*Lam-Chen* model) to predict the initial velocity closest to the turbine, which were derived based on the axial momentum theory and dimensional analysis providing a solution as shown in Figure 2-14 (also utilizing the top-hat assumption). The term efflux velocity (V_0) is used to define the minimum velocity taken from a time-averaged velocity distribution along the initial turbine plane, which in turn is the point of lowest velocity (V_{min}) in the wake (maximum velocity deficit) and the point where recovery starts. For the *Lam -Chen* model the efflux velocity is then used in a defined set of equations to calculate the respective minimum velocities at points downstream.

Free Stream Velocity V_∞
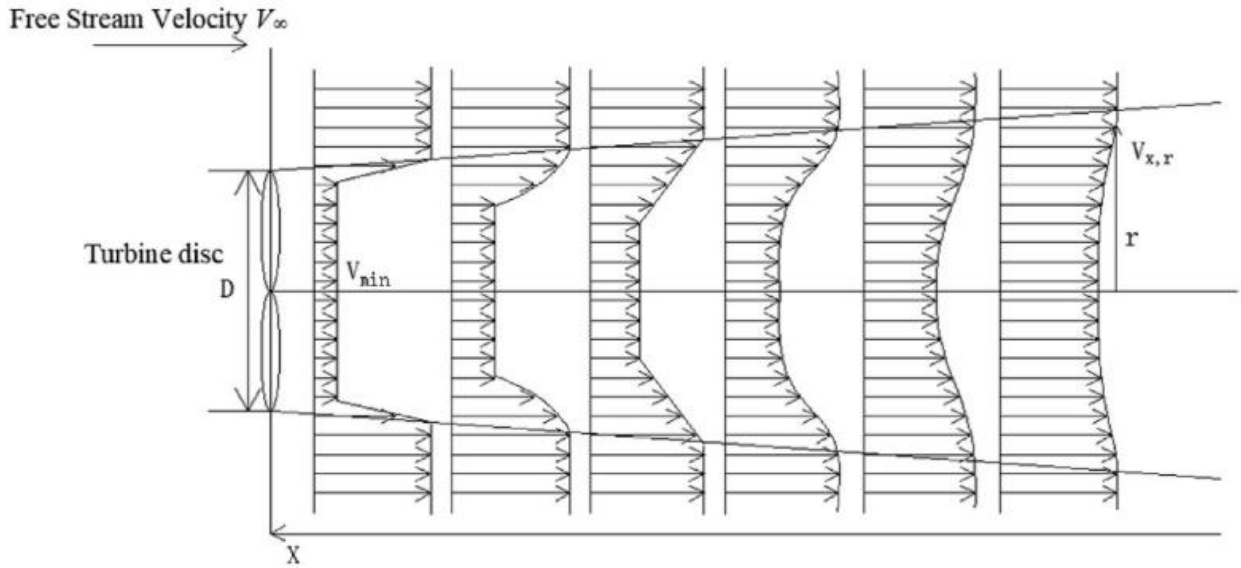
Figure 2-14: Turbine wake based on the Lam-Chen model (Lam and Chen, 2014)

For the *Lam-Chen* model the equations for V_0 are primarily based on turbine thrust, and stem from the analytical propeller jet theory (Hamill and Kee, 2016). The turbine thrust (T) can be expressed in the following equation through use of Bernoulli's energy equation:

$$C_T = \frac{T}{\rho n^2 D^4} \tag{14}$$

In terms of rotation (n), diameter (D) and density (ρ). Substituting the properties of a HAHT into these equations the efflux velocity (V_o) can be derived as a function of the free stream velocity (V_∞) based on the propeller jet theory:

$$V_0 = \sqrt{(V_\infty)^2 - (1.59nD\sqrt{C_T})^2} \tag{15}$$

Lam, Chen & Hashim (2015) then further adapted this equation to include less inputs. By assuming, due to the much lower rotation rates of a turbine comparing to propeller jets, the thrust coefficient (C_T) can be defined as :

$$C_T = \frac{T}{\frac{1}{2}\rho AU^2} \tag{16}$$

And therefore, the efflux velocity allows a much simpler formulation. Empirical coefficients were added, calibrated from a set of experimental results, resulting in the following formulation for velocity deficit (V_{min}) in the wake (at distance x downstream):

$$V_{min} = \left(0.0927\left(\frac{x}{D}\right) + 0.993\right) \times V_\infty\sqrt{1 - C_T} \tag{17}$$

Wang *et al.* (2018) noted the importance of considering turbine solidity and tip speed ratio (λ) when calculating the efflux velocity and adapted the *Lam-Chen* model to include an additional

energy term (E), which is a function of λ, also providing radial solutions to meet the Gaussian profile in the wake (visual representation shown in Figure 2-15).

$$V_0 = \sqrt{V_\infty{}^2 - (nD\sqrt{EC_T})^2} \tag{18}$$

$$E = 16.174\lambda^{-1.837} \tag{19}$$
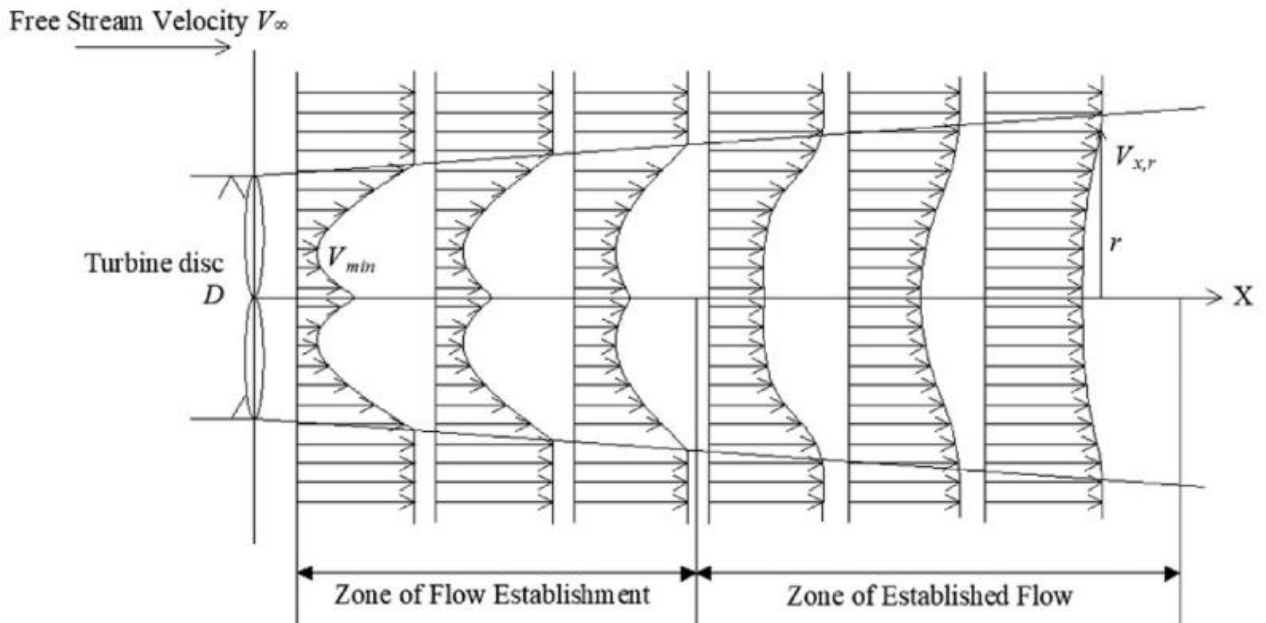
Figure 2-15: Turbine wake model proposed by Lam-Wang (Wang *et al.*, 2018)

It is important to determine not only the efflux velocity but also the point where this will occur. When comparing to the propeller jet theory, Berger *et al.* (1981) mentioned a point relevant to turbines: "*When comparing a ships propeller to a plain water jet, the wake differs due to the presence of the hub*". Therefore, although Hamill, McGarvey and Hughes (2004) suggested the position of maximum velocity for a water jet is located along its axis, this may not be true to propeller jets.

Berger *et al.* (1981) suggested for a ship propeller the position of maximum velocity (R_{mo}) can be predicted as a function of the radius of the propeller *(R)* and the radius of the propeller hub (R_h):

$$R_{mo} = 0.67(R - R_h) \tag{20}$$

Prosser (1968) proposed a position at 60% of the blade radius from the hub. Hamill, McGarvey and Hughes (2004) proposed rather 0.7 in place of 0.67 shown in the formula by Berger *et al.* (equation (20)). Through studies completed by Lam, Chen and Hashim (2015) comparing results to experimental results for HAHTs the equation by Berger *et al.* (1981) was found to correlate best and recommended for determination of the point of lowest velocity in the wake of a HAHT.

Although the previously developed wake models may have a different field of application, or need further validation, the initial development and factors considered may be used to give an

indication of the variables which have most weight and effect of wake development and recovery. A summary of wake models which have been considered, developed, or adapted for HK turbines as well as the variables considered in each model are listed in Table 2-2.

Table 2-2: Wake models and factors considered in each model

Model	Governing equation	Considered variables
Larson model (Larsen, 1988) adapted for tidal turbines	$U_c = 1 - \dfrac{V_x}{U_o} = \dfrac{1}{9}(C_T A_d x^{-2})^{\frac{1}{3}}\left(\left(\dfrac{35}{2\pi}\right)^{\frac{3}{10}}(3c_1{}^2)^{\frac{-1}{5}}\right)^2$	Downstream velocity (V_x), Thrust coefficient (C_T), non-dimensional mixing length (c_l) Rotor diameter (A_d)
Jensen model (Jensen, 1983) adapted for tidal turbines	$V_x = U_o(1 - 2a\left(\dfrac{R}{R + \alpha x}\right)^2)$ $a = 1 - \sqrt{\dfrac{1 - C_T}{2}}$	Free stream velocity (U_o), Thrust coefficient (C_T), empirical coefficient (α), axial induction factor (a) (in terms of C_T) and Rotor radius (R)
Lam & Chen model. (Lam and Chen, 2014; Lam, Chen and Hashim, 2015)	$V_{min} = (0.0927\left(\dfrac{x}{D}\right) + 0.993) \times V_\infty \sqrt{1 - C_T}$	Free stream velocity (V_∞), thrust coefficient (C_T)
Adapted Jensen and Larson coefficients (Pyakurel *et al.*, 2017)	$\alpha = 0.00003TI^4 - 0.0009TI^3 + 0.0097TI^2 - 0.0396TI + 0.0763$ $c_1 = 0.0406e^{0.1361TI}$	Turbulence intensity (TI) additional to the terms considered in Larsen and Jensen models.
Wang, Lam, Cui, Zhang, Jiang, Sun, Guo, Ma and Hamill. (Wang *et al.*, 2018)	$V_0 = \sqrt{V_\infty{}^2 - (nD\sqrt{EC_T})^2}$ $E = 16.174\lambda^{-1.837}$	Free stream velocity (V_∞), thrust coefficient (C_T), rotation rate (n), and tip speed ratio (λ)
Multiple turbine wake model. (Oppong *et al.*, 2020)	$V_o = \sqrt{(V_\infty)^2 - (1.59(n_o - n)D\sqrt{C_T})^2}$	Free stream velocity (V_∞), thrust coefficient (C_T), rotation rate (n) and turbine diameter (D)

2.6 Water surface deformation effects of HAHTs

HAHTs in bounded flow fields may result in significant free surface deformation above the device. Provided subcritical flow regimes hold, this may result in water level changes at significant distances upstream. A simple schematic of the primary principles occurring in the flow and resulting in a free surface effect can be seen in Figure 2-16. The increase in the free surface (Δh) occurs due to the pressure changes in the turbine region (Whelan *et al.*, 2009).
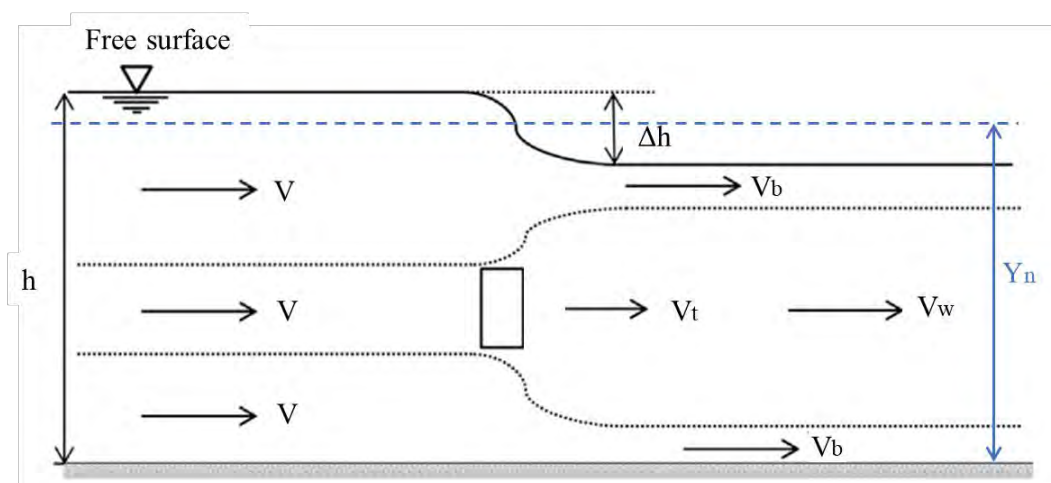
Figure 2-16: 2D approximation of the flow past a turbine (Birjandi *et al.*, 2013)

Previous studies into the free-surface effects of HAHTs have indicated extreme near-field effects and flow deformation directly upstream and downstream of the HAHT. Myers and Bahaj (2007) investigated a 1:30 scale HAHT model (rotor diameter = 0.4 m) and observed a clear difference in the water surface during energy extraction. Water depths increased immediately upstream of the rotor and decreased downstream for about 2 d_t. Observations of the water surface profiles can be seen in Figure 2-17. The results indicated a standing wave between 7-8 d_t downstream (it should be noted this was for the high freestream velocity case).
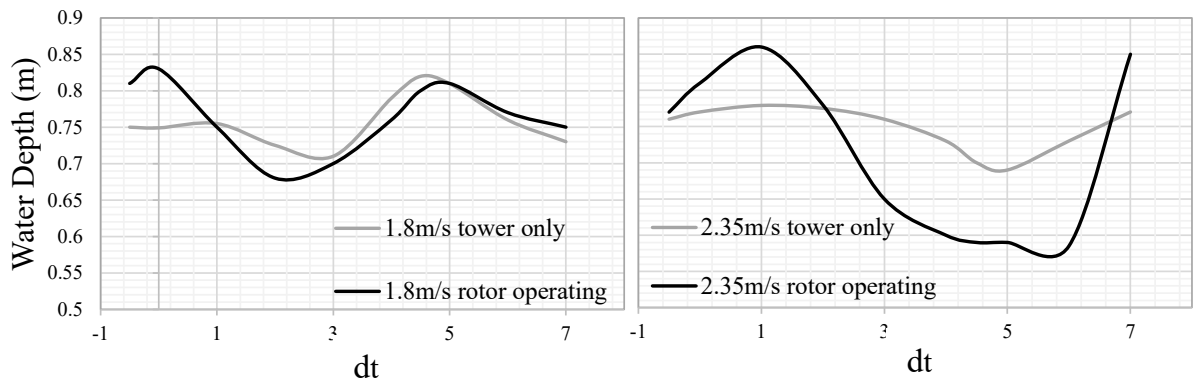
Figure 2-17: Water surface profile through a scaled turbine operating at 2 different velocities, comparing to the no energy extraction stage (Myers and Bahaj, 2007)

Understanding the specific energy and flow regime is imperative to allow flow behaviour prediction after HK deployment. Here a Froude number based on turbine diameter ($Fr_D = \frac{U}{\sqrt{gD}}$ where U is the mean velocity, and D the turbine diameter) may be more useful, which has also been linked to the free-surface effects (Adamski, 2013).

The flow effects observed can be explained using the specific energy of the flow section, which is a function of water depth and velocity. When ignoring friction losses (from the channel sides and bed) the specific energy may be defined as:

$$E = y + \frac{\alpha Q^2}{2gA^2} \tag{21}$$

Through the water depth (y), the energy coefficient (α), the volumetric flow rate (Q in m³/s), the cross-sectional area (A in m²) and gravitational acceleration (g). The energy coefficient can then be defined as:

$$\alpha = \frac{\sum u^3 \Delta A}{U^3 A} \tag{22}$$

Where u is the velocity measured within an elemental area, ΔA. The flow regime (sub- or supercritical) and thus the Froude number of the flow will govern the behaviour of the flow (Henderson, 1966).

A parameter of specific interest is the critical depth of the channel in which the turbine is placed. When the water surface decreases to critical or below critical depth, flow phenomena such as the formation of a hydraulic jump may occur downstream to allow recovery to a

normal flow depth. Even for subcritical conditions, previous research has indicated that for high blockage ratios (above 30%) the bypass flow may become supercritical, this is however dependent on the exact free stream flow conditions (Whelan *et al.*, 2009).

Simplification of crucial free surface parameters in inland HK installations can be summarised by two fundamental effects (Figure 2-18):

- Free-surface effects in the form of a possible standing wave formed, or decreased water surface above the turbine (due to a pressure drop).
- Potential backwater effects caused (damming upstream up to a distance, defined by the flow regime).

As shown in the organogram (Figure 2-18) the blockage resulting from the HK device (in typical subcritical, flat-sloped channels) may have multiple subsequent effects influencing downstream installations (within an array) as well as upstream flow conditions. Neglecting the free surface effects in high blockage ratio cases may result in exposed downstream turbines (freeboard reduced), hydraulic jump (HJ) formation (enforced critical flow), upstream damming effects and may lead to potential blade tip cavitation problems. Accurately quantifying the water surface effects is a challenge, and clearer guidelines to avoid unfavourable conditions would be valuable.
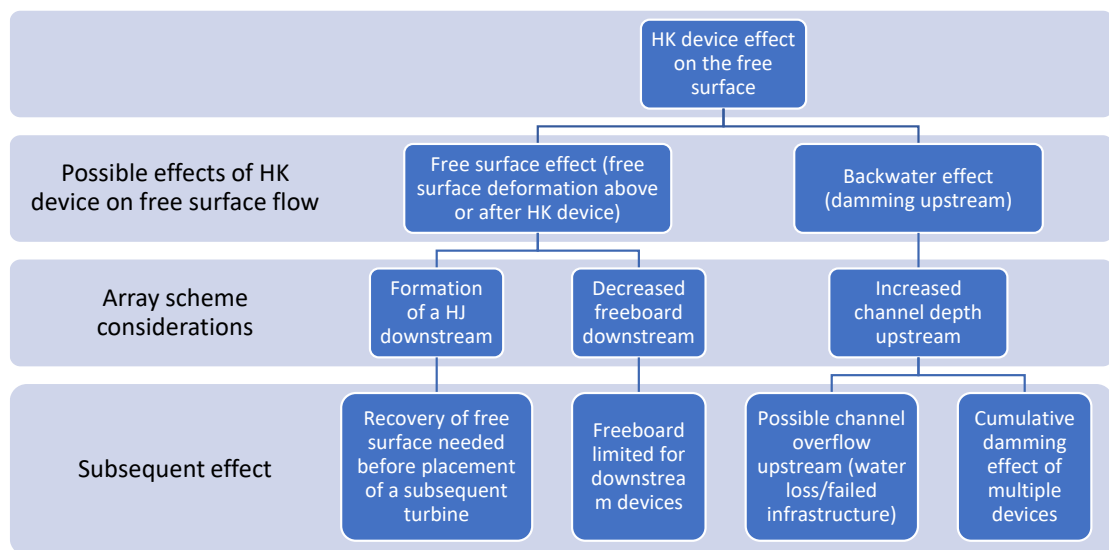
Figure 2-18: Water surface deformation from HK devices in inland flow infrastructure

2.6.1 Free surface effects of HAHTs

Free surface effects are a critical aspect in riverine and tidal turbine array design as the standing wave formed downstream of the turbine may affect turbine submergence as well as additional downstream turbines. Previous studies have concluded the depth of the downstream water surface is strongly dependant on the Fr_D. Additionally, the β also affects this free surface change, however not as strongly as Fr_D (Adamski, 2013).

Myers and Bahaj (2007) found when imposing an assumed wake expansion estimation on the water surface, this coincided with the increased elevation observed 4-5 d_t downstream of the turbine rotor (as shown in Figure 2-19). In addition, due to the wake expansion coincident

with the free surface, cumulative turbine placement at intervals smaller than the recovery length may cause the flow to approach critical depth causing severe undulations in the water surface profiles (WSP's). Turbine operation and efficiency may also vary due to decreasing flow velocity over the blades during operation. Accurate quantification of the WSPs around an array may be a challenge due to multiple effects of turbulence, wake mixing and superposition of WSP effects (Myers and Bahaj, 2007).
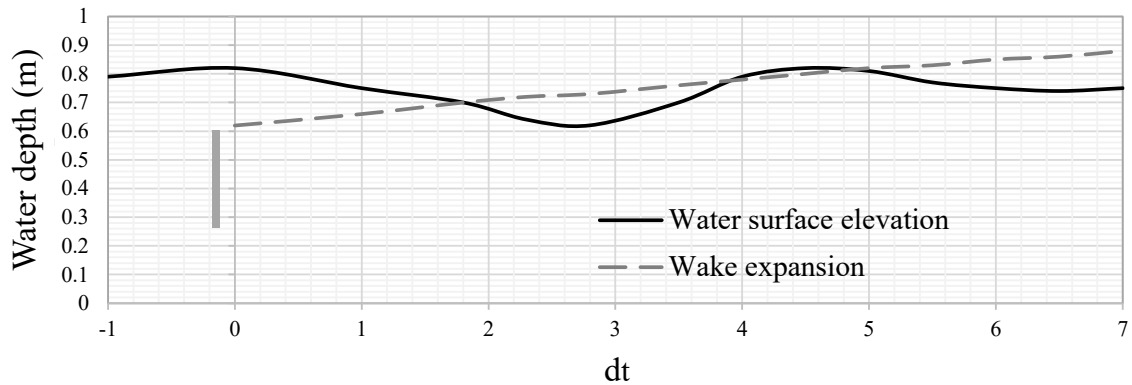
Figure 2-19: Wake expansion effect with free surface (Myers and Bahaj, 2007)

The presence of a support structure (tower/stanchion) may also alter the free surface effect (Myers and Bahaj, 2007) (also see Figure 2-17). The same experiment proved the strong possibility of the formation of a hydraulic jump downstream of the turbine when flow is forced to a supercritical regime due to the presence of the turbine together with the support structure.

Free surface effects may be more pronounced for shallow turbines compared to turbines installed well below the free surface. It is also important to consider possible cross-sectional changes in the infrastructure where the turbine is placed, as this may alter/dampen/exaggerate these effects. Specified clearance coefficients have been previously investigated for tidal turbines to limit the severity of decreased depths downstream of the turbine, or possible exposure of the turbine. Birjandi *et al*. (2013) proposed a clearance coefficient, C_h defined as:

$$C_h = \frac{h_c}{L} \tag{23}$$

where h_c is the turbine submergence depth (height between the top of the turbine and water surface) and L the rotor diameter. The recommended clearance coefficients for commercially available tidal turbines can be seen in Table 2-3.

Table 2-3: Clearance coefficients for commercial HAHTs (Birjandi *et al.*, 2013)

Turbine name	Turbine details	Clearance coefficient
Seaflow	2-bladed, 300kW	0.18-0.64
SeaGen	2-bladed, 1.2MW (2x 600kW)	0.25-0.38
HS300	3-bladed, 300kW	0.75
AK-1000	3-bladed, 1MW	1.02

2.6.2   Backwater effects

Backwater effects refer to a phenomenon experienced in subcritical flow conditions where downstream blockages in the flow field result in a flow disturbance travelling both upstream and downstream. This is attributed to the nature of the free stream velocity at subcritical flow conditions where the flow disturbance is propagated at a wave speed of $c = \sqrt{gy}$, (where y is the channel depth and g the gravitational acceleration) exceeding the flow velocity and thus moving upstream (Chadwick, Morfett and Borthwick, 2013).

A HK device acts as a blockage as well as energy loss in the channel. When $Fr << 1$ and subcritical flow is prevalent, the backwater effect may extend a large distance upstream and cause significant damming. This depends greatly on the blockage ratio (β) as well as theoretical to actual efficiency (Whelan *et al.*, 2009).

In a study on a pilot HAHT installation placed in an irrigation canal, the backwater effect from the presence of the turbine extended up to 2.7 km upstream, due to the flat slope and subcritical flow present in the channel (Niebuhr, van Dijk and Bhagwan, 2019) (Figure 2-20). The clearance coefficient for this installation had not yet been defined. The specific turbine studied in the project included grids upstream of the turbine, which trapped debris and caused further increase in the backwater effect to the point of channel overtopping. The blockage ratio for the installation was around 12.5%.
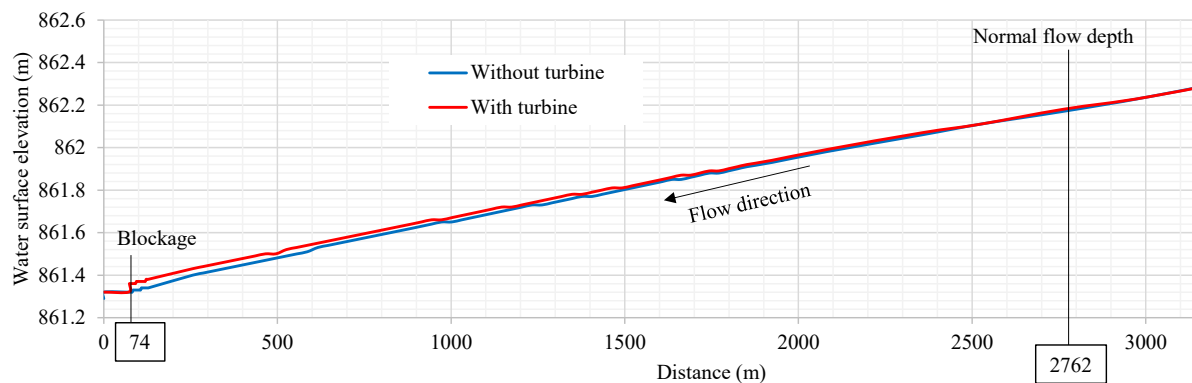
Figure 2-20: Backwater effect due to turbine blockages (Niebuhr, van Dijk and Bhagwan, 2019)

Additional to the blockage ratio, the Fr or Fr_D of the flow can influence the backwater effect. A previous study analysing this effect drew the following conclusions (Adamski, 2013):
1. The upstream free surface deformation increased with Fr_D.
2. The location of maximum damming (highest water level) moved closer to the turbine as Fr_D increased.

2.7   Review of previously developed backwater models

Previous studies have investigated the hydrodynamic effects of HAHTs both experimentally (e.g. in canals (Gunawan, Roberts and Neary, 2015), investigating boundary layers (Bahaj *et al.*, 2011) and varying Reynolds numbers (Bachant and Wosnik, 2016)) and computationally (both CFD applications in (Kartezhnikova and Ravens, 2014) and (Turnock *et al.*, 2011)).

However, most of the studies are performed under constant operational conditions and are site specific.

Only a few previous studies have attempted to quantify the effective blockage of a HAHT within a flow area to allow determination of the backwater effect. Some have addressed this through using the relationship of overall power extracted to total power dissipated by the devices (Polagye, 2009), analytical relationships (Lalander and Leijon, 2011) and even enhanced manning n-values where the energy loss is included as a friction loss (Kartezhnikova and Ravens, 2014).

Generally, backwater calculations utilise a blockage size (typical backwards facing step, weir or pier shape) or energy loss function (quantified energy losses) to predict the backwater effect. Due to the novelty of HK energy, a streamlined procedure for determining the backwater effect has not yet been determined. This may be attributed to the variability of turbine types, operational conditions, and efficiencies, all of which result in a different effective blockage.

The extraction of energy resulting from the HK device may also be analytically incorporated through the use of the momentum equation (Bryden, Grinsted and Melville, 2004) where the power extraction term is added as a shear stress component (added to the effective shear stress caused by bed friction). Assuming gradually varied steady-state flow, the conservation of mass and momentum can be used to adjust the standard open channel flow equation (Chanson, 2004) with the addition of a term for artificial energy extraction (Bryden, Grinsted and Melville, 2004):

$$\left(1 - \frac{Q^2}{h^3 b^2 g}\right)\frac{\partial h}{\partial x} = \frac{\partial h}{\partial x}\frac{Q^2}{gh^2 b^3} - \frac{1}{\rho gbh}P\,\tau_{eff} \qquad (24)$$

which is defined by the channel flow depth (h) width (b) and flow rate (Q) at streamline position x. The effective shear (τ_{eff}) is defined as a combination of bed shear (τ_o) and power extraction added as a shear term (τ_{add}):

$$\tau_{eff} = \tau_o + \tau_{add} = \rho\frac{g}{C^2}U^2 + \frac{P_x R}{U} \qquad (25)$$

where P is the wetted perimeter, C the Chezy friction coefficient, and P_x the term added for power extraction, which may be more useful to express in terms of P_A being the power extracted per unit area. As the flow passes through a plane where $P_x = \frac{P_A}{\Delta x}$ (Δx being the change in distance) the free surface deformation is calculated. Such an effect can be seen graphically in Figure 2-21 where a 10% energy extraction term was added.
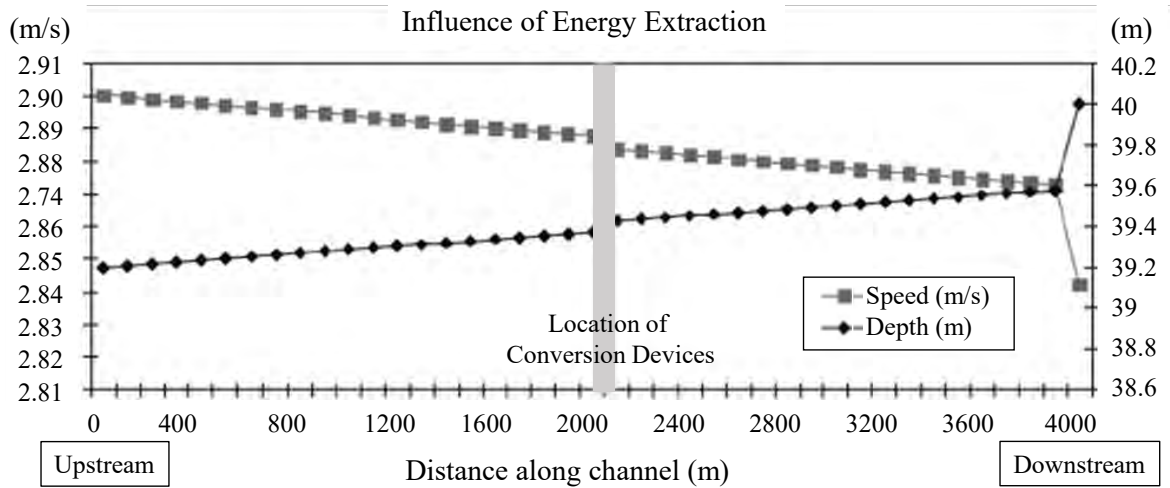
Figure 2-21: Influence of artificial energy extraction on speed and depth of flow (Bryden, Grinsted and Melville, 2004)

Mańko (2018) attempted to determine the backwater curve for instances when either the cross-section varied, the channel slope changed or when there was an obstacle in the channel and gradually varied flow was present. The model was based on the Bernoulli equation between two cross-sections. The energy loss between the cross-sections (related to distance) was termed the hydraulic loss, I, which can be calculated using

$$I = \frac{n^2 U^2}{R_h^{\frac{4}{3}}}$$

(26)

where n is the Manning roughness (s/ m$^{1/3}$), R_h is the hydraulic radius of the channel in (m) and U is the velocity of water in (m/s). The change in water levels (Δz) between two sections can then be determined between two significant cross sections (e.g., 0 and 1) and calculated as shown in the equation below, where $\propto$ is the Coriolis coefficient and U_0 and U_1 are the average velocities, over distance ΔL:

$$\Delta z = \Delta L \left(\frac{I_0 + I_1}{2} \right) + \frac{\propto}{2g} (U_0^2 - U_1^2)$$

(27)

Very few models have been developed to attempt to predict the backwater effect. Most studies have focussed on tidal arrays and using free-surface effects to determine the optimum number and placement of turbines (Garrett and Cummins, 2005, 2007). Within tidal applications free-surface effects are only of concern for tip-clearance and therefore these models have limitations within the application in steady inland channels where spatial constraints are of primary concern.

In the study by Kartezhnikova and Ravens (2014) an increased manning roughness coefficient is used on the channel section representing the HAHT. The n-value used is a function of the actual channel n-value, slope, water depth, device efficiency, blockage ratio and device deployment density. The method can then be used to determine the hydraulic impact as well as impact of various device configurations.

The head loss associated with the channel friction (h_{Lt}) (used in the energy conservation equation) is written as a function of cross-sectional area (A_0), channel hydraulic radius (R_h), discharge (Q_n), and the length over which the loss is applied (L):

$$h_{Lt} = \left(\frac{Q_n}{A_0 R_h^{2/3}} \right)^2 L \tag{28}$$

Based on the assumption that the upstream and downstream velocity and pressure heads are equal and assuming the drag loss is negligible, the following equation for an enhanced bottom roughness (n_t) can be derived as a function of the total power dissipated (h_p), change in elevation (Δz) and channel Manning roughness coefficient (n):

$$n_t = n \left(1 - \frac{h_p}{\Delta z} \right)^{-1/2} \tag{29}$$

This approach required assumptions on L as well as n which strongly affect results.

Lalander and Leijon (2011) investigated the use of numerical and analytical models to determine the effects on upstream water levels in a river. The analytical model is dependent on the channel blockage (β of the HK device) and determining energy loss from the energy capture and the energy losses in the wake. The analytical models are based on the same theory, that energy is removed, causing a power loss, thus energy capture is a component of the total friction in the channel.

The total head loss can be determined as the sum of friction loss (Δh_f) and the head loss caused by the presence of the turbine (Δh_t) and P_t is the total power of the turbine. The formulation of the stress term τ_f, where f is equal to the Darcy-Weisbach coefficient and U is the velocity of water is included as:

$$\Delta h_{tot} = \Delta h_f + \Delta h_t = \frac{L}{\rho g R_h} * \tau_f + \frac{P_t}{\rho g Q} \tag{30}$$

Where:

$$\tau_f = \frac{f\rho}{8} * U^2 \tag{31}$$

Although some attempts have been made at backwater calculation models, the strong dependence on input parameters which are difficult to predict, or not available during the design phase (e.g. Bypass flow characteristics) is a major setback. Although the work provides a theoretical base to develop a future approach, there is still work to be done. It is also important to consider the blockage effect, which may increase the turbine power output (Garrett and Cummins, 2007; Ross and Polagye, 2020) as this will alter the energy loss or momentum change experienced.

2.8 Numerical models of HAHTs

Analytical and numerical models have been used in recent years to offer an alternative analysis to modelling the HAHT surrounding flow. These techniques may be used as a tool to assess possible concerns, problem areas and identify unforeseen hydrodynamic effects in the

HK turbine flow field. Laboratory tests are often expensive and prove difficult to accurately scale the flow environment (Hill *et al.*, 2020). Although few studies on a range of numerical modelling approaches of HK devices have been investigated, multiple studies have been performed into effective modelling of wind turbine models, and a similar theory may be applied to HK device analysis.

The simplest approach to modelling the wake is the employment of analytical models (Lam and Chen, 2014; Lo Brutto *et al.*, 2015; Lam, Chen and Hashim, 2015), where the self-similar nature of the far wake is exploited to obtain expressions for velocity deficit and turbulence intensity. The *Jensen* model (Jensen, 1983) is most often used in wake analysis. It models the velocity deficit in the wake as radially independent. The model provides a one-dimensional (1D) mathematical expression for the wake velocity deficit downwind of a single wind turbine. The wake speed is assumed to be the only variable in the function of the downstream dissipation distance, this means the predicted wake profile at a certain distance downstream is assumed to be uniform (Tian *et al.*, 2015). Due to the simplistic approach effects of a retaining structure, confined flow and onset turbulence are not included.

Due to recent developments in tidal energy, multiple large-scale analyses of tidal turbine arrays have been reported. The majority of these studies utilise simplified numerical models for array scheme analysis (Nishino and Willden, 2012, 2013; Adcock, Draper and Nishino, 2015; Gotelli *et al.*, 2019). The blade element momentum theory is often used for simplified performance analysis, however does not include any effect in the wake from the freestream or bounded flow (Whale *et al.*, 2000). This theory uses global momentum balance together with 2D blade elements to calculate aerodynamic blade characteristics (Sanderse, van der Pijl and Koren, 2011).

Vortex-lattice and vortex-particle methods (Fabrice *et al.*, 2008; Pinon *et al.*, 2012) describe the wake vorticity in concentrated sheets of particles. Generalised actuator disk (AD) as well as direct method are commonly referred to as computational fluid dynamics (CFD) methods which are newer more accurate methods taking into account external effects, retaining structures and wall effects (Sanderse, van der Pijl and Koren, 2011). A summary of these models with the method of blade and wake modelling are shown in Table 2-4.

Table 2-4: Classification of models (Sanderse, van der Pijl and Koren, 2011)

Method	Blade model	Wake model
Kinematic	Thrust coefficient	Self-similar solutions
Blade element momentum (BEM)	Actuator disk + blade element	Quasi one-dimensional momentum theory
Vortex lattice, vortex particle	Lifting line/surface + blade element	Free/fixed vorticity sheet, particles
Generalised actuator	Actuator disk/line/surface	Volume mesh/RANS/LES
Direct	Volume mesh	Volume mesh, Euler/RANS/LES

CFD models may be used to resolve the effect of turbulence at sub-grid scale level. As larger computational options are becoming more readily available these models are being used more often for first order analysis or design. Various orders of complexity and thus computational cost required are available to resolve these turbulence scales. As CFD models are used for

generation of data in this study, a literature review of common approaches and findings relevant to HK energy is included.

2.9   Computational fluid dynamics modelling of HAHT

CFD modelling has become the method of choice of HK turbine device analysis. Additionally, studies on similar energy generation mechanisms such a wind energy and tidal energy development allow a broad spectrum of studies where CFD is used for analysis of performance and wake interaction. Virtually all flows are turbulent and thus require a competent turbulence model for correct capture of the flow field. Models capturing the complexities of turbulent flow are especially important in the presence of flow separation, vortex shedding and fluid-structure interaction. All of which are present in the flow surrounding HK turbines.

The Navier-Stokes (NS) equations are most suitable to describe the hydrodynamics around HK devices. However, these equations are not easily solved as the difficulty lies in the presence of non-linear convective terms creating a wide range of time and length scales, especially in the small scales existing in the blade boundary layers (Davidson, 2004).

The range of scales can be identified by the Reynolds number (Re) which indicates the ratio of convective to viscous forces in the flow. Large Re values lead to large ranges in scales resulting in a large computational expensive. Resolving all these scales is referred to as a direct numerical simulation (DNS) which, due to the inherent scaling laws of turbulence, are only applicable at very low Re and very simple geometries, and therefore not feasible in HK applications (Menter, 2011).

Due to this, turbulence models are developed to model the unresolved small scales through the known behaviour of the resolved large scales. Common approaches to simplify solving the NS equations include Large-Eddy simulations (LES), Reynolds-averaged Navier Stokes (RANS) models and detached eddy simulation (DES), all of which have different applications and vary in computational demand.

Uniformity laws and "scales of modelling" are important considerations within computational models of HK flows. This ensures dependant variables are included and computational resources are focussed on key aspects. For tidal applications scales of hydrodynamic modelling have previously been developed to address the required accuracy at each scale (Adcock, Draper and Nishino, 2015). A similar approach may be applied to inland HK systems. The four primary scales of modelling are represented in Figure 2-22. Each scale has a focus and may be more specifically defined as:

1] Device scale (blade scale):
   a. Focus on the flow around the turbine blades, lift and drag, performance analysis (Adcock, Draper and Nishino, 2015; Fontaine *et al.*, 2020; Hill *et al.*, 2020)
   b. Important to capture the 'dynamic stall' due to the massive flow separation (Fontaine *et al.*, 2020) to accurately predict turbine performance.
   c. Important to capture effects of blade roughness (fouling), e.g., (Walker *et al.*, 2014; Fontaine *et al.*, 2020)

    d.   Important to capture effects of submergence and cavitation (Bahaj, Molland, *et al.*, 2007; Fontaine *et al.*, 2020)

    e.   Important to capture blade wakes and tip vortices, e.g., (Fontaine *et al.*, 2020; Hill *et al.*, 2020)

    f.   Requires highly accurate simulations resolving the large eddies not only in the wake, but also the boundary layer still attached to the blades (Churchfield, Li and Moriarty, 2013; Mannion *et al.*, 2019).

2] Device scale (rotor scale) flow field analysis:

    a.   Analysing the bulk thrust load and wake resulting from specific operating conditions (Sanderse, van der Pijl and Koren, 2011).

    b.   Effect of local flow conditions e.g. ambient turbulence (Maganga *et al.*, 2010; Mycek *et al.*, 2014)

    c.   Prerequisite to determining placement of array schemes.

3] Array scale (channel scale) analysis:

    a.   Turbine inter-effect (Interaction of multiple turbines).

    b.   Effect of local flow conditions, e.g., ambient turbulence (Mycek *et al.*, 2014)

    c.   Simplified techniques such as porous disk method (Myers and Bahaj, 2012) or blade element momentum theory applied on an actuator disk (BEM-AD) together with Reynolds-averaged Navier-Stokes (RANS) equation models (Edmunds *et al.*, 2014; Malki *et al.*, 2014) or actuator line large eddy simulations (LES) (Churchfield, Li and Moriarty, 2013)

4] Far field flow analysis (full system analysis):

    a.   Analysis of far field backwater effects, blockage effects, erosion, sedimentation.

    b.   Simplified 1-dimensional or 2-dimensional modelling using simplified numerical or analytical models (Kartezhnikova and Ravens, 2014; Lam and Chen, 2014; Pyakurel, Vanzwieten, Wenlong, *et al.*, 2017; Dai *et al.*, 2018)
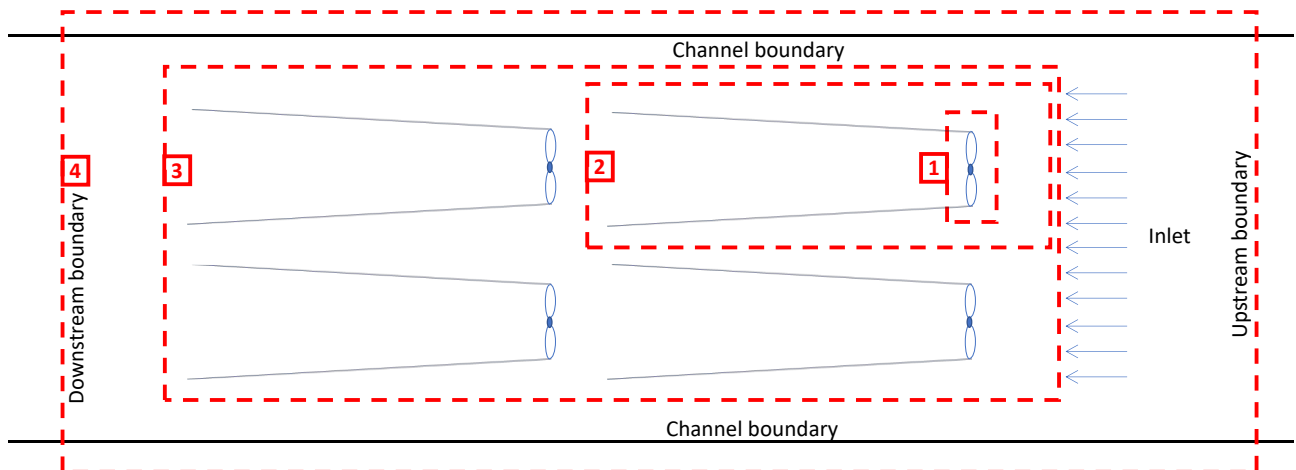
Figure 2-22: Scales of modelling inland HK schemes (Niebuhr *et al.*, 2022)

As summarised in Fontaine at al. (2020), numerous physical modelling studies have investigated device scale physics. Including wake generation, dissipation and flow recovery downstream of a single turbine. Similar numerical modelling investigations have been performed (Bahaj, Myers, *et al.*, 2007; Harrison *et al.*, 2010; Silva *et al.*, 2016; Boudreau and Dumas, 2017; Chen, Lin, Lin and Wang, 2017) however, clear guidelines on suitable computational approaches and methods to avoid inaccuracies and errors are lacking.

2.9.1 Turbulence modelling

As mentioned before, the flow surrounding a HAHT is turbulent due to the fluid-structure interaction and strong vorticity in the wake. For an accurate model depicting the flow and the turbulent nature, the behaviour needs to be captured. Turbulence itself is difficult to define and can be described as irregular, diffusive three dimensional, dissipative, and continuous. It is a property of the fluid flow and not a fluid property. Turbulence is often treated as a random process arising when flow is sufficiently high in Re and disturbed by an instability, such as a HK device. The turbulent state is then maintained by taking the energy from shear flow (Rose, 2018).

For CFD models, a range of turbulence models are available to model the turbulent structures in the wake which ultimately drive wake dissipation. This is the most limiting factor in accurate computational simulations of engineering flows (Menter, 2011). To incorporate the best performing models an understanding of the flow behaviour is necessary.

Accurately representing turbulent flow in CFD remains a large challenge due to its strong dependence on initial conditions as well as the wide range of scales (eddies) present in the flow. Most often statistical approaches based on RANS, with eddy viscosity models for turbulence closure, are used (Contreras, Lopez and Lain, 2017; Pyakurel, Tian, *et al.*, 2017). RANS methods aim to describe flow statistically where flow quantities (e.g., Velocity, pressure, density, and temperature (x)) are split into averaged $\bar{u}(x)$ and fluctuating $u'(x,t)$ terms, referred to as Reynolds decomposition:

$$u(x,t) = \bar{u}(x) + u'(x,t) \tag{32}$$

The Reynolds decomposition is then substituted into the NS equation which is then averaged. During this substitution a term referred to as the Reynolds stress tensor appears as a consequence of the non-linearity of the convective term (terms of the underlying NS equations). These essentially represents the averaged momentum transfer due to turbulent fluctuations (or turbulent diffusive forces). These are especially large in turbine wakes.

To allow closure of the system of equations, models are needed to express these Reynolds stresses in terms of mean flow quantities (Sanderse, van der Pijl and Koren, 2011). The RANS concept is to model turbulence and compute mean flow (not resolve the turbulent structures in time and space) Although this can be seen as a shortcoming, RANS modelling has had great success in modelling accuracy in almost all industrial CFD simulations (Menter, 2011).

In terms of closure models RANS models may be divided into two principles of development, the first is the Boussinesq hypothesis, providing a simpler relationship between the Reynolds stresses and velocity gradients through eddy viscosity, these conditions are isotropic. Closure models such as the two-equation shear stress transport (SST) k-ω and k-ε models fall within this category, defined as eddy viscosity models.

It is often observed (Wilcox, 1994) that for the reason of lack of anisotropy, eddy viscosity models may not be suitable for predicting flows with rotating or strong curvature effects as those present in HK wakes. However, these isotropic RANS models yield robust solutions at

relatively low computational resources (Edmunds *et al.*, 2017; Gajardo, Escauriaza and Ingram, 2019), but may yield high dissipation rates reducing the ability to predict detailed unsteady features on the flow field. Previously, Shives & Crawford (2014) concluded the k-ε model predicts much faster wake recovery than those observed in experimental results. Employing the SST k-ω model improved on this. However, it overcompensates, resulting in a delayed wake recovery.

Freestream turbulence defining input factors may vary over different CFD codes. Many assign default values and allow the user to override these if desired, however usually little guidance is available on the effect of these choices on decay rates (Spalart and Rumsey, 2007). This is especially true for the SST k-ω and k-ε models where the specified turbulent dissipation rate strongly affects the development of the wake and dissipation curve.

In many scenarios eddy viscosity models are an attractive, well-calibrated option (specifically performance focussed studies). However, cases where flows with strong swirl or streamline curvature exist, or where secondary motion is driven by turbulence anisotropies, these models cannot provide the information required to accurately compute physical effects (Menter, 2011). In the past this problem has been alleviated by moving beyond the eddy viscosity models to Reynolds Stress model's (RSM).

The Reynolds stress transport (RST) equations (used in RSM) are derived directly from manipulating the NS equations. These still contain unknown quantities (constants) however hold no assumptions of isotropy. Comparing to models centred on the Boussinesq hypothesis these are very complicated and expensive to solve due to the equation complexities, each computed independently. The RSM's have the potential to predict more complex flows than other eddy viscosity models due to the transport equations accounting for the effects of turbulence anisotropy, streamline curvature, swirl rotation and high strain rates.

Due to the RSM approach, modelling of the transient, convective, and molecular diffusion terms is not required. The turbulent diffusion term, dissipation term and pressure-strain term are then modelled. The most complicated of these is the pressure strain term which have resulted in decades of research and the development of different approaches such as the Linear pressure strain model, quadratic pressure-strain model and elliptical blending model (Sarkar and Lakshmanan, 1991; Speziale, Sarkar and Gatski, 1991). However, the six partial differential equations must be modelled again, and the closure relations often resemble the Boussinesq hypothesis. Additionally, disappearance of the eddy viscosity term (which stabilises the problem) can lead to numerical problems.

Gibson & Launder (1978) reviewed the pressure fluctuation effects of capturing the boundary layer and noted the importance of an accurate capture of boundary layer formation and thus developed a two layer formulation which may be applied to the linear pressure strain model. The RSM was developed from the modelled Reynolds stress transport equation, which assumes the individual Reynolds stress advection term minus the diffusion term can be expressed as the product of the kinetic energy component *(K)* and the individual Reynolds stresses normalised by *K*.

This implicit relation replaces the Boussinesq hypothesis. By applying the Boussinesq hypothesis the linearity of this equation results in excluding any dependence on the rotational

mean velocity gradient tensor. However the RSM, although it is known to have more accuracy in the correct description of turbulence, also has limitations in predicting turbulence for complicated flows, especially in describing the effects of rotation (Wallin and Johansson, 2000).

An example of the improved separation flow prediction using RSM can be seen in Figure 2-23. Here the effect of including anisotropy into a simulation for a wing-body junction can be seen. The SST model (eddy viscosity model) tends to over predict the size of the corner separation, where the WJ-BSL-EARSM (RSM) allowed improved predictions of the separation. A more pronounced effect of this may be present in turbomachinery blades (Menter, 2011), and should be considered for HK application.
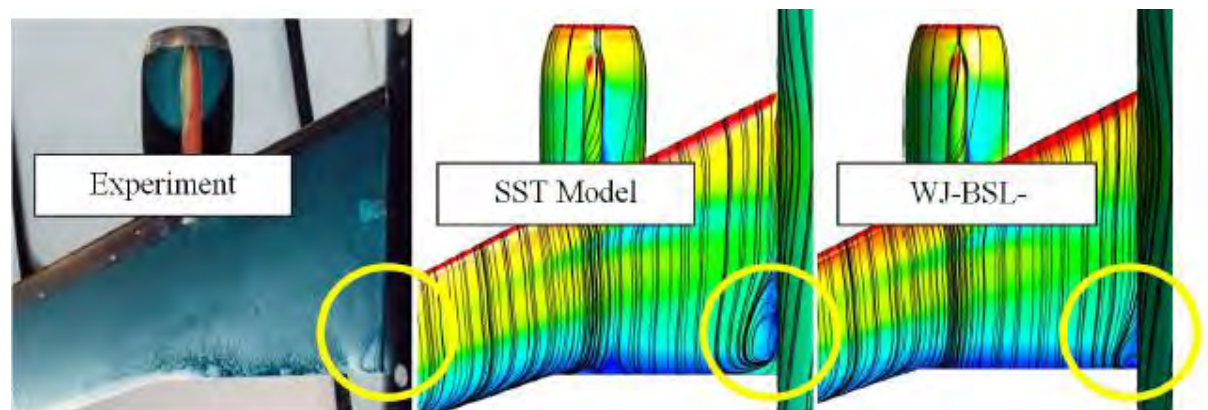
Figure 2-23: Separation zone comparison of experimental, SST and RS models (Menter, 2011)

McNaughton *et al.* (2012) performed a comparative analysis (near wake and turbine performance) using two 2-equation eddy viscosity models and the LRR Reynold stress model. The model used a sliding mesh to replicate the 3-bladed turbine and concluded further testing needs to be completed on requirements of grid refinement in the wake. Additionally, the requisite to correctly model the support structure. The study concluded the SST and LRR methods performed best comparing to LES results.

A higher-level solution is possible with LES which is a scale-resolving simulation. This means a portion of the turbulence spectrum is resolved, not modelled, as in RANS (Sanderse, van der Pijl and Koren, 2011). However, this is yet to replace RANS due to the high-resolution and consequent high-computational demands for wall-bounded flows. Even though LES has remained a research tool to applications not much affected by wall boundary layers (e.g. Combustion chambers) (Sanderse, van der Pijl and Koren, 2011; Kang *et al.*, 2012), it may be useful when analysing details in the flow features (Kang *et al.*, 2012; Churchfield, Li and Moriarty, 2013). The computational demand required for LES can be seen in a comparison in Figure 2-24 when laminar turbulent transition and complete 3-D geometry are included.

	Number of cells	Number of time steps	Number of inner loops per time step	Effort relative to RANS
RANS	$\sim 10^6$	$\sim 10^2$-10^3	1	1
LES	$\sim 10^9$	$\sim 10^5$	1-10	$\sim 10^5$-10^6

Figure 2-24: Comparison of LES and RANS CPU resources required for a single turbine blade estimate (Menter, 2011)

Actuator disk (AD) embedded CFD methods may be useful where large scale flow effects (such as those in multi-turbine arrays) are of interest (Harrison *et al.*, 2010). Blackmore, Batten and Bahaj (2014) used a LES approach coupled with an AD to model the wake of a horizontal axis turbine. The results correlated well with published experimental data beyond 3 d_t. Kang, Yang and Sotiropoulos (2014) analysed a detailed comparison of AD embedded LES showing that this is not sufficient to correctly reproduce the development of an actual turbine wake. They have proven even in fully turbulent open channel flow; the development of the far wake is sensitive to the stability of the vortical structures in the near wake region. As a result, models need to be resolved in detail in the near wake region to predict an accurate far wake result (Adcock, Draper and Nishino, 2015). The AD concept is not applicable for detailed design of a turbine rotor. It may however be useful for wake analysis and allows a significant reduction in computational size and cost (Bai *et al.*, 2013; Lain, Contreras and Lopez, 2019).

Detached Eddy Simulations (DES) proposed by Spalart (2000) utilises a hybrid RANS-LES approach. This approach allows a decreased grid resolution, eliminating the main limitations of LES. This means the wall boundary layers are covered by a RANS model and free-shear flows computed in LES. DES may result in a reduction of the eddy viscosity without proper generation of turbulent content (which occurs for wall boundary layers) (Menter, 2011). Salunkhe *et al.* (2019) compared unsteady-RANS (URANS) to improved Delayed-DES (IDDES) for a full rotor geometry model and found that although all models overpredicted the wake diffusion after 4 d_t, URANS performed better than IDDES. DES also suffers from a modelled stress depletion issue in the wake, resulting in inaccuracies.

2.9.2   Rotor representation

A representation of the turbine blades or subsequent effect of the turbine in the modelled CFD flow field is necessary. As the blades rotate the surrounding fluid exerts a force (torque) on the blades, as a result the fluid behind the rotor loses kinetic energy (the wake) and a pressure differential is generated across the blades. The torque enforced is counteracted by the generator keeping a constant angular velocity (Vermeer, Sørensen and Crespo, 2003). Various options to model this behaviour exist, ranging in complexity.

The turbine may be modelled using the full turbine geometry (FRG), (sliding mesh interface) where the presence of the blades is taken into account by discretising the actual blades on a computational mesh (Gajardo, Escauriaza and Ingram, 2019). Previous studies indicated this method predicts turbine performance well for lower water speeds and tip speed ratio's (λ), but underpredicts the power at higher velocities. This can be explained by the strongly separated flow not being correctly captured by insufficient mesh resolutions and limitations of the turbulence model employed (Sanderse, van der Pijl and Koren, 2011).

An alternative may be employing a VD approach. The AD model is the least computationally expensive and applies a uniform force to the flow, however employing this model comes at the cost of losing important representations such a rotor swirl. Coupling the Blade element momentum (BEM) theory within the VD may be seen as middle ground, incorporating rotational components, and using real turbine geometric data. A limitation is that it is still unable to represent the discrete blade effects such as tip vortices. BEM has been widely used in wind turbine array models and has shown good representation of the wake (Malki *et al.*, 2011; Edmunds *et al.*, 2017). Most recent studies use this simplified motor modelling embedded in a CFD model.

The BEM theory embodies the simplified assumption that the wake behind a turbine may be represented as a set of stream-tubes. This is modelled as a distribution of momentum sources and lift and drag coefficients as well as other geometric characteristics of the blade which are required as inputs. Lift is defined as the force perpendicular to the free stream flow and drag parallel and thus opposing the free stream flow. The lift and drag forces (F_L and F_D) are thus calculated using the following relationships (Edmunds *et al.*, 2017)

$$F_L = 0.5 \, \rho V^2 A C_L \tag{33}$$

$$F_D = 0.5 \, \rho V^2 A C_D \tag{34}$$

where V is defined as the fluid velocity, A the area and, and C_L and C_D the lift and drag co-efficient's. The relevant coefficients are dependent on the angle of attack, geometric properties of the hydrofoil and the flow Reynolds number. The axial and tangential forces on the blade element are then calculated for flow angle φ as shown in Figure 2-25 (Guo, Zhou and Wang, 2015):

$$F_a = F_L cos\varphi + F_D sin\varphi \tag{35}$$

$$F_t = F_L sin\varphi + F_D cos\varphi \tag{36}$$

(a) Disk model and rotor   (b) Blade element and regions   (c) Blade element velocities and forces
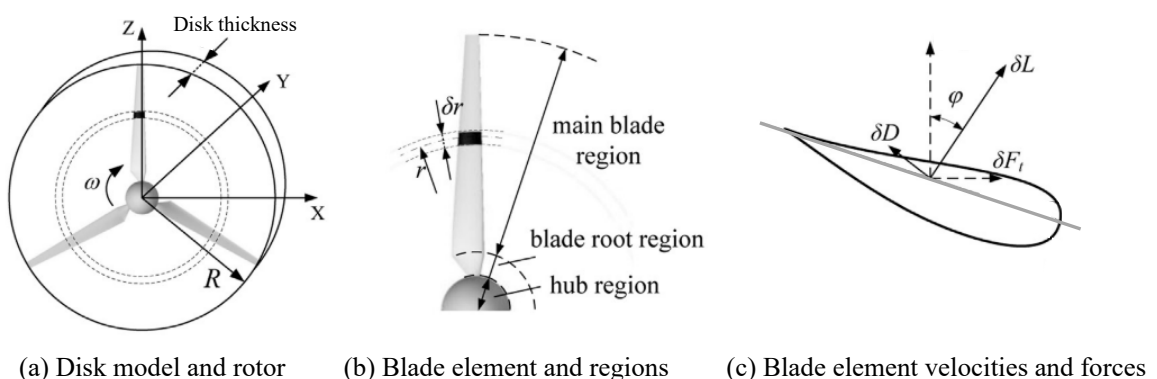
Figure 2-25: Schematic of the virtual disk model, hydrofoil and blade element characteristics. (Guo, Zhou and Wang, 2015)

The assumption of an infinite number of blades is also corrected when using the BEM method by locally changing the induced velocity.

When this is solved together with a Reynolds averaged solution, transient flow features resulting from the hydrofoil position are not resolved (including tip vortices, laminar to turbulent transition on the blade surface, flow separation and turbulence generation along the downstream part of the hydrofoil) (Edmunds *et al.*, 2017).

Fully resolved HK turbine models for a fully developed wake is computationally expensive. Edmunds *et al.* (2017) explored the use of a coupled BEM-CFD method which uses an enhanced AD and reduces computational time by simulating a time averaged downstream velocity field. The model indicated results similar in wake to the experimental results (Figure 2-26).
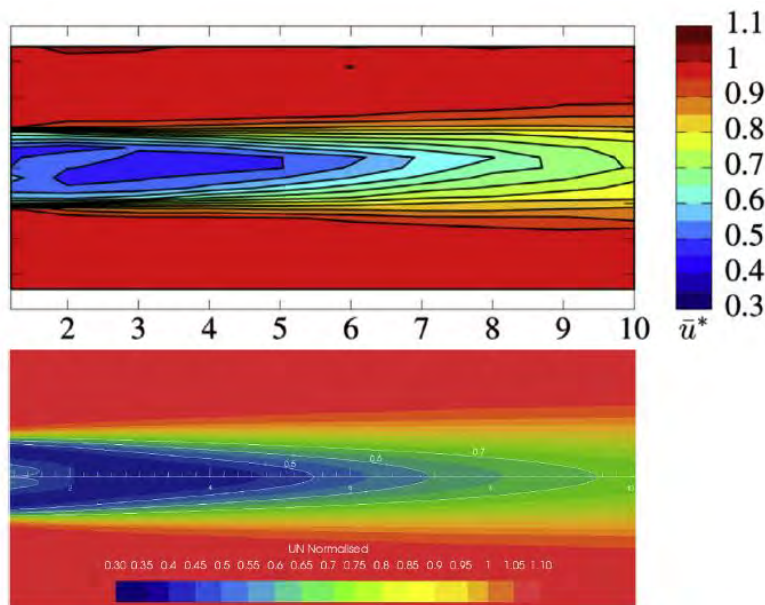
Figure 2-26: A comparison of experimental and numerical results from a BEM-CFD model (Edmunds *et al.*, 2017)

Most applications of the BEM theory showed over predictions in the simulated power co-efficient (C_P) and thrust coefficient (C_T) values. Various theories exist to explain this over prediction and solutions have been previously implemented. One such solution is the blade tip-loss correction. Tip loss occurs when the flow induction factor is large at the blade position, then the lift force will be almost normal to the rotor plane, thus the tangential component of lift will be small, and so will its contribution to torque. This means reduced torque and reduced power output (known as tip loss) as it only occurs on the outermost part of the blades. This correction is beyond the abilities of the BEM theory (Burton *et al.*, 2011).

Various methods of incorporating tip loss exist through azimuthal variation of the induction factor for several radial positions. Various methods may be seen in Figure 2-27. Where a factor F indicates the reduction applied (tip loss correction). Commonly the Prandtl approximation for tip loss correction is applied, which is a relatively simple analytical formula. Details for this can be seen in Burton *et al.* (2011), and are not explored in detail here.
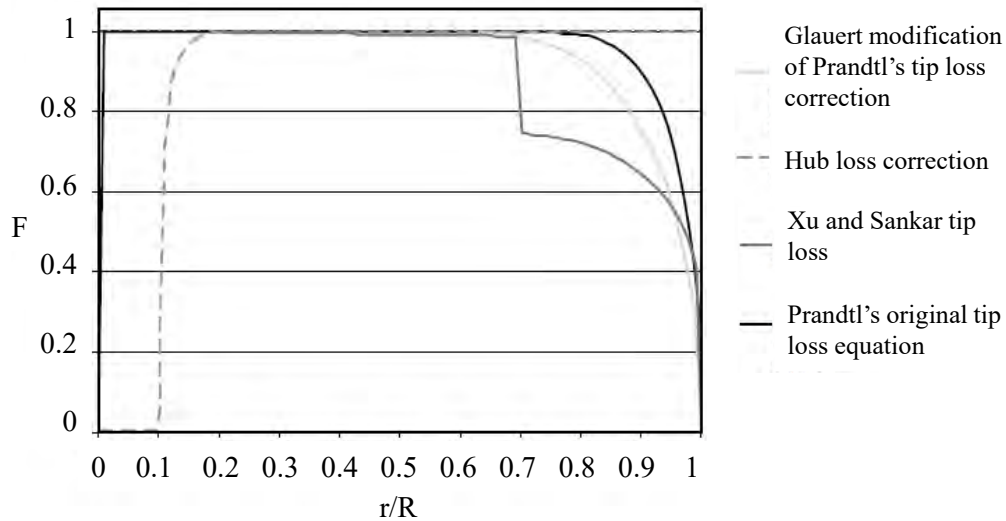
Figure 2-27: Comparison of tip and hub loss equations for a normalised blade radius (Masters *et al.*, 2014)

A number of recent studies use the BEM-CFD method (Turnock *et al.*, 2011; Malki *et al.*, 2013; Masters *et al.*, 2014; Guo, Zhou and Wang, 2015). Various authors (Masters *et al.*, 2013, 2015) have used this method to analyse the flow field of turbines arranged in arrays, specifically for tidal optimisation. The SST k-ω model coupled with BEM has been found capable of predicting the flow velocity structures in the far wake regions to an acceptable level of accuracy (Masters *et al.*, 2013; Edmunds *et al.*, 2017). Gotelli *et al.* (2019) and Gajardo, Escauriaza and Ingram (2019) found better agreement of a coupled BEM-DES method than the BEM-RANS method on a 3-bladed HAHT. However, Gotelli *et al.*(2019) predicted large variances in the near wake due to the BEM approach but showed better agreement from a distance 3 d_t downstream.

2.9.3 Bounded flow and free-surface modelling

The consideration of environmental variables on wake prediction and modelling, such as bounded flow and depth below the free surface, is also necessary. Previous studies have specifically addressed the concern of distance to the free surface, as well as blockage ratio (Whelan *et al.*, 2009; Myers and Bahaj, 2010; Birjandi *et al.*, 2013; Kolekar and Banerjee, 2015). Complexities arise when turbines are placed near the free-surface, as the boundary may modify the turbine flow-field and affect device performance. Generally, this causes significant flow acceleration, its magnitude depending on the blockage ratio.

El Fajri *et al.*, (2020) investigated the effects of shallow water on the near wake recovery through a validated CFD model with a tip clearance of 0.35 diameters. The stanchion holding the turbine in place (Figure 2-28) initiated the free-surface wake interaction and a significant wake deformation can be seen at 7 d_t. The results found suggest the free-surface blockage enhances wake recovery in the near or intermediate wake by accelerating the flow in the upper bypass region. However, the wake recovery rate (specifically in the intermediate-far wake) was not affected significantly as shown in (c) in Figure 2-28. Kolekar and Banerjee (Kolekar and Banerjee, 2015) studied this effect and found that smaller tip clearances retarded wake propagation, but accelerated the flow in the upper bypass region causes a skewed wake. Experimental investigations proved that small clearances may also cause free surface

deformation resulting in a free-surface drop behind the turbine. However, clearances avoiding this behaviour are usually prescribed by turbine manufacturers to prevent performance degradation. Additionally, an optimal clearance depth (depth form blade tip to free surface) exists, resulting in improved turbine performance (Kolekar and Banerjee, 2015).
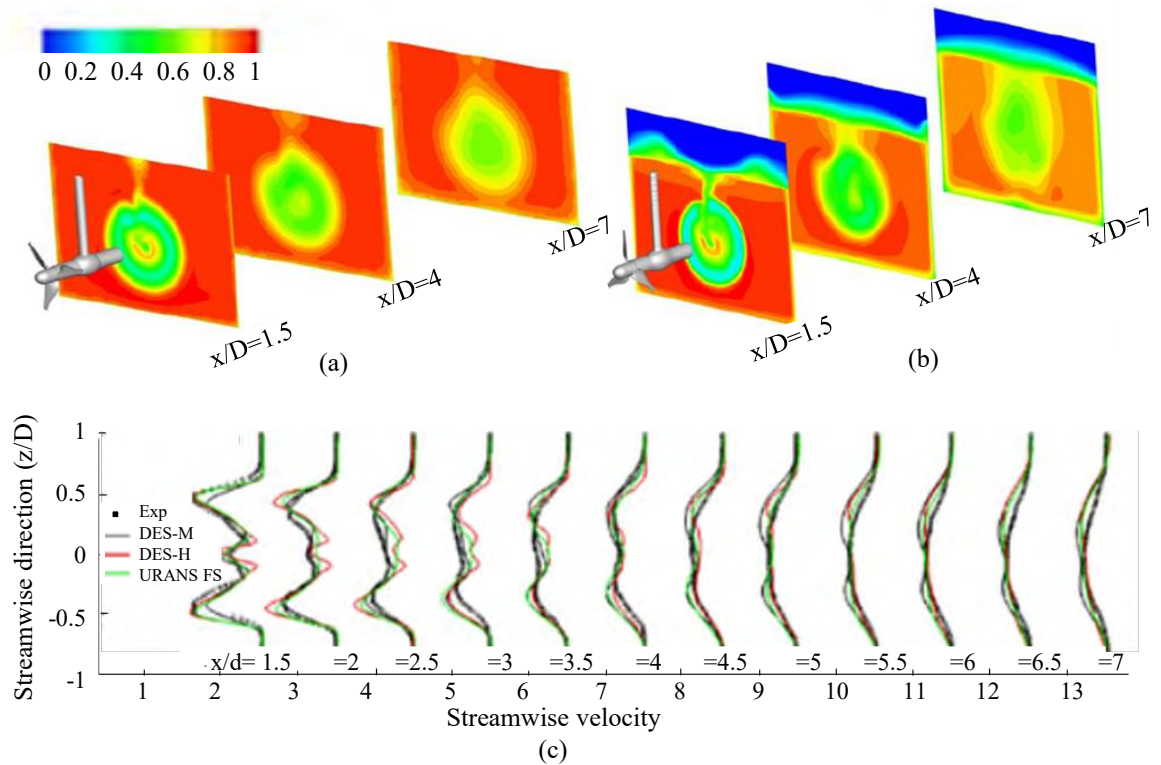
Figure 2-28: Free surface effect on wake indicated by the differences in (a) single phase-*DES-M/H* and (b) multiphase-*URANS* (El Fajri *et al.*, 2020) (c) comparisons of velocity profiles

When a turbine is placed in bounded flow, the flow velocity in the bypass region around the turbine will be increased due to the spatial restrictions of the channel bed and walls as well as the free surface. This change may lead to an altered wake velocity deficit comparing to unbounded flow cases. This effect is caused by changes in the rate of mixing between the wake and the bypass flow (which is the driving force for flow recovery) and thus affects the wake recovery length scale (Stallard *et al.*, 2013). To ensure accurate prediction of this behaviour it should be ensured that wall effects and boundary layers are accurately modelled.

Simulating the water-air interface (free surface) has been approached in various ways in literature. Most often the free surface is assumed to be a significant distance from the turbine and so free surface deformation is neglected and a symmetry boundary condition is used (Masters *et al.*, 2014). Computational cost is saved using this approach. Alternatively, the free surface may be modelled using a multiphase modelling approach. This is usually divided by two separate approaches, the Eulerian multiphase approach and the Lagrangian multiphase approach, the difference being in the perception of phases. The Volume of Fluid (VOF) surface tracking model approach proposed by Hirt and Nichols (Hirt and Nichols, 1981) has shown to perform better for complicated free-boundary configurations such as deformations

between fluid and deformable structures. This is often used and has proved to correlate well to experimental free surface observations (Oggiano *et al.*, 2017; López *et al.*, 2018), also in HK applications (Benchikh Le Hocine, Jay Lacey and Poncet, 2019).

2.9.4 Considerations in computational modelling of HAHTs

The effects of a HK turbine on ambient inflow conditions has been studied in recent years. These studies include the velocity deficit (Malki *et al.*, 2011; Lam and Chen, 2014); the complex three-dimensional flow structure (including hub and tip vortices) (Myers and Bahaj, 2009); increase in turbulence intensity and anisotropy (Chamorro *et al.*, 2013; Mycek *et al.*, 2014; Ahmadi, 2019); effects of ambient turbulence levels; unsteady loading; flow depth to turbine diameter; and turbine operating conditions affecting thrust (e.g., tip-speed-ratio) (Morris *et al.*, 2016; Siddiqui *et al.*, 2017). In all such studies, correct capturing of the inflow conditions is imperative.

In a study (Nezu, Nakagawa and Jirka, 1994) measured vertical profiles of the mean velocity and turbulence stresses reported in literature for rivers and large canals are compared along with classical models developed for turbulent flat plate boundary layer flows. The vertical mean velocity profiles are modelled reasonably well with a power law (exponent = 1/6), and similarly vertical profiles of turbulence (Reynolds) stresses with semi-empirical exponential decay formulae derived from classical open channel hydraulics experiments. Nevertheless, a significant amount of scatter is observed about these modelled profiles due to variations in bedforms, complex bathymetry, non-stationary (unsteady) phenomena, and potentially, three-dimensional flow structures, e.g., large coherent motions emanating from natural and manmade obstructions (Neary *et al.*, 2013).

For CFD modelling, and specifically simplified rotor modelling techniques, the rotation rate of the turbine is specified. This may pose a challenge where operational rotation rates are unknown.

Some turbines may operate at fixed rotational speeds (except starting or stopping), which significantly simplifies system operation when using a synchronous generator, this also prevents excessive turbine rotational speeds (at higher than predicted velocities) and essentially protects turbine integrity. However this also means a fixed maximum performance is only available at one particular speed, and performance is lower for all other speeds (Johnson, 2001).

The shaft power is a function of shaft rotational speed (as shown in Figure 2-29). The maximum power (P_m) rises to a maximum value for each water speeds at a particular rotational speed (n). The torque also rises to a maximum at a particular rotational speed (for each flow speed), however this is reached at a lower rotational speed than the peak shaft power (Figure 2-29). The relationship between shaft torque and maximum load (T_L) can usually be defined by shaft power varying by the cube of rotational speed, where K is selected to allow the curve to pass through the peaks of the curves (Johnson, 2001).

$$T_L = Kn^2 \tag{37}$$

This graph of power vs rotational speed is necessary to program variable speed operation, as well as predicting the operation of the turbine at various operational conditions.
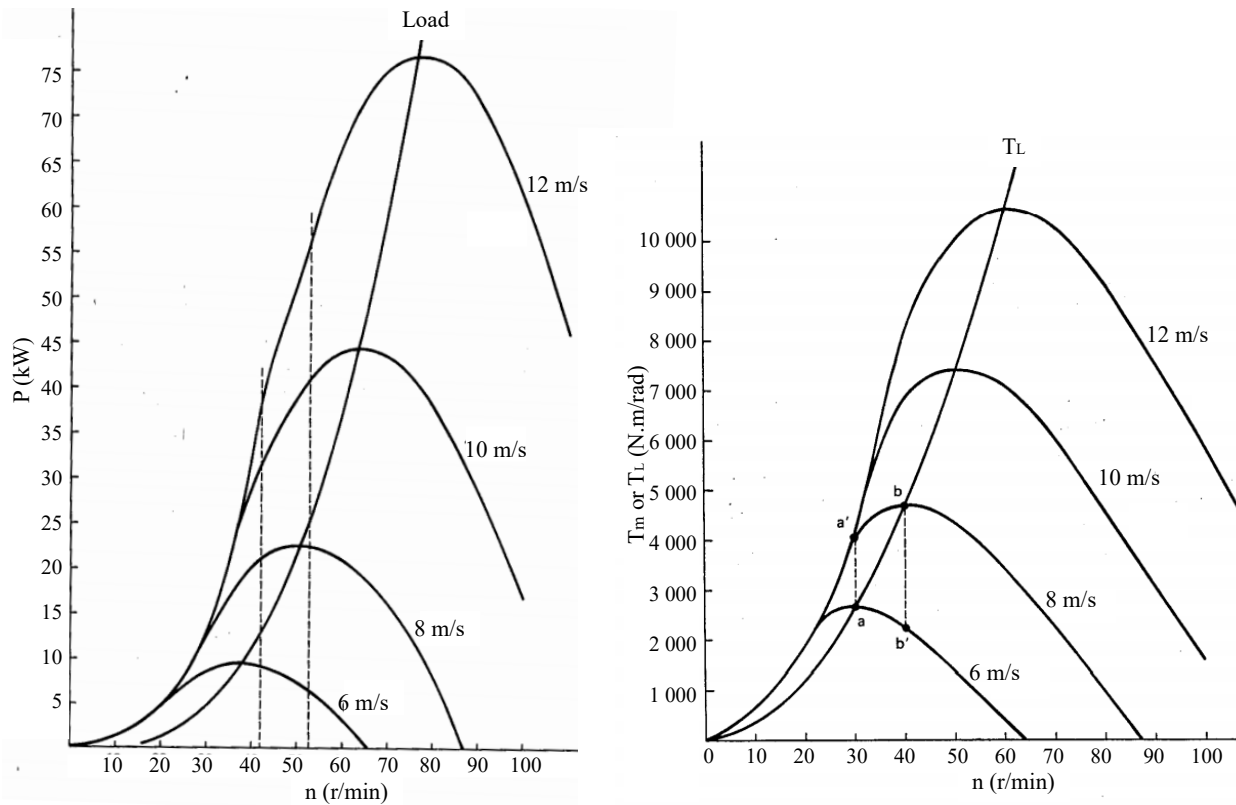
Figure 2-29: Shaft power output and torque of a Darrieus variable speed operation wind turbine (Johnson, 2001)

Ensuring Reynolds (*Re*) uniformity is important within wake studies. Models validated further from the Reynolds number experienced at full-scale *Re* results in a lack of confidence in the models (Bachant and Wosnik, 2014). A previous analysis to observe Re dependence using towing tank tests (Bachant and Wosnik, 2014) indicated that near-wake statistics (mean velocity, turbulence intensity, Reynolds stress) were less Re dependant than the performance measurements of the turbine. However, it is important to consider Re dependencies when scaled models are used for numerical validation. The study also found that when scaling experimental tests, no significant Re dependence was found for velocity profiles, however a small Re dependence existed for turbulence intensity and Reynolds stresses. Numerical results (specifically using the SST *k-ω* solution) indicated a stronger *Re* dependence, over predicting performance due to the increased blockage and exclusion of tip effects.

Previous results have also indicated that power coefficients (C_P) are more sensitive to *Re* dependency than the thrust coefficient (C_T), the same is true for blockage ratios (Ross and Polagye, 2020). In conclusion low blockage may alter the Re (comparing to non-blocked cases) for scaled tests, and in turn alter the turbine performance. Re uniformity should therefore be included if scaled testing is used.

2.10   Summary of literature

Investigations into the flow effects of HAHT deployment have provided an overview into the numerous considerations and factors affecting the overall hydrodynamic changes imposed by such a device. Although multiple complexities lie around the effects of these systems in water infrastructure, such as effect on aquatic life, bed scour and water properties. The primary considerations that require understanding prior to design or rollout are the possible inter-effect between devices, where the upstream wake affects downstream turbines. As well as possible backwater effect, or cumulative backwater effect through installation of multiple turbines in a channels section.

It is found that the complex turbulent wake region behind a HAHT is highly dependent on not only the turbine design, but also the environmental conditions. Although turbine characteristics such as the turbine thrust and tip speed ratio form the initial vortical wake structure, flow properties such as ambient turbulence, retaining structure and blockage ratio drive the wake dissipation further downstream. Previous studies have indicated that specifically ambient turbulence values strongly alter the wake dissipation rate.

An obvious need exists for a simplified wake calculation method without complex numerical modelling. A few attempts at semi-empirical and empirical models have been previously developed for simplified wake prediction. However, most of these models consider only the turbine characteristics. Some recent models have incorporated the effect of ambient turbulence, however as the model was empirical and calibrated to a single operational case, the use over a range of turbines and flow conditions is limited.

Similarly, rudimentary backwater models based on turbine drag or energy loss have been attempted. However, a lack of model validation as well as requirements of complex model input parameters and assumptions on input parameters limit the usability of these approaches. Although no specific solution exists, the investigations provide an insight into simplification techniques and the possibilities in developing a backwater modelling approach.

A primary limitation faced in the previous attempts at developing simplified wake and backwater models found in literature is the lack of experimental data, or lack of operational scenarios considered. As computational resources are becoming more accessible, CFD models have shown to predict the hydrodynamic behaviour around HK turbines well using simplified RANS modelling techniques. Although these models are primarily used for performance analysis, wake dissipation prediction has also shown positive results and may open the door for faster generation of wake dissipation results over various operational conditions which may be difficult to model, or control in laboratory studies.

The literature study indicated the possibilities of simplified models for hydrodynamic effect prediction and provides guides on theoretical principles such as the axial momentum theory or actuator disk method which have proved to be useful principles in deriving models. The novelty of HK energy, especially in wall confined inland systems leaves a large gap in research. Analysis of driving factors specific to these scenarios is necessary, and experimental results are needed to paint a broader picture of the affects over numerous turbine designs and geometries

3. PART 1: COMPUTATIONAL MODEL DEVELOPMENT

3.1 Introduction

An adequate numerical modelling approach for the use of computation fluid dynamics (CFD) modelling for HK flow fields is required for the development of a wake (Part 2) and backwater (Part 3) model. This chapter describes the development of a suitable CFD modelling approach. The approach is based on successful modelling strategies found in literature as well as final model validation and benchmark studies with an available experimental dataset. Due to the scarcity of experimental data, over the course of the study additional models with parameters found to be of interest for wake and backwater development were added. Therefore, ongoing benchmark validation and model adjustments were made.

Testing a CFD modelling approach ensures correct prescription of input variables and correct selection of physics models governing the flow. The testing process consists of two steps: verification and validation. Verification includes evaluating numerical errors. One such technique is a grid independence study. This results in adequate mesh sizes to capture the necessary detail. Validation of the model includes comparison to experimental data (benchmark tests) to investigate the validity of the model.

Laboratory tests on rotating horizontal axis hydrokinetic turbines (HAHT) yield suitable experimental data for validation as they are measured in a controlled environment. However, these conditions vary from environmental conditions, typically in terms of blockage ratio, ambient turbulence intensities and the effect of channel wall roughness. In this study numerous experimental results are modelled each with a specific purpose of ensuring environmental changes are captured in the models.

The Reference model 1 (RM1) turbine was constructed and tested at Sadia Laboratories to provide results for the purpose of numerical calibration/verification (Hill and Neary, 2014). The RM1 design and testing environment allows a Reynolds (Re) uniform analysis of the inter-effect between the two closely spaced turbine rotors as well as incorporating the effect of turbine wake interaction with the center stanchion itself. The rotor diameter and blade profile resemble those often used in inland HK applications. The channel conditions as well as the blockage ratio also hold value for the analysis of inland schemes.

Additional published laboratory test results were used for further validation of the CFD approach. Wake results from the French Research Institute for exploration of the Sea (IFREMER) wave and flume tank of the so called LOMC 3-bladed turbine model (Mycek *et al.*, 2014) allowed the capture of variations of environmental turbulence intensities. Experimental performance results from a study of a 2, 3 and 4-bladed HAHT tested at Liverpool University (Mason-jones, 2010; Tedds, Owen and Poole, 2014) allowed testing of the CFD approach at different turbine solidities as well as rotation rates. Additionally a 3-bladed HAHT tested at the Southampton University towing tank and cavitation channel (Bahaj, Batten and McCann, 2007) (referred to as the BBMC turbine) was included.

Modelling the turbulent vortex structures in the wake region of a HK device is extremely challenging, the shortfalls when employing models within this regime are an important consideration and should be well understood before simulation. Benchmark validation of the turbine performance alone, which has been proven to be modelled well with even lower fidelity models, does not necessarily result in correct capture of the wake formation. The turbulent nature of the wake varies to the approach flows where small eddies play a larger role in breaking down the strong tip and root vortices in the wake effectively, leading to wake dissipation.

The purpose of this work was to bring light to the shortcomings of each computational approach and find the most accurate solution capable of capturing the flow behaviour changes through HAHT placement in a typical inland channel. The broad range of operational parameters tested in the validation cases is expected to present a robust approach to allow the necessary data generation of wake and backwater effects for the development of a wake and backwater models. Benchmark validation and correct capture of the wake region were imperative in this study.

3.2   Methodology

The following methodology was used in this chapter:
1. A laboratory case study (Reference model 1- RM1 turbine) with available performance and wake flow field results was used to develop a CFD modelling approach through the following steps:
    a. A CFD model was build replicating experimental testing conditions.
    b. Performance metrics measured during the RM1 laboratory tests were compared to generated CFD results from various modelling approaches (e.g. rotor modelling techniques and turbulence models).
    c. Wake dissipation rates measured during the RM1 laboratory testing were compared to the best performing CFD model wake results. Fundamental principles and literature findings of each approach were analysed to determine the best approach for the study.
    d. The sensitivity to input parameters for the CFD approaches were tested to ensure accuracy over various operational conditions (e.g., multiphase vs. single phase boundary conditions; inlet and outlet specifications and distances; mesh resolution effects).
    e. The prescribed approach was used to model the IFREMER-LOMC 3-bladed turbine which was tested over a range of onset flow turbulence values, measured experimentally. Special attention to operational condition changes were ensured to test the model's ability to capture wake behaviour correctly at a variety of ambient turbulence intensities.
2. The final CFD approaches were used to model various other HAHTs to include a variety of turbine geometries and operational conditions in the dataset. Less emphasis was placed on these models as only experimental performance measurements were available. The following turbines which have been previously tested and optimised experimentally were used:
    a. The BBMC 3-bladed turbine was modelled, and performance metrics were compared.

b. A 3-bladed turbine built and tested at Liverpool University was modelled to experimental test conditions and tested for performance and near wake accuracy. 2-bladed and 4-bladed variations of this turbine were also modelled, and available performance results were compared.

3. A final CFD approach to use for testing and development of the wake and backwater models was determined.

3.3   RM1 Benchmark validation case

The RM1 test setup can be seen in Figure 3-1 with the range of test conditions as well as optimal conditions (highest power output). Mean and fluctuating velocity fields were measured using three Nortek vectrino ADV's sampled at 200 Hz data output at hub height. To ensure volume rotation was considered all ADV measurement, the channel was ponded with water and a towing test performed to determine the rotation. The rotation matrix was then applied to all measured data before calculation of flow statistics. Additionally, time series data was filtered to remove erroneous samples (Gunawan, Neary and McNutt, 2011).

The measured turbulence intensity in the rotor region was approximately 5 %. Wake vertical velocity profiles were taken downstream of the turbine from 1 diameter length (d_t) to 10 d_t at intervals of 1 d_t. These were collected for 3 min at 200 Hz. A horizontal plane was collected from 1 d_t to 10 d_t also with 1 d_t spacing, the cross stream ADV point locations were assumed to have provided enough spatial resolution to capture key characteristics of the wake. The velocity time series was decomposed into mean and fluctuating components through Re decomposition, the fluctuating velocity components were used to calculate flow statistics such as turbulence intensity, Re stresses and turbulent kinetic energy (TKE). Details may be seen in experimental reports (Hill and Neary, 2014; Hill *et al.*, 2020).

Parameter	RM1:
Fixed parameters:	
Diameter	0.5 m
NACA profile	4415
Velocity (U_∞)	1.05 m/s
Blockage ratio (β)	17%
Depth to hub	0.5 m
Froude number (Fr)	0.28
Flow rate (Q)	2.425 m³/s
Flow depth	1 m
Testing conditions:	
Tips peed ratio (λ) (fixed U_∞)	1.51 - 9.05
Optimum operation:	
Tip speed ratio (λ)	5.1
C_P	0.48
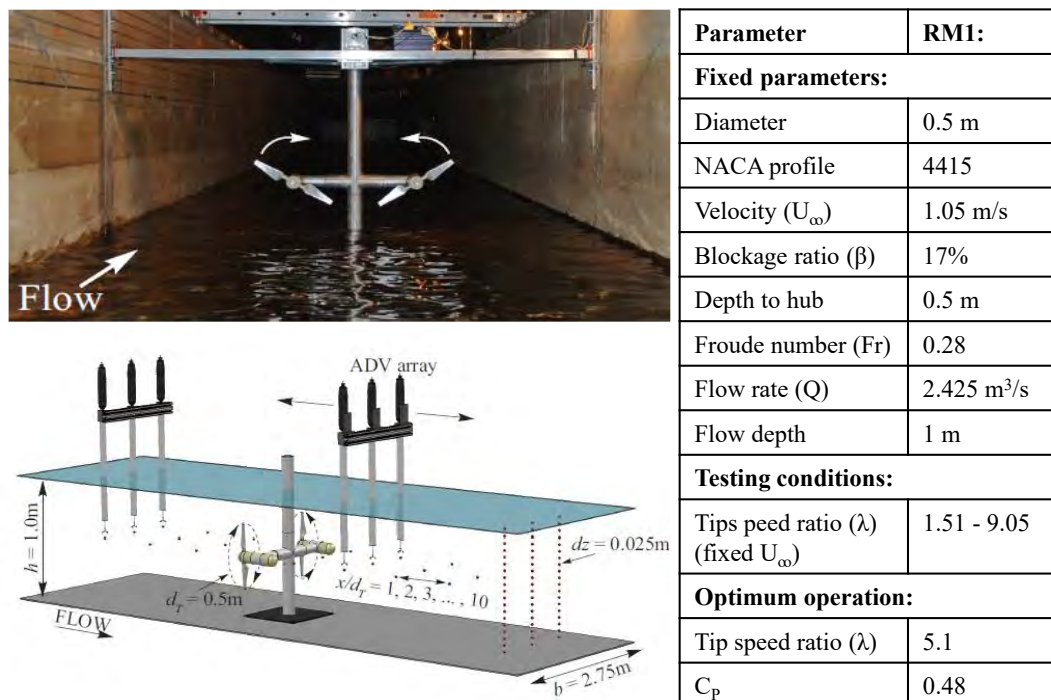
Figure 3-1: 2-bladed RM1 duo rotor test conditions (Hill and Neary, 2014; Hill et al., 2020)

Each rotor had an Interface Force 20 Nm miniature reaction torque sensor mounted inside the hub, to enable torque measurement. During performance measurements all ADVs were placed 3 d_t upstream and synchronised with the turbine torque and angular position measurements. The turbine performance was measured using synchronous velocity, torque, and rotor position measurements. The rotor position was used to calculate turbine angular velocity ω, which was then used to calculate the turbine power P_T. This is possible together with the torque measurement (τ) applied over the stepper motor and measured using the positional encoder integrated with the drive system. This can then be compared to available power using the approach flow upstream of the rotor (P_A)

$$P_T = \tau\omega \tag{38}$$

$$P_A = \frac{1}{2}\rho A_T U^3 \tag{39}$$

where ρ, is the density of water the A_T cross sectional rotor area and U the approach flow mean velocity measured 3 d_t upstream.

Both rotors (counter-rotating) were identical but performed differently (Figure 3-2). The flow complexity in the channel, as well as the slight asymmetry in the approach flow could have affected this change. Because of the performance sensitivity to velocity (U^3) a slight difference in approach velocity (3-5 % e.g., 0.03 m/s) could cause a 10 % change in performance (at optimal λ). A variation of wake results in the near wake were also observed, with a 17 % higher peak velocity deficit for the left rotor at 2 d_t downstream. This emphasises the strong variability in near wake results from small operational changes, asymmetric inflow conditions or manufacturing flaws.
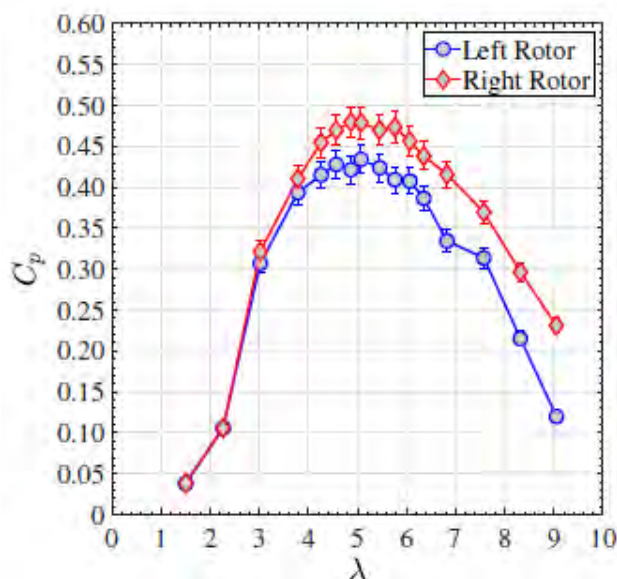
Figure 3-2: Calculated power coefficient (C_p) versus tip speed ratio (λ) for left and right rotors, dashed lines represent results before calibration (Hill *et al.*, 2020)

3.4 Computational modelling of the RM1 HAHT

Siemens STAR-CCM+ software was used to simulate a wall bounded three-dimensional model replicating the experimental conditions. A variety of approach combinations, as shown in Figure 3-3, were considered. Combinations of model properties were varied with the goal of understanding the limitations as well as capabilities of each approach.
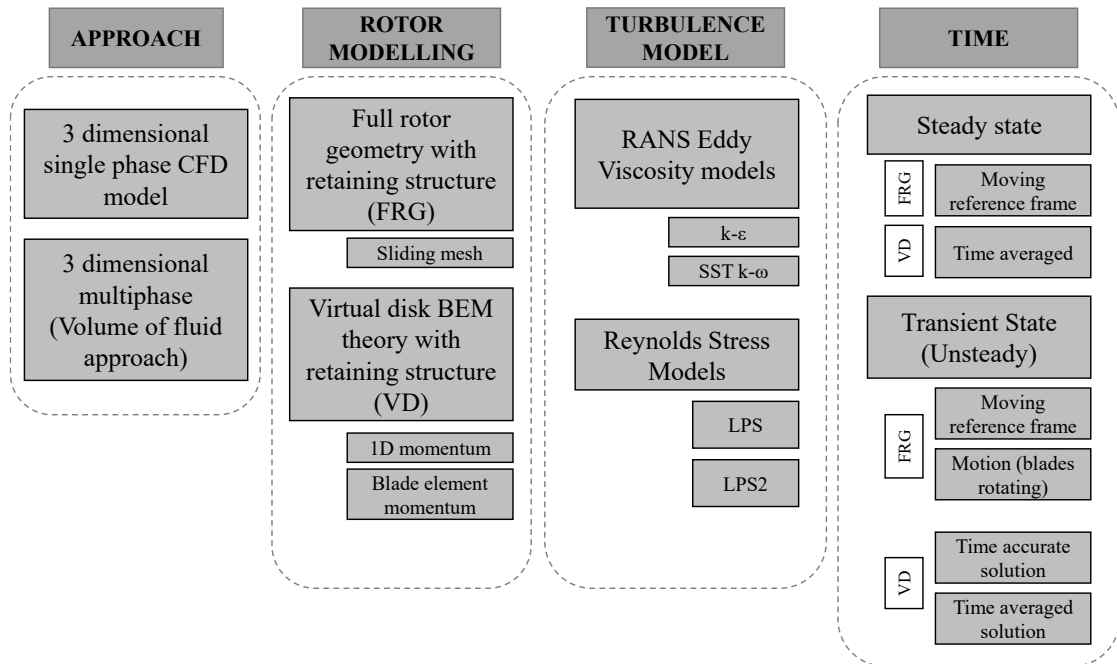
Figure 3-3: Summary of CFD approaches considered

3.4.1 Rotor modelling approach

The rotor was modelled using two widely used methods. First the overset (sliding) mesh technique (Figure 3-5a) was used to deal with the blade movement, this method was employed in numerous validated axial turbine studies (Boudreau and Dumas, 2017). This is referred to here as full rotor geometry (FRG) modelling. The presence of the blades is taken into account by discretising the blade geometry on a computational mesh (Boudreau and Dumas, 2017; Gajardo, Escauriaza and Ingram, 2019). During each time step interpolation of the flow field is performed between the first cell mesh of the moving body and the background mesh region (shown in Figure 3-10c). The sliding mesh boundary can be seen on Figure 3-10a. The rotating mesh continua should be a minimal size to ensure numerical efficiency whilst also ensuring numerical stability. A cylindrical area 10% larger than the turbine diameter was used here.

Second, a virtual disk (VD) was used to represent the rotor (Figure 3-5b and Figure 3-11) and a blade element momentum (BEM) model was employed. This VD-BEM modelling approach has demonstrated good accuracy at reduced computational cost (Turnock *et al.*, 2011; Malki *et al.*, 2013; Masters *et al.*, 2014; Guo, Zhou and Wang, 2015). A BEM tip-loss correction was incorporated using the Prandtl tip loss correction method (Shen, Mikkelsen and Sorensen, 2005). The vorticity map shown in Figure 3-5b indicates the time accurate approach used in the URANS model for rotor enforcement. In this approach the source term is only added on

the blade through motion tracking (simulating the blade movement) the virtual blades can be seen on the figure.

The virtual disk required rotor geometry and aerodynamics performance metrics (lift and drag coefficients). The rotor geometry metrics in terms of chord length, twist, pitch and number of blades was included in the model. Lift and drag coefficients (C_L and C_D) generated in XFOIL software as well as past experimental results on the NACA4415 blade profile over a range of Re's (200 000 < Re < 3 000 000) were added to the VD-BEM model as shown in Figure 3-4.
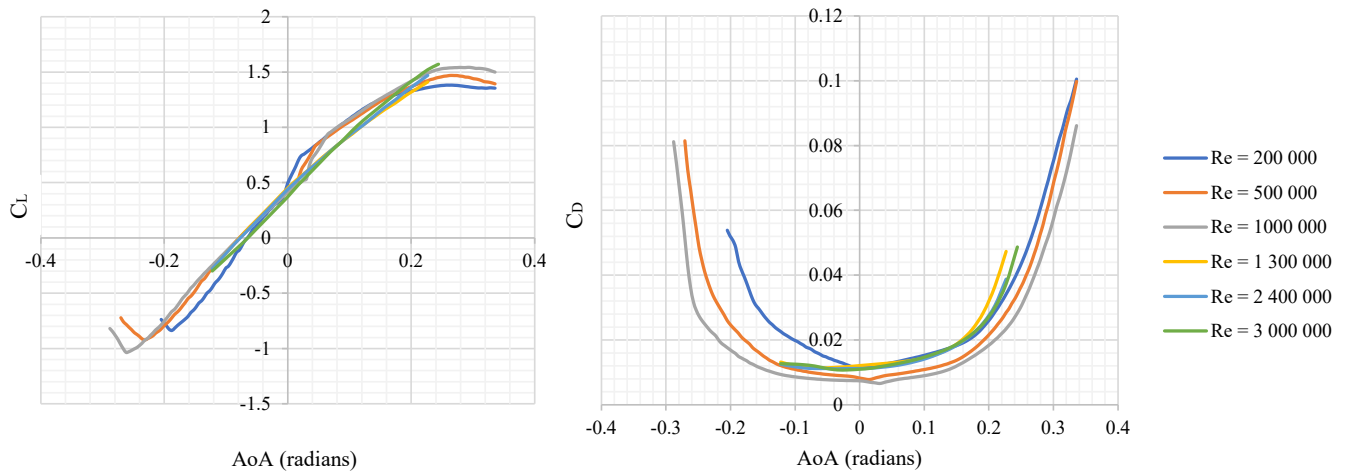
Figure 3-4: Lift and drag coefficient for the NACA 4415 profile
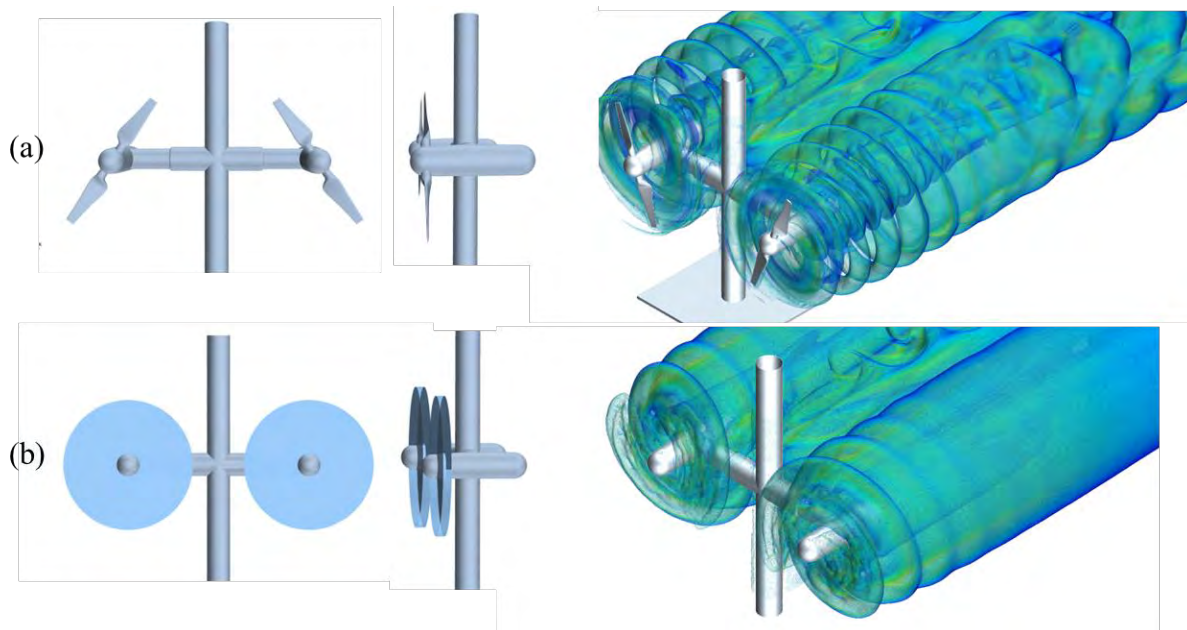
Figure 3-5: a) Full rotor geometry and b) virtual disk blade modelling approaches and vorticity maps

3.4.2   Computational domain and boundary conditions

A wall bounded 3-dimenional model was built replicating experimental conditions. Two domains were built for the specific requirements of the single phase and multiphase model. The first domain extended from -8 d_t upstream to 30 d_t downstream of the propeller center of rotation (Figure 3-6). Walls were modelled with non-slip conditions which allowed formation

of a boundary layer, and incorporation of bounded flow effects. The final inlet length was based on full flow and boundary layer development before the turbine operational point is reached. The length to the downstream boundary was selected to allow analysis of far wake effects (up to 25 d_t). This also ensured the boundary conditions did not change wake formation or dissipation.

Due to the necessity of free-surface measurements in this analysis, in a second approach the free surface is modelled using a Volume-of-Fluid (VOF) approach. The approach uses a 2nd-order discretization to compute a clear interface between the air and water. A volume-fraction variable is used to specify the spatial distribution of each phase. Cells with multiple phases are treated as a mixture, and the method is highly dependent on adequate mesh resolution. The domain extends further upstream (14 d_t selected after a sensitivity analysis) to allow proper formation of the backwater effect after the prescribed inflow conditions. The downstream length is also reduced due to the requirements of this model (only backwater determination/benchmark validation) as around 15 d_t downstream is adequate for correct capture of the turbine near wake.
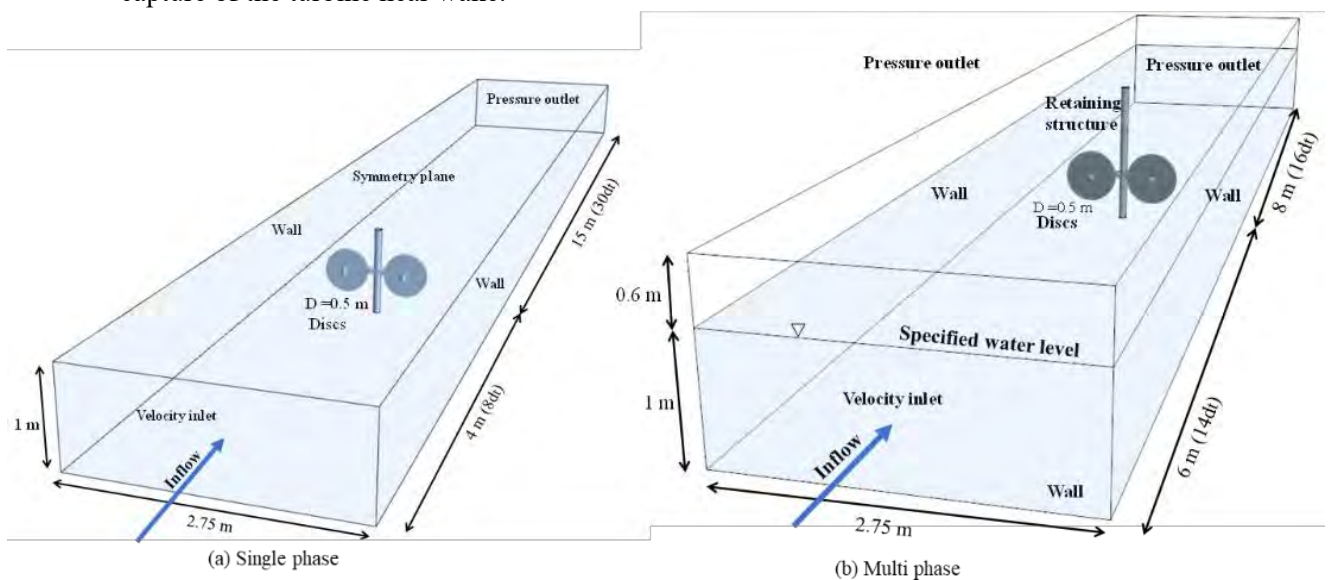
Figure 3-6: Computational domain

The upstream boundary was specified as a velocity inlet, with a constant velocity distribution. Although the vertical distribution of the inflow velocity was measured experimentally the model was found to perform better when the boundary layers were allowed to form freely (by extending the inlet length) based on the non-slip wall condition specified. The fully developed flow velocity distribution comparisons to the measured velocity (3 d_t upstream as shown in Figure 3-7) show a similar nature before the propeller inflow once boundary layers have fully developed (Figure 3-7).
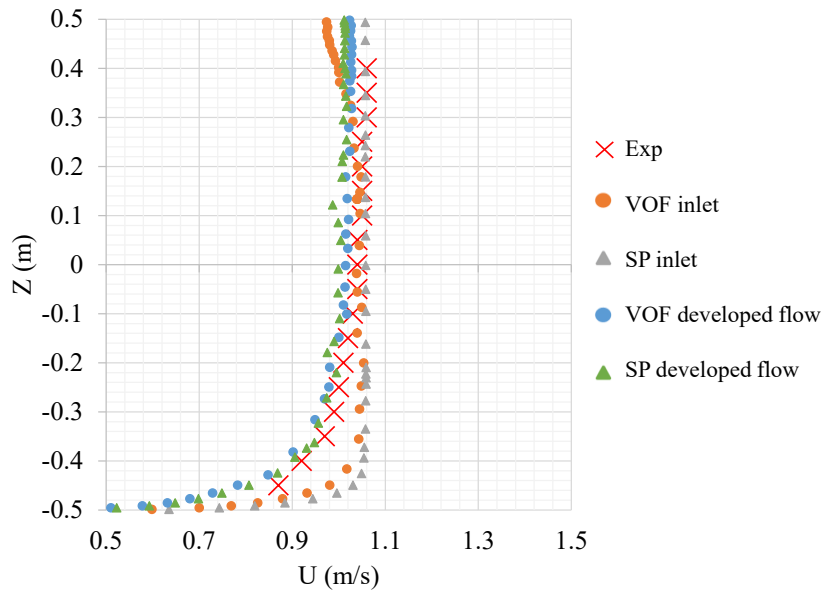
Figure 3-7: Flow properties for experimental, single phase (SP) and multiphase (VOF) inlet flow development

A pressure outlet was used to simulate the model outflow conditions with an environmental condition specified (to prevent backflow). Full development of the boundary layer on all surfaces (boundary walls, blades, and stanchion) was ensured through the specific turbulence model wall treatment and mesh resolution for each test case.

The boundary conditions for the free surface varied over the single phase and multiphase (VOF) models. As seen in Figure 3-6 for the single-phase model the free surface was modelled as a symmetry plane, which is a method often used in literature. For the multiphase-VOF approach the air water interphase is modelled as a phase change (volume fraction of water change in each cell) and the top outlet is specified as a pressure outlet. This limits interference from the top boundary.

Figure 3-8 highlights the slight differences in water surface boundary condition. A variation is seen just downstream of the stanchion structure where the water surface elevation is decreased. This is not observed in the single-phase model where a more drastic decrease in velocity occurs instead, this also results in a slight increase of velocities closer to the air-water interface. Additionally, a stronger vortex street is seen on the top boundary on the single-phase model. However, no relevant difference in turbine wake results is observed which also agrees with previous findings on a similar HAHT model (El Fajri *et al.*, 2022).
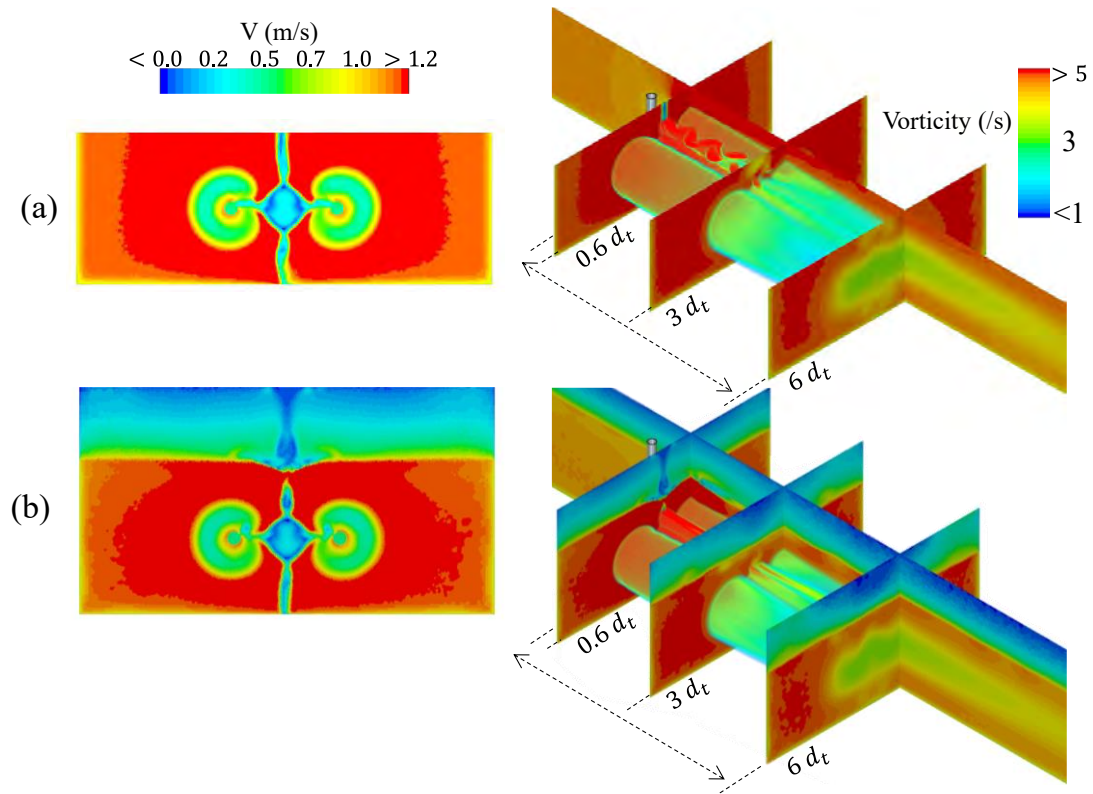
Figure 3-8: Comparison between a) single phase and b) multiphase velocity contour and wake vorticity maps representing the HAHT RM1 model flow field.

3.4.3 Solution domain and mesh generation

Steady and transient simulations are performed for all models where unsteady terms are discretised using a 2nd order implicit scheme. A time step ensuring Courant numbers less than 1 in all regions is ensured as far as possible. The time steps are around 0.002 % of the total time to complete one rotation for the FRG simulations and 0.01 % for the BEM-CFD models. However, timesteps varied over each approach depending on the grid sizes.

Careful selection of flow physics, and comparisons of commonly used models is a crucial factor in accurate modelling of these complex flow fields. A RANS approach is selected due to the reduced computational demand (when comparing to LES or DES) whilst allowing a large variety of approaches and complexity within these equations. As described in section 2.9, unsteady RANS is based on triple decomposition of time-dependant variables, with various closure models available.

RANS eddy viscosity models are most often used for turbine analysis (Miller and Schaefer, 2010; Afgan *et al.*, 2013; Shives and Crawford, 2014; Daskiran *et al.*, 2017). The k-ε turbulence model was compared to Menter's SST k-ω turbulence model (Menter, 1994) which typically predicts adverse pressure gradients in the near wall region better than the k-ε turbulence model. More complex Reynolds stress models (RSM) were then employed to allow more accuracy in prediction of possible flow anisotropy, these have shown positive results in HK wakes but require further validation (McNaughton *et al.*, 2012). The RS Linear pressure strain two-layer (RS-LPS2) model (Sarkar and Lakshmanan, 1991; Speziale, Sarkar and Gatski, 1991) was selected which allows near wake accuracy with a low y^+ wall treatment on the turbine and turbine structure.

The computational domain consists of a polyhedral mesh with grid refinements in the near wake, far wake and surrounding the retaining structure. Past results indicate the importance of fine grids to track the tip vortices when using simplified RANS models (Sanderse, van der Pijl and Koren, 2011). Simulations are performed on various meshes with similar base sizes and increased resolution over volumetric controls in regions of high turbulence. An adaption of the GCI (Roache, 1994) was used due to the variance in grid sensitivity in the different wake regions, therefore separate regions were decreased incrementally, starting from the near wake region, until no changes in wake behaviour was observed. An example of this can be seen in Table 3-1 with the refinement regions shown in Figure 3-9. Details of the grid independence studies for each model can be seen in Appendix A.

Table 3-1: Refinement domain for mesh independent models for the RM1 turbine k-ω BEM case.

	Mesh 1	Mesh 2	Mesh 3	Mesh 4
Base size (m)	0.07	0.07	0.07	0.07
VC_1 (m)	0.0035	0.0042	0.0049	0.0063
VC_2 (m)	0.007	0.0084	0.0065	0.0119
VC_3 (m)	0.0105	0.0126	0.0154	0.0189
No of cells	25 114 182	15 287 880	9 729 511	5 910 121

Performance metrics (Torque)

	Mesh 1	Mesh 2	Mesh 3	Mesh 4
Torque (N.m)	2.45	2.45	2.46	2.46

Wake hub height point velocities

	Mesh 1	Mesh 2	Mesh 3	Mesh 4
U_{avg} 2 d_t (m/s)	0.75	0.75	0.71	0.72
U_{avg} 4 d_t (m/s)	0.90	0.91	0.85	0.86
U_{avg} 6 d_t (m/s)	0.97	0.98	0.93	0.93
U_{avg} 8 d_t (m/s)	0.98	0.99	0.97	0.94
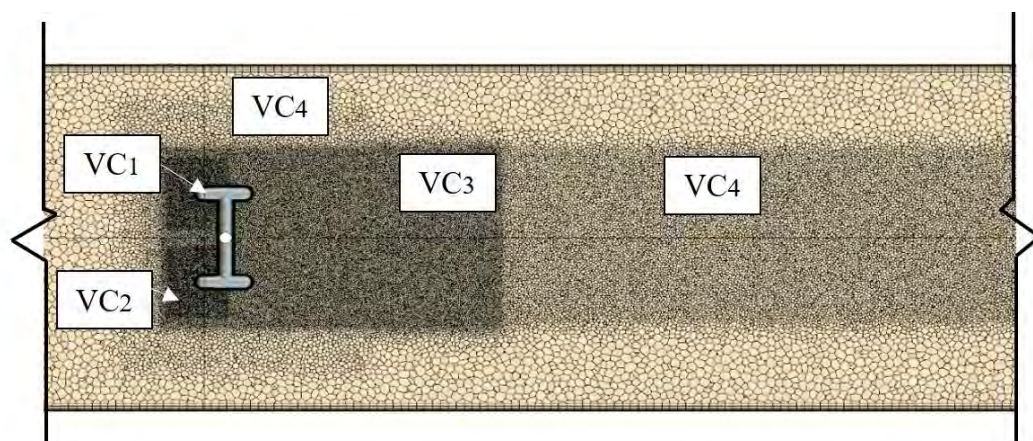
Figure 3-9: Plan view of the volumetric controls over the domain.

For the optimum turbine operation conditions ($\lambda = 5.07$) results showed grid sensitivity up to a minimum cell size of 3 mm (0.6 % D) around the blades for FRG modelling. However, a further 30 % increase in cell size showed only a 1 % change in wake dissipation rate. For the

FRG case a small mesh size is inevitable to capture the geometry of the blades (under high rotation) as well as boundary layer formation. RS models also required finer grids comparing to eddy viscosity models. For the RM1 turbine the advancing prism layer Mesher proved to be best for the complex geometry and customization of the prism layer thickness on the upstream and downstream side of the blades. The mesh can be seen in Figure 3-10 with final mesh sizes being around 19 million cells.

For the VD model (Figure 3-11) a 10 mm minimum cell size (2 % D) proved adequate for a BEM-RANS analysis. The finite number of blades across the virtual disk should ensure introduction of the effects of the propeller on the computational domain. A minimum of 4 cells over the blade thickness is ensured with all meshes, no performance or wake result effect is seen for further refinement or change in thickness. Both rotor modelling techniques solutions converged for near wake cell sizes of 8 mm. Increasing this near wake grid by only 4 % (2 mm cell size change) resulted in a 5 % change in wake velocity deficit results. Therefore, near wake grid sensitivity was carefully considered. A far wake cell size of around 8-15 mm showed no significant change. A 14 mm (2.8 % D) base size in the far wake was selected. Final mesh sizes amounted to around 13 million cells. A high-resolution mesh (Figure 3-11c) is ensured on the free surface, with a final size cell determined through a GCI study focussed on a free-surface profile analysis (Details in Appendix A).
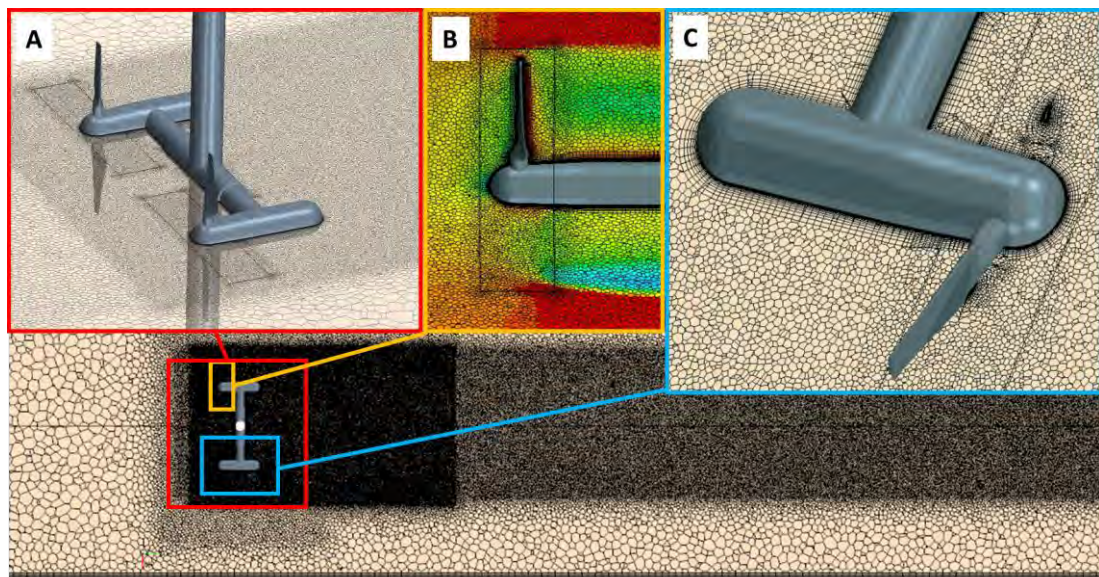
Figure 3-10: FRG Mesh indicating A-Near wake refinement regions B- Sliding mesh refinement and C- Sliding mesh prism layers.
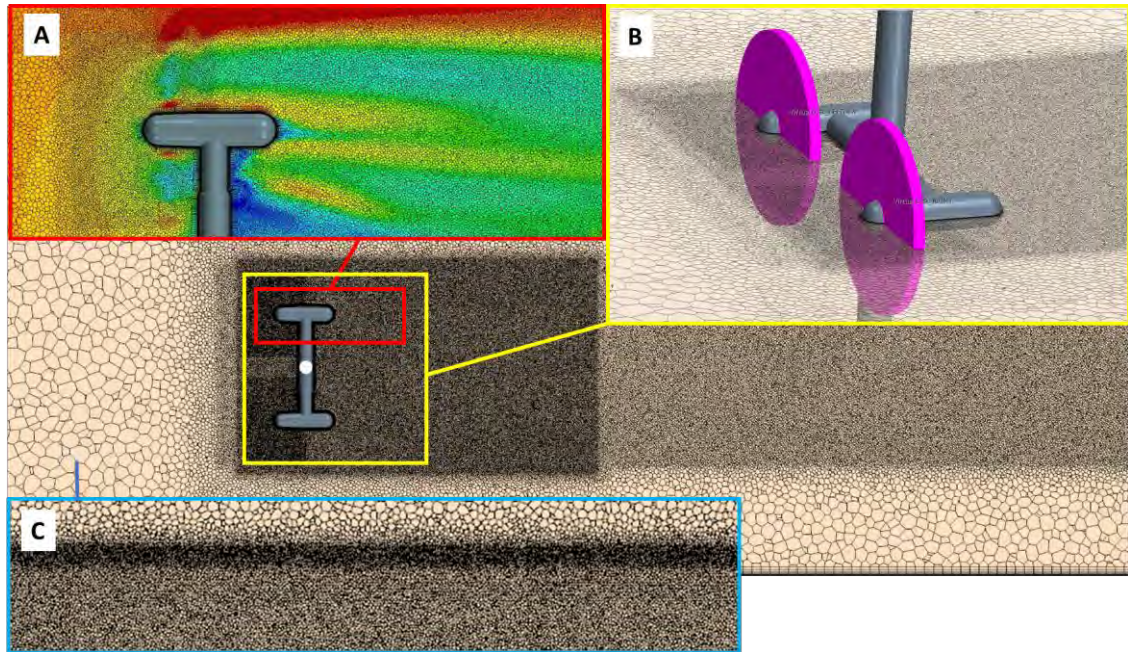
Figure 3-11: BEM-VD model mesh with A- Refinement regions around VD, B- VD placement and refinements and C- Free surface refinement (for the multiphase model).

Prism layers were built according to the wall treatment requirements applicable to each turbulence modelling approach. For the SST k-ω models a high y^+ wall treatment ($30 < y^+ < 300$) on the channel walls, and a layer resolving low y^+ ($y^+ < 1$) approach on the turbine and retaining structure was required, fully resolving the viscous sub-layer. Mesh refinement, specifically in the near wall region of the boundary layer was ensured for accurate near wake region development, especially where both separated and attached flow exists (Silva *et al.*, 2016). Gibson & Launder (1978) investigated the pressure fluctuation effects of capturing the boundary layer and noted the importance of an accurate capture of boundary layer formation and thus developed a two-layer formulation which may be applied to the linear pressure strain model (LPS2 model). Thus, all other models use the two-layer formulation.

3.5   Computational model validation

For HK turbine performance analysis both steady and transient FRG and BEM rotor modelling approaches are often employed and have proven good correlation to experimental results with the approaches used in Section 3.4 (Malki *et al.*, 2013; Masters *et al.*, 2014; Allmark *et al.*, 2020). Numerous studies have assessed which models are best for performance tests (Lavaroni *et al.*, 2014; Contreras, Lopez and Lain, 2017; Daskiran *et al.*, 2017; Lain, Contreras and Lopez, 2019), and this is often used as adequate validation even without comparison of wake results. However, the driving variables in wake dissipation (turbulent dissipation and breaking up of vortex structures) vary to those of turbine performance (fluid-structure interaction) and therefore the correct approach is unclear without proper experimental verification of both the turbine performance and wake dissipation rate.

The mesh independent study (covered in section 3.4.3) and analysis of the level of uncertainty in terms of modelling assumptions and approximations also including the uncertainty due to input parameters. The validation process includes direct comparison to experimental measurements.

3.5.1 Performance analysis

Table 3-2 includes the torque (T) and power coefficient (C_P) measurements and model results for the RM1 device modelled at its optimum tip speed ratio. The CFD results for both counterrotating rotors (left and right) showed identical results and thus only one set of results is listed. Due to the uncertainties of accuracy of the experimental performance results, specifically on the left rotor (mentioned in section 3.3) a certain degree of uncertainty lies on the measured values. However, the CFD results all lie well within the measured range and within 5 % of the measured results with similar conclusions found by Masters *et al.* (2015). The experimental systematic and random measurement errors existing on the torque sensors are also included, these were calculated based on measured and expected value comparisons.

Table 3-2: Performance comparison

Rotor	Experimental		
	T (N.m)	T difference (%) (sensor calibration)	C_P (%)
Left	2.081	3.80%	41.20%
Right	2.603	0.69%	47.60%
Turbulence model	FRG-CFD		
	Steady (moving reference frame)		Transient (motion)	
	T (N.m)	C_P (%)	T (N.m)	C_P (%)
RS-LPS2	2.35	44%	2.39	45%
SST kw	2.35	44%	2.45	46%
k-ε	2.16	41%	2.28	43%
Turbulence model	BEM-CFD		
	Steady state (time averaged)		Transient (Time accurate)	
	T (N.m)	C_P (%)	T (N.m)	C_P (%)
RS-LPS2	2.43	46%	2.38	45%
SST kw	2.43	46%	2.39	45%

Although Table 3-2 indicates most approaches predicted the performance to a certain degree of accuracy, the current study is more concerned with accurate performance in the near and far wake zone. By modelling the FRG using the sliding mesh technique, the vorticity in the wake is replicated (Figure 3-12). The tight vortical structures observed in Figure 3-12 correlate with the expected near wake behaviour prevalent in past LES studies (Churchfield, Li and Moriarty, 2013).

For steady state analysis a moving reference frame (MRF) is used to enforce the turbine rotation, however the solution lacks adequate capture of the vorticity and rotation in the wake. From the wake results it is clear the transient solutions better capture the wake. Although it may seem that steady state results better align with the left rotor it should be noted that during laboratory testing the left rotor did not perform to the expected degree of accuracy and has a larger degree of error (Hill *et al.*, 2014) (hypothesised to be a result of approach flow asymmetry (Hill *et al.*, 2020)).

The steady solution indicated a high initial turbulence with an overpredicted velocity deficit in the near wake. This resulted in an accelerated and inaccurate wake dissipation rate. Accelerated decay of the TKE in the bypass flow was prevalent in the near wake region. This may be attributed to the simplification of eddy viscosity model and its inability to resolve small eddies forming at the tip and root vortices. The eddy-viscosity model showed a strong vortex structure extending from the blade tips which is maintained up to 6 d_t downstream due to inadequate mixing in the model (McNaughton *et al.*, 2012). This leads to inadequate wake dissipation as the TKE in the bypass flow is too weak to break these structures down in the near wake.
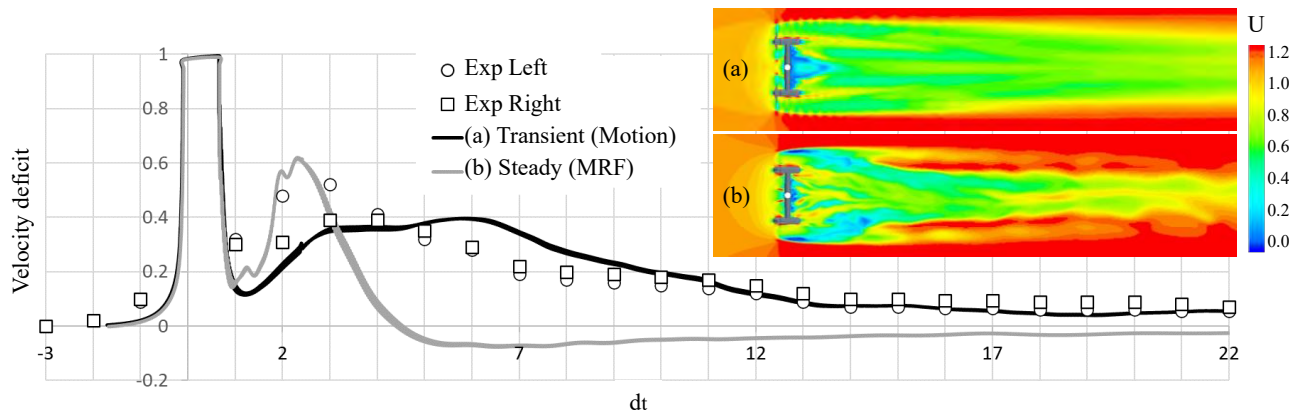
Figure 3-12: Comparison of steady state vs transient results for the FRG-RSM wake dissipation rate as well as velocity magnitude and vorticity scalar scenes (CFD results are identical for left and right rotor).
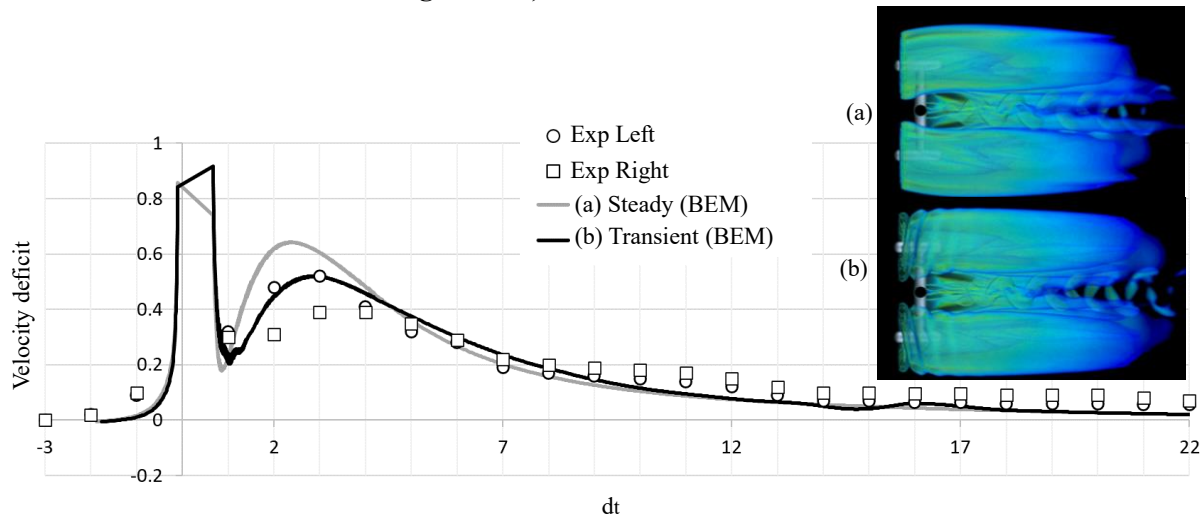
Figure 3-13: Comparison of steady state vs transient results for BEM-RSM dissipation rate and vorticity scalar scenes (CFD results are identical for left and right rotor).

Although simplified rotor modelling using a VD reduces computational time, the simplification results in the lack of tip and root vortices formation (seen on the vorticity plots in Figure 3-13). This is as a result of the BEM-VD theory, where a force (which is a function of the rotor hydrofoil geometry) is applied at all locations along the disk and blade tips are not resolved. The BEM-VD time accurate approach available in most commercial software improves this prediction. This method tracks the motion of the blades adding a source term only to the volume of cells corresponding to the location of the blades (specified as input

values to the VD). The improvement when using a time-accurate transient approach can be seen in Figure 3-13b. Similar behaviour as that shown in FRG modelling occurs, however the effect is not as pronounced.

For BEM-VD rotor modelling a sensitivity analysis on drag (C_D) and lift (C_L) coefficients comparing experimental (Hoffmann, Reuss Ramsay and Gregorek, 1996; Fouatih, Imine and Medale, 2019) and numerical data (XFOIL data shown previously in Figure 3-4) is necessary to ensure correct input data. The results indicate a significant variation in turbine performance, wake formation and wake dissipation rate in the near and far wake. Better results were obtained when using numerical coefficients over a broad range of Re numbers (including the operational range) and angle of attacks. This proves it is crucial that extensive and well approximated data be used in simplified rotor modelling techniques. All BEM-VD results utilised the Prandtl cosine tip loss function, not considering the tip loss effect of the turbine results in a further 12 % overestimation of the near wake velocity deficit.

Although modelling the FRG should improve the quality of the approximation when comparing to a VD approach, it is hypothesised that the complexities in fully modelling the geometry with these lower fidelity closure models results in a less reliable wake simulation. Meaning the VD approach couples better with RS models as the modelled wake vorticity from the VD is easily broken down by the TKE present in the wake and does not depend on resolving the smaller eddies which are present and important in real wake conditions. Higher fidelity models such as LES's have shown FRG modelling gives a better approximation of the wake behaviour. It is also important to note that although steady state models may be sufficient for performance analysis, wake analysis requires a transient approach.
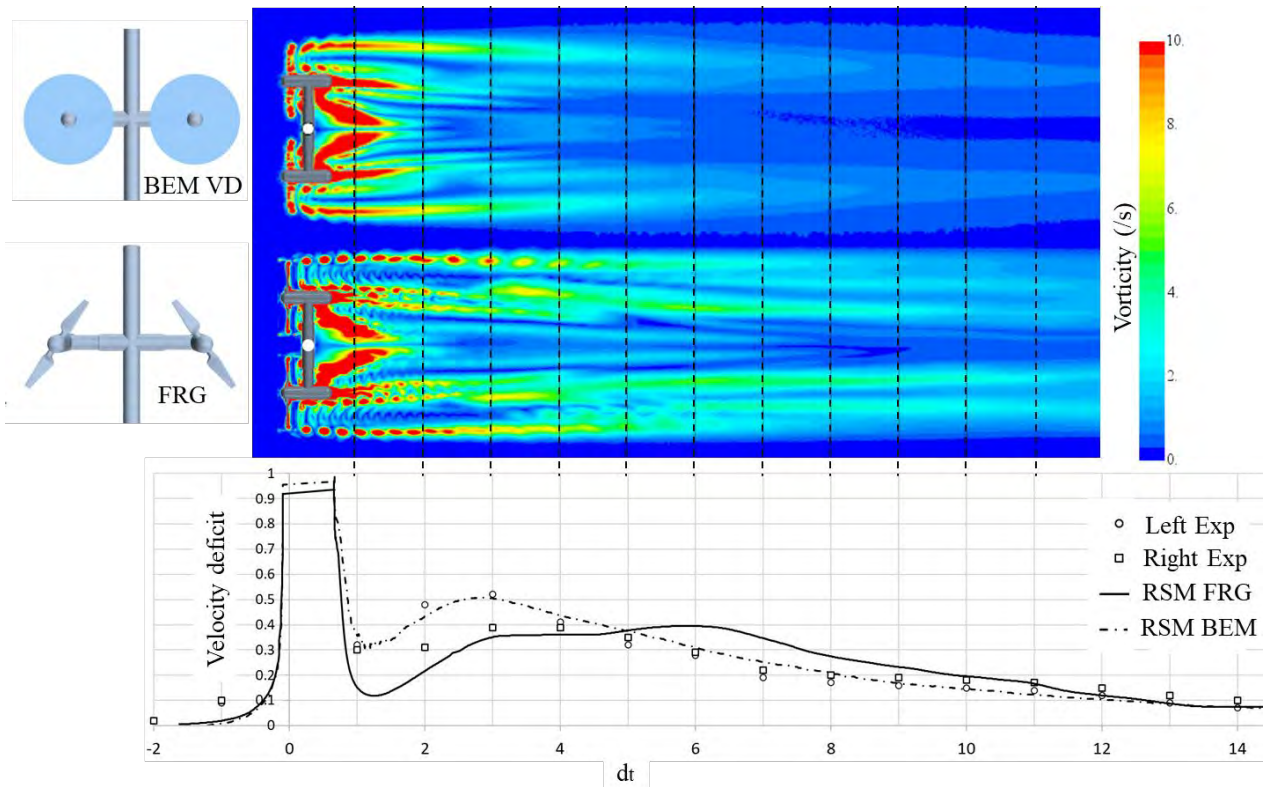
Figure 3-14: Rotor modelling approach comparison for RSM turbulence modelling

3.5.2 Wake prediction

Hub height velocity measurements are often used as an indicator of wake recovery. A CFD approach accurately capturing the recovery rate and behaviour would be most useful for device scale analysis of HAHT systems (as required in this study). A summary of the hub height velocity deficits for the various transient modelling approaches investigated in this study can be seen in Figure 3-15. No velocity deficit difference is observed in wake results between left and right rotors in the CFD models, thus only one set of numerical results are plotted together with both left and right rotor results from the experimental analysis. The discretion between rotors in the experimental wake velocity deficit becomes almost insignificant after 4 d_t after which little variation is observed.
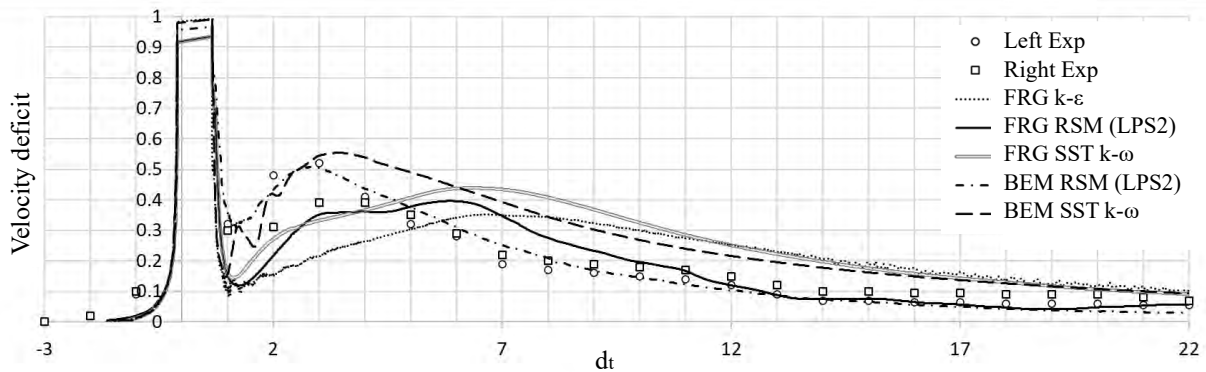
Figure 3-15: Comparison of RANS modelling approaches for left and right rotors.

The wake behaviour observed is characterised by a tight vortex formation in the near wake which starts to mix with the bypass flow further downstream. This mixing behaviour results in dissipation of the wake as it is carried downstream. Mixing is then slowed after about 10 d_t downstream where approximately 80 % wake recovery has occurred. The remaining deficit is carried a significant distance downstream.

For the FRG modelling all RANS solutions prove to have the similar problem of accelerated decay of the TKE in the bypass flow. Comparison of the wake width, vortex formation as well as dissipation rate indicate eddy viscosity models (k-ε and SST k-ω) predict the largest dissimilarity to experimental results in terms of dissipation rate. Although turbine performance is adequately determined, adequate capture of the wake dissipation rate is limited. The SST k-ω showed wake better prediction than the k-ε model. However, it still overpredicts the wake by up to 20 % between 6 d_t and 10 d_t downstream and significantly delays wake recovery.

Employing the RS-LPS2 turbulence model significantly improvs predictions with an improved mixing rate in the near wake and good correlation to experimental results after 10 d_t (Figure 3-16). The improvement could be attributed to the RSM's transport equations accounting for the effects of turbulence anisotropy (Sarkar and Lakshmanan, 1991; Speziale, Sarkar and Gatski, 1991). Whereas eddy viscosity models use the Boussinesq hypothesis (Menter, 2011) which assumes isotropic conditions. For the LPS2 model results, accelerated TKE decay in the bypass flow is still observed with inaccurate prediction of dissipating wake behaviour up to 10 d_t.

Although the RS models are known to have more accuracy within turbulence description, they also have limitations in predicting turbulence for complicated flows, especially in describing the effects of rotation (Wallin and Johansson, 2000). Curvature correction factors are available in some commercial codes and may be a useful tool in some cases. For this investigation, the correction did not have a significant effect. For all RANS solutions inaccurate wake results may also be attributed to the lack of resolving small eddies, which can only be resolved by employing higher fidelity models such as DES or LES.

When coupling BEM-AD with SST k-ω or LPS2 similar behaviour is observed. For the SST k-ω solution, a high velocity deficit is observed in the near wake, resulting in a delayed wake dissipation, and predicting inaccuracies up to 17 d_t downstream. An accumulated effect is observed through the shortcomings of the VD, which generally over estimates the turbulent eddy viscosity in the high shear flow within the VD and near wake (Shives and Crawford, 2014). This induces rapid mixing in the near wake and a higher peak velocity deficit.

The BEM-LPS2 model approach correlates best to experimental results behind the turbine rotor, with a maximum difference of 4% between 3 d_t and 17 d_t downstream (Figure 3-16). The theoretical modelling of the turbine rotor (using a VD) does not produce strong tip vortices. Although this is a shortcoming of utilizing the BEM-VD approach, when coupled with a RANS solution, the weaker vorticity requires less TKE in the bypass flow to break up the rotating wake structure. As a result, inadequate mixing is less of a problem when combining RANS with this simplified rotor technique (Figure 3-16).

The better correlation of the BEM-CFD model may be attributed to the shortcomings of the RANS approaches in the FRG rotating body-fluid interaction rather than greater accuracy when using the VD. When using the BEM-CFD approach less accuracy in resolution of the fluid-blade interaction is needed as the rotation effect on the flow is modelled using the BEM theory and therefore only requires correct resolution of the wake beyond the turbine.

Further validation cases are needed to investigate the consistency of this effect for variations of operating conditions (which is described in chapter 3.6).
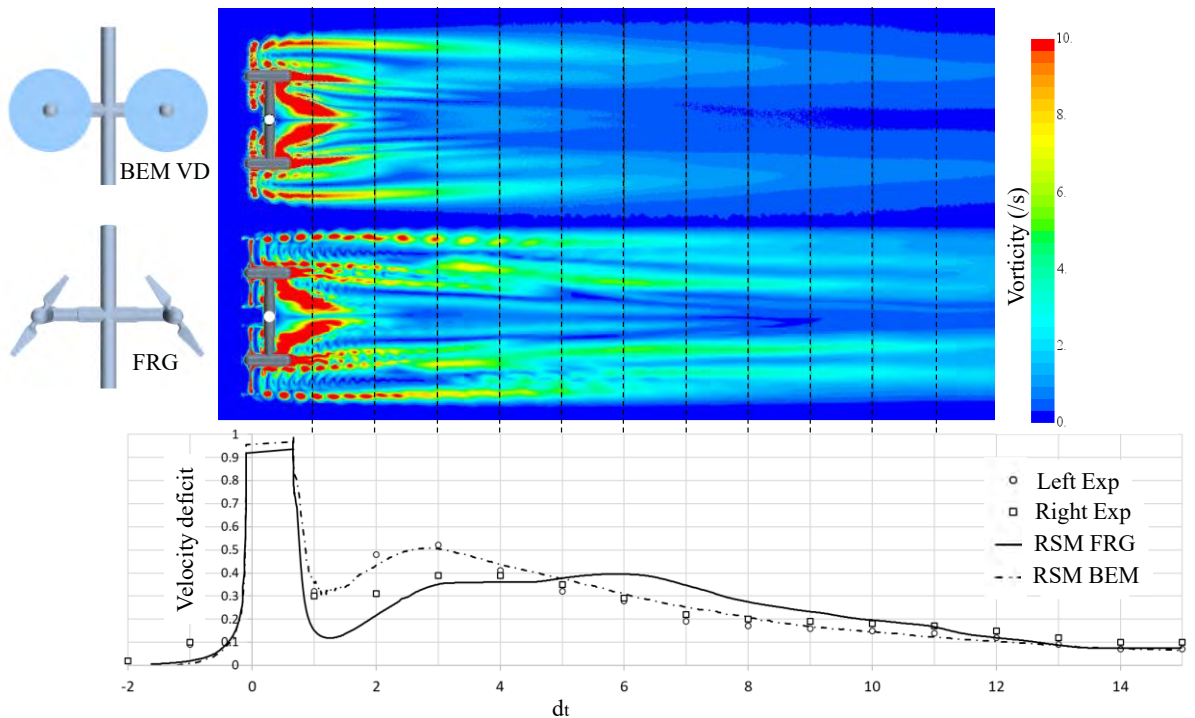
Figure 3-16: Vortical structure comparison for the rotor modelling techniques (using RS-LPS2 turbulence model)

3.5.3 Free surface prediction

Simulation of the air-water interface (multi-phase flow) may be approached in various ways. A multiphase analysis ensures a robust approach, but demands a higher computational load, and therefore a symmetry boundary condition is often used in a single-phase model.

Due to the necessity of free-surface measurements in this analysis for verification of the backwater measurement approach (Chapter 5), the free surface was modelled using a VOF approach. The approach uses a 2nd-order discretization to compute a clear interface between the air and water. A volume-fraction variable is used to specify the spatial distribution of each phase. Cells with multiple phases are treated as a mixture, and the method is highly dependent on adequate mesh refinement. A high-resolution mesh is ensured on the free surface. The final cell refinement around the free surface was determined through a gradual refinement of the free surface mesh size until no free-surface change was observed (mesh shown previously in Figure 3-11c). The remaining domain was modelled to the same resolution as verified in the single-phase analysis.

To allow verification of the immediate backwater in the model, the free-surface measurements from a multiphase model are compared. An image of the free surface effects both experimentally, with the data obtained from personal communication with Craig Hill, June 4, 2021, and modelled in CFD, can be seen in Figure 3-17 indicating the qualitative similarity.
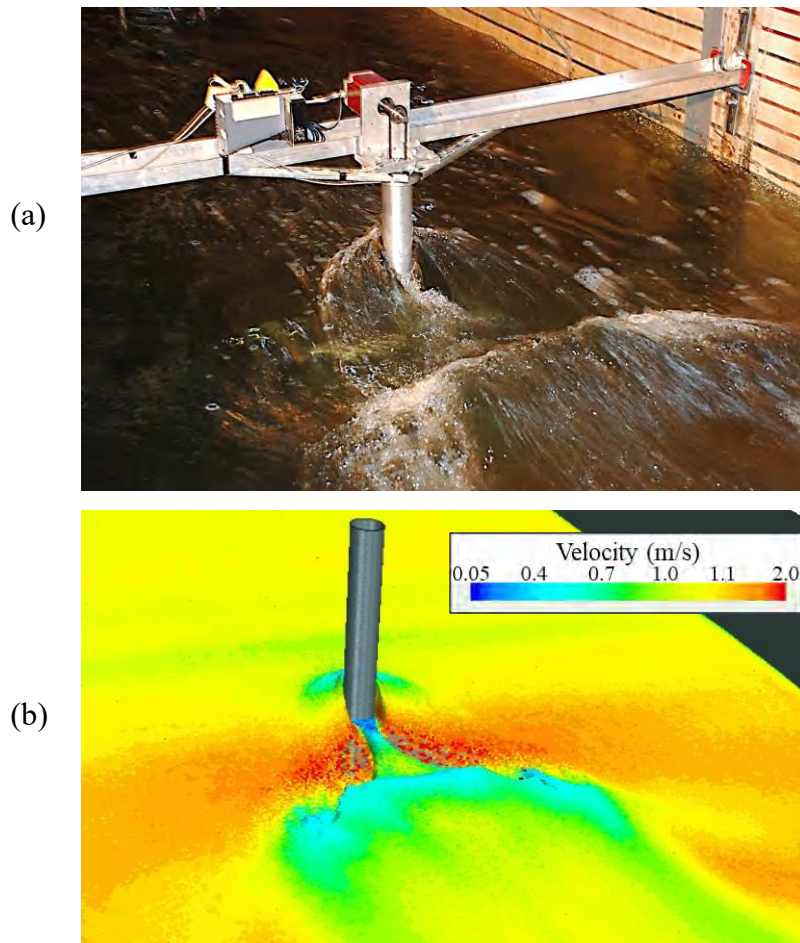
Figure 3-17: free-surface a) experimental data obtained from personal communication with Craig Hill, June 4, 2021, b) CFD model

During the experimental testing, free surface measurements were taken at a resolution of 500 mm (1 d_t) in the streamwise direction and 200 mm (0.4 d_t) in the cross-stream direction. An area from 5 d_t upstream to 10 d_t downstream was scanned. Comparison of the experimental and CFD free-surface measurements can be seen in Figure 3-18. The CFD results are recorded over one rotation and plotted as an envelope (Figure 3-18b).

In Figure 3-18a the free-surface depth on lateral points at the measurement points 3 d_t upstream to 1 d_t downstream is compared. The model purpose for this study was to observe the ability of the BEM-CFD multiphase model to indicate the backwater caused through the addition of the turbine. The maximum backwater at 1 d_t upstream is predicted within 1 mm of the measured values, indicating good prediction of the upstream damming effect and free-surface resolution. Discrepancies between the experimental and modelled values are seen primarily at 3 d_t upstream where the asymmetry of the approach flow observed in the experimental setup may have resulted in free-surface effects. This is also observed in the -1 d_t measurements between $300 < Y < 1000$. The prediction of the average deformation downstream of the turbine also correlated well to experimental measurements.
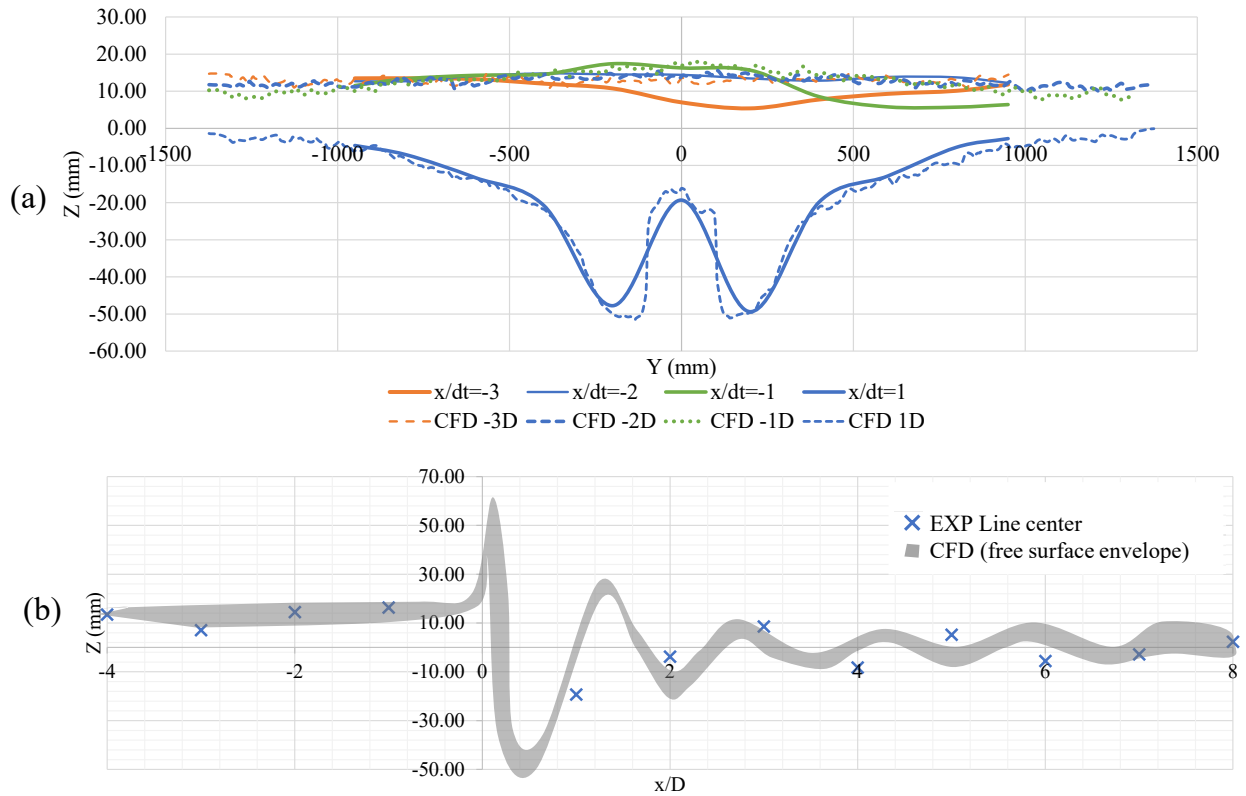
Figure 3-18: Comparison of experimental and computational water surface profiles for the RM1 tests (a) Lateral WSE comparison (b) longitudinal centreline WSE comparison

3.5.4 Sensitivity to input parameters and boundary conditions

A major challenge in CFD analysis is the prescription of inlet conditions, especially when validating models with experimental results. Correctly replicating the experimental conditions, including the anisotropy of the turbulence within the inflow boundary is a challenge. It is clear from the equations used to solve the turbulence dissipation rate in the SST k-ω model that the chosen freestream values of turbulence quantities have a strong influence on the rate of decay of turbulence (Spalart and Rumsey, 2007). Spalart & Rumsey (2007) also demonstrated that eddy viscosity models facilitate more rapid decay of turbulence at higher freestream turbulence intensities (TI), and the same is true for low levels of freestream eddy viscosity.

The factor which most affected the recovery rate for all RANS approaches, especially in the near wake, is the specified inlet turbulence. This effect is portrayed in Figure 3-19 where the dissipation rate for a high TI case (15%) as well as the assumed experimental TI case (5%) is compared. Higher TI's reduced the peak velocity deficit in the near wake, which agrees with previous LES results (Ahmadi, 2019) as well as similar experimental results comparing turbulence cases (Mycek *et al.*, 2014).
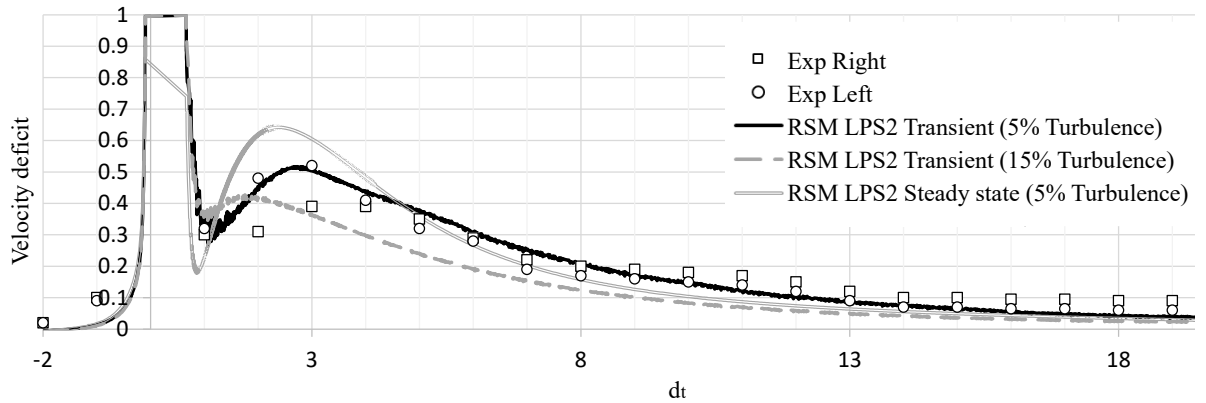
Figure 3-19: Turbulence input specification effect on wake dissipation rate for BEM-CFD analyses.

The experimental turbulent and velocity profiles (Figure 3-20) showed a slight asymmetry about the rotor center. This indicates that the free surface as well as channel bed may have an influence on the wake. Although a slight asymmetry is seen in the numerical wake, the effect is more pronounced in experimental conditions (Hill and Neary, 2014). Incorporating an air/water interface increases the accuracy of capturing the asymmetric effect (Figure 3-20c), but also significantly increases computational overhead. The vertical profile of a multiphase model using the experimentally measured free surface profile at the inlet is shown in Figure 3-20c.

When comparison is drawn to a single-phase model with a symmetry plane boundary condition (in Figure 3-20b) a slight difference in the velocity profile close to the free surface is observed. Additionally, a slightly accelerated recovery region is seen between 6 d_t and 10 d_t downstream in the bypass flow between the wake and free surface. Although the effect is minimal in this case, it may be necessary to perform a multiphase analysis when the turbine is in closer proximity to the free surface. Blockage and free surface effects may play a bigger role at higher blockage ratios and cases where turbine performance near the free surface is of importance. When BEM-VD theory is used for scaled tests, blockage correction factors may be incorporated (Whelan *et al.*, 2009).
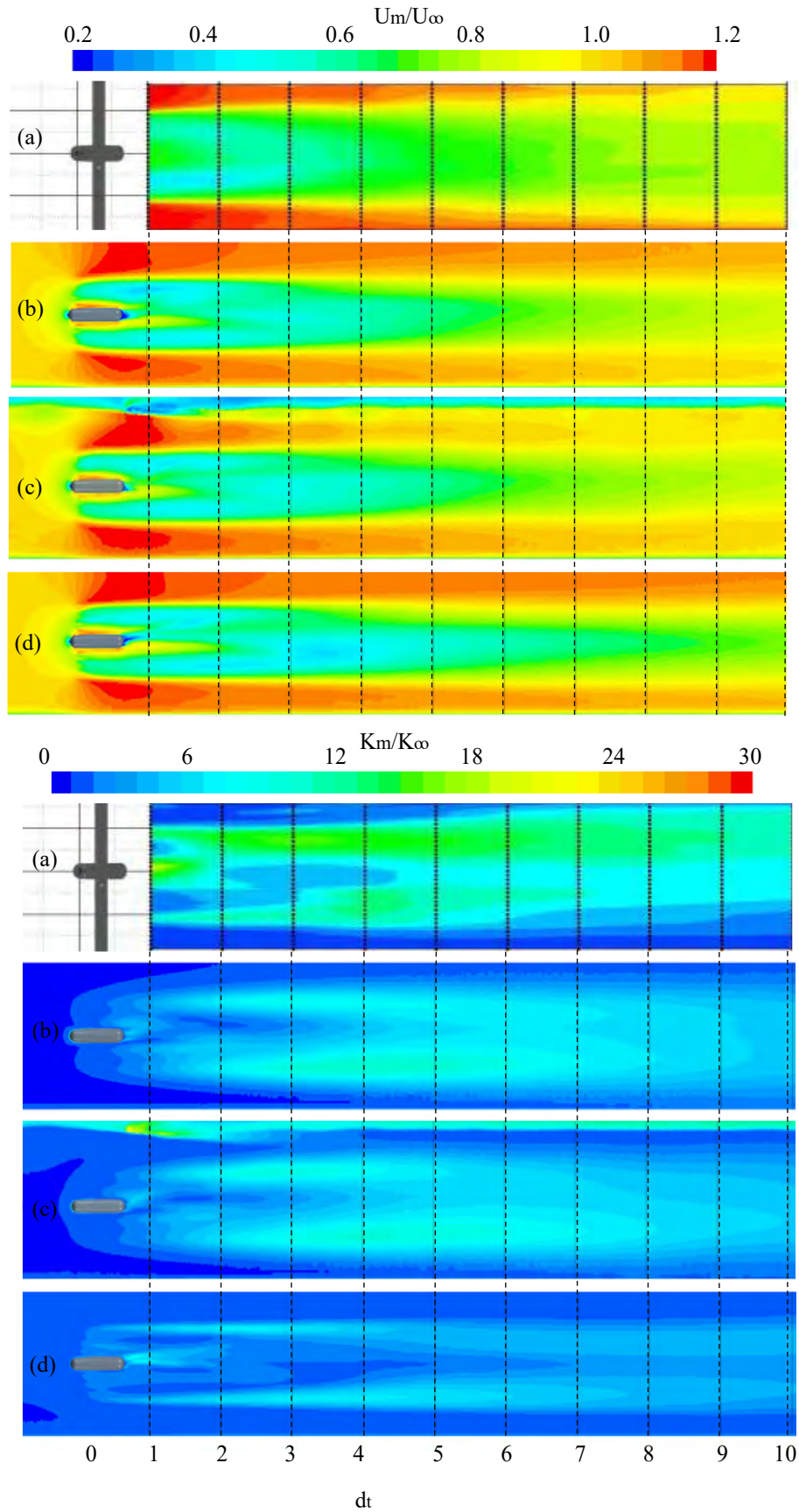
Figure 3-20: Vertical velocity (left) and turbulence (right) profiles comparing a) Experimental results b) Single phase BEM-RS(LPS2) c) Multiphase BEM-RS (LPS2) and d) Single phase BEM-SST k-ω CFD results.

Utilizing a constant pressure outlet (used in the single-phase analyses) showed negligible effects when compared to the realistic pressure distributions used in the multiphase downstream boundary. However, a distance of at least 10 d_t to the outlet was ensured here **(**Figure 3-20).

Although this study has shown better results using RS models, due to the reduced computational expense of two-equation eddy viscosity models it may be beneficial to use these models as a first order estimate and adjust for differences (especially when FRG modelling is necessary). A solution is to prevent accelerated TKE decay. As mentioned previously, eddy viscosity models result in more rapid decay of turbulence at higher freestream TI's, and the same is true for low levels of freestream eddy viscosity. Therefore, to achieve a reasonable turbulence decay rate, very low TI, or very high eddy viscosity value should be chosen for the freestream.

A solution to this may be "controlled decay" where an ambient turbulence source term is enforced over the domain to prevent decay. This may be done by utilising the SST k-ω equation but increasing the turbulent production term or adding a turbulence source term equal to the measured TKE or TI present in the flow field, over the whole domain. This limits turbulence dissipation by subtracting the inflow decay specified and counter-acting turbulent decay.

In the validation case, addition of the source term significantly improved results to within 5 % accuracy between 4 d_t and 12 d_t downstream for the FRG case, where the maximum eddy viscosity model error is observed as shown in Figure 3-21. Shives & Crawford (2014) recommended a more precise solution. To augment the production term in the near wake, specifically for results when a simplified rotor modelling technique is used, and tip vortices are not resolved. However, this is complex and may vary between testing cases. Olczak *et al.* (2016) also improved BEM-CFD results by around 25 % through an added turbulence source.
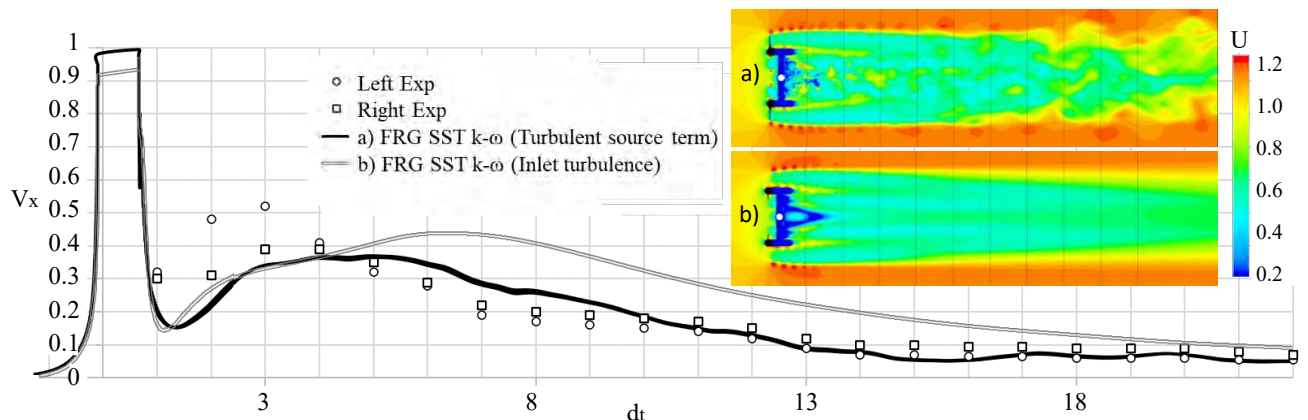
Figure 3-21: Turbulence source term SST k-ω improvement

3.5.5 Benchmark validation of the IFREMER-LOMC HAHT model

To allow further verification of the computational approach an additional turbine tested under laboratory conditions is modelled and the wake results compared. A 3-bladed HAHT was built and tested at the French Research Institute for exploration of the Sea (IFREMER) wave and

flume tank of the so called LOMC 3-bladed turbine model (Mycek *et al.*, 2014) with properties shown at Figure 3-22. The turbine was tested over a range of tip speed ratios (λ) and found to have a maximum power output at $\lambda = 3.67$ when tested in a flow velocity of 0.8 m/s. Laser Doppler Velocimetry (LDV) wake velocity and turbulence measurements were taken for these conditions under two ambient turbulence intensities. The first was a higher ambient turbulence measured as 15% which is the naturally occurring TI in the flume. A honeycomb inlet structure was then used to smooth the flow to a TI = 3 %.

Description	Variable
Rotor diameter	0.7 m
Blade profile	NACA 63418
Flow depth	2 m
Tip speed ratios measured	0-10
Flow velocity (V_{hub})	0.8 m/s
Sense of rotation	Counter clockwise

Figure 3-22: Turbine details and picture (Mycek *et al.*, 2014)

A computational model replicating the experimental test cases is constructed. The mesh resolution (relative to turbine diameter and λ) as well as solution domain is kept consistent with the approach presented in the RM1 model. Boundary layers are altered where needed to ensure the correct wall treatment is implemented on each boundary, the final mesh can be seen in Figure 3-23 (grid convergence tests are shown in Appendix A). A timestep of 0.001s is used to ensure a Courant number less than 1 over all cells in the mesh. A transient LPS2-RS turbulence model approach is followed. The TI is specified as a TKE over the inlet boundary.

The performance correlated well with experimental results with a C_p error of 1.2 % found in the TI = 3 % results and 2 % in the TI = 15 % results as shown on Figure 3-24.
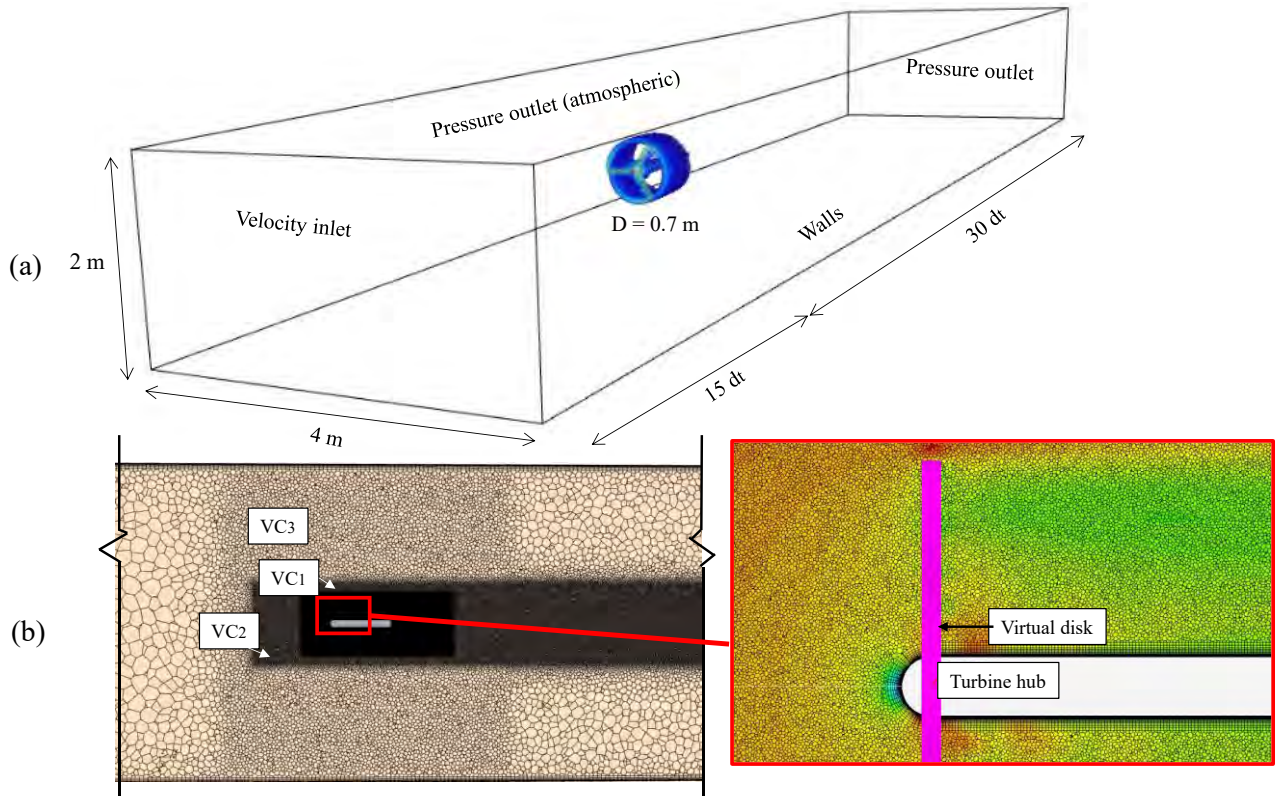
Figure 3-23: IFREMER-LOMC turbine CFD model final mesh refinement
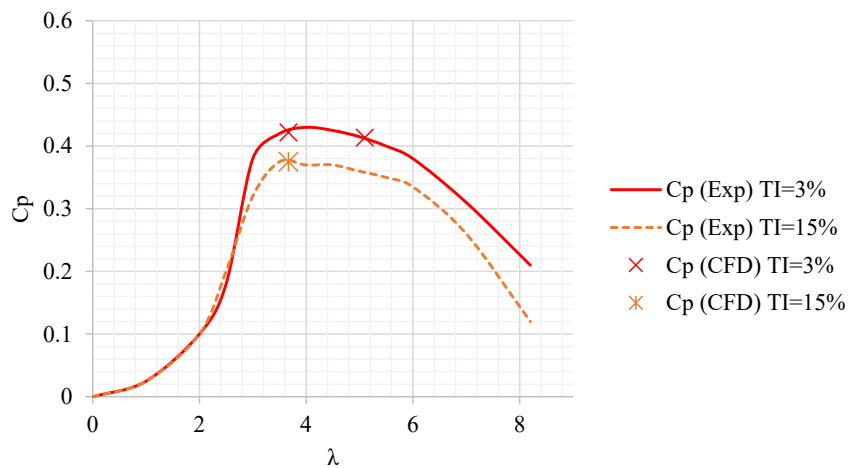
Figure 3-24: Performance validation with experimental results

The wake contour maps of two varying ambient TI measurements are shown in Figure 3-25. The TI is well represented in the TI = 3 % case where the high TI zone in the wake seen in the experimental results is also observed in the CFD results. The higher inlet TI case (Figure 3-25b) highlights the issue with RANS models, namely the fast dissipation of the TKE, which can be seen on the edges of the wake towards 10 d_t. However, although wake spreading is limited, the TI dissipation in the wake still correlates well to experimental results, capturing the increased dissipation rate.

(a) Turbulence intensity map (inlet TI= 3%)   (b) Turbulent intensity map (inlet TI= 15%)
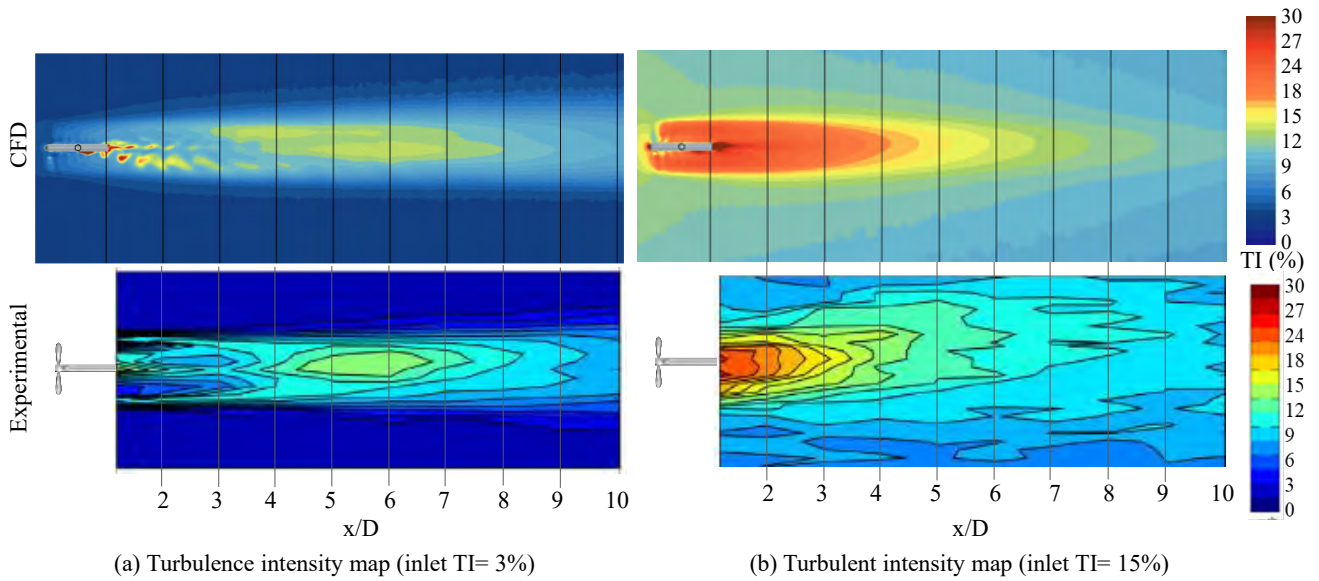
Figure 3-25: Wake TI map comparisons of CFD and experimental results (Mycek *et al.*, 2014)

Comparison of the wake velocity contours are shown in Figure 3-26 where hub height point velocity measurements behind the turbine are also compared. For both the low and high turbulence scenarios a slightly higher velocity deficit is predicted by the CFD model in the near wake (1 d_t to 3 d_t). This discrepancy could be attributed to multiple factors, such as mesh size, implemented turbulence model (for the CFD model) as well as experimental measurement unquantified uncertainties.
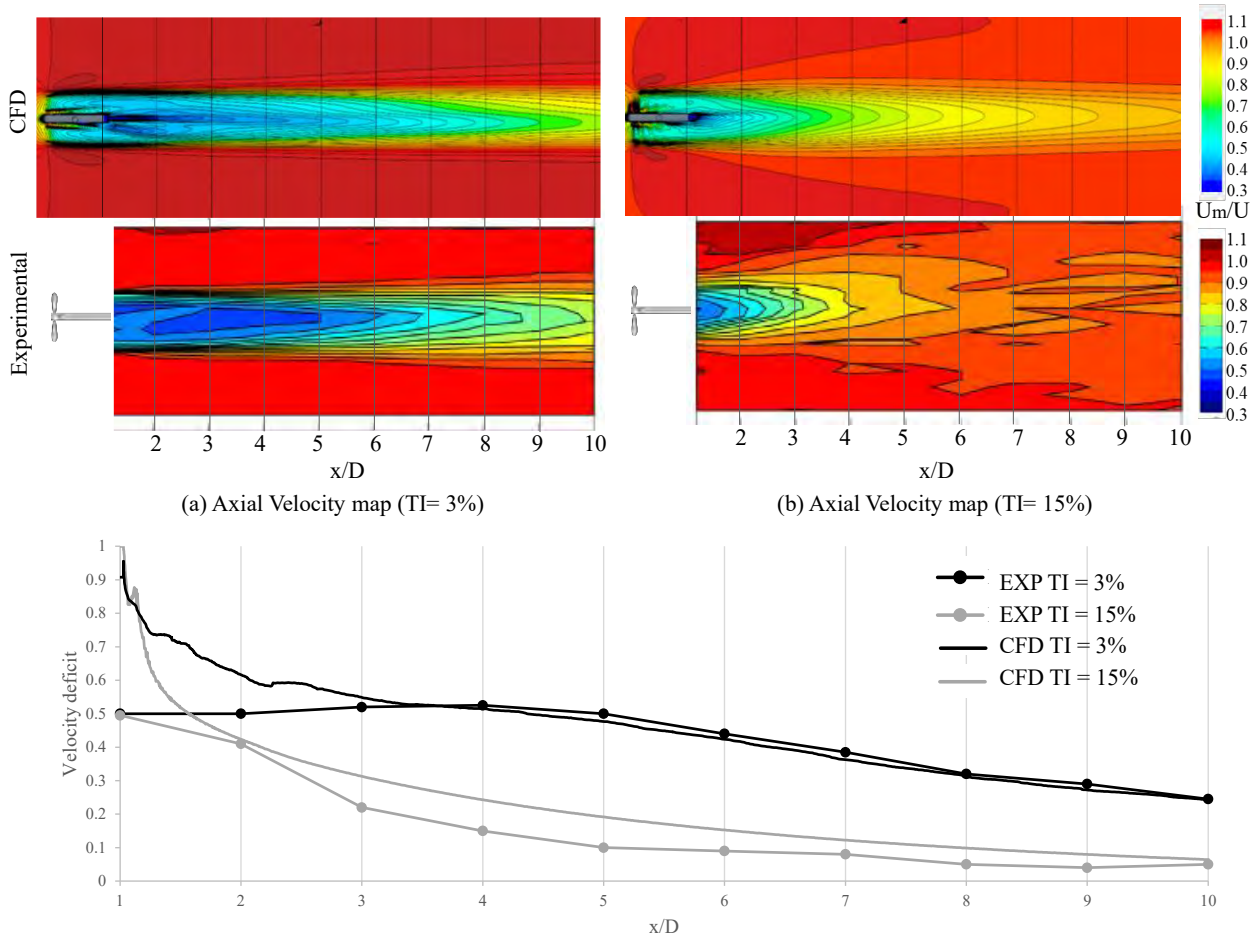
Figure 3-26: Comparative results of the downstream lines and contour plots for (a) TI= 3 % and (b) TI = 15 % for CFD and experimental (Mycek *et al.*, 2014) results.

On close inspection of the wake behind the turbine hub, which begins at 1.02 d_t behind the turbine, a very low velocity zone can is observed directly behind the hub (Figure 3-28), which is to be expected as flow passes a blunt body. The Karman vortex street behaviour is also seen behind the hub and results in a highly turbulent zone. If this behaviour is predicted correctly, it would make accurate experimental point velocity measurements using probes quite difficult and could thus result in lower velocity measurements.

An example of this can be seen in Figure 3-28 where the mean flow velocity measured on lines slightly offset from the centreline are shown over a single rotation. The results vary significantly in the near wake and when used, showed closer correlation to the experimental measurements. This indicates velocity deficit changes up to 50 % could occur in the near wake by probe placement inaccuracies of only 50 mm (0.07 d_t). This inaccuracy may be eliminated by using the area averaged velocities (Figure 3-27) where measurements of velocity deficit were averaged over an area equivalent to the turbine swept area (Y_r). This analysis would more likely remove errors made in point velocity measurements and could therefore result in the better correlation observed.
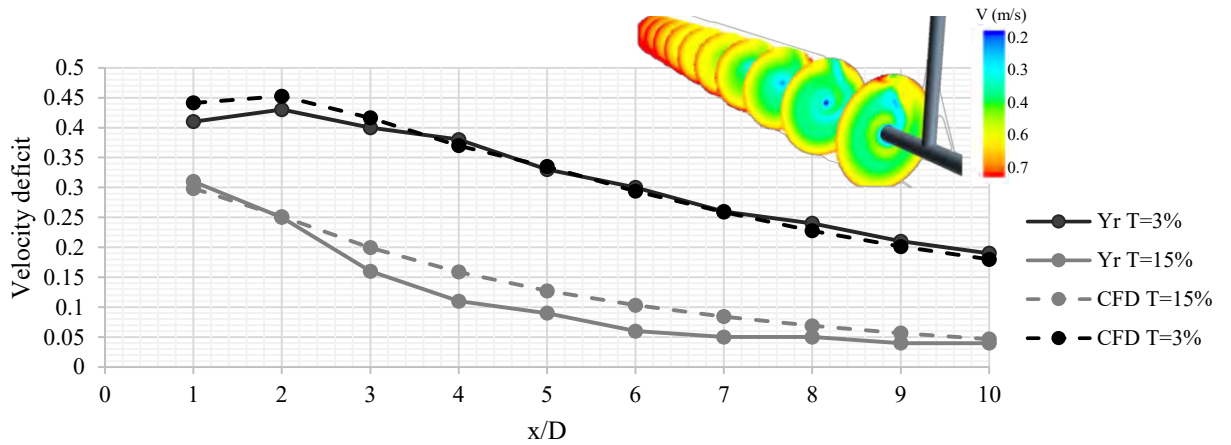
Figure 3-27: Results for the velocity deficit averaged over the turbine swept area at points downstream
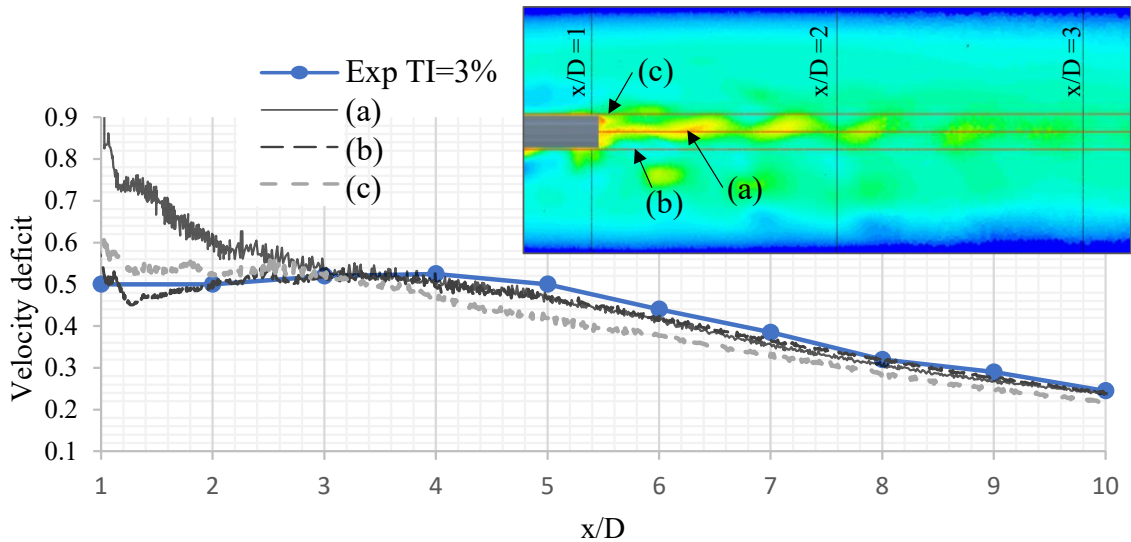
Figure 3-28: Downstream mean velocity deficit for (a) centreline (b) left offset 0.07 D and (c) right offset 0.07 D and instantaneous velocity contour plot

A slight underestimation of the velocity deficit in the high TI scenario (TI = 15 %) is observed. This could be attributed to the overly rapid dissipation of turbulence resulting from the use of the RS models which also reduced the wake spreading effect observed in the experimental case Figure 3-26b. This effect may be more pronounced in higher turbulence cases. Despite this difference the CFD modelling approach seems to predict the wake dissipation rate to a relatively high degree of accuracy after 3 d_t downstream (max error of 4.5 % for the TI = 3 % case and 9 % for the TI = 9 % case). The model also captures the change in wake behaviour when the inlet turbulence is altered, which is an important input variable in wake analysis. This meets the requirements necessary for the study and is therefore deemed acceptable.

3.6 Additional computational modelling case studies

As concluded in the previous section, utilizing a RSM together with a VD-BEM rotor modelling approach indicated good correlation to experimental results in terms of

performance and wake dissipation rate for both the two-bladed RM1 turbine and the three-bladed IFREMER-LOMC turbine over a range of ambient TI's.

To allow proper development of a wake and damming model two further turbine designs which have been previously tested, and the optimal operational points found and reported, were built in CFD using the same approach which is validated in the previous section. Although these turbines did not have detailed wake results for benchmark validation it is assumed the approach validated previously allows a relatively accurate depiction of the wake to allow testing and generation of wake data. Where available, some details on turbine performance or published wake analysis results were used to validate the results obtained as well as further verification through grid independence studies.

3.6.1 Case studies

Only turbines with a known optimal operating point were included to ensure the models developed are true for optimal operation. Two such cases were found and are described below.

A HAHT was optimised and tested at the University of Liverpool recirculating water flume (Mason-Jones *et al.*, 2012). The working section in which the turbine was tested is 3.7 m long 1.4 m wide and 0.85 m in depth. A honeycomb and contraction guide vane were used to correct the streamline direction upstream and ensure uniform flow as far as possible. Laser Doppler Anemometry (LDA) measurements were used to measure turbulence (found to be around 3%) at the measured water speed. Morris (2014) further tested this design by also adjusting the blade numbers (2, 3 and 4 bladed setups) and finding the optimal operation point for each turbine solidity. The turbine characteristics can be seen in Figure 3-29.

Description	Variable
Rotor diameter	0.5 m
Blade profile	FX63-137
Flow depth	0.85 m
Tip speed ratios measured	0 - 8
Flow velocity (V_{hub})	1 m/s
Sense of rotation	Clockwise

Figure 3-29: Liverpool turbine test setup (Mason-jones, 2010; Morris, 2014)

An additional three-bladed HAHT turbine (referred to as the BBMC turbine) was constructed and tested in a cavitation tunnel at Southampton Solent University (Bahaj *et al.*, 2005; Bahaj, Batten and McCann, 2007). The cavitation tunnel working section used, measured 2.4 m in width by 1.2 m height over a 5 m length with the rotor centred within the tunnel. The details of the turbine and experimental test are shown in Figure 3-30. An in-line strain gauge dynamometer was used to measure turbine thrust and torque over a range of tip speed ratios (Bahaj *et al.*, 2005).

Description	Variable
Rotor diameter	0.8 m
Blade profile	NACA 63-8xx
Flow depth	1.2 m
Tip speed ratios measured	4.2-10
Flow velocity (V_{hub})	1.0-1.7 m/s
Sense of rotation	Clockwise
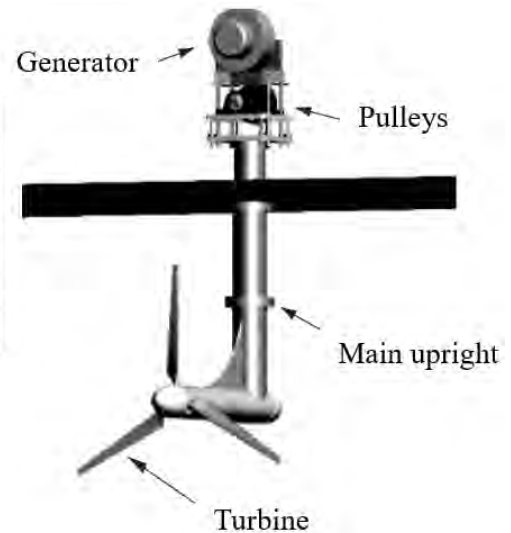
Figure 3-30: BBMC turbine test setup (Bahaj, Batten and McCann, 2007)

The BBMC represents an elongated thin blade shape compared to the larger chord and thicker shape used in the IFREMER turbine. The turbine was tested over various blade pitch angles (15⁰ to 30⁰), λ's and water tunnel speeds (U_∞ = 0.8 to 2.0 m/s) (Bahaj *et al.*, 2005). The lowest pitch was found to perform best and the optimal power output was found to be at around λ = 5.07 (tested at U_∞= 1.36 m/s). Bahaj *et al.* (2007) further tested the turbine over a pitch of 0⁰ - 15⁰, with a maximum power output found to be at a pitch of 5⁰.

3.6.2   Computational models

Both turbine designs described in section 3.6.1 were modelled using a wall bounded single phase BEM-CFD model with the validated approach described in 3.5. Validation of the performance metrics was carried out for the various optimal operational cases tested experimentally. Additional verification is completed through a mesh independent study to ensure the mesh is fine enough to capture both performance and wake dissipation (details included in Appendix A). For all model's airfoil section properties (lift and drag coefficients) as well as propeller blade properties (geometry, chord and twist distribution) were included. These were found from various publications, as well as generated values from XFOIL software (for specific profiles around the operational Re). These properties and airfoil details are included in Appendix A.

The 2-, 3- and 4- bladed turbines tested at Liverpool University are modelled with a final mesh size shown in Figure 3-31. The domain extended from 15 d_t upstream to 30 d_t downstream. A stanchion extending from the turbine hub through the upper boundary was included with similar dimensions to that used in the experimental tests. The final mesh size was around 11,2 million cells.

(a)

(b)
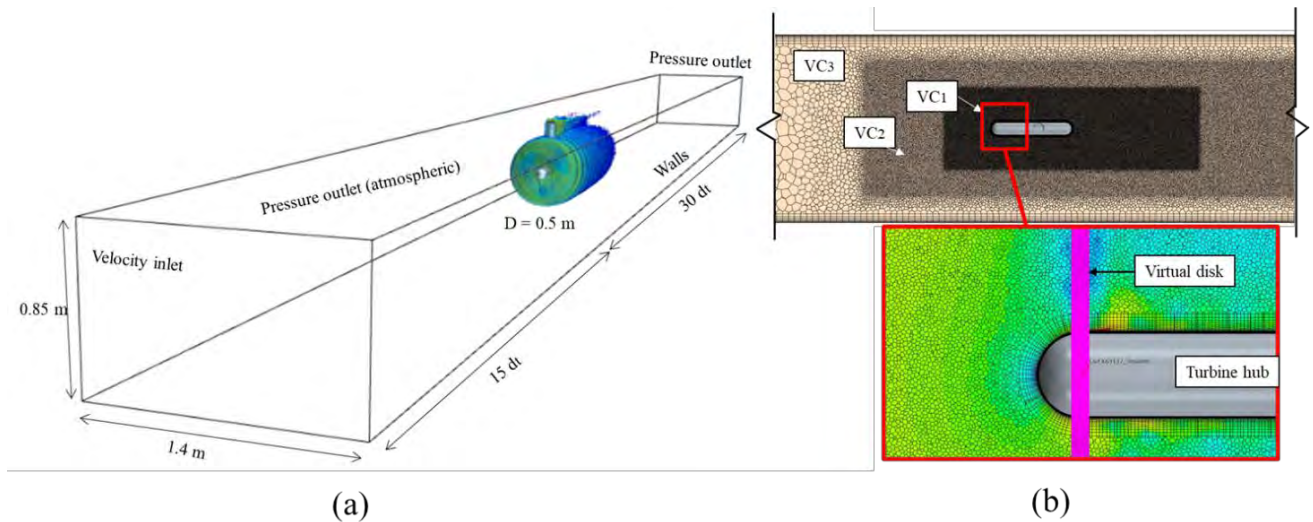
Figure 3-31: Liverpool University turbine model (a) domain and (b) mesh details and volumetric controls (VC)

The turbine performance was measured and compared to experimental values reported by Morris (2014). For the 3-bladed turbine, three operational points were included, where the lower λ showed better correlation to experimental results (Figure 3-32b). The 2- and 4-bladed models were modelled at optimal λ and found to correlate well to experimental measurements (within 2.5 % accuracy). As the blade numbers increased, the higher thrust and thus more disruptive wake was prevalent in the velocity contours (seen in Figure 3-32a). the slight asymmetry in the wake due to the direction of rotation is also prevalent as well as the effect of wall boundaries and confined flow around the turbine.
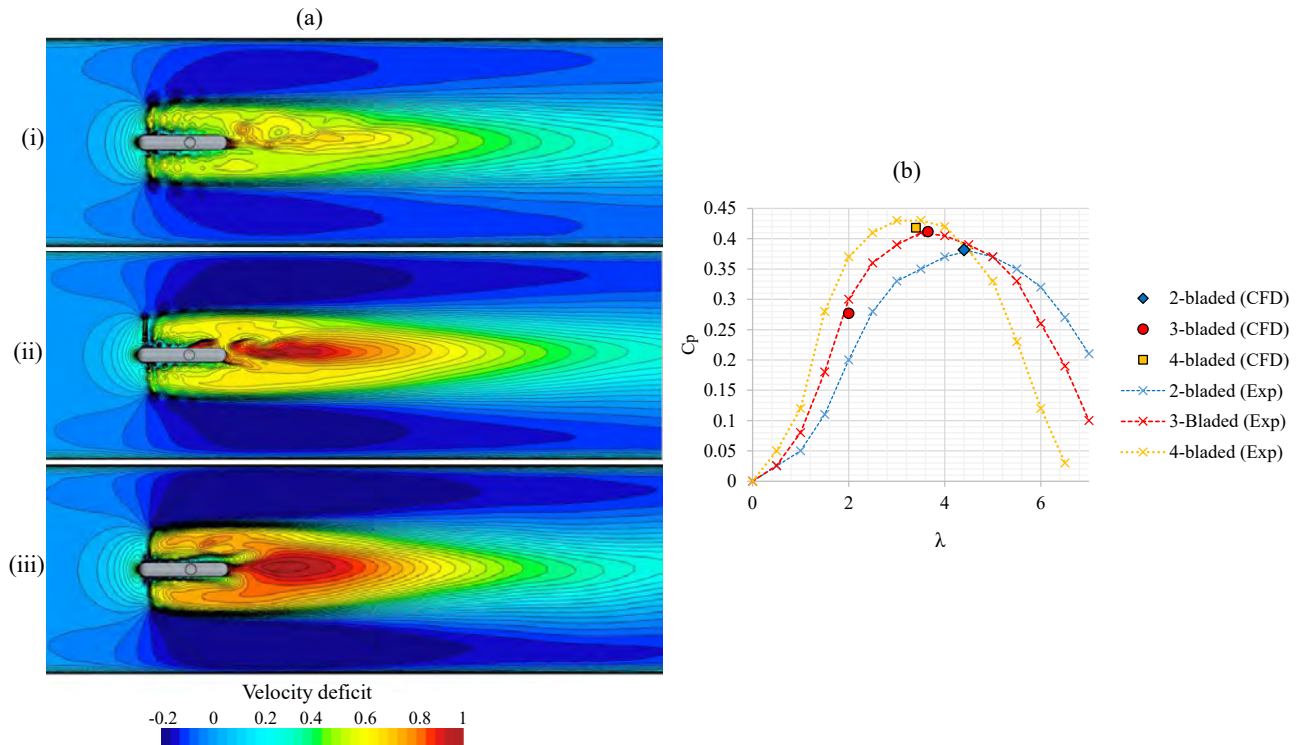
Figure 3-32: Liverpool University turbine model (a) (i) 2-bladed (ii) 3-bladed and (iii) 4-bladed velocity contour and (b) performance comparison to experiment results

A 3-bladed model replicating the BBMC turbine in the cavitation tunnel (also described in 3.6.1) is built with the turbine operating at its optimal point as well as two additional λ's lower and higher than the optimal point (for benchmark validation purposes). The model extends 15 d_t upstream and 30 d_t downstream to ensure full development of the inlet flow and proper wake formation without secondary effects from the outlet boundary. The final mesh size was around 21,2 million cells.
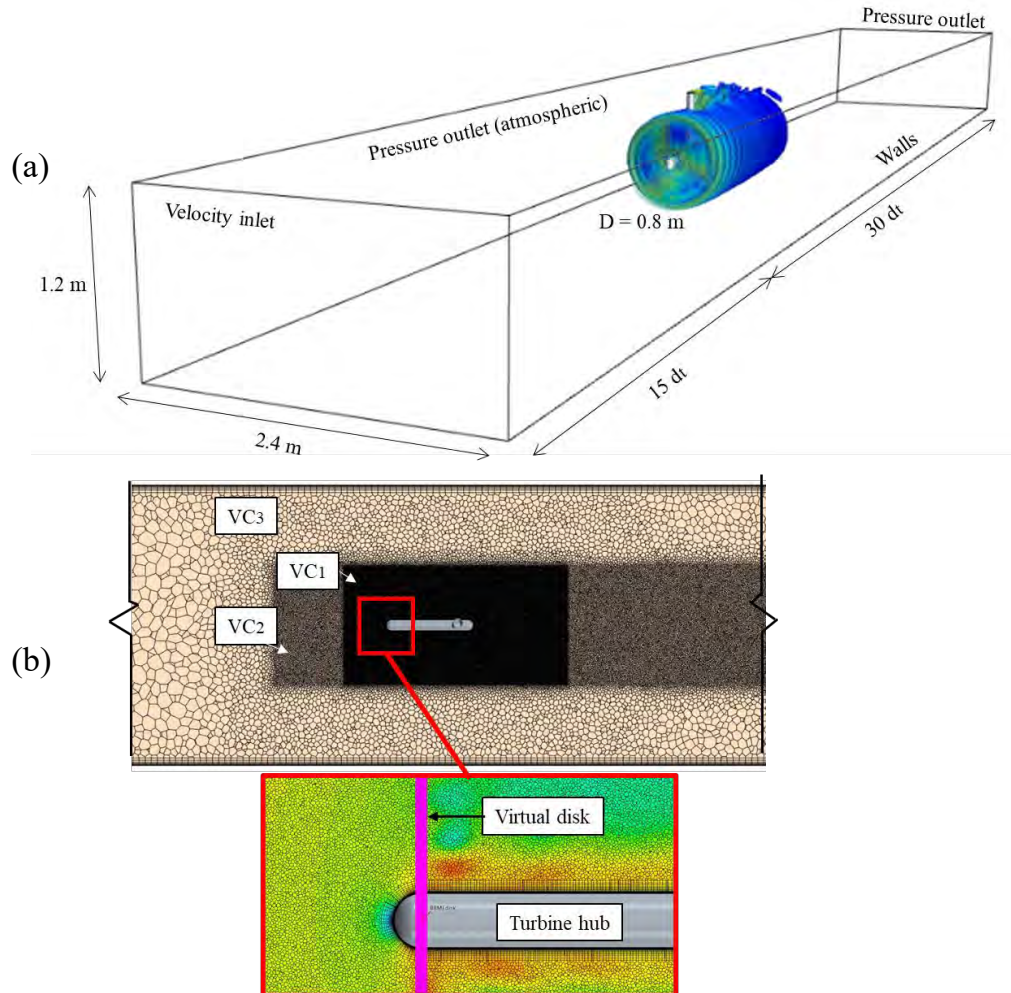
Figure 3-33: BBMC turbine model (a) Domain and (b) mesh details and volumetric controls (VC)

A comparison of the performance metrics (C_p) to experimental measurements (Bahaj *et al.*, 2005) is provided in Figure 3-34. In CFD the λ was varied through altering the rotation rates. At lower λ's the model showed lower performance than was found experimentally. However, the scatter in experimental measurements also indicates variance and unpredictability in experimental measurements. At the optimal λ of 4.8 the performance metric showed good correlation also indicating this as the point of highest power output. The lower thrust and wake disruption are seen in Figure 3-34a when compared to the previous models, this result is expected due to the long thin nature of the blades.
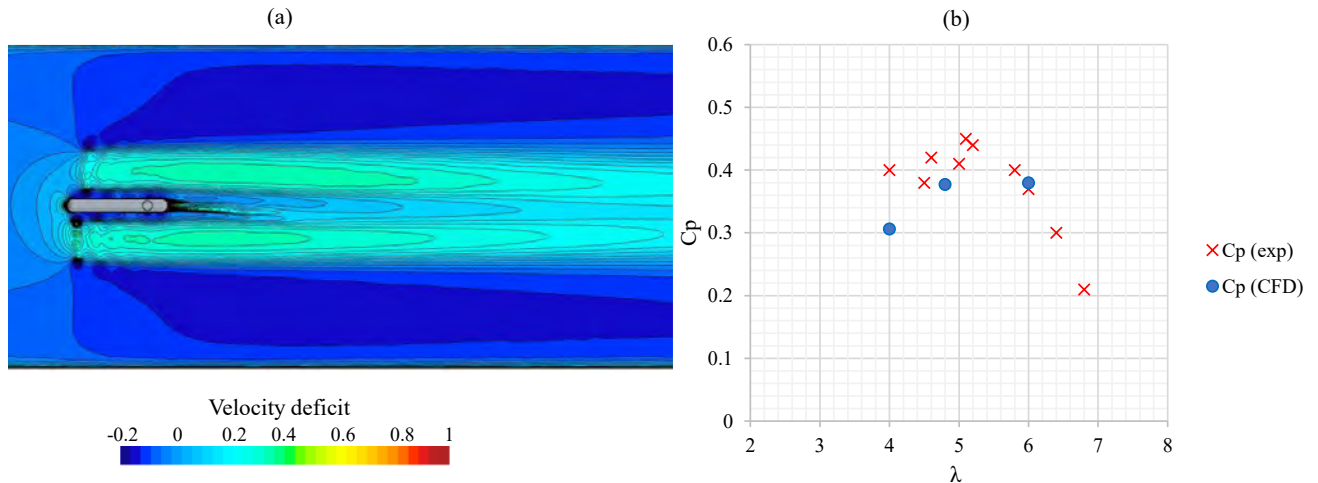
Figure 3-34: Three bladed BBMC turbine CFD model (a) velocity deficit contour and (b) performance metric comparison

All models were found to model the turbine performance well indicating the input variables of the BEM disk used to model the rotor were adequate for the replication of experimental conditions. This also further validated the modelling approach.

3.7 Summary and conclusions

HAHT deployment in inland systems have typical operating conditions (flow conditions as discussed in section 2.2), due to the nature of computational models, full scale modelling is possible, avoiding discrepancies in scaling laws and disregard of possible effects from scaling. Many laboratory scaled models of tidal turbine applications fall within the typical conditions of full-scale inland HAHT schemes (found in rivers and canals). These test cases were used for model validation in this section.

The primary flow conditions found to be most common to inland HAHT conditions and thus included in the verified models are shown in Table 3-3. The computational models were kept within these constraints.

Table 3-3: Range of inland flow conditions for HAHT application validated by experimental results.

Variable	Range of values considered in the study	
	Min value	Max value
Flow velocity (U_∞)	0.8 m/s	3 m/s
Turbulence intensity (TI)	5%	20%
Froude number (Fr)	0.1	0.6
Channel flow Reynolds number ($Re_{channel}$)	300 000	900 000
Radius based Reynolds number (Re_D)	140 000	680 000
Blockage ratio (β)	5%	25%
Turbine diameter (D)	0.5 m	1 m

For computational models a verified mesh is imperative for correct solution over all parameters, the following rules for correct grid refinement were found through a GCI process.

Details on the grid studies for the models can be seen in Appendix A. It should be noted that the following summarises only the parameters considered:

a. For performance measurements a surrounding rotor mesh of 0.8 % of the turbine diameter is found to correctly capture performance. This is true for tip speed ratios up to 5.1, higher values could possibly require smaller grid refinements.

b. For proper formation of the near wake a near wake mesh size of 1.5 % of the turbine diameter is necessary, however up to 2.5 % of the diameter was found to provide 5 % accuracy of wake dissipation up to 6 d_t downstream. After 10 d_t the dissipation rate is predicted within 1% accuracy for the courser mesh with the near wake effects not being as prevalent.

c. To ensure correct incorporation of ambient turbulence (especially for higher TI values) the flow field and far wake should be a maximum of 1.3 % of the turbine diameter (as found for the IFREMER 15 % TI case).

The CFD model study highlights the importance of a rigorous validation process and using tested computational methods when analysing the effects of HK turbines on wake generation and flow recovery. The following points summarise the key findings:

a. The shortcomings of the each employed modelling technique should be understood and carefully considered. Often too much confidence is placed on results from simplified techniques that have not been properly validated.

b. Simplified techniques may be used where the intention of the model is a specific part/scale where uniformity laws are focused on only relevant areas to decrease the required computational resources. Here, the consideration of scales of modelling and ensuring proper validation of the analysis region is important.

c. Correct description of the boundary conditions as well as quantifying the sensitivity of such boundary conditions are crucial for CFD models. In this work the free-surface and blockage effects as well as upstream development of wall boundary layers are of importance. The complex inlet condition (velocity and turbulent distribution) should be carefully modelled. This is even more important for inland HK device application where spatial constraints give rise to many design limitations.

d. The correct selection and application of turbulence models is important. Research on the applicability of turbulence models within the HK flow environment has increased in recent years, many of which are summarised in Chapter 2. The importance of understanding the applicability and limitations of each model prior to application remains critical, especially as commercial modelling software becomes an increasingly common tool for feasibility studies and design. A carefully researched and prescribed method should be used in such cases.

e. Rotor modelling techniques in CFD applications should be selected together with turbulence models and based on the analysis region. FRG modelling performs well for performance tests but has shown to have shortcomings in wake dissipation accuracy when coupled with RANS models. Simplified disk techniques should only be used when well-defined input parameters (lift and drag coefficients etc.) are available.

A collective review of literature and comparison of approaches together with proper model validation and verification ensures an evolution of techniques and improved application of modelling software.

4. PART 2: HAHT SEMI-EMPIRICAL WAKE MODEL DEVELOPMENT

4.1 Introduction

This chapter describes the development of a semi-empirical analytical wake model for simple prediction of the wake dissipation behind a HAHT using minimal input parameters. The primary purpose is to provide insight into the wake strength and propagation which impact array planning, and placement of turbines in inland systems. Metrics governing wake behaviour are identified and investigated to ensure all important driving factors are included in the model.

The result is a model accounting for the effects of blockage and turbulence in combination, which has previously not been investigated or developed. In addition, the model is tested over a range of turbine geometries and is therefore not limited to one specific design but applicable over a range of typical geometries.

4.2 Methodology

The following methodology is followed in this chapter:
1. The validated CFD models (Chapter 3) were used to test possible metrics that, when varied, cause changes in the wake behaviour:
    a. The metrics found to affect wake formation and dissipation in literature were investigated to determine the extremity of their influence on the wake.
    b. Additional parameters (not found in literature) thought to have an effect were tested for their effect on the wake.
2. A simplified analytical wake model was developed through the following procedure:
    a. A conservation of momentum and energy-based formulation for determination of the point of minimum velocity in the wake was developed, tested, and calibrated to experimental results (Also based on theoretical models found in literature).
    b. The point of occurrence of the minimum velocity was investigated and a strategy for incorporation of this value determined.
    c. Empirical relationships for the dissipation rate of the wake past the point of minimum velocity was developed through regression analysis. This accounts for wake results over a variety of turbines and operational conditions.
    d. Model limitations and considerations were investigated and listed.
    e. Simplified nomographs of the typical wake lengths for turbines under certain operational conditions were developed to allow quick reference to expected wake behaviour.
3. A final simplified semi-empirical HAHT wake model for inland flow conditions is prescribed.

4.3 Semi-empirical wake model development

The solution objective of the wake model is to determine the wake recovery over a diametrically proportional distance downstream of the turbine blades ($x/D = d_t$) averaged over an area equivalent to the swept area of the blades (A_D) as shown in Figure 4-1. The average velocity over the A_D downstream of the turbine is selected as the primary parameter of interest

of the model due to its influence on turbine power output. The asymmetric nature of the wake is shown in Figure 4-1 and the averaged value over the area is shown, projected over the swept area. This also allows better correlation to the theoretical principles of the actuator disk (AD) theory which also uses the average velocity over the disk (swept area). The differential between the minimum velocity (at a point) over the A_D and the average velocity over A_D reduces with d_t.

(a)   (b)
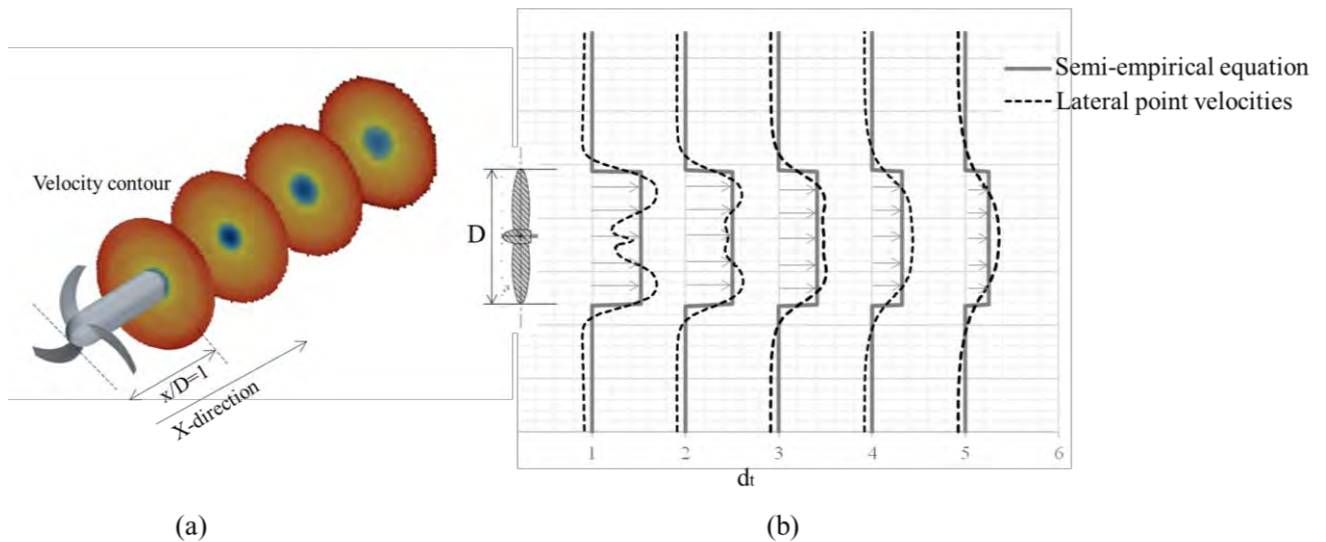
Figure 4-1: Wake model diagram (a) velocity map over swept area (b) averaged wake deficit values vs true lateral wake measurements.

A HAHT wake is extremely complex. Hence, it is not straightforward to derive a simple wake dissipation equation solely based on hydrodynamic laws and derivations. Rather, a semi-empirical approach is adopted, which is an approach most often used in literature for similar studies (Lam and Chen, 2014; Lo Brutto *et al.*, 2016; Pyakurel, Tian, *et al.*, 2017). Here, an experimental dataset of wake formations at various operational conditions is utilised. The analysis focuses on the independent examination of wake defining parameters, which are considered as metrics of interest. Then, a set of equations is derived to enable a reliable estimation of the dissipation behaviour of wakes in inland flow.

To allow simple application of the wake model with minimal input parameters, the wake is characterised and grouped based on three properties as seen in Figure 4-2:
1. The minimum velocity point (averaged over the turbine swept area) V_{OD}.
2. The point at which this low velocity zone occurs (X_{min}).
3. The dissipation rate after V_{OD}.
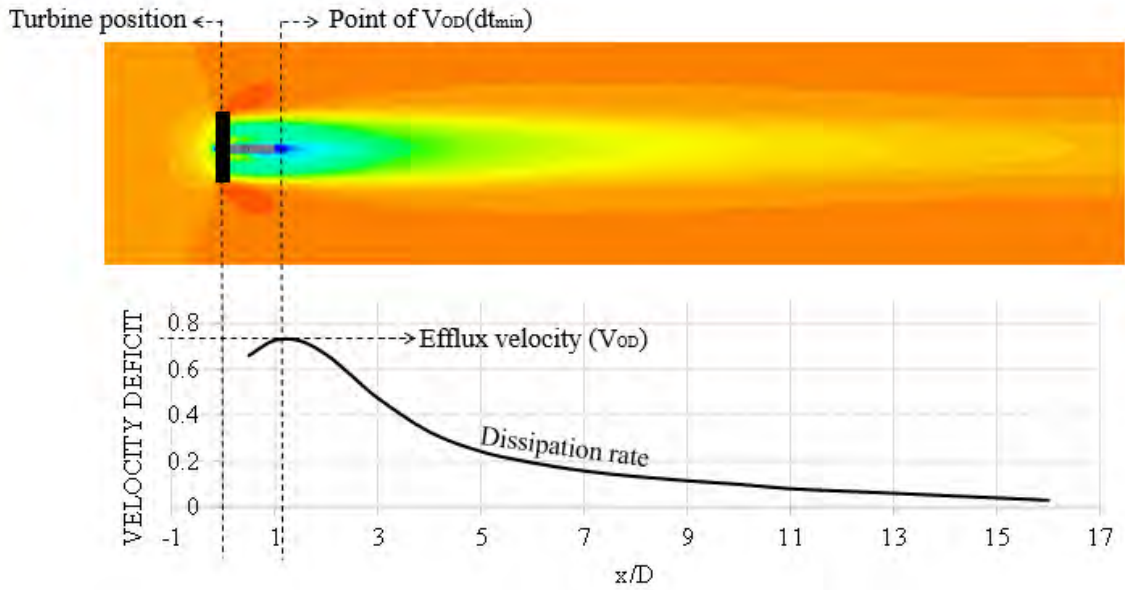
Figure 4-2: Wake model parameters

The preceding chapters describe the determination of these three properties through analysis of wake behaviour of various turbine geometries analysed at various operational conditions.

4.4 Metrics of consideration

As mentioned in section 2.4 multiple factors around the turbine operating conditions and environmental flow field affect the wake formation and dissipation. The extent of some of these effects have previously been quantified, however most still required clarifications. Factors which were thought to affect wake behaviour were varied over the CFD test cases to see which most significantly affect wake formation and should therefore be considered in the wake model.

The following section summarises the investigated properties (referred to as wake metrics) and aims to indicate which result in significant changes in the wake and should therefore be included in the wake model.

4.4.1 Turbine operating point

The importance of ascertaining the operational tip speed ratio (λ) and thrust coefficient (C_T) for accurate wake determination was emphasised in literature (Ma *et al.*, 2018; Wang *et al.*, 2018). The formation of the spiral vortex structure downstream of a HAHT differs over the λ's as shown in Figure 4-3. Although the difference in wake formation is drastic over the λ's shown in Figure 4-3 it is favourable to design a turbine to operate most efficiently (highest C_p, described in section 2.2.2). This typically results in the similar conditions to the range seen in Figure 4-3 (b), (c) and (d). The presence of distinct and tightly formed vortical structures, which are not merged into a single structure, is a prominent characteristic. Within this operational range of acceptable power outputs, a variation of near wake values is observed and indicated in Figure 4-4.

Typically, at higher λ's, there is a noticeable frequency variation in the vortical structures within the wake. This frequency change consequently leads to a more pronounced initial wake velocity deficit. A parabolic velocity distribution is observed over the swept area and the high deficit in the centreline of the wake. At λ's at or below the optimum C_p (Figure 4-4, $\lambda < 5.1$) a symmetric gaussian velocity distribution is prevalent over the swept area, also resulting in loose vortical structures breaking up faster in the wake.
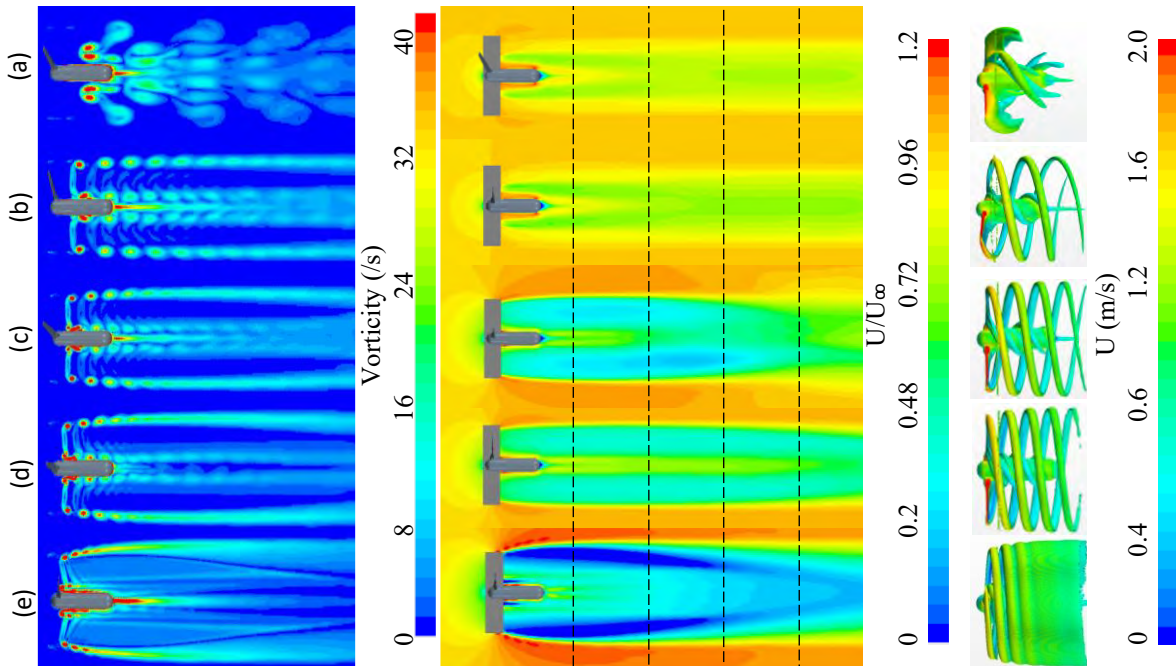
Figure 4-3: Vorticity, mean normalised velocity and vortex profiles of a single 2-bladed NACA 4415 HAHT with a λ of (a) 1.5 (b) 4.2 (c) 5.1 (d) 6 and (e) 9.1.
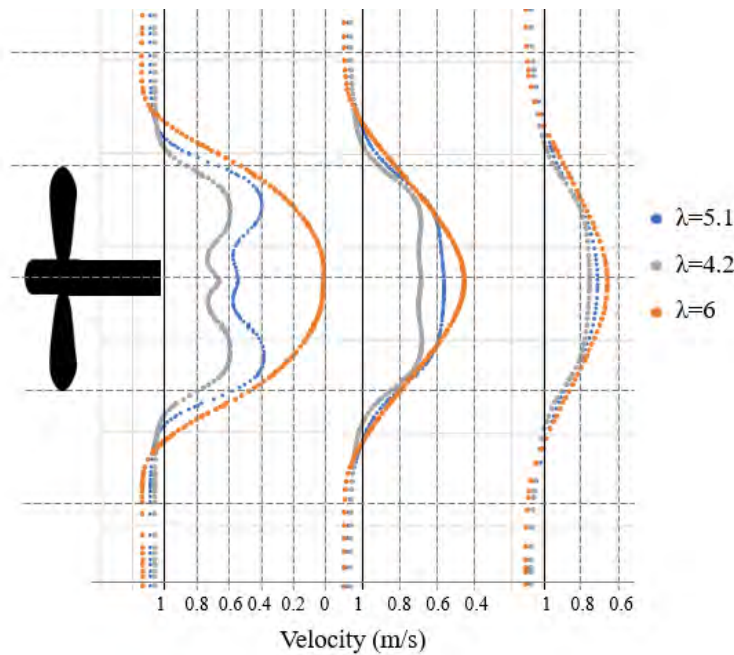
Figure 4-4: Velocity distribution of a single 2-bladed NACA 4415 HAHT wake over a range of λ (optimal λ = 5.1)

HAHT units are designed for specific operational conditions best suited for the turbine, and usually retrofitted to a site. Although in some cases the applied resistance from the generator (torque) may be altered to suit the operational conditions, the turbine is generally provided with a set control system and pre-determined power curve (Niebuhr, van Dijk and Bhagwan, 2019). The turbine may operate at slightly higher or lower λ's than the optimal conditions but should not operate too far from optimal conditions. Due to flow separation, self-starting abilities of typical HAHT geometries the λ operating range is typically limited to between 3 and 6.

Turbine thrust, and the subsequent thrust coefficient, was found to be a useful metric to measure the overall initial disturbance in the flow field. As mentioned, the optimum design, or selected turbine, may depend on supplier preference or availability. However, as the number of blades increases, the optimum λ decreases, which is expected as the as the total swept area of water in contact with the blades increases. This is also seen when comparing the C_p curves of a 2, 3 and 4-bladed turbine shown in Figure 4-5.
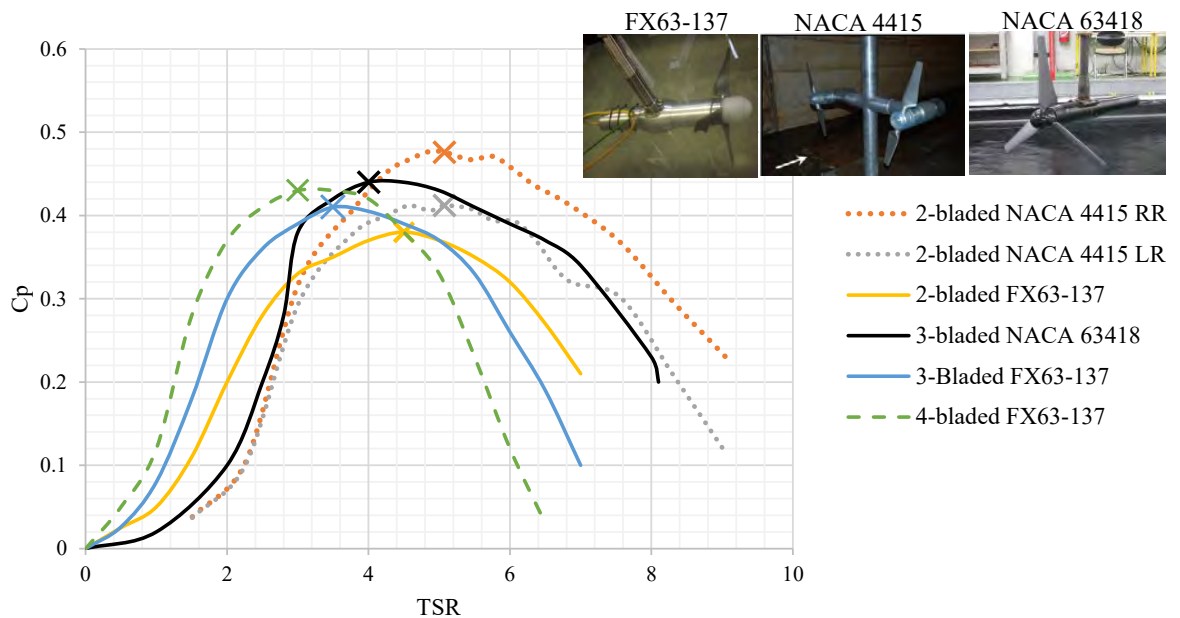
Figure 4-5: Turbine performance comparison between the measured experimental results of the HAHT with NACA4415 (Hill and Neary, 2014), NACA 63418 (Mycek *et al.*, 2014) and FX63-137 (Morris, 2014) blade profiles.

The optimum λ is typically consistent over a range of inlet conditions (changes are only prevalent at large changes in inflow velocity). This can also be observed through the 2-bladed NACA 4415 HAHT curves, where the left rotor (LR) and right rotor (RR) performed differently, however the λ for optimal performance is still consistent. A similar trend was observed throughout literature.

4.4.2 Blockage ratio effect

As found in literature (detailed in subsection 2.4.3), blockage ratio (β) has proven to significantly alter turbine performance at ratios exceeding 5 – 10 % (Kolekar and Banerjee,

2015). The β is calculated as $\beta = (A_D + A_S)/A_C$ where A_S is the projected area of the support structure and A_C the projected area of the channel cross section perpendicular to the flow direction.

During initial testing the blockage ratio is found to strongly affect the minimum velocity in the wake (V_{OD}) and thus the subsequent dissipation rate as shown in Figure 4-6. The power output results also indicate a significantly higher power output from higher blockage ratios, which also aligns with literature findings (Ross and Polagye, 2020). With the case shown in Figure 4-6, a $C_P = 0.15$ is obtained in the $\beta = 7\%$ case, compared to $C_P = 0.26$ in the $\beta = 16\%$ case.
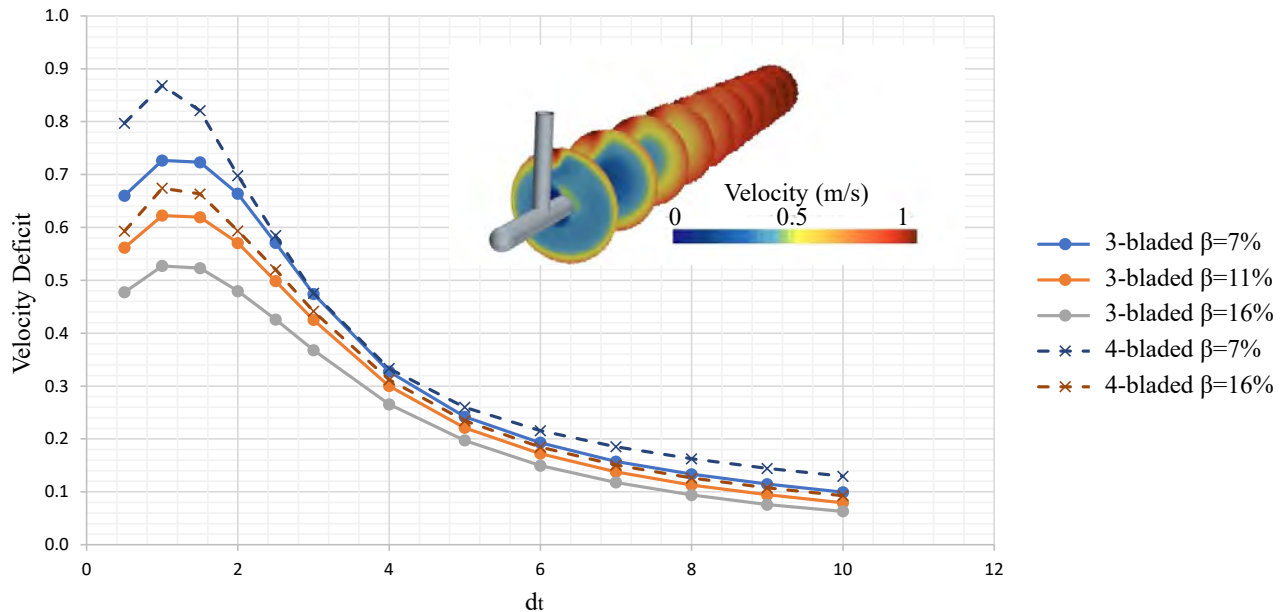
Figure 4-6: Effect of blockage ratio on the velocity deficit of 3- and 4-bladed FX63-137 turbines

The effect of blockage ratio seems to lower the dissipation rate, but does not alter the dissipation rate relative to the minimum velocity point (V_{OD}), this can be observed through the normalised velocity deficit (V_x/V_{OD}) shown in Figure 4-7. Therefore, it is assumed that β affects V_{OD} and due to this the dissipation behaviour is altered.

Only at extremely high blockage ratios ($\beta > 20\%$) the wake dissipation rate is accelerated by the blockage effect and contact with the channel wall boundary layers. Although at lower β the effect of a higher bypass flow slightly increases wake dissipation, the effect is small. For analysis of high blockage ratios, multiphase analysis and modelling of the air-water interface is necessary (as shown in Part 1).
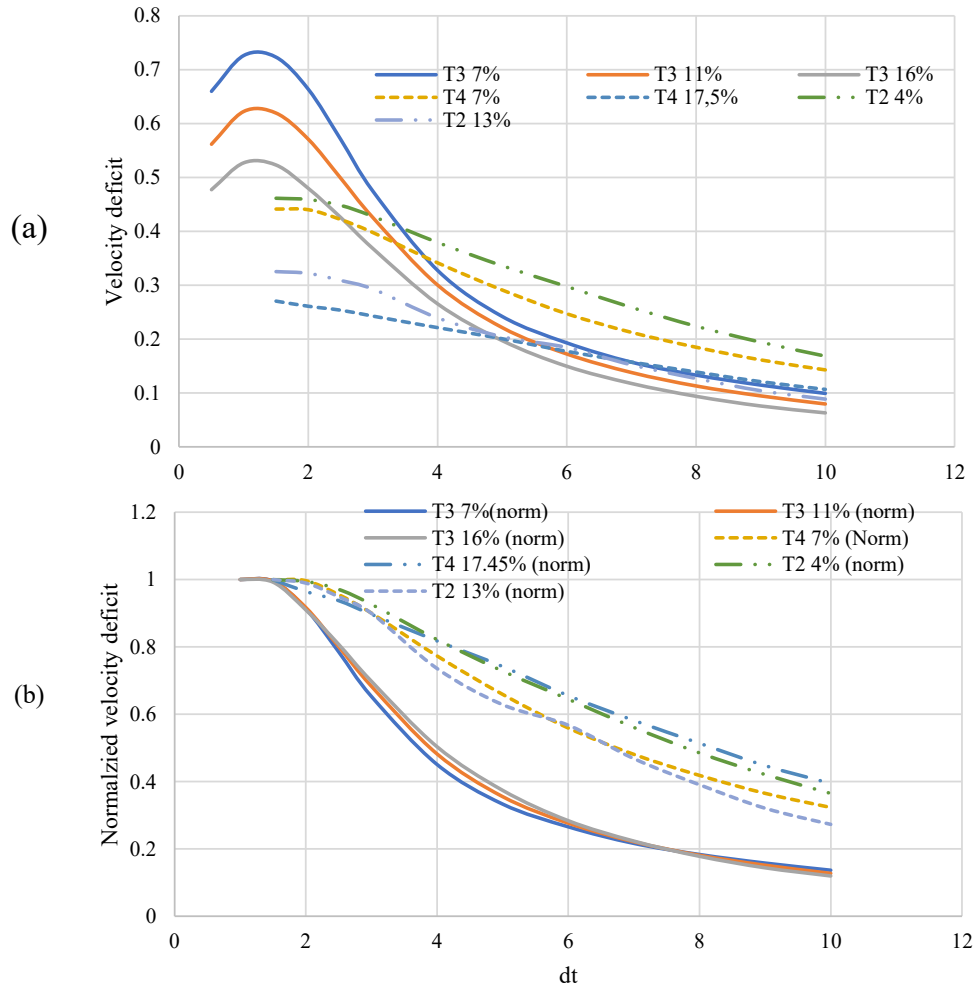
Figure 4-7: Effect of blockage ratio on dissipation rate.

The comparison of a 3-bladed turbine in a multiphase BEM-CFD analysis in a β of 23 % vs β of 5 % flow field can be seen in Figure 4-8. The effects of the free surface (at the top of Figure 4-8 c & d) as well as wall boundaries (at the bottom of Figure 4-8 c & d) are prevalent here and affect performance due to the wall boundary layer confinement effect. The free surface plays a larger role in the presence of a support structure as was shown by El Fajri *et al.* (2020) and described in Chapter 2.4.3. The blockage in Figure 4-8 resulted in a normalised velocity deficit differential of around 20 %, compared to almost no differential seen in Figure 4-7. The gives an indication of more extreme wake dissipation rate at $\beta \gg 20$ %. However, these high β's are typically avoided due to backwater effects or clearance depth requirements.
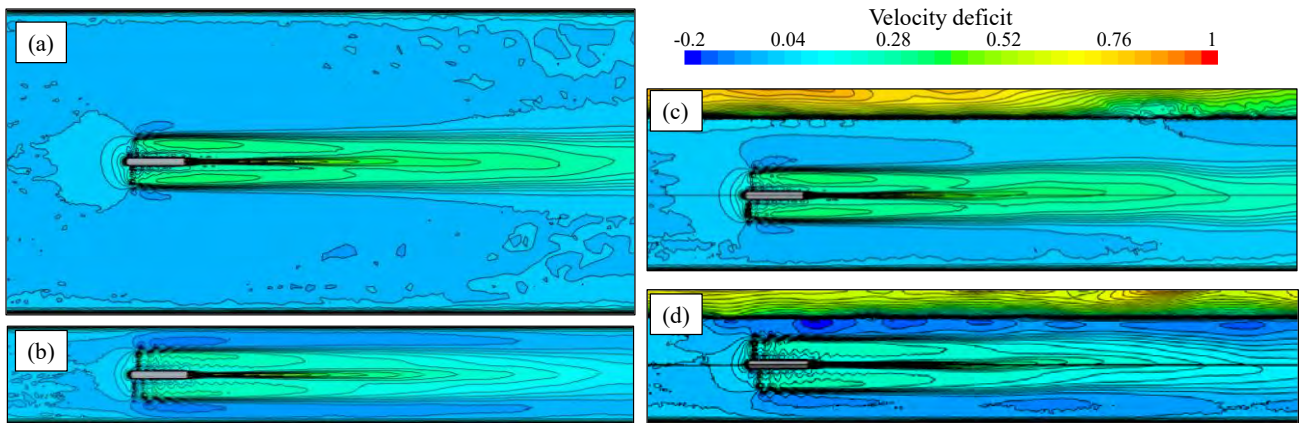
Figure 4-8: Velocity deficit distribution surrounding a 3-bladed HAHT for a β = 5% (a) horizontal and (c) vertical profiles; a β = 23% (b) horizontal and (d) vertical profiles

The analysis included channel aspect ratios (CA = W/H with W = Channel width and H = channel height) of CA = 0.5 to CA = 1 with most analysis in the range of CH = 0.6 – 0.7. Only smaller differences were attributed to aspect ratio variations, and therefore assumed negligible in this case. Future studies on a larger variation of aspect ratios would prove beneficial to validate this result. Further conclusions on aspect ratios were limited due to the scope limitation of available laboratory test results.

4.4.3 Effect of turbulence

As mentioned in section 2.4, higher turbulence intensity (TI) in a channel resulted in accelerated wake dissipation. The overall V_{OD} is decreased as formation of the strong vortex structure is prevented and the position of the highest V_{OD} (X_{min}) is decreased (position of X_{min} is closer to the turbine).

The measure of turbulence in a channel or river section is usually indicated by streamwise TI. Transverse and vertical intensities typically vary in different ratios (Milne *et al.*, 2013), with streamwise turbulence being magnitudes greater. Turbulence intensities in a smooth river or canal section is usually between 5 – 20 %. Although Li *et al*. (2010) reported turbulence intensities in the East River, New York in shallow water of 25 – 30 % (where U_∞= 2 m/s).

Neary *et al.*, (2013) investigated the longitudinal turbulence intensity in rivers, canals and laboratory flumes to understand the TI's that HK turbines may be exposed to. The study also suggested a power law which may be used for first order approximations for TI profiles in rivers. Determining TI's in relevant installation sections is not only important for wake development, but also for structural design calculations (or turbine life) as well as energy production of the HK device.

The primary behaviour observed from higher TI's in the flow is a reduction of X_{min} where the occurrence of V_{OD} moves closer to the turbine due to accelerated wake formation and dissipation as seen in Figure 4-9. The wake model is adapted for values typical to inland water reticulation systems which range from 5 % to 20 %. Although higher TI's may be found, this usually results in unfavourable installation conditions and is therefore not included in the study.

Although many results on the effect of TI on wake formation are available (summarised in subsection 2.4.1), few far field analyses have been conducted. CFD models in this study were modelled at various TI values, to ensure effects are captured and to develop a usable dataset for the semi-empirical wake model development,
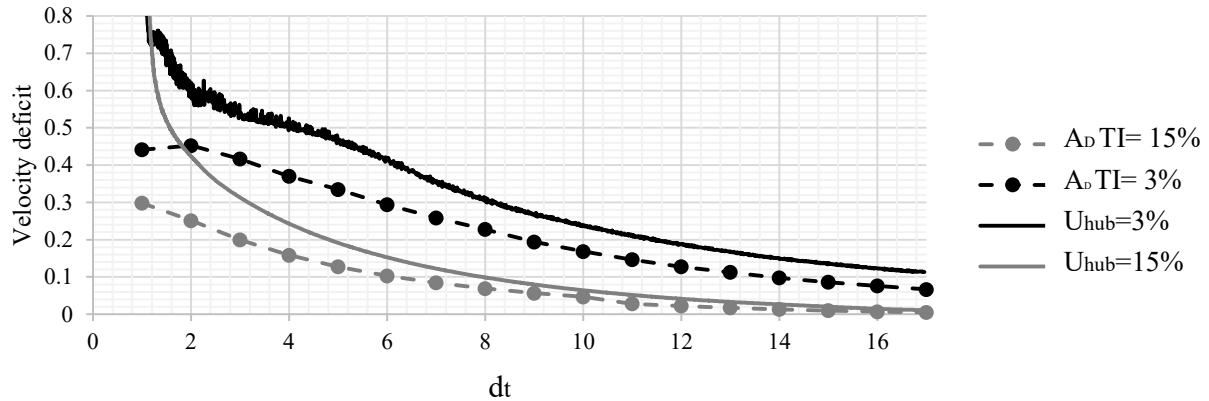
Figure 4-9: 3-bladed NACA63418 turbine results showing hub height velocity measurements vs. averaged velocity over the turbine swept area

4.4.4 Consideration of grids and retaining structures and lateral turbines

Turbine placement usually requires significant bracing, consideration of debris or debris removal (grid) as well as utilizing a greater swept area through lateral turbine placement. Although the wake model is not developed to include specific installation conditions, some effects of retaining structures and lateral turbines were analysed through the RM1 test case to provide some insight into these effects.

Previous studies have indicated wake effects of a retaining structure are not significant in the far wake (Lam and Chen, 2014). The center stanchion effect present in the RM1 validation case can be seen in Figure 4-10. Despite the existence of various designs for retaining structures, and potential variations that could affect the results, the RM1 stanchion stands out due to its large size and substantial reduction in flow area. Consequently, it is presumed that significant wake effects resulting from such a structure would be observed in this particular case study.
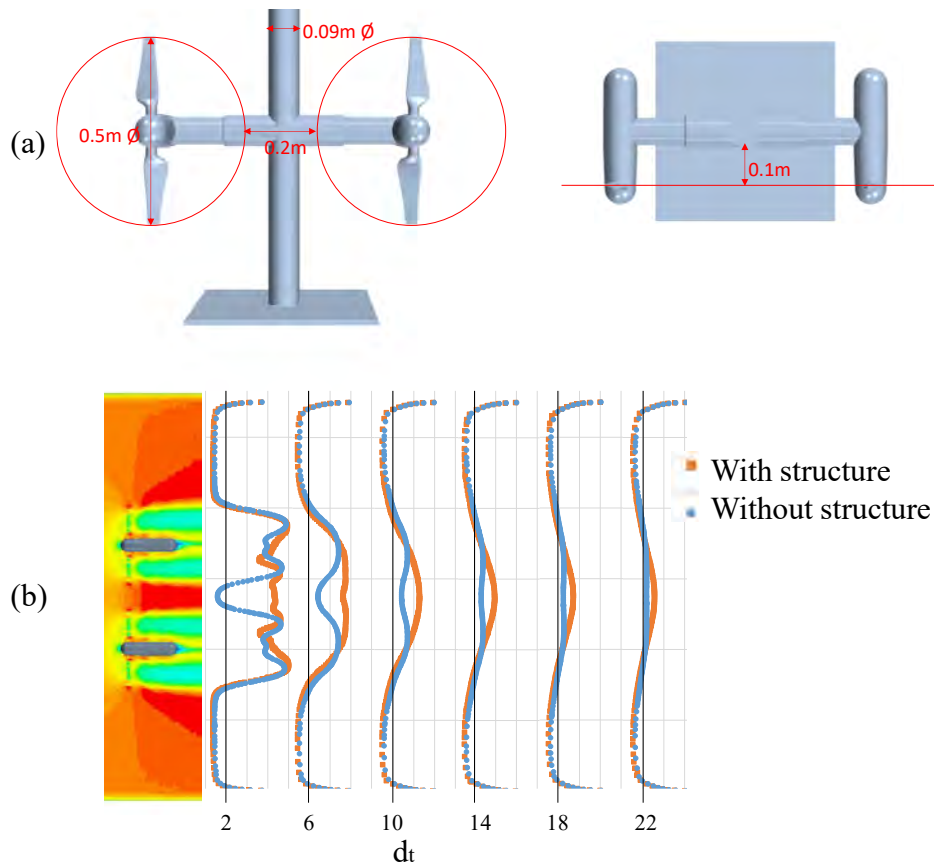
Figure 4-10: Wake velocity deficit results of the RM1 geometry with and without the stanchion structure.

In the test case, the stanchion and cross-bracing were removed, leaving only the turbine generator and blades intact. The findings revealed that there was no substantial impact observed within the wake recovery behind each turbine. However, the presence of the additional center blockage resulted in the most severe blockage, causing a deficit that propagated into the far wake region and generated its own wake Therefore, although no significant effect (in terms of faster or slower recovery within the rotor wake) is seen, the positioning of the stanchion (if such a structure is used) should be carefully selected not to interfere with possible downstream turbines placed in the stanchion wake.

When comparing the RM1 duo-turbine case (two turbines and retaining structure) with a single turbine within the same flow area (large enough to ensure insignificant blockage ratio effects), no significant difference is noted within the wake dissipation rate (Figure 4-11). This could indicate that the wake inter-effect between two turbines when placed more than 1.4 dt (between hub centrelines) apart could be insignificant.
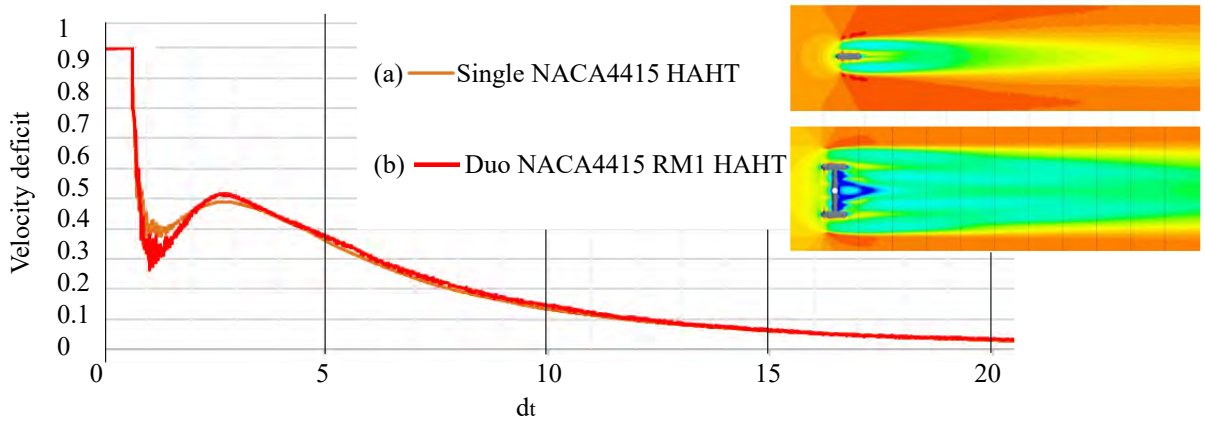
Figure 4-11: Hub height centreline measurements of the wake dissipation of duo-rotor turbine with retaining structure wake compared to a single turbine

4.5 Integration of considered metrics into the developed wake model

The primary factors governing and significantly altering the wake formation and dissipation were investigated through CFD studies as well as literature findings. These primary factors were found to be:

- The thrust experience in the turbine, which accounts for the operational λ and blade profile;
- The blockage ratio (β), which affects the power output and therefore also the maximum V_{OD} in the wake as well as dissipation rate;
- And lastly the turbulence intensity (TI) in the flow field, which significantly accelerates the wake recovery at higher TI values.

These metrics were included in each wake model property as shown in Table 4-1.

Table 4-1: Model considerations

Property	Variable	Metrics of consideration	Section
Minimum velocity point (over A)	V_{OD}	C_T, β	4.6
Point at which minimum velocity occurs	X_{min}	V_{OD}, TI	4.7
Dissipation rate (at points d_t downstream)	V_x ($d_t = x/D$)	V_{OD}, TI, β	4.8

In installation cases involving significant retaining structures, the placement of grids upstream, or installations situated near the free surface, it is essential to consider the potential alterations in the wake behaviour. However, due to the wide variability in installation possibilities and the observed effects primarily occurring in the near wake, these factors were not incorporated into the scope of this study.

4.6 Determination of minimum velocity in the wake

The minimum velocity over the turbine swept area projected downstream (V_{OD}) is primarily a function of turbine thrust. However, additional operational conditions affect the extent of V_{OD}

(As proven in Section 4.4). This section explains the derivation of a V_{OD} equation and empirical inclusion of the metrics of consideration mentioned in Table 4-1.

A simple approximation for the lowest velocity downstream of a HAHT can be found through the actuator disk (AD) theory. Figure 4-12 shows the application of the axial momentum theory using an AD principle, often used in wind turbine analysis (Eggleston and Stoddard, 1987). Applying the Bernoulli energy equation over this disk allows approximation of the minimum velocity downstream of the disk.
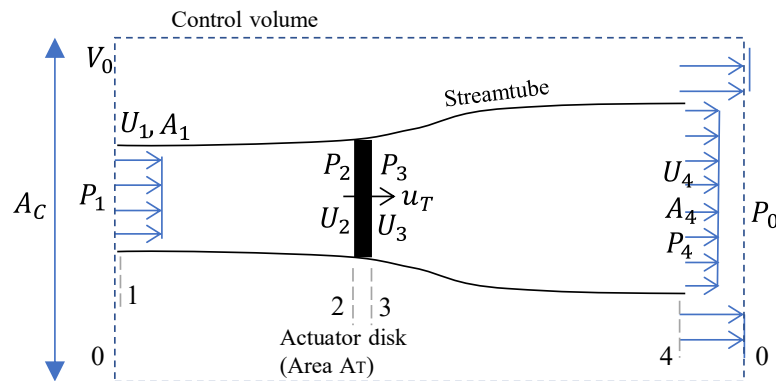
Figure 4-12: Actuator disk model

Assuming a very flat slope (thus ignoring the reference to a datum height) the energy upstream of the disk can be described as follows:

$$\frac{P_1}{\rho g} + \frac{U_1{}^2}{2g} = \frac{P_2}{\rho g} + \frac{U_2{}^2}{2g} \tag{40}$$

The same relationship applies downstream:

$$\frac{P_3}{\rho g} + \frac{U_3{}^2}{2g} = \frac{P_4}{\rho g} + \frac{U_4{}^2}{2g} \tag{41}$$

where P_1, P_2, P_3 and P_4 are the pressures at points 1, 2, 3 and 4 (Figure 4-12) and U_1, U_2, U_3 and U_4 the velocities (m/s), ρ the density of water and g the gravitational acceleration.

As continuity must hold within the streamtube the following holds:

$$U_1 A_1 = u_T A_T = U_4 A_4 \tag{42}$$

Continuity holds over the control volume (upstream and downstream) and a net flow exists:

$$\Delta Q = V_0[(A_c - A_1) - (A_c - A_4)] = V_0(A_4 - A_1) \tag{43}$$

To quantify the change in momentum over the disk the effect of the disk can be simply expressed as a thrust (T) which is essentially the force (F) on the disk. This force can be incorporated as a static pressure drop over the disk to slow the water, similar to the AD approach, (assume no periodicity or pressure variation with time):

$$T = F = A_T(P_2 - P_3) \tag{44}$$

Assuming the far upstream and far downstream pressure (P_1 and P_4) are equal and assuming the velocities directly upstream and downstream of the disks remain the same ($U_2 = U_3$). The Bernoulli energy equation can be combined with the thrust approximation and the following relationship is obtained:

$$T = \frac{1}{2}\rho A(U_1{}^2 - U_4{}^2) \tag{45}$$

From the propeller jet theory it is known that axial thrust is produced through shaft torque by increasing the rearward momentum of the surrounding fluid (Stewart, 1992). This induces a reaction forward force from the fluid on the propeller (used for propulsion). By representing the propeller as an AD consisting of an infinite number of rotating blades and assuming energy is supplied to the system as water passes through the jet. The change of momentum due to the energy supplied results in a net thrust on the fluid. Dimensional analysis of the propeller thrust allows the following relationship:

$$T = C_T \rho n^2 D^4 \tag{46}$$

where n is the propeller rotation rate (rev/s), C_T the propeller thrust co-efficient and D the propeller diameter.

Combining this equation with equation (43) the minimum velocity in the wake (U_4) can be expressed as:

$$U_4 = \sqrt{U_1{}^2 - \frac{2C_T n^2 D^4}{A}} \tag{47}$$

However, this relationship does not hold well for turbines as ship propellers have exponentially higher rotation rates than HK turbines in channel flows, and therefore an alternative definition for the thrust coefficient (equation 48) is used. This approximation is commonly used for the thrust of a wind turbine (Eggleston and Stoddard, 1987) and defined as the non-dimensional ratio of axial force to incoming flow momentum with U_∞ representing the freestream velocity:

$$C_T = \frac{T}{\frac{1}{2}\rho U_\infty{}^2 A_D} \tag{48}$$

By considering U_∞ equal to U_1 (in Figure 4-12) and combining equations (45) and (48) the following relationship for U_4 is obtained, which would refer to the minimum velocity in the wake:

$$U_4 = \sqrt{U_\infty{}^2(1 - C_T)} \tag{49}$$

This minimum velocity in the wake (U_4) is often referred to as the efflux velocity (Lam, Chen and Hashim, 2015). As mentioned, in the current study it was found that the average velocity over the cylindrical area (V_{OD}) is most useful when determining turbine spacing (average velocity over disk area) which is according to the equation derivation equivalent to U_4, being an expression of the average velocity downstream of the disk (over its swept area).

Although this equation is useful in determining the minimum velocity in the wake based on the turbine C_T and flow velocity, it is over simplified and does not include any effects of ambient TI or blockage effects (β) which have been shown to affect the minimum velocity (Section 4.4).

In section **Error! Reference source not found.**, it was found that the turbine thrust is affected by β, which may account for the changes in the maximum V_{OD} observed in the wake (when β is not excessively high). Previous research has focused on correcting for blockage in laboratory tests with higher blockage ratios, which is relevant for tidal energy applications and unconfined installations. These studies are based on Glauert's (1983) concept of performance change effects in wind turbine wind tunnel testing and use blockage correction models that rely on the momentum-balance/AD model. These models typically adjust the thrust coefficient approximation (equation (48)) with a predicted freestream velocity ($U\infty'$) that would result in the same thrust as measured in bounded flow scenarios in unconfined conditions. In principle, these blockage correction principles could be applied to adapt V_{OD} for higher blockage ratios and were therefore investigated.

Most blockage correction methods such as those proposed by Mikkelsen and Sorensen (2002) as well as Barnsley and Wellicome (1990) require prior knowledge of the bypass flow velocity, as well as the velocity through the turbine which are both unknown when following the current model (Barnsley and Wellicome, 1990; Mikkelsen and Sorensen, 2002). The approach proposed by Werle (2010) provides an adapted C_T based on the blockage ratio for wind turbines (Werle, 2010). This approach accounts for the confined flow effect on the thrust coefficient and the same theory holds for water flow.

The application of the wind turbine blockage correction model to the results in this study overestimated the results. This was found to agree with previous testing of the same model on HK turbines (Ross and Polagye, 2020). However, a trend correlation was prevalent and through an empirical adjustment to the model an acceptable correlation to experimental results was observed. The blockage correction formation was thus adjusted and incorporated into the minimum velocity (V_{OD}) equation as follows:

$$V_{OD} = U_\infty \sqrt{1 - \frac{(1 - \Delta\beta)^2}{1 + \Delta\beta} C_T}$$

(50)

where the $\Delta\beta$ is calculated as follows:

$$\Delta\beta = \beta - 0.07$$

(51)

This V_{OD} equation (50) allows calculation through only the turbine thrust, swept area and inflow velocity. This indicates a clear relationship between the thrust coefficient and V_{OD}.

Predictions of seven experimental test cases at low TI's are shown in Figure 4-13 where the distribution between V_{OD} deficit (Vx_{OD}) values calculated through equation (50) and measured from wake results are compared. The results indicate the general trend of higher V_{OD} deficit values for turbines operating at higher thrust coefficients (indicated by the linear trendline) with predictions of Vx_{OD} values with a maximum differential of 5 %.
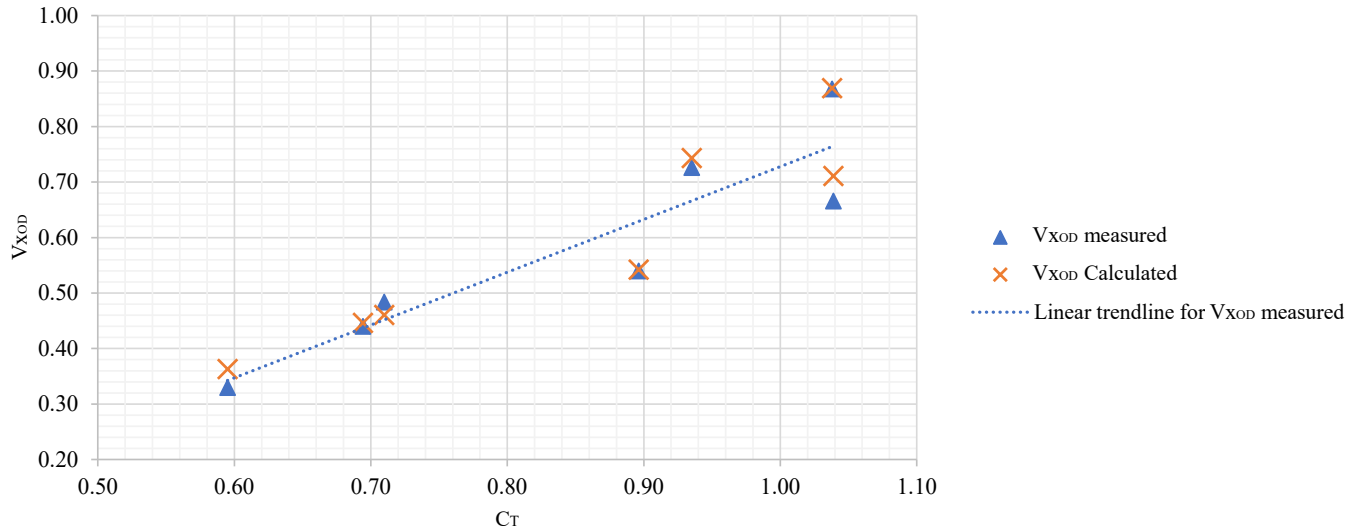
Figure 4-13: Relationship between C$_T$ and V$_{OD}$ for the 7 modelled turbines operating at optimal λ

Slight variations in wake behaviour were observed over a range of turbine solidities, specifically linked to blade numbers (2, 3 or 4 blades). In the past, changes to the efflux velocity were investigated over a range of turbine solidities and λ's. Wang *et al.* (2018) attempted to include an empirical co-efficient based on the propeller theory for the inclusion of operational λ (based on experimental results for a turbine tested as various solidities (Maganga *et al.*, 2010)). The efflux velocity equation used the propeller theory with a similar equation as shown in equation (51), with empirical coefficient *E*:

$$U_0 = \sqrt{U_\infty^2 - (nD\sqrt{EC_T})^2}$$
(52)

$$E = 16.174\lambda^{-1.837}$$
(53)

Using these equations with the available dataset showed a larger difference in V_{OD} than found when applying equation (50) (details shown in Appendix B) . As the developed V_{OD} equation proved to show good correlation to experimental results for low blockage and low onset turbulence values this was used not further adapted. For turbines operating outside of the optimum λ, effects of wake behaviour as shown in section 4.4.1 should be expected.

4.7   Point of minimum velocity in the wake

The downstream section with minimum velocity in the wake depends not only on the *β* and TI, but on the extent of the C_T value. HAHTs with higher C_T's cause a larger disturbance in the flow, resulting in a higher V_{OD}. As seen in Figure 4-14 this larger disturbance results in a faster mixing rate in the near wake due to the larger differential velocity between the wake and bypass flow. Therefore, a general trend in X_{min} is observed (as seen in Figure 4-14)

indicating the movement of X_{min} further downstream for cases with lower V_{OD}'s. This relationship only holds true for low TI values. As the TI increases the X_{min} also moves further upstream (as shown previously in 4.4.3).
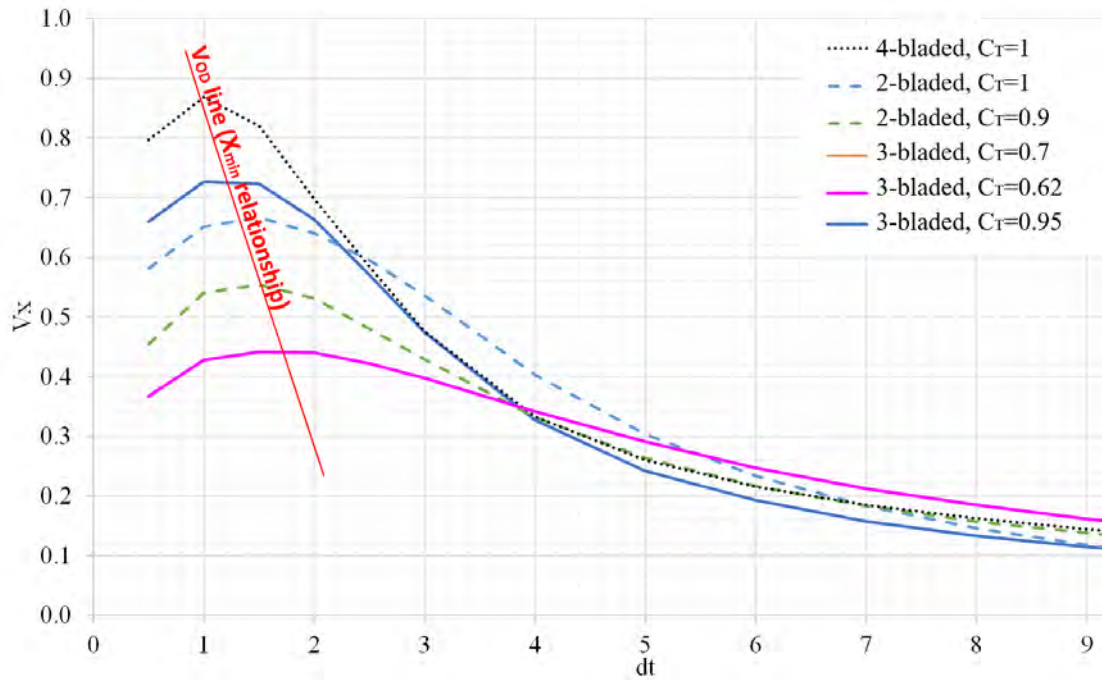
Figure 4-14: X_{min} values for low TI experimental test cases

Previous analyses have concluded with a set point for the efflux velocity, occurring around 1.1 dt downstream (Whale *et al.*, 1996; Lam and Chen, 2014). Berger *et al.* (1981) suggested for a ship propeller the position of maximum velocity (R_{mo}) can be predicted as a function of the radius of the propeller *(R)* and the radius of the propeller hub (R_h):

$$R_{mo} = 0.67(R - R_h) \tag{54}$$

Prosser (1968) proposed 60 % of the blade radius from the hub. Hamill, McGarvey and Hughes (2004) proposed rather 0.7 in place of 0.67 shown in the formula by Berger *et al.* (1981). Through studies completed by Lam, Chen and Hashim (2015) comparing empirical to experimental results for HAHTs, the equation by Berger *et al.* (1981) was found to correlate best and recommended for determination of the point of lowest velocity in the wake of a HAHK device.

In all experiments in the current study the X_{min} occurred between 1.1 and 1.5 d_t downstream. As near wake results are not of primary importance in the current model, the X_{min} point is chosen to be at a maximum of 1.5 d_t. This significantly simplifies the process of wake prediction and allows simpler incorporation of TI through the dissipation rate. However, it should be noted when determining the X_{min} in higher V_{OD} cases the position of X_{min} is generally closer to $d_t = 1$. Where the location of V_{OD} is of importance the equation by Berger *et al.* (1981) should be used.

4.8 Dissipation rate

After the initial near wake formation, where the lowest velocity point (V_{OD}) exists, the wake continues to dissipate a distance downstream. From the experimental wake results (subsection 4.4) it was observed that the dissipation rate after V_{OD} is observed to be governed by the environmental conditions such as ambient TI and β as well as the initial extremity of the disturbance (magnitude of V_{OD}).

Regression analysis is used to incorporate parameters of importance into a usable dissipation equation. In literature, linear relationships between V_{OD}/V_∞ and x/D have previously been determined through an experimental dataset (Lam, Chen and Hashim, 2015; Oppong *et al.*, 2020). Although this approach was tested, it did not result in a satisfactory result. Additionally, large variations in wake behaviour were observed when testing the model by Lam, Chen and Hashim (2015) which is based on a linear approach (also seen in Appendix B). In this study a non-linear regression analysis is used instead.

The dissipation rate is determined as a function of the minimum cylindrically averaged velocity deficit in the near wake (Vx_{OD}). The dissipation rate is calculated from an assumed X_{min} of 1.5 d$_t$ downstream of the hub. The velocity deficit averaged over the turbine swept area, at various distances downstream (V_x) is determined as follows:

$$V_x = Vx_{OD} \times C_a \times e^{-Vx_{OD} \times C_b \times x} \tag{55}$$

Where C_a and C_b are coefficients determined through the non-linear regression analysis of the metrics of consideration (section 4.4), where x is the distance downstream as a function of turbine diameter ($x = d_t$).

The coefficient's were determined as follows:

$$C_a = 1.37 - 0.035 \times TI \tag{56}$$

$$C_b = (1.25 \times \beta^{\frac{1}{8}})(0.0031 \times TI^2 - 0.033TI + 0.3463) \tag{57}$$

where TI is the turbulence intensity, β is the blockage ratio percentage.

The dissipation rate was tested over the following ranges which are typical for installation conditions:
- Turbulence intensities of 5 % to 20 %
- Blockage ratios of 4 % to 18 %.

The maximum differential in velocity deficit in the wake at various distances downstream of the turbine can be seen in Table 4-2 for a variation of TI values and Table 4-3 over a range of β's. Full details of the model testing can be seen in Appendix B.

Table 4-2: Percentage difference at various TI's at a low blockage ratio

Ambient Turbulence intensity (TI%)	Percentage difference at a given distance from the turbine hub (%)									
	2 d_t	4 d_t	6 d_t	8 d_t	10 d_t	12 d_t	14 d_t	16 d_t	18 d_t	20 d_t
4-6 %	1.9	4.3	4.4	3.1	1.9	1.0	0.9	1.7	2.5	0.1
9-11 %	5.9	2.3	1.4	1.2	1.0	0.7	0.4	0.2	0.2	0.1
16-18 %	2.9	0.9	1.1	1.2	1.0	0.7	0.3	0.2	0.1	0.1
Maximum differential in dataset	**8.1**	**9.3**	**8.7**	**5.4**	**2.5**	**1.4**	**1.4**	**1.6**	**2.5**	**0.1**

Table 4-3: Percentage difference at various blockage ratios (measured over a range of TI's)

Blockage ratio β (%)	Percentage difference at a given distance from the turbine hub (%)									
	2 d_t	4 d_t	6 d_t	8 d_t	10 d_t	12 d_t	14 d_t	16 d_t	18 d_t	20 d_t
< 7 %	3.3	2.8	2.6	2.0	1.4	0.8	0.6	0.5	0.6	0.1
13 %	0.5	0.1	0.4	0.9	1.4	0.7	0.5	0.1	0.1	0.1
17 %	4.8	3.0	1.9	1.7	1.6	1.4	1.1	0.7	0.3	0.1
Maximum differential in dataset	**12.6**	**6.0**	**2.5**	**3.1**	**3.1**	**2.8**	**2.5**	**1.9**	**0.6**	**0.1**

The modelled values proved to be within 10 % of the experimental results past 4 d_t downstream, with very few cases showing slightly higher differences in the V_x approximation in the near wake.

4.9 Model testing

The final model is tested over a range of conditions and turbine types. Due to the large computational requirements per CFD model, a combination of operational conditions and turbines were tested to ensure specifically turbine thrust, ambient TI and β in various combinations were included both independently and as a combined effect. All model results and comparisons to experimental conditions can be seen in Appendix B.

As an indication of the model accuracy the root mean squared error (*rmse*) of the experimental velocity deficit ($V_{x,exp}$) and predicted velocity deficit ($V_{x,model}$) at distances downstream relative to the turbine diameter (d_t) were analysed. The *rmse* for each turbine dataset used as well as the overall *rmse* over all datasets can be seen in Figure 4-15.

$$rmse = \sqrt{\frac{\sum_{i=1}^{n}(V_{x,exp} - V_{x,model})^2}{n}}$$

(58)

The predicted wakes of the 3-bladed and 2-bladed turbines shown in Figure 4-15 indicated good correlation to experimental results and trends in wake dissipation. The largest variations

were found in the T3 models, which has extremely high thrust and therefore the initial near wake indicated some variations in behaviour. The comparison of the 4-bladed turbines (T3_4b) resulted in under predictions of the extent of velocity deficits in the near wake. However, a lack of data on 4-bladed turbines prevented further model calibration. All other datasets proved to be within 10 % of experimental values past 4 d_t downstream indicating good prediction of the wake behaviour for typical inland conditions.
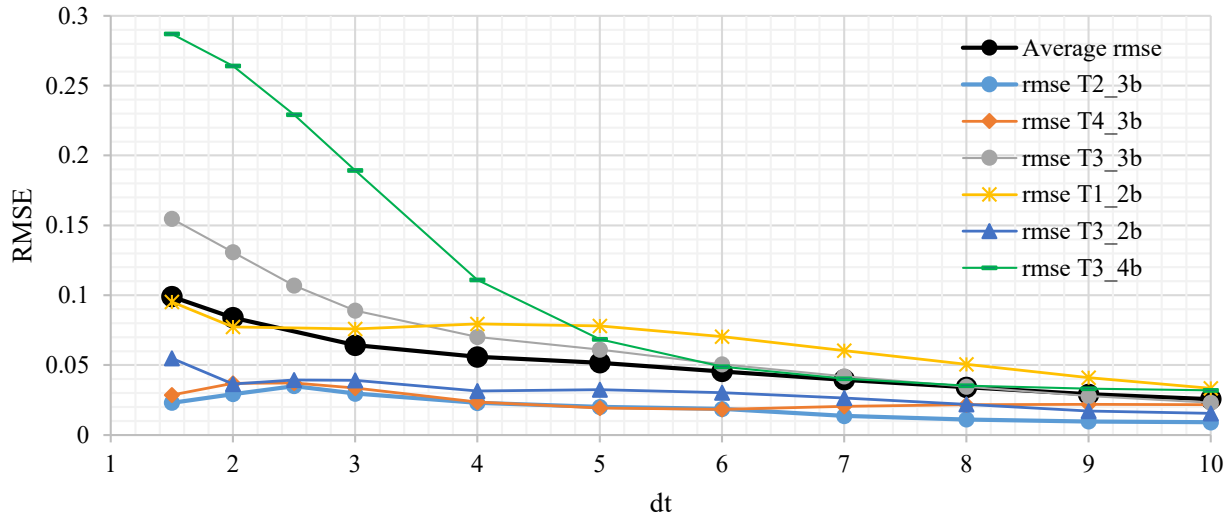
Figure 4-15: Wake model prediction *rmse* of experimental measurements

4.10   Model limitations and considerations

The semi-empirical model was aimed to allow approximation of the wake deficit to within 10 % accuracy. However, several limitations should be considered due to the nature of the model development, simplification of wake metric effect, and use of RANS-CFD for experimental data set generation. Some specific limitations include:

- Wake results from laboratory tests were used for benchmark validation of the CFD models. Few of these laboratory tests have wake results exceeding 10 d_t downstream. Model behaviour after this point is assumed to be correct, but a consideration of possible inaccuracies in the far wake must be considered. However, the assumption is that the inaccuracies would be slower dissipation due to the lack of high turbulence values in the bypass flow in the far wake, and therefore the model is predicted to result in a conservative prediction.

- Additional environmental and operational effects such as drastic differences in turbine geometry (e.g., blade numbers) may alter wake formation. The model was developed in a way that allows further calibration and addition of any further parameters affecting the wake development. The current model is not tested over a wide range of turbine solidities and most turbines tests were 3-bladed (as these are currently most efficient and most produced).

- As the model is developed to allow simple use in the preliminary design or site assessment phases where just minimal turbine details are known, some inaccuracies may result from the oversimplification of the model. This should be considered where exact wake propagation is relevant or wake width is of importance (e.g., for possible scour or sedimentation analysis or where spacing is a limited parameter). More complex and

detailed wake models should be used when more details are available on the specific turbine planned for installation. Especially as wake width is not considered here.

- For array schemes the inter-effect of coinciding wakes was not included. Variations of these effects have been investigated in the past and could be referred to (Nuernberg and Tao, 2018; Gajardo, Escauriaza and Ingram, 2019).

All existing HK wake models do not consider blockage ratio, and only few have included two or three variations of TI's. The current model provides a significant improvement to HAHT analytical wake models. Through including model validation over multiple turbine types and operational conditions it was possible to ascertain the model applicability over a range of results.

4.11   Typical HAHT wake in inland flow

A prediction of wake dissipation rates in canal systems through the developed semi-empirical model can be seen in Figure 4-16 and Figure 4-17. Figure 4-16 indicates specifically the effect of C_T and TI, where Figure 4-17 shows the effect of a variation of TI and β for a turbine operating at optimal λ at a relatively high C_p (high efficiency). The plot shows a variation over TI (typically between 5 – 20 % in canal systems) which can be used as a visual reference guide.
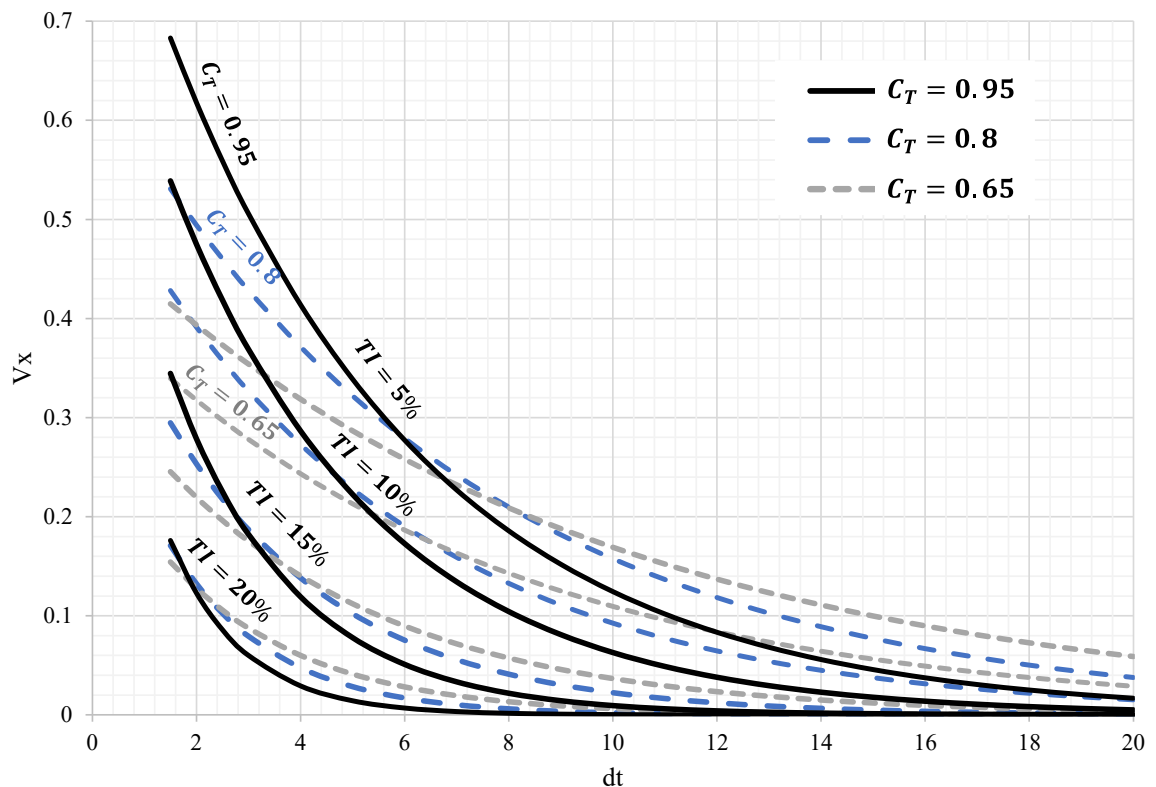
Figure 4-16: Typical wake dissipation for varying C_T and turbulence intensities (TI) for a 3-bladed turbine
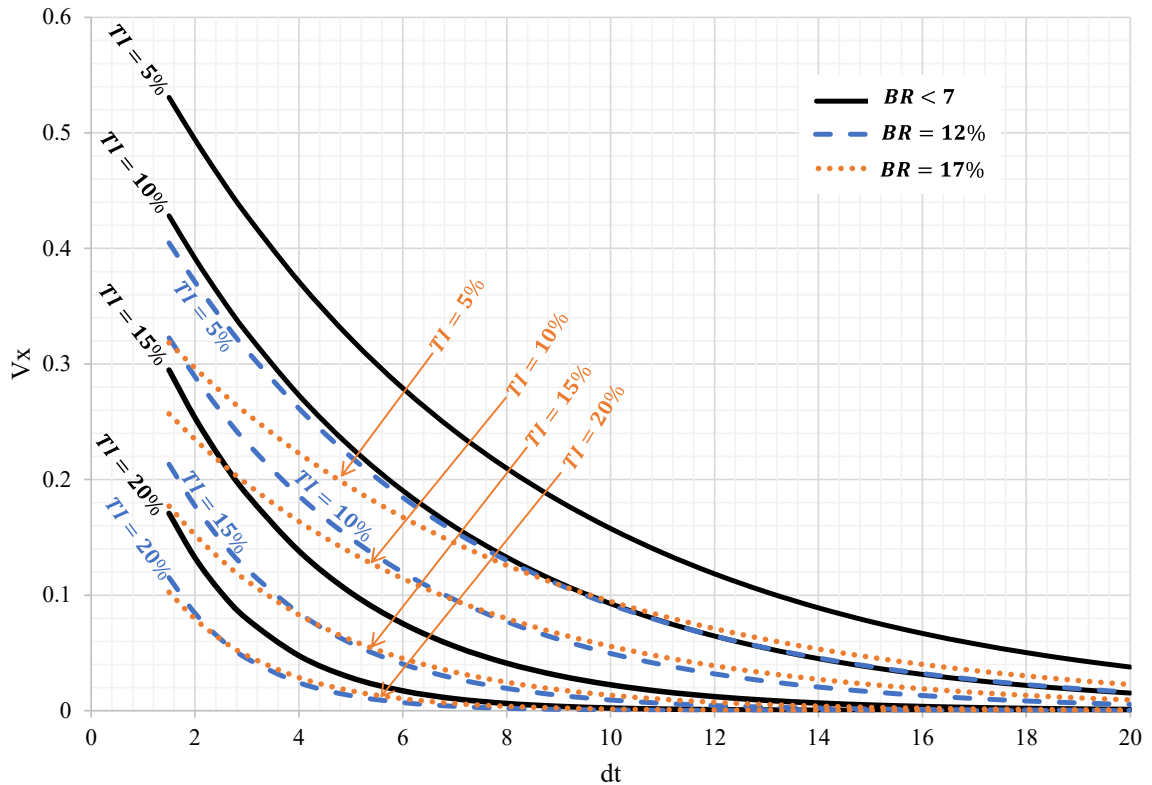
Figure 4-17: Typical wake dissipation for varying Blockage ratios and turbulence intensities (TI) at a typical C_T of 0.8 for a 3-bladed turbine

4.12   Summary and conclusions

A semi-empirical calculation method for the decay of a single HAHT wake is formulated for uniform unbounded flow and adjusted for bounded flow and ambient turbulence conditions. The mean momentum integral relationship proves the momentum deficit in the wake may be determined through the thrust of the turbine. Previous models have concluded this may be exclusively determined through thrust; however, the current experimental results show blockage ratio and TI should also be considered. A semi-empirical relationship for the wake dissipation rate in the near and far wake is determined through typical hydraulic principles in combination with non-linear regression analysis using an experimental dataset obtained from various validated CFD models.

The findings and semi-empirical model allow a description of the wake characteristics and assist in estimating the wake dissipation with minimum input variables. Additionally, this assists in providing an overview of wake changes for important parameters of consideration (referred to as wake change metrics) which are primarily the turbine thrust at the operating point (C_T), the ambient turbulence intensity of the flow and the blockage ratio. The following summarises these primary effects on the wake dissipation:

- Higher C_T's result in a higher efflux velocity and thus higher disturbance in the flow field.
- Higher TI values result in faster wake dissipation and thus also cause the point of minimum velocity to move further upstream in the wake.
- Higher blockage ratios result in an overall faster wake dissipation due to the confined bypass flow causing it to slow, and therefore wake dissipation is accelerated. Although

this effect may vary depending on channel shapes and width to height ratios, the overall effect of wall distance is included in the semi-empirical model.

The solution for wake model prediction is noticeably a simplification of the extreme complexities in the downstream flow field. However, it allows an overview of the general wake behaviour and limits over estimation of wake lengths leading to long distances required between turbines in inland array designs. Whilst limiting the complexity of application of the model, making it useful as a reference guide. It also includes typical flow conditions experienced in channels and favourable installation conditions for inland HAHT devices.

5. PART 3: HAHT BACKWATER MODEL DEVELOPMENT

5.1 Introduction

Prediction of the hydrodynamic effects of hydrokinetic turbines in canal systems remain an important pre-development objective. Due to the nature of canal design, these systems usually have flat slopes and subcritical flow regimes. Therefore, the analysis of backwater effects from turbines are critical for the prevention of flooding and water loss. This is especially important in array schemes where the cumulative upstream damming effect of multiple devices can exceed the available freeboard and cause upstream flooding.

A literature review indicated that no applicable backwater prediction model for inland horizontal axis hydrokinetic turbine (HAHT) analysis is available (Chapter 2.6 and 2.7). This chapter describes the development of a simplified method for calculating the backwater effect of HK turbines in canal systems. An analytical approximation based on turbine performance metrics and inflow conditions is tested using validated computational fluid dynamics (CFD) models. These models allow a larger dataset to validate the recommended analytical approximation.

5.2 Methodology

The following methodology was used in this chapter:
1. A validated multiphase CFD model of a HAHT (Subsection 3.5.3) was used to build the required dataset necessary for the development and testing of the backwater prediction model.
2. Relevant data indicating the extend of damming caused by the deployment of a HAHT device in a flow field was extracted from the validated CFD models:
    a. The relationship between the pressure drop measured at a specific distance upstream and downstream of a modelled HAHT and extent of maximum backwater effect was verified (based on the Bernoulli energy equation).
    b. The pressure drop was measured over a range of turbines and operational conditions.
    c. Experimental backwater effects were calculated based on the pressure drop over the modelled HAHTs.
3. A mathematical approach for determining the maximum backwater effect based on turbine performance was determined.
4. The backwater prediction model was verified:
    a. The maximum backwater effect was calculated for the existing turbine models.
    b. Predicted backwater values were compared to the measured experimental data (from step 2c).
5. An approach for the inclusion of a stanchion structure was proposed and verified.
6. A final backwater prediction model is prescribed for HAHTs in channel flow.

5.3 Backwater model approach

Backwater effects are often prevalent in subcritical channelised flow. Any blockage or disturbance in a uniform flow area results in an effect which may be characterised as gradually varied flow (GVF) or rapidly varied flow (RVF) depending on the extent of the disturbance (Chadwick, Morfett and Borthwick, 2013). The disturbance experienced by the deployment

of a HAHT in a channel will depend on the flow regime (flow characterises and channel slope) as well as the blockage ratio (β). High blockage ratios may result in RVF behaviour, acting similar to a weir structure which may result in the formation of a hydraulic jump (as seen in section 2.6). However even at small blockage ratios channels with subcritical flow regimes portray backwater effects great distances upstream (GVF phenomenon).

For theoretical approximation of the effects of a HAHT in a channel, the device may be defined primarily as an energy loss in the system. Energy losses in a channel are accounted for in several ways. An example of such a loss is friction losses due to channel wall roughness. Friction formulae have been developed to account for the shear force imposed by channel wall friction such as the well know manning equation (Chadwick, Morfett and Borthwick, 2013). Additionally, sudden losses due to channel features such as piers, bends and drop structures have also been defined/estimated empirically and can be included as form losses (Henderson, 1966). These are typically defined as eddy losses (h_e) included as an energy loss:

$$h_e = C_L \frac{V_\infty^2}{2g} \tag{59}$$

where C_L is the loss coefficient pre-defined for typical losses in a channel, as a function of flow velocity (V_∞) and gravitational acceleration (g). The drop in water level due to a particular loss can be quantified/included by either applying the conservation of momentum or energy over a channel section, between upstream and downstream sections (in which the energy loss exists). Additionally an empirical approach may be used, where experimental results determine an empirical relationship, such as the well-known relationships developed by Yarnell in 1934 for bridge piers (Yarnell, 1934).

Both the momentum and energy approach were investigated for the inclusion of the HAHT energy loss and subsequent effective blockage and resultant backwater effect. Approximations of the loss due to the presence of the turbine have been attempted (e.g., the models mentioned in section 2.7). However, no existing models provide a simplified applied applicable to inland flow.

5.3.1 Momentum approach

A conservation of momentum-based approach is often used to investigate the effect of an object/structure on the flow area and subsequent free surface effect. Energy losses occur due to flow separation, vortex generation, friction and turbulence all associated with the changes in velocity due to the presence of the HAHT. As mentioned in some cases, the presence of the turbine may also result in formation of a hydraulic jump on the water surface, resulting in additional energy losses. Applying the momentum approach avoids the need for inclusion of these individual energy losses by considering the change in momentum between a section upstream and downstream of the device. Additionally, if the resultant drag enforced by the presence of the turbine can be quantified, the momentum approach may be favourable.

Figure 5-1 and equation (60) indicate how the turbine may be quantified as a momentum change over a section upstream (1) and downstream (2) of the HAHT. The change in momentum is quantified by the hydrostatic forces upstream (F_1) and downstream (F_2) of the device (including the water level change), as well as friction from the channel bed and walls

(F_f) and the force due to the turbine (F_D). This can then be re-written to equation (61), in terms of the drag force (F_D) due to the presence of the turbine, where channel width (b) and height (h) define the cross sections of the channel.

$$F_1 - F_2 - F_D - F_f = \rho Q(V_2 - V_1) \tag{60}$$

$$F_D = \frac{1}{2}\rho g b h_1{}^2 - \frac{1}{2}\rho g b h_2{}^2 - \rho Q(V_2 - V_1) \tag{61}$$
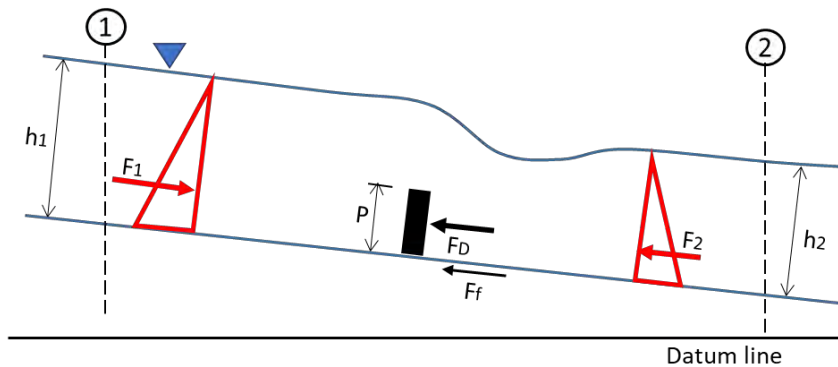
Figure 5-1: Schematic of the consideration of a disturbance using the momentum approach.

The drag coefficient for the HK device can be re-written to allow determination of the upstream water level through knowledge of the drag coefficient and downstream flow conditions. However, this requires knowledge of the downstream conditions which is not always known. An alternative conservative analysis would be to use the channel normal flow depth as the downstream value. However, the result seems overly conservative and thus an energy approach was considered instead.

5.3.2 Energy approach

The energy approach is more often used to determine backwater effects in typical open channel flow scenarios. This is a common approach, and has previously been applied to bridge piers (Henderson, 1966) when modelling the backwater effect of arch bridges (Martín-Vide *et al.*, 2005) and even irregular structures such as wood jams (Follett, Schalko and Nepf, 2020). This approach however requires calibration and empirical analysis due to the unknown losses surrounding the operating HK device (and therefore a dataset).

The energy approach can be seen in equation (62) and Figure 5-2. All energy losses between a point upstream and downstream of a HK device or blockage are quantified as terms which contribute to either the friction losses (h_f) or local losses (h_l).

$$\frac{U_1{}^2}{2g} + h_1 + Z_1 = \frac{U_4{}^2}{2g} + h_4 + Z_4 + \sum h_{f_{1-4}} + \sum h_{l_{1-4}} \tag{62}$$

All terms are defined in terms of flow velocity (U_∞), water depth (h) and distance from a datum (Z). The total energy (TEL), energy grade line (EGL) and water level/hydraulic grade line (HGL) are shown in Figure 5-2.
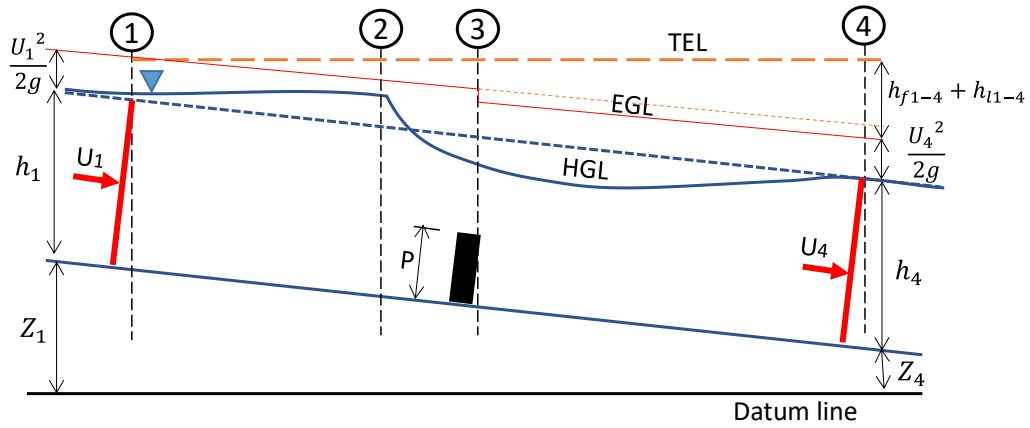
Figure 5-2: Schematic of the consideration of a disturbance using energy approach

The simplest method of including the turbine loss in the energy equation is to quantify it in terms of a loss coefficient that has been calibrated to the turbine type and operating conditions. The energy loss due to the presence of the turbine (h_t) can be written as a function of this loss coefficient (λ_T) and included in the Bernoulli energy equation. This considers the full effect of the turbine and effective blockage area as well as the freestream velocity (U_∞), as shown in equation (63). The loss coefficient requires proper calibration over a range of turbines and operational conditions to ensure a realistic outcome.

$$h_t = \lambda_T \frac{U_\infty^2}{2g} \tag{63}$$

5.4 Formulation of the loss coefficient

The energy approach allows inclusion of an energy loss through a kinetic energy or potential energy loss (similar to the approach for defining obstructions (Manko, 2018) mentioned in section 2). The Rankine Froude actuator disk theory may be applied to approximate the extracted energy through the terms indicated in Figure 5-3. The HAHT power can be written as follows (with flow velocity (u) through the rotor with area (A_u)):

$$Power = \frac{1}{2}\rho U_0^2 A_u - \frac{1}{2}\rho U_1^2 A_u \tag{64}$$

which is also most commonly used to define the maximum power output from a turbine according to the Betz limit (Eggleston and Stoddard, 1987). This allows characterisation of the energy loss in terms of pressure and velocity relationships as shown in Figure 5-3.
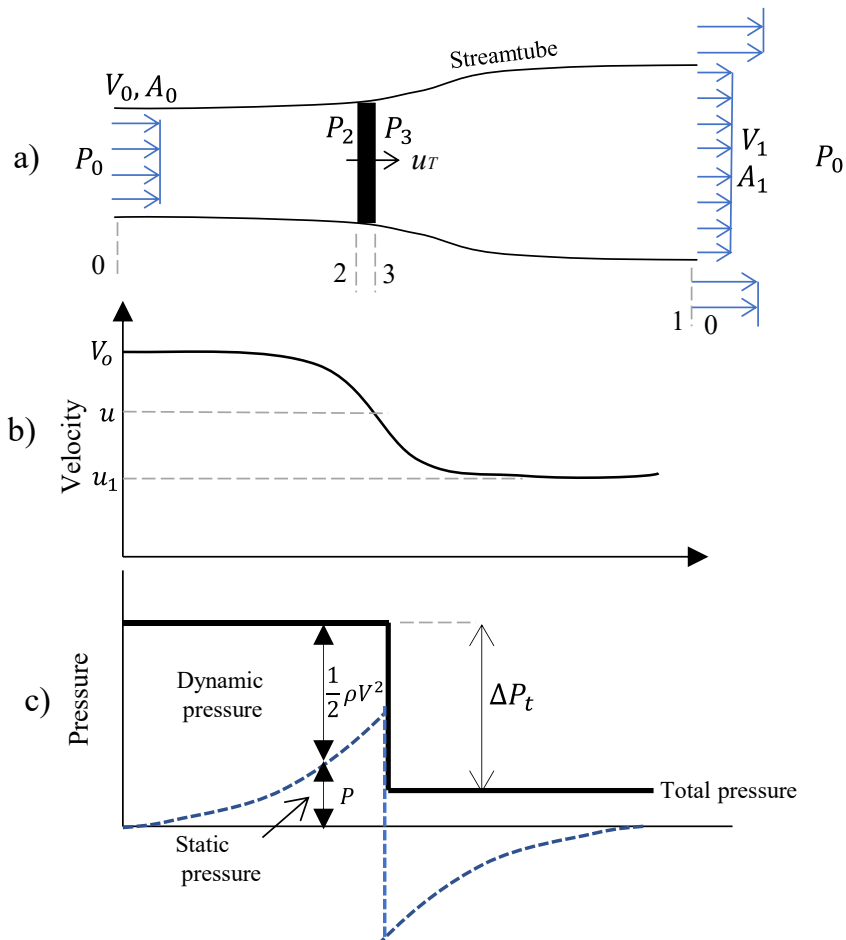
Figure 5-3: Pressure and velocity relationships shown graphically around a turbine (adapted from (Eggleston and Stoddard, 1987))

Again, using the definition of the thrust in terms of a force manifested as a pressure drop across the disk as seen in Figure 5-3:

$$T = A_u(P_3 - P_2) \tag{65}$$

where P_3 and P_2 are the static pressure just behind and ahead of the disk.

It is important that this simplification assumes the pressure does not vary with time and is also not periodic. Considering the momentum theorem for a cylindrical control volume as well as continuity between the flow upstream (0) and near downstream (1) the thrust can be further defined as (Eggleston and Stoddard, 1987):

$$T = \rho A_1 U_1(U_0 - U_1) \tag{66}$$

These relationships used in the actuator disk theory indicate that the pressure drop across a disk may be directly related to the turbine thrust. If the thrust coefficient (C_T equation (48))

with thrust represented as in equation (66), together with the turbine blockage ratio (β), are used as representation for the loss coefficient (λ_T). One is left with an energy loss represented as a pressure drop:

$$\lambda_T \frac{U_\infty^2}{2g} = C_T \beta \frac{U_\infty^2}{2g} = \frac{A(P_3 - P_2)}{\frac{1}{2}\rho U_\infty^2 A} \beta \frac{U_\infty^2}{2g} = \frac{(P_3 - P_2)}{\rho g} \beta \qquad (67)$$

The use of C_T allows determination of the effective pressure drop experienced over the turbine rotor, allowing inclusion of an energy loss term in the commonly used Bernoulli energy approach in GVF. It is important to note the implication of the assumptions and simplifications used. For one, no wake rotation is considered. This means no energy is dissipated (or pressure drop considered) due to the twirling wake as shown in Figure 5-4 (additional loss between 2 and 4).
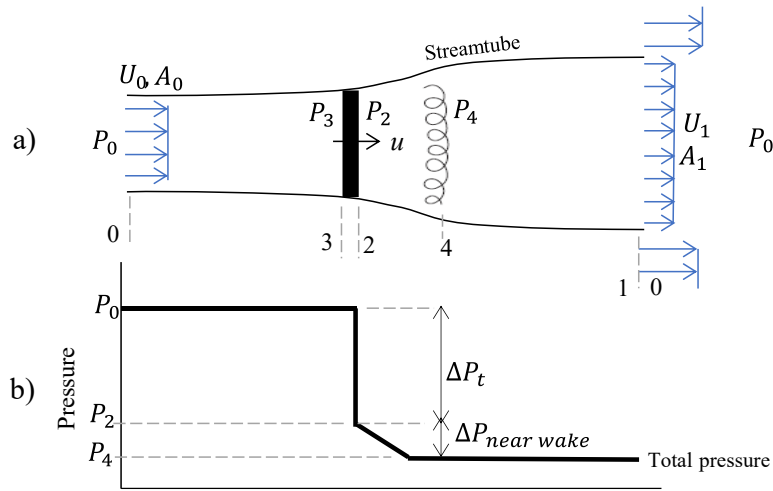
Figure 5-4: Turbine blockage expressed as an adapted pressure drop including near wake energy losses.

To include all possible effects and losses, a loss co-efficient is defined as a function of the following:
1. C_T which includes the primary losses as a function of turbine type.
2. Blockage ratio (β) to include the effective blockage of the turbine in the channel area.
3. And empirical coefficient c_3 which adjusts the C_T value to include additional energy due to kinetic energy dissipation in the near wake.

The loss coefficient is thus proposed as shown in equation (68):

$$\lambda_T = c_3 \times C_T \times \frac{A_t}{A} = c_3 \times C_T \times \beta \qquad (68)$$

For HAHT these C_T values usually range from 0.52 to 0.95 (Stallard *et al.*, 2013; Mycek *et al.*, 2014; Jeffcoate *et al.*, 2016; Morandi *et al.*, 2016). Theoretically it is also known that ideally according to the Betz limit, $a = \frac{1}{3}$, and therefore the ideal and highest attainable C_T would be 0.88. According to the BEM theory this should result in the highest velocity deficit in the near wake and therefore the "worst case" scenario for the operational conditions. Realistically the values lie at an upper limit of $C_T = 0.8$.

As mentioned in the literature review, rotor states (Eggleston and Stoddard, 1987) may exist where higher thrust coefficients are obtained and thus the momentum theory does not hold. Analysis in these regions is recommended for future work and improvement in the model accuracy and range of application.

5.5 Calibration of the loss coefficient

CFD models have previously been used to measure the backwater effects from blockages such as bridge piers (Kocaman, 2014) with computed and measured levels showing almost identical results. Multiple similar methods have been be used to determine the backwater effect of common structures found in river channels (Ranga Raju *et al.*, 1983; Martín-Vide *et al.*, 2005; Azinfar and Kells, 2011). A calibration process was carried out for the loss coefficient using experimental results, following a similar procedure.

As mentioned previously the energy loss due to the presence of the turbine *(h_t)* may also be quantified as a pressure drop (ΔP_t) (Figure 5-3c), which may be directly converted to a quantifiable energy loss through the following relationship:

$$h_t = \frac{\Delta P_t}{\rho g} \times \frac{A_t}{A} \tag{69}$$

Utilizing this approach allows a measurable pressure drop (ΔP_t) in the computational models (experimental results). Other than the losses due to the direct pressure drop over the turbine, there are additional losses in the near wake, due to the turbulent flow. Using the ΔP_t approximation allows measurement of the pressure drop over the turbine and near wake area. This approach allows the use of single phase CFD models to approximate energy loss due to the presence of the turbine. This provides the possibility of a larger set of experimental results for calibration of the loss coefficient without large computational expense.

To ensure a realistic backwater approximation in single-phase CFD models, it is necessary to validate the relationship using the ΔP_t measurements.

5.5.1 Validation of *ΔP_t* parameter measurement

The ΔP_t was measured in the single phase CFD model for the RM1 validation case, to determine if the approximation for h_t holds true. The calculated loss (h_t) through the relationship shown in equation (69) is compared to the measured backwater effect measured in the laboratory tests and multiphase CFD analysis. As these measurements include the stanchion support structure, the effective blockage due to the support structure was incorporated using the Yarnell approximation. This also validates a possible method of inclusion of support structures within the loss coefficient (equation (68)).

The Yarnell approximation for a single circular bridge pier (most similar to the support stanchion) was implemented for the RM1 case study (Yarnell, 1934):

$$\left[\frac{\Delta y}{y}\right]_{empirical} = K(K + 5\text{Fr}^2 - 0.6)(15\alpha^4)Fr^2 \tag{70}$$

where Δy is the backwater generated by the pier, y is the undisturbed flow depth, Fr the downstream Froude number and α here is the ratio of flow area obstructed by the piers to the total flow area downstream of the pier (also referred to as blockage ratio). K is used as a coefficient reflecting the pier shape. The RM1 modelled free-surface deformation was measured with and without the stanchion structure (Figure 5-5) to ensure the Yarnell approximation and pressure loss (ΔP_t) calculation work independently. The results were compared to the backwater calculation using only the measured pressure drop and including the stanchion through the Yarnell approximation.
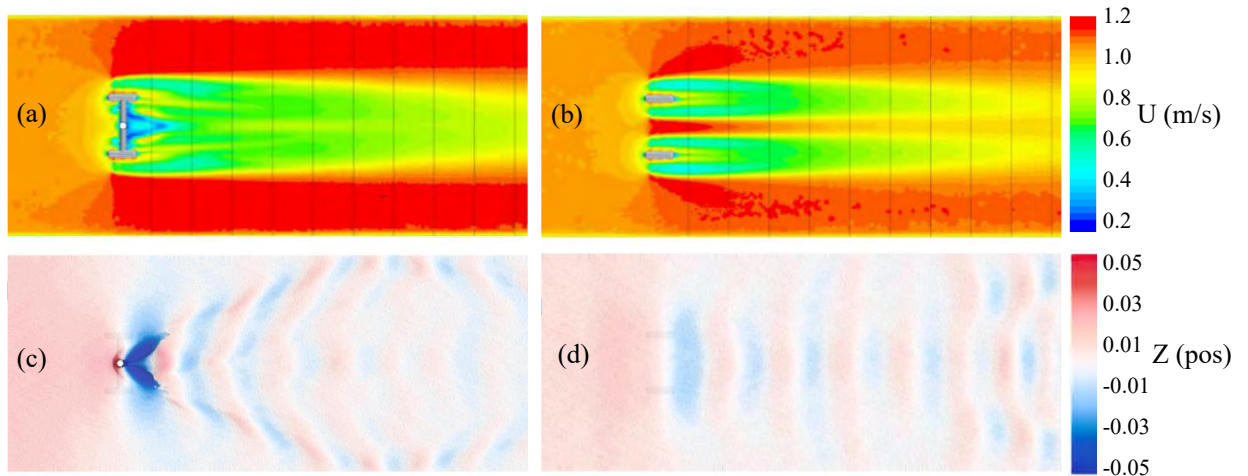
Figure 5-5: Multiphase CFD results velocity (a & b) and surface water measurements (c & d) graphics for the RM1 full model vs RM1 rotor and nacelle only.

Additionally, the CFD models allowed measurement of the pressure loss over the turbine alone, as well as measurement of added losses in the near wake. It was important to ascertain the lowest pressure zone in the near wake to ensure all losses are measured and included. An investigation was conducted, revealing that this minimum pressure point occurs when measured approximately 1 diameter (dt) upstream from the undisturbed incoming flow and extends to around 1.1 diameters (dt) downstream (visual example in Figure 5-7). This location was pushed further downstream with the addition of the propeller mount pole attached to the nacelle (such as the pole present in the T2, T3 and T4 tests). CFD comparisons with and without the pole confirmed this (Figure 5-6). Inclusion of the pole was added by the Yarnell approximation and therefore removed for the calibration of coefficient c_3.
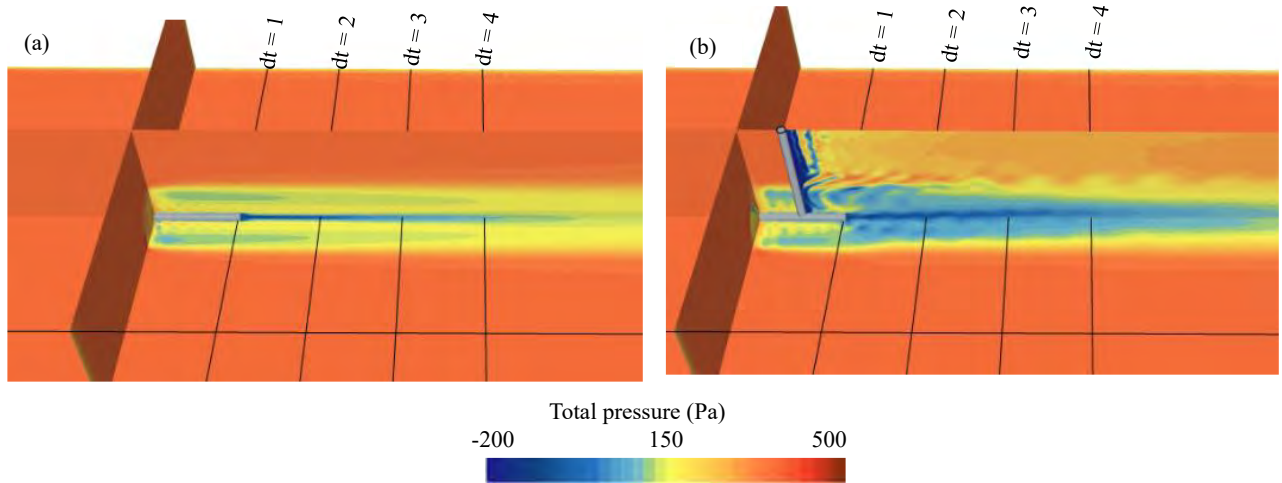
Figure 5-6: T2 turbine pressure gradient (a) without propeller mount and (b) with propeller mount
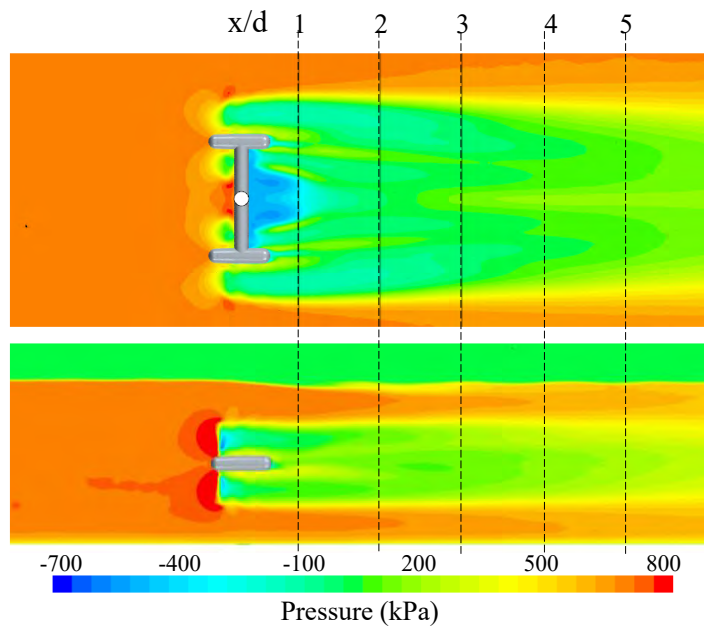
Figure 5-7: Pressure measurements over the horizontal and vertical planes (at the turbine hub height centreline)

The calculated backwater was then compared to the measured backwater and the results are included in Table 5-1. These results are calculated from the average disk pressure drop as shown in Figure 5-8. For the inclusion of the stanchion the pressure drop over the whole cross section is used instead (also seen in Figure 5-8).
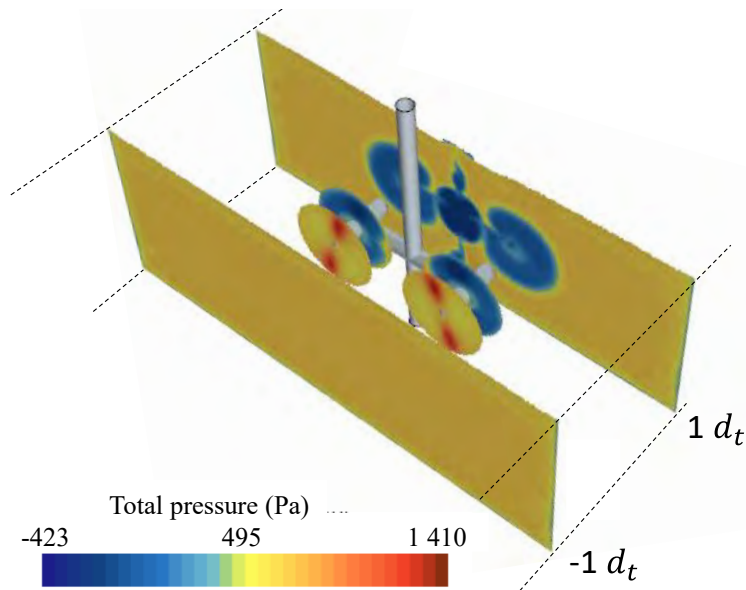
Figure 5-8: Pressure measurements over the disk and planes upstream and downstream of the RM1 turbine and retaining structure.

The results in Table 5-1 indicate a maximum differential of 0.13 % between the measured backwater and the calculated h_t through the ΔP_t assumption. This validates the approach and measurement technique, allowing the use of single phase CFD model results as an experimental dataset which require an exponentially lower computation expense with acceptable precision compared to multiphase modelling.

Table 5-1: Comparison of measured and predicted backwater levels

CFD model	ΔP_t disk (Pa)	ΔP_t plane (Pa)	Calculated h_t (mm)	Yarnell approx. (mm)	Measured h_t (mm)	$h_{t,meas} - h_{t,calc}$(%)
RM1 (no stanchion)	570	57.73	8.30	-	9.60	0.13%
RM1 (with stanchion)	530	74.09	7.72	4.36	12.00	0.01%
			12.66			

5.5.2 Calibration of the near wake coefficient

The additional energy loss experienced in the near wake due to the turbulent vortex structures has not been previously quantified and may differ for different turbine types, propeller profiles and operational parameters. Measurement of the pressure loss directly after the turbine, as well as to the distance of maximum pressure loss further downstream indicated this value varies from 4% to 10% for the turbine models included in this study.

As this value is highly dependent on the operational λ, turbine design, exact hub shape and type of retaining structure, determining an exact value can be highly complex. During attempts to quantify the extremity of the energy loss in the near wake the following was found (measurements included in Appendix C):

- Turbines operating at higher λ's indicate a lower ratio of energy loss in the near wake compared to the turbine itself. Although it has previously been deduced that turbines with higher rotation rates result in greater kinetic energy losses in the near wake, the turbine thrust effects are larger, therefore reducing the effect on the ratio of near wake loss.

- No clear link is found to blade solidity in the current dataset, however the deductions made by Eggleston and Stoddard (1987) on wind turbines, namely generally slow turning turbines with high solidities waste considerable energy in the wake rotation, are also observed here. The 4-bladed turbine indicated considerably more near wake losses than found by the 3- and 2-bladed devices (30-40% losses compared to 4-10% with 3-bladed). However as only one 4-bladed turbine was modelled this result cannot be seen as a general trend and could be bias to the specific design.

For simplicity in this study a value of $c_3 = 1.08$ is selected as a conservative metric adjusting for the near wake losses. This provides the best fit to the experiential results used in the study. Adjusting c_3 for specific operational cases proved ineffective as a detailed study and larger dataset would be necessary for this. As near wake losses were a small component of the total loss, a constant c_3 is regarded as acceptable for the scope and purpose of the study. For turbines operating at higher λ or designed with higher solidity, an adjustment to the c_3 value should be considered.

5.5.3 Verification of the proposed backwater prediction model

A verification of the proposed backwater prediction equation is required, to ensure the Yarnell approximation and pressure loss (ΔP_t) calculation work independently This was completed through a comparative analysis of experimental results and backwater predictions determined by the proposed equation.

Acceptable correlation between the experimental and calculated values over an initial dataset created confidence to proceed with the model and build a larger dataset to analyse the model accuracy at a larger operational variance from optimum conditions. As the λ_T is strongly dependant on C_T, and a single C_T value (as would have been specified by the manufacturer) should be applicable over all operational ranges, testing over a range of environmental conditions was necessary.

A regression to the mean approach was used to accumulate the necessary dataset for the analysis of the aforementioned calculation procedure and assumptions. This is required to reduce computational cost and compensate for the lack of available data on HAHT operating over a variety of operational conditions.

The dataset is created through CFD results from the cases described in Part 1 (Chapter 3). The models' environmental conditions were varied in five primary operational states, namely:
- Inlet velocity changes ($0.4 < U_\infty < 2.8$)
- Blockage ratio changes (Swept area to flow area) ($4\% < BR < 23\%$)
- Tip speed ratio changes (lower or higher load applied) ($3 < TSR < 6$)
- Froude number ($0.18 < Fr < 0.34$) (within the subcritical flow regime).
- Froude number based on turbine diameter ($0.15 < Fr_D < 0.9$).

These primary variables have been previously investigated and shown to potentially influence the turbine thrust imposed on the flow area and may therefore influence the backwater effect. Constraints were set to the variation of these variables to ensure the computational models remain within realistic operational scenarios, whilst allowing insight into the effect of operational states. The primary objective of the model verification is to ensure a relative level

of accuracy is obtained, and more importantly, a conservative approach in predicting the possible backwater effect caused by such a device.

The metrics of consideration investigated in section 4.4 can be applied in this analysis, as the turbine thrust is also affected by certain changes in operation. For example, a turbine operating at a lower β results in less thrust measured over the turbine for the same operational λ. The same blockage correction model applied in section 4.7 could be applied to the C_T value for better correlation to true conditions.

A measure of accuracy of the methods is indicated by the mean square absolute error. The absolute error (MAE) rather than relative error (RMSE) is used to place greater emphasis on the larger backwater values (at higher blockage ratios) rather than uniform predictions over the range of backwater predictions (h_t). Additionally, as the sample size changes in the analysis, the strength of the sample size effect is minimised when comparing MAE. The variance is also included to give an indication of the test condition with greater variability. Also indicating under which test conditions, the equations (and assumptions) perform best. The MAE is calculated as a function of the backwater level increase, channel depth (y) and sample size (N) shown in equation 71.

$$\sigma = \sqrt{\frac{1}{N}\sum\left(\frac{h_{t,exp}}{y} - \frac{h_{t,calc}}{y}\right)^2} \tag{71}$$

First the h_t results are calculated using equation (68) (excluding near wake effects, $c_3 = 1$) and compared to the energy loss experienced over the turbine blades only. The thrust coefficient is calculated for each experimental case using the thrust coefficient equation shown previously in equation (48). The results showed good correlation to experimental measurements over a range of test conditions. Details of the results and comparisons can be seen in Appendix C.

The validity of the recommended energy loss calculation (equation (69)) is then tested through comparison to measured energy loss over the turbine and near wake. It is important to note that the C_T value for each specific turbine was kept constant (as calculated for unconfined conditions at the optimal λ).

The calculated values were compared to the primary validation cases described in Part 1 (Chapter 2) can be seen in Table 5-2. The point of maximum pressure drop was determined for each model independently, occurring at different distances downstream of the turbine. This value typically ranged between dt = 1.1 to 1.6 downstream.

The results using the correct C_T value for each turbine proved to have a good correlation to experimental results with a MAR of only 0.96 mm and variance of 1.11 mm. Results using the Betz limit assumption of a maximum C_T of 0.88 were included to test this assumption. The assumption proved to function well for most test cases, however the T3 turbine (tested at Liverpool University) showed underestimated results due to the high thrust due to the turbine design.

Table 5-2: Backwater prediction results on six turbine test cases

Test case	β (%)	Flow depth (y)	C_T	Δh_t exp (mm)	C_T = Correct Δh_t (mm)	C_T = 0.88 Δh_t (mm)
T2_3b.1	4.8%	2	0.73	1.20	1.36	1.49
T1_2b.1	7.1%	1	0.91	4.15	3.99	3.81
T3_3b.1	16.5%	0.85	1.16	11.30	12.40	7.99
T3_2b.1	16.5%	0.85	1.06	9.82	10.69	7.99
T3_2b.1	16.5%	0.85	0.87	7.96	9.30	7.99
T4_3b.1	17.5%	1.2	0.73	12.45	11.77	16.57
				σ	0.96	2.30
				Variance	1.11	6.34

The variations between experimental and approximated h_t for variations of flow velocity's (U) and Fr_D's are shown graphically in Figure 5-9 to allow a better overview of specific operational effects on the predictions. As would be expected due to the strong dependency on C_T, at lower operational velocities the equation overpredicted backwater estimations. Also, at higher velocities the model slightly underpredicted results resulting in a larger MAE for the variation on inlet velocities.
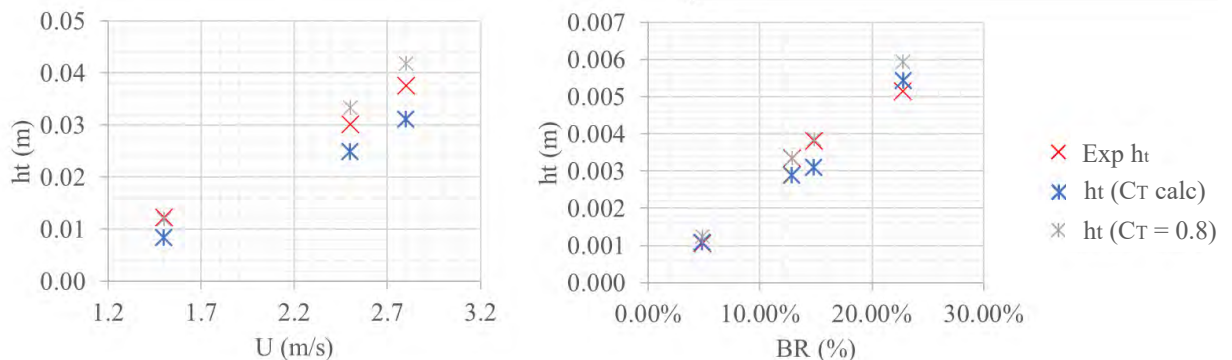
Figure 5-9: Effect of a) U_∞ and b) Fr_D on the determined h_t values (excluding near wake losses)

All backwater predictions using equation (68) and comparisons to experimental results are included in Table 5-3. Again, the Betz limit approximation of C_T was included.

Table 5-3: Comparative analysis results for the backwater prediction equation

Test condition	N	C_T	MAE (mm)	Variance (mm)
All tests conducted	18	Measured	1.37	1.99
	18	0.88 assumption	2.02	4.34
Validation case test conditions (operating at optimal λ)	6	Measured	0.96	1.11
	6	0.88 assumption	2.30	0.61
Variation of blockage ratios (β= 4%-22%) at optimum operational point	6	Measured	0.69	0.58
	6	0.88 assumption	1.85	4.12
Variation of flow velocities (0.8 to 2 m/s)	4	Measured	0.17	0.04
	4	0.88 assumption	0.24	0.08

Variation of inlet velocities at optimum tip speed ratios.	6	Measured	0.96	1.11
	6	0.88 assumption	0.71	0.61
Slight variation of tip speed ratios (+-25%)	3	Measured	2.70	10.93
	3	0.88 assumption	3.89	22.75

From the results in Table 5-3 the following observations are drawn:

1. The energy approach allows inclusion of the increase in velocity through the V^2 component of the loss coefficient. The validity of this is tested through comparison of predicted values to experimental test cases. The turbines were kept at optimal λ's and the inlet flow velocities were varied. A MAE of 0.96 mm was observed with a smaller error from the Betz assumption. This can however be explained through the dataset, as the C_T increases at higher velocities and the dataset used for the velocity tests were the T1 and T2 turbine's both with a general C_T value of around 0.8.

2. Test cases at low operational velocities (low Froude numbers) resulted in larger errors in approximating h_t, however it is important to note that these are unfavourable installation conditions and far removed from a feasible installation. The turbines may have low performance at these low operational velocities and therefore pose an unrealistic scenario. Here, the C_T calculation results in a more realistic value, due to the reduced performance.

3. To test the validity of the model over higher blockage ratios the T2 turbine results were compared to a high blockage ratio of 23% and the original turbine thrust coefficient was used to determine if this assumption holds. It is observed that as the β increased, the measured pressure drop increased- counteracting the increase in performance. Therefore, the equation still performed well, specifically in the critical cases (at higher β's).

4. The measured pressure decreased with an increase in ambient turbulence. This could be attributed to the faster recovery and therefore lower kinetic energy loss in the near wake.

5. The C_T approximation results in underprediction of the h_t at higher TSR's. As the turbine thrust is significantly higher, this C_T assumption does not hold. A large MAE and variance is observed for these tests. However, as these are not optimal conditions and result in significantly lower power output, it is assumed that turbines would not operate under these conditions. Therefore, the model was not adjusted for λ. which is a limitation to the model.

6. The C_T approximation gave significantly better results for the 3-bladed turbines and 2-bladed turbines tested. A larger dataset of 4-bladed models are needed to validate the use over higher solidity turbines. As most available turbines are 3-bladed, a focus was kept on an accurate prediction of these geometries.

The backwater model performed well and provided an approximation based only on basic operational conditions and turbine performance. This indicates the usefulness of this approximation.

5.6   Summary and conclusions

Quantifying the backwater resulting from the effective blockage of an operating turbine remains a challenge for the deployment of HK turbines in inland infrastructure such as canal systems. The use of a simple analytical model based on overall turbine thrust, to estimate the effective blockage and backwater effect from HK devices was explored here. The development of the model followed a similar approach to what was previously used for bridge pier modelling and quantifying blockages from such structures.

Variations of typical examples of HK devices were modelled using a recommended CFD approach and conditions were varied to allow testing over a range of operational conditions. The water surface profile measurements from the Reference model 1 (RM1) scaled model experiments allowed validation of the water surface deformation obtained when using a VOF approach coupled with a RS-LPS2 closure model and BEM-VD blade modelling approach.

The developed backwater model allows a conservative approach with various levels of certainty attainable, depending on the input parameters installed. This approximation allows backwater determination through minimal unknowns using only the basic turbine properties planned in the design. The thrust coefficient C_T is typically calculated during HAHT testing and design, and usually provided from the turbine manufacturer.

Although the recommended procedure is a simplified approximation, the results obtained were significantly closer to available dataset of backwater effects, and the procedure is significantly less complex than the methods found in literature. The ease of use also makes this method useful to engineers and developers when detailed numerical models are not feasible.

This model allows cumulative estimation of backwater, with simple inclusion of blockage structures or multiple turbines using available approximations for solid structures such as the Yarnell equation (the validity of this was also proven in this study). Additionally due to the nature of flow in canals (flat slopes), subcritical conditions govern, and backwater effects extend a large distance upstream. This allows simple cumulative inclusion of blockages without complex computational modelling, making this approach simple and relatively accurate (or at the least favourably conservative).

The approach allows room for further development and determination of calibrated thrust coefficients for typical turbines or typical operational conditions (similar to what was previously completed for pier shapes etc.). Additionally, a similar approach may be investigated for crossflow turbines where experimental results are available.

6. FINAL CONCLUSIONS AND PROPOSED FUTURE WORK

6.1 Summary

When a horizontal axis hydrokinetic turbine is deployed in water conveyance infrastructure such as a canal, two primary disturbances occur in the flow field. First, a downstream turbulent wake region, and second, a possible backwater effect. For planned deployment of multiple devices in series or parallel these effects may govern the number of devices or spacing of these devices. Therefore, the study aimed to investigate these effects, and identify simple analytical approximations for feasibility studies, planning and design.

The strong link between the turbulent wake region and turbine thrust has been used as a basis for determination of analytical wake models in the past (Lam, Chen and Hashim, 2015; Pyakurel, Vanzwieten, Wenlong, *et al.*, 2017). This relationship is found through simplified theoretical principles based on the momentum theory and the actuator disk method. Although a similar approach has been used in wind turbine analysis, environmental conditions present in channel flow such as ambient turbulence, blockage ratio and operational tip speed, strongly govern wake dissipation rates (Mycek *et al.*, 2014). Only a few of these effects have been quantified, or included in wake approximations. Therefore, a new analytical wake model, considering all relevant effects, was derived. A semi-empirical model is used to eliminate the complexities in the turbulent flow, depending on experimental wake results for calibration.

Similarly, the presence of the turbine and subsequent thrust, result in an effective blockage in the flow area. This causes a local pressure drop or energy loss at the turbine deployment region. When multiple turbines are placed in a channel flowing under a subcritical flow regime, backwater effects become a problem, resulting in damming which can extend a great distance upstream (Niebuhr, van Dijk and Bhagwan, 2019). A few attempts at quantifying the energy loss or drag due to the turbine have been made. However, a tested and calibrated approach over a range of turbines and environmental conditions does not exist. A simple approximation of energy loss due to the presence of the turbine, which can be incorporated into gradually varied flow analyses was determined.

For both the wake and backwater models, an experimental dataset over a range of environmental conditions as well as turbine geometries was required. Laboratory tests are limited in terms of controlling independent variables such a turbulence intensity, and few laboratories have the facilities to model ranges of blockage ratios, flow velocities (and tip speed ratios) or Reynolds and Froude conditions. A carefully validated Computational fluid dynamics (CFD) model is used, to create the necessary dataset. A rigorous benchmark validation study with five different turbine geometries with captured laboratory test results was undertaken, to evaluate the CFD approach. For turbulence modelling, a Reynolds stress model together with a virtual disk rotor modelling technique was found to capture the flow behaviour well, with a dedicated focus on capturing the wake dissipation rate. For hydrokinetic CFD models typically lower fidelity eddy viscosity models are used but were found to cause delayed wake dissipation due to the lack of turbulent kinetic energy in the wake.

The derived wake and backwater prediction approaches were tested and calibrated over a dataset relevant to the model constraints. A specific focus on correct model behaviour over a range of blockage ratios and flow conditions (with a focus on turbulence intensity) were ensured.

6.2 Conclusions

Based on the analysis and testing completed during the study the following conclusions were made which relate to the objectives of the study mentioned in Chapter 1:

- A CFD approach employing a Reynolds stress model resolving the flow surrounding a HAHT with a virtual disk blade modelling technique was found to model turbine performance as well as wake dissipation rate to a good degree of accuracy of the experimental values over a range of validation cases. A comparison of various modelling techniques found in literature allowed determination of a useful technique using lower fidelity single phase RANS models.

- A multiphase CFD modelling approach also compared well to experimental free surface measurements, replicating free surface deformation as well as backwater effects.

- Three-dimensional CFD model results allowed analysis of the effects and driving factors behind wake formation and dissipation. Factors most affecting wake formation and dissipation were found to be the operational tip-speed ratio and turbine solidity in the near wake and turbulence intensity and blockage ratio in the far wake. Blockage ratio was also found to affect the turbine performance, which agrees with blockage correction theories found in literature.

- A semi-empirical wake prediction approach was developed and tested over an experimental dataset. The wake model replicated wake dissipation rates of turbines operating at their optimum tip speed ratio to within 10 % accuracy. With even better accuracy in the far wake. Dissipation rates were predicted well over a range of blockage ratios and turbulence intensities.

- A backwater approximation based on turbine thrust (through C_T) was developed and found to function well over a range of operational cases and turbine geometries. Limitations over a variety of turbine solidities and tip speed ratios outside of the optimal range were observed. The backwater model indicated good results when combined with the Yarnell equation, allowing simple inclusion of a stanchion support structure.

- The models proved to provide a good approximation of hydrodynamic effects prevalent in channels where HAHT are deployed. The models allow flexible application and are based on coefficients with room for further calibration where a larger dataset is available.

6.3 Recommendations and proposed future work

The exploration of factors affecting the flow hydrodynamics in far from complete. Combinations of future laboratory and numerical testing will provide more insight into the factors affecting wake dissipation. Also assisting in the design of new systems to minimise wake effects, thereby increasing the densities of array systems.

The same is true for CFD approaches, where the ever-increasing availability of computational resources allows the use of higher fidelity models with a higher level of accuracy and reduced uncertainty. Further measurements and publication of laboratory tests is imperative to allow

proper validation and comparison of CFD approaches. The flexibility and control of variables in CFD opens up many doors in understanding the complexities around hydrokinetic turbines.

The models were developed keeping in mind possible improvements and calibration, similar to what past models have allowed for the current study. Work on improving these models to eliminate the need for complex CFD models pre-development would result in great advancements in installations of hydrokinetic turbines, as well as ease in regulatory exercises.

The following research is suggested to further improve the models:
- Research into the effect of blockage ratio on performance or investigation into the best blockage model to use to correctly calibrate C_T at other blockage ratios.
- Prescribed C_T values for specific cases/ turbine geometries. All flow disturbances are highly dependent on turbine thrust, and subsequently on C_T, therefore more knowledge into typical C_T values would be useful.
- Increasing the experimental dataset to include various other turbines and see if the model still works. Further calibration of the empirical coefficients.
- Although this section focussed on backwater determination, other free-surface effects such as the water level drop over the turbine, or possible hydraulic jumps downstream are important considerations for array designs. Recommendations on clearance coefficients and turbine spacing (due to wake recovery) should be carefully considered prior to deployment. Determination of guidelines are further investigations would further assist market-readiness.

7. REFERENCES

Adamski, S. J. (2013) Numerical Modelling of the Effects of a Free Surface on the Operating Characteristics of Marine Hydrokinetic Turbines. University of Washington.

Adcock, T. A. A., Draper, S. and Nishino, T. (2015) 'Tidal power generation – A review of hydrodynamic modelling', Journal of Power and Energy, 0(0), pp. 1–17. doi: 10.1177/0957650915570349.

Afgan, I., Mcnaughton, J., Rolfo, S., Apsley, D. D., Stallard, T. and Stansby, P. (2013) 'Turbulent flow and loading on a tidal stream turbine by LES and RANS', International Journal of Heat and Fluid Flow. Elsevier Inc., 43, pp. 96–108. doi: 10.1016/j.ijheatfluidflow.2013.03.010.

Aghsaee, P. and Markfort, C. D. (2018) 'Effects of flow depth variations on the wake recovery behind a horizontal-axis hydrokinetic in-stream turbine', Renewable Energy, 125, pp. 620–629. doi: 10.1016/j.renene.2018.02.137.

Ahmadi, M. H. B. (2019) 'Influence of upstream turbulence on the wake characteristics of a tidal stream turbine', Renewable Energy. Elsevier Ltd, 132, pp. 989–997. doi: 10.1016/j.renene.2018.08.055.

Ahmadian, R. and Falconer, R. A. (2012) 'Assessment of array shape of tidal stream turbines on hydro-environmental impacts and power output', Renewable Energy. Elsevier Ltd, 44(2012), pp. 318–327. doi: 10.1016/j.renene.2012.01.106.

Ainslie, J. F. (1988) 'Calculating the flow field in the wake of wind turbines', Journal of Wind Engineering and Industrial Aerodynamics, 27, pp. 213–224. Available at: http://linkinghub.elsevier.com/retrieve/pii/0167610588900372.

Allmark, M., Ellis, R., Lloyd, C., Ordonez-Sanchez, S., Johannesen, K., Byrne, C., Johnstone, C., O'Doherty, T., Mason-Jones, A., (2020) 'The development, design and characterisation of a scale model Horizontal Axis Tidal Turbine for dynamic load quantification', Renewable Energy. Elsevier Ltd, 156, pp. 913–930. doi: 10.1016/j.renene.2020.04.060.

Azinfar, H. and Kells, J. A. (2011) 'Drag force and associated backwater effect due to an open channel spur dike field', Journal of Hydraulic Research, 49(2), pp. 248–256. doi: 10.1080/00221686.2011.552470.

Bachant, P. and Wosnik, M. (2014) 'Reynolds Number Dependence of Cross-Flow Turbine Performance and Near- Wake Characteristics', in Proceedings of the 2nd Marine Energy Technology Symposium. Seattle, WA.

Bachant, P. and Wosnik, M. (2016) 'Effects of Reynolds Number on the Energy Conversion and Near-Wake Dynamics of a High Solidity Vertical-Axis Cross-Flow Turbine', Energies, 9(73). doi: 10.3390/en9020073.

Bahaj, A. S., Batten, W.M.J., Molland, A.F. and Chaplin, J.R. (2005) Experimental Investigation into the Hydrodynamic Performance of Marine Current Turbines, Sustainable Energy Series, Report 3.

Bahaj, A. S., Myers, L. E., Thomson, M. D., Jorge, N (2007) 'Characterising the wake of horizontal axis marine current turbines', 7th European Wave and Tidal Energy Conference, (January).

Bahaj, A. S., Molland, A. F., Chaplin, J. R., Batten, W. M. J. (2007) 'Power and thrust measurements of marine current turbines under various hydrodynamic flow conditions in a cavitation tunnel and a towing tank', Renewable Energy, 32(3), pp. 407–426. doi: 10.1016/j.renene.2006.01.012.

Bahaj, A. S. Myers, L. E., Rawlinson-Smith, R. I., Thomson, M. (2011) 'The effect of boundary proximity upon the wake structure of horizontal axis marine current turbines', Journal of Offshore Mechanics and Arctic Engineering, 134(2), pp. 1–8. doi: 10.1115/1.4004523.

Bahaj, A. S., Batten, W. M. J. J. and McCann, G. (2007) 'Experimental verifications of numerical predictions for the hydrodynamic performance of horizontal axis marine current turbines', Renewable Energy, 32(15), pp. 2479–2490. doi: 10.1016/j.renene.2007.10.001.

Bahaj, A. S. and Myers, L. E. (2013) 'Shaping array design of marine current energy converters through scaled experimental analysis', Energy. Elsevier Ltd, 59, pp. 83–94. doi: 10.1016/j.energy.2013.07.023.

Bai, G., Li, J., Fan, P., Li, G. (2013) 'Numerical investigations of the effects of different arrays on power extractions of horizontal axis tidal current turbines', Renewable Energy. Elsevier Ltd, 53, pp. 180–186. doi: 10.1016/j.renene.2012.10.048.

Barnsley, M. J. and Wellicome, J. F. (1990) Final report on the 2nd phase of development and testing of a horizontal axis wind turbine rig for the investigation of stall regulation aerodynamics.

Batten, W. M.J., Bahaj, A. S., Molland, A. F., Chaplin, J. R. (2007) 'Experimentally validated numerical method for the hydrodynamic design of horizontal axis tidal turbines', Ocean Engineering, 34(7), pp. 1013–1020. doi: 10.1016/j.oceaneng.2006.04.008.

Behrouzi, F., Nakisa, M., Maimun, A., Ahmed, Y. M. (2016) 'Renewable energy potential in Malaysia: Hydrokinetic river/marine technology', Renewable and Sustainable Energy Reviews. Elsevier, 62, pp. 1270–1281. doi: 10.1016/j.rser.2016.05.020.

Benchikh Le Hocine, A. E., Jay Lacey, R. W. and Poncet, S. (2019) 'Multiphase modeling of the free surface flow through a Darrieus horizontal axis shallow-water turbine', Renewable Energy, 143, pp. 1890–1901. doi: 10.1016/j.renene.2019.06.010.

Behrouzi, F., Nakisa, M., Maimun, A., Ahmed, Y.M. (1981) 'Courant provoque par les bateaux protection des berges et solution pour eviter l'erosion du lit du haut rhin', in PIANC, 25th Congress. Edinburgh. (in French).

Bigillon, F., Niño, Y. and Garcia, M. H. (2006) 'Measurements of turbulence characteristics in an open-channel flow over a transitionally-rough bed using particle image velocimetry', Experiments in Fluids, 41(6), pp. 857–867. doi: 10.1007/s00348-006-0201-2.

Birjandi, A.H., Bibeau, E. L., Chatoorgoon, V., Kumar, A. (2013) 'Power measurement of hydrokinetic turbines with free-surface and blockage effect', Ocean Engineering. Elsevier, 69, pp. 9–17. doi: 10.1016/j.oceaneng.2013.05.023.

Birjandi, A. H., Woods, J. and Bibeau, E. L. (2012) 'Investigation of macro-turbulent flow structures interaction with a vertical hydrokinetic river turbine', Renewable Energy, 48, pp. 183–192. doi: 10.1016/j.renene.2012.04.045.

Blackmore, T., Batten, W. M. J. and Bahaj, A. S. (2014) 'Influence of turbulence on the wake of a marine current turbine simulator', Proceedings of the Royal Society A: Mathematical, Physical and Engineering Sciences, 470(2170), pp. 1–17. doi: 10.1098/rspa.2014.0331.

Boudreau, M. and Dumas, G. (2017) 'Comparison of the wake recovery of the axial-flow and cross-flow turbine concepts', Journal of Wind Engineering and Industrial Aerodynamics, 165(October 2016), pp. 137–152. doi: 10.1016/j.jweia.2017.03.010.

Brasil Junior, A. C. P., Mendes, R. C. F., Wirrig, T., Noguera, R., Oliveira, T. F. (2019) 'On the design of propeller hydrokinetic turbines : the effect of the number of blades', Journal of the Brazilian Society of Mechanical Sciences and Engineering, 41, p. 253.

Bryden, I. G., Grinsted, T. and Melville, G. T. (2004) 'Assessing the potential of a simple tidal channel to deliver useful energy', Applied Ocean Research, 26(5), pp. 198–204. doi: 10.1016/j.apor.2005.04.001.

Burton, T., Jenkins, N., Sharpe, D., Bossanyi, E. (2011) Wind Energy Handbook (2nd Edition). 2nd edn, Environmental Science and Engineering (Subseries: Environmental Science). 2nd edn. John Wiley and Sons. doi: 10.1007/978-3-540-88258-9-1.

Cardona-Mancilla, C., Rio, J. S., Hincapié-zuluaga, D., Chica, E. (2018) 'A Numerical Simulation of Horizontal Axis Hydrokinetic Turbine with and without Augmented Diffuser', International journal of renewable energy research, 8(4).

Castelli, M. R. and Benini, E. (2011) 'Comparison between Lift and Drag-Driven VAWT Concepts on Low-Wind Site AEO', International Journal of Environmental and Ecological Engineering, 5(11), pp. 669–674. Available at: https://doi.org/10.5281/zenodo.1083101.

Chadwick, A., Morfett, J. and Borthwick, M. (2013) Hydraulics in Civil and Environmental Engineering. 5th edn. CRC Press.

Chamorro, L. P., Hill, C., Morton, S., Ellis, C., Arndt, R. E.A., Sotiropoulos, F. (2013) 'On the interaction between a turbulent open channel flow and an axial-flow turbine', Journal of Fluid Mechanics, 716, pp. 658–670. doi: 10.1017/jfm.2012.571.

Chamorro, L. P., Troolin, D. R., Lee, S. J. Arndt, R. E. A., Sotiropoulos, F. (2013) 'Three-dimensional flow visualization in the wake of a miniature axial-flow hydrokinetic turbine', Experiments in Fluids, 54(2). doi: 10.1007/s00348-013-1459-9.

Chanson, H. (2004) Hydraulics of Open Channel Flow. 2nd edn. Elsevier Science and Technology.

Chawdhary, S. Hill, C., Yang, X., Guala, M., Corren, D., Colby, J. and Sotiropoulos, F. (2017) 'Wake characteristics of a TriFrame of axial-flow hydrokinetic turbines', Renewable Energy, 109, pp. 332–345. doi: 10.1016/j.renene.2017.03.029.

Chen, Lin, B., Lin, J. and Wang, S. (2017) 'Experimental study of wake structure behind a horizontal axis tidal stream turbine', Applied Energy, 196, pp. 82–96.

Churchfield, M. J., Li, Y. and Moriarty, P. J. (2013) 'A large eddy simulation study of wake propagation and power production in an array of tidal-current turbines', Philosophical Transactions of the Royal Society A, 371(14), pp. 1–15.

Consul, C. A., Willden, R. H. J. and McIntosh, S. C. (2013) 'Blockage effects on the hydrodynamic performance of a marine cross-flow turbine', Philosophical Transactions of the Royal Society A, 371(1985). doi: 10.1098/rsta.2012.0299.

Contreras, L. T., Lopez, Y. and Lain, S. (2017) 'CFD Simulation of a Horizontal Axis Hydrokinetic Turbine', Renewable Energy and Power Quality Journal, 1(15), pp. 512–517. doi: 10.24084/repqj15.376.

Dai, Y., Ren, Z., Wang, K., Li, W., Li, Z. and Yan, W., (2018) 'Optimal sizing and arrangement of tidal current farm', IEEE Transactions on Sustainable Energy. IEEE, 9(1), pp. 168–177. doi: 10.1109/TSTE.2017.2719042.

Daskiran, C, Riglin, J., Schleicher, W. and Oztekin. A. (2017) 'Transient analysis of micro-hydrokinetic turbines for river applications', 129(August 2016), pp. 291–300.

Davidson, P. A. (2004) Turbulence - An Introduction for Scientists and Engineers. Oxford: Oxford University Press.

De Dominicis, M., O'Hara Murray, R. and Wolf, J. (2017) 'Multi-scale ocean response to a large tidal stream turbine array', Renewable Energy. Elsevier Ltd, 114, pp. 1160–1179. doi: 10.1016/j.renene.2017.07.058.

Edmunds, M, Malki, R., Williams, A J., Masters, I., and Croft T. N. (2014) 'Aspects of tidal stream turbine modelling in the natural environment using a coupled BEM – CFD model', 7, pp. 20–42.

Edmunds, M., Williams, A. J., Masters, I. and Croft, T. N. (2017) 'An enhanced disk averaged CFD model for the simulation of horizontal axis tidal turbines', 101, pp. 67–81.

Eggleston, D. M. and Stoddard, F. (1987) Wind turbine engineering design. New York: Van Nostrand Reinhold Company Inc.

Fabrice, M., Gregory, P., Gregory, G., and Elie. R. (2008) 'Numerical simulation of the wake of marine current turbines with a particle method', in World Renewable Energy Congress X. Glasgow.

Fajri, O. E., Bhushan, S., Thompson, D. S. and O'Doherty. T. (2020) 'Numerical investigation of shallow-water effects on hydrokinetic turbine wake recovery', International Marine Energy Journal, 3(1), pp. 25–35. doi: 10.36688/imej.3.25-35.

Fajri, O. E., Bowman, J., Bhushan, S., Thompson, D. and O'Doherty. T. (2022) 'Numerical study of the effect of tip-speed ratio on hydrokinetic turbine wake recovery', Renewable Energy. Elsevier Ltd, 182(January 2022), pp. 725–750. doi: 10.1016/j.renene.2021.10.030.

Ferraiuolo, R., Gharib-Yosry, A., Fernández-Jiménez, A., Espina-Valdés, R., Álvarez-Álvarez, E., Del Giudice, G. and Giugni. M. (2022) 'Design and Experimental Performance Characterization of a Three-Blade Horizontal-Axis Hydrokinetic Water Turbine in a Low-Velocity Channel', in Environmental sciences proceedings. doi: 10.3390/environsciproc2022021062.

Follett, E., Schalko, I. and Nepf, H. (2020) 'Momentum and Energy Predict the Backwater Rise Generated by a Large Wood Jam', Geophysical Research Letters, 47(17). doi: 10.1029/2020GL089346.

Fontaine, A. W., Straka, W., Meyer, R., Jonson, M. and Neary, V. S. (2020) 'Performance and wake flow characterization of a 1:8.7 scale reference USDOE MHKF1 hydrokinetic turbine to establish a verification and validation test database', Renewable Energy.

Fouatih, O. M., Imine, B. and Medale, M. (2019) 'Numerical/experimental investigations on reducing drag penalty of passive vortex generators on a NACA 4415 airfoil', Wind Energy, 22(7), pp. 1003–1017. doi: 10.1002/we.2330.

Frandsen, S., Barthelmie, R., Pryor, S., Rathmann, O. and Larsen. S. (2006) 'Analytical modelling of wind speed deficit in large offshore wind farms', Wind Energy, 9, pp. 39–53.

Gajardo, D., Escauriaza, C. and Ingram, D. M. (2019) 'Capturing the development and interactions of wakes in tidal turbine arrays using a coupled BEM-DES model', Ocean Engineering. Elsevier Ltd, 181(November 2018), pp. 71–88. doi: 10.1016/j.oceaneng.2019.03.064.

Garrett, C. and Cummins, P. (2005) 'The power potential of tidal currents in channels', Proceedings of the Royal Society A: Mathematical, Physical and Engineering Sciences, 461(2060), pp. 2563–2572. doi: 10.1098/rspa.2005.1494.

Garrett, C. and Cummins, P. (2007) 'The efficiency of a turbine in a tidal channel', Journal of Fluid Mechanics, 588, pp. 243–251. doi: 10.1017/S0022112007007781.

Ge, M., Wu, Y., Liu, Y., and Yang. X. I. A. (2019) 'A two-dimensional Jensen model with a Gaussian-shaped velocity deficit', Renewable Energy, 141, pp. 46–56. doi: 10.1016/j.renene.2019.03.127.

Gibson, M. M. and Launder, B. E. (1978) 'Ground effects on pressure fluctuations in the atmospheric boundary layer', Journal of Fluid Mechanics, 86(3), pp. 491–511. doi: 10.1017/S0022112078001251.

Glauert, H. (1983) The Elements of Aerofoil and Airscrew Theory. Cambridge: Cambridge University Press. doi: 10.1017/CBO9780511574481.

Gotelli, C. Musa, M., Guala, M. and Escauriaza. C. (2019) 'Experimental and Numerical Investigation of Wake Interactions of Marine Hydrokinetic Turbines', Energies, 12(3188), pp. 1–17. doi: 10.3390/en12163188.

Goward Brown, A. J., Neill, S. P. and Lewis, M. J. (2017) 'Tidal energy extraction in three-dimensional ocean models', Renewable Energy. Elsevier Ltd, 114, pp. 244–257. doi: 10.1016/j.renene.2017.04.032.

Guerra, M. and Thomson, J. (2019) 'Wake measurements from a hydrokinetic river turbine', Renewable Energy, 139, pp. 483–495. doi: https://doi.org/10.1016/j.renene.2019.02.052.

Gunawan, B., Neary, V. S. and McNutt, J. R. (2011) ORNL ADV Post-Processing Guide and MATLAB Algorithms for MHK Site Flow and Turbulence Analysis. Oak Ridge, Tennessee: US Department of Energy.

Gunawan, B., Roberts, J. and Neary, V. (2015) 'Hydrodynamic Effects of Hydrokinetic Turbine Deployment in an Irrigation Canal', 3rd Marine Energy Technology Symposium, (Figure 2), pp. 1–6.

Guo, Q., Zhou, L. and Wang, Z. (2015) 'Comparison of BEM-CFD and full rotor geometry simulations for the performance and flow field of a marine current turbine', Renewable Energy, 75, pp. 640–648.

Hamill, G. A. and Kee, C. (2016) 'Predicting axial velocity profiles within a diffusing marine propeller jet', Ocean Engineering. Elsevier, 124, pp. 104–112. doi: 10.1016/j.oceaneng.2016.07.061.

Hamill, G. A., McGarvey, J. A. and Hughes, D. A. B. (2004) 'Determination of the efflux velocity from a ship's propeller', Proceedings of the Institution of Civil Engineers- Maritime Engineering, 157(2), pp. 83–91.

Hansen, O. L. (2008) Aerodynamics of wind turbines. Earthscan.

Harrison, M. E. et al. (2010) 'Comparison between CFD simulations and experiments for predicting the far wake of horizontal axis tidal turbines', IET Renewable Power Generation, 4(6), p. 613. doi: 10.1049/iet-rpg.2009.0193.

Henderson, F. M. (1966) Open channel Flow. New York: The Mcmillan Company.

Hill, C., Neary, V. S., Gunawan, B., Guala, M. and Sotiropoulos, F. (2014) U. S. Department of Energy Reference Model Program RM1 : Experimental Results, Sandia National Laboratories. Minneapolis.

Hill, C, Neary, V. S., Guala, M. and Sotiropoulos F. (2020) 'Performance and Wake Characterization of a Model Hydrokinetic Turbine: The Reference Model 1 (RM1) Dual Rotor Tidal Energy Converter', in Energies, pp. 1–21. doi: 10.3390/en13195145.

Hill, C. and Neary, V. S. (2014) 'U. S. Department of Energy Reference Model Program RM1 : Experimental Results', Sandia National Laboratories.

Hirt, C. W. and Nichols, B. D. (1981) 'Volume of fluid (VOF) method for the dynamics of free boundaries', Journal of Computational Physics, 39(1), pp. 201–225. doi: 10.1016/0021-9991(81)90145-5.

Hoffmann, M. J., Reuss Ramsay, R. and Gregorek, G. M. (1996) Effects of grit roughness and pitch oscillations on the NACA 4415 airfoil, NREL/TP-442-7817. doi: 10.2172/266691.

Ibrahim, W. I., Mohamed, M. R., Ismail, R. M. T. R., Leung, P. K., Xing, W. W. and Shah. A. A. (2021) 'Hydrokinetic energy harnessing technologies: A review', Energy Reports. Elsevier Ltd, 7(May), pp. 2021–2042. doi: 10.1016/j.egyr.2021.04.003.

Jeffcoate, P., Whittaker, T., Boake, C. and Elsaesser. B. (2016) 'Field tests of multiple 1/10 scale tidal turbines in steady flows', Renewable Energy. Elsevier Ltd, 87, pp. 240–252. doi: 10.1016/j.renene.2015.10.004.

Jensen, N. O. (1983) 'A note on wind generator interaction', Risø-M-2411 Risø National Laboratory Roskilde, pp. 1–16. Available at: http://www.risoe.dk/rispubl/VEA/veapdf/ris-m-2411.pdf.

Johansson, P. B. V. (2002) The axisymmetric turbulent wake. Chalmers University of Technology.

Johnson, G. L. (2001) 'Wind Turbine power, energy and Torque', in Wind Turbine Systems, pp. 1–54.

Kang, S., Borazjani, I., Colby, J. A. and Sotiropoulos. F. (2012) 'Numerical simulation of 3D flow past a real-life marine hydrokinetic turbine', Advances in Water Resources, 39, pp. 33–43. doi: 10.1016/j.advwatres.2011.12.012.

Kang, S., Yang, X. and Sotiropoulos, F. (2014) 'On the onset of wake meandering for an axial flow turbine in a turbulent open channel flow', Journal of Fluid Mechanics, 744, pp. 376–403. doi: 10.1017/jfm.2014.82.

Kartezhnikova, M. and Ravens, T. M. (2014) 'Hydraulic impacts of hydrokinetic devices', Renewable Energy, 66, pp. 425–432. doi: 10.1016/j.renene.2013.12.034.

Keulegan, G. H. (1938) 'Laws of turbulent flow in open channels', Journal of Research of the National Bureau of Standards, 21(6), p. 707. doi: 10.6028/jres.021.039.

Kinsey, T. and Dumas, G. (2017) 'Impact of channel blockage on the performance of axial and cross- flow hydrokinetic turbines', Renewable Energy, 103, pp. 239–254.

Kironoto, B. A. and Graf, W. H. (1995) 'Turbulence characteristics in rough non-uniform open-channel flow', Proceedings of the Institution of Civil Engineers: Water, Maritime and Energy, 112(4), pp. 336–348. doi: 10.1680/iwtme.1995.28114.

Kocaman, S. (2014) 'Prediction of backwater profiles due to bridges in a compound channel using CFD', Advances in Mechanical Engineering, 2014. doi: 10.1155/2014/905217.

Kolekar, N., Hu, Z., Banerjee, A. and Du, X. (2013) 'Hydrodynamic Design and Optimization of Hydro - kinetic Turbines using a Robust Design Method', in Proceedings of the 1st Marine Energy Technology Symposium, pp. 1–10.

Kolekar, N. and Banerjee, A. (2015) 'Performance characterization and placement of a marine hydrokinetic turbine in a tidal channel under boundary proximity and blockage effects', Applied Energy. Elsevier Ltd, 148, pp. 121–133. doi: 10.1016/j.apenergy.2015.03.052.

Lain, S., Contreras, L. T. and Lopez, O. (2019) 'A review on computational fluid dynamics modeling and simulation of horizontal axis hydrokinetic turbines', Journal of the Brazilian Society of Mechanical Sciences and Engineering, (August). doi: 10.1007/s40430-019-1877-6.

Lalander, E. and Leijon, M. (2011) 'In-stream energy converters in a river - Effects on upstream hydropower station', Renewable Energy, 36(1), pp. 399–404. doi: 10.1016/j.renene.2010.05.019.

Lam, W., Chen, L. and Hashim, R. (2015) 'Analytical wake model of tidal current turbine', 79, pp. 512–521.

Lam, W. H. and Chen, L. (2014) 'Equations used to predict the velocity distribution within a wake from a horizontal-axis tidal-current turbine', Ocean Engineering, 79, pp. 35–42. doi: 10.1016/j.oceaneng.2014.01.005.

Lam, W. H., Chen, L. and Hashim, R. (2015) 'Analytical wake model of tidal current turbine', Energy, 79(C), pp. 512–521. doi: 10.1016/j.energy.2014.11.047.

Larsen, G. C. (1988) 'A Simple Wake Calculation Procedure', Risø-M, No. 2760, p. 58. Available at: http://orbit.dtu.dk/ws/files/55567186/ris_m_2760.pdf.

Lavaroni, L., Watson, S. J., Cook, M. J., and Dubal, M. R. (2014). A comparison of actuator disc and BEM models in CFD simulations for the prediction of offshore wake losses. Journal of Physics: Conference Series, 524(1). https://doi.org/10.1088/1742-6596/524/1/012148

Li, W., Zhou, H., Liu, H., Lin, Y., and Xu, Q. (2016) 'Review on the blade design technologies of tidal current turbine', Renewable and Sustainable Energy Reviews. Elsevier, 63, pp. 414–422. doi: 10.1016/j.rser.2016.05.017.

Li, Y., Colby, J. A., Kelley, N., Thresher, R., Jonkman, B., Hughes, S. (2010) 'Inflow measurements in a tidal strait for deploying tidal current turbines: lessons, opportunities and

challenges', in proceedings of the 29th International conference on Ocean, Offshore and Artic Engineering (OMAE2010). Shanghai, China: ASME.

Lloyd, T. P., Turnock, S. R. and Humphrey, V. F. (2014) 'Assessing the influence of inflow turbulence on noise and performance of a tidal turbine using large eddy simulations', Renewable Energy. Elsevier Ltd, 71, pp. 742–754. doi: 10.1016/j.renene.2014.06.011.

Lo Brutto, O. A., Nguyen, V. T., Guillou, S. S., Gualous, H., Boudart, B. (2015) 'Reanalyse of an Analytical Model for One Tidal Turbine Wake Prediction', in Proceedings of the 11th European Wave and Tidal Energy Conference. Nantes, France.

López, I., Rosa-Santos, P., Moreira, C., and Taveira-Pinto, F. (2018) 'RANS-VOF modelling of the hydraulic performance of the LOWREB caisson', Coastal Engineering. Elsevier, 140(July), pp. 161–174. doi: 10.1016/j.coastaleng.2018.07.006.

Ma, Y., Lam, W. H., Cui, Y., Zhang, T., Jiang, J., Sun, C., Guo, J., Wang, S., Lam, S. S., Hamill, G. (2018) 'Theoretical vertical-axis tidal-current-turbine wake model using axial momentum theory with CFD corrections', Applied Ocean Research, 79(March), pp. 113–122. doi: 10.1016/j.apor.2018.07.016.

Macleod, A. J., Barnes, S., Rados, K. G., and Bryden, I. G. (2002) 'Wake effects in tidal current turbine farms', in MAREC 2002.

Maganga, F., Germain, G., King, J., Pinon, G., and Rivoalen, E. (2010) 'Experimental characterisation of flow effects on marine current turbine behaviour and on its wake properties', IET Renewable Power Generation, 4(6), pp. 498–509. doi: 10.1049/iet-rpg.2009.0205.

Malki, R, Masters, I., Williams, A. J., and Croft, N. (2011) 'The variation in wake structure of a tidal stream turbine with flow velocity', in International Conference on Computational Methods in Marine Engineering. Barcelona. doi: 10.1007/978-94-007-6143-8.

Malki, R, Williams, A. J., Croft, T. N., Togneri, M., and Masters, I. (2013) 'A coupled blade element momentum – Computational fluid dynamics model for evaluating tidal stream turbine performance', Applied Mathematical Modelling. Elsevier Inc., 37(5), pp. 3006–3020. doi: 10.1016/j.apm.2012.07.025.

Malki, Rami, Masters, I., Williams, A. J., and Croft, T. N. (2014) 'Planning tidal stream turbine array layouts using a coupled blade element momentum e computational fluid dynamics model', Renewable Energy, 63, pp. 46–54.

Mańko, R. (2018) 'Ranges of Backwater Curves in Lower Odra', Civil and Environmental Engineering Reports, 28(4), pp. 25–35. doi: 10.2478/ceer-2018-0048.

Mannion, B., McCormack, V., Leen, S. B., and Nash, S. (2019) 'A CFD investigation of a variable-pitch vertical axis hydrokinetic turbine with incorporated flow acceleration', Journal of Ocean Engineering and Marine Energy, 5(1), pp. 21–39. doi: 10.1007/s40722-019-00130-1.

Martín-Vide, J. P., Prió, J. M., Martin-Vide, J. P., and Prio, J. M. (2005) 'Backwater of arch bridges under free and submerged condition', Journal of Hydraulic Research, 43(5), pp. 515–521. doi: 10.1080/00221680509500149.

Mason-jones, A. (2010) Performance assessment of a Horizontal Axis Tidal Turbine in a high velocity shear environment. Cardiff University.

Mason-Jones, A., O'Doherty, D. M., Morris, C. E., O'Doherty, T., Byrne, C. B., Prickett, P. W., Grosvenor, R. I., Owen, I., Tedds, S., Poole, R. J. (2012) 'Non-dimensional scaling of tidal stream turbines', Energy. Elsevier, 44(1), pp. 820–829. doi: 10.1016/j.energy.2012.05.010.

Masters, Ian, Malki, R., Williams, A. J., and Croft, T. N. (2013) 'The influence of flow acceleration on tidal stream turbine wake dynamics : A numerical study using a coupled BEM – CFD model', Applied Mathematical Modelling. Elsevier Inc., 37, pp. 7905–7918. doi: 10.1016/j.apm.2013.06.004.

Masters, I, Chapman, J. C., Willis, M. R., and Orme, J. A. C. (2014) 'A robust blade element momentum theory model for tidal stream turbines including tip and hub loss corrections', Journal of Marine Engineering and Technology, 10(1), pp. 25–35. doi: 10.1080/20464177.2011.11020241.

Masters, Ian, Williams, A., Croft, T. N., Togneri, M., Edmunds, M., Zangiabadi, E., Fairley, I., Karunarathna, H. (2015) 'A comparison of numerical modelling techniques for tidal stream turbine analysis', Energies, 8(8), pp. 7833–7853. doi: 10.3390/en8087833.

McNaughton, J., Rolfo, S., Apsley, D. D., Afgan, I., Stansby, P. K., and Stallard, T. (2012) 'CFD prediction of turbulent flow on an experimental tidal stream turbine using RANS modelling', 1st Asian Wave and Tidal Conference Series. doi: 10.1017/CBO9781107415324.004.

McQuivery, R. S. and Richardson, E. V (1969) 'Some Turbulence Measurements in Open-Channel Flow', Journal of the Hydraulics Division, 95(1), pp. 209–224.

Menter, F. R. (1994) 'Two-equation eddy-viscosity turbulence models for engineering applications', AIAA Journal, 32(8), pp. 1598–1605.

Menter, F. R. (2011) Turbulence Modelling for Engineering Flows, A Technical Paper from ANSYS, Inc. Available at: http://cfd.spbstu.ru/agarbaruk/c/document_library/DLFE-41517.pdf.

Mikkelsen, R. and Sorensen, J. N. (2002) 'Modelling of wind tunnel blockage', in Global Wind-power conference. Paris, France.

Miller, V. B. and Schaefer, L. A. (2010) 'Dynamic modelling of hydrokinetic energy extraction', Journal of Fluids Engineering, Transactions of the ASME, 132(9), pp. 1–7. doi: 10.1115/1.4002431.

Milne, I. A., Sharma, R. N., Flay, R. G. J., and Bickerton, S. (2013) 'Characteristics of the turbulence in the flow at a tidal stream power site', Philosophical Transactions of the Royal Society A: Mathematical, Physical and Engineering Sciences, 371(1985). doi: 10.1098/rsta.2012.0196.

Morandi, B., Di Felice, F., Costanzo, M., Romano, G. P., Dhomé, D., and Allo, J. C. (2016) 'Experimental investigation of the near wake of a horizontal axis tidal current turbine', International Journal of Marine Energy. Elsevier Ltd, 14, pp. 229–247. doi: 10.1016/j.ijome.2016.02.004.

Morris, C. E. (2014) 'Influence of Solidity on the Performance, Swirl Characteristics, Wake Recovery and Blade Deflection of a Horizontal Axis Tidal Turbine'.

Morris, C. E., O'Doherty, D. M., Mason-Jones, A., and O'Doherty, T. (2016) 'Evaluation of the swirl characteristics of a tidal stream turbine wake', International Journal of Marine Energy. Elsevier Ltd, 14, pp. 198–214. doi: 10.1016/j.ijome.2015.08.001.

Mycek, P., Gaurier, B., Germain, G., Pinon, G., and Rivoalen, E. (2014) 'Experimental study of the turbulence intensity effects on marine current turbines behaviour. Part II: Two interacting turbines', Renewable Energy. Elsevier Ltd, 68, pp. 876–892. doi: 10.1016/j.renene.2013.12.048.

Myers, L. and Bahaj, A. S. (2007) 'Wake studies of a 1 / 30th scale horizontal axis marine current turbine', Ocean Engineering, 34, pp. 758–762. doi: 10.1016/j.oceaneng.2006.04.013.

Myers, L. and Bahaj, A. S. (2009) 'Near wake properties of horizontal axis marine current turbines', in Eighth European wave and tidal energy conference. Uppsala, Sweden, pp. 558–565.

Myers, L. E. and Bahaj, A. S. (2010) 'Experimental analysis of the flow field around horizontal axis tidal turbines by use of scale mesh disk rotor simulators', Ocean Engineering. Elsevier, 37(2–3), pp. 218–227. doi: 10.1016/j.oceaneng.2009.11.004.

Myers, L. E. and Bahaj, A. S. (2012) 'An experimental investigation simulating flow effects in first generation marine current energy converter arrays', Renewable Energy, 37(1), pp. 28–36. doi: 10.1016/j.renene.2011.03.043.

Neary, V S, Gunawan, B., and Sale, D. C. (2013) 'Near and far field flow disturbances induced by model hydrokinetic turbine: ADV and ADP comparison', Renewable Energy, 60, pp. 1–6. doi: 10.1016/j.renene.2013.03.030.

Neary, V. S., Gunawan, B. and Sale, D. C. (2013) 'Turbulent inflow characteristics for hydrokinetic energy conversion in rivers', Renewable and Sustainable Energy Reviews. Elsevier, 26, pp. 437–445. doi: 10.1016/j.rser.2013.05.033.

Nezu, I., Nakagawa, H. and Jirka, G. H. (1994) 'Turbulence in Open-Channel flows', Journal of Hydraulic Engineering, 120(10).

Nezu, I. and Rodi, W. (1986) 'Open-channel Flow Measurements with a Laser Doppler Anemometer', Journal of Hydraulic Engineering, 112(5).

Niebuhr, C. M., van Dijk, M., Neary, V. S., and Bhagwan, J. N. (2019) 'A review of hydrokinetic turbines and enhancement techniques for canal installations: Technology, applicability and potential', Renewable and Sustainable Energy Reviews, 113. doi: 10.1016/j.rser.2019.06.047.

Niebuhr, C. M., van Dijk, M. and Bhagwan, J. N. (2019) 'Development of a design and implementation process for the integration of hydrokinetic devices into existing infrastructure in South Africa', Water SA, 45(3), pp. 434–446. doi: 10.17159/wsa/2019.v45.i3.6740.

Niebuhr, C. M., Schmidt, S., van Dijk, M., Smith, L., and Neary, V. S. (2022) 'A review of commercial numerical modelling approaches for axial hydrokinetic turbine wake analysis in channel flow', Renewable and Sustainable Energy Reviews. Elsevier Ltd, 158(March 2021), p. 112151. doi: 10.1016/j.rser.2022.112151.

Nishino, T. and Willden, R. H. J. (2012) 'Effects of 3-D channel blockage and turbulent wake mixing on the limit of power extraction by tidal turbines', International Journal of Heat and Fluid Flow. Elsevier Inc., 37, pp. 123–135. doi: 10.1016/j.ijheatfluidflow.2012.05.002.

Nishino, T. and Willden, R. H. J. (2013) 'Two-scale dynamics of flow past a partial cross-stream array of tidal turbines', pp. 220–244. doi: 10.1017/jfm.2013.340.

Nuernberg, M. and Tao, L. (2018) 'Experimental study of wake characteristics in tidal turbine arrays', Renewable Energy. Elsevier Ltd, 127(2018), pp. 168–181. doi: 10.1016/j.renene.2018.04.053.

Oggiano, L., Pierella, F., Nygaard, T. A., De Vaal, J., and Arens, E. (2017) 'Reproduction of steep long crested irregular waves with CFD using the VOF method', in Energy Procedia. Trondheim, Norway: Elsevier B.V., pp. 273–281. doi: 10.1016/j.egypro.2017.10.351.

Olczak, A., Stallard, T., Feng, T., and Stansby, P. K. (2016) 'Comparison of a RANS blade element model for tidal turbine arrays with laboratory scale measurements of wake velocity and rotor thrust', Journal of Fluids and Structures. Elsevier, 64, pp. 87–106. doi: 10.1016/j.jfluidstructs.2016.04.001.

Olivieri, D. and Ingram, D. (2013) Tidal array scale numerical modelling. Interactions within a farm (Unsteady Flow). Edinburgh.

Oppong, S., Lam, W. H., Guo, J., Tan, L. M., Ong C. O., Tey, W. Y., Lee, Y. F., Ujang, Z., Dai, M., Robinson, D., Hamill, G. (2020) 'Predictions of Wake and Central Mixing Region of Double Horizontal Axis Tidal Turbine', KSCE Journal of Civil Engineering, 24, pp. 1983–1995. doi: 10.1007/s12205-020-1910-4.

Pinon, G., Mycek, P., Germain, G., and Rivoalen, E. (2012) 'Numerical simulation of the wake of marine current turbines with a particle method', Renewable Energy, 46, pp. 111–126. doi: 10.1016/j.renene.2012.03.037.

Polagye, B. L. (2009) Hydrodynamic effects of kinetic power extraction by in-stream tidal turbines, Thesis/Dissertation. University of Washington.

Prosser, M. J. (1968) Propeller induced scour.

Pyakurel, P., Vanzwieten, J. H., Wenlong, T., and Ananthakrishnan, P. (2017) 'Analytic Characterization of the Wake Behind In-stream Hydrokinetic Turbines', Marine Technology Society Journal, 51(6), pp. 58–71.

Pyakurel, P., Tian, W., VanZwieten, J. H., and Dhanak, M. (2017) 'Characterization of the mean flow field in the far wake region behind ocean current turbines', Journal of Ocean Engineering and Marine Energy, 3(2), pp. 113–123. doi: 10.1007/s40722-017-0075-9.

Pyakurel, P., Vanzwieten, J. H., Dhanak, M., and Xiros, N. I. (2017) 'Numerical modeling of turbulence and its effect on ocean current turbines', International Journal of Marine Energy, 17, pp. 84–97. doi: 10.1016/j.ijome.2017.01.001.

Raichlen, F. (1967) 'Some Turbulence Measurements in Water', Journal of the Engineering Mechanics Division, 93(2), pp. 73–98.

Ranga Raju, K. G., Rana, O. P. S., Asawa, G. L., and Pillai, A. S. N. (1983) 'Rational assessment of blockage effect in channel flow past smooth circular cylinder', Journal of Hydraulic Research, 21(4), pp. 289–302. doi: 10.1080/00221688309499435.

Riglin, J., Carter, F., Oblas, N., Schleicher, W. C., Daskiran, C., and Oztekin, A. (2016) 'Experimental and numerical characterization of a full-scale portable hydrokinetic turbine prototype for river applications', Renewable Energy, 99, pp. 772–783.

Riglin, J. D. (2016) Design, Manufacture and Prototyping of a Hydrokinetic Turbine Unit for River Application. Lehigh University. Available at: http://preserve.lehigh.edu/etdhttp://preserve.lehigh.edu/etd/2747.

Roache, P. J. (1994) 'Perspective: A method for Uniform Reporting of Grid Refinement Studies', Journal of Fluids Engineering, Transactions of the ASME, 116(3), pp. 405–413.

Rose, S. M. (2018) In the Wake of a Tidal Turbine. University of Strathclyde.

Ross, H. and Polagye, B. (2020) 'An experimental assessment of analytical blockage corrections for turbines', Renewable Energy, 152, pp. 1328–1341.

Rowell, M. (2013) Experimental evaluation of a mixer-ejector marine hydrokinetic turbine at two open-water test sites and in a tow tank, Master's Theses and Capstones. doi: 10.4031/MTSJ.47.4.15.

Salunkhe, S., Fajri, O. El, Bhushan, S., Thompson, D., O'Doherty, D., O'Doherty, T., and Mason-Jones, A. (2019) 'Validation of tidal stream turbine wake predictions and analysis of

wake recovery mechanism', Journal of Marine Science and Engineering, 7(10). doi: 10.3390/jmse7100362.

Sanderse, B. (2009) Aerodynamics of wind turbine wakes: Literature review. doi: 10.1002/we.

Sanderse, B., van der Pijl, S. P. and Koren, B. (2011) 'Review of computational fluid dynamics for wind turbine wake aerodynamics', Wind Energy, 14, pp. 799–819. doi: 10.1002/we.

Sarkar, S. and Lakshmanan, B. (1991) 'Application of a Reynolds stress turbulence model to the compressible shear layer', AIAA Journal, 29(5), pp. 743–749. doi: 10.2514/3.10649.

Shen, W. Z., Mikkelsen, R. and Sorensen, J. N. (2005) 'Tip loss corrections for wind turbine Computations', Wind Energy, 8, pp. 457–475. doi: 10.1002/we.153.

Shives, M. and Crawford, C. (2014) 'Turbulence Modelling for Accurate Wake Prediction in Tidal Turbine Arrays', in 5th International Conference on Ocean Energy. Halifax, Canada.

Siddiqui, M. S., Rasheed, A. . di., Kvamsdal, T., and Tabib, M. (2017) 'Influence of Tip Speed Ratio on Wake Flow Characteristics Utilizing Fully Resolved CFD Methodology', Journal of Physics: Conference Series, 854(1). doi: 10.1088/1742-6596/854/1/012043.

Silva, P. A. S. F., De Oliveira, T. F., Brasil Junior, A. C. P., Vaz, J. R. P. P., Oliveira, T. F. D. E., Junior, A. C. P. B., and Vaz, J. R. P. P. (2016) 'Numerical Study of Wake Characteristics in a Horizontal-Axis Hydrokinetic Turbine', Annals of the Braziian Academy of Sciences, 88(4), pp. 2441–2456. doi: 10.1590/0001-3765201620150652.

Spalart, P. R. (2000) 'Strategies for Turbulence Modelling and Simulations', International Journal of heat and fluid flow, 21, pp. 252–263.

Spalart, P. R. and Rumsey, C. L. (2007) 'Effective inflow conditions for turbulence models in aerodynamic calculations', AIAA Journal, 45(10), pp. 2544–2553. doi: 10.2514/1.29373.

Speziale, C. G., Sarkar, S. and Gatski, T. B. (1991) 'Modelling the pressure-strain correlation of turbulence : An invariant dynamical systems approach', Journal of Fluid Mechanics, 227, pp. 245–272. doi: 10.1017/S0022112091000101.

Stallard, T., Collings, R., Feng, T., and Whelan, J. (2013) 'Interactions between tidal turbine wakes: Experimental study of a group of three-bladed rotors', Philosophical Transactions of the Royal Society A: Mathematical, Physical and Engineering Sciences, 371(1985). doi: 10.1098/rsta.2012.0159.

Stewart, D. P. J. (1992) Characteristics of a ship's screw wash and the influence of quay wall proximity, Doctoral dissertation, Queen's University of Belfast. Queen's University of Belfast.

Tedds, S. C., Owen, I. and Poole, R. J. (2014) 'Near-wake characteristics of a model horizontal axis tidal stream turbine', Renewable Energy. Elsevier Ltd, 63, pp. 222–235. doi: 10.1016/j.renene.2013.09.011.

Tian, L., Zhu, W., Shen, W., Zhao, N., and Shen, Z. (2015) 'Development and validation of a new two-dimensional wake model for wind turbine wakes', Journal of Wind Engineering and Industrial Aerodynamics, 137, pp. 90–99. doi: 10.1016/j.jweia.2014.12.001.

Tian, W., Mao, Z. and Ding, H. (2018) 'Design, test and numerical simulation of a low-speed horizontal axis hydrokinetic turbine', International Journal of Naval Architecture and Ocean Engineering, 10, pp. 782–793.

Turnock, S. R., Phillips, A. B., Banks, J., and Nicholls-Lee, R. (2011) 'Modelling tidal current turbine wakes using a coupled RANS-BEMT approach as a tool for analysing power capture of arrays of turbines', Ocean Engineering, 38(11–12), pp. 1300–1307. doi: 10.1016/j.oceaneng.2011.05.018.

Vermeer, L. J., Sørensen, J. N. and Crespo, A. (2003) 'Wind turbine wake aerodynamics', Progress in Aerospace Sciences, 39(6–7), pp. 467–510. doi: 10.1016/S0376-0421(03)00078-2.

Walker, J., Flack, K., Lust, E., MP, S., and Luznik, L. (2014) 'Experimental and numerical studies of blade roughness and fouling on marine current turbine performance', Renewable Energy, 66, pp. 257–267.

Wallin, S. and Johansson, A. V. (2000) 'An explicit algebraic Reynolds stress model for incompressible and compressible turbulent flows', Journal of Fluid Mechanics, 403, pp. 89–132. doi: 10.1017/S0022112099007004.

Wang, S., Lam, W. H., Cui, Y., Zhang, T., Jiang, J., Sun, C., Guo, J., Ma, Y., Hamill, G. (2018) 'Novel energy coefficient used to predict efflux velocity of tidal current turbine', Energy, 158, pp. 730–745. doi: 10.1016/j.energy.2018.06.032.

Werle, M. J. (2010) 'Wind turbine wall-blockage performance corrections', Journal of Propulsion and Power, 26(6), pp. 1317–1321. doi: 10.2514/1.44602.

Whale, J., Papadopoulos, K. H., Anderson, C. G., Skyner, D. J., and Helmis, C. G. (1996) 'A study of the near wake structure of a wind turbine comparing measurements from laboratory and full-scale experiments', Solar Energy, 56(6), pp. 621–633.

Whale, J., Anderson, C. G., Bareiss, R., and Wagner, S. (2000) 'An experimental and numerical study of the vortex structure in the wake of a wind turbine', Journal of Wind Engineering and Industrial Aerodynamics, 84(1), pp. 1–21. doi: 10.1016/S0167-6105(98)00201-3.

Whelan, J. I., Graham, J. M. R. R., Peiro, J., and Peiró, J. (2009) 'A free-surface and blockage correction for tidal turbines', Journal of Fluid Mechanics, 624, pp. 281–291. doi: 10.1017/S0022112009005916.

Wilcox, D. (1994) Modelling for CFD. 2nd edn. DCW Industries inc.

Yarnell, D. (1934) Bridge piers as channel obstructions. Washington, D.C: United States Department of Agriculture.

Yuce, M. I. and Muratoglu, A. (2015) 'Hydrokinetic energy conversion systems : A technology status review', Renewable and Sustainable Energy Reviews. Elsevier, 43, pp. 72–82. doi: 10.1016/j.rser.2014.10.037.

Zhang, Y., Zhang, J., Lin, X., Wang, R., Zhang, C., and Zhao, J. (2020) 'Experimental investigation into downstream field of a horizontal axis tidal stream turbine supported by a mono pile', Applied Ocean Research. Elsevier, 101(June), p. 102257. doi: 10.1016/j.apor.2020.102257.

Appendix A:

Input variables and grid convergence details of CFD case studies

A-1. CFD model input details

This section includes the necessary input details for the computational fluid dynamics models used, specifically pertaining to blade profile details and airfoil properties..

A-1.1. RM1 turbine model (T1)

The RM1 turbine was simulated to replicate laboratory test conditions. Various CFD approaches were compared, mainly turbulence models. The final modelling approach adopted a BEM-CFD RSM model (specifically the Linear Pressure Strain 2-layer model). This required input of turbine geometry and airfoil characteristics including lift and drag coefficients (C_L and C_D values).

For the full rotor geometry modelling the full CAD geometry of the rotor was included in the model. For the virtual disk approach, a set of input parameters was required. These are shown in Table A-1, and the airfoil properties generated through XFOIL software are shown in Figure A-1 and Figure A-2.

Table A-1: RM1 blade properties (Hill *et al.*, 2014)

r/R	Radius (mm)	Twist (rad)	Chord (m)	Thickness (m)	t/c (%)
0.21	53.3	0.22968533	0.0300	0.0300	100
0.24	60	0.22968533	0.0300	0.0300	100
0.27	66.7	0.22968533	0.0342	0.0290	84.9
0.29	73.3	0.22968533	0.0468	0.0242	51.8
0.32	80	0.22968533	0.0572	0.0178	31.1
0.35	86.7	0.22968533	0.0626	0.0121	19.4
0.37	93.3	0.22968533	0.0645	0.0097	15
0.40	100	0.19687314	0.0644	0.0097	15
0.43	106.7	0.17872171	0.0632	0.0095	15
0.45	113.3	0.16458454	0.0615	0.0092	15
0.48	120	0.15289084	0.0595	0.0089	15
0.51	126.7	0.14259340	0.0574	0.0086	15
0.53	133.3	0.13334315	0.0553	0.0083	15
0.56	140	0.12496557	0.0532	0.0080	15
0.59	146.7	0.11693706	0.0511	0.0077	15
0.61	153.3	0.10943214	0.0492	0.0074	15
0.64	160	0.10227629	0.0473	0.0071	15
0.67	166.7	0.09529497	0.0456	0.0068	15
0.69	173.3	0.08848819	0.0440	0.0066	15
0.72	180	0.08185594	0.0424	0.0064	15
0.75	186.7	0.07522369	0.0409	0.0061	15
0.77	193.3	0.06859144	0.0395	0.0059	15
0.80	200	0.06195918	0.0382	0.0057	15
0.83	206.7	0.05532693	0.0370	0.0055	15
0.85	213.3	0.04852015	0.0358	0.0054	15
0.88	220	0.04153883	0.0346	0.0052	15
0.91	226.7	0.03455751	0.0335	0.0050	15
0.93	233.3	0.02740166	0.0323	0.0049	15
0.96	240	0.01989675	0.0312	0.0047	15
1.00	250	0.01221730	0.0300	0.0045	15
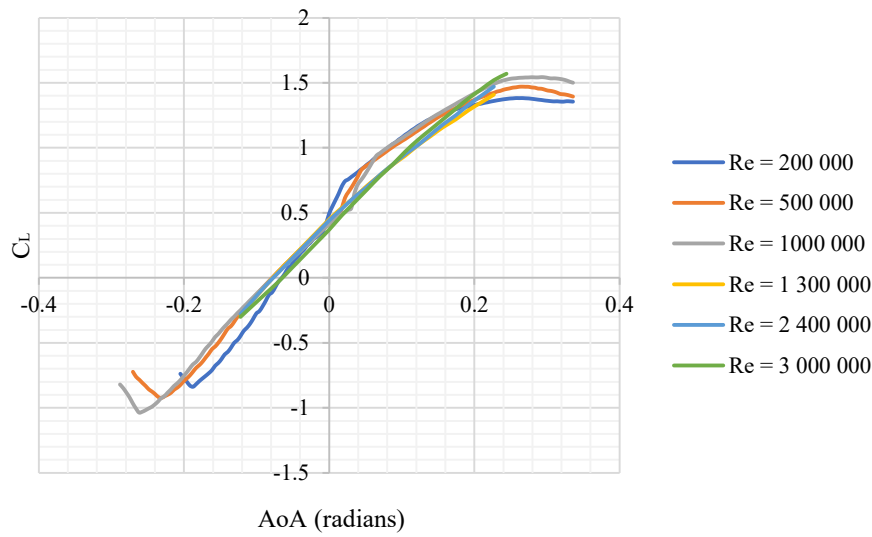
Figure A-1: NACA 4415 C_L over AoA (sourced from: XFOIL)
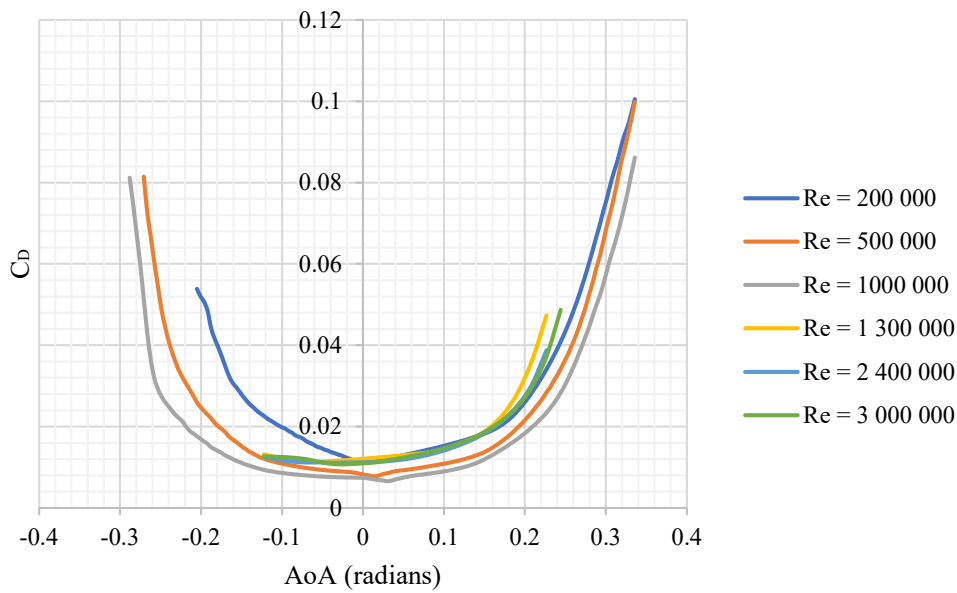
Figure A-2: NACA 4415 C_D over AoA (sourced from: XFOIL)

A-2.1 IFREMER LOMC turbine model (T2)

The IFREMER turbine model was constructed using the same CFD approach that was determined to be the most effective for the RM1 turbine case.

The BEM component required geometric details as shown in Table A-2.

The lift and drag coefficients included in the model were a combination of results sourced from a numerical study on the blade profile (Zhuang *et al.*, 2012) and results generated in XFOIL software (Figure A-3 and Figure A-4).

Table A-2: IFREMER LOMC blade properties (Mycek *et al.*, 2014)

r/R	Radius (mm)	c/R	Chord (m)	Pitch (rad)	T/c (%)
0.1333	46.7	0.0567	0.0198	0.5160	80
0.15	52.5	0.0567	0.0198	0.5160	100
0.155	54.3	0.0567	0.0198	0.5160	100
0.1983	69.4	0.1521	0.0532	0.4473	36
0.2417	84.6	0.2474	0.0866	0.3866	21.3
0.285	99.8	0.2375	0.0831	0.3369	21.4
0.3283	114.9	0.2259	0.0791	0.2962	21.7
0.3717	130.1	0.2141	0.0749	0.2627	22
0.415	145.3	0.2029	0.0710	0.2349	22.2
0.4583	160.4	0.1925	0.0674	0.2115	22.4
0.5017	175.6	0.1829	0.0640	0.1917	22.5
0.545	190.8	0.1743	0.0610	0.1747	22.5
0.5883	205.9	0.1665	0.0583	0.1602	22.4
0.6317	221.1	0.1594	0.0558	0.1475	22.2
0.675	236.3	0.1529	0.0535	0.1365	21.9
0.7183	251.4	0.1471	0.0515	0.1268	21.5
0.7617	266.6	0.1418	0.0496	0.1182	20.9
0.805	281.8	0.137	0.0480	0.1106	20.2
0.8483	296.9	0.1325	0.0464	0.1039	19.5
0.8917	312.1	0.1285	0.0450	0.0978	18.6
0.935	327.3	0.1247	0.0436	0.0924	18
0.9783	342.4	0.1213	0.0425	0.0875	18
1	350.0	0.0655	0.0229	0.0851	25
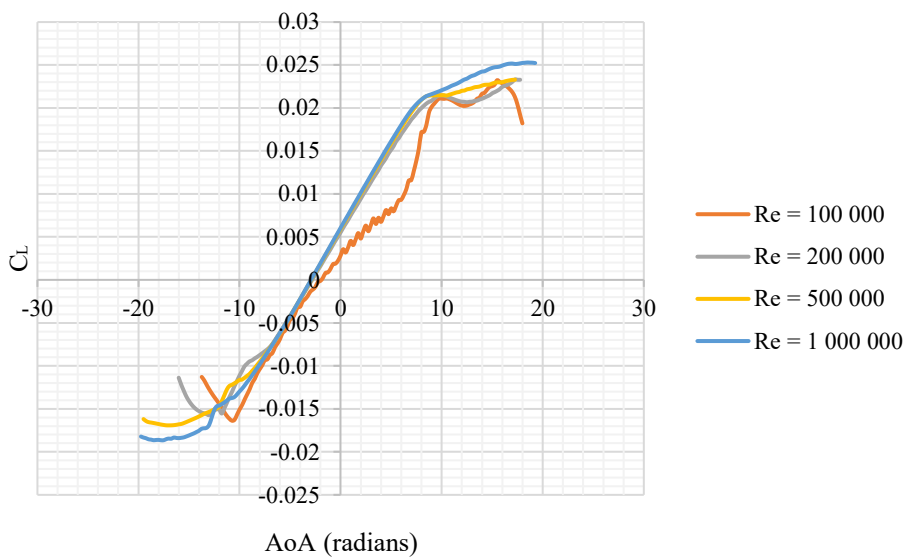
Figure A-3: NACA 63418 C_L over AoA (sourced from XFOIL and Zhuang et al. (2012))
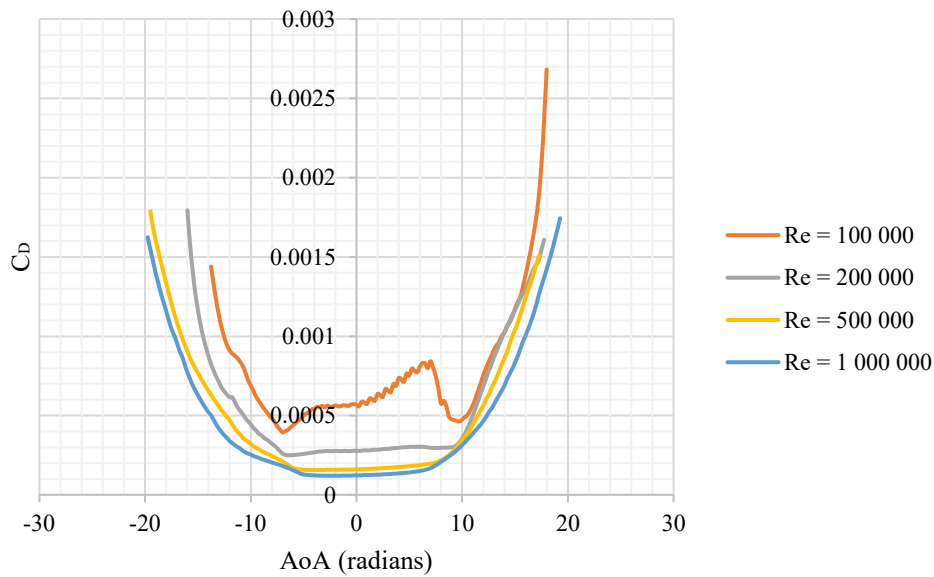
Figure A-4: NACA 63418 C_D over AoA (sourced from XFOIL and Zhuang et al. (2012))

A-3.1 Liverpool University turbine model (T3)

Geometric input parameters for the Liverpool University turbine are shown in Table A-3. Multiple pitch angles were tested, and different pitch angles were used for the benchmark validation of specific experimental results. For all tests used in the study the optimum pitch angle of 6 degrees (as found in the laboratory testing by Mason-Jones (2010) and Morris (2014)). The airfoil properties implemented in the model are shown in Figure A-5 and Figure A-6.

Table A-3: Liverpool University turbine blade properties (at various pitch angles)

| r/R | Radius (mm) | Baseline Pitch (rad) | Other pitch angles (degrees) | | | | | | | | | Chord (mm) |
			2	3	4	5	5.5	6	8	9	10	
0.989	247.25	1.570796	88	87	86	85	84.5	84	82	81	80	0.0295
0.912	228	1.566433	87.75	86.75	85.75	84.75	84.25	83.75	81.75	80.75	79.75	0.03165
0.836	209	1.54898	86.75	85.75	84.75	83.75	83.25	8275	80.75	79.75	78.75	0.035
0.76	190	1.51512	84.81	83.81	8281	81.81	81.31	80.81	78.81	77.81	76.81	0.03904
0.684	171	1.474454	8248	81.48	80.48	79.48	78.98	78.48	76.48	75.48	74.48	0.04525
0.608	152	1.424014	79.59	78.59	77.59	76.59	76.09	75.59	73.59	7259	71.59	0.056
0.53	132.5	1.368338	76.4	75.4	74.4	73.4	729	724	70.4	69.4	68.4	0.0635
0.454	113.5	1.303935	7271	71.71	70.71	69.71	69.21	68.71	66.71	65.71	64.71	0.07
0.378	94.5	1.224174	68.14	67.14	66.14	65.14	64.64	64.14	6214	61.14	60.14	0.0745
0.302	75.5	1.116836	61.99	60.99	59.99	58.99	58.49	57.9	55.99	54.99	53.99	0.0755
0.226	56.5	0.979304	54.11	53.11	5211	51.11	50.61	50.11	48.11	47.11	46.11	0.075
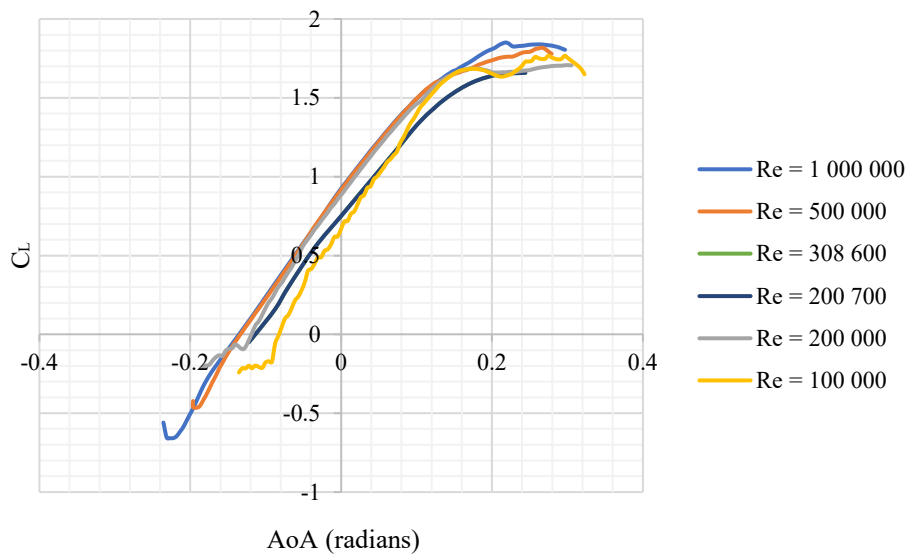
Figure A-5: FX 63-137 C_L over AoA (sourced from: XFOIL)
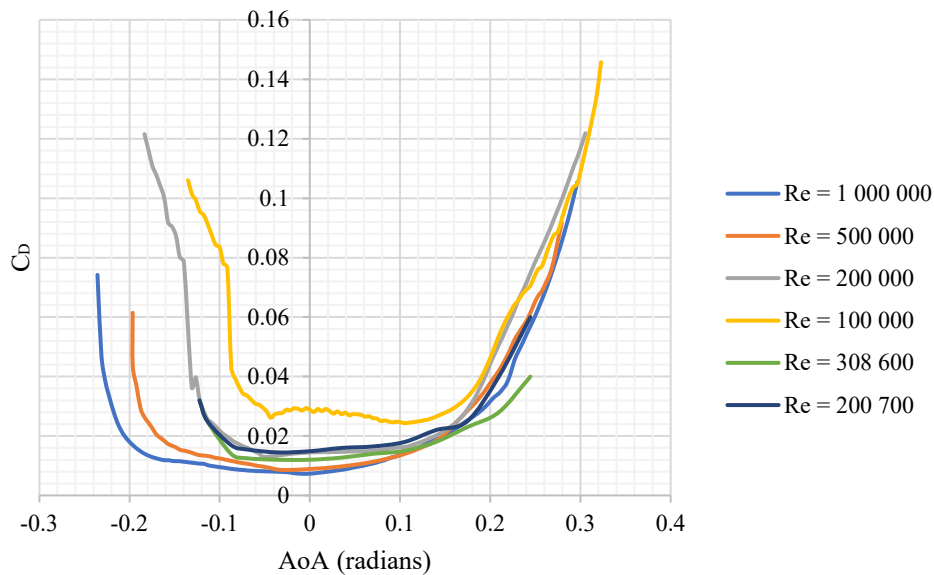
Figure A-6: FX 63-137 C_D over AoA (sourced from: XFOIL)

A-4.1 BBMC turbine model (T4)

The BBMC turbine blades were manufactured through interpolated coordinate-based data for NACA 63-812, 63-815, 63-818, 63-821 and 638-24 profiles (Final propeller details are shown in Table A-4). Lift and drag measurements were collected from published XFOIL results (Bahaj, Batten and McCann, 2009). The C_D and C_L coefficients are shown on Figure A-7 and Figure A-8.

Table A-4: Turbine blade and hub details (Bahaj et al., 2005)

r/R	Radius (mm)	c/R (%)	Pitch (degrees)	t/c (%)
0.20	80	0.125	15	24.0
0.25	100	0.116	12.1	22.5
0.30	120	0.1203	9.5	20.7
0.35	140	0.1156	7.6	19.5
0.40	160	0.1063	6.1	18.7
0.45	180	0.1016	4.9	18.1
0.50	200	0.0969	3.9	17.6
0.55	220	0.0922	3.1	17.1
0.60	240	0.0875	2.4	16.6
0.65	260	0.0828	1.9	16.1
0.70	280	0.0781	1.5	15.6
0.75	300	0.0734	1.2	15.1
0.80	320	0.0688	0.9	14.6
0.85	340	0.0641	0.6	14.1
0.90	360	0.0594	0.4	13.6
0.95	380	0.0547	0.2	13.1
1.00	400	0.05	0.0	12.6
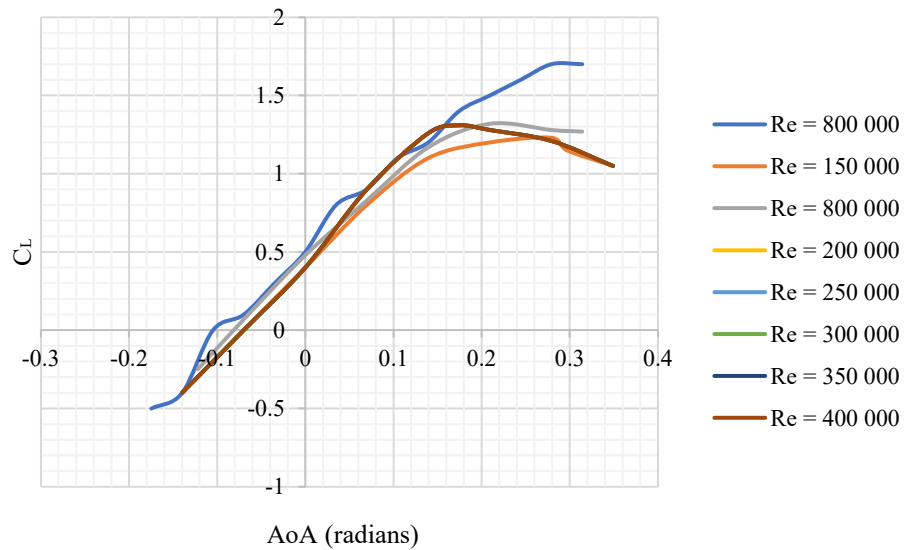
Figure A-7: C_L over AoA (sourced from results generated by Bahaj, Batten and McCann, (2009))
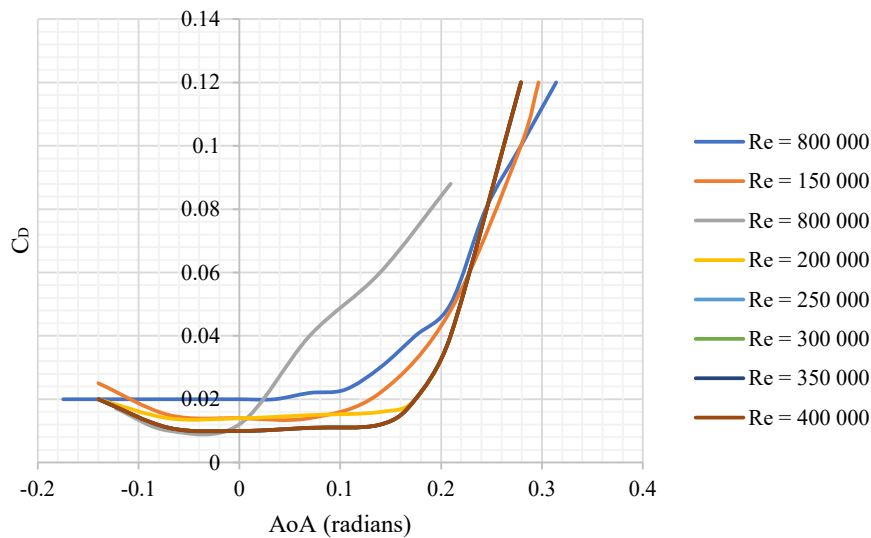
Figure A-8: C_D over AoA (sourced from results generated by Bahaj, Batten and McCann, (2009))

A-2. Grid independence study

Multiple grid independence studies were completed during the study. For initial testing a very fine grid was used, and the grid was varied to the specific requirements of the turbulence model employed. As models with higher rotation rates, inlet velocities or input turbulence values were modelled, a sensitivity study on a finer mesh was completed to ensure the mesh resolution is adequate.

An example of the grid study is shown in Table A-5 for the SST k-ω model case. Larger mesh sizes were required to capture the FRG modelling technique. The importance of the fine mesh resolution for the FRG models can be seen in the vorticity plots on Figure A-9. All FRG models ensured fine meshes as described in the dissertation.

Table A-5: RM1 validation case single phase model using full rotor geometry modelling and the SST k-ω model.

		Mesh 1	Mesh 2	Mesh 3	Mesh 4
	Base size (m)	0.07	0.07	0.07	0.07
	VC1 (m)	0.0063	0.0049	0.0042	0.0035
	VC2 (m)	0.0119	0.0065	0.0084	0.007
	VC3 (m)	0.0189	0.0154	0.0126	0.0105
	No of cells	5 910 121	9 729 511	15 287 880	25 114 182
	Torque left rotor	2.47	2.46	2.45	2.45
	Torque right roto	2.47	2.45	2.45	2.45
Left rotor					
Average velocities (m/s)	Vel 2D	0.72	0.72	0.73	0.75
	Vel 4D	0.86	0.85	0.91	0.90
	Vel 6D	0.93	0.93	0.98	0.97
	Vel 8D	0.94	0.97	0.99	0.98
Right rotor					
Average velocities (m/s)	Vel 2D	0.72	0.72	0.73	0.75
	Vel 4D	0.86	0.87	0.85	0.91
	Vel 6D	0.94	0.93	0.98	0.97
	Vel 8D	0.95	0.96	0.99	0.98
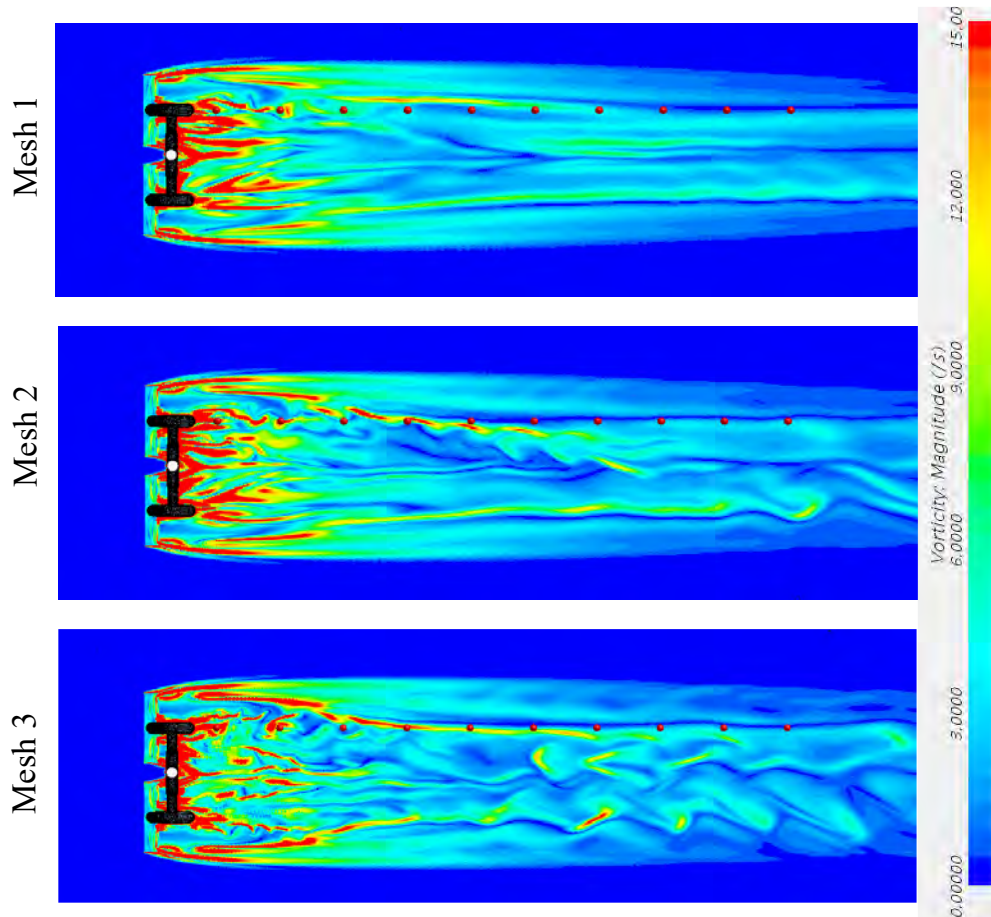
Figure A-9: FRG SST k-ω model wake vorticity comparison over mesh resolution.

It was determined that a lower resolution mesh was sufficient when using the selected turbulence model (Reynolds stress LPS 2-layer model) in conjunction with the VD blade modelling technique (details in Table A-6). A final mesh of around 15 million cells (Mesh 3) was selected for the model analysis.

Table A-6: Grid study using a VD-CFD approach with a LPS2 turbulence model.

		Mesh 1	Mesh 2	Mesh 3	Mesh 4
	Base size (m)	0.075	0.068	0.06	0.0525
	VC1 (m)	0.007	0.006	0.005	0.005
	VC2 (m)	0.010	0.009	0.008	0.007
	VC3 (m)	0.015	0.014	0.012	0.011
	No of cells	4 322 556	8 794 523	13 889 123	26 582 451
	Torque left rotor	2.03	2.04	2.04	2.04
	Torque right rotor	2.03	2.04	2.04	2.04
Left rotor					
Average velocities (m/s)	Vel 2D	0.61	0.60	0.61	0.61
	Vel 4D	0.73	0.73	0.75	0.75
	Vel 6D	0.83	0.84	0.85	0.85
	Vel 8D	0.90	0.90	0.90	0.90
Right rotor					
Average velocities (m/s)	Vel 2D	0.61	0.60	0.61	0.61
	Vel 4D	0.73	0.73	0.75	0.75
	Vel 6D	0.83	0.84	0.85	0.85
	Vel 8D	0.90	0.91	0.90	0.90

For the multiphase models, grid independence was focussed on the free surface. The same grid properties as those for Mesh 3 were applied and only the free surface was refined. The results can be seen in Figure A-10. Very little difference in free surface behaviour was observed. However, there were slight differences in deformation downstream of the stanchion structure only visible when utilising Mesh 2 and 3. Therefore the Mesh 2 properties were selected for the final mesh.
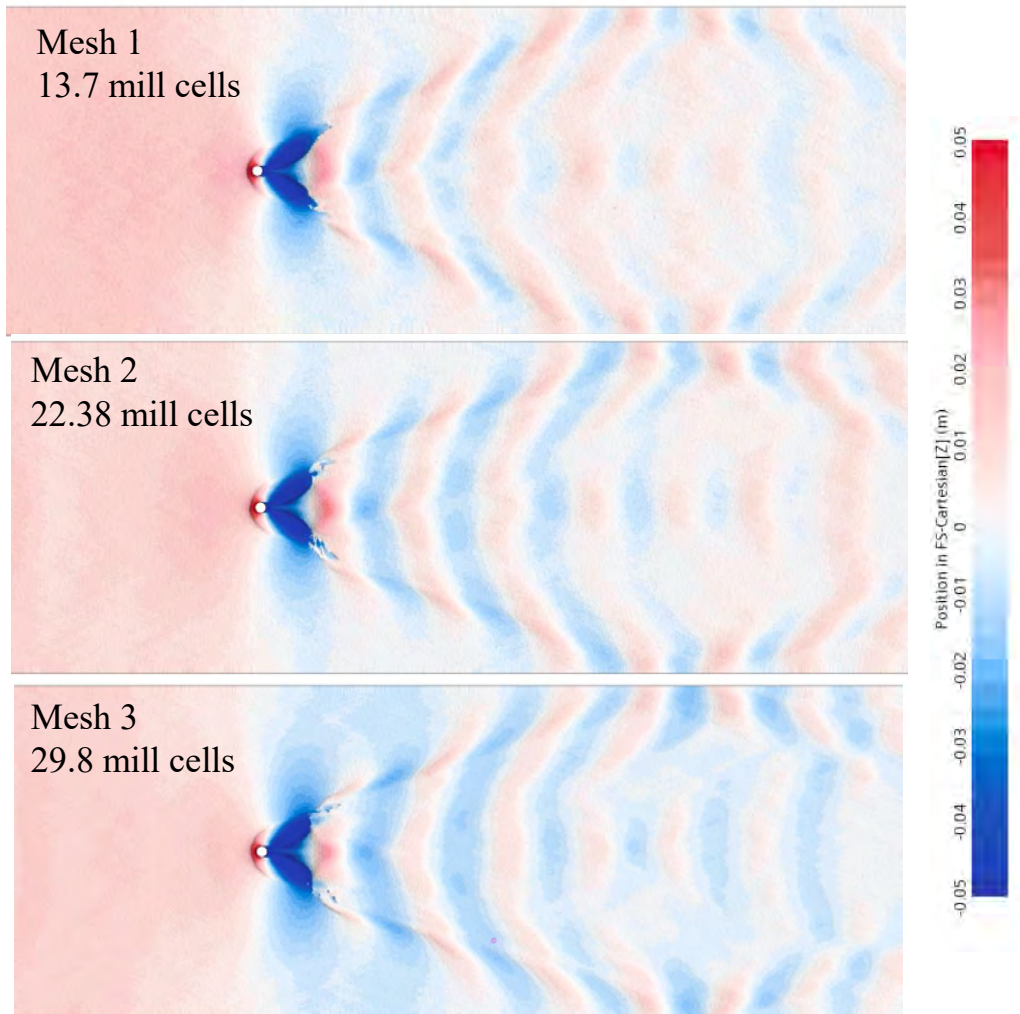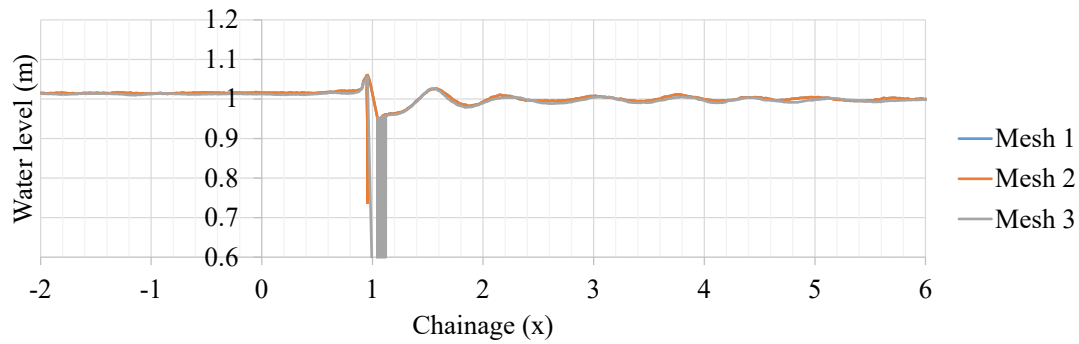
Figure A-10: Free surface grid convergence check, VOF-BEM CFD model

For the IFREMER LOMC turbine testes (T2), the same mesh resolution relative to the rotor diameter was used. Due to the significantly slower rotation rate (and tip speed ratio) compared to the RM1 case study, it was conjectured that a finer mesh, as determined in the RM1 study, would not be necessary to capture the flow effect. However, to ensure this is a true deduction of the behaviour a finer mesh (mesh 2 and 3) was compared to ensure the assumption holds. This proved the adequacy of a courser mesh for wake behaviour, however more accurate performance results were possible when a finer mesh was used to model the flow around the blades.

Careful consideration to the higher turbulence case was ensured (Table A-7 and Figure A-11). As a finer resolution mesh may be required to adequately capture the flow effects of the highly turbulence flow. This was also found to limit the over-dissipative behaviour of the inflow TI specified. To ensure consistency and no error in mesh results for the lower TI cases the high-resolution mesh was kept consistent for all results (final mesh: Mesh 2).

Table A-7: T2 modelled at TI=15%

		Mesh 1	Mesh 2	Mesh 3
	Base size (m)	0.06	0.0525	0.045
	VC1 (m)	0.0055	0.0048125	0.004125
	VC2 (m)	0.012	0.0105	0.009
	VC3 (m)	0.045	0.039375	0.03375
	No. of cells	11 771 782	17 924 502	23 859 452
	Torque (N.m)	5.65	5.76	5.76
Avg vel def (Vx)	Vel 2D	0.23	0.23	0.23
	Vel 4D	0.15	0.15	0.15
	Vel 6D	0.10	0.10	0.11
	Vel 8D	0.07	0.07	0.07
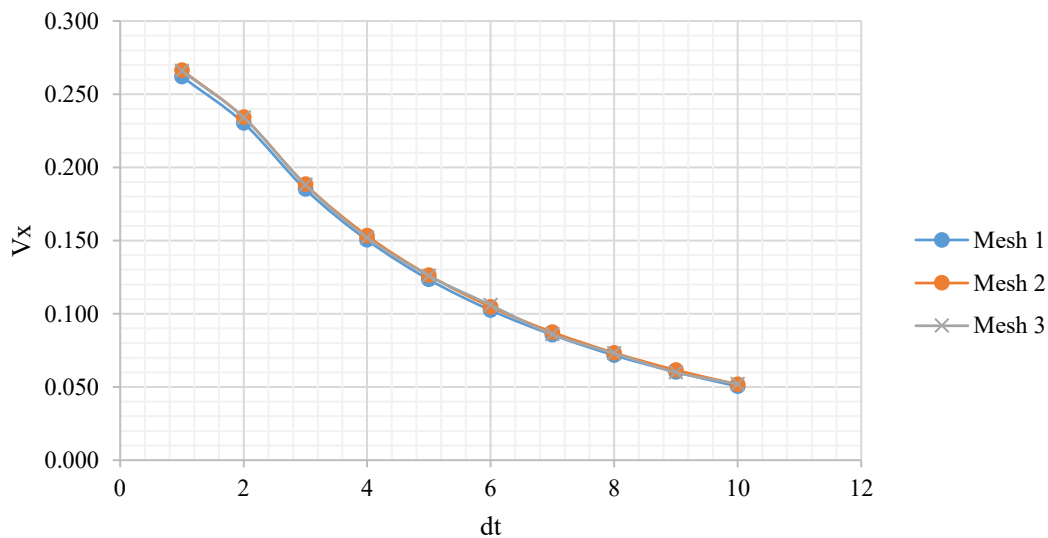
Figure A-11: T2 mesh wake deficit for TI=15%

Where domain and operational conditions allowed lower resolution meshes, additional grid tests and result comparisons were carried out to optimize computational usage. The mesh resolution for the T3 turbine can be seen in Table A-8 and Figure A-12. This indicated a mesh larger than the characteristics of mesh 2 is not favourable.

Table A-8: T3 mesh resolution check

	Mesh 1	Mesh 2	Mesh 3
Base size (m)	0.06	0.0525	0.045
VC1 (m)	0.0055	0.0048125	0.004125
VC2 (m)	0.012	0.0105	0.009
VC3 (m)	0.045	0.039375	0.03375
No. of cells	5 749 482	11 180 664	17 628 517
Torque (N.m)	2.52	2.71	2.71

		Mesh 1	Mesh 2	Mesh 3
Avg vel def (Vx)	**Vel 2D**	0.52	0.56	0.57
	Vel 4D	0.32	0.37	0.38
	Vel 6D	0.18	0.21	0.22
	Vel 8D	0.12	0.13	0.13
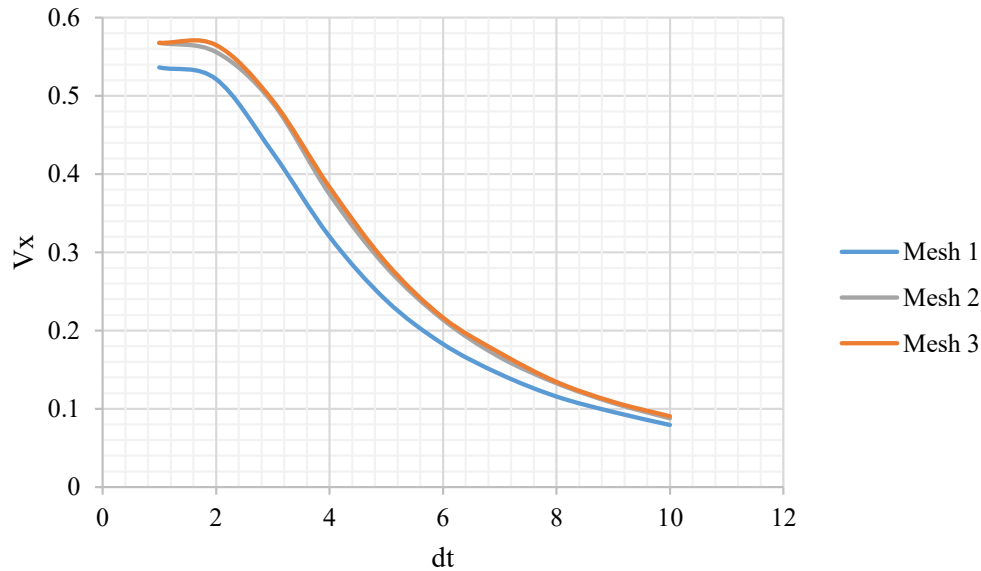
Figure A-12: T3 wake velocity deficit mesh comparison.

In order to address discrepancies observed between steady-state and transient results, mesh convergence tests were conducted exclusively on transient models. This approach imposed a significant computational demand. To optimize computational resources, an adaptive procedure was employed wherein mesh results from previous models served as the foundation for subsequent models. This enabled an efficient utilization of computational resources.

Appendix B:

Wake model determination

B-1. Collection of experimental wake data

The experimental cases tested using the verified CFD approach described in the study are summarized in Table B-1.

Table B-1: Overview of CFD test cases

No.	Turbine	D (m)	U_∞ (m/s)	TI (%)	β (%)
1	T1_2b.1	0.5	1.05	2.7	7.1
2	T1_2b.2	0.5	1.05	7.0	7.1
3	T1_2b.3	0.5	1.05	11.0	7.1
4	T3_2b.1	0.5	1.00	4.5	7.0
5	T3_2b.2	0.5	1.00	4.5	16.5
6	T2_3b.1	0.7	0.80	3.7	4.0
7	T2_3b.2	0.7	0.80	16.0	4.0
8	T2_3b.3	0.7	0.80	3.7	13.0
9	T2_3b.4	0.7	0.80	3.0	4.0
10	T2_3b.5	0.7	0.83	15.0	4.0
11	T2_3b.6	0.7	0.80	5.0	22.7
12	T3_3b.1	0.5	1.00	4.5	7.0
13	T3_3b.2	0.5	1.00	4.5	16.0
14	T3_3b.3	0.5	1.00	13.0	16.0
15	T3_3b.4	0.5	1.00	11.5	7.0
16	T3_3b.5	0.5	1.00	13.0	7.0
17	T4_3b.1	0.8	1.36	2.7	7.0
18	T4_3b.2	0.8	1.36	8.9	17.5
19	T4_3b.3	0.8	1.36	2.7	17.5
20	T3_4b.1	0.5	1.00	2.6	16.5
21	T3_4b.2	0.5	1.00	9.3	16.5
22	T3_4b.3	0.5	1.00	4.8	7.0

B-2. Testing of developed model

Figure B-1 to Figure B-6 visually depict the prediction results of wake development, as calculated by the development wake model outlined in Section 4-CALC TX_XX for various test cases. These are compared to experimental measurements of the wake deficits for each test case (TX_XX).
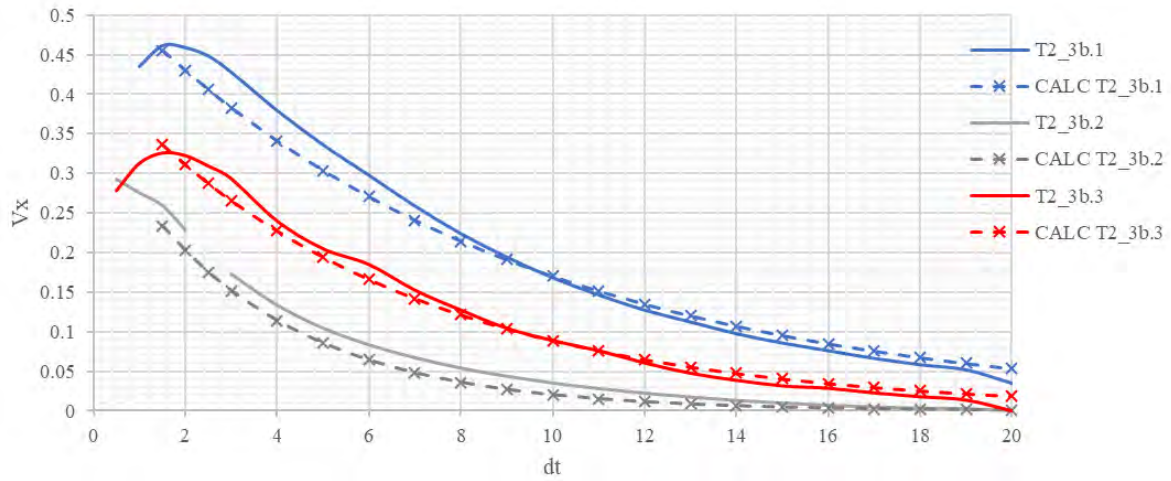
Figure B-1: T2_3b tests
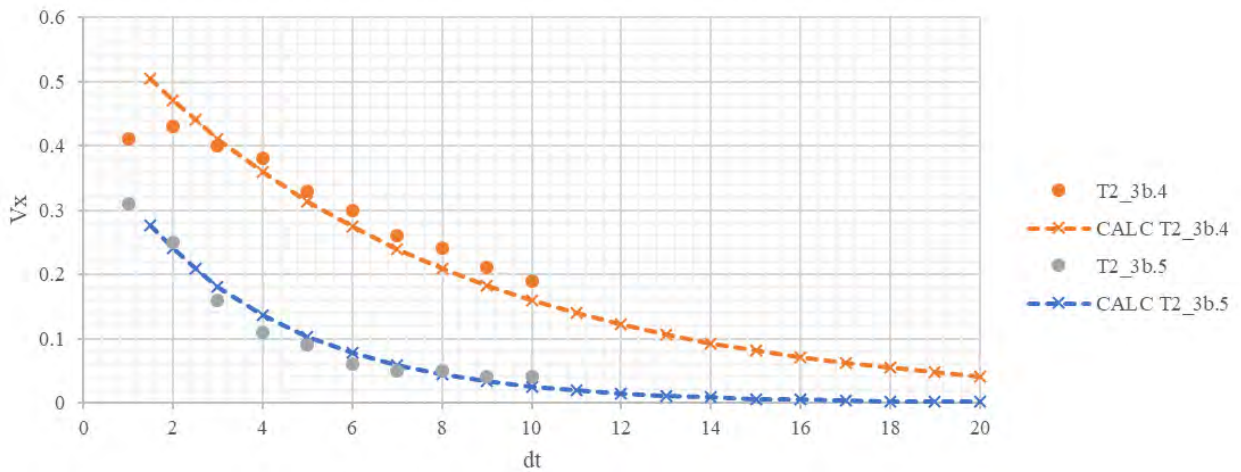
Figure B-2: T2_3b Literature result comparison (experimental results from Mycek et al., (2014))
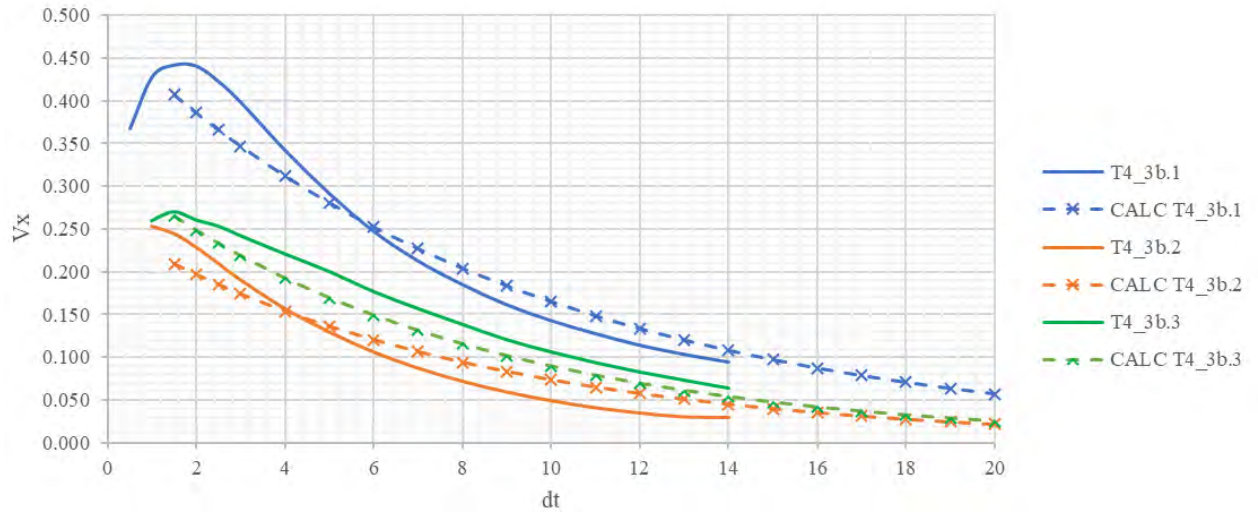
Figure B-3: T4_3b tests
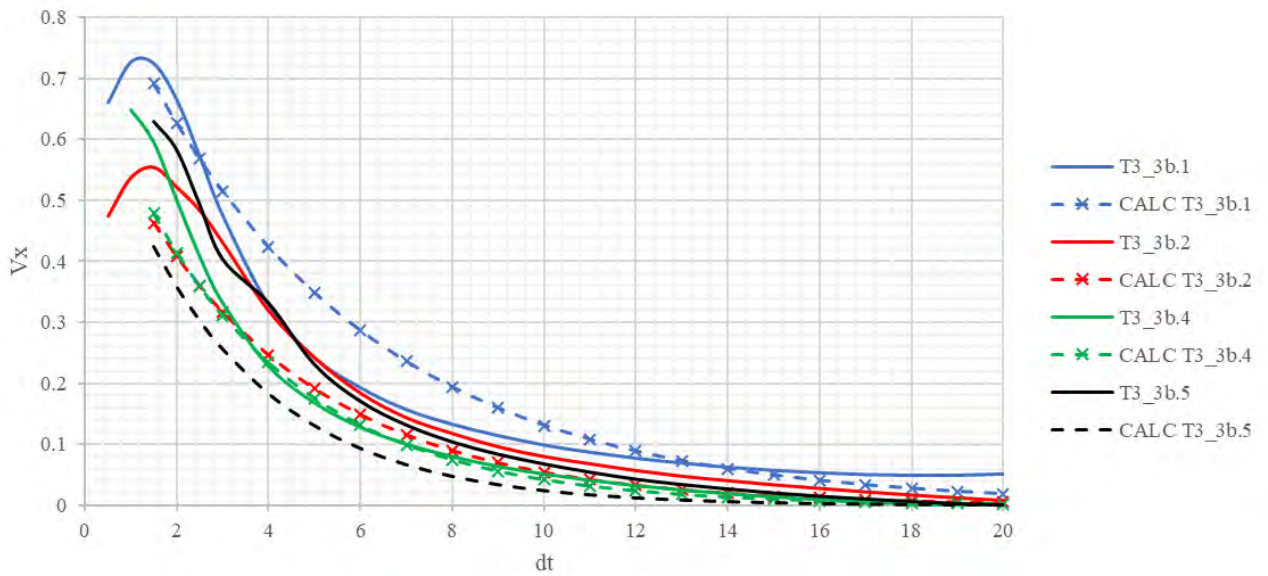
Figure B-4: T3_3b tests
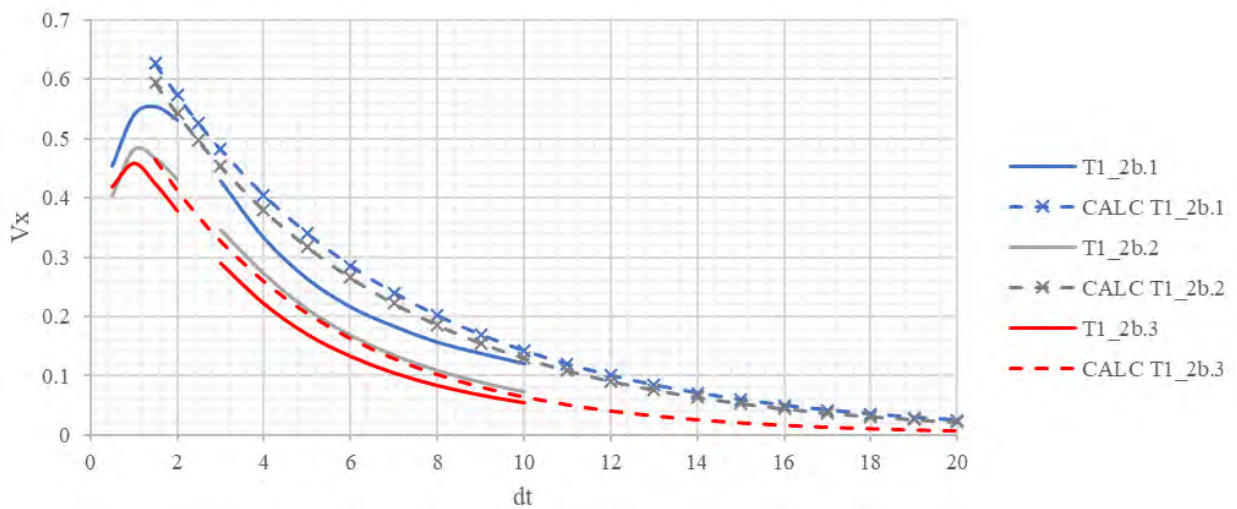
Figure B-5: T1_2b tests
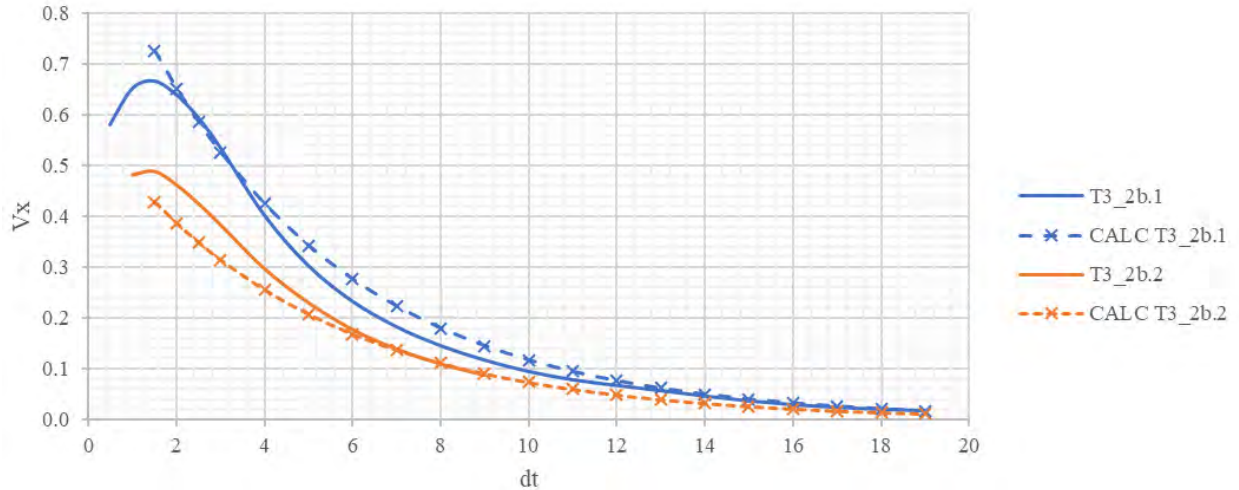
Figure B-6: T3_2b tests

B-3. Comparative results to approaches found in literature

Prior to developing a new approach to predict the wake behind a HAHT, existing approaches were continuously tested (as described in the dissertation). A visual and quantitative representation of the comparisons mentioned in the study are included here as reference for the statements made with regard to model behaviour and accuracy. All existing turbine tests used in the study are shown in Table B-2, the laboratory test conditions are also included.

To initiate the study, a preliminary comparative analysis was conducted, which involved evaluating wake prediction models documented in literature, against a set of published experimental results. This analysis served as an initial step in assessing the performance and accuracy of the models by comparing their predictions to the experimental data. This provided a basis for the study development and ascertained the need for a new model development which included a larger dataset and input parameters. The experimental dataset used for this analysis is shown graphically in Figures B-7 to B-10. An overview of the overall error in velocity deficit prediction is summarized in Table B-3.

Table B-2: Experimental results used for the first order analysis.

Result name	Exp 1	Exp 2	Exp 3	Exp 4a	Exp 4b
Test turbine and literature reference	IFREMER LOMC (T2) (Mycek *et al.*, 2014)		BBMC (T4) (Myers and Bahaj, 2009; Bahaj and Myers, 2013)	RM1 Right Rotor (Hill *et al.*, 2014)	RM1 Left Rotor Hill *et al.*, 2014)
Turbulence (%)	3	15	6	5	5
Inflow velocity (m/s)	0.8	0.83	0.8	1.05	1.05
C_T	0.82	0.82	0.77	0.52	0.52
Diameter (m)	0.7	0.7	0.8	0.5	0.5
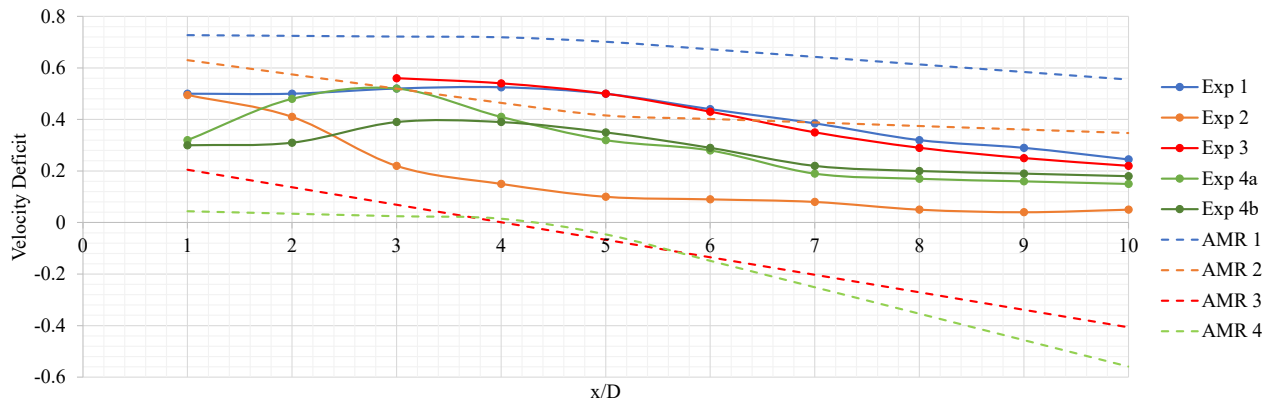
Figure B-7: Comparative analysis to the analytical model result (AMR) by Wang et al., (2018)
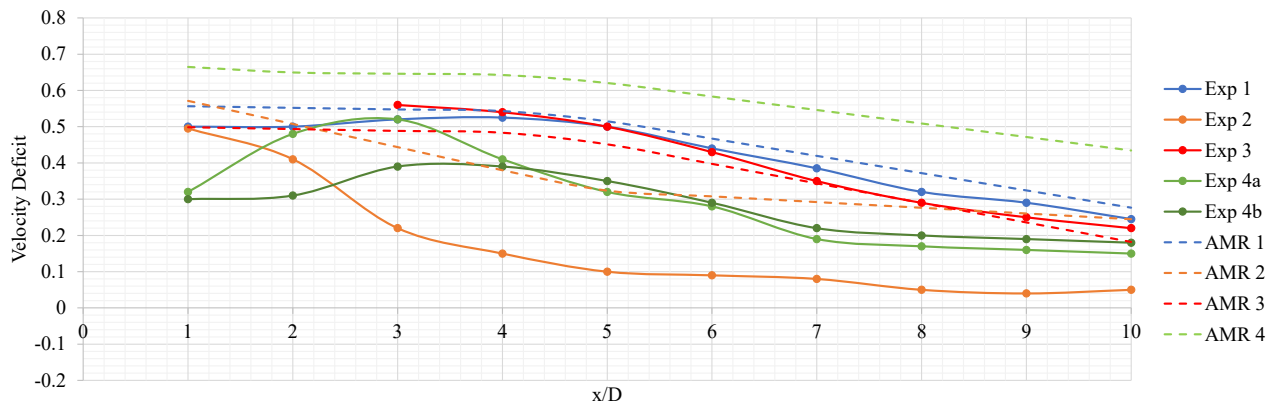
Figure B-8: Comparative analysis to the analytical model result (AMR) by Lam & Chen (2014)
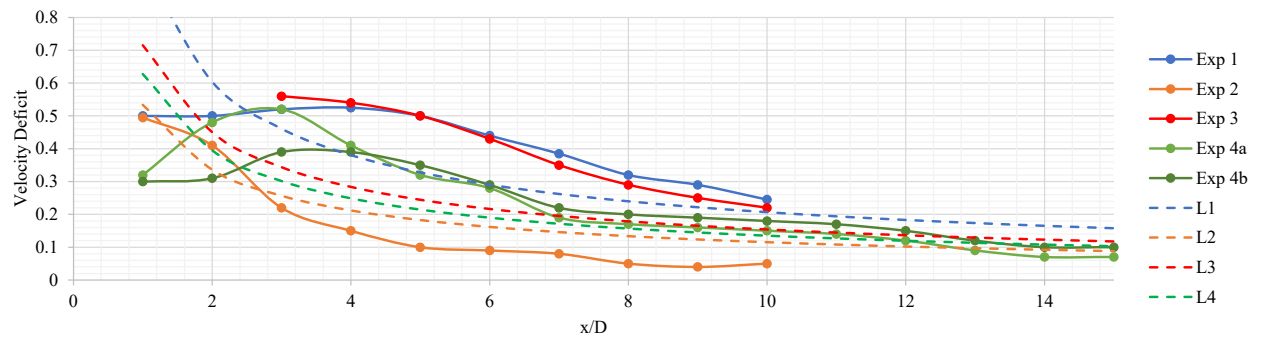
Figure B-9: Comparative analysis to the adapted Larson model result (L) by Pyakurel et al. (2017)
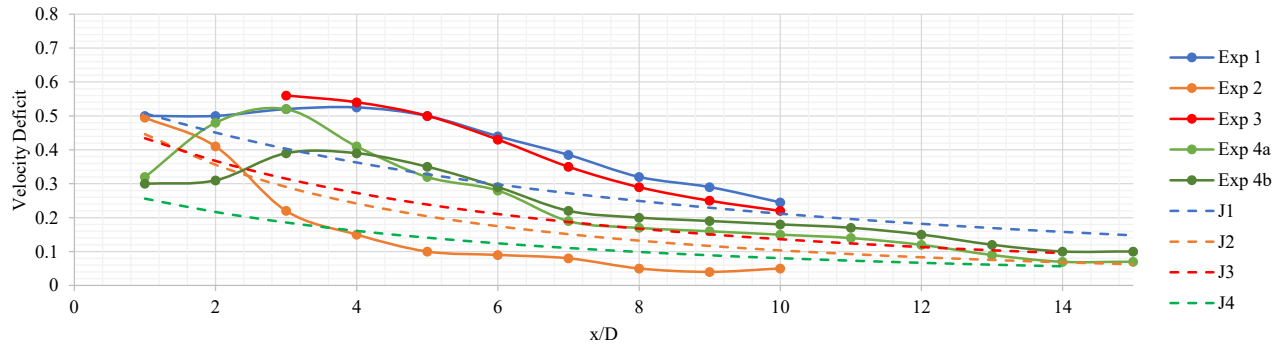
Figure B-10: Comparative analysis to the adapted Jenson model result (J) by Pyakurel et al. (2017)

Table B-3: Quantitative comparison on wake model predictions

Model used	Comparison		Error in data comparison (% of V_x)		
	Exp test Case	Model test case	V_{min} error	Max error between 1-4 D	Max error between 5-10 D
Wang, Lam, Cui, Zhang, Jiang, Sun, Guo, Ma and Hamill. (Wang *et al.*, 2018)	Exp 1	AMR 1	3.1	-5.6	-5.2
	Exp 2	AMR 2	-7.6	-23.0	-22.6
	Exp 3	AMR 3	6.2	7.2	4.9
	Exp 4a	AMR 4	9.0	14.3	36.2
	Exp 4b	AMR 4	22.0	25.9	33.2
Lam-Chen model. (Lam, Chen and Hashim, 2015)	Exp 1	AMR 1	3.1	-5.6	-5.2
	Exp 2	AMR 2	-7.6	-23.0	-22.6
	Exp 3	AMR 3	6.2	7.2	4.9
	Exp 4a	AMR 4	-27.5	-25.3	-25.4
	Exp 4b	AMR 4	-14.5	-12.6	-28.4
Adapted Larson model (Pyakurel *et al.*, 2017)	Exp 1	L1	43.4	-45.9	3.8
	Exp 2	L2	-3.9	-6.2	-8.3
	Exp 3	L3	-15.5	25.6	25.5
	Exp 4a	L4	-23.7	14.1	13.5
	Exp 4b	L4	-10.7	21.8	10.5
Adapted Jensen model (Pyakurel *et al.*, 2017)	Exp 1	J1	-1.7	-0.8	3.4
	Exp 2	J2	4.9	-9.2	-10.4
	Exp 3	J3	12.6	26.7	26.1
	Exp 4a	J4	13.4	22.9	20.9
	Exp 4b	J4	26.4	33.4	17.9

The Vx_{OD} equation comparison developed by Wang *et al.* (2018) and tested on the experimental dataset can be seen in Figure B-11.
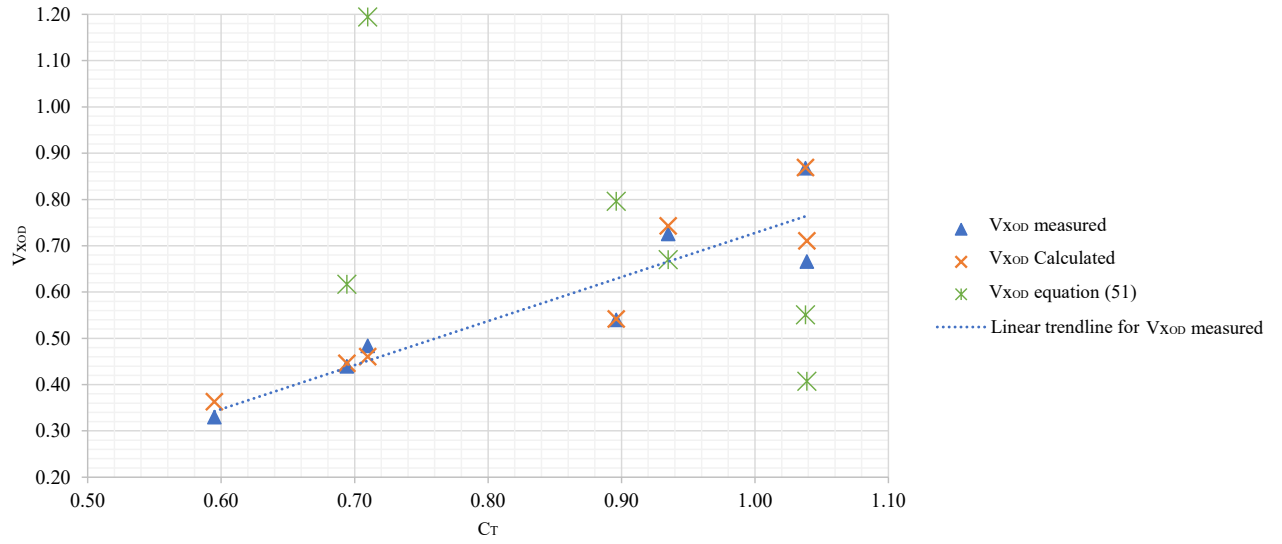
Figure B-11: Scatter in VOD values using the prescribed equation (developed in this dissertation) vs the equation found in literature (equation (52))

Appendix C:

Backwater model verification and testing results

C-1. Backwater prediction model testing

This section offers additional details regarding the test cases and specific results, which are referenced in the analysis and conclusions presented in the dissertation.

Table C-1 presents the test cases utilized for the calibration of the backwater prediction method. Furthermore, the included information on near wake measurements provides an overview of the observations. It should be noted that the effects of turbine retaining structures are not depicted in this section. However, it is worth mentioning that higher near wake pressure drops were observed when the CFD models incorporated the pole structure.

Table C-1: Pressure drop over turbine test cases (including near wake effects)

Test case ID	y (m)	β (%)	D (m)	U∞ (m/s)	TSR	Fr_D	Fr (channel)	ΔP_t (Pa)	$\Delta P_{t+near\ wake}$ (Pa)	% near wake loss
T2_3b.1	2	4.81%	0.7	0.80	3.67	0.31	0.18	231	244	5.8
T2_3b.2	2	4.81%	0.7	0.83	3.67	0.32	0.19	197	200	1.5
T2_3b.3	1.3	22.77%	0.7	0.80	3.67	0.31	0.22	178	191	7.3
T2_3b.4	2	4.81%	0.7	0.80	3.67	0.31	0.18	187	207	10.5
T2_3b.7	2	4.81%	0.7	2.00	3.67	0.76	0.45	1599	1641	2.6
T2_3b.8	2	4.81%	0.7	1.50	3.67	0.57	0.34	883	908	2.8
T1_2b.4	1	7.14%	0.5	1.05	5.10	0.47	0.34	513	570	11.1
T1_2b.5	1	7.14%	0.5	1.05	5.10	0.47	0.34	495	513	3.6
T1_2b.6	1	7.14%	0.5	1.50	5.10	0.68	0.48	1049	1177	12.2
T1_2b.7	1	7.14%	0.5	1.80	5.10	0.81	0.57	1529	1720	12.5
T1_2b.8	1	19.63%	0.5	1.05	5.10	0.47	0.34	496	546	10.1
T3_3b.2	0.85	16.50%	0.5	1.00	3.65	0.45	0.35	637	672	5.5
T3_3b.1	1.3	7.00%	0.5	1.00	3.65	0.45	0.28	625	657	5.1
T3_2b.2	0.85	16.50%	0.5	1.00	2.13	0.45	0.35	574	584	1.7
T3_4b.2	0.85	16.50%	0.5	1.00	3.02	0.45	0.35	337	473	40.4
T4_3b.3	1.2	17.45%	0.8	1.40	4.80	0.50	0.41	671	700	4.3
T4_3b.4	1.2	17.45%	0.8	1.40	4.00	0.50	0.41	509	540	6.1
T4_3b.5	1.2	17.45%	0.8	1.40	6.00	0.50	0.41	854	950	11.2

In Section 5 of the dissertation, a backwater prediction approach was developed and described. Tables C-2 to C-7 summarize all the test results utilized to assess the suitability and accuracy of the backwater prediction approach.

Table C-2: Backwater approach testing over all test cases

Test ID	β (%)	D (m)	U∞ (m/s)	C_T	Δh EXP (mm)	Δh calculated (mm)		(htexp-htcalc)/y	
						C_T	$C_T = 0.88$	C_T	$C_T = 0.88$
T2_3b.1	4.81%	0.7	0.8	0.8	1.20	1.36	1.49	0.01	0.02
T2_3b.2	4.81%	0.7	0.83	0.8	0.98	0.73	1.61	0.02	0.10
T2_3b.3	22.77%	0.7	0.8	0.6	4.43	3.83	7.06	0.22	4.08
T2_3b.4	4.81%	0.7	0.8	0.6	1.02	0.53	1.49	0.06	0.06
T2_3b.5	4.81%	0.7	2	0.8	8.05	4.24	9.32	3.63	0.40
T2_3b.6	4.81%	0.7	1.5	0.8	4.45	2.38	5.24	1.07	0.16
T1_2b.1	7.14%	0.5	1.05	0.9	4.15	3.99	3.81	0.03	0.11
T1_2b.2	7.14%	0.5	1.05	0.9	3.73	3.99	3.81	0.06	0.01
T1_2b.3	7.14%	0.5	1.5	0.9	8.57	8.14	7.78	0.19	0.62
T1_2b.4	7.14%	0.5	1.8	0.9	12.52	11.72	11.21	0.65	1.73
T1_2b.5	19.63%	0.5	1.05	0.9	10.93	10.96	10.49	0.00	0.20
T3_3b.1	16.50%	0.5	1	1.2	11.30	12.40	7.99	1.65	15.16
T3_3b.2	7.00%	0.5	1	1.2	4.69	3.44	3.39	0.92	1.00
T3_2b.1	16.50%	0.5	1	1	9.82	10.69	7.99	1.03	4.64
T3_2b.1	16.50%	0.5	1	0.9	7.96	9.30	7.99	2.49	0.00
T4_3b.1	17.45%	0.8	1.4	0.8	12.45	11.77	16.57	0.33	11.76
T4_3b.2	17.45%	0.8	1.4	0.8	9.61	11.77	16.57	3.24	33.66
T4_3b.3	17.45%	0.8	1.4	0.8	16.90	11.77	16.57	18.29	0.08
						N	18		18
						MAR	1.4		2.0
						variance	2.0		4.3

Table C-3: Backwater approach testing over primary validation cases

Test ID	β (%)	D (m)	U∞ (m/s)	C_T	Δh EXP (mm)	Δh calculated (mm)		(htexp-htcalc)/y	
						C_T	$C_T = 0.88$	C_T	$C_T = 0.88$
T2_3b.1	4.81%	0.7	0.8	0.8	1.20	1.36	1.49	0.01	0.02
T1_2b.1	7.14%	0.5	1.05	0.9	4.15	3.99	3.81	0.03	0.11
T3_3b.1	16.50%	0.5	1	1.2	11.30	12.40	7.99	1.65	15.16
T3_2b.1	16.50%	0.5	1	1	9.82	10.69	7.99	1.03	4.64
T3_2b.1	16.50%	0.5	1	0.9	7.96	9.30	7.99	2.49	0.00
T4_3b.1	17.45%	0.8	1.4	0.8	12.45	11.77	16.57	0.33	11.76
						N	6		6
						MAR	1.0		2.3
						variance	1.1		6.3

Table C-4: Backwater approach testing over blockage ratio variations

Test ID	β (%)	D (m)	U∞ (m/s)	C_T	Δh EXP (mm)	Δh calculated (mm) C_T	C_T= 0.88	(htexp-htcalc)/y C_T	C_T= 0.88
T2_3b.3	22.77%	0.7	0.8	0.6	4.43	3.83	7.06	0.22	4.08
T2_3b.4	4.81%	0.7	0.8	0.6	1.02	0.53	1.49	0.06	0.06
T1_2b.5	19.63%	0.5	1.05	0.9	10.93	10.96	10.49	0.00	0.20
T1_2b.1	7.14%	0.5	1.05	0.9	4.15	3.99	3.81	0.03	0.11
T3_3b.2	7.00%	0.5	1	1.2	4.69	3.44	3.39	0.92	1.00
T3_3b.1	16.50%	0.5	1	1.2	11.30	12.40	7.99	1.65	15.16
							N	6	6
							MAR	0.7	1.9
							variance	0.6	4.1

Table C-5: Backwater approach testing over variations of inlet turbulence

Test ID	β (%)	D (m)	U∞ (m/s)	C_T	Δh EXP (mm)	Δh calculated (mm) C_T	C_T= 0.88	(htexp-htcalc)/y C_T	C_T= 0.88
T2_3b.1	4.81%	0.7	0.8	0.8	1.20	1.36	1.49	0.01	0.02
T2_3b.2	4.81%	0.7	0.83	0.8	0.98	0.73	1.61	0.02	0.10
T1_2b.1	7.14%	0.5	1.05	0.9	4.15	3.99	3.81	0.03	0.11
T1_2b.2	7.14%	0.5	1.05	0.9	3.73	3.99	3.81	0.06	0.01
							N	4	4
							MAR	0.2	0.2
							variance	0.0	0.1

Table C-6: Backwater approach testing over inlet velocity variations

Test ID	β (%)	D (m)	U∞ (m/s)	C_T	Δh EXP (mm)	Δh calculated (mm) C_T	C_T= 0.88	(htexp-htcalc)/y C_T	C_T= 0.88
T2_3b.1	4.81%	0.7	0.8	0.8	1.20	1.36	1.49	0.01	0.02
T2_3b.5	4.81%	0.7	2	0.8	8.05	4.24	9.32	3.63	0.40
T2_3b.6	4.81%	0.7	1.5	0.8	4.45	2.38	5.24	1.07	0.16
T1_2b.1	7.14%	0.5	1.05	0.9	4.15	3.99	3.81	0.03	0.11
T1_2b.3	7.14%	0.5	1.5	0.9	8.57	8.14	7.78	0.19	0.62
T1_2b.4	7.14%	0.5	1.8	0.9	12.52	11.72	11.21	0.65	1.73
							N	6	6
							MAR	0.9	0.7
							variance	1.1	0.6

Table C-7: Backwater approach testing over TSR variations

Test ID	β (%)	D (m)	U∞ (m/s)	C_T	Δh EXP (mm)	Δh calculated (mm)		(htexp-htcalc)/y	
						C_T	C_T = 0.88	C_T	C_T = 0.88
T4_3b.1	17.45%	0.8	1.4	0.8	12.45	11.77	16.57	0.33	11.76
T4_3b.2	17.45%	0.8	1.4	0.8	9.61	11.77	16.57	3.24	33.66
T4_3b.3	17.45%	0.8	1.4	0.8	16.90	11.77	16.57	18.29	0.08
							N	3	3
							MAR	2.7	3.9
							variance	10.9	22.8

Appendix D:

Published papers by the author

D-1. Structure of publications

The dissertation was structured to provide three studies which would be submitted for publication in three separate peer-reviewed articles in reputable journals. The following papers are included, and directly linked to parts 1, 2 and 3 of the study as described in the dissertation.

1] Niebuhr, CM., Schmidt, S., van Dijk, M., Smith, L. and Neary, VS., "A review of commercial numerical modelling approaches for axial hydrokinetic turbine wake analysis in channel flow", *Renewable and Sustainable Energy Reviews*, 158(112151), 2022.

2] Niebuhr CM., van Dijk, M., and Smith, L., "Development of a semi-empirical wake formation and dissipation prediction model for HAHT placed in channel flow", *Ocean Engineering*, 285(115249), 2023..

3] Niebuhr CM., Hill, C., van Dijk, M. and Smith, L., "Development of a Hydrokinetic Turbine Backwater Prediction Model for Inland Flow through Validated CFD Models", *Processes*, 10(1310), 2022.

Additional peer-reviewed articles that formed part of the study include:

4] Niebuhr, CM., Van Dijk, M. and Bhagwan, JN., "Development of a design and implementation process for the integration of hydrokinetic devices into existing infrastructure in South Africa." *Water SA*, 45(3):434-446, 2019.

5] Niebuhr, CM., van Dijk, M. and de Wet, C. „Investigating the Hydrokinetic Turbine wake effects as a result of operational parameter variations through validated CFD models." *7th Oxford Tidal Energy Workshop*, Oxford, UK. 8-9 April 2019.

6] Niebuhr, CM. and van Dijk, M., "Monitoring operation and maintenance of hydrokinetic schemes through pilot installations in South Africa." *HYDRO 2021*, Strasbourg, France. 25-27 April 2022.

The papers mentioned above are included in this Appendix in the same order as mentioned above.

Check for updates

A review of commercial numerical modelling approaches for axial hydrokinetic turbine wake analysis in channel flow

C.M. Niebuhr [a,*], S. Schmidt [b], M. van Dijk [a], L. Smith [c], V.S. Neary [d]

[a] Department of Civil Engineering, University of Pretoria, Pretoria, 0001, South Africa
[b] Institute of Aerodynamics and Fluid Mechanics, Technical University of Munich, D-85748, Munich, Germany
[c] Department of Mechanical Engineering, University of Pretoria, Pretoria, 0001, South Africa
[d] Sandia National Laboratories, Albuquerque, NM, 87185, USA

ABSTRACT

Computational fluid dynamics is employed for detailed prediction of the hydrokinetic turbine performance and wake modelling. Of these, Reynolds-averaged Navier-Stokes (RANS) models are most widely used due to their ability to resolve power performance and detailed flow features at relatively low computational costs and acceptable accuracy. The limitations of these models are often not well understood when applied to complex turbine and wake dynamics which could lead to potential inaccurate and inappropriate conclusions. This paper focuses on the prediction of the wake generation, dissipation and flow recovery using commercially available modelling software. The approach and findings of previous numerical investigations on this matter are reviewed and compared to experimental measurements reported for a dual-rotor reference turbine. The shortcomings of these models are discussed and appropriate modelling techniques for the preliminary design or analysis of hydrokinetic turbines and inland energy generation schemes are identified. Commercially available RANS models show a good correlation of turbine performance. However, prediction of the wake behaviour is improved by using a virtual disk model with the blade element momentum theory, employing Reynolds stress closure models. These models allow for modelling the anisotropic conditions in the wake unlike the more popular eddy viscosity models. In addition, simplified rotor geometry models using blade element momentum theory are found to adequately model wake development and dissipation at a modest computational expense. The shortcomings of other approaches in terms of wake dissipation prediction and the effect of boundary and inflow conditions are analysed, emphasizing the importance of correct prescriptions of model parameters.

1. Introduction

1.1. Inland hydrokinetic energy

Inland hydrokinetic energy has seen increased research and development activity in the last ten years. This includes studies that assess the resource for regional and national renewable energy portfolios, e.g. Ref. [1], studies characterizing the ambient turbulent inflow conditions and wake effects, e.g. Refs. [2,3], studies demonstrating hydrokinetic (HK) turbine technologies [4,5] and specific focus on characterization and assessment of the spatiotemporal variation in the current velocity and turbulence acting on the turbine rotor [2].

For inland horizontal axis hydrokinetic turbines (HAHT) schemes, like wind farms, devices are placed in arrays to increase the annual energy production and optimize the techno-economic performance [5]. Within array schemes, prediction of the upstream wake effects on the ambient inflow conditions is of primary importance [6]. Disregard of these effects can result in reduced efficiencies of downstream turbines [7,8]. and a combined large scale effect of the array on the environment [9,10]. A thorough review of these complex wake dynamics are reported by Fontaine et al. [4].

The current advancements in computational efficiency and capacity incentivise the use of complex CFD models for inland HK turbines modelling to expand on the existing knowledge base. Computational investigations on both performance and wake effects are providing a much clearer picture of the flow-structure interaction and power output of HK installations. The impact environmental effects such as blockage [11], flow speed [12], yawed flow [13] have on turbine performance may be better understood through computational modelling.

Abbreviations

λ	Tip speed ratio
AD	Actuator disk
ADV	Acoustic Doppler velocimetry
BEM	Blade element momentum
CFD	Computational fluid dynamics
Cp	Calculated power coefficient
D	Diameters
DES	Detached eddy simulation
ECA	Energy capture area
FRG	Full rotor geometry
GCI	Grid convergence index
HAHT	Horizontal axis hydrokinetic turbine
HK	Hydrokinetic
IDDES	Improved delayed-detached eddy simulation
LDV	Laser Doppler velocimetry
LES	Large eddy simulation
LPS	Linear pressure strain
LRR	Launder-Reece-Rodi
PIV	Particle image velocimetry
RANS	Reynolds-averaged Navier-Stokes
RM1	Reference model 1
RSM	Reynolds stress model
SST	Shear stress transport
TI	Turbulence intensity
TKE	Turbulent kinetic energy
URANS	Unsteady Reynolds-averaged Navier-Stokes
VD	Virtual disk

Additionally the primary wake recovery mechanisms [14] and wake interactions [15] have also been analysed. A more informed understanding of these complex flow effects enables an improvement of the design and installation of HK devices. This also provides more clarity on site selection [16], proper array spacing [17] and other challenges surrounding operations and maintenance.

1.2. Modelling of hydrokinetic devices

Numerical/computational modelling techniques may be used as a tool to assess possible concerns, problem areas and unforeseen hydrodynamic effects in the HK turbine flow field. Laboratory tests are often expensive and prove difficult to accurately scale the flow environment [16]. Inland hydrokinetic turbines or turbine arrays are often placed in constrained flow areas that are only one or two orders of magnitude larger than their energy extraction planes [17], therefore accurate modelling of blockage and free surface effects are important [18].

Uniformity laws and "scales of modelling" are important considerations within computational models. This ensures dependant variables are included and computational resources are focussed on key aspects. For tidal applications scales of hydrodynamic modelling have previously been developed to address the required accuracy at each scale [19]. A similar approach may be applied to inland HK systems. The four primary scales of modelling are represented in Fig. 1. Each scale has a focus and may be more specifically defined as:

1] Device scale (blade scale):
   a. Focus on the flow around the turbine blades, lift and drag, performance analysis [4,16,19].
   b. Important to capture the 'dynamic stall' due to the massive flow separation [4] to accurately predict turbine performance.
   c. Important to capture effects of blade roughness (fouling), e.g. [4, 20],
   d. Important to capture effects of submergence and cavitation [4, 13].
   e. Important to capture blade wakes and tip vortices, e.g. [4,16],
   f. Requires highly accurate simulations resolving the large eddies not only in the wake, but also the boundary layer still attached to the blades [21,22].

2] Device scale (rotor scale) flow field analysis:
   a. Analysing the bulk thrust load and wake resulting from specific operating conditions [23].
   b. Effect of local flow conditions e.g. ambient turbulence [24,25].
   c. Prerequisite to determining placement of array schemes.

3] Array scale (channel scale) analysis:
   a. Turbine inter-effect (Interaction of multiple turbines).
   b. Effect of local flow conditions, e.g., ambient turbulence [26].
   c. Simplified techniques such as porous disc method [7] or Blade element momentum theory applied on an actuator disk (BEM-AD) together with Reynolds-averaged Navier-Stokes (RANS) equation models [27,28] or Actuator line Large eddy simulations (LES) [29].

4] Far field flow analysis (full system analysis):
   a. Analysis of far field backwater effects, blockage effects, erosion, sedimentation.
   b. Simplified 1-dimensional or 2-dimensional modelling using simplified numerical or analytical models [30–33].

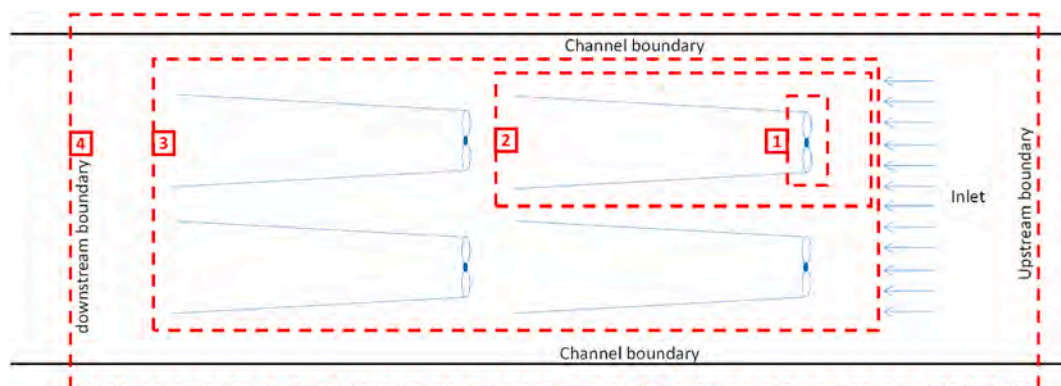As summarized in Ref. [4], numerous physical modelling studies

Fig. 1. Scales of modelling inland HK schemes.

have investigated device scale physics, including wake generation, dissipation and flow recovery downstream of a single turbine, e.g., Refs. [15,21–23]. Similar numerical modelling investigations have been performed [34–38]. Clear guidelines on suitable computational approaches and methods to avoid inaccuracies and errors are lacking. This paper serves to address the limitations of the approaches and methods usually employed in the modelling of specifically the device scale flow field. This is of crucial importance for inland schemes, where spatial constraints are restrictive and optimal spacing is essential to maximize power generation and annual energy production.

1.3. Hydrokinetic wake development for channel flow

Placing a turbine in a moving flow field causes a disturbance in the downstream region. This region is characterized by intense turbulent mixing, helical movements and a complex eddy system referred to as the wake [39].

Understanding wake formation is critical in HK installation and array optimisation. Like wind turbines, water turbine wake dynamics and structures exhibit wake rotation, wake meandering [40], the evolution of the shear layer, significant momentum transport across this shear layer, and dynamic interaction and breakdown of hub, tip and stanchion vortices within and at the interface of the coherent wake structure [4, 40]. However, there are clear differences for water turbine wake structures operating in depth-limited boundary layer flows. Including changes in fluids interacting with the bounding surfaces/free surface [36]. Additionally, far wake velocity deficits do not have the symmetric Gaussian profiles typically found downstream of wind turbines in unconfined atmospheric boundary layer flows, and these constraints can strongly affect flow recovery (as proven in previous studies [41,42]).

Fig. 2 may be used to describe a turbine wake and propagation thereof. Consider a turbine of area A in channel cross sectional area A_c Consider cross section A_o as the stream tube area in upstream undisturbed flow where the pressure is p_o and flow speed u_o. The stream tube pressure is p_1 just upstream of the turbine and p_2 just downstream (assumed uniform as in the Lanchester-Betz formulation). The stream tube then continues to expand downstream of the turbine before settling to a constant area A_3 with speed u_3. The speed of flow outside the wake is u_4 and pressure p_4. As indicated on the sketch as A_c approaches infinity $p_4 = p_0$ and $u_4 = u_o$ (depending on the blockage ratio). The flow further downstream allows lateral mixing which results in a change of pressure to p_5 which varies from p_0 [43]

The energy extraction is obtained through applying the momentum and Bernoulli equations to the flow field in Fig. 2 [43]. For a channel in an infinitely large domain, the maximum efficiency has been found to be around 0.59 (however the effect of confinement on this efficiency has not been investigated). Immediately downstream of the turbine the

wake physics is complex, and is influenced by the bypass flow, induced flow rotor and specific tip vortex interaction with the supporting structure [44]. Further downstream the wake starts mixing with the bypass flow and causes wake expansion inducing velocity recovery occurring over a long distance downstream.

The typical wake structure of a HK device can be split into two zones with different primary behaviour, namely the near and far wake. The end of the near wake may be categorized as the point with highest velocity deficit as indicated in Fig. 3. Further downstream the wake starts mixing with the bypass flow, resulting in wake expansion and velocity recovery. This wake region is characterized by intense turbulent mixing, helical movements, and a complex eddy system. This may be attributed to two phenomena, the instability of boundary layers on the blades due to the adverse pressure gradient along the rotor plane and a spiral vortex structure which is shed outwards from the blade tip and rotor root. The latter produces large eddies in the flow which last a long distance downstream (far wake region) [34].

Multiple physical processes exist in the flow affecting the performance and wake of a HK device. These include the onset shear and turbulence, interaction with the retaining structure, tip vortices and wake rotation (as indicated in Fig. 3). The near wake is characterised and affected by the turbine geometry, whilst the far wake, less so [32]. To allow accurate prediction of the near and far wake numerical models may be used, and care should be taken to ensure all factors affecting the wake as well as the complex flow in the wake itself are captured.

Results from previous studies on HK turbines placed in channels with similar Reynolds numbers to typical inland installation may be used as an indication of the development and length of a typical HAHT wake. These studies have indicated wake velocity deficits exceeding 10–20 rotor diameters (D) downstream [25,26]. Chamorro et al. [40] observed a wake propagating further than 15 D downstream. Bahaj et al. [36] presented wake centreline measurements indicating a velocity deficit for distances exceeding 20 D. A study by Edmunds et al. [46] drew a comparison of experimental and numerical results at a tip-speed ratio (TSR) of 3.7 where the wake spread and reduced from a 22% velocity deficit at 1.2 D to a 12% deficit at 10 D. In one of the few documented far field experimental studies completed on an three-bladed HAHT, the far field wake measurements indicated a velocity deficit propagating further than 35 D downstream [8]. With wake measurements indicating an 80% recovery at around 10 D downstream. Studies showed similar trends where the velocity deficit decays exponentially starting at 3 D downstream and reaches approximately 80% recovery between 9 and 10 D before maintaining a almost constant value until 35 D downstream (indicated in Ref. [8]). However, the large velocity deficit variations observed in the near wake indicates the sensitivities of HK turbine wakes to environmental/operational parameters. A good understanding of how these parameters drive wake formation and flow recovery is needed for
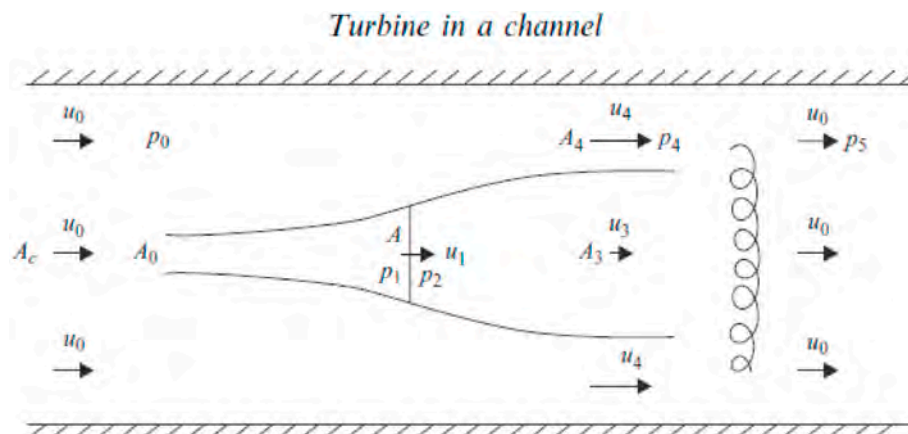

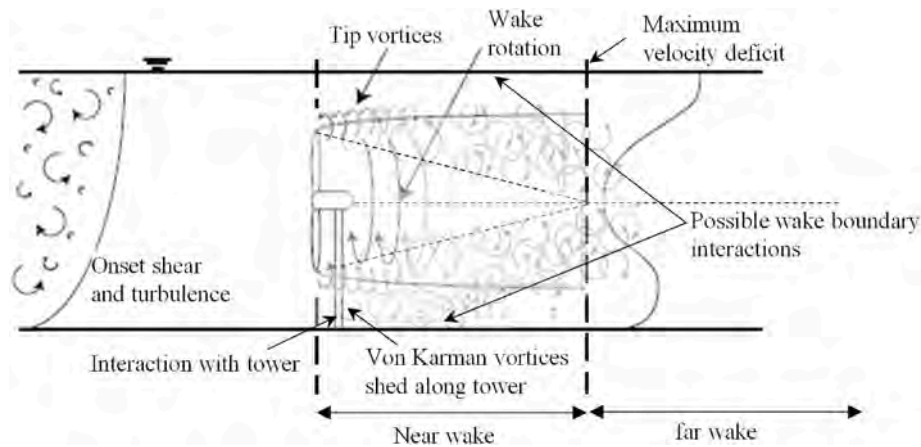**Fig. 2.** Definition for single turbine in a channel [43].

Fig. 3. Schematic of flow affecting the loading and wake of a HK device (adapted from Refs. [44,45]).

accurate wake predictions.

2. Computational and numerical modelling of HAHT

The key to determining the spacing between HK turbines in arrays is to address challenges faced in numerically modelling the flow physics resulting from complex geometries, moving boundaries, and the complex flow conditions as those illustrated in Fig. 3.

2.1. Numerical and analytical modelling of HAHT

Analytical and numerical models offer an alternative to physical scale models for simulating the complex flow physics, including wake dynamics. A number of studies have investigated effective modelling approaches for wind turbine wakes [47–49] and employing a similar approach for hydrokinetic flow fields seems reasonable. For analytical models, e.g. Refs. [32,50,51], the self-similar nature of the far wake is exploited to obtain expressions for velocity deficit and turbulence intensity. However, the calculated dissipation rate from these one-dimensional models is a function of wake speed only, resulting in uniform downstream wake profiles [52] independent of the effects of the retaining structure, confined flow and relative turbulence.

Due to recent developments in tidal energy, multiple large-scale analyses of tidal turbine arrays have been reported. The majority of the studies utilise simplified numerical models for array scheme analysis [19,53–55]. BEM theory is often used for simplified performance analysis. However, this method does not include any wake effect from the freestream or bounded flow [56]. Vortex-lattice and vortex-particle methods [57,58] may be used to describe the wake vorticity in concentrated sheets of particles. Computational Fluid Dynamics (CFD) simulations make use of generalized actuator disk (AD) or direct geometry modelling techniques to model complex external effects and more accurately retain fluid structure and wall effects [23]. Additionally, BEM may be embedded in the CFD domain.

CFD models may be used to resolve the effect of turbulence at subgrid scale level. Due to this, they are being used more often for first order analysis or design, many without experimental validation. However, they have the potential to offer more comprehensive solutions and insight when their limitations are understood.

2.2. CFD modelling for HAHT

For CFD wake analysis turbulence models are selected to model the turbulent structures in the wake which ultimately drive wake dissipation. The near wake may be characterized as a connected structure associated with vortex shedding similar to the Karman vortex street behaviour [59]. In the far wake two primary features exist in the wake,

low water speed and high turbulence intensity [60] the former of which reduces the power output of any subsequent turbine placed in its wake. Accurately representing turbulent flow in CFD remains a large challenge due to its strong dependence on initial conditions as well as the wide range of scales (eddies) present in the flow. Most often statistical approaches based on the RANS equations, with eddy viscosity models for turbulence closure, are used [61,62].

Previously, Shives & Crawford [63] indicated the k-ε model predicts much faster wake recovery than experimental results. Employing the shear stress transport (SST) k-ω model improved on this. However, it overcompensates, resulting in a delayed wake recovery. In summary the spatial pattern of turbulence in the wake was improved but the intensity was still too low. A possible solution may be to specify minimum turbulence intensities or limit decay [63]. Freestream turbulence defining input factors may vary over different CFD codes. Many assign default values and allow the user the override these if desired, however usually little guidance is available on the effect of these choices on decay rates [48]. This is especially true for the SST, k-ω and k-ε models where the specified turbulent dissipation rate strongly affects the development of the wake and dissipation curve.

In many scenarios eddy viscosity models are an attractive, well-calibrated option (specifically performance focussed studies). However, cases where flows with strong swirl or streamline curvature exist, or where secondary motion is driven by turbulence anisotropies, these models cannot provide the information required to accurately compute physical effects [64]. In the past this problem has been alleviated by moving beyond the eddy viscosity models to Reynolds Stress model's (RSM). However, these models have shown reduced numerical robustness especially when equations are integrated through the viscous sublayer [64]. McNaughton [65] performed a comparative analysis (near wake and turbine performance) using two 2-equation eddy viscosity models and the Launder-Reece-Rodi (LRR) Reynold stress model and concluded further testing needs to be completed on requirements of grid refinement in the wake when utilizing RSM's. The study found the SST and LRR methods performed well when compared to Large Eddy Simulation (LES) results.

A higher-level solution is possible with LES which is a scale-resolving simulation. This means a portion of the turbulence spectrum is resolved, not modelled, as in RANS [23]. However, this is yet to replace RANS due to the high-resolution and consequent high-computational demands for wall-bounded flows. Even though LES has remained a research tool to applications not much affected by wall boundary layers (e.g. Combustion chambers) [23,66], it may be useful when analysing details in the flow features [29,66].

Detached Eddy Simulation (DES) proposed by Spalart et al. [67] utilizes a hybrid RANS-LES. This approach allows a decreased grid resolution, eliminating the main limitations of LES. This means the wall

boundary layers are covered by a RANS model and free-shear flows computed in LES. DES may result in a reduction of the eddy viscosity without proper generation of turbulent content (which occurs for wall boundary layers) [64]. Salunkhe et al. [14] compared unsteady-RANS (URANS) to improved Delayed-DES (IDDES) for a full rotor geometry model and found that although all models overpredicted the wake diffusion after 4 D downstream, URANS performed better than IDDES. DES also suffers from a modelled stress depletion issue in the wake, resulting in inaccuracies.

Actuator disk (AD) embedded CFD methods may be useful where large scale flow effects (such as those in multi-turbine arrays) are of interest [35]. Blackmore et al. [68] used a LES approach coupled with an AD to model the wake of a horizontal axis turbine, the results correlated well with published experimental data beyond 3 D downstream. Kang et al. [69] analysed a detailed comparison of AD embedded LES showing that this is not sufficient to correctly reproduce the development of an actual turbine wake. They have proven even in fully turbulent open channel flow; the development of the far wake is sensitive to the stability of the vortical structures in the near wake region. As a result models need to be resolved in detail in the near wake region to predict an accurate far wake result [19]. The AD concept is not applicable for detailed design of a turbine rotor. It may however be useful for wake analysis and allows a significant reduction in computational size and cost [70,71].

Wake formation may not be extremely sensitive to small changes in turbine operation. However, power production has been proven to directly affect the wake velocity deficit, where higher power production produces a higher deficit in the wake [14]. Therefore, the turbine representation should be correctly captured when employing CFD models for wake analysis by incorporating the rotation of the blades and its effect on the surrounding flow field. As the blades rotate the surrounding fluid exerts a force (torque) on the blades, as a result the fluid behind the rotor loses kinetic energy (the wake) and a pressure differential is generated across the blades. The torque enforced is counteracted by the generator keeping a constant angular velocity [72]. Options ranging in complexity and varying in input requirements may be selected. The most accurate rotor modelling technique is modelling the full turbine rotor geometry (FRG). Previous studies indicated this method predicts turbine performance well for lower water speeds and tip speed ratios; however, underprediction of power output may occur at higher velocities. This can be explained by incorrect capture of the strongly separated flow by insufficient mesh resolutions and limitations of the employed turbulence model [23].

Another rotor modelling approach is to distribute a theoretical approach or source term over a virtual disk (VD), replicating the effects of the turbine action and coupling this with a CFD environment. The AD treatment is the least computationally expensive method and applies a uniform force to the flow. However due to the low fidelity modelling option important representations such a rotor swirl are lost [73]. BEM theory on the VD as a mid-fidelity modelling method, incorporating rotational components, and using real turbine geometric data. A limitation of this method is the inability to represent the discrete blade effects such as tip vortices [46]. The BEM-CFD method requires pre-determined lift and drag coefficients (F_L and F_D as inputs as shown in Fig. 4).

An important aspect when utilizing the BEM method is incorporating the tip loss correction factor [74–76]. Tip-loss correction compensates when the flow induction factor is large at a specific blade position, meaning the lift force will be almost normal to the rotor plane. Thus, the tangential component of lift will be small, and so will its contribution to torque. The result is a reduced torque and reduced power output (known as tip loss as it only occurs on the outermost part of the blades) [77]. Details of the BEM-CFD method are covered in Ref. [46].

A number of recent studies use the BEM-CFD method [76,78–80]. It has been widely used in wind turbine array models with good representation of the wake [46,81]. Various authors [73,82] have used this method to analyse the flow field of turbines arranged in arrays, specifically for tidal optimisation. The SST k-ω model coupled with BEM has been found capable of predicting the flow velocity structures in the far wake regions to an acceptable level of accuracy [46,82]. Gotelli et al. [55] and Gajardo et al. [83] found better agreement of a coupled BEM-DES method than the BEM-RANS method on a 3-bladed horizontal axis turbine. However, Gotelli et al. [55] predicted large variances in the near wake due to the BEM approach but showed better agreement from a distance 3 D downstream.

2.3. Ambient inflow and environmental conditions

The effects of a HK turbine on ambient inflow conditions has been studied in recent years as reviewed in Ref. [4]. These studies include the velocity deficit [32,81]; the complex three-dimensional flow structure (including hub and tip vortices) [84]; increase in turbulence intensity and anisotropy [26,40,85]; effects of ambient turbulence levels; unsteady loading; flow depth to turbine diameter; and turbine operating conditions affecting thrust (e.g., tip-speed-ratio) [86,87].

Turbulent, ambient inflow characteristics of depth-limited flows and their implications for HK turbine deployments, are detailed in Ref. [2]. Measured vertical profiles of the mean velocity and turbulence stresses reported in literature for rivers and large canals are compared along with classical models developed for turbulent flat plate boundary layer flows. The vertical mean velocity profiles are modelled reasonably well with a power law (exponent = 1/6), and similarly vertical profiles of turbulence (Reynolds) stresses with semi-empirical exponential decay formulae derived from classical open channel hydraulics experiments [88]. Nevertheless, a significant amount of scatter is observed about these modelled profiles due to variations in bedforms, complex bathymetry, non-stationary (unsteady) phenomena, and potentially, three-dimensional flow structures, e.g., large coherent motions emanating from natural and manmade obstructions [89].

Additional to inlet conditions, the consideration of environmental variables on wake prediction and modelling, such as bounded flow and depth below the free surface, is also necessary. Previous studies have specifically addressed the concern of distance to the free surface, as well
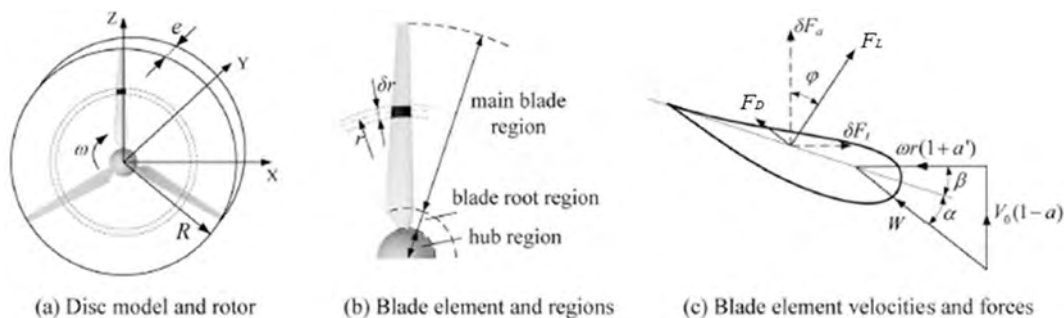

Fig. 4. Schematic of the virtual disc model, hydrofoil and blade element characteristics [78].

(a) Disc model and rotor   (b) Blade element and regions   (c) Blade element velocities and forces

as blockage ratio [17,18,90,91]. Complexities arise when turbines are placed near the free-surface, as the boundary may modify the turbine flow-field and affect device performance. Generally, this causes significant flow acceleration, its magnitude depending on the blockage ratio.

El Fajri et al. [92], investigated the effects of shallow water on the near wake recovery through a validated CFD model with a tip clearance of 0.35D. The stanchion holding the turbine in place (Fig. 5) initiated the free-surface wake interaction and a significant wake deformation can be seen at 7 D. The results found suggest the free-surface blockage enhances wake recovery in the near or intermediate wake by accelerating the flow in the upper bypass region. However, the wake recovery rate (specifically in the intermediate-far wake) was not affected significantly as shown in (c) in Fig. 5. Kolekar and Banerjee [17] studied this effect and found that smaller tip clearances retarded wake propagation, but accelerated the flow in the upper bypass region. This caused a skewed wake. Experimental investigations proved that small clearances may also cause free surface deformation resulting in a free-surface drop behind the turbine. However, clearances avoiding this behaviour are usually be prescribed by turbine manufacturers to prevent performance degradation. Additionally, an optimal clearance depth (depth form blade tip to free surface) exists, resulting in improved turbine performance [17].

When a turbine is placed in bounded flow, the flow velocity in the bypass region around the turbine will be increased due to the spatial restrictions of the channel bed and walls as well as the free surface. This change may lead to an altered wake velocity deficit comparing to unbounded flow cases. This effect is caused by changes in the rate of mixing between the wake and the bypass flow (which is the driving force for flow recovery) and thus affects the wake recovery length scale [93]. To ensure accurate prediction of this behaviour it should be ensured that wall effects and boundary layers are accurately modelled.

Ensuring Reynolds uniformity is important within wake studies. Models validated further from the Reynolds number experienced at full-scale results in a lack of confidence in the models [94]. A previous analysis to observe Reynolds dependence using towing tank tests [94] indicated that near-wake statistics (mean velocity, turbulence intensity, Reynolds stress) were less Reynolds dependant than the performance measure of the turbine. However, it is important to consider Reynolds dependencies when scaled models are used for numerical validation. The study also found that when scaling experimental tests, no significant Reynolds number dependence was found for velocity profiles, however a small Reynolds dependence existed for turbulence intensity and Reynolds stresses. Numerical results (specifically using the SST k-ω solution) indicated a stronger Reynolds dependence, overpredicting performance due to the increased blockage and exclusion of tip effects. Previous results have also indicated that power coefficients (C_P) are more sensitive to Reynolds dependency than the thrust coefficient (C_T), the same is true for blockage ratios [95]. In conclusion low blockage may alter the Reynolds number (comparing to non-blocked cases) for scaled tests, and in turn alter the turbine performance. Reynolds uniform + mity should therefore be included if scaled testing is used.

3. Methods

3.1. RM1 validation case

To allow accurate development of a CFD model, verification (correct numerical model) and validation is necessary. The latter requires comparison with experimental data or numerical data. The Reference model 1 (RM1) turbine [96] with properties as seen in Fig. 6 was used as a validation case. The RM1 design and testing environment allows a Reynolds uniform analysis of the inter-effect between the two closely spaced turbine rotor wakes as well as incorporating the effect of turbine wake interaction with the center stanchion itself. The rotor diameter and blade profile resemble those often used in inland hydrokinetic applications. Channel conditions as well as the blockage ratio also hold value for the analysis of inland schemes (see Fig. 7).

Mean and fluctuating velocity fields were measured using three Nortek vectrino ADV's sampled at 200 Hz data output at hub height. To ensure any ADV measurement volume rotation was considered, the channel was ponded with water and a towing test performed to determine the rotation. The rotation matrix was then applied to all measured data before calculation of flow statistics. Additionally, time series data was filtered to remove erroneous samples [97]. The measured turbulence intensity in the rotor region was approximately 5%. Wake vertical velocity profiles were taken downstream of the turbine from 1 D to 10 D at intervals of 1 D. These were collected for 3 min at 200 Hz. A horizontal plane was collected from 1 D to 10 D also with 1 D spacing, the cross stream ADV point locations were assumed to have provided enough spatial resolution to capture key characteristics of the wake. The
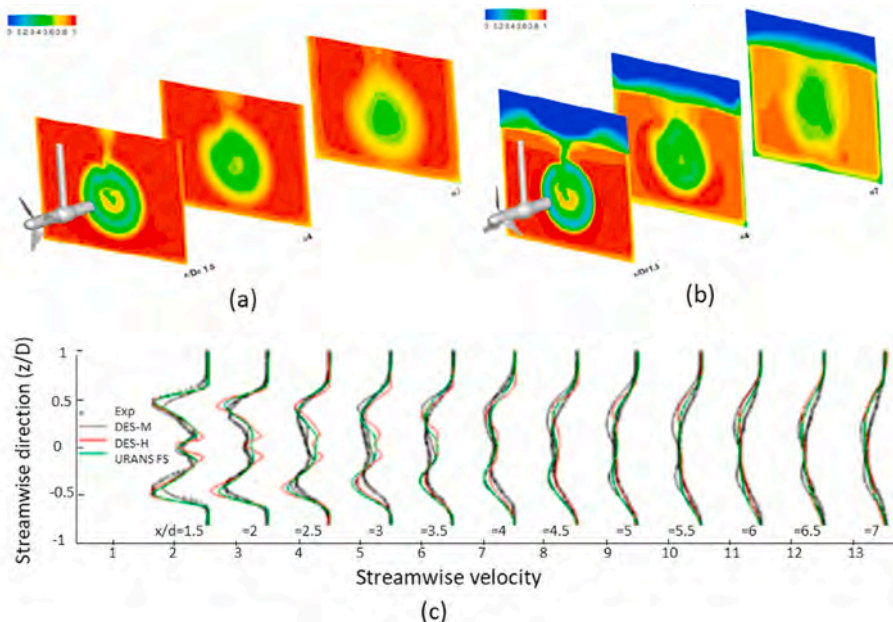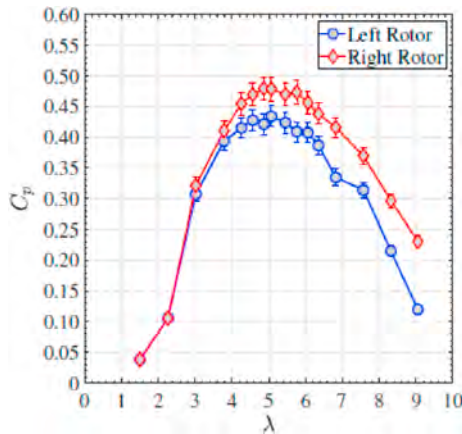

Fig. 5. Free surface effect on wake indicated by the differences in (a) single phase-*DES-M/H* and (b) multiphase- *URANS FS* [92].

Parameter	Scaled model
Flow rate	2.425 m³/s
Depth	1.0 m
Velocity (hub)	1.04 m/s
Froude number	0.28
Re_c at $C_{p\text{-}Opt}$	3.1×10^5
Re_D	4.4×10^5
NACA	4415
Diameter	0.5 m
Depth to hub (h_{hub})	0.5 m
Tip speed ratio	1-9

Fig. 6. RM1 laboratory setup details [16].

Fig. 7. Calculated power coefficient (C_p) versus tip speed ratio (λ) for left and right rotors, dashed lines represent results before calibration [16].

Fig. 8. Computational domain.

velocity time series was decomposed into mean and fluctuating components through Reynolds decomposition, the fluctuating velocity components were used to calculate flow statistics such as turbulence intensity, Reynolds stresses and turbulent kinetic energy. Details may be seen in experimental reports [16,96].

Both rotors (counter-rotating) were identical but performed differently (Fig. 4). The flow complexity in the channel, as well as the slight asymmetry in the approach flow could have affected this change. Because of the performance sensitivity to velocity (U^3) a slight difference in approach velocity (3–5% e.g., 0.03 m/s) could cause a 10% change in performance (at optimal TSR). A variation of wake results in the near wake was also observed, with a 17% higher peak velocity deficit for the left rotor at 2 D downstream. This emphasizes the strong variability in near wake results from small operational changes, asymmetric inflow conditions or manufacturing flaws.

3.2. Numerical domain

Commercial modelling software Siemens STAR-CCM+ was used to simulate the wake effects of the turbine. This allows comparison of commercial software used in HAHT design. The computational domain can be seen in Fig. 8. The RM1 dimensions were replicated using a wall bounded model. The domain extended from −8 D upstream to 30 D downstream of the axis of rotation. The inlet length was selected to allow full flow development (including wall boundary layer development) before the rotor is reached. Similarly, the outlet length ensured the channel outlet boundary has no influence on the wake dynamics, although this large distance is not necessary for performance analysis (around 15 D is adequate [98,99]). The large downstream length was selected to allow analysis of far wake accuracy. A velocity inlet and downstream pressure outlet were specified as boundary conditions. The
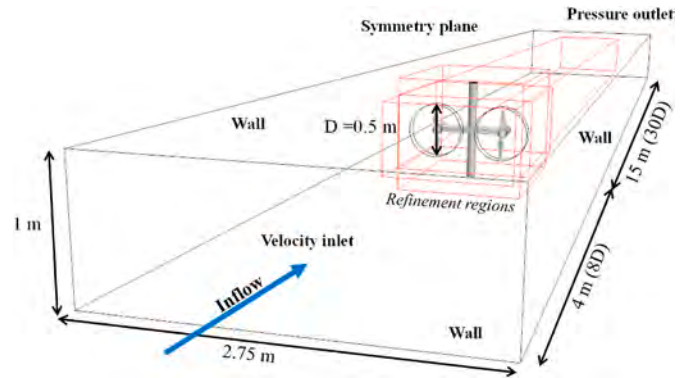
turbulence and velocity values measured in the experimental analysis were specified at the inlet. Full development of the boundary layer on all surfaces (boundary walls, blades, and stanchion) was ensured through the specific turbulence model wall treatment and mesh resolution for each test case.

The rotor was modelled using two widely used methods. First the overset (sliding) mesh technique was used to deal with the blade movement, this method was employed in numerous validated axial turbine studies [37]. The presence of the blades is taken into account by discretising the blade geometry on a computational mesh [37,83]. During each time step interpolation of the flow field is performed between the first cell mesh of the moving body and the background mesh region (Fig. 10C). The sliding mesh boundary can be seen on Fig. 10B. The rotating mesh continua should be a minimal size to ensure numerical efficiency whilst also ensuring numerical stability. A cylindrical area 10% larger than the turbine diameter was used here. Second, a VD was used (Fig. 11B) and a BEM model was employed. This VD-BEM modelling approach has demonstrated good accuracy at reduced computational cost [76,78–80]. A BEM tip-loss correction was incorporated using the Prandtl tip loss correction method [75].

Careful selection of flow physics, and comparisons of commonly used models is a crucial factor in accurate modelling of these complex flow fields. RANS eddy viscosity models are most often used for turbine analysis [63,100–102]. The k-ε turbulence model was compared to Menter's SST k-ω turbulence model [103] which typically predicts adverse pressure gradients in the near wall region better than the k-ε turbulence model. The near wall region is defined as the viscous sub-layer in the region y⁺<5, where y⁺ = yu*/ν, y is the normal distance from the wall in wall coordinates, u* is the friction velocity and ν is the fluid kinematic viscosity [103,104]. Both models were built with a different mesh, specifically in the wall regions, the k-ε model was built using a high y⁺ approach and resolving boundary layers, whilst for the SST k-ω turbulence model a low y⁺ approach was used, fully resolving the viscous sub-layer. More complex Reynolds stress models (RSM) were

then employed to allow more accuracy in prediction of possible flow anisotropy, these have shown positive results in HK wakes but require further validation [65]. The RS Linear pressure strain two-layer (RS-LPS2) model [105,106] was selected which allowed near wake accuracy with a low y^+ wall treatment on the turbine and turbine structure.

Steady and transient simulations were performed (for both RANS and RSM) where unsteady terms were discretized using a 2nd order implicit scheme. A time step ensuring Courant numbers less than 1 in all regions was ensured as far as possible. The time steps were around 0.002% of the total time to complete one rotation for the FRG simulations and 0.01% for the BEM-CFD models. However, timesteps varied over each approach depending on the results of the grid convergence index (GCI). All approaches are shown in Fig. 9, where combinations of model properties were varied with the goal of understanding the limitations as well as capabilities of each approach.

3.3. Mesh

The computational domain (Fig. 8) consisted of a polyhedral mesh with grid refinements in the near wake, far wake and surrounding the retaining structure. Past results indicate the importance of fine grids to track the tip vortices when using simplified RANS models [23]. Simulations were performed on various meshes with similar base sizes and increased resolution over volumetric controls in regions of high turbulence. An adaption of the GCI [107] was used due to the variance in grid sensitivity in the different wake regions, therefore separate regions were decreased incrementally, starting from the near wake region, until no changes in wake behaviour was observed. For the optimum flow conditions ($\lambda = 5.07$) results showed grid sensitivity up to a minimum cell size of 3 mm (0.6% D) around the blades for FRG. However, a further 30% increase in cell size showed only a 1% change in wake dissipation rate. For FRG a small mesh size is inevitable to capture the geometry of the blades (under high rotation) as well as boundary layer formation. RS models also required finer grids comparing to eddy viscosity models. For the RM1 turbine the advancing prism layer Mesher proved to be best for the complex geometry and customization of the prism layer thickness on the upstream and downstream side of the blades. The mesh can be seen in Fig. 10. Final mesh sizes were around 19 million cells.

For the VD model (Fig. 11) a 10 mm minimum cell size (2% D) proved adequate for a BEM-RANS analysis. The finite number of blades across the virtual disk should ensure introduction of the effects of the propeller on the computational domain. A minimum of 4 cells over the blade thickness were ensured with all meshes, further refinement or change in thickness did not affect results. Both rotor modelling techniques showed converged solutions for near wake cell sizes of 8 mm. Increasing this near wake grid by only 4% (2 mm cell size change) resulted in a 5% change in wake velocity deficit results. Therefore, near wake grid sensitivity should be carefully considered. A far wake cell size of around 8–15 mm showed no significant change. In this paper, a 14 mm (2.8% D) base size in the far wake was selected. Final mesh sizes were around 13 million cells.

3.4. Boundary conditions

Walls were modelled with non-slip conditions which allowed formation of a boundary layer, and incorporation of bounded flow effects. Prism layers were built according to the wall treatment requirements applicable to each model. For the SST k-ω models high y^+ treatment ($30 < y^+ < 300$) on the channel walls, and a layer resolving low y^+ ($y^+ < 1$) approach on the turbine and retaining structure was built. Mesh refinement, specifically in the near wall region of the boundary layer is crucial for accurate near wake region development, especially where both separated and attached flow exists [34]. Gibson & Launder [108] investigated the pressure fluctuation effects of capturing the boundary layer and noted the importance of an accurate capture of boundary layer formation and thus developed a two layer formulation which may be applied to the linear pressure strain model (LPS2 model). All analyses used the two-layer formulation.

Simulating the water-air interface (free surface) has been approached in various ways in literature. Most often the free surface is assumed to be a significant distance from the turbine and so free surface deformation is neglected and a symmetry boundary condition is used. Computational cost is saved using this approach [76] compared to a more accurate boundary condition where the free surface is modelled. Both were analysed in this study.

4. Results and discussion

4.1. Performance comparison

For HK turbine performance analysis both steady and transient FRG and BEM rotor modelling approaches are often employed and have proven good correlation to experimental results with the approaches used in Section 3 [76,79,109]. Numerous studies have assessed which models are best for performance tests [62,71,101,110]. Although the

APPROACH	ROTOR MODELLING	TURBULENCE MODEL	TIME
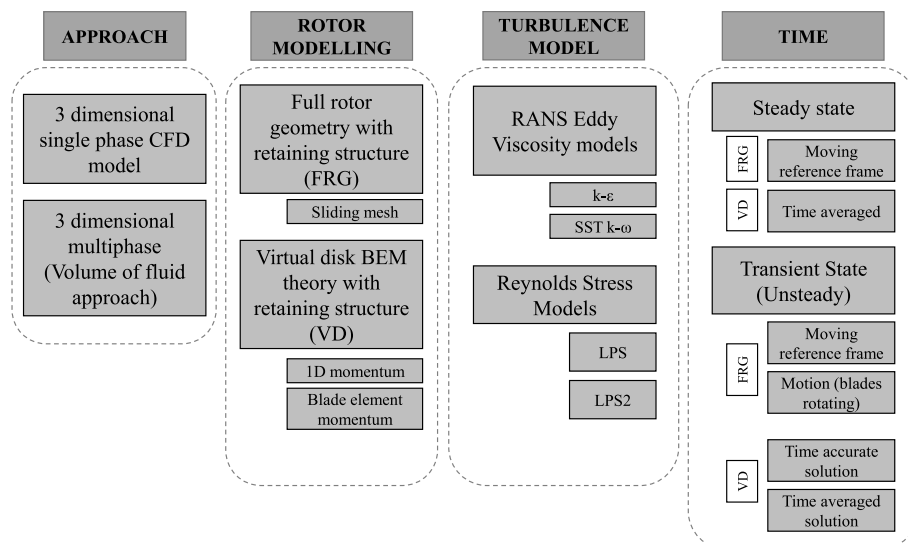
Fig. 9. Summary of CFD approaches.
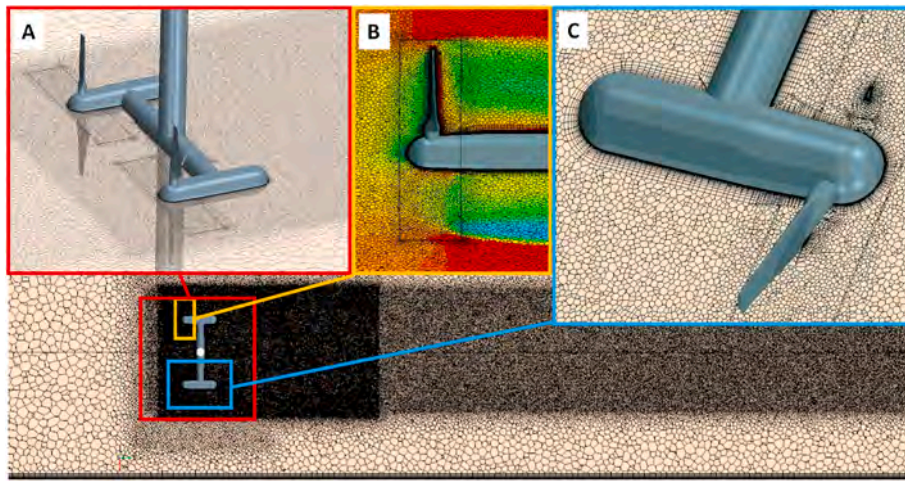
Fig. 10. Full rotor geometry mesh A) full rotor B) Sliding mesh interface C) Dynamic mesh.
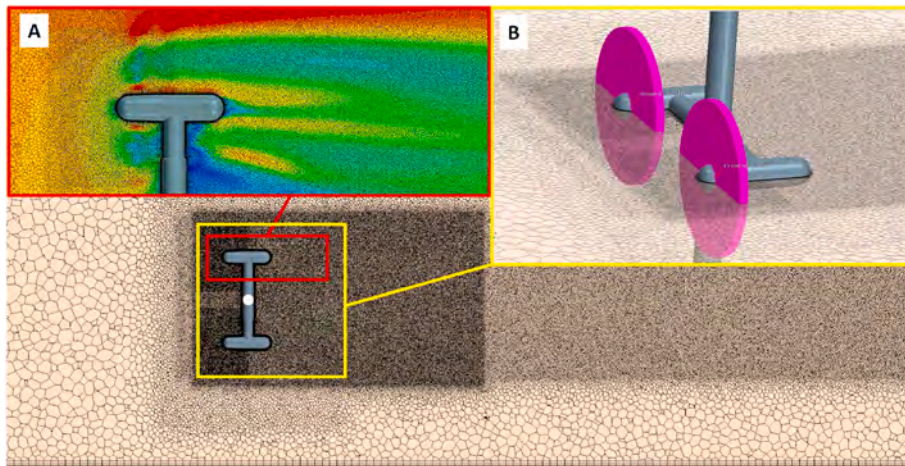
Fig. 11. BEM-RANS Mesh A) velocity contour on BEM mesh B) Virtual disks.

focus of this paper is on modelling of the wake dissipation rate, accuracy of each model's energy capture was ensured through comparison to experimental performance variables. Table 1 includes the torque (T) and power co-efficient's (C_P) measurements and model results for the optimum TSR. The CFD results for both rotors showed identical results and thus only one set of results is listed. Due to the uncertainties of accuracy of the experimental performance results, specifically on the left rotor (mentioned in 3.1) a certain degree of uncertainty lies on the measured values. However, the CFD results all lie well within the measured range and within 5% of the measured results. A similar conclusion was found by Masters et al. [73]. The experimental systematic and random measurement errors existing on the torque sensors were also included, these were calculated based on measured and expected value comparisons.

4.2. Rotor modelling

By modelling the FRG using the sliding mesh technique, the vorticity in the wake is simulated (Fig. 13). The tight vortical structures observed in Fig. 12 correlates with the expected near wake behaviour prevalent in past LES studies [22]. For steady state analysis a moving reference frame (MRF) is used to enforce the turbine rotation, however the solution lacks adequate simulation of the vorticity and rotation in the wake. From Fig. 13 it is clear the transient solutions better capture the wake. Although it may seem that steady state results better align with the left rotor it should be noted that during laboratory testing the left rotor did not perform to the expected degree of accuracy and has a larger degree of error [111] (hypothesized to be a result of approach flow asymmetry [16]). The steady solution indicates a high initial turbulence with an overpredicted velocity deficit in the near wake. This resulted in an accelerated and inaccurate wake dissipation rate. Accelerated decay of

Table 1
Performance comparison.

ROTOR	Experimental		
	T (N.m)	T Error (%) (sensor calibration)	CP (%)
left	2.081	3.80%	41.20%
right	2.603	0.69%	47.60%
Turbulence model	FRG-CFD		
	Steady (moving reference frame)		Transient (motion)
	T (N.m)	C_P (%)	T (N.m)	C_P (%)
RS-LPS2	2.35	44%	2.39	45%
SST kw	2.35	44%	2.45	46%
k-ε	2.16	41%	2.28	43%
Turbulence model	BEM-CFD		
	Steady state (time averaged)		Transient (Time accurate)
	T (N.m)	C_P (%)	T (N.m)	C_P (%)
RS-LPS2	2.43	46%	2.38	45%
SST kw	2.43	46%	2.38	45%

Fig. 12. Comparison of steady state vs transient results for the FRG-RSM dissipation rate as well as velocity magnitude and vorticity scalar scenes (CFD results are identical for left and right rotor).

Fig. 13. Comparison of steady state vs transient results for BEM-RSM dissipation rate and vorticity scalar scenes (CFD results are identical for left and right rotor).

the turbulent kinetic energy (TKE) of the bypass flow was prevalent in the near wake region. This may be attributed to the simplification of eddy viscosity model and its inability to resolving small eddies forming at the tip and root vortic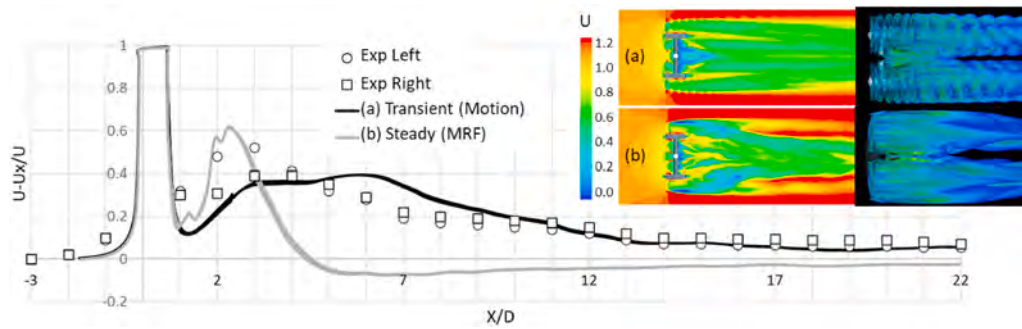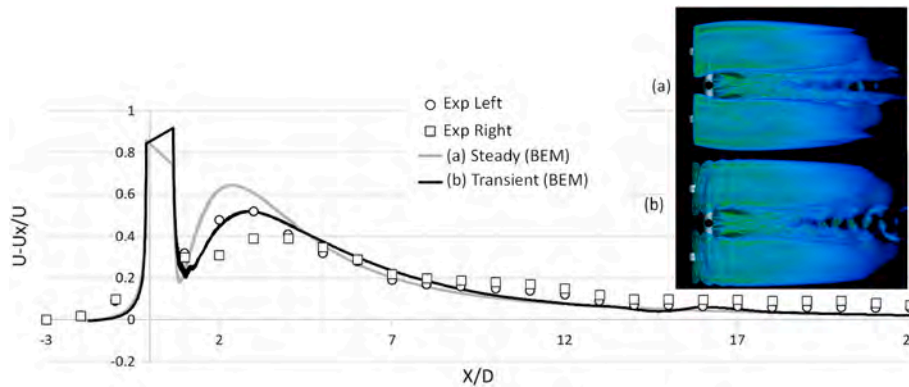es. The eddy-viscosity model showed a strong vortex structure extending from the blade tips which is maintained up to 6 D downstream due to inadequate mixing in the model [65]. This leads to inadequate wake dissipation as the TKE in the bypass flow is too weak to break these structures down in the near wake.

Although simplified rotor modelling using a VD reduces computational time, the simplification results in the lack of tip and root vortices formation (seen on the vorticity plots in Fig. 13). This is a result of the BEM-VD theory, where a force (which is a function of the rotor hydrofoil geometry) is applied at all locations along the disk and blade tips are not resolved. The BEM-VD time accurate approach available in most commercial software improves this prediction. This method tracks the motion of the blades adding a source term only to the volume of cells corresponding to the location of the blades (specified as input values to the VD). The improvement when using a time-accurate transient approach can be seen in Fig. 13. Similar behaviour as that shown in FRG modelling occurs, however the effect is not as pronounced.

For BEM-VD rotor modelling a sensitivity analysis was done using drag (C_D) and life (C_L) coefficients comparing experimental [112,113] and numerical data (XFOIL data). The results indicated a significant variation in turbine performance, wake formation and wake dissipation rate in the near and far wake. Better results were obtained when using numerical coefficients over a broad range of Reynolds numbers (including the operational range) and angle of attacks. Therefore, it is crucial that extensive and well approximated data be used. All BEM-VD results utilized the Prandtl cosine tip loss function, not considering the tip loss effect of the turbine resulted in a further 12% overestimation of the near wake velocity deficit.

Although modelling the full rotor geometry should intuitively increase the accuracy when comparing to a VD approach, it is

hypothesized that the complexities in fully modelling the geometry with these lower fidelity closure models results in a less accurate wake solution. Meaning the VD approach couples better with RS models as the modelled wake vorticity from the VD is easily broken down by the TKE present in the wake and does not depend on resolving the smaller eddies which are present and important in real wake conditions. Higher fidelity models such as LES's have shown FRG modelling gives a better approximation of the wake behaviour. It is also important to note that although steady state models may be sufficient for performance analysis, wake analysis requires a transient approach.

4.3. Dissipation rate

Hub height velocity measurements are often used as an indicator of wake recovery. A CFD approach accurately capturing the recovery rate and behaviour would be most useful for device scale analysis of HAHT systems. A summary of the hub height velocity deficits for the various transient modelling approaches investigated in this study can be seen in Fig. 14. No velocity deficit difference was observed in wake results between left and right rotors in the CFD models, thus only one set of numerical results are plotted together with both left and right rotor results from the experimental analysis. The discretion between rotos in the experimental wake velocity deficit becomes almost insignificant after 4 D after which little variation is observed.

The wake behaviour observed is characterized by a tight vortex formation in the near wake which starts to mix with the bypass flow further downstream. This mixing behaviour results in dissipation of the wake as it is carried downstream. Mixing is then slowed after about 10 D downstream where approximately 80% wake recovery has occurred. The remaining deficit is carried a significant distance downstream.

For the FRG modelling all RANS solutions proved to have the similar problem of accelerated decay of the TKE in the bypass flow. Comparison of the wake width, vortex formation as well as dissipation rate indicated
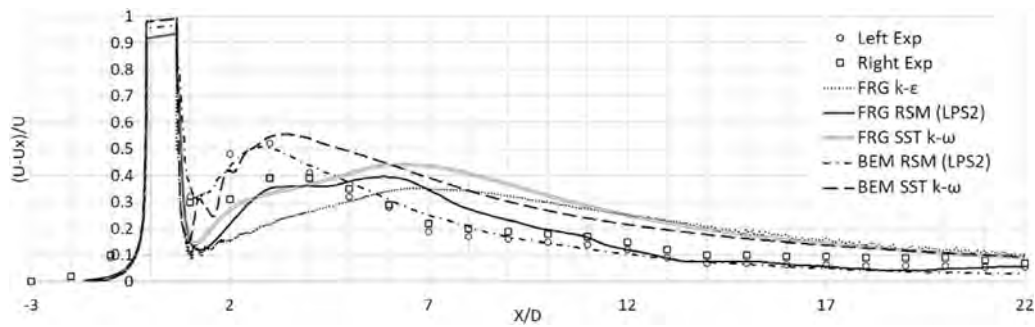
Fig. 14. Comparison of RANS modelling approaches for left and right rotors.

these models (k-ε and SST k-ω) predicted the largest dissimilarity to experimental results in terms of dissipation rate. Although turbine performance was adequately determined, adequate capture of the wake dissipation rate was limited. The SST k-ω showed better prediction than the k-ε model. However, it still overpredicted the wake by up to 20% between 6 D and 10 D downstream and significantly delayed wake recovery.

Employing the RS-LPS2 turbulence model significantly improved predictions with an improved mixing rate in the near wake and good correlation to experimental results after 10 D (Fig. 15). The improvement could be attributed to the RSM's transport equations accounting for the effects of turbulence anisotropy [105,106]. Whereas eddy viscosity models use the Boussinesq hypothesis [64] which assumes isotropic conditions. For LPS2 results accelerated TKE decay in the bypass flow is still observed with inaccurate prediction of dissipating wake behaviour up to 10 D. Although the RS models are known to have more accuracy within turbulence description, they also have limitations in predicting turbulence for complicated flows, especially in describing the effects of rotation [114]. Curvature correction factors are available in some commercial codes and may be a useful tool in some cases. For this investigation, the correction did not have a significant effect. For all RANS solutions inaccurate wake results may also be attributed to the lack of resolving small eddies, which can only be fixed by employing higher fidelity models such as DES or LES.

When coupling BEM-AD with SST k-ω or LPS2 similar behaviour is observed. For the SST k-ω solution, a high velocity deficit is observed in the near wake, resulting in a delayed wake dissipation, and predicting inaccuracies up to 17 D downstream. An accumulated effect is observed through the shortcomings of the VD, which generally over estimates the turbulent eddy viscosity in the high shear flow within the VD and near wake [63]. This induces rapid mixing in the near wake and a higher peak velocity deficit.

The BEM-LPS2 turbulence model showed best correlation to experimental results behind the turbine rotor with a maximum difference of 4% between 3 D and 17 D downstream (Fig. 15). The theoretical modelling of the turbine rotor (using a VD) does not produce strong tip vortices. Although this is a shortcoming of utilizing the BEM-VD approach, when coupled with a RANS solution, the weaker vorticity requires less TKE in the bypass flow to break up the rotating wake structure. As a result, inadequate mixing is less of a problem when combining RANS with this simplified rotor technique (Fig. 15). The better correlation of the BEM-CFD model may be attributed to the shortcomings of the RANS approaches in the FRG rotating body-fluid interaction rather than greater accuracy when using the VD. When using the BEM-CFD approach less accuracy in resolution of the fluid-blade interaction is needed as the rotation effect on the flow is modelled using the BEM theory and therefore only requires correct resolution of the wake beyond the turbine. Further validation cases should investigate the consistency of this effect for variations of operating conditions.
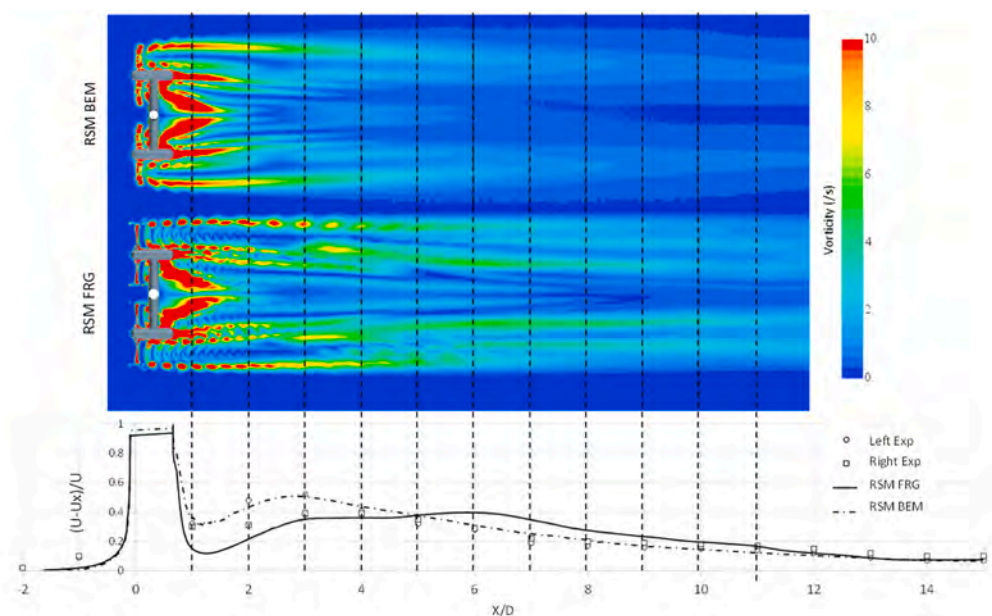

Fig. 15. Vortical structure comparison for the rotor modelling techniques (using RS-LPS2 turbulence model).

4.4. Sensitivity to input parameters and boundary conditions

A major challenge in CFD analysis is the prescription of inlet conditions, especially when validating models with experimental results. Correctly replicating the experimental conditions, including the anisotropy of the turbulence within the inflow boundary is a challenge. It is clear from the equations used to solve turbulence dissipation rate in the SST k-ω model that the chosen freestream values of turbulence quantities have a strong influence on the rate of decay of turbulence [48]. Spalart & Rumsey [48] also demonstrated that eddy viscosity models facilitate more rapid decay of turbulence at higher freestream turbulence intensities (TI), and the same is true for low levels of freestream eddy viscosity. The factor which most affected the recovery rate for all RANS approaches, especially in the near wake, is the specified inlet turbulence. This effect is portrayed in Fig. 16 where the dissipation rate for a high turbulence case (15%) as well as the assumed experimental turbulence case (5%) is compared. Higher turbulence reduced the peak velocity deficit in the near wake, which agrees with previous LES results [85] as well as similar experimental results comparing turbulence cases [24,26].

The experimental turbulent and velocity profiles (Fig. 17) indicate a slight asymmetry about the rotor center. This indicates the free surface as well as channel bed may have an influence on the wake. Although a slight asymmetry is seen in the numerical wake, the effect is more pronounced in experimental conditions [96]. Incorporating an air/water interface may increase the accuracy of capturing the asymmetric effect, but also significantly increases computational overhead [115]. The vertical profile of a multiphase model using the experimentally measured free surface profile at the inlet is shown in Fig. 17c. When comparison is drawn to a single-phase model with a symmetry plane boundary condition (in Fig. 17b) a slight difference in the velocity profile close to the free surface is observed. Additionally, a slightly accelerated recovery region is seen between 6D-10D downstream in the bypass flow between the wake and free surface. Although this effect was minimal in this case, it may be necessary to perform a multiphase analysis when the turbine is in closer proximity to the free surface. The wake effects of depth variation have been previously investigated for a shallow turbine and can be seen in Ref. [42]. Blockage and free surface effects may play a bigger role at higher blockage ratios and cases where turbine performance near the free surface is of importance. When BEM-VD theory is used for scaled tests, blockage correction factors may be incorporated [90].

The inlet and outlet boundary conditions should correctly model the environmental conditions. Any wall boundaries should be modelled to capture the boundary layer formation upstream of the turbine. If a constant velocity is applied at the inlet, full boundary layer formation (ensuring accurate velocity distribution over the flow area) should be reached before the analysis region. More realistic boundary conditions such as those shown in Neary et al. [2] may be used as inlet conditions to reduce mesh sizes (inlet lengths). Utilizing a constant pressure outlet (used in the single-phase analyses) showed negligible effects when compared to the realistic pressure distributions used in the multiphase downstream boundary. However, a distance of at least 10 D to the outlet was ensured here (Fig. 17).

Although this paper has shown better results using RS models, due to the reduced computational expense of two-equation eddy viscosity models, it may be beneficial to use these models as a first order estimate and adjust for differences (especially when FRG modelling is necessary). The solution is to prevent accelerated TKE decay. As mentioned previously, eddy viscosity models result in more rapid decay of turbulence at higher freestream TI's, and the same is true for low levels of freestream eddy viscosity. Therefore, to achieve a reasonable turbulence decay rate, very low TI, or very high eddy viscosity value should be chosen for the freestream.

A solution to this may be "controlled decay" where an ambient turbulence source term is enforced over the domain to prevent decay. This may be done by utilizing the SST k-ω equation but increasing the turbulent production term or adding a turbulence source term equal to the measured TKE or TI present in the flow field, over the whole domain. This limits turbulence dissipation by subtracting the inflow decay specified and counter-acting turbulent decay. In the validation case, addition of the source term significantly improved results to within 5% accuracy between 4 D and 12 D downstream for the FRG case, where the maximum eddy viscosity model error is observed as shown in Fig. 18. Shives & Crawford [63] recommended a more precise solution. To augment the production term in the near wake, specifically for results when a simplified rotor modelling technique is used, and tip vortices are not resolved. However, this is complex and may vary between testing cases. Olczak et al. [44] also improved BEM-CFD results by around 25% through an added turbulence source.

4.5. Further validation of prescribed method

For further assurance of the accuracy of the method which is prescribed in this paper an additional bounded flow HAHT experiment was modelled for comparative purposes. The laboratory test results from Mycek et al. [24,26], were used for comparison. The turbine in Fig. 19 was modelled using the same approach mentioned in Section 3. Two cases with varying inlet TI's were modelled and the wake dissipation rate results were compared.

The mesh resolution was consistent with the ratios used in the RM1 validation case. Boundary layers were altered where needed to ensure the correct wall treatment was implemented on each boundary. A timestep of 0.001s was used ensuring a Courant number less than 1 over all cells in the mesh. A transient LPS2-RS turbulence model was used. A result comparison was drawn. The results indicate the hub height centreline velocity deficit downstream of the turbine and contour plots (Fig. 20) and the average velocity measured over an area equivalent to the turbine swept area (Yr) at ten points downstream of the turbine (1 D to 10 D as shown in Fig. 21). Two sets of experimental results were compared, a low inlet turbulence scenario (with turbulence intensity T = 3%) and a higher inlet turbulence scenario (T = 15%).
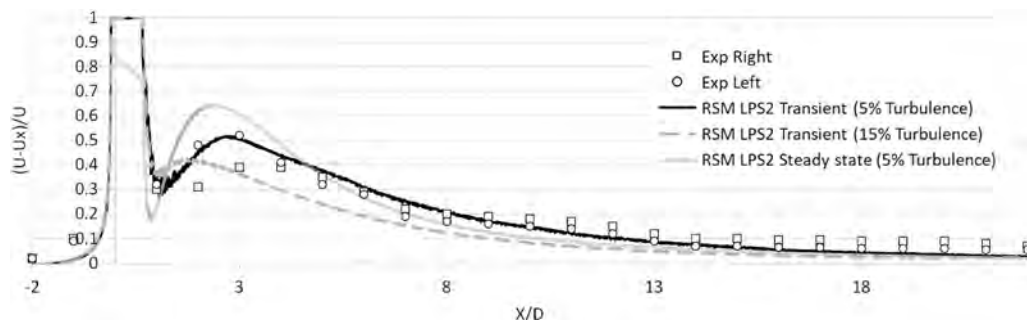
Fig. 16. Turbulence input specification effect on wake dissipation rate for BEM-CFD analyses.
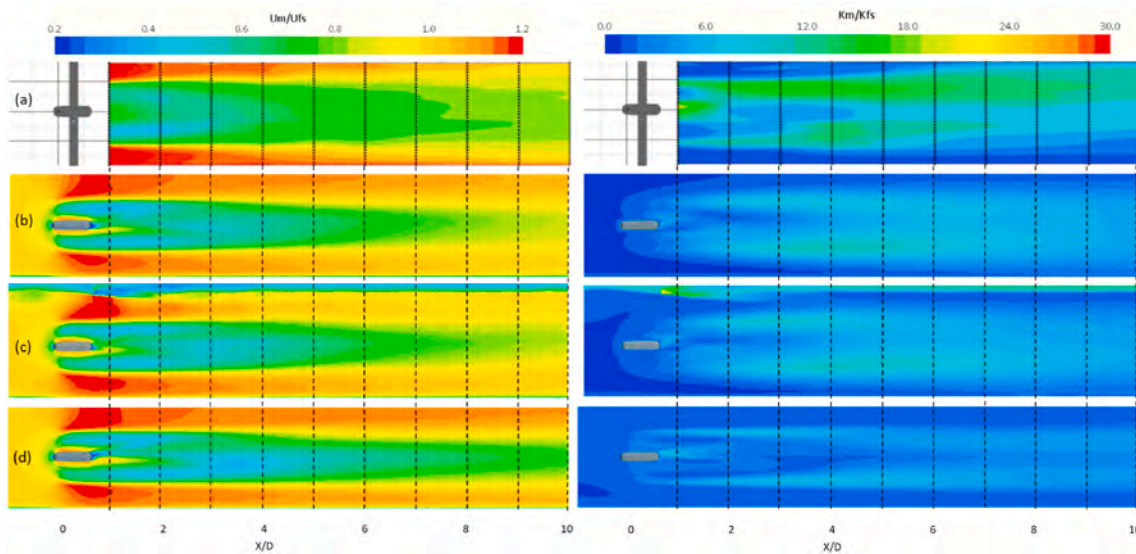
Fig. 17. Vertical velocity (left) and turbulence (right) profiles comparing a) Experimental results b) Single phase BEM-RS (LPS2) c) Multiphase BEM-RS (LPS2) and d) Single phase BEM-SST k-ω
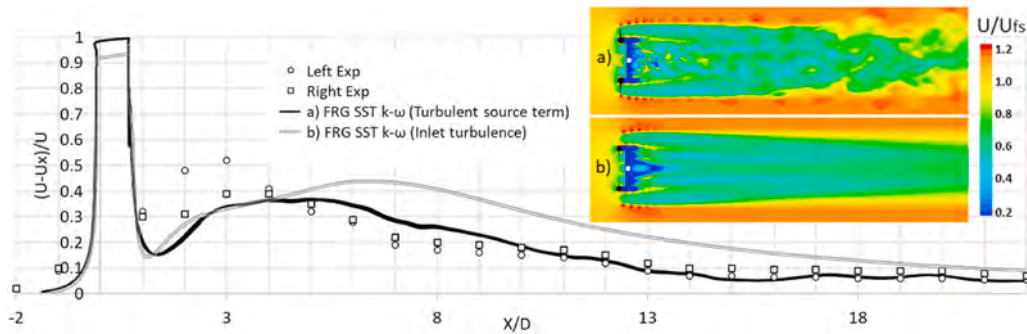
Fig. 18. Turbulence source term SST k-ω improvement.

Description	Variable
Rotor diameter	0.7 m
Blade profile	NACA 63418
Flow depth	2 m
Tip speed ratios measured	0-10
Flow velocity (V_{hub})	0.8 m/s
Reynolds number	$1.4–4.2 \times 10^5$
Sense of rotation	Counter clockwise

Fig. 19. Turbine details and picture [24].

For both the low and high turbulence scenarios a slightly higher velocity deficit was predicted by the CFD model in the near wake (1 D to 3 D). This discrepancy could be attributed to multiple factors, such as mesh size, implemented turbulence model (for the CFD model) as well as experimental measurement error. On close inspection of the wake behind the turbine hub, which extended 1.02 D behind the turbine, a very low velocity zone can is observed directly behind the hub (Fig. 22), which is to be expected as flow passes a blunt body. The Karman vortex street behaviour is also seen behind the hub and results in a highly turbulent zone. If this behaviour is predicted correctly, it would make accurate experimental point velocity measurements using probes quite difficult and could thus result in lower velocity measurements. An example of this can be seen in Fig. 22 where lines slightly offset from the centreline were used to measure the mean flow velocity downstream over a single rotation. The results varied significantly in the near wake

and when used, showed closer correlation to the experimental measurements. This indicates velocity deficit changes up to 50% could occur in the near wake by probe placement inaccuracies of only 50 mm (0.07 D). This inaccuracy may be eliminated by using the area averaged velocities (Fig. 21) where measurements of velocity deficit were averaged over an area equivalent to the turbine swept area (Yr). This analysis would more likely remove errors made in point velocity measurements and could therefore result in the better correlation observed.

A slight underestimation of the velocity deficit in the high TI scenario (T = 15%) is observed. This could be attributed to the overly rapid dissipation of turbulence resulting from the use of the RS models which also reduced the wake spreading effect observed in the experimental case Fig. 20b. This effect may be more pronounced in higher turbulence cases. Despite this difference the CFD model seems to predict the wake dissipation rate to a relatively high degree of accuracy after 3 D
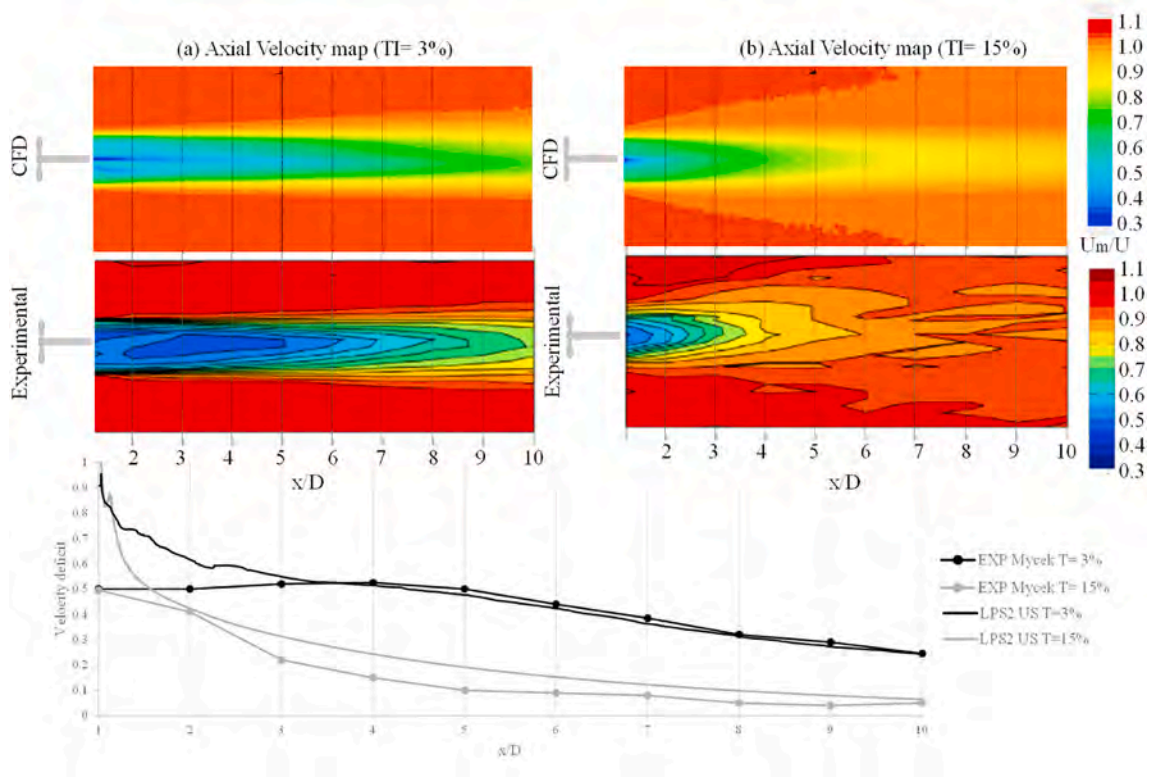
Fig. 20. Comparative results of the downstream lines and contour plots for (a) T = 3% and (b) T = 15%.

Fig. 21. Results for the velocity deficit averaged over the turbine swept area at points downstream.

Fig. 22. Downstream mean velocity deficit for (a) centreline (b) left offset 0.07 D and (c) right offset 0.07 D and instantaneous velocity contour plot.

downstream (max error of 4.5% for the T = 3% case and 9% for the T = 9% case). The model also captures the change in wake behaviour when the inlet turbulence is altered, which is an important input variable in wake analysis.

4.6. Discussion of findings

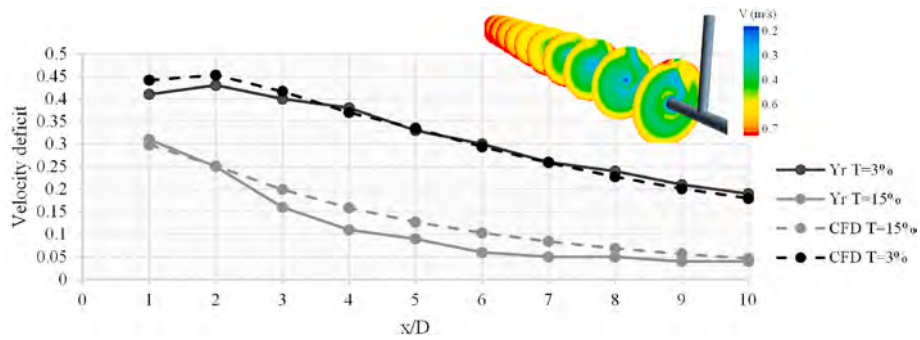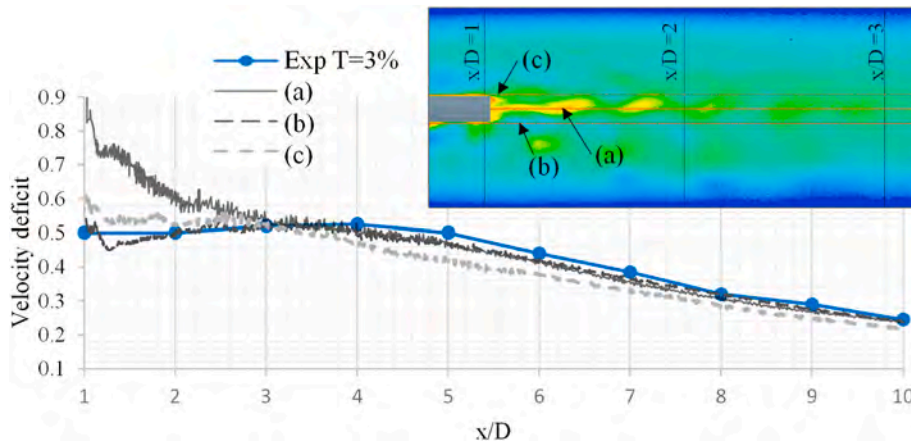The review study highlights the importance of a rigorous validation process and using tested computational methods when analysing the effects of HK turbines on wake generation and flow recovery. The following points summarize the key findings:

1] The shortcomings of the employed modelling technique (analytical models, simplified numerical models, CFD models) should be understood and carefully considered. Often too much confidence is placed on results from simplified techniques that have not been properly validated.

2] Simplified techniques may be used where the intention of the model is a specific part/scale where uniformity laws are focused on only relevant areas to decrease required computational resources. Here, the consideration of scales of modelling and ensuring proper validation of the analysis region is important.

3] Correct description of the boundary conditions as well as quantifying the sensitivity of such boundary conditions are crucial for CFD models. In this work the free-surface and blockage effects as well as upstream development of wall boundary layers were of important concern. The complex inlet condition (velocity and turbulent distribution) should be carefully modelled. This is even more important for inland HK device application where spatial constraints give rise to many design limitations.

4] The correct selection and application of turbulence models is important. Research on the applicability of turbulence models within the HK flow environment has increased in recent years, many of which are summarized in this paper. The importance of understanding the applicability and limitations of each model prior to application remains critical, especially as commercial modelling software becomes an increasingly common tool for feasibility studies and design. A carefully researched and prescribed method should be used in such cases (as is a primary purpose of this review).

5] Rotor modelling techniques in CFD applications should be selected together with turbulence models and based on the analysis region. FRG modelling performs well for performance tests but has shown to have shortcomings in wake dissipation accuracy when coupled with RANS models. Simplified disk techniques should only be used when well-defined input parameters (lift and drag coefficients etc.) are available.

A collective review of literature and comparison of approaches ensures an evolution of techniques and improved application of modelling software. Often available literature is not considered prior to design testing, or isolated studies with fitted validation cases are used resulting in incorrectly predicted flow behaviour. This collection and revision of findings serves to provide a "fuller-picture" of commonly applied modelling techniques, shortcomings, and possible solutions.

5. Conclusions

A growing number of researchers and design engineers are using CFD for wake analysis of hydrokinetic turbine design. This is often done without sufficient model validation. Although investigation into simplified analytical models for tidal energy applications has been extensively researched, for inland schemes design spacing may be governed by blockage ratios, confinement, and spatial limitations. Therefore, a more descriptive analysis of the system characteristics and their effects in the complex wake field is necessary. The use of CFD and 3-D modelling of the flow field offers a more in-depth result, which is an

advantage over traditional BEM. Here the wake interactions may also be analysed. This paper examines the limitations of commercially available CFD models and methods used in HAHT wake analysis.

Higher order models such as LES and DES are becoming more affordable as computational resources increase in availability. However, a simplified BEM-RANS analysis serves as a lower-cost computational tool which can adequately model the wake dissipation, including effects of retaining structures as well as inlet conditions (e.g., Turbulence). There are however limitations in accurately predicting the near wake, including underestimation of the TKE present in the flow and a sensitivity to input variables. These limitations must be understood prior to application.

All RANS models and rotor modelling techniques indicated good representations of the turbine performance metrics, which are also often used in literature. However, the performance of these modelling techniques varies when simulating more complex wake dissipation behaviour. Despite the slight inaccuracies, which could be a result of one or more of the mentioned factors, the present study indicates under current available commercial CFD approaches the BEM-CFD approach using RSM-LPS2 model allows a fairly accurate analysis of the near and far wake dissipation rate. The rate of decay of the wake indicated a maximum of 4% difference when the model is analysed using the prescribed conditions without further calibration from validation case discrepancies. The sensitivity of the VD to input parameters and foil properties should be considered and care should be taken to ensure accurate and extensive input data. The model was also shown to be sensitive to turbulent inflow conditions and may therefore be a better tool to employ when analysing flow over a range of operating conditions.

A second validation case with different operational parameters and ambient turbulences showed adequate accuracy in the velocity deficit in the near and far wake. Further, validation cases should investigate the consistency of the BEM-LPS2 solution. However, accuracy and good characterization of uncertainties in experimental results is imperative to proper validation and recommending useful computational modelling methods.

When the full geometry of the turbine is used for analysis, care should be taken in the selection of turbulence models and mesh refinement, specifically in the near wake where small changes in mesh size significantly influence results. This study has highlighted some inaccuracies in wake dissipation rates resulting from the use of full rotor geometry when coupled with the analysed approaches. This may be due to the lack of resolution in the small eddies in the wake, or inaccuracies in the fluid body interaction with the rotating blades. The result is stronger vortices in the near wake and rapidly degrading TKE in the bypass flow which delays wake dissipation. Thus, it may be preferential to use a disk approach rather than the full rotating geometry when employing RANS models.

Although higher fidelity Reynolds Stress models are preferable to accurately model the wake, computational time and expense may not allow this. Solutions to offset the poor performance of eddy viscosity models due to accelerated TKE depletion can be counteracted by limiting the minimum value of TI in the flow field. A few investigations into possible solutions have been examined, and a simple solution may be to specify an ambient turbulent source term in the investigated validation case. However, this solution should be used with care and requires further investigation.

It is known in experimental wake studies and validation cases that scaling parameters and keeping to required uniformity laws are of concern. This is especially true when considering the Reynolds number and the lack of confidence in models validated further from the Reynolds number experienced at full-scale. Although Reynolds number dependence was not relevant here, as no scaling was carried out, numerical models have shown to have strong Reynolds dependencies.

CFD is a useful tool for wake analysis and provides detailed results of the wake structure and dissipation rate when coupled with the correct

input parameters and solvers required to simulate the complexities of wake flow. CFD is preferable over simplified numerical tools, e.g., analytical models because it resolves the effects of wake interaction, retaining structures and blockage effects, which can be significant in inland hydrokinetic schemes due to spatial limitations. Hence, it is a useful tool for design and analysis of inland HAHT schemes.

Funding

Declaration of competing interest

The authors declare that they have no known competing financial interests or personal relationships that could have appeared to influence the work reported in this paper.

Acknowledgements

References

[1] EPRI. Assessment and Mapping of the Riverine Hydrokinetic Resource in the Continental United States. 2012. Palo Alto, CA.
[2] Neary VS, Gunawan B, Sale DC. Turbulent inflow characteristics for hydrokinetic energy conversion in rivers. Renew Sustain Energy Rev 2013;26:437–45. https://doi.org/10.1016/j.rser.2013.05.033.
[3] Guerra M, Thomson J. Wake measurements from a hydrokinetic river turbine. Renew Energy 2019;139:483–95. https://doi.org/10.1016/j.renene.2019.02.052.
[4] Fontaine AW, Straka W, Meyer R, Jonson M, Neary VS. Performance and wake flow characterization of a 1:8.7 scale reference USDOE MHKF1 hydrokinetic turbine to establish a verification and validation test database. Renew Energy 2020;159:451–67. https://doi.org/10.1016/j.renene.2020.05.166. In press.
[5] Niebuhr CM, van Dijk M, Neary VS, Bhagwan JN. A review of hydrokinetic turbines and enhancement techniques for canal installations: Technology, applicability and potential. Renew Sustain Energy Rev 2019;113. https://doi.org/10.1016/j.rser.2019.06.047.
[6] Niebuhr CM, van Dijk M, Bhagwan JN. Development of a design and implementation process for the integration of hydrokinetic devices into existing infrastructure in South Africa. WaterSA 2019;45:434–46.
[7] Myers LE, Bahaj AS. An experimental investigation simulating flow effects in first generation marine current energy converter arrays. Renew Energy 2012;37: 28–36. https://doi.org/10.1016/j.renene.2011.03.043.
[8] Neary VS, Gunawan B, Hill C, Chamorro LP. Near and far field flow disturbances induced by model hydrokinetic turbine: ADV and ADP comparison. Renew Energy 2013;60:1–6. https://doi.org/10.1016/j.renene.2013.03.030.
[9] De Dominicis M, O'Hara Murray R, Wolf J. Multi-scale ocean response to a large tidal stream turbine array. Renew Energy 2017;114:1160–79. https://doi.org/10.1016/j.renene.2017.07.058.
[10] Goward Brown AJ, Neill SP, Lewis MJ. Tidal energy extraction in three-dimensional ocean models. Renew Energy 2017;114:244–57. https://doi.org/10.1016/j.renene.2017.04.032.
[11] Consul CA, Willden RHJ, McIntosh SC. Blockage effects on the hydrodynamic performance of a marine cross-flow turbine. Philos. Trans. R. Soc. A. 2013;371. https://doi.org/10.1098/rsta.2012.0299.
[12] Riglin J, Carter F, Oblas N, Schleicher WC, Daskiran C, Oztekin A. Experimental and numerical characterization of a full-scale portable hydrokinetic turbine prototype for river applications. Renew Energy 2016;99:772–83.
[13] Bahaj AS, Molland AF, Chaplin JR, Batten WMJ. Power and thrust measurements of marine current turbines under various hydrodynamic flow conditions in a cavitation tunnel and a towing tank. Renew Energy 2007;32:407–26. https://doi.org/10.1016/j.renene.2006.01.012.
[14] Salunkhe S, El Fajri O, Bhushan S, Thompson D, O'Doherty D, O'Doherty T, Mason-Jones A. Validation of tidal stream turbine wake predictions and analysis of wake recovery mechanism. J Mar Sci Eng 2019;7. https://doi.org/10.3390/jmse7100362.
[15] Olivieri D, Ingram D. Tidal array scale numerical modelling . Interactions within a farm (unsteady Flow). 2013. Edinburgh.
[16] Hill C, Neary VS, Guala M, Sotiropoulos F. Performance and wake characterization of a model hydrokinetic turbine: the reference model 1 (RM1) dual rotor tidal energy converter. Energies 2020:1–21. https://doi.org/10.3390/en13195145.
[17] Kolekar N, Banerjee A. Performance characterization and placement of a marine hydrokinetic turbine in a tidal channel under boundary proximity and blockage effects. Appl Energy 2015;148:121–33. https://doi.org/10.1016/j.apenergy.2015.03.052.
[18] Birjandi AH, Bibeau EL, Chatoorgoon V, Kumar A. Power measurement of hydrokinetic turbines with free-surface and blockage effect. Ocean Eng 2013;69: 9–17. https://doi.org/10.1016/j.oceaneng.2013.05.023.
[19] Adcock TAA, Draper S, Nishino T. Tidal power generation – a review of hydrodynamic modelling. J. Power Energy. 2015:1–17. https://doi.org/10.1177/0957650915570349.
[20] Walker J, Flack K, Lust E, Mp S, Luznik L. Experimental and numerical studies of blade roughness and fouling on marine current turbine performance. Renew Energy 2014;66:257–67.
[21] Mannion B, McCormack V, Leen SB, Nash S. A CFD investigation of a variable-pitch vertical axis hydrokinetic turbine with incorporated flow acceleration. J. Ocean Eng. Mar. Energy. 2019;5:21–39. https://doi.org/10.1007/s40722-019-00130-1.
[22] Churchfield MJ, Li Y, Moriarty PJ. A large eddy simulation study of wake propagation and power production in an array of tidal-current turbines. Philos. Trans. R. Soc. A. 2013;371:1–15.
[23] Sanderse B, van der Pijl SP, Koren B. Review of computational fluid dynamics for wind turbine wake aerodynamics. Wind Energy 2011;14:799–819. https://doi.org/10.1002/we.
[24] Mycek P, Gaurier B, Germain G, Pinon G, Rivoalen E. Experimental study of the turbulence intensity effects on marine current turbines behaviour. Part I: one single turbine. Renew Energy 2014;66:729–46. https://doi.org/10.1016/j.renene.2013.12.048.
[25] Maganga F, Germain G, King J, Pinon G, Rivoalen E. Experimental characterisation of flow effects on marine current turbine behaviour and on its wake properties. IET Renew Power Gener 2010;4:498–509. https://doi.org/10.1049/iet-rpg.2009.0205.
[26] Mycek P, Gaurier B, Germain G, Pinon G, Rivoalen E. Experimental study of the turbulence intensity effects on marine current turbines behaviour. Part II: two interacting turbines. Renew Energy 2014;68:876–92. https://doi.org/10.1016/j.renene.2013.12.048.
[27] Edmunds M, Malki R, Williams AJ, Masters I, Croft TN. Aspects of tidal stream turbine modelling in the natural environment using a coupled. BEM – CFD model 2014;7:20–42.
[28] Malki R, Masters I, Williams AJ, Croft TN. Planning tidal stream turbine array layouts using a coupled blade element momentum e computational fluid dynamics model. Renew Energy 2014;63:46–54.
[29] Churchfield MJ, Li Y, Moriarty PJ. A large-eddy simulation study of wake propagation and power production in an array of tidal-current turbines. Philos. Trans. R. Soc. A. 2013;371.
[30] Dai Y, Ren Z, Wang K, Li W, Li Z, Yan W. Optimal sizing and arrangement of tidal current farm. IEEE Trans Sustain Energy 2018;9:168–77. https://doi.org/10.1109/TSTE.2017.2719042.
[31] Kartezhnikova M, Ravens TM. Hydraulic impacts of hydrokinetic devices. Renew Energy 2014;66:425–32. https://doi.org/10.1016/j.renene.2013.12.034.
[32] Lam WH, Chen L. Equations used to predict the velocity distribution within a wake from a horizontal-axis tidal-current turbine. Ocean Eng 2014;79:35–42. https://doi.org/10.1016/j.oceaneng.2014.01.005.
[33] Pyakurel P, Vanzwieten JH, Wenlong T, Ananthakrishnan P. Analytic characterization of the wake behind in-stream hydrokinetic turbines. Mar Technol Soc J 2017;51:58–71.
[34] Silva PASF, De Oliveira TF, Brasil Junior ACP, Vaz JRPP, Oliveira TFDE, Junior ACPB, Vaz JRPP. Numerical study of wake characteristics in a horizontal-Axis hydrokinetic turbine. Ann. Brazilian Acad. Sci. 2016;88:2441–56. https://doi.org/10.1590/0001-3765201620150652.
[35] Harrison ME, Batten WMJ, Myers LE, Bahaj AS. Comparison between CFD simulations and experiments for predicting the far wake of horizontal axis tidal turbines. IET Renew Power Gener 2010;4:613. https://doi.org/10.1049/iet-rpg.2009.0193.
[36] Bahaj AS, Myers LE, Thomson MD, Jorge N. Characterising the wake of horizontal axis marine current turbines. In: 7th Eur. Wave Tidal Energy Conf.; 2007.
[37] Boudreau M, Dumas G. Comparison of the wake recovery of the axial-flow and cross-flow turbine concepts. J Wind Eng Ind Aerod 2017;165:137–52. https://doi.org/10.1016/j.jweia.2017.03.010.

[38] Chen B, Lin, Lin J, Wang S. Experimental study of wake structure behind a horizontal axis tidal stream turbine. Appl Energy 2017;196:82–96.

[39] Silva PASF, De Oliveira TF, Brasil Junior ACP, Vaz JRP. Numerical study of wake characteristics in a horizontal-axis hydrokinetic turbine. An Acad Bras Cienc 2016;88:2441–56. https://doi.org/10.1590/0001-3765201620150652.

[40] Chamorro LP, Hill C, Morton S, Ellis C, Arndt REA, Sotiropoulos F. On the interaction between a turbulent open channel flow and an axial-flow turbine. J Fluid Mech 2013;716:658–70. https://doi.org/10.1017/jfm.2012.571.

[41] Bahaj AS, Myers LE, Rawlinson-Smith RI, Thomson M. The effect of boundary proximity upon the wake structure of horizontal axis marine current turbines. J Offshore Mech Arctic Eng 2011;134:1–8. https://doi.org/10.1115/1.4004523.

[42] Aghsaee P, Markfort CD. Effects of flow depth variations on the wake recovery behind a horizontal-axis hydrokinetic in-stream turbine. Renew Energy 2018;125:620–9. https://doi.org/10.1016/j.renene.2018.02.137.

[43] Garrett C, Cummins P. The efficiency of a turbine in a tidal channel. J Fluid Mech 2007;588:243–51. https://doi.org/10.1017/S0022112007007781.

[44] Olczak A, Stallard T, Feng T, Stansby PK. Comparison of a RANS blade element model for tidal turbine arrays with laboratory scale measurements of wake velocity and rotor thrust. J Fluid Struct 2016;64:87–106. https://doi.org/10.1016/j.jfluidstructs.2016.04.001.

[45] Sanderse B. Aerodynamics of wind turbine wakes: Literature review. 2009. https://doi.org/10.1002/we.

[46] Edmunds M, Williams AJ, Masters I, Croft TN. An enhanced disk averaged CFD model for the simulation of horizontal axis tidal turbines 2017;101:67–81.

[47] Mehta D, Van Zuijlen AH, Koren B, Holierhoek JG, Bijl H. Large Eddy Simulation of wind farm aerodynamics : a review. J Wind Eng Ind Aerod 2014;133:1–17. https://doi.org/10.1016/j.jweia.2014.07.002.

[48] Spalart PR, Rumsey CL. Effective inflow conditions for turbulence models in aerodynamic calculations. AIAA J 2007;45:2544–53. https://doi.org/10.2514/1.29373.

[49] Mikkelson R, Sorensen JN, Schen WZ. Modelling and analysis of the flow field around a coned rotor. Wind Energy 2001;4:121–35.

[50] a Lo Brutto O, Nguyen VT, Guillou SS, Gualous H, Boudart B. Reanalyse of an analytical model for one tidal turbine wake prediction. In: Proc. 11th Eur. Wave Tidal Energy Conf.; 2015. Nantes, France.

[51] Lam WH, Chen L, Hashim R. Analytical wake model of tidal current turbine. Energy 2015;79:512–21. https://doi.org/10.1016/j.energy.2014.11.047.

[52] Tian L, Zhu W, Shen W, Zhao N, Shen Z. Development and validation of a new two-dimensional wake model for wind turbine wakes. J Wind Eng Ind Aerod 2015;137:90–9. https://doi.org/10.1016/j.jweia.2014.12.001.

[53] Nishino T, Willden RHJ. Effects of 3-D channel blockage and turbulent wake mixing on the limit of power extraction by tidal turbines. Int J Heat Fluid Flow 2012;37:123–35. https://doi.org/10.1016/j.ijheatfluidflow.2012.05.002.

[54] Nishino T, Willden RHJ. Two-scale dynamics of flow past a partial cross-stream array of tidal turbines. 2013. p. 220–44. https://doi.org/10.1017/jfm.2013.340.

[55] Gotelli C, Musa M, Guala M, Escauriaza C. Experimental and numerical investigation of wake interactions of marine hydrokinetic turbines. Energies 2019;12:1–17. https://doi.org/10.3390/en12163188.

[56] Whale J, Anderson CG, Bareiss R, Wagner S. An experimental and numerical study of the vortex structure in the wake of a wind turbine. J Wind Eng Ind Aerod 2000;84:1–21. https://doi.org/10.1016/S0167-6105(98)00201-3.

[57] Pinon G, Mycek P, Germain G, Rivoalen E. Numerical simulation of the wake of marine current turbines with a particle method. Renew Energy 2012;46:111–26. https://doi.org/10.1016/j.renene.2012.03.037.

[58] Fabrice M, Gregory P, Gregory G, Elie R. Numerical simulation of the wake of marine current turbines with a particle method. Glasgow: World Renew. Energy Congr. X; 2008.

[59] Tian W, Mao Z, Ding H. Design, test and numerical simulation of a low-speed horizontal axis hydrokinetic turbine. Int. J. Nav. Archit. Ocean Eng. 2018;10:782–93.

[60] Ge M, Wu Y, Liu Y, Yang XIA. A two-dimensional Jensen model with a Gaussian-shaped velocity deficit. Renew Energy 2019;141:46–56. https://doi.org/10.1016/j.renene.2019.03.127.

[61] Pyakurel P, Tian W, VanZwieten JH, Dhanak M. Characterization of the mean flow field in the far wake region behind ocean current turbines. J. Ocean Eng. Mar. Energy. 2017;3:113–23. https://doi.org/10.1007/s40722-017-0075-9.

[62] Contreras L, Lopez Y, Lain S. CFD simulation of a horizontal Axis hydrokinetic turbine. Renew. Energy Power Qual. J. 2017;1:512–7. https://doi.org/10.24084/repqj15.376.

[63] Shives M, Crawford C. Turbulence modelling for accurate wake prediction in tidal turbine arrays. In: 5th Int. Conf. Ocean Energy. Halifax: Canada; 2014.

[64] Menter FR. Turbulence Modeling for Engineering Flows. 2011. http://cfd.spbstu.ru/agarbaruk/c/document_library/DLFE-41517.pdf.

[65] McNaughton J, Rolfo S, Apsley DD, Afgan I, Stansby PK, Stallard T. CFD prediction of turbulent flow on an experimental tidal stream turbine using RANS modelling. 1st Asian Wave Tidal Conf. Ser.; 2012. https://doi.org/10.1017/CBO9781107415324.004.

[66] Kang S, Borazjani I, Colby JA, Sotiropoulos F. Numerical simulation of 3D flow past a real-life marine hydrokinetic turbine. Adv Water Resour 2012;39:33–43. https://doi.org/10.1016/j.advwatres.2011.12.012.

[67] Spalart PR. Strategies for turbulence modeling and simulations. Int J Heat Fluid Flow 2000;21:252–63.

[68] Blackmore T, Batten WMJ, Bahaj AS. Influence of turbulence on the wake of a marine current turbine simulator. Proc. R. Soc. A Math. Phys. Eng. Sci. 2014;470:1–17. https://doi.org/10.1098/rspa.2014.0331.

[69] Kang S, Yang X, Sotiropoulos F. On the onset of wake meandering for an axial flow turbine in a turbulent open channel flow. J Fluid Mech 2014;744:376–403. https://doi.org/10.1017/jfm.2014.82.

[70] Bai G, Li J, Fan P, Li G. Numerical investigations of the effects of different arrays on power extractions of horizontal axis tidal current turbines. Renew Energy 2013;53:180–6. https://doi.org/10.1016/j.renene.2012.10.048.

[71] Lain S, Contreras LT, Lopez O. A review on computational fluid dynamics modeling and simulation of horizontal axis hydrokinetic turbines. J. Brazilian Soc. Mech. Sci. Eng. 2019;41(9):1–24. https://doi.org/10.1007/s40430-019-1877-6. In this issue.

[72] Vermeer LJ, Sørensen JN, Crespo A. Wind turbine wake aerodynamics. Prog Aero Sci 2003;39:467–510. https://doi.org/10.1016/S0376-0421(03)00078-2.

[73] Masters I, Williams A, Croft TN, Togneri M, Edmunds M, Zangiabadi E, Fairley I, Karunarathna H. A comparison of numerical modelling techniques for tidal stream turbine analysis. Energies 2015;8:7833–53. https://doi.org/10.3390/en8087833.

[74] El khchine Y, Sriti M. Tip loss factor effects on aerodynamic performances of horizontal Axis wind turbine. In: 2nd Int. Conf. Adv. Berlin, Germany: . Clean Energy Res.; 2017. p. 2–6.

[75] Shen WZ, Mikkelsen R, Sorensen JN. Tip loss corrections for wind turbine Computations. Wind Energy 2005;8:457–75. https://doi.org/10.1002/we.153.

[76] Masters I, Chapman JC, Willis MR, Orme JAC. A robust blade element momentum theory model for tidal stream turbines including tip and hub loss corrections. J. Mar. Eng. Technol. 2014;10:25–35. https://doi.org/10.1080/20464177.2011.11020241.

[77] Burton T, Jenkins N, Sharpe D, Bossanyi E. Wind Energy Handbook (2nd Edition). second ed. John Wiley & Sons; 2011. https://doi.org/10.1007/978-3-540-88258-9-1.

[78] Guo Q, Zhou L, Wang Z. Comparison of BEM-CFD and full rotor geometry simulations for the performance and flow field of a marine current turbine. Renew Energy 2015;75:640–8.

[79] Malki R, Williams AJ, Croft TN, Togneri M, Masters I. A coupled blade element momentum – computational fluid dynamics model for evaluating tidal stream turbine performance. Appl Math Model 2013;37:3006–20. https://doi.org/10.1016/j.apm.2012.07.025.

[80] Turnock SR, Phillips AB, Banks J, Nicholls-Lee R. Modelling tidal current turbine wakes using a coupled RANS-BEMT approach as a tool for analysing power capture of arrays of turbines. Ocean Eng 2011;38:1300–7. https://doi.org/10.1016/j.oceaneng.2011.05.018.

[81] Malki R, Masters I, Williams AJ, Croft N. The variation in wake structure of a tidal stream turbine with flow velocity. In: Int. Conf. Comput. Methods Mar. Eng.; 2011. https://doi.org/10.1007/978-94-007-6143-8. Barcelona.

[82] Masters I, Malki R, Williams AJ, Croft TN. The influence of flow acceleration on tidal stream turbine wake dynamics : a numerical study using a coupled BEM – CFD model. Appl Math Model 2013;37:7905–18. https://doi.org/10.1016/j.apm.2013.06.004.

[83] Gajardo D, Escauriaza C, Ingram DM. Capturing the development and interactions of wakes in tidal turbine arrays using a coupled BEM-DES model. Ocean Eng 2019;181:71–88. https://doi.org/10.1016/j.oceaneng.2019.03.064.

[84] Myers L, Bahaj AS. Near wake properties of horizontal axis marine current turbines. In: Eighth Eur. Wave Tidal Energy Cnference. Uppsala: Swedeb; 2009. p. 558–65.

[85] Ahmadi MHB. Influence of upstream turbulence on the wake characteristics of a tidal stream turbine. Renew Energy 2019;132:989–97. https://doi.org/10.1016/j.renene.2018.08.055.

[86] Morris CE, O'Doherty DM, Mason-Jones A, O'Doherty T. Evaluation of the swirl characteristics of a tidal stream turbine wake. Int. J. Mar. Energy. 2016;14:198–214. https://doi.org/10.1016/j.ijome.2015.08.001.

[87] Siddiqui MS, Rasheed A di, Kvamsdal T, Tabib M. Influence of tip speed ratio on wake flow characteristics utilizing fully resolved CFD methodology. J. Phys. Conf. Ser. 2017;854. https://doi.org/10.1088/1742-6596/854/1/012043.

[88] Nezu I, Nakagawa H, Jirka GH. Turbulence in open-channel flows. J Hydraul Eng 1994;120.

[89] Neary VS, Gunawan B, Hill C, Chamorro LP. Near and far field flow disturbances induced by model hydrokinetic turbine: ADV and ADP comparison. Renew Energy 2013;60:1–6. https://doi.org/10.1016/j.renene.2013.03.030.

[90] Whelan JI, Graham JMR, Peiró J. A free-surface and blockage correction for tidal turbines. J Fluid Mech 2009;624:281–91. https://doi.org/10.1017/S0022112009005916.

[91] Myers LE, Bahaj AS. Experimental analysis of the flow field around horizontal axis tidal turbines by use of scale mesh disk rotor simulators. Ocean Eng 2010;37:218–27. https://doi.org/10.1016/j.oceaneng.2009.11.004.

[92] El Fajri O, Bhushan S, Thompson DS, O'Doherty T. Numerical investigation of shallow-water effects on hydrokinetic turbine wake recovery. Int. Mar. Energy J. 2020;3:25–35. https://doi.org/10.36688/imej.3.25-35.

[93] Stallard T, Collings R, Feng T, Whelan J. Interactions between tidal turbine wakes: experimental study of a group of three-bladed rotors. Philos. Trans. R. Soc. A Math. Phys. Eng. Sci. 2013;371. https://doi.org/10.1098/rsta.2012.0159.

[94] Bachant P, Wosnik M. Reynolds number dependence of cross-flow turbine performance and near- wake characteristics. In: Proc. 2nd Mar. Energy Technol. Symp.; 2014. Seattle, WA.

[95] Ross H, Polagye B. An experimental assessment of analytical blockage corrections for turbines. Renew Energy 2020;152:1328–41.

[96] Hill C, Neary VS. U. S. Department of Energy Reference Model Program RM1 : Experimental Results. Sandia Natl. Lab.; 2014.

[97] Gunawan B, Neary VS, McNutt JR. ORNL ADV Post-Processing Guide and MATLAB Algorithms for MHK Site Flow and Turbulence Analysis. Oak Ridge, Tennessee: US Department of Energy; 2011.

[98] Nasef MH, El-Askary WA, AbdEL-hamid AA, Gad HE. Evaluation of Savonius rotor performance: static and dynamic studies. J Wind Eng Ind Aerod 2013;123:1–11. https://doi.org/10.1016/j.jweia.2013.09.009.

[99] Franke J, Hirsch C, Jensen AG, Krus HW, Schatzmann PS, Miles SD, Wisse JA, Wright NG. Recommendations on the use of CFD in wind engineering, COST Action C14 Impact Wind Storm City Life Urban Environ. 2004.

[100] Miller VB, Schaefer LA. Dynamic modeling of hydrokinetic energy extraction. J. Fluids Eng. Trans. ASME. 2010;132:1–7. https://doi.org/10.1115/1.4002431.

[101] Daskiran C, Riglin J, Schleicher W, Oztekin A. Transient analysis of micro-hydrokinetic turbines for river applications 2017;129:291–300.

[102] Afgan I, Mcnaughton J, Rolfo S, Apsley DD, Stallard T, Stansby P. Turbulent flow and loading on a tidal stream turbine by LES and RANS. Int J Heat Fluid Flow 2013;43:96–108. https://doi.org/10.1016/j.ijheatfluidflow.2013.03.010.

[103] Menter FR. Two-equation eddy-viscosity turbulence models for engineering applications. AIAA J 1994;32:1598–605.

[104] Menter FR, Kuntz M, Langtry R. Ten years of industrial experience with the SST turbulence model. Turbul Heat Mass Transf 2003;4:625–32.

[105] Speziale CG, Sarkar S, Gatski TB. Modelling the pressure-strain correlation of turbulence : an invariant dynamical systems approach. J Fluid Mech 1991;227:245–72. https://doi.org/10.1017/S0022112091000101.

[106] Sarkar S, Lakshmanan B. Application of a Reynolds stress turbulence model to the compressible shear layer. AIAA J 1991;29:743–9. https://doi.org/10.2514/3.10649.

[107] Roache PJ. Perspectvie: a method for uniform reporting of grid refinement studies. J. Fluids Eng. Trans. ASME. 1994;116:405–13.

[108] Gibson MM, Launder BE. Ground effects on pressure fluctuations in the atmospheric boundary layer. J Fluid Mech 1978;86:491–511. https://doi.org/10.1017/S0022112078001251.

[109] Allmark M, Ellis R, Lloyd C, Ordonez-Sanchez S, Johannesen K, Byrne C, Johnstone C, O'Doherty T, Mason-Jones A. The development, design and characterisation of a scale model Horizontal Axis Tidal Turbine for dynamic load quantification. Renew Energy 2020;156:913–30. https://doi.org/10.1016/j.renene.2020.04.060.

[110] Lavaroni L, Watson SJ, Cook MJ, Dubal MR. A comparison of actuator disc and BEM models in CFD simulations for the prediction of offshore wake losses. J. Phys. Conf. Ser. 2014;524. https://doi.org/10.1088/1742-6596/524/1/012148.

[111] Hill C, Neary VS, Gunawan B, Guala M, Sotiropoulos F. U. S. Department of Energy Reference Model Program RM1 : Experimental Results. 2014. Minneapolis.

[112] Hoffmann MJ, Reuss Ramsay R, Gregorek GM. Effects of grit roughness and pitch oscillations on the NACA 4415 airfoil. 1996. https://doi.org/10.2172/266691.

[113] Fouatih OM, Imine B, Medale M. Numerical/experimental investigations on reducing drag penalty of passive vortex generators on a NACA 4415 airfoil. Wind Energy 2019;22:1003–17. https://doi.org/10.1002/we.2330.

[114] Wallin S, Johansson AV. An explicit algebraic Reynolds stress model for incompressible and compressible turbulent flows. J Fluid Mech 2000;403:89–132. https://doi.org/10.1017/S0022112099007004.

[115] McBride D, Croft TN, Cross M. A coupled finite volume method for the computational modelling of mould filling in very complex geometries, Comput. Fluid 2008;37:170–80.

Development of a semi-empirical wake formation and dissipation prediction model for HAHT placed in channel flow

C.M. Niebuhr [a,*], M. van Dijk [a], L. Smith [b]

[a] Department of Civil Engineering, University of Pretoria, Pretoria, 0001, South Africa
[b] Department of Mechanical Engineering, University of Pretoria, Pretoria, 0001, South Africa

ARTICLE INFO

ABSTRACT

Hydrokinetic (HK) energy production has been primarily developed for use in tidal energy applications. However, where inland water infrastructure systems with sufficient velocities and spatial requirements exist, HK energy may hold great potential. A first order estimate of the wake length and dissipation rate behind a device is necessary for installation design and analysis. Some analytical approximations have been developed to estimate the wake field, although the majority of these approximations do not consider operational conditions in confined flow settings. This paper focuses on the development of a new semi-empirical model for the prediction of the wake formation, dissipation, and flow recovery. Various HK turbines are modelled, and benchmark validated using commercially available computational fluid dynamics software. The developed semi-empirical wake model adequately predicts wake behaviour over a range of performance conditions (linked to the specific turbine thrust), ambient turbulence conditions as well as blockage ratios, which are all important parameters in inland flow applications. The model enables an approximation of the wake behaviour with an accuracy of within 10% over the tested range of turbines. This approximation is valuable for facilitating the planning of turbine placement and determining the spatial requirements for inland hydrokinetic (HK) schemes.

1. Introduction

Renewable energy technologies, such as small-scale hydropower systems, provide a clean energy source with a dependable base load. The climate crises and increasing electricity demand calls for new solutions and a need to capture "hidden" renewable energy sources. One example exists within hydrokinetic (HK) micro-hydro systems (Williams and Jain, 2011).

The kinetic energy in channels/canals with a sufficient flow velocity provides a predictable and extractable energy source (Guerra and Thomson, 2019). A HK turbine is designed to directly capture the kinetic energy of flowing water and generate electricity through thrust induced rotating blades. Although this type of hydropower does not necessitate civil works or modifications to water courses, the presence of the turbine leads to a disturbance that induces a pressure drop. Consequently, an axial pressure gradient is formed, giving rise to the formation of the wake (Sanderse et al., 2011). This wake is characterized by a significant velocity deficit and turbulent flow field (Lam et al., 2011). A comprehensive understanding of the hydrodynamics of these systems is crucial to ensure the safeguarding of watercourses and the surrounding areas.

Additionally, it plays a vital role in turbine design and resource assessment (Guerra and Thomson, 2019), to harness this energy and allow a larger rollout of commercial HK devices. Accurate prediction of the wake length and dissipation rate is essential for optimising the energy extraction of turbine arrays (Chawdhary et al., 2017).

In recent years, several analytical and empirical approaches have been developed to allow simpler and faster approximations of the wake downstream of HK devices. Most have been developed for tidal applications (Ma et al., 2018; Pyakurel et al., 2017a) and thus unbounded flow. These analytical models are based on equations derived through the axial momentum theory, multiple stream tube theory and the lifting line theory. In the past, these were utilised for simplified performance analysis and have only recently been employed for wake characterization and turbine spacing (Lam and Chen, 2014).

A thorough understanding of the driving factors behind wake formation and dissipation is necessary to develop analytical wake models. The following factors have been considered in literature:

- Operational parameters such as tip speed ratio (λ) (Mourad et al., 2015) (Siddiqui et al., 2017) and turbine thrust have been linked to near wake formation.

Nomenclature

A	Area
AD	Actuator disk
b	Channel width
BEM	Blade element momentum
C	Empirical coefficient
CA	Channel aspect ratio
CFD	Computational fluid dynamics
D	Turbine diameter
dt	Rotor diameter length metric
Fr	Froude number
g	gravitational acceleration
HAHT	Horizontal axis hydrokinetic turbine
HK	Hydrokinetic
LPS2	Linear pressure strain 2-layer turbulence model
LR	Left rotor
$P_{position}$	Pressure
RANS	Reynolds averaged Navier Stokes
Re	Reynolds number
R	Rotor radius
rmse	Root mean square error
RR	Right rotor

RSM	Reynolds stress model
T	Thrust
TI	Turbulence intensity
TKE	Turbulent kinetic energy
U	Velocity
URANS	Unsteady Reynolds averaged Navier Stokes
VC	Volumetric control
VD	Virtual disk
V	Point velocity
V_x	Velocity deficit
W	Channel width
X	Position
β	Blockage ratio
λ	Tip speed ratio
ρ	Density

Subscripts

D	Drag
∞	Freestream
w	Wake
T	Thrust
P	Power
o	Available

- Additional parameters such a flow velocity, Reynolds number and additional blockage caused by turbine retaining structures or grids have been found to affect wake formation.
- It has been observed that ambient turbulence has a significant impact on the overall dissipation rate of the wake (experientially (Milne et al., 2013) (Lo Brutto et al., 2015) and numerically (Ahmadi, 2019) (Pyakurel et al., 2017b)).
- Blockage ratio (β) (Consul et al., 2013a; Koh and Ng, 2017) and depth below the free surface (Whelan et al., 2009) have been shown to influence turbine performance as well as wake dissipation rate and wake symmetry.

The consideration of these effects vary depending on specific installations, such as tidal or inland channels, where spatial constraints and array configurations differ.

The past studies mentioned are valuable for simplifying wake prediction. However, a simplified methodology for predicting wake lengths specifically for inland applications is currently unavailable. This paper aims to utilise a combination of literature findings and validated computational fluid dynamics (CFD) analyses to develop a new semi-empirical wake model. This model will be specifically designed to account for the typical installation conditions and turbine operating conditions in inland channels.

2. Background

2.1. Wake formation

Placing a turbine in a moving flow field causes a disturbance in the downstream region. This region is characterized by intense turbulent mixing, helical movements, and a complex eddy system, referred to as the wake. The wake characteristics may be attributed to two distinct phenomena. The first is the instability of the boundary layers on the blades caused by the adverse pressure gradient along the rotor plane. The second is the formation of a spiral vortex structure that emanates from the blade tip and rotor root, resulting in the generation of long-lasting large eddies in the downstream flow field (Silva et al., 2016) (as portrayed in Fig. 1).

The theoretical principles in Fig. 2 may be used to describe a turbine wake and propagation thereof. Consider a turbine of area A in a channel with cross sectional area A_c. Cross section A_o is the streamtube area of the upstream undisturbed flow, with the pressure p_o and flow speed u_o.
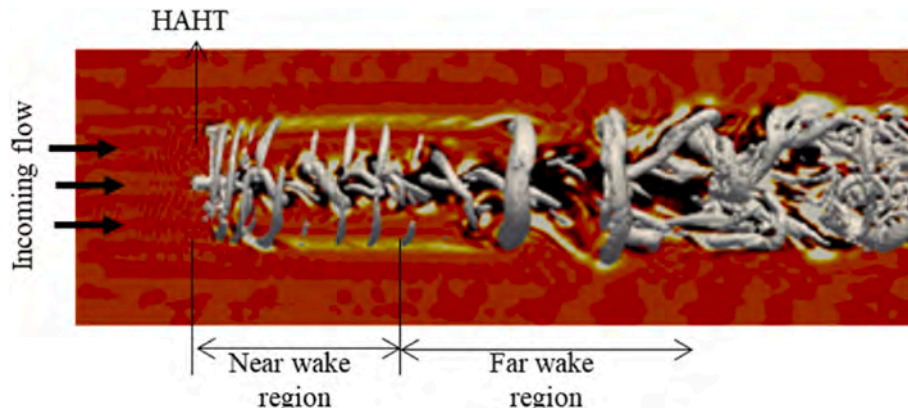

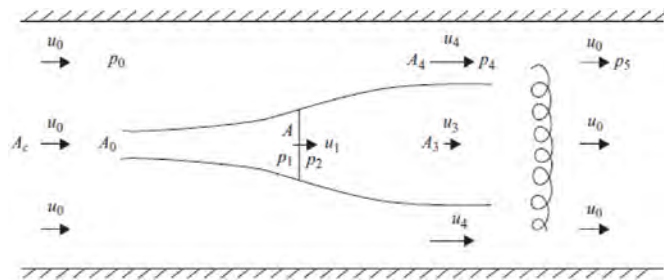**Fig. 1.** HAHT wake (adapted from (Lloyd et al., 2014)).

Fig. 2. Definition for single turbine in a channel (Garrett and Cummins, 2007).

The streamtube pressure is p_1 just upstream of the turbine and p_2 just downstream (assumed uniform as in the Lanchester-Betz formulation (Garrett and Cummins, 2007)). The streamtube expands downstream of the turbine and continues to do so before settling to a constant area A_3 with speed u_3. The flow speed outside the wake zone is defined by parameters u_4 and pressure p_4.

As portrayed on the sketch, when A_c approaches infinity, $p_4 = p_0$ and $u_4 = u_0$ (depending on the blockage ratio). The flow further downstream allows lateral mixing, resulting in a pressure change to p_5, which varies from p_0. The equation for energy extraction is derived (Garrett and Cummins, 2007) by applying the conservation momentum and conservation of energy to the above mentioned flow. In a channel with an infinitely large domain the maximum efficiency for power extraction has been determined to be approximately 59% commonly known as the Betz limit. Nevertheless, the impact of confinement on this efficiency has not been extensively studied, and it has been observed to surpass this limit (Cardona-Mancilla et al., 2018).

In the immediate downstream region of the turbine, the wake physics becomes complex and is influenced by various factors, including the bypass flow, induced flow from the rotor and the interaction of specific tip vortices with the supporting structure (Olczak et al., 2016). Further downstream the wake begins to mix with the bypass flow, leading to the expansion of the wake and gradual recovery of velocity over an extended distance. This defines the two predominant behaviours and regions which are more generally referred to as the near wake and far wake. The near wake may be characterized as a connected structure associated with vortex shedding behaviour. The far wake is associated with global instabilities and inhibits a slow movement of the whole mean velocity field. The near wake is specifically characterised and affected by the turbine geometry, whilst the far wake is not (Lam and Chen, 2014). The presence of tip vortices is clearly seen in this region. The formed tip and root vortices result in sharp velocity gradients and peaks in turbulence intensity. For extremely high tip speed ratio's, a vortex street may form downstream as the tip vortices join, forming a shear layer (Sanderse

et al., 2011) and slower rotations. As a result, this process exhibits a behaviour similar to that of the Karman vortex street (Tian et al., 2018).

In the far-wake region, turbulence intensifies and the interaction between the bypass flow and wake flow regions become more stochastic, leading to increased mixing. Two primary features exist in the wake, low water speeds and a high turbulence intensity (Ge et al., 2019), the former of which reduces the power output of any subsequent turbine in its wake.

2.2. Factors affecting wake formation and recovery

The wake behaviour of a turbine is influenced by several physical processes present in the flow. These include the onset shear and turbulence, interaction with retaining structures, tip vortices, and wake rotation (as indicated in Fig. 3). However, there have been limited studies that have extensively investigated the impact of these factors on the far wake.

The inlet/ambient turbulence intensity (TI) acts as an effective mixer. This leads to wake recovery and thus a decrease in overall turbulence intensity. TI is the primary driver to wake dissipation and recovery. Multiple studies have investigated the effect of wake dissipation and wake extents at different levels of ambient TI (Lo Brutto et al., 2015; Pyakurel et al., 2017b; Birjandi et al., 2012; Mycek et al., 2014). These studies found that as turbulence levels were increased, the wake dissipation rate increased, reaching lower velocity deficits closer to the turbine. It was also found that wake expansion increased closer to the turbine at higher TI levels (Lo Brutto et al., 2015) (Pyakurel et al., 2017c). Maganga et al. (2010) tested the effect of ambient TI on the wake for a 3-bladed horizontal axis turbine at $\lambda = 9$, placed in two different ambient turbulence scenarios namely 8% and 25%. Wake comparison indicated a maximum recovery of close to 60% by 4.4 d_t (diameter downstream) for a TI $= 8\%$, and 60% by 1.4 d_t downstream for a TI $= 25\%$. Similarly, an 80% recovery in streamwise velocity was found at 9 d_t for a test case with onset TI $= 8\%$ and 3 d_t for onset TI $= 25\%$.

Blockage ratio (β) has been shown to significantly alter turbine performance at ratios exceeding 5–10% (Kolekar and Banerjee, 2015). Generally for turbines operating at a given tip speed ratio, higher β results in an increased streamwise flow speed through and around the rotor which in turn increases the turbine torque and thrust (Ross and Polagye, 2020). Details of the effects on turbine hydrodynamics are given in (Houlsby et al., 2017; Consul et al., 2013b). Significant increases is C_P and C_T have also been attributed to the acceleration of the bypass flow (Nishino and Willden, 2012). A major challenge exists in experimental validation of β effects, encompassing both turbine behaviour and multiple analytical corrections. This is due to the difficulty in conducting experiments requiring varying β's whilst controlling
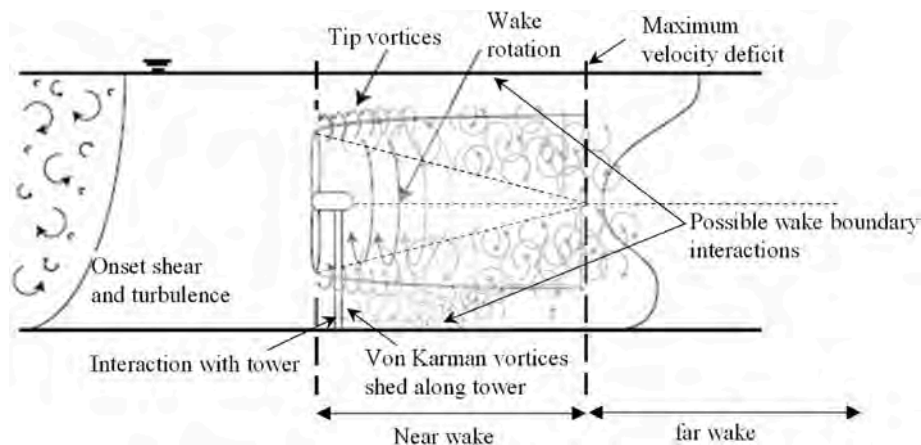

Fig. 3. Schematic of flow affecting the loading and wake of a HK device (adapted from (Niebuhr et al., 2022)).

Reynolds dependence and considering the effects of the free surface (submergence depth) and Froude number (Fr) (Ross and Polagye, 2020). An example of the β effect on the power and thrust curves for axial turbines can be seen in Fig. 4. Past studies have also reported the insensitivity of C_p to β at low λ's (Kolekar et al., 2013) (Kinsey and Dumas, 2017). Generally, turbines perform better at higher blockage coefficients, but this has a limit.

The effect of the depth the HK device is placed below the free surface may influence turbine performance as well as wake recovery. Complexities arise when turbines are placed near the free-surface, as the boundary may modify the turbine flow-field and affect device performance. In general, this causes significant flow acceleration, with the magnitude of acceleration depending on the blockage ratio. Kolekar and Banerjee (2015) found that there exists an optimal clearance depth (depth from blade tip to free surface) resulting in improved turbine performance, which should be considered during relevant installations.

The shape and size of the retaining structure as well as a grid or any other element placed in the flow field may affect the wake propagation downstream. Even more so in inland HK applications where blockage ratios are high. Many studies have concluded that turbine geometry may affect the shape of the near wake but have negligible effect on the far wake (Lam and Chen, 2014). Siddiqui et al. (2017) found a faster recovery rate due to the presence of a turbine tower. Zhang et al. (2020) investigated the wake of a horizontal axis tidal stream turbine supported by a monopile and found that the monopile strongly affects the flow field within three rotor diameters downstream, this resulted in an asymmetric recovery trend for the velocity. An interesting finding noted the high disturbance in the near wake of a HK device due to the turbine hub, body and support structure at a low ambient TI (TI = 8%) which was not noticeable at a high ambient TI case (TI = 25%). This phenomenon can be attributed to the faster decrease in velocity deficit and the subsequent absence of wake development caused by the hub. The vertical structure of the wake is also more prevalent at lower TI's (Maganga et al., 2010).

A summary of the factors found to affect wake recovery, as well as references to literature investigating these effects can be seen in Table 1.

2.3. Existing wake models

Studies have demonstrated that HK wakes result in downstream velocity deficits ranging from 10 to 20 rotor diameters downstream (Mycek et al., 2014) (Maganga et al., 2010). Therefore, quantifying the dissipation rate of turbine wakes is crucial for conducting performance and placement analyses of turbine arrays (Pyakurel et al., 2017c).

Previously, analytical wake prediction models have been developed through various approaches. These have been developed based on the axial momentum theory, actuator disk model (CFD approach) and empirical relationships through experimental work. Lam & Chen (Lam and Chen, 2014) proposed a set of equations to predict the lowest velocity closest to the turbine, which were derived from the axial momentum theory combined with a dimensional analysis. The term efflux

Table 1
Factors investigated for wake effects.

	Quantified significant effect on the wake	Quantified insignificant effect on the wake	Investigation and unquantified effect on the wake
Free stream turbulence	(Lo Brutto et al., 2015) (Pyakurel et al., 2017b) (Birjandi et al., 2012) (Mycek et al., 2014) (Pyakurel et al., 2017c) (Blackmore et al., 2014)		Maganga et al. (2010)
Depth below free surface	Silva et al. (2016)	(El Fajri et al., 2020) (Myers and Bahaj, 2007) 13]	Stallard et al. (2013)
Blockage ratio	Stallard et al. (2013).		(Stallard et al., 2013) (Nishino and Willden, 2012)
Turbine geometry/ retaining structure			Lam and Chen (2014)
Debris protection grids	-	-	-
Turbine operational conditions (thrust/λ)	(Wang et al., 2018) (Tian et al., 2018) (Harrison et al., 2010)		
Turbine array effect	(Stallard et al., 2013) (Macleod et al., 2002) (Stallard et al., 2013)		(Churchfield et al., 2013) (Gotelli et al., 2019)
Reynolds number			Bachant and Wosnik (2016)

velocity is used to define the minimum velocity taken from a time-averaged velocity distribution along the initial turbine plane. This is also the point of lowest velocity in the wake (maximum velocity deficit) and the point where wake recovery starts. For Lam & Chen's model the efflux velocity is used in a defined equation to calculate the minimum velocities at respective points downstream. The efflux velocity was derived as a function of the free stream velocity based on the propeller jet theory.

Wang et al. (2018) noted the importance of considering turbine solidity and λ when calculating the efflux velocity and adapted the Lam & Chen model to include an additional term E, which is a function of λ. Lam et al. (2015a) noted the strong effect of TI on the wake and therefore suggested a separate set of equations for low TI (3%) and high TI (14%) cases, based on the distance from the hub.

Several analytical wake models have previously been used to model the wake behind a wind turbine, such as the Jensen (1983), Larsen (1988) and Frandsen (Frandsen et al., 2006) model's. Pyakurel et al.
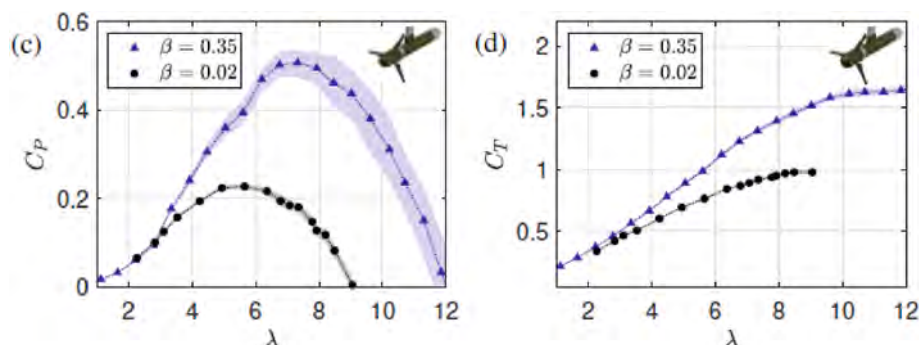
Fig. 4. Confined and unconfined power and thrust coefficient for axial flow turbines (shading represents uncertainty) (Ross and Polagye, 2020).

(2017a) developed an analytical HK wake prediction model based on three wind turbine models (Larsen, Jensen and Ainslie approach) and adjusted the models to account for ambient turbulence. CFD analyses were used to optimize the coefficients α (Jensen model) and c_1 (Larsen model). The model was developed for tidal installations with no blockage ratio incorporated due to the lack of experimental data (Pyakurel et al., 2017c). The study found the Larsen model exhibited superior performance for ambient turbulence intensities (TI) of 3%, whilst the Jensen model was more suitable for TI values of 6% and 9%. Although both models did not show good correlation to CFD results.

Lo Brutto et al. (2015) used an adaptation of the Jensen model to calculate the axial velocity profiles in the wake of turbines with small diameter to depth ratios (20%). Their work aimed to improve the work by Palm et al., 2010, 2011 by taking into account the thrust coefficient (C_T) and the ambient turbulence in comparison to CFD data. Using these equations, it was possible to estimate the velocity in the wake of the turbine for difference values of ambient turbulence (I_0).

While the previously developed wake models might have been designed for different applications, such as wind turbines, or may require additional validation, their initial development and the factors considered can still provide insight into the variables that have the most significant impact on wake development and recovery. This information can be valuable in assessing and understanding wake characteristics across different turbine geometries and applications. A summary of wake models which have been considered or developed for HK turbines as well as the variables considered in each model are listed in Table 2.

Whilst each model mentioned in Table 2 is valuable for open flow applications, they provide inadequate results for inland HK turbines operating in bounded flow conditions. This inadequacy results from the models lack of inclusion of consideration for blockage (in all models) and ambient turbulence (in most models). The objective of this study is to address these limitations by incorporating the necessary variables and advancing the development of analytical models. This was achieved by collecting a more extensive dataset of wake formations and building upon the prior research mentioned in Table 2.

3. Method

A semi-empirical approach was employed in this study, wherein fundamental hydrodynamic laws were utilised to derive basic equations. Metrics found to significantly alter the wake formation and dissipation were included empirically. These equations were then employed to develop a simplified wake model.

3.1. Semi-empirical wake model development

The solution objective of the wake model is to determine the wake recovery over a diametrically proportional distance downstream of the turbine blades ($x/D = d_t$) averaged over an area equivalent to the swept area of the blades (A_D) as shown in Fig. 5. This particular quantification

was chosen because the primary objective of the model is to determine the inlet velocity of a downstream turbine. The asymmetric nature of the wake is evident in Fig. 5 and the averaged value over the area is indicated, projected over the swept area.

To simplify the wake model, the wake is characterized into 3 properties as seen in Fig. 6:

1. The minimum velocity point (averaged over the turbine swept area) V_{OD}.
2. The point at which this low velocity zone occurs (X_{min}).
3. The dissipation rate after V_{OD}.

3.2. Collection of wake data

A limitation in the development of analytical models is the availability of a reliable wake dataset. CFD modelling was used to generate a significant dataset on a range of turbine types and operational conditions. A rigorous validation procedure was completed to ensure a reliable dataset.

Siemens STAR-CCM + software was used to model wall bounded three-dimensional models at full scale. Firstly, replications of the benchmark validation cases were modelled for verification of the CFD approach, after which input parameters were varied to create a larger dataset. Careful selection of flow physics, and comparisons of commonly used models is a crucial factor in accurate modelling of these complex flow fields. A Reynolds averaged Navier Stokes (RANS) approach was selected due to the reduced computational demand. A Reynolds stress model (RSM), specifically the Linear pressure strain 2-layer (LPS2) turbulence model, was employed, as this proved to best replicate experimental results. Transient simulations were performed for all models where unsteady terms were discretised using a 2nd order implicit scheme. The upstream boundary was specified as a velocity inlet, with a constant velocity distribution. The model was found to perform best when the boundary layers were allowed to form freely (by extending the inlet length) based on the non-slip wall condition specified. A pressure outlet was used to simulate the model outflow conditions with an environmental condition specified (to prevent backflow). Full development of the boundary layer on all surfaces was ensured through the specific turbulence model wall treatment and mesh resolution for each test case.

A virtual disk (VD) was used to represent the rotor, and a blade element momentum (BEM) model was employed. A BEM tip-loss correction was incorporated using the Prandtl tip loss correction method (Shen et al., 2005). The virtual disk required rotor geometry and aerodynamics performance metrics (lift and drag coefficients). The rotor geometry metrics in terms of chord length, twist, pitch and number of blades was included in the model. Lift and drag coefficients (C_L and C_D) generated in XFOIL software as well as past experimental results on the blade profile over a range of Re's (200 000 < Re < 3 000 000) were added to the VD-BEM model. A detailed description of the CFD approach

Table 2
Wake models and factors considered in each model.

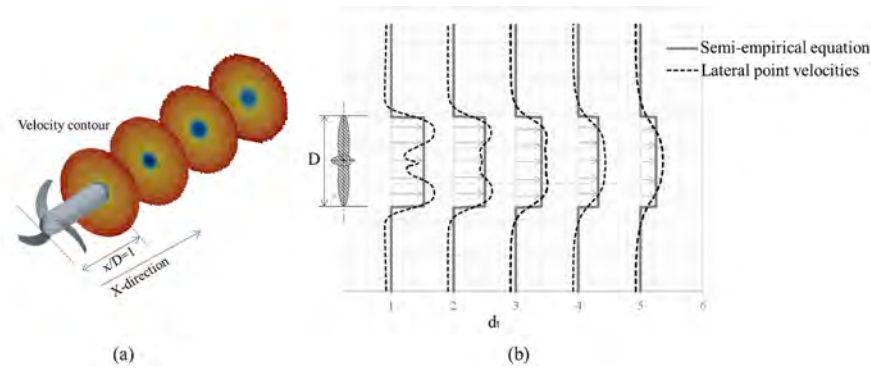| Model	Governing equation	Considered variables f{}
Larsen, 1988 (Larsen, 1988)	$U_c = 1 - \frac{V_x}{U_o} = \frac{1}{9}(C_T A_d x^{-2})^{\frac{1}{3}}\left(\left(\frac{35}{2\pi}\right)^{\frac{3}{10}}(3c_1^2)^{\frac{-1}{5}}\right)^2$	Downstream velocity (V_x), Thrust coefficient (C_T), non-dimensional mixing length (c_1) Rotor diameter (A_d)
Jensen, 1983 (wind turbine model) (Jensen, 1983)	$V_x = U_o\left(1 - 2a\left(\frac{R}{R + \alpha x}\right)^2\right)$ $a = 1 - \sqrt{\frac{1 - C_T}{2}}$	Free stream velocity (U_o), empirical coefficient (α), axial induction factor (a) (in terms of C_T) and Rotor radius (R)
Lam and Chen. 2015 (Lam et al., 2015b)	$V_{min} = \left(0.0927\left(\frac{x}{D}\right) + 0.993\right) \times V_\infty \sqrt{1 - C_T}$	Free stream velocity (V_∞), thrust coefficient (C_T)
Pyakurel et al., 2017 (Adapted Jensen and Larson coefficients) (Pyakurel et al., 2017a)	$\alpha = 0.00003TI^4 - 0.0009TI^3 + 0.0097TI^2 - 0.0396TI + 0.0763$ $c_1 = 0.0406e^{0.1361TI}$	Turbulence intensity (TI)
Oppong et al., 2020 (Oppong et al., 2020)	$V_o = \sqrt{(V_\infty)^2 - (1.59(n_o - n)D\sqrt{C_T})^2}$	Free stream velocity (V_∞), thrust coefficient (C_T), rotation rate (n) and turbine diameter (D)

Fig. 5. Wake model diagram (a) velocity map over swept area (b) averaged wake deficit values vs true lateral wake measurements.
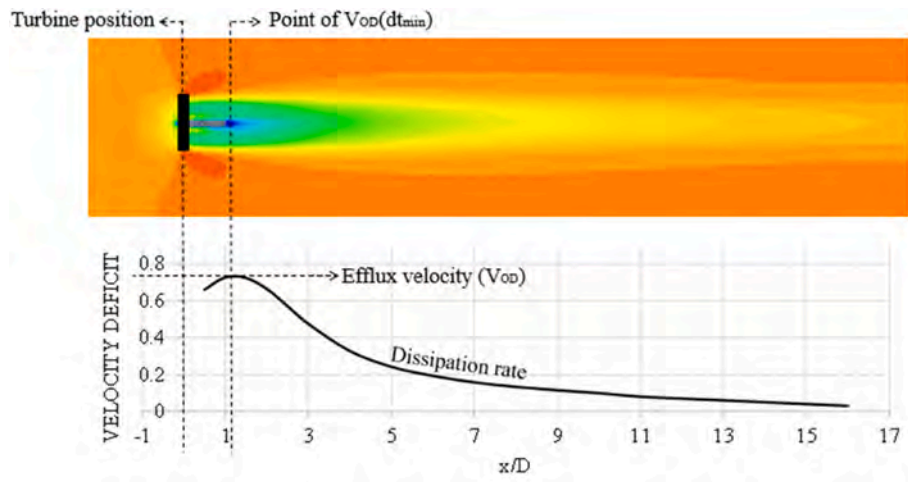

Fig. 6. Wake model parameters.

used can be seen in previous work (Niebuhr et al., 2022).

Six HK turbines with existing laboratory or experimental wake and/ or performance results were used as benchmark validation cases. CFD models using a RANS-Reynolds stress approaches were simulated (see full method in (Niebuhr et al., 2022)):

- **T1 model:** The RM1 2-bladed (Hill et al., 2014, 2020) laboratory test turbines were modelled in CFD. Benchmark validation of wake dissipation was done through a comparison of wake velocity and turbulence profiles (d_t = 1–22). Power output and performance metrics were also compared (see (Niebuhr et al., 2022)).
- **T2 model:** The IFREMER-LOMC 3-bladed (Mycek et al., 2014) turbine laboratory setup was modelled. Benchmark validation was completed through wake velocity contour comparisons (d_t = 1–10), power output (W) comparisons and C_P and C_T results.
- The 2, 3 and 4-bladed 0.5 m diameter turbines built and tested at Liverpool University (Morris, 2014; El Fajri et al., 2022; Tedds et al., 2014; Morris et al., 2016) (**T3 model**) as well as a 3-bladed BBMC 0.8 m diameter turbine (Bahaj and WMJJMcCann, 2007) (**T4 model**) were modelled. C_p and C_T results were used to validate the model applicability.

An example of the modelling approach and mesh can be seen in Figs. 7 and 8. A virtual disk (VD) was used to model the turbine rotor. The experimental performance results (Fig. 9b) indicated that the virtual disk model adequately captured the turbine performance and validated the correctness of the parameters incorporated in the virtual disk model.

For computational models, it is crucial to conduct a mesh-independent study and utilise a validated mesh to ensure appropriate
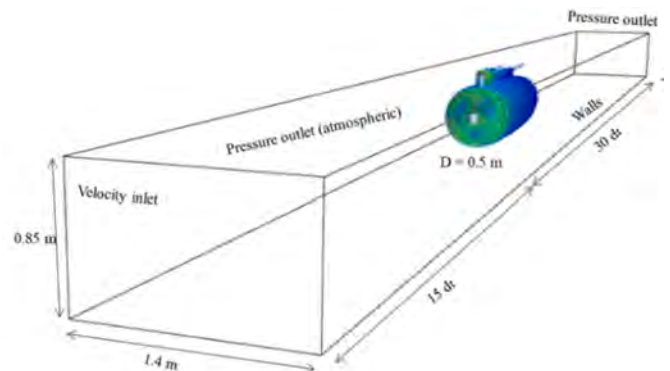
Fig. 7. T3 turbine model domain.

solutions across all parameters. The correct grid refinement rules were determined through a grid convergence test process. A polyhedral mesh with volumetric refinements in the near and far wake was used to ensure the wake effects were captured. Surrounding the VD, a local mesh refinement of 0.8% of the turbine diameter was found to adequately capture performance. This is true for λ's up to 5.1, higher values could possibly require smaller grid refinements due to changes in local courant numbers. For proper formation of the near wake a mesh size of 1.5% of the turbine diameter was necessary. A minimum mesh of 2.5% of the diameter provided an accuracy of within 5% of experimental wake dissipation rates up to 6 d_t downstream. After 10 d_t the dissipation rate was predicted within 1% accuracy for the courser mesh as the near wake
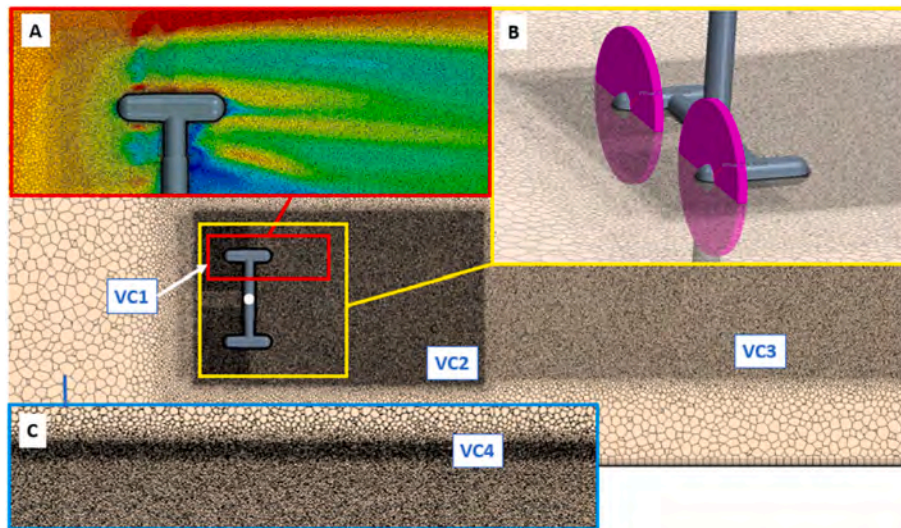
Fig. 8. BEM-VD model mesh with A- Refinement regions around the VD, B- VD placement and refinements and C- Free surface refinements (for multiphase models).
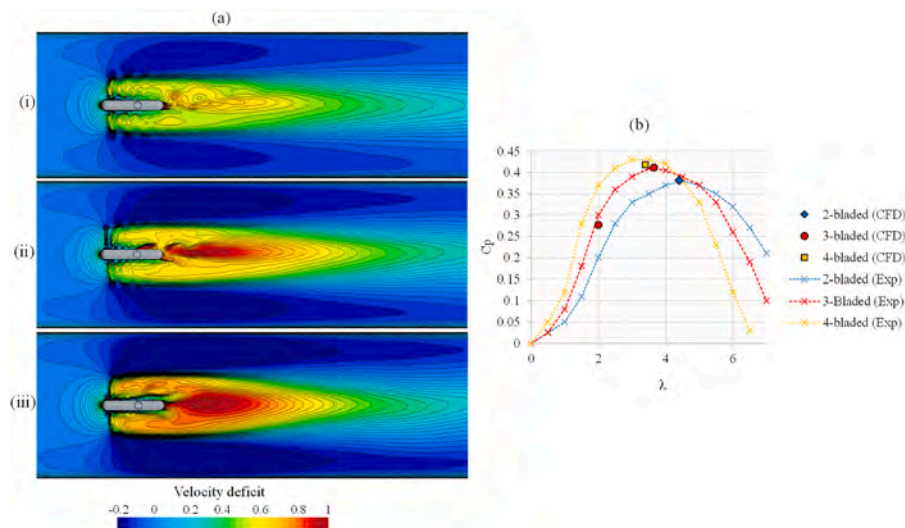
Fig. 9. T3 model turbine model (a) (i) 2-bladed (ii) 3-bladed and (iii) 4-bladed velocity contour and (b) performance comparison to experiment results.

effects became less prevalent. The flow field and far wake should be a maximum of 1.3% of the turbine diameter (as found for the IFREMER 15% TI case) to ensure correct incorporation of ambient turbulence (especially for higher TI values). Final mesh sizes of around 15 million cells were used in a transient analysis.

In summary, the primary flow conditions found to be most common to inland HAHT conditions and thus included in the verified models are

Table 3
Range of inland flow conditions for HAHT application verified and validated by experimental results.

Variable	Range of values considered in the study	
	Min value	Max value
Flow velocity (U_∞)	0.8 m/s	3 m/s
Turbulence intensity (TI)	5%	20%
Froude number (Fr)	0.1	0.6
Channel flow Reynolds number ($Re_{channel}$)	300 000	900 000
Radius based Reynolds number (Re_D)	140 000	680 000
Blockage ratio (β)	5%	25%
Turbine diameter (Ø)	0.5 m	1 m

shown in Table 3. The computation models were kept within these constraints.

3.3. Metrics of consideration

As mentioned in section 2.2, multiple factors around the turbine operating conditions and environment affect the wake formation and dissipation. Many of these potential factors were varied over the CFD test cases to see which most affected the wake formation and should therefore be included in the model.

HAHT units are typically designed for specific operational conditions best suited for the turbine and retrofitted to a site. Although in some cases the applied resistance from the generator (torque) may be altered to suit the operational conditions, the turbine is usually provided with a set control system (maximum power point tracker) and pre-determined power curve (Niebuhr et al., 2019). Therefore, the turbine may operate at slightly higher or lower λ's than the optimal conditions. Due to flow separation, self-starting abilities, as well as defined optimal operational conditions of previously tested turbines, the λ may be limited to a typical range of between 3 and 6.

Turbine thrust, and subsequent thrust coefficient, were found to be a

useful metric to measure the overall initial disturbance in the flow field. As mentioned, the optimum design, or selected turbine, may depend on supplier preference or availability. However, as the number of blades increases, the optimum λ decreases. This is also seen when comparing the C_p curves of a 2, 3 and 4-bladed turbine shown in Fig. 10. The optimum λ is typically consistent over a range of inlet conditions. The results from the 2-bladed NACA 4415 HAHT curves showed the left rotor (LR) and right rotor (RR) performed differently, however the λ for optimal performance is still consistent. A similar trend was observed throughout literature.

Similar to literature results (Kolekar and Banerjee, 2015) in this study the blockage ratio (β) was found to significantly alter the turbine performance at ratios exceeding 5–10%. The β is calculated as $\beta = (A_D + A_S)/A_C$ where A_S is the projected area of the support structure and A_C the projected area of the channel cross section perpendicular to the flow direction. During initial testing the blockage ratio was found to have a significant influence on the minimum velocity in the wake (V_{OD}) and thus also on the subsequent dissipation rate. The performance measurements also indicated that a significantly higher power output is achieved at higher blockage ratios, which also aligns with literature findings. For the case shown in Fig. 11 a C_P of 15% was obtained for a β of 7% case, compared to $C_P = 0.26$ in the 16% β case.

The effect of blockage ratio seems to lower the dissipation rate, but does not alter the dissipation relative to the minimum velocity point (V_{OD}), this can be observed through the normalized velocity deficit (*Velocity deficit*/V_{OD}) shown in Fig. 11. The clearest observed of this phenomenon is evident in the T3 results, although a similar result is also exhibited by the results of the other three turbines tested. Therefore, it can be concluded that β primarily affects the V_{OD} value and the dissipation behaviour is altered proportionally.

At extremely high blockage ratios ($\beta > 20\%$) the wake dissipation rate is accelerated by the blockage effect and the channel wall boundary layers. Although at lower β's the effect of a higher bypass flow slightly increases wake dissipation, the effect is small. A comparison of the same 3-bladed turbine in a multiphase BEM-CFD analysis in a β of 23% vs β of 5% flow field can be seen in Fig. 12. The effects of the free surface as well as wall boundaries are prevalent. The free surface plays a larger role in the presence of a support structure as was shown by El Fajri et al. (El Fajri et al., 2020). The blockage in Fig. 12 resulted in a normalized velocity deficit differential of around 20%, compared to almost no differential at lower β's as those included in Fig. 11. The gives an indication of more extreme wake dissipations in cases of $\beta \gg 20\%$. As turbine placement depths are usually limited by manufacturers the effect of near free surface turbines and higher β's ($\beta > 16\%$) was not considered in this

study, however this should be considered in a future study and the model adapted accordingly.

The analysis included channel aspect ratios ($CA = W/H$ with $W =$ Channel width and $H =$ Channel height) of a CA of 0,5 to 1. Most analysis were in the range of $CH = 0.6$ to 0.7. Only smaller differences were attributed to aspect ratio variations, and therefore assumed negligible in this case. Future studies on a larger variation of aspect ratios would prove beneficial to validate this result. Further conclusions on aspect ratios were limited due to the scope limitation of available laboratory test results.

Higher turbulence intensities (TI) in a channel result in accelerated wake dissipation. The overall V_{OD} is decreased as the strong vortex structure is not allowed to form, and the position of the highest V_{OD} ($X_{\min}$) is decreased (the position of $X_{\min}$ moves closer to the turbine).

Streamwise turbulence intensity is commonly employed as a measure of turbulence in a channel or river section. Transverse and vertical intensities usually exhibit different ratios (Milne et al., 2013), with streamwise turbulence often being significantly greater in magnitude. Turbulence intensities in a smooth river or canal section are usually between 5 and 20%. Li et al. (2010) reported turbulence intensities of 25–30% in shallow water in the East River, New York (where $U_\infty = 2$ m/s).

In flow regions with higher TI's a reduction of $X_{\min}$ is commonly observed, where the occurrence of V_{OD} moves closer to the turbine due to accelerated wake formation and dissipation. The wake model was adjusted to account for typical behaviour observed in inland water reticulation systems, where the TI ranges from 5% to 20%. Although higher TI's may exist, they often lead to unfavourable installation conditions, and as a result, they were not included in the study. Although numerous previous studies have explored the impact of TI on wake formation, there have been relatively few analyses conducted on the far field characteristics of wakes. To ensure accurate capture of these effects, CFD tests were conducted across a range of TI values. This was done to generate a comprehensive dataset that could be utilised for the development of the semi-empirical wake model.

In summary, the primary factors considered to govern the wake formation and dissipation in the flow field of a HK turbine were: turbine thrust, which accounts for the operational λ and blade profile; The blockage ratio (β) which affects the power output and therefore also the maximum V_{OD} in the wake; as well as dissipation rate, which is accelerated at higher blockage ratios due to the confined bypass flow; And lastly the turbulence intensity (TI) in the flow field, which significantly accelerated the wake recovery at higher TI values. These metrics were included in each property as shown in Table 4.
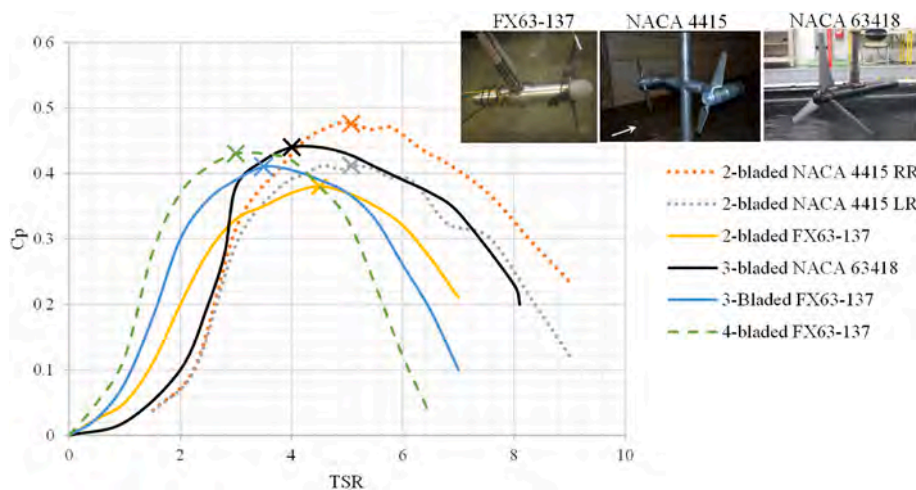
Fig. 10. Turbine performance comparison between the measured experimental results of the HAHT with NACA4415 (Hill and Neary, 2014), NACA 63418 (Mycek et al., 2014) and FX63-137 (Morris, 2014) blade profiles.
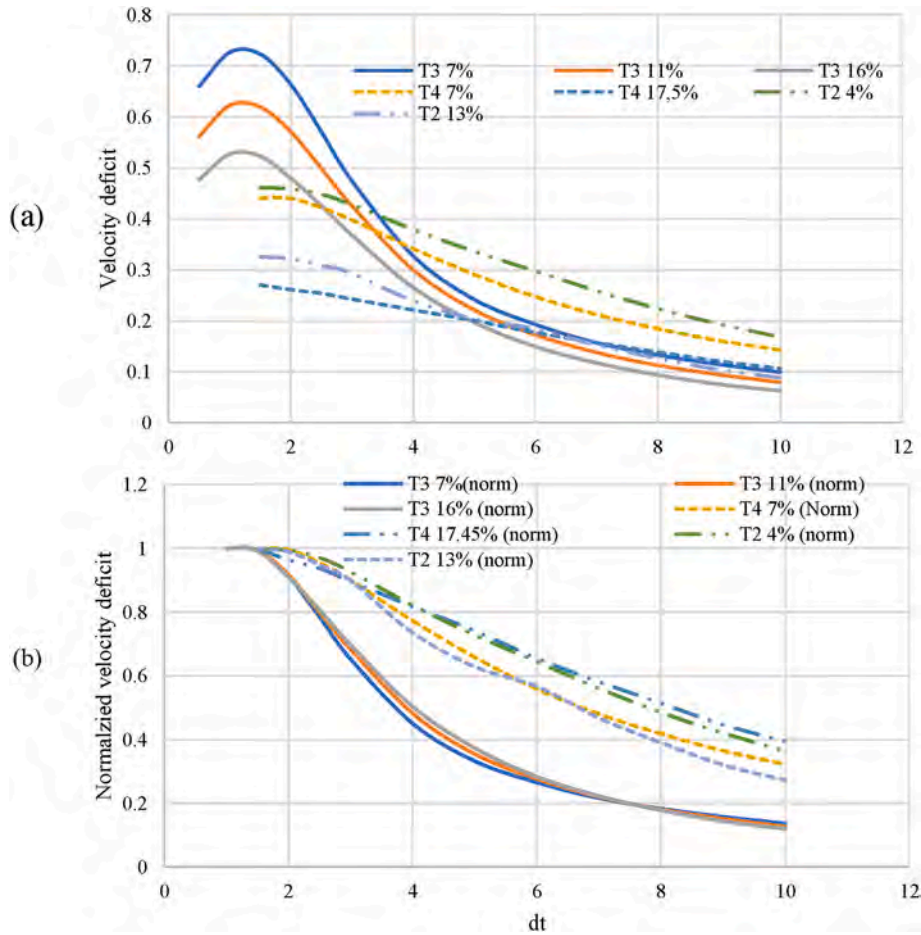
Fig. 11. Effect of blockage ratio (at 7%, 11% and 16%) on dissipation rate comparing (a) Velocity deficit and (b) normalized velocity deficit.
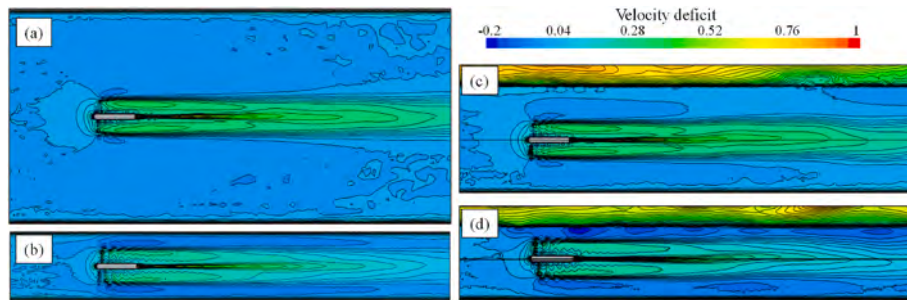
Fig. 12. Velocity deficit distribution surrounding a 3-bladed HAHT for a $\beta = 5\%$ (a) horizontal and (c) vertical profiles; a $\beta = 23\%$ (b) horizontal and (d) vertical profiles.

Table 4
Model considerations.

Property	Variable	Metrics of consideration
Minimum velocity point (over A)	V_{OD}	C_T, β, TI
Point at which minimum velocity occurs	X_{min}	V_{OD}, TI
Dissipation rate (at points d_t downstream)	V_x $(d_t = x/d)$	V_{OD}, TI, β

3.4. Determination of minimum velocity in the wake (V_{OD})

A simple approximation for the minimum velocity just downstream of a HAHT is possible through the actuator disk theory. Fig. 13 shows the
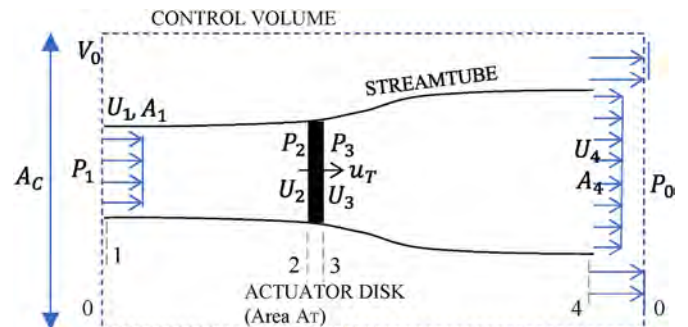
Fig. 13. Actuator disk model.

application of the axial momentum theory using an actuator disk principle, often used in wind turbine analysis (Eggleston and Stoddard, 1987). Applying the conservation of energy over this disk allows approximation of the minimum velocity downstream of the disk.

Assuming a very flat slope (thus ignoring the reference to a datum height) the energy upstream of the disk can be described with P_1, P_2, P_3 and P_4 are the pressures at points 1,2,3 and 4 (Fig. 13) and U_1, U_2, U_2 and U_4 the relevant velocities (m/s), ρ the density of water and g the gravitational acceleration.

As continuity must hold within the streamtube we know that:

$$U_1 A_1 = u_T A_T = U_4 A_4 \tag{1}$$

We also know that continuity holds over the control volume (upstream and downstream) and a net flow exists:

$$\Delta Q = V_0[(A_c - A_1) - (A_c - A_4)] = V_0(A_4 - A_1) \tag{2}$$

To quantify the change in momentum over the disk the effect of the disk can be simply expressed as a thrust (T) which is essentially the force (F) on the disk. To slow the water the force can be written as a static pressure drop over the disk, similar to the actuator disk approach, (assuming no periodicity or pressure variation with time).

Assuming the far upstream and far downstream pressure (P_1 and P_4) are equal and assuming the velocities directly upstream and downstream of the disks remain the same ($U_2 = U_3$). The Bernoulli energy equation can be combined with the thrust approximation and the following relationship is obtained:

$$T = \frac{1}{2}\rho A \left(U_1{}^2 - U_4{}^2\right) \tag{3}$$

From the propeller jet theory it is known that axial thrust is produced through shaft torque by increasing the rearward momentum of the surrounding fluid (Stewart, 1992). This induces a reactive forward force from the fluid on the propeller (used for propulsion). By representing the propeller as an actuator disk consisting of an infinite number of rotating blades and assuming energy is supplied to the system as water passes through the jet. The change of momentum due to the energy supplied results in a net thrust on the fluid. Dimensional analysis of the propeller thrust allows the following relationship.

$$T = C_T \rho n^2 D^4 \tag{4}$$

Where n is the propeller rotation rate (rev/s), C_T the propeller thrust coefficient and D the propeller diameter. Combining this equation with equation (3) the minimum velocity in the wake (U_4) can be expressed as:

$$U_4 = \sqrt{U_1{}^2 - \frac{2 C_T n^2 D^4}{A}} \tag{5}$$

However, this relationship does not translate well to turbines, as ship propellers typically operate at exponentially higher rotation rates compared to HK turbines in channel flows. As a result, an alternative definition for the thrust coefficient is employed. This approximation is commonly used to define the thrust of a wind turbine (Eggleston and Stoddard, 1987) and is described as the non-dimensional ratio of axial force to incoming flow momentum with U_∞ representing the freestream velocity:

$$C_T = \frac{T}{\frac{1}{2}\rho U_\infty{}^2 A_D} \tag{6}$$

By considering U_∞ equal to U_1 and combining equations (3) and (6) the following relationship for U_4 is determined, which would refer to the minimum velocity in the wake:

$$U_4 = \sqrt{U_\infty{}^2(1 - C_T)} \tag{7}$$

This minimum velocity in the wake (U_4) is often referred to as the efflux velocity (Lam et al., 2015a). As mentioned, in the current study it

was found that the average velocity over the cylindrical area (V_{OD}) is most useful when determining turbine spacing (average velocity over disk area) which is, according to the equation derivation, equivalent to U_4, being an expression of the average velocity downstream of the disk (over the propeller swept area). Although this equation is useful in determining the minimum velocity in the wake based on the turbine C_T and flow velocity, it does not include any effects of ambient TI or blockage (β) which have been proven to affect the minimum velocity.

The β influences the turbine thrust and could therefore account for variations in the maximum V_{OD} in the wake. Previous studies have been conducted to explore blockage correction methods that account for laboratory test results for higher β's. These approaches are based on a concept introduced by (Glauert, 1983) for performance change effects in wind turbine wind tunnel testing. Typically, the model adapts the thrust coefficient approximation (equation (6)) with a new predicted freestream velocity ($U_\infty{}'$) which would, in unconfined conditions, result in the same thrust as measured in the bounded flow scenarios. In theory these same blockage correction principles should be useful in adapting V_{OD} for higher blockage ratios and were therefore investigated.

Most blockage correction methods such as those proposed by Mikkelsen and Sorensen (2002) and Barnsley and Wellicome (1990), typically rely on prior knowledge of the bypass flow velocity and flow velocity through the turbine. However, these values are often unknown during the time of analysis. The approach proposed by Werle (2010) provides an adapted C_T for wind turbines based on the blockage ratios. This approach accounts for the confined flow effect on the thrust coefficient. The same theory holds for water flow. Applying this wind turbine blockage correction model to the HK results in this study indicated exaggerated estimations of the results, this was found to agree with previous testing of this model on HK turbines (Ross and Polagye, 2020). However, a correlation trend was prevalent, and through an empirical model adjustment, acceptable correlation to experimental results was observed. The blockage correction formation was adjusted and incorporated into the minimum velocity (V_{OD}) equation as follows:

$$V_{OD} = U_\infty \sqrt{1 - \frac{(1 - \Delta\beta)^2}{1 + \Delta\beta} C_T} \tag{8}$$

Where the $\Delta\beta$ is calculated as follows:

$$\Delta\beta = \beta - 0.07 \tag{9}$$

The V_{OD} equation (8) allows an approximation of this value through only the turbine thrust, swept area and inflow velocity. This indicates a clear relationship between the thrust coefficient and V_{OD}. Seven experimental test cases at low TI's are shown in Fig. 14 where the distribution between V_{OD} values calculated through the V_{OD} approximation and measured from wake results are compared. The results indicate the good approximation of the calculated minimum velocity through to the values measured experimentally. The general trend of higher V_{OD} values for turbines operating at higher thrust coefficients is also indicated by the linear trendline.

The point of V_{OD} occurrence (X_{min}) depends not only on the β and TI, but on the extent of the C_T value. HAHT's with higher C_T's cause a larger disturbance in the flow, resulting in a higher V_{OD}. Within the dataset it was observed that larger disturbance resulted in a faster mixing rate in the near wake due to the larger differential velocity between the wake and bypass flow. Therefore, a general trend was observed, indicating that X_{min} moved further downstream for cases with lower V_{OD}'s. This relationship only holds true for low TI values. As the TI increased the X_{min} also moved further upstream.

Previous analyses have concluded with a set point for the efflux velocity, occurring around 1.1 d_t downstream (Lam and Chen, 2014; Whale et al., 1996). Berger et al. (1981) suggested for a ship propeller the position of maximum velocity (R_{mo}) can be predicted as a function of the radius of the propeller (R) and the radius of the propeller hub (R_h):
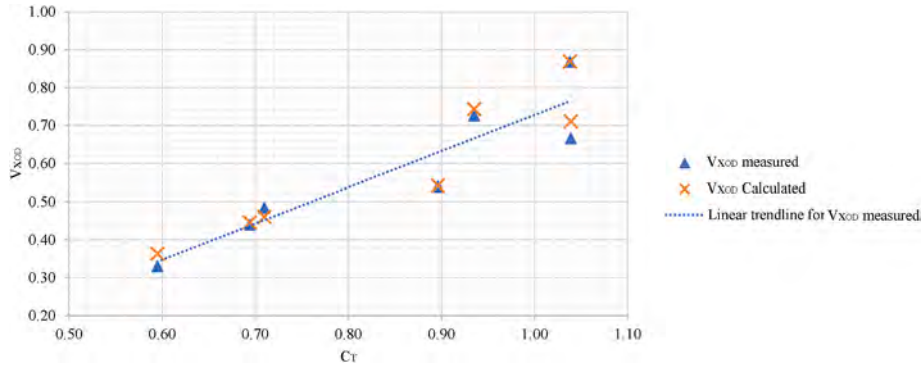
Fig. 14. Relationship between C_T and V_{OD} for the 7 modelled turbines operating at optimal λ.

$$R_{mo} = 0.67(R - R_h) \tag{10}$$

Prosser (1968) proposed a value of 60% of the blade radius from the hub be used. Hamill et al. (2004) proposed rather 0.7 in place of 0.67 shown in the formula by Berger et al. (1981). Lam et al. (2015b) compared empirical equations to experimental results for HAHT's and the equation by Berger et al. (1981) has the closest correlation. Lam et al. (2015b) recommended the equation by Berger et al. (1981) to determine the point of lowest velocity occurrence in the wake of a HAHK device.

In all experiments in the current study the X_{min} occurred between 1.1 and 1.5 dt downstream. As near wake results are not of primary importance in the current model, the X_{min} point is chosen to be at a maximum of $1.5d_t$. This significantly simplifies the wake determination and allows simpler incorporation of TI through the dissipation rate. However, it should be noted when determining the X_{min} in higher V_{OD} cases the position of X_{min} is generally closer to $d_t = 1$. Where the location of V_{OD} is important, the equation by Berger et al. (1981) should be utilised.

3.5. Dissipation rate

After the initial near wake formation, where the lowest velocity point (V_{OD}) exists, the wake continues to dissipate for a distance downstream. Based on the experimental wake results it was observed that the dissipation rate after V_{OD} is primarily governed by the environmental conditions such as ambient turbulence intensity (TI) and blockage ratio (β), as well as the initial magnitude of the disturbance (magnitude of V_{OD}).

A regression analysis was used to incorporate these parameters of importance into a useable dissipation equation. In literature, linear relationships between V_{OD}/V_∞ and x/D have previously been determined through an experimental dataset (Lam et al., 2015b; Oppong et al., 2020). Although this approach was tested, it did not result in a satisfactory wake prediction. Additionally, large variations in wake behaviour (>20%) were observed when testing the model by Lam et al. (2015a) which is based on a linear approach. In this study a non-linear regression analysis is used instead.

The dissipation rate is determined as a function of the minimum cylindrically averaged velocity deficit in the near wake (Vx_{OD}). The dissipation rate is calculated from a conservative assumed X_{min} of 1.5 d_t downstream of the hub. The velocity deficit averaged over the turbine swept area (unitless), at various distances downstream (V_x) was determined as:

$$V_x = Vx_{OD} \times C_a \times e^{-Vx_{OD} \times C_b \times dt} \tag{11}$$

where C_a and C_b are coefficients determined through a non-linear regression analysis of the metrics of consideration and d_t is the distance downstream as a function of turbine diameter. The coefficients were determined as:

$$C_a = 1.37 - 0.035 \times TI \tag{12}$$

$$C_b = \left(1.25 \times \beta^{\frac{1}{8}}\right)\left(0.0031 \times TI^2 - 0.033TI + 0.3463\right) \tag{13}$$

The dissipation rate was tested over the following ranges which are representative of installation conditions:

- Turbulence intensities of 5%–20%
- Blockage ratios of 4%–18%.

The maximum differential in velocity deficit in the wake at various distances downstream of the turbine can be seen in Table 5 for a variation of TI values and Table 6 over a range of β's. The modelled values proved to be within 10% of the experimental results past 4 d_t downstream, with very few cases showing slightly higher differences in the V_x approximation in the near wake.

3.6. Model testing

The final model was tested over a range of conditions and turbine types. Due to the large computational requirements per model, a combination of varying operational conditions and turbine geometries were tested to ensure that specifically the turbine thrust, ambient TI and β were included both independently and as a combined effect. As an indication of the model accuracy, the root mean squared error (*rmse*) of the experimental velocity deficit ($V_{x,exp}$) and predicted velocity deficit ($V_{x,model}$) at incremental distance downstream relative to the turbine diameter (d_t), were analysed. The *rmse* for each turbine dataset used as well as the overall *rmse* over all datasets can be seen in Fig. 15.

$$rmse = \sqrt{\frac{\sum_{i=1}^{n}\left(V_{x,exp} - V_{x,model}\right)^2}{n}} \tag{14}$$

As depicted in Fig. 15, the predicted wakes of the 3-bladed (*_3b) and 2-bladed (*_2b) turbines exhibited a strong correlation with the experimental results, accurately capturing the trends in wake dissipation. The largest variations were found in the T3 models (form validation case (Morris, 2014)), which had extremely high turbine thrust measurements resulting in certain variations in the behaviour of the initial near wake. The comparison of the 4-bladed turbines (T3_4b) results showed under prediction of the extent of velocity deficits in the near wake. However, a lack of data on 4-bladed turbines prevented further model calibration. Despite this near wake effect all datasets proved to be within 10% of experimental values past 4 d_t downstream indicating good prediction of the wake behaviour for typical inland conditions.
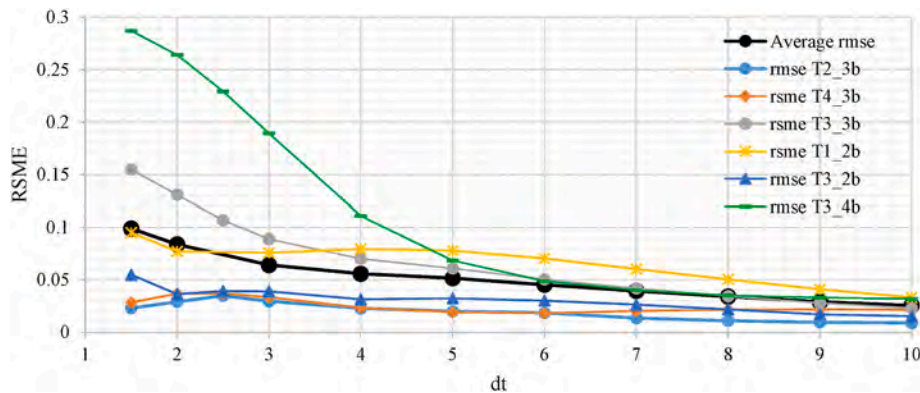
3.7. Model limitations and considerations

The goal of the semi-empirical model was to provide an approximation of the wake deficit with an accuracy of within 10%. However, it

Table 5
Velocity deficit percentage difference at various TI's at a low blockage ratio.

Ambient Turbulence intensity (TI%)	Percentage difference at a given distance from the turbine hub (%)									
	$d_t = 2$	$d_t = 4$	$d_t = 6$	$d_t = 8$	$d_t = 10$	$d_t = 12$	$d_t = 14$	$d_t = 16$	$d_t = 18$	$d_t = 20$
4–6%	1.9	4.3	4.4	3.1	1.9	1.0	0.9	1.7	2.5	0.1
9–11%	5.9	2.3	1.4	1.2	1.0	0.7	0.4	0.2	0.2	0.1
16–18%	2.9	0.9	1.1	1.2	1.0	0.7	0.3	0.2	0.1	0.1
Maximum differential in dataset	**8.1**	**9.3**	**8.7**	**5.4**	**2.5**	**1.4**	**1.4**	**1.6**	**2.5**	**0.1**

Table 6
Velocity deficit percentage difference at various blockage ratios (measured over a range of TI's).

Blockage ratio β (%)	Percentage difference at a given distance from the turbine hub (%)									
	$d_t = 2$	$d_t = 4$	$d_t = 6$	$d_t = 8$	$d_t = 10$	$d_t = 12$	$d_t = 14$	$d_t = 16$	$d_t = 18$	$d_t = 20$
<7%	3.3	2.8	2.6	2.0	1.4	0.8	0.6	0.5	0.6	0.1
13%	0.5	0.1	0.4	0.9	1.4	0.7	0.5	0.1	0.1	0.1
17%	4.8	3.0	1.9	1.7	1.6	1.4	1.1	0.7	0.3	0.1
Maximum differential in dataset	**12.6**	**6.0**	**2.5**	**3.1**	**3.1**	**2.8**	**2.5**	**1.9**	**0.6**	**0.1**

Fig. 15. Wake model prediction error over a range of test conditions.

is important to consider several limitations due to the nature of the model development, simplification of wake metric effect, and the use of RANS-CFD for generating the experimental data. Some specific limitations to be noted include:

- Wake results from laboratory tests were used for the benchmark validation of the CFD models, however, few of these laboratory tests have wake results exceeding 10 d_t downstream of the turbine. Model behaviour after this point appears to be a reasonable approximation, but a consideration of possible inaccuracies in the far wake is necessary. It is assumed that any inaccuracies in the model would be attributed to slower dissipation, as a result of the absence of high turbulence values in the bypass flow within the far wake. Consequently, the model is anticipated to yield conservative predictions.
- Additional environmental and operational effects such as drastic differences in turbine geometry (e.g., blade numbers) may alter wake formation. However, the model was developed in a way that allows further calibration and inclusion of any further parameters affecting the wake development. The current model was not tested over a wide range of turbine solidities and most turbine tests were 3-bladed (as these are currently most efficient and most produced).
- As the model was developed for simplistic application in the preliminary design or site assessment stages where minimal turbine details are known, it is expected that some inaccuracies may result from the oversimplification of the model. This should be considered where exact wake propagation is relevant (e.g., for possible scour or sedimentation analysis or where spacing is a limited parameter). More complex and detailed wake models should be used when more

details are available on the specific turbine planned for installation, especially as wake width is not considered here.
- The model was built with the assumption that sufficient submergence depths have been ensured. In cases where the turbine is near to the free surface the water surface boundary may affect wake propagation.
- For array schemes the inter-effect of coinciding wakes was not included. Variations of these effects have been investigated in the past and could be referred to (Nuernberg and Tao, 2018; Gajardo et al., 2019).

Previous HK wake models have typically overlooked the impact of blockage ratio, and only a limited number of studies have included two or three variations of TI's. The current model provides a significant improvement to existing HAHT analytical wake models by incorporating these important factors. Through including multiple turbine types and operational conditions it was possible to ascertain the model applicability over a range of results.

3.8. Typical HAHT wake in inland flow

A prediction of wake dissipation in canal systems based on the developed semi-empirical model can be seen in Figs. 16 and 17. Fig. 16 specifically indicates the effect of C_T and TI where Fig. 17 depicts wake propagation over the variation of TI and β for a turbine operating at optimal λ and at a relatively high C_p (high efficiency). The plots depict a range of TI's between 5 to 20%, which is commonly observed in canal systems. These plots can serve as a visual reference guide on typical
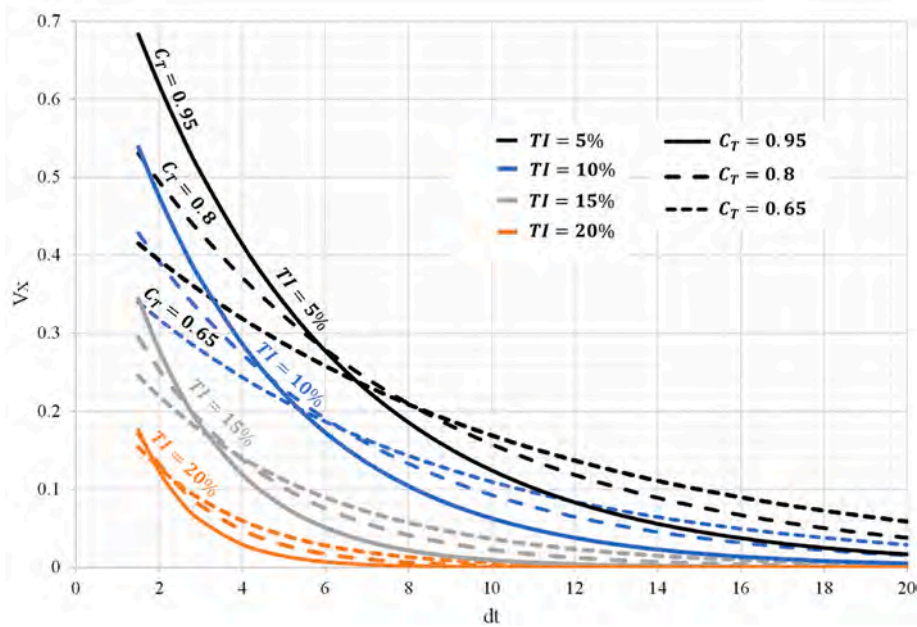
Fig. 16. Typical wake dissipation for varying C_T and turbulence intensities (TI) for a 3-bladed turbine.
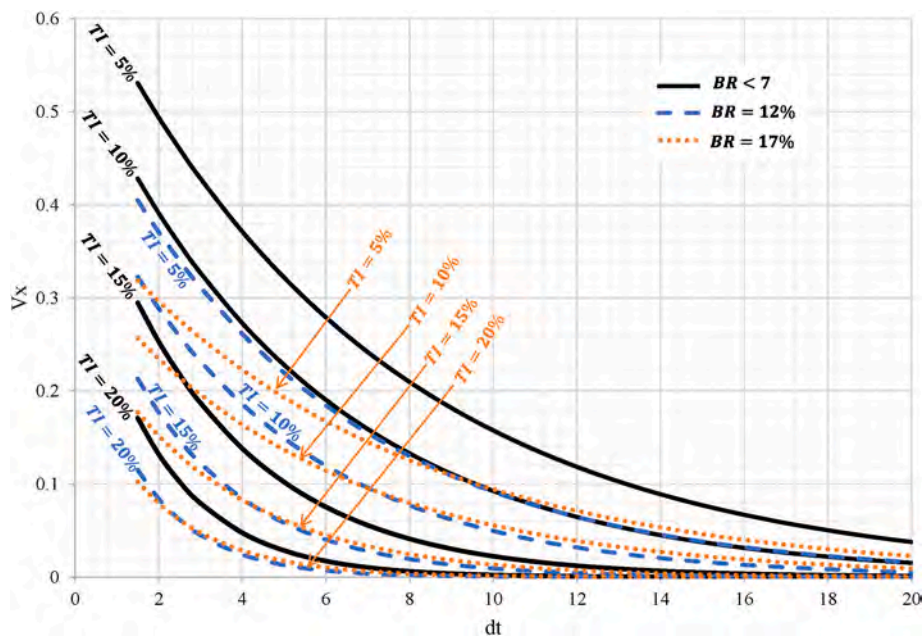
Fig. 17. Typical wake dissipation for varying Blockage ratios and turbulence intensities (TI) at a typical C_T of 0.8 for a 3-bladed turbine.

wake behaviour.

4. Conclusions

A semi-empirical calculation method for the decay of a single hydrokinetic turbine wake is formulated for uniform unbounded flow, and then adjusted for bounded flow and changes in turbulence changes. The mean momentum integral, which demonstrates the momentum deficit in the wake, can be estimated through the thrust of the turbine. Previous models have concluded this may be exclusively determined through thrust; however, the current experimental results show blockage ratio and TI should also be considered. A semi-empirical relationship for the wake dissipation rate in the near and far wake is determined through theoretical relationships and experimental data from various validated

CFD models.

The findings and consequently developed model allow a description of the wake characteristics and assist in estimating the wake dissipation with the minimum required information. It also assists in providing an overview of wake changes for important parameters of consideration (referred to here as wake change metrics) which are primarily the turbine thrust at operating point (C_T), the ambient turbulence intensity of the flow (TI) and the blockage ratio, being the ratio of turbine swept area over the channel flow area. The following summarizes these primary effects on the wake dissipation:

- Higher C_T results in a higher efflux velocity and thus higher disturbance in the flow field.

- Higher TI values result in faster wake dissipation and thus also cause the $X_{\min}$ (point of minimum velocity) to move further upstream in the wake.
- Higher blockage ratios lead to faster wake dissipation overall, as there is limited space for the bypass flow to decelerate. Consequently, the wake dissipation process is accelerated. Although this effect may vary depending on channel shapes and width to height ratios, the overall effect of wall distance is included in the semi-empirical model.

This wake model solution is a simplified approach to predicting the extreme complexities in the flow field downstream of a HK device. It however allows an overview of the general wake behaviour and limits over estimation of wake lengths leading to long distances required between turbines in inland array designs. Additionally, the proposed model limits the application complexities, making it useful as a reference guide. It also includes typical flow conditions experienced in channels with favourable installation conditions for inland HAHT devices.

Declaration of competing interest

The authors declare the following financial interests/personal relationships which may be considered as potential competing interests: Chantel Niebuhr reports equipment, drugs, or supplies was provided by University of Pretoria. Chantel niebuhr reports equipment, drugs, or supplies was provided by Center for high performance computing cape town.

Data availability

Data will be made available on request.

Acknowledgements

References

Ahmadi, M.H.B., 2019. Influence of upstream turbulence on the wake characteristics of a tidal stream turbine. Renew. Energy 132, 989–997.

Bachant, P., Wosnik, M., 2016. Effects of Reynolds number on the energy conversion and near-wake dynamics of a high solidity vertical-Axis cross-flow turbine. Energies. https://doi.org/10.3390/en9020073.

Bahaj, A.S., Wmjj, Batten, McCann, G., 2007. Experimental verifications of numerical predictions for the hydrodynamic performance of horizontal axis marine current turbines. Renew. Energy 32, 2479–2490.

Barnsley, M.J., Wellicome, J.F., 1990. Final Report on the 2nd Phase of Developmeent and Testing of a Horizontal axis Wind Turbine Rig for the Investigation of Stall Regulation Aerodynamics.

Berger, W., FelKel, K., Hager, M., Oebius, H., Schale, E., 1981. Courant provoque par les bateaux protection des berges et solution pour eviter l'erosion du lit du haut rhin. PIANC, 25th Congr.

Birjandi, A.H., Woods, J., Bibeau, E.L., 2012. Investigation of macro-turbulent flow structures interaction with a vertical hydrokinetic river turbine. Renew. Energy 48, 183–192.

Blackmore, T., Batten, W.M.J., Bahaj, A.S., 2014. Influence of turbulence on the wake of a marine current turbine simulator. Proc R Soc A Math Phys Eng Sci 470, 1–17.

Cardona-Mancilla, C., Rio, J.S., Hincapié-zuluaga, D., Chica, E., 2018. A numerical simulation of horizontal Axis hydrokinetic turbine with and without augmented diffuser. Int. J. Renew. Energy Resour. 8.

Chawdhary, S., Hill, C., Yang, X., Guala, M., Corren, D., Colby, J., Sotiropoulos, F., 2017. Wake characteristics of a TriFrame of axial-flow hydrokinetic turbines. Renew. Energy 109, 332–345.

Churchfield, M.J., Li, Y., Moriarty, P.J., 2013. A large eddy simulation study of wake propagation and power production in an array of tidal-current turbines. Philos Trans R Soc A 371, 1–15.

Consul, C.A., Willden, R.H.J., McIntosh, S.C., 2013a. Blockage effects on the hydrodynamic performance of a marine cross-flow turbine. Philos Trans R Soc A Math Phys Eng Sci. https://doi.org/10.1098/rsta.2012.0299.

Consul, C.A., Willden, R.H.J., McIntosh, S.C., 2013b. Blockage effects on the hydrodynamic performance of a marine cross-flow turbine. Philos Trans R Soc A. https://doi.org/10.1098/rsta.2012.0299.

Eggleston, D.M., Stoddard, F., 1987. Wind Turbine Engineering Design. Van Nostrand Reinhold Company Inc., New York.

El Fajri, O., Bhushan, S., Thompson, D.S., O'Doherty, T., 2020. Numerical investigation of shallow-water effects on hydrokinetic turbine wake recovery. Int Mar Energy J 3, 25–35.

El Fajri, O., Bowman, J., Bhushan, S., Thompson, D., O'Doherty, T., 2022. Numerical study of the effect of tip-speed ratio on hydrokinetic turbine wake recovery. Renew. Energy 182, 725–750.

Frandsen, S., Barthelmie, R., Pryor, S., Rathmann, O., Larsen, S., 2006. Analytical modelling of wind speed deficit in large offshore wind farms. Wind Energy 9, 39–53.

Gajardo, D., Escauriaza, C., Ingram, D.M., 2019. Capturing the development and interactions of wakes in tidal turbine arrays using a coupled BEM-DES model. Ocean Eng. 181, 71–88.

Garrett, C., Cummins, P., 2007. The efficiency of a turbine in a tidal channel. J. Fluid Mech. 588, 243–251.

Ge, M., Wu, Y., Liu, Y., Yang, X.I.A., 2019. A two-dimensional Jensen model with a Gaussian-shaped velocity deficit. Renew. Energy 141, 46–56.

Glauert, H., 1983. The elements of aerofoil and airscrew theory. https://doi.org/10.1017/CBO9780511574481.

Gotelli, C., Musa, M., Guala, M., Escauriaza, C., 2019. Experimental and numerical investigation of wake interactions of marine hydrokinetic turbines. Energies 12, 1–17.

Guerra, M., Thomson, J., 2019. Wake measurements from a hydrokinetic river turbine. Renew. Energy 139, 483–495.

Hamill, G.A., McGarvey, J.A., Hughes, D.A.B., 2004. Determination of the efflux velocity from a ship's propeller. Proc Inst Civ Eng Marit Eng 157, 83–91.

Harrison, M.E., Batten, W.M.J., Myers, L.E., Bahaj, A.S., 2010. Comparison between CFD simulations and experiments for predicting the far wake of horizontal axis tidal turbines. IET Renew. Power Gener. 4, 613.

Hill, C., Neary, V.S., 2014. U. S. Department of energy reference model program RM1 : experimental results. Sandia Natl. Lab.

Hill, C., Neary, V.S., Gunawan, B., Guala, M., Sotiropoulos, F., 2014. U. S. Department of Energy Reference Model Program RM1 : Experimental Results (Minneapolis).

Hill, C., Neary, V.S., Guala, M., Sotiropoulos, F., 2020. Performance and wake characterization of a model hydrokinetic turbine: the reference model 1 (RM1) dual rotor tidal energy converter. In: Energies, pp. 1–21.

Houlsby, G., Vogel, C., 2017. In: Civ, Proc Inst, Water, Eng (Eds.), The Power Available to Tidal Turbines in an Open Channel Flow. Marit. Energy, pp. 12–21.

Jensen, N.O., 1983. A note on wind generator interaction. Risø-M-2411 Risø Natl Lab Roskilde 1–16.

Kinsey, T., Dumas, G., 2017. Impact of channel blockage on the performance of axial and cross- flow hydrokinetic turbines. Renew. Energy 103, 239–254.

Koh, W.X.M., Ng, E.Y.K., 2017. A CFD Study on the Performance of a Tidal Turbine under Various Fl Ow and Blockage Conditions, 107, pp. 124–137.

Kolekar, N., Banerjee, A., 2015. Performance characterization and placement of a marine hydrokinetic turbine in a tidal channel under boundary proximity and blockage effects. Appl. Energy 148, 121–133.

Kolekar, N., Hu, Z., Banerjee, A., Du, X., 2013. Hydrodynamic design and optimization of hydro - kinetic turbines using a robust design method. In: Proc. 1st Mar. Energy Technol. Symp, pp. 1–10.

Lam, W.H., Chen, L., 2014. Equations used to predict the velocity distribution within a wake from a horizontal-axis tidal-current turbine. Ocean Eng. 79, 35–42.

Lam, W., Hamil, G.A., Song, Y.C., Robinson, D.J., Raghunathan, S., 2011. A review of the equations used to predict the velocity distribution within a ship's propeller jet. Ocean Eng. 38, 1–10.

Lam, W., Chen, L., Hashim, R., 2015a. Analytical Wake Model of Tidal Current Turbine, 79, pp. 512–521.

Lam, W.H., Chen, L., Hashim, R., 2015b. Analytical wake model of tidal current turbine. Energy 79, 512–521.

Larsen, G.C., 1988. A Simple Wake Calculation Procedure, 2760. Risø-M No, p. 58.

Li, Y., Colby, J.A., Kelley, N., Thresher, R., Jonkman, B., Hughes, S., 2010. Inflow measurements in a tidal strait for deploying tial current turbines: lessons, opportunities and challenges. Proc. 29th Int. Conf. Ocean. Offshore Artic Eng.

Lloyd, T.P., Turnock, S.R., Humphrey, V.F., 2014. Assessing the influence of inflow turbulence on noise and performance of a tidal turbine using large eddy simulations. Renew. Energy 71, 742–754.

Lo Brutto, O.A., Nguyen, V.T., Guillou, S.S., Gualous, H., Boudart, B., 2015. Reanalyse of an analytical model for one tidal turbine wake prediction. Proc. 11th Eur. Wave Tidal Energy Conf.

Ma, Y., Lam, W.H., Cui, Y., Zhang, T., Jiang, J., Sun, C., Guo, J., Wang, S., Lam, S.S., Hamill, G., 2018. Theoretical vertical-axis tidal-current-turbine wake model using axial momentum theory with CFD corrections. Appl. Ocean Res. 79, 113–122.

Macleod, A.J., Barnes, S., Rados, K.G., Bryden, I.G., 2002. Wake effects in tidal current turbine farms. MAREC 2002.

Maganga, F., Germain, G., King, J., Pinon, G., Rivoalen, E., 2010. Experimental characterisation of flow effects on marine current turbine behaviour and on its wake properties. IET Renew. Power Gener. 4, 498–509.

Mikkelsen, R., Sorensen, J.N., 2002. Modelling of wind tunnel blockage. Glob. Wind. Conf.

Milne, I.A., Sharma, R.N., Flay, R.G.J., Bickerton, S., 2013. Characteristics of the turbulence in the flow at a tidal stream power site. Philos Trans R Soc A Math Phys Eng Sci. https://doi.org/10.1098/rsta.2012.0196.

Morris, C., 2014. Influence of Solidity on the Performance, Swirl Characteristics, Wake Recovery and Blade Deflection of a Horizontal Axis Tidal Turbine.

Morris, C.E., O'Doherty, D.M., Mason-Jones, A., O'Doherty, T., 2016. Evaluation of the swirl characteristics of a tidal stream turbine wake. Int J Mar Energy 14, 198–214.

Mourad, M.G., Ayad, S.S., Abdellatif, O.E., Abdelaziz, A.A., 2015. An experimental study of the near wake of horizontal axis wind turbines. 13th Int Energy Convers Eng Conf. https://doi.org/10.2514/6.2015-3714.

Mycek, P., Gaurier, B., Germain, G., Pinon, G., Rivoalen, E., 2014. Experimental study of the turbulence intensity effects on marine current turbines behaviour. Part II: two interacting turbines. Renew. Energy 68, 876–892.

Myers, L., Bahaj, A.S., 2007. Wake studies of a 1/30th scale horizontal axis marine current turbine. Ocean Eng. 34, 758–762.

Niebuhr, C.M., van Dijk, M., Bhagwan, J.N., 2019. Development of a design and implementation process for the integration of hydrokinetic devices into existing infrastructure in South Africa. WaterSA 45, 434–446.

Niebuhr, C.M., Schmidt, S., van Dijk, M., Smith, L., Neary, V.S., 2022. A review of commercial numerical modelling approaches for axial hydrokinetic turbine wake analysis in channel flow. Renew. Sustain. Energy Rev. 158, 112151.

Nishino, T., Willden, R.H.J., 2012. Effects of 3-D channel blockage and turbulent wake mixing on the limit of power extraction by tidal turbines. Int. J. Heat Fluid Flow 37, 123–135.

Nuernberg, M., Tao, L., 2018. Experimental study of wake characteristics in tidal turbine arrays. Renew. Energy 127, 168–181.

Olczak, A., Stallard, T., Feng, T., Stansby, P.K., 2016. Comparison of a RANS blade element model for tidal turbine arrays with laboratory scale measurements of wake velocity and rotor thrust. J. Fluid Struct. 64, 87–106.

Oppong, S., Haur, W., Guo, J., et al., 2020. Predictions of wake and central mixing region of double horizontal Axis tidal turbine. KSCE J. Civ. Eng. 24, 1983–1995.

Palm, M., Huijsmans, R., Pourquie, M., Sijtstra, A., 2010. Simple wake models for tidal turbines in farm arrangement. In: ASME 2010 29th Int. Conf. Ocean. Offshore Arct. Eng. Am. Soc. Mech. Eng., pp. 577–587.

Palm, M., Huijsmans, R., Pourquie, M., Sijtstra, A., 2011. The applicability of semiempirical wake models for tidal farms. Proc. 9th Eur. Wave Tidal Energy Conf.

Prosser, M.J., 1968. Propeller Induced Scour.

Pyakurel, P., Vanzwieten, J.H., Wenlong, T., Ananthakrishnan, P., 2017a. Analytic characterization of the wake behind in-stream hydrokinetic turbines. Mar. Technol. Soc. J. 51, 58–71.

Pyakurel, P., Vanzwieten, J.H., Dhanak, M., Xiros, N.I., 2017b. Numerical modeling of turbulence and its effect on ocean current turbines. Int J Mar Energy 17, 84–97.

Pyakurel, P., Tian, W., VanZwieten, J.H., Dhanak, M., 2017c. Characterization of the mean flow field in the far wake region behind ocean current turbines. J Ocean Eng Mar Energy 3, 113–123.

Ross, H., Polagye, B., 2020. An experimental assessment of analytical blockage corrections for turbines. Renew. Energy 152, 1328–1341.

Sanderse, B., van der Pijl, S.P., Koren, B., 2011. Review of computational fluid dynamics for wind turbine wake aerodynamics. Wind Energy 14, 799–819.

Shen, W.Z., Mikkelsen, R., Sorensen, J.N., 2005. Tip loss corrections for wind turbine Computations. Wind Energy 8, 457–475.

Siddiqui, M.S., Rasheed, A. di, Kvamsdal, T., Tabib, M., 2017. Influence of tip speed ratio on wake flow characteristics utilizing fully resolved CFD methodology. J Phys Conf Ser. https://doi.org/10.1088/1742-6596/854/1/012043.

Silva, P.A.S.F., De Oliveira, T.F., Brasil Junior, A.C.P., Vaz, J.R.P.P., Oliveira, T.F.D.E., Junior, A.C.P.B., Vaz, J.R.P.P., 2016. Numerical study of wake characteristics in a horizontal-Axis hydrokinetic turbine. Ann Braziian Acad Sci 88, 2441–2456.

Stallard, T., Collings, R., Feng, T., Whelan, J., 2013. Interactions between tidal turbine wakes: experimental study of a group of three-bladed rotors. Philos Trans R Soc A Math Phys Eng Sci. https://doi.org/10.1098/rsta.2012.0159.

Stewart, D.P.J., 1992. Characteristics of a Ship's Screw Wash and the Influence of Quay Wall Proximity. Queen's University of Belfast.

Tedds, S.C., Owen, I., Poole, R.J., 2014. Near-wake characteristics of a model horizontal axis tidal stream turbine. Renew. Energy 63, 222–235.

Tian, W., Mao, Z., Ding, H., 2018. Design, test and numerical simulation of a low-speed horizontal axis hydrokinetic turbine. Int. J. Nav. Archit. Ocean Eng. 10, 782–793.

Wang, S., Lam, W.H., Cui, Y., Zhang, T., Jiang, J., Sun, C., Guo, J., Ma, Y., Hamill, G., 2018. Novel energy coefficient used to predict efflux velocity of tidal current turbine. Energy 158, 730–745.

Werle, M.J., 2010. Wind turbine wall-blockage performance corrections. J. Propul. Power 26, 1317–1321.

Whale, J., Papadopoulos, K.H., Anderson, C.G., Skyner, D.J., Helmis, C.G., 1996. A study of the near wake structure of a wind turbine comparing measurements from laboratory and full-scale experiments. Sol. Energy 56, 621–633.

Whelan, J.I., Graham, J.M.R.R., Peiro, J., Peiró, J., 2009. A free-surface and blockage correction for tidal turbines. J. Fluid Mech. 624, 281–291.

Williams, G., Jain, P., 2011. Renewable energy strategies. Sustain a J Environ Sustain issues 29–42.

Zhang, Y., Zhang, J., Lin, X., Wang, R., Zhang, C., Zhao, J., 2020. Experimental investigation into downstream field of a horizontal axis tidal stream turbine supported by a mono pile. Appl. Ocean Res. 101, 102257.

Article

Development of a Hydrokinetic Turbine Backwater Prediction Model for Inland Flow through Validated CFD Models

Chantel Monica Niebuhr [1,*], Craig Hill [2], Marco Van Dijk [1] and Lelanie Smith [3]

1 Department of Civil Engineering, University of Pretoria, Pretoria 0001, South Africa; marco.vandijk@up.ac.za
2 Mechanical and Industrial Engineering Department, University of Minnesota-Duluth, Duluth, MN 55812, USA; cshill@d.umn.edu
3 Department of Mechanical Engineering, University of Pretoria, Pretoria 0001, South Africa; lelanie.smith@up.ac.za
* Correspondence: chantel.niebuhr@up.ac.za; Tel.: +27-79-427-5190

Abstract: Hydrokinetic turbine deployment in inland water reticulation systems such as irrigation canals has potential for future renewable energy development. Although research and development analysing the hydrodynamic effects of these turbines in tidal applications has been carried out, inland canal system applications with spatial constraints leading to possible blockage and backwater effects resulting from turbine deployment have not been considered. Some attempts have been made to develop backwater models, but these were site-specific and performed under constant operational conditions. Therefore, the aim of this work was to develop a generic and simplified method for calculating the backwater effect of HK turbines in inland systems. An analytical backwater approximation based on assumptions of performance metrics and inflow conditions was tested using validated computational fluid dynamics (CFD) models. For detailed prediction of the turbine effect on the flow field, CFD models based on Reynolds-averaged Navier–Stokes equations with Reynolds stress closure models were employed. Additionally, a multiphase model was validated through experimental results to capture the water surface profile and backwater effect with reasonable accuracy. The developed analytical backwater model showed good correlation with the experimental results. The model's energy-based approach provides a simplified tool that is easily incorporated into simple backwater approximations, while also allowing the inclusion of retaining structures as additional blockages. The model utilizes only the flow velocity and the thrust coefficient, providing a useful tool for first-order analysis of the backwater from the deployment of inland turbine systems.

Keywords: hydrokinetic; computational fluid dynamics; backwater; inland hydrokinetic; axial flow turbines

1. Introduction

Research and development of hydrokinetic (HK) devices in canal systems is increasing in popularity due to increasing electricity costs and the drive towards finding renewable energy sources with unconventional applications [1–3]. Although most development has focussed on tidal applications, multiple opportunities exist for the deployment of HK systems within inland water infrastructure (e.g., canal systems) [1]. However, the placement of such a device can have significant water level and hydrodynamic energy loss effects [4].

Prediction of the hydrodynamic effects of hydrokinetic turbines in canal systems remains an important pre-development objective. Due to the nature of canal design, these systems usually have flat slopes and subcritical flow regimes. Therefore, the analysis of backwater effects from blockages is critical for the prevention of flooding and water loss. This is especially important in array schemes where the cumulative effect of multiple devices can exceed the top of the channel and cause it to overtop.

Generally, backwater calculations utilize a blockage size (e.g., typical backwards-facing step, weir or pier shape) or energy loss function (quantified energy losses) to predict the backwater effect. Due to the novelty of HK energy, a streamlined procedure for determining the backwater effect has not yet been determined. This may be attributed to the variability of turbine types, operational conditions, and efficiencies, all of which result in a different effective blockage.

Previous studies have investigated the hydrodynamic effects of horizontal-axis hydrokinetic turbines (HAHTs) both experimentally (e.g., in canals [5], investigating boundary layers [6] and varying Reynolds numbers [7]) and computationally (e.g., both CFD applications in [4,8]). However, most of the studies are performed under constant operational conditions, and are site-specific (e.g., three-bladed [9] and two-bladed [9,10] turbines under optimal conditions). Some attempts have been made in the past to develop backwater models using roughness values [4] or analytical relationships [11], but the lack of experimental results over a range of turbine designs and operational conditions has resulted in site-specific models. Additionally, use of the models without in-depth knowledge of input variables limits their utility.

This study aimed to develop a simplified method for calculating the backwater effect of HK turbines in canal systems. An analytical approximation based on assumptions of performance metrics and inflow conditions was tested using validated computational fluid dynamics (CFD) models. These models allow a larger dataset and, thus, validation of the analytical approximation recommended.

2. Background

Placement of an HK device extracting energy in confined flow may affect water surfaces and water surface profiles. This is especially true in array schemes, and must be considered to ensure that the clearance between the rotor blades and the surface is sufficient. Myers and Bahaj [12] investigated a 1:30 scale HAHT model (rotor diameter, $d_T = 0.4$ m), and observed a clear difference in the water surface once energy was extracted. Water depths increased immediately upstream of the rotor and decreased downstream for about 2 d_T. Details of the water surface profiles can be seen in Figure 1. The results observed a standing wave 7–8 d_T downstream (it should be noted that this was for the high-freestream-velocity case).
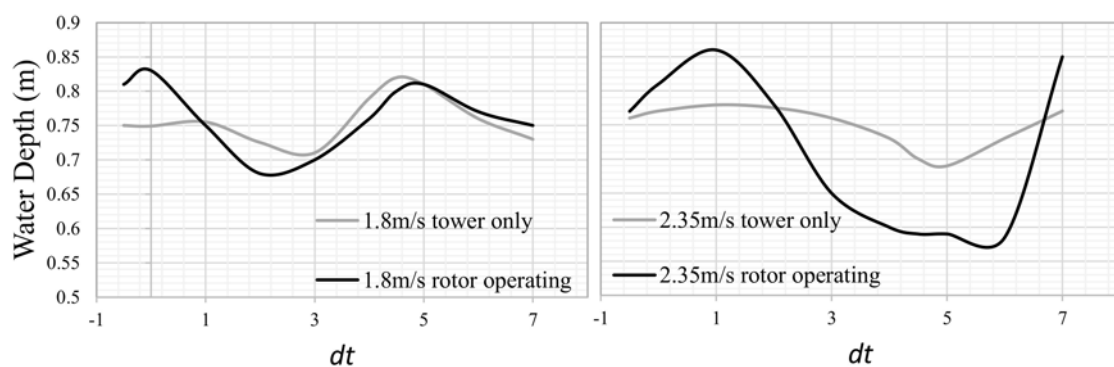
Figure 1. Water surface profile through a scaled turbine operating at 2 different velocities, compared to the no-energy-extraction stage [12].

Prediction of such occurrences requires understanding of the specific energy and flow regime (Froude number) to predict flow behaviour after HK deployment; here, a Froude number based on turbine diameter ($Fr_D = \frac{U}{\sqrt{gd_t}}$, where U is the mean velocity and d_t is the turbine diameter) may be more useful, which has also been found to govern the free-surface effects [13].

The flow effects observed can be explained using the specific energy of the flow section, which is a function of water depth and velocity. When ignoring friction losses (e.g., from the channel sides and bed), the specific energy may be defined as follows:

$$E = y + \frac{\alpha Q^2}{2gA^2} \tag{1}$$

where y is the water depth, α is the energy coefficient, Q is the volumetric flow rate, A is the cross-sectional area, and g is the gravitational acceleration. The energy coefficient can then be defined as follows:

$$\alpha = \frac{\sum u^3 \Delta A}{U^3 A} \tag{2}$$

where A is the total flow area and u is the velocity measured within an elemental area, ΔA. The flow regime (sub- or supercritical) and, thus, the Froude number of the flow govern the behaviour of the flow [14].

A parameter of specific interest is the critical depth of the channel in which the turbine is placed. When the water surface decreases to critical or subcritical depth, flow phenomena such as hydraulic jumps may form downstream to allow recovery to normal flow depth.

Simplification of crucial free-surface parameters in inland HK installations can be summarized by two fundamental effects:

- Free-surface effects in the form of a possible standing wave formed, or decreased water surface above the turbine (due to decreasing pressure).
- Potential backwater effects caused (e.g., damming upstream).

2.1. Free-Surface Effects of HK Turbines

Free-surface effects are a critical aspect in riverine and tidal turbine array design, as the standing wave formed downstream of the turbine affects additional downstream turbines. Previous studies have concluded that the depth of the downstream water surface is strongly dependant on the Fr_D. Additionally, the blockage ratio also affects this free-surface change, albeit not as strongly as Fr_D [13].

Myers and Bahaj [12] found that when imposing the typical wake expansion on the water surface, this coincided with the increased elevation observed 4–5 d_t downstream of the turbine rotor (as shown in Figure 2). In addition, due to the wake expansion coincident with the free surface, cumulative turbine placement at intervals smaller than the recovery length may cause the flow to approach critical depth, causing severe undulations in the water surface profiles (WSPs). Turbine operation and efficiency may also vary due to decreasing fluid velocity over the blades during operation. Accurate quantification of the WSPs around an array may be a challenge due to the multiple effects of turbulence, wake mixing, and superposition of WSP effects [12].
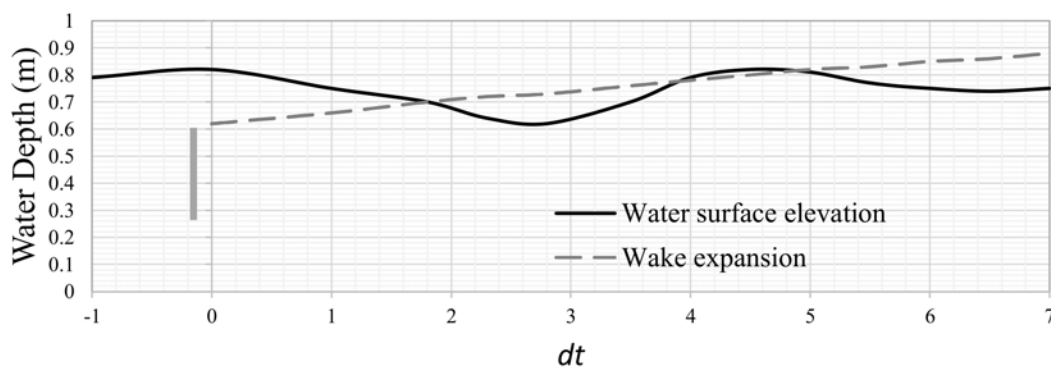

Figure 2. Wake expansion effect with free surface [12].

The presence of a support structure (tower/stanchion) also strongly affects the free-surface effect [12] (Figure 1). The same experiment also indicated the strong possibility of the formation of a hydraulic jump downstream of the turbine when flow is forced to a supercritical level due to the presence of the turbine and support structure.

Free-surface effects may be more pronounced for shallow turbines compared to turbines installed well below the free surface. It is also important to consider possible cross-sectional changes in the infrastructure where the turbine is placed, as this may alter/dampen/exaggerate these effects. Specified clearance coefficients have been investigated to limit the severity of decreased depths downstream of the turbine, or possible exposure of the turbine. Birjandi [15] proposed a clearance coefficient, C_h, defined as follows:

$$C_h = \frac{H}{L} \tag{3}$$

where H is the turbine submergence depth (i.e., the height between the top of the turbine and the water surface) and L is the rotor diameter. The recommended clearance coefficients for commercially available turbines can be seen in Table 1.

Table 1. Clearance coefficients for commercial HAHTs.

	Turbine	Clearance Coefficient
Seaflow	2-Bladed, 300 kW	0.18–0.64
SeaGen	2-Bladed, 1.2 MW (2× 600 kW)	0.25–0.38
HS300	3-Bladed, 300 kW	0.75
AK-1000	3-Bladed, 1 MW	1.02

2.2. Backwater Effect

A turbine acts as a blockage in the channel and results in energy loss in inland flow infrastructure (where flow is constrained). When Fr << 1 and subcritical flow is prevalent, the backwater effect (damming upstream) may extend a large distance upstream as well as causing significant damming. This depends greatly on the blockage ratio, which is a function of the turbine swept area (A_T), channel flow area (A_o) ($BR(\%) = \frac{A_T}{A_o}$), and additional constrictions [16], as well as the theoretical to actual efficiency [17].

In a study on a pilot HK installation in an irrigation canal, the backwater effect from the presence of the turbine extended up to 2.7 km upstream, due to the flat slope and subcritical flow present in the channel [1] (Figure 3). The clearance coefficient for this installation had not yet been defined. The specific turbine studied in that project contained grids upstream of the turbine, which trapped debris and caused a further increase in the backwater effect, to the point of channel overtopping. The blockage ratio for the installation was around 12.5%.
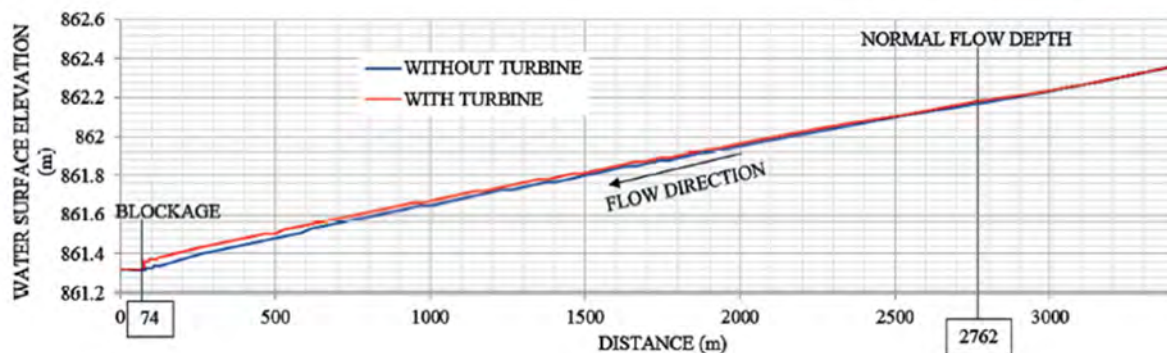
Figure 3. Backwater effect due to turbine blockages [1].

Additional to the blockage ratio, the Froude number (*Fr*) or Froude number based on turbine diameter (*Fr_D*) of the flow can influence the backwater effect. A previous study analysing this effect drew the following conclusions [13]:

1. The upstream free-surface deformation increased with Fr_D.
2. The location of maximum damming (i.e., the highest water level) moved closer to the turbine as Fr_D increased.

Previous studies have attempted to quantity the effective blockage of an HK device. Some have addressed this through the relationship of power extracted to total power dissipated by the devices [18], analytical relationships [11], and even enhanced Manning n-values quantifying the energy loss as a friction loss [4]. However, a simple formula quantifying the effective blockage for different turbine types and operational conditions is yet to be determined, and provides the motivation for this paper.

2.3. Backwater Calculations

The extraction of energy resulting from the HK device may also be analytically incorporated through the use of the momentum equation [19], where the power extraction term is added as a shear stress component (added to the effective shear stress caused by bed friction). Assuming gradually varied steady-state flow, the conservation of mass and momentum can be used to adjust the standard open-channel flow equation [20] with the addition of a term for artificial energy extraction [19]:

$$\left(1 - \frac{Q^2}{h^3 b^2 g}\right) \frac{\partial h}{\partial x} = \frac{\partial h}{\partial x} \frac{Q^2}{g h^2 b^3} - \frac{1}{\rho g b h} P \, \tau_{eff} \tag{4}$$

The effective shear (τ_{eff}) is defined as a combination of the bed shear (τ_o) and power extraction added as a shear term (τ_{add}):

$$\tau_{eff} = \tau_o + \tau_{add} = \rho \frac{g}{C^2} U^2 + \frac{P_x R}{U} \tag{5}$$

where P is the wetted perimeter, C is the Chezy friction coefficient, and P_x is the term added for power extraction, which may be more useful to express in terms of P_A being the power extracted per unit area, as the flow passes through a plane where $P_x = \frac{P_A}{\Delta x}$ (Δx being the change in distance). Such an effect can be seen graphically in Figure 4, where a 10% energy extraction term has been added.
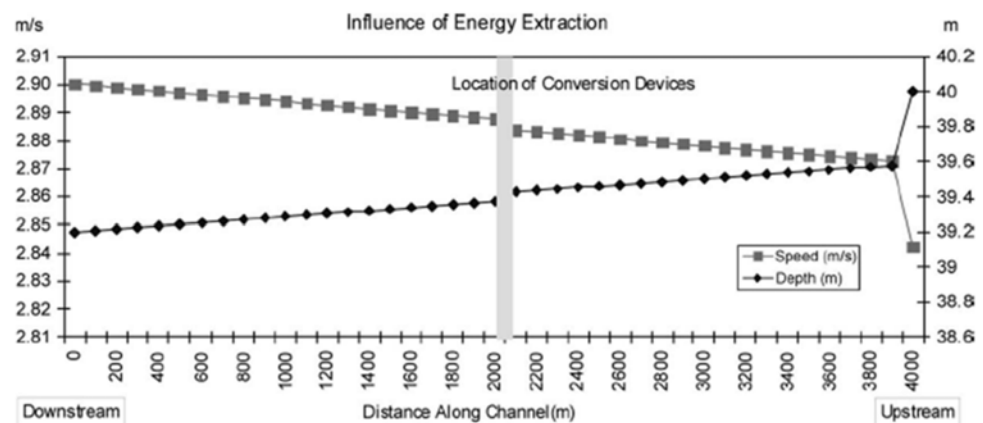

Figure 4. Influence of artificial energy extraction on speed and depth of flow [19].

A previous study [21] attempted to determine the backwater curve for instances when either the cross-section varied, the channel slope changed, or there was an obstacle in the channel and gradually varied flow was present. The model was based on the Bernoulli

equation between two cross-sections. The energy loss between the cross-sections (related to distance) was termed the hydraulic loss, *I*, which can be calculated as follows:

$$I = \frac{n^2 U^2}{R_H^{\frac{4}{3}}} \tag{6}$$

where n is the Manning roughness (s/m$^{1/3}$), R_h is the hydraulic radius of the channel (m), and U is the velocity of the water (m/s). The change in water levels (Δz) between two sections can then be determined between two significant cross-sections (e.g., 0 and 1) and calculated as shown in Equation (7), where α is the Coriolis coefficient and U_0 and U_1 are the average velocities over distance ΔL:

$$\Delta z = \Delta L \left(\frac{I_0 + I_1}{2} \right) + \frac{\alpha}{2g} \left(U_0^2 - U_1^2 \right) \tag{7}$$

Very few models have been developed to attempt to predict the backwater effect—mostly 1D analytical models [4,11]. Most studies have focussed on tidal arrays and using free-surface effects to determine the optimal number and placement of turbines [22,23]. Within tidal applications, free-surface effects are only of concern for tip clearance; therefore, these models have limitations within the application in steady inland channels where spatial constraints are of primary concern.

In a study by Kartezhnikova and Ravens [4], an increased Manning roughness coefficient was used on the channel section representing the hydrokinetic device. The *n*-value used was a function of the actual channel *n*-value, slope, water depth, device efficiency, blockage ratio, and device deployment density. This method can then be used to determine the hydraulic impact, as well as the impact of various device configurations.

The head loss associated with the channel friction (h_{Lt}) (used in the energy conservation equation) can be written as shown in Equation (8), as a function of cross-sectional area (A_0), channel hydraulic radius (R_h), discharge (Q_n), and the length over which the loss is applied (L).

$$h_{Lt} = \left(\frac{Q_n}{A_0 R_h^{2/3}} \right)^2 L \tag{8}$$

Based on the assumption that the upstream and downstream velocity and pressure heads are equal, and assuming that the drag loss is negligible, the following equation for an enhanced bottom roughness (n_t) can be derived as a function of the total power dissipated (h_p), change in elevation (Δz), and channel Manning roughness coefficient (n).

$$n_t = n \left(1 - \frac{h_p}{\Delta z} \right)^{-1/2} \tag{9}$$

Lalander and Leijon [11] investigated the use of numerical and analytical models to determine the effects on upstream water levels in a river. The analytical models are dependent on the channel blockage (of the HK device) determining energy loss from the energy capture, as well as the energy losses in the wake. The numerical models are based on the same theory—that energy is removed, causing a power loss; thus, energy capture is a component of the total friction in the channel. The total head loss can be determined as the sum of the friction loss (Δh_f) and head loss caused by the turbine (Δh_t), and P_t is the total power of the turbine (W). The formulation of the stress term τ_f is shown in Equation (11), where f is equal to the Darcy–Weisbach coefficient (unitless) and U is the velocity of water (*m/s*).

$$\Delta h_{tot} = \Delta h_f + \Delta h_t = \frac{L}{\rho g R_h} * \tau_f + \frac{P_t}{\rho g Q} \tag{10}$$

$$\tau_f = \frac{f\rho}{8} * U^2 \tag{11}$$

It is also important to consider the blockage effect, which can increase the turbine power output [22,24].

2.4. Summary of Literature

When HK devices are placed in array schemes in inland channels/rivers, the cumulative effect and inter-effect of these devices should be well understood to avoid unfavourable free-surface effects. As shown in the organogram (Figure 5), the blockage resulting from the HK device (in typical subcritical, flat-sloped channels) may have multiple subsequent effects influencing downstream installations (within the array) as well as upstream flow conditions. Neglecting the free-surface effects in high-blockage cases may result in exposed downstream turbines (i.e., freeboard reduced), hydraulic jump formation (enforced critical flow), and upstream damming effects, and may also lead to potential blade-tip cavitation problems. Accurately quantifying the water surface effects is a challenge, and guidelines to avoid unfavourable conditions may be extremely useful.
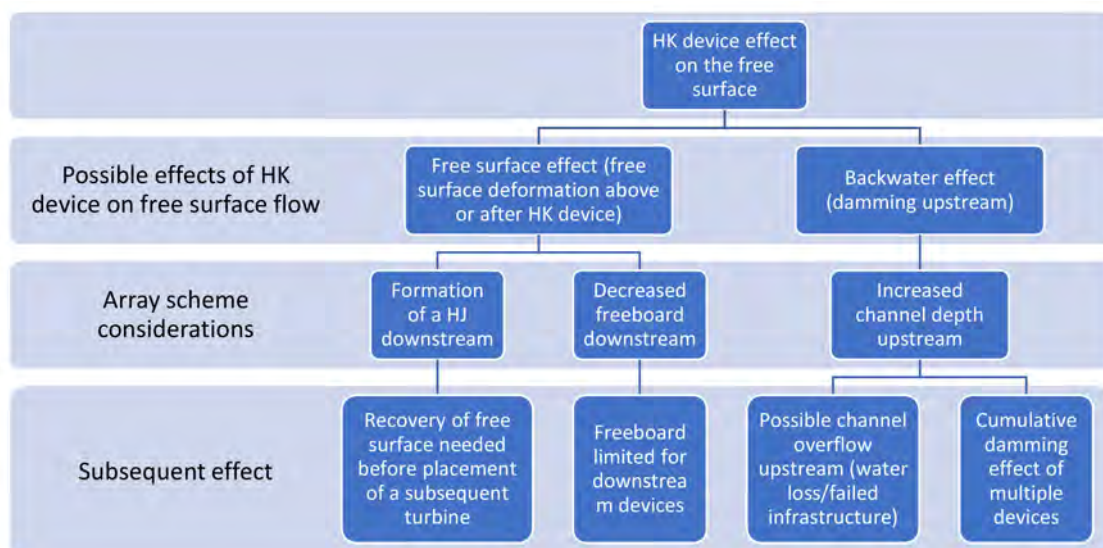
Figure 5. Water surface deformation from HK devices in inland flow infrastructure.

For inland systems, the backwater effect and the calculation thereof are of primary concern. Existing models include multiple unknowns and assumptions of values required as inputs that may not be available to users. Development of a clear, simple, effective blockage approximation of an HK device that can be applied to typical backwater calculations is necessary.

3. Validation of CFD Models

Comprehensive validation of a developed analytical model requires a dataset from a range of turbine styles under various operational conditions. Computational models offer an alternative to physical scale models to simulate the complex flow physics around HK devices. However, the importance of model validation through a physical model dataset should not be neglected. A number of studies have tested and validated modelling approaches for HK turbines [25,26].

Developments in tidal energy have led to multiple large-scale analyses of tidal turbine arrays, where simplified numerical models are used for array schemes [27–30]. With the ever-increasing availability and reliability of computational power, computational fluid dynamics (CFD) simulations are being used to model complex external effects and more accurately resolve fluid dynamic and wall effects [31]. Additionally, blade element

momentum (BEM) theory is often used as a rotor modelling technique that also significantly reduces computational load [32].

CFD models may be used to resolve the effects of turbulence at the sub-grid-scale level, and are being used more often for first-order analysis or design. They have the potential to offer more comprehensive solutions and insights when their limitations are understood. Accurately representing turbulent flow in CFD is imperative due to its strong dependence on initial conditions, as well as the wide range of scales (eddies) present in the flow. Most often, statistical approaches based on the Reynolds-averaged Navier–Stokes (RANS) equations, with eddy viscosity models for turbulence closure, are used [33].

CFD models are valuable tools in flow-field analysis, especially at the sub-grid-scale level and for resolving turbulent length scales. When they are correctly applied and their limitations are understood, they offer useful insights and an alternative to laboratory testing. Correctly representing the turbulent flow, along with prescription of initial conditions, is important—especially due the wide range of scaled eddies present in the flow. Approaches based on the Reynolds-averaged Navier–Stokes (RANS) equations are most often used with various turbulence closure models incorporated, such as eddy viscosity models (k-Epsilon and SST k-ω).

A number of recent studies have used the BEM embedded in CFD method [8,34,35], which is also widely used in wind turbine array models, with good representation in terms of experimental results [36,37]. Various authors [38,39] have used this method to analyse the flow field of turbines arranged in arrays—specifically for tidal turbine optimization. A study analysing the accuracy of RANS approaches revealed good correlation with the experimental data found when using a Reynolds stress turbulence model (RSM) coupled with a BEM blade modelling technique (RSM-BEM) [40]. The study also highlights the importance of using an RSM rather than standard eddy viscosity models, due to the strong anisotropic flow in the wake.

3.1. CFD Models

Three different turbines (shown in Table 2) were modelled using CFD and validated with experimental results (a variation of free-surface, wake, and performance measurements). The primary validation case used was the U.S. Department of Energy's Reference Model 1 (RM1) dual-rotor axial flow turbine, which was modelled in the St. Anthony Falls Laboratory (SAFL) at the University of Minnesota [10]. Free-surface measurements allowed validation of the multiphase CFD model and free-surface deformation.

Additionally, two three-bladed turbine models with experimental results found in the literature [41] and tested on site [1] were modelled as specified in [40], for further measurements and validation of the backwater calculation methods. Where possible, BEM-VD (virtual disk) models were used to reduce the computational expense required. However, for the turbines which customized NACA profiles (Smart Hydropower turbine used in [1]) the full rotor geometry was modelled using a sliding mesh.

Table 2. Turbines modelled in CFD.

Turbine	Name	Blades	Diameter (m)	CFD Model
T1	RM1 [10]	2-Bladed NACA4415	0.5	Multiphase RSM-BEM model
T2	IFREMER [9]	3-Bladed NACA63418	0.7	Single-phase RSM-BEM model
T3	SHP [1]	3-Bladed custom blade	1	Single-phase RSM-FRG model

3.2. RM1 Model Validation

A 0.5 m diameter dual-rotor axial flow tidal turbine was investigated in a laboratory setup. The relevant details of the experiment can be seen in Table 3, with additional details available in [42]. The experimental results [42] provide high-resolution wake measurements

of the near- and far-wake flow field surrounding the turbine from -5 to $10\ d_t$. These were used previously to validate the CFD procedure for a single-phase analysis [40].

Table 3. RM1 laboratory setup details [42].

Description	Variable
Rotor diameter	0.5 m
Blade profile	NACA 4415
Flow depth	1 m
Flow rate	2.425 m^3/s
Tip speed ratios measured	1 to 9
Flow velocity (U_{hub})	1.05 m/s
Turbulence intensity	5%
Froude number	0.28
Reynolds number (chord)	$\sim 3.0 \times 10^5$

Although the velocity profiles and performance metrics were adequately modelled with both the single-phase and multiphase models, correct approximation of the backwater effect through the multiphase modelling required validation. For this, free-surface measurements were collected for the optimal operational case (*TSR* = 5.1, *U* = 1.05 m/s) of the RM1 experimental setup, at a resolution of 1 d_t (diameters) in the streamwise direction, and 0.4 d_t in the cross-stream direction. The measurement zone was $-5\ dt$ to $10\ dt$ downstream. Elevation data were sampled at 50 Hz for 120 seconds at each location using a Massa ultrasonic range sensor, allowing for both time-averaged and fluctuating water surface elevation analysis and CFD validation.

Siemens STAR-CCM+ Commercial modelling software was used to simulate the turbines. The computational domain representing the RM1 laboratory model is shown in Figure 6. A wall-bounded model was used, extending from $-14\ d_t$ upstream to $16\ d_t$ downstream of the axis of rotation. The specified inlet length allowed full flow development prior to reaching the turbine axis of rotation. The outlet length ensured that no effects from the downstream boundary condition affected the near-wake behaviour. Previous studies have found that around 15 d_t is usually adequate for the outlet boundary length [43,44].

A velocity inlet and downstream pressure outlet were specified as boundary conditions. The laboratory test turbulence and velocity values that were measured experimentally were specified at the inlet. Full development of the boundary layer on all surfaces (i.e., boundary walls, blades, and stanchion) was ensured through the specific turbulence model wall treatment and mesh resolution for each test case (details seen in [40]).

A virtual disk (VD) rotor modelling technique was used, and a BEM model was employed over the VD. This VD-BEM modelling approach has demonstrated good accuracy in the past, also significantly reducing computational costs [8,34,35,45,46]. A BEM tip-loss correction was incorporated using the Prandtl tip-loss correction method [47].

A Reynolds stress model (RSM) was used to allow more accuracy in prediction of possible flow anisotropy. The RS linear pressure strain two-layer (RS-LPS2) model [48,49] was found to model the near wake accurately, with a low y$^+$ wall treatment on the turbine and turbine structure (y$^+$ < 1).

Only transient simulations were performed, where unsteady terms were discretized using a 2nd-order implicit scheme. A time step ensuring Courant numbers of less than 1 over the domain was ensured as far as possible (some cells exceeded 1 at the blade tips, where smaller time steps did not change results and, therefore, larger Courant numbers were allowed to reduce computational time). The time steps were around 0.003 s for the BEM-CFD models. However, the time steps varied over each approach, depending on the results of the grid convergence index (GCI).
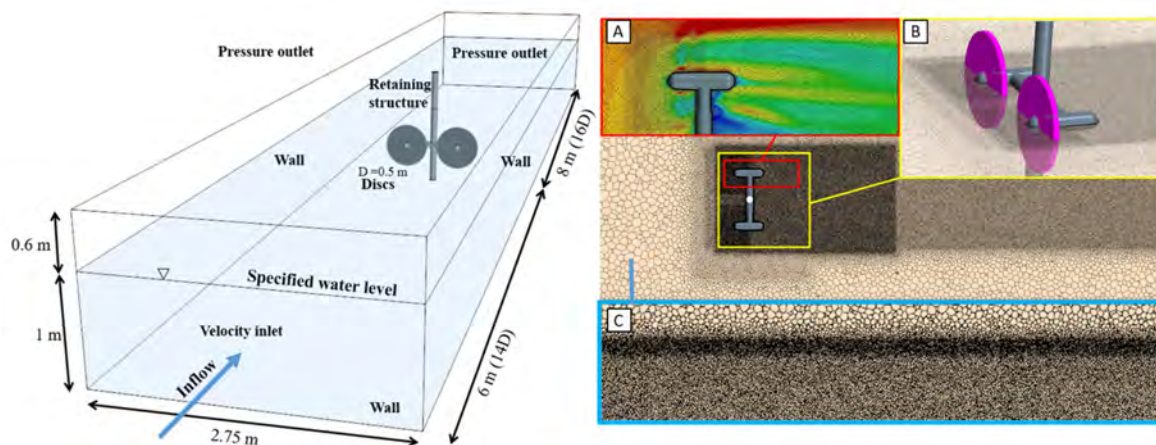
Figure 6. Computational domain with grid refinements: (**A**) near wake, (**B**) blades, and (**C**) free surface.

The computational domain (Figure 6) consisted of a polyhedral mesh with grid refinements in the free surface, near wake, far wake, and surrounding the turbine structure. In the past, results indicated the importance of fine grids to track the tip vortices when using simplified RANS models [31]. For grid refinement, an adapted GCI method [50] was used, due to the variance in grid sensitivity in the different regions. Separate regions' mesh sizes were incrementally decreased, until no changes in turbine performance, free surface, or wake behaviour were observed. As depicted in Figure 6, the final mesh sizes were around 14 million cells.

The smallest cell sizes were specified at the near wake and free surface, where a 10 mm minimum size proved to be adequate. Refinement in the near-wake region is imperative for accurate development of the complex near-wake behaviour, where both separated and attached flow exist [51]. Gibson and Launder [52] investigated the pressure fluctuation effects of capturing the boundary layer surrounding the turbine, and noted the importance of an accurate capture of boundary layer formation. For the VD rotor modelling technique, a minimum of four cells over the blade thickness was ensured for all meshes, which is the recommended minimum when using the VD method. A mesh base size of 14 mm (2.8% d_t) proved adequate in the far-wake region.

The channel walls around the turbine were modelled as non-slip walls using a high-y+ wall treatment to ensure that the effects of the wall boundary layer were included in the simulation. A two-layer formulation may be applied to the linear pressure strain model (LPS2 model). All analyses used the two-layer formulation.

Simulation of the air–water interface (multiphase flow) may be approached in various ways. A multiphase analysis ensures a robust approach, but demands a higher computational load; therefore, a symmetry boundary condition is often used in a single-phase model [40].

Due to the necessity of free-surface measurements in this analysis, the free surface was modelled using a volume-of-fluid approach. This approach uses a 2nd-order discretization to compute a clear interface between the air and water. A volume-fraction variable is used to specify the spatial distribution of each phase. Cells with multiple phases are treated as mixtures, and the method is highly dependent on adequate mesh resolution. A high-resolution mesh (Figure 6C) was ensured on the free surface, with the final cell size determined through a GCI test focussed on a free-surface profile analysis.

Validation of the modelled wake and performance can be seen in [40]. Due to the importance of the backwater approximation, and correct modelling of the backwater effect caused by the turbine blockage, the free-surface measurements from a multiphase model were compared in this paper. Comparison of the experimental and CFD results can be seen in Figure 7. The results correlated well, with the computed free-surface behaviour

fitting well with the experimental tests. The CFD results were recorded over one rotation and plotted as an envelope. The backwater effect was predicted well, with a maximum of 12 mm damming occurring upstream.
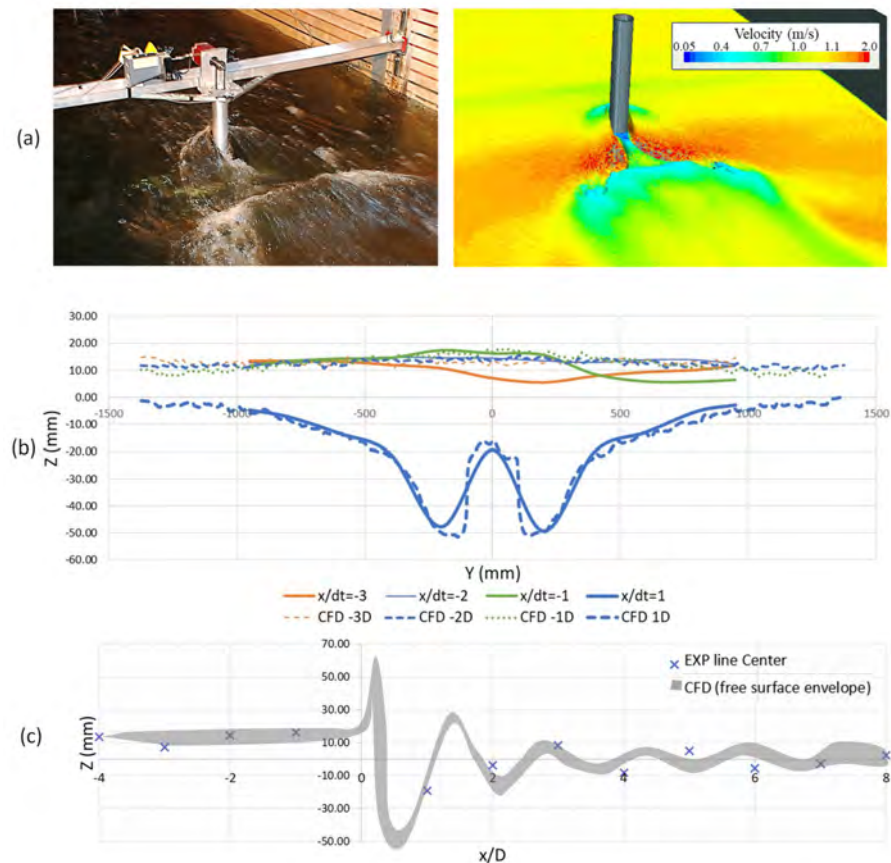
Figure 7. Comparison of experimental and computational water surface profiles for the RM1 tests: (**a**) experiment and CFD water surface graphics; (**b**) lateral WSE comparison; (**c**) longitudinal centre-line WSE comparison.

4. Methods

The primary objective of the development of a backwater model is to allow a usable model with only basic inputs required. Thus, a mathematical formulation based on existing models, basic hydrodynamic principles, and a set of recommended assumptions (where/if information is not yet available) was carried out. The workflow for the backwater model's development can be seen in Figure 8, and is explained in the following subsections.
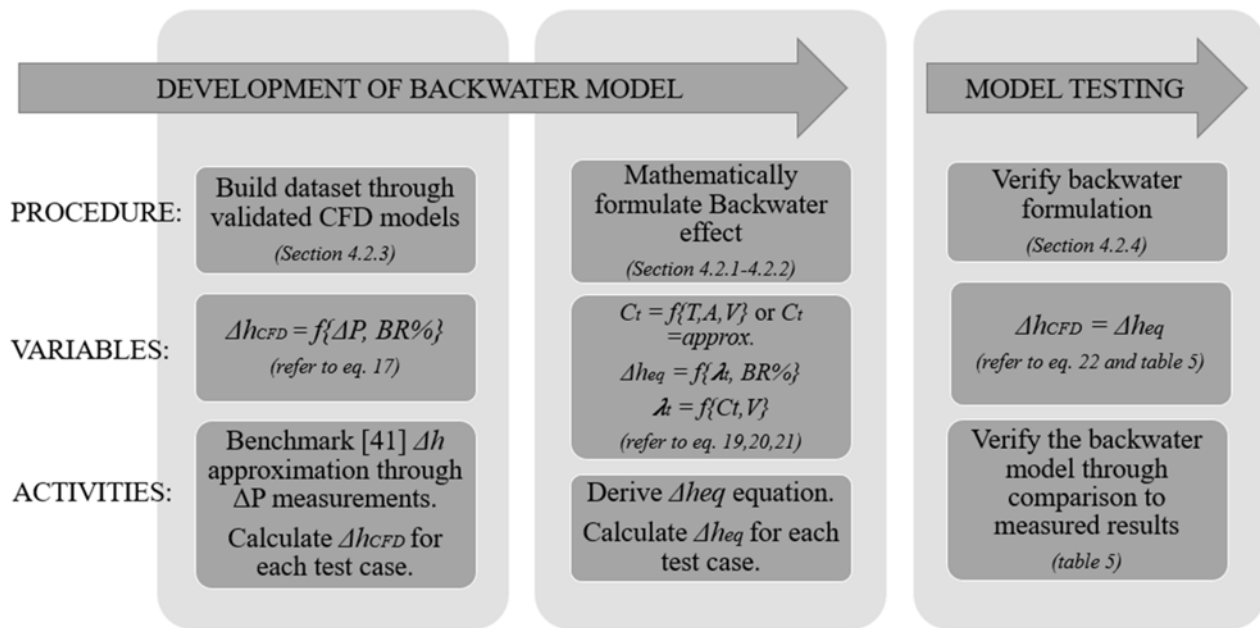
Figure 8. Workflow of backwater model development.

4.1. Assumptions and Exclusions

It is important to state the limitations of the model. Operational condition boundaries were set to within the typical canal operating conditions, where deployment of HK devices would be considered. Scenarios outside of these boundaries were not considered, as it was assumed that the use of such a model would not be necessary outside of these conditions (e.g., at supercritical flow conditions) [1,14,53].

The following limitations on flow conditions were set:

- Subcritical flow regime (Fr < 1);
- 5000 < Re < 1,500,000;
- Typical operational velocities of channels (0.8–2.8 m/s);
- Manning n-value around 0.016–0.023 s/m$^{1/3}$ (lined channel).

4.2. Mathematical Formulation

Energy losses in a channel are categorized and included with various approximations. For channel roughness, the friction losses can be accounted for by the Manning equation. Additionally, sudden losses due to channel features such as piers, bends, and drop structures have also been defined/estimated empirically, and can be included as form losses [14]. These are typically defined as eddy losses (h_e), included as an energy loss:

$$h_e = C_L \frac{V^2}{2g}$$

(12)

where C_L is the loss coefficient predefined for typical losses in a channel. The drop in water level due to a particular loss can be quantified/included by applying either the momentum or energy equation over a channel section, and the upstream and downstream sections (in which the energy loss exists). Additionally, an empirical approach may be used, where experimental results are used to determine an empirical relationship, such as that done by Yarnell in 1934 for bridge piers [54].
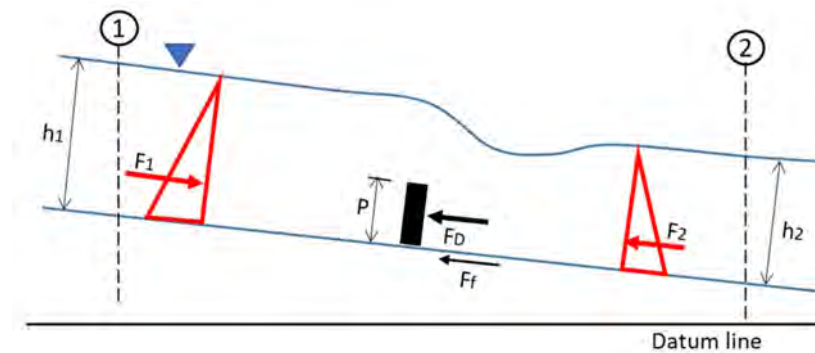
4.2.1. Approach 1: Momentum Approach

A possible approach often used to determine the effect of an object/structure on the free surface (backwater effect) is the momentum approach. Energy losses occur due to flow separation, vortex generation, friction, and turbulence—all associated with the changes

in velocity due to the presence of the turbine. In some cases, the presence of the turbine may also result in the formation of a hydraulic jump on the water surface, resulting in additional energy losses. Applying the momentum approach avoids inclusion of these individual energy losses by considering the change in momentum between an upstream and downstream section. Additionally, if drag can be quantified, the momentum approach may be favourable.

The simple momentum formulation between two flow sections can be used with the resistance of the turbine represented as a drag coefficient, as shown in Figure 9 and Equation (13), where the change in momentum is quantified by the hydrostatic forces upstream (F_1) and downstream (F_2) of the device (water level change), as well as the friction from the channel bed and walls (F_f) and the force due to the turbine (F_D). This can then be rewritten to Equation (14), in terms of the drag force (F_D) due to the presence of the turbine.

$$F_1 - F_2 - F_D - F_f = \rho Q(\beta_2 V_2 - \beta_1 V_1) \tag{13}$$

$$F_D = \frac{1}{2}\rho g B h_1{}^2 - \frac{1}{2}\rho g B h_2{}^2 - \rho Q(\beta_2 V_2 - \beta_1 V_1) \tag{14}$$

Figure 9. Momentum approach schematic (adapted form [55]).

The drag coefficient for the HK device can be rewritten, which allows the determination of h_1 (the upstream water level) through knowledge of the drag coefficient and downstream flow conditions. However, this requires knowledge of the downstream conditions, which is not always possible in feasibility studies in the design phase. An alternative conservative analysis would be to use the normal flow depth as the downstream value.

4.2.2. Approach 2: Energy Approach

The energy approach is more often used to determine backwater effects in typical open-channel flow scenarios. This is also a common approach in bridge pier modelling [14] when modelling the backwater effect of arch bridges [56], bridge piers, and even irregular structures such as wood jams [57].

The energy approach can be seen in Equation (15) and Figure 10. All energy losses between a point upstream and downstream of an HK device or blockage are quantified as terms that contribute to either the friction losses (h_f) or local losses (h_l).

$$\frac{V_1{}^2}{2g} + h_1 + Z_1 = \frac{V_4{}^2}{2g} + h_4 + Z_4 + \sum h_{f1-4} + \sum h_{l1-4} \tag{15}$$

All terms are defined in terms of velocity U), water depth (h), and distance from a datum (Z). The total energy (*TEL*), energy grade line (*EGL*), and water level/hydraulic grade line (*HGL*) are shown in Figure 10.
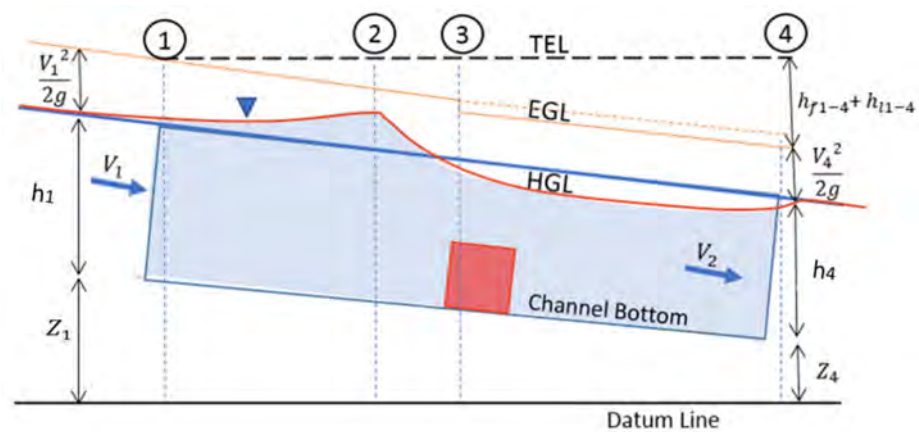
Figure 10. Energy approach.

Approximations of the loss due to the presence of the turbine have been attempted, such as those mentioned in Sections 2 and 3. However, preliminary tests of these methods indicated inaccuracies over a range of varying turbines and operational scenarios.

A method of including the turbine loss in the energy equation includes quantifying it in terms of a loss coefficient that has been calibrated to the turbine type and operating conditions. The energy loss due to the presence of the turbine (h_t) can be written as a function of a loss coefficient (α), the freestream velocity (U), and the blockage ratio of the turbine, as shown in Equation (16).

$$h_t = \alpha \frac{U^2}{2g} \times \frac{A_t}{A} \tag{16}$$

Although this approach is most often used in the literature, the loss (h_t) may also be quantified as a pressure drop, which is then directly converted to an energy loss as follows:

$$h_t = \frac{\Delta P_t}{\rho g} \times \frac{A_t}{A} \tag{17}$$

The pressure change (ΔP_t) is measured in the computational models as the pressure drop across the turbine, and applied (with consideration to the blockage ratio) to the channel area. This approach was followed to allow the use of CFD models to approximate energy loss due to the presence of the turbine. Other than the losses due to the direct pressure drop over the turbine, there are additional losses in the near wake, due to the turbulent flow. Using the ΔP_t approximation (Equation (17)) allows measurement of the pressure drop over the turbine and near-wake area, thus including additional losses.

4.2.3. Validation of Pressure Drop Measurement in CFD Results

CFD has previously been used to measure the backwater effects from blockages such as bridge piers [58], with computed and measured levels showing almost identical results. Multiple methods have also been analysed and validated for determining the backwater effects of common structures found in river channels [59–61]. To validate whether the approximation for h_t shown in Equation (17) holds true, the ΔP_t was measured in the CFD model for the RM1 validation case. The subsequently calculated loss (h_t) was then compared to the measured backwater effects in the laboratory tests (as well as multiphase CFD analysis). Inclusion of the support structure blockage was incorporated using the Yarnell approximation. The Yarnell approximation for a single circular bridge pier (similar to the support stanchion) was implemented:

$$\left[\frac{\Delta y}{y}\right]_{empirical} = K\left(K + 5F_r^2 - 0.6\right)\left(15\alpha^4\right)Fr^2 \tag{18}$$

where Δy is the backwater generated by the pier, y is the undisturbed flow depth, F_{r} is the downstream Froude number, and α is the ratio of the flow area obstructed by the pier to the total flow area downstream of the pier (also referred to as the blockage ratio). K is used as a coefficient reflecting the pier's shape. To ensure that the Yarnell approximation and pressure loss (ΔP_t) calculation work independently, the RM1 model free-surface deformation was measured with and without the stanchion structure (Figure 11), and the results were compared to the backwater calculation using only the pressure drop, as well as including the stanchion through the Yarnell approximation.
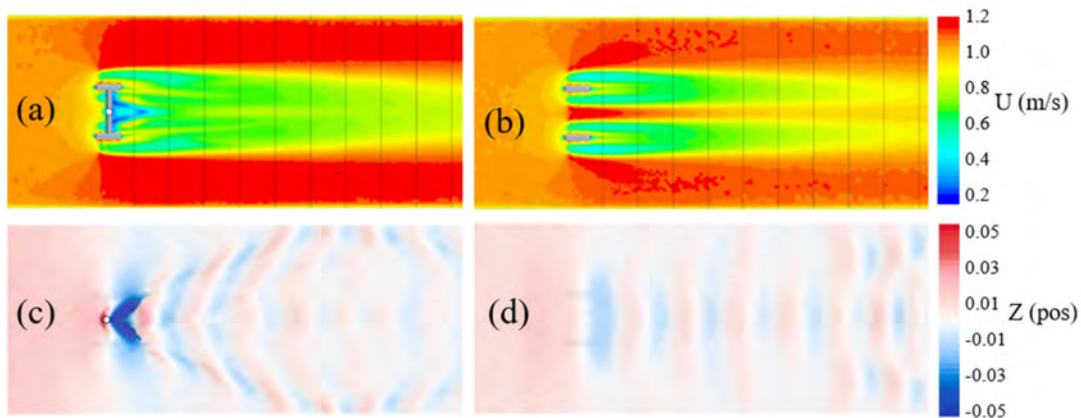
Figure 11. (**a**,**b**) Velocity and (**c**,**d**) surface water measurements graphics for the RM1 full model vs. the RM1 rotor and nacelle only.

The pressure drop due to the presence of the HK device was found to be maximal when measured over the size of the turbine-swept area from 1 D upstream to 1.5 D downstream (Figure 12). The calculated backwater (Equation (17)) was then compared to the measured backwater (Table 4), which was calculated from the average disk pressure drop, as shown in Figure 13.
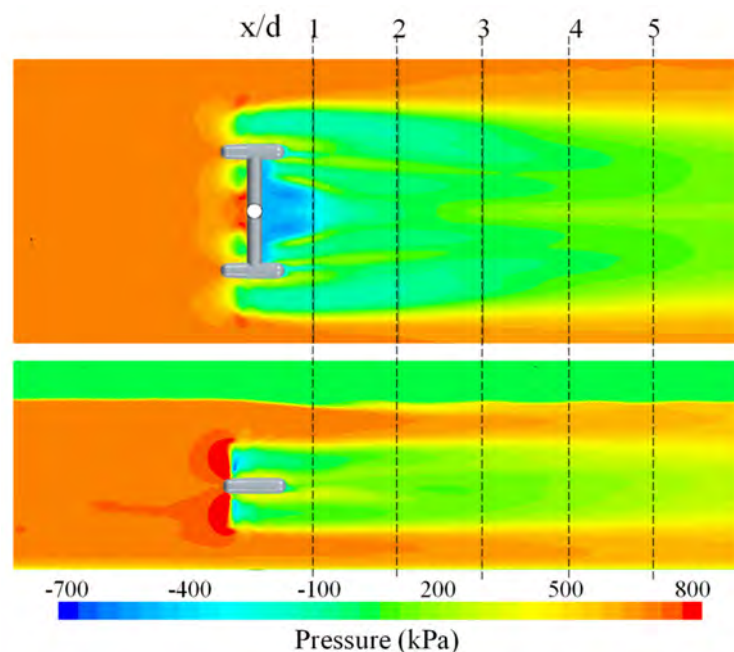
Figure 12. Pressure measurements over the horizontal and vertical planes (at the turbine hub height centerline).
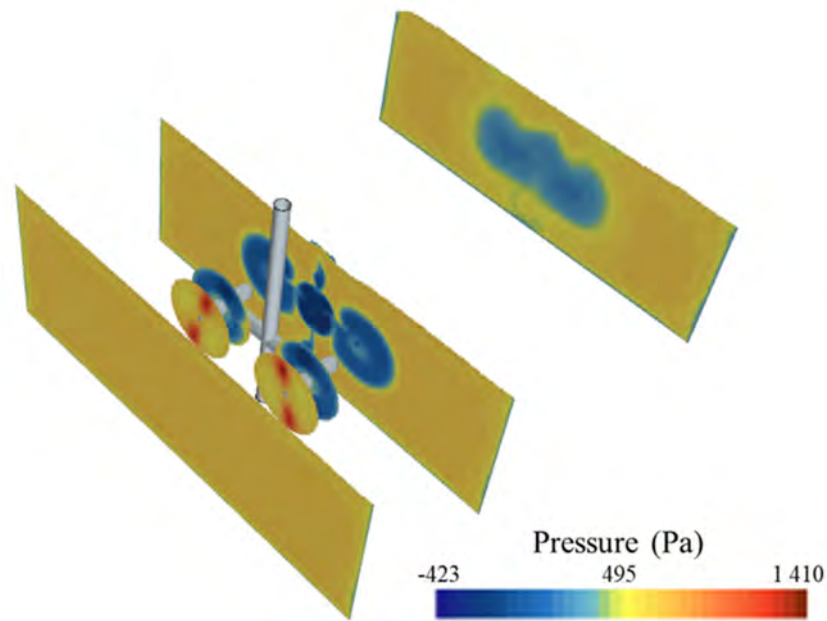
Figure 13. Pressure measurements over the disk and planes upstream and downstream of the RM1 turbine and retaining structure.

Table 4. Comparison of measured and predicted backwater levels.

	ΔP_t Disk (Pa)	ΔP_t Plane (Pa)	Calculated h_t (mm)	Yarnell Approx. (mm)	Measured h_t (mm)	$\frac{ht\ meas - ht\ calc}{y}$ (%)
RM1 (no stanchion)	570	57.73	8.30	-	9.60	0.13%
RM1 (with stanchion)	530	74.09	7.72 / 12.66	4.36	12.00	0.01%

As shown in Table 4, the calculated analytical backwater values from Equation (17) and the computational reading for disk ΔP result in a very similar h_t, as would be the result of the RM1 device in channel flow.

4.2.4. Lambda Approximation

To allow a simple empirical model for the determination of the energy loss due to the turbine, λ_T was selected as the energy loss coefficient used in the energy equation:

$$h_t = \lambda_T \times \frac{A_t}{A} \frac{U^2}{2g} \tag{19}$$

where h_t is included as a loss in the energy equation (Equation (15)), and λ_T is calculated as a function of the thrust coefficient (C_t):

$$\lambda_T = \frac{C_t \times U^2}{2g} \tag{20}$$

where C_t is a value that can be obtained from the manufacturer, calculated, or assumed in the pre-feasibility stage. For HAHTs, these thrust coefficients (C_t) usually range from 0.52 to 0.89 [9,62–64]. According to the actuator disk theory, C_t may be written in terms of the induction factor a [65]. It is also known that ideally, according to the Betz limit, $a = \frac{1}{3}$; therefore, the ideal and highest attainable C_t would be 0.88. Theoretically, according to the BEM theory, this should result in the highest velocity deficit in the near wake and, therefore, the "worst case" scenario for the operational conditions. Realistically, the values lie at an

upper limit of $C_t = 0.8$. The thrust coefficient can be calculated directly if the thrust force (T), inlet velocity (U), and swept area (A) are known:

$$C_t = \frac{T}{\left(\frac{1}{2}\right)\rho U^2 A} \tag{21}$$

To justify the use of the λ_T approximation, the validated CFD models were analysed, the pressure drop/total thrust was measured, and the subsequent backwater effect was determined. The calculated h_t (through Equation (19)) was then compared to the h_t determined through the ΔP_t (Equation (17)) results, as validated in Section 4.2.3.

Two approximations for λ_T were included (calculated and assumed C_t). The model should be usable with only basic knowledge of the turbine installation and operating parameters; therefore, simple available metrics could be used to obtain a conservative result. Acceptable correlation between the experimental and calculated values created confidence to proceed with the model and build a larger dataset to analyse the model's accuracy at a larger operational variance from optimal conditions.

A regression to the mean approach was used to accumulate the necessary dataset for the analysis of the aforementioned calculation procedure and assumptions. This was required to reduce computational costs, and due to the lack of available data on various input parameters. The dataset was created through results from three models of turbines typically used for inland installations (Table 2). These CFD models were validated through benchmark validation using experimental results obtained at optimal performance points. The models were then varied in five primary operational states, namely:

1. Inlet velocity changes (0.4 < U < 2.8);
2. Blockage ratio changes (Swept area to flow area) (4% < BR < 23%);
3. Tip speed ratio changes (lower or higher load applied) (3 < TSR < 6);
4. Froude number (0.18 < Fr < 0.34) (within the subcritical flow regime);
5. Froude number based on turbine diameter (0.15 < Fr_D < 0.9).

These primary variables have been previously investigated and shown to influence the turbine thrust imposed on the flow area, and may therefore influence the backwater effect. Constraints were set to the variation of these variables to ensure that the computational models remained within realistic scenarios, whilst allowing insight into the effects of changes. The primary objective of the model validation was to ensure that a relative level of accuracy was obtained and, more importantly, a conservative approach to predicting the possible backwater effects caused by such a device.

A measure of accuracy of the methods is indicated by the mean square absolute error. The absolute error (MAE), rather than relative error (RMSE), was used to place greater emphasis of the larger backwater values (at higher blockage ratios) rather than uniform predictions over the range of backwater predictions (h_t). Additionally, as the sample size changed in the analysis, the strength of the sample size effect was minimized when comparing MAE. The variance was also included to give an indication of the test conditions with greater variability, and under which test conditions the model (and assumptions) performed best.

$$\sigma = \sqrt{\frac{1}{N}\sum\left(\frac{h_t}{y}_{exp} - \frac{h_t}{y}_{calc}\right)^2} \tag{22}$$

The MAE (σ) and variance values calculated for various scenarios are shown in Table 5. The variations between experimental and approximated h_t for variations in blockage ratio (*BR*) velocity (*U*) and Fr_D are shown in Figure 14.

Table 5. Mean absolute error and variance for test cases.

Test Condition	C_t	N	MAE	Variance
All tests conducted	Equation (21)	14	1.45	2.26
	0.8	14	1.42	2.17
	0.89	14	1.99	4.27
Optimal operational point	Equation (21)	3	1.26	1.85
	0.8	3	1.25	1.83
Variation of blockage ratios (BR = 4–22%) at optimal operational point	Equation (21)	4	0.35	0.16
	0.8	4	0.27	0.09
Variation of inlet velocities at optimal tip speed ratios	Equation (21)	4	2.4	7.65
	0.8	4	1.36	2.47
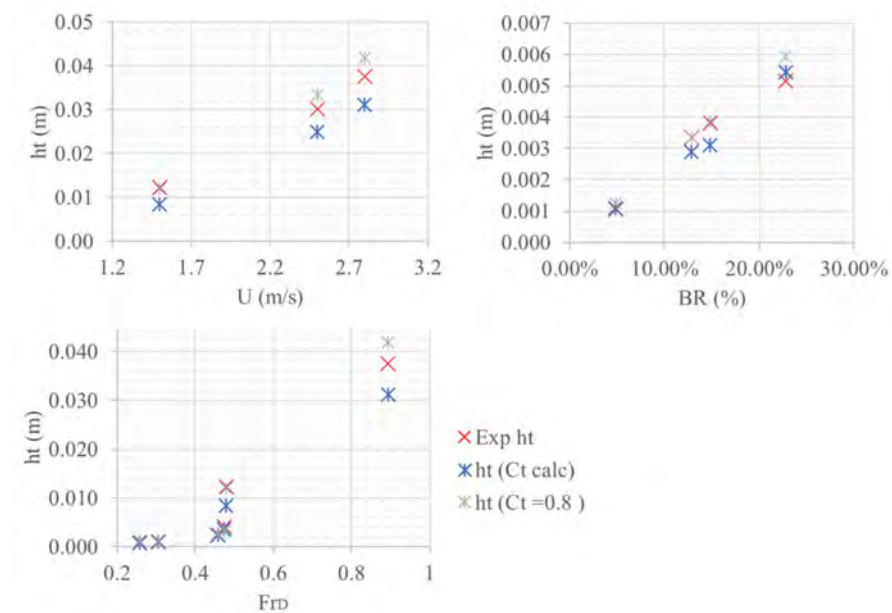
Figure 14. Effects of U, BR, and F_{rD} on the determined h_t values.

From the results in Table 5 and Figure 14, the following observations can be drawn:

1. At turbine optimal operational points, a maximum deviation of 13% from the predicted backwater was obtained when using the correct C_t value. This deviation increased to 19% for the $C_t = 0.8$ approximation.

2. When utilizing the C_t assumption of 0.8, a conservative result was obtained, with the backwater estimation generally overestimating the measured blockage.

3. Calculating C_t based on the turbine thrust (measured thrust) lowered the h_t approximation. However, for test cases operating close to the optimal performance and highest C_t value, the backwater was underestimated by up to 20%.

4. Test cases at low operational velocities (low Froude numbers) resulted in larger errors in approximating h_t; however, it is important to note that these are unfavourable installation conditions and far from typical installations. The turbines may have low performance at these low operational velocities and, therefore, pose an unrealistic scenario. Here, the C_t calculation resulted in a more realistic value, due to the reduced performance.

5. The C_t approximation resulted in large overestimations of the h_t at lower TSRs. However, the C_t equation (Equation (22)) performed well in these scenarios, as the turbine thrust was significantly lower, and the C_t assumption did not hold.

6. The C_t approximation gave significantly better results for the three-bladed turbines. The two-bladed (T1) case predicted better results with the C_t calculation, which

was also higher than the 0.8 approximation, indicating that the turbine operates closer to the Betz limit and ideal induction factor (*a*), which could be further tested and calibrated. The C_t calculation performed better in this case, predicting $C_t = 0.89$. Therefore, utilizing this assumption may be favourable for avoiding errors—especially when turbines with higher operational tip speed ratios are used.

Based on the small dataset obtained from the three turbine models, a C_t value for each turbine can be determined empirically, which could be improved with a larger dataset.

The recommended model also performed significantly better than models found in the literature, as well as needing less input data and background knowledge on specific turbine performance. This indicates the usefulness of this approximation.

5. Conclusions

Quantifying the backwater resulting from the effective blockage caused by the operating turbine remains a challenge for the deployment of HK turbines in inland infrastructure, such as canal systems. This paper shows a simple analytical model to estimate the effective blockage and backwater effect from HK devices. The development of the model followed a similar approach to what has been previously used for bridge pier modelling and quantifying blockages from such structures.

Three variations of typical examples of commercially available HK devices were modelled using a recommended CFD approach, and conditions were varied to allow testing over a range of operational conditions. The water surface profile measurements from the Reference Model 1 (RM1) scaled model experiments allowed validation of the water surface deformation obtained when using a VOF approach coupled with an RS-LPS2 Reynolds stress closure model and BEM-VD blade modelling approach. This highlights the usefulness of CFD models in HK energy development.

The developed backwater model allows a conservative approach with various levels of certainty attainable, depending on the input parameters installed. Although the recommended procedure is an extremely simplified approximation, the results obtained were significantly closer to available dataset of backwater effects than the methods found in the literature. The ease of use also makes this method useful for engineers and developers when detailed numerical models are not feasible.

This model also allows cumulative estimation of backwater, with simple inclusion of blockage structures or multiple turbines using available approximations such as the Yarnell equation. Additionally, due to the nature of flow in canals (flat slopes), subcritical conditions govern, and backwater effects extend a large distance upstream. This allows simple cumulative inclusion of blockages without complex computational modelling, making this approach simple and relatively accurate (or at least favourably conservative).

This approach allows room for further development and determination of calibrated thrust coefficients for typical turbines or typical operational conditions (similar to what was previously done for pier shapes, etc.). Additionally, a similar approach may be investigated for cross-flow turbines where experimental results are available.

Although this paper focussed on backwater determination, other free-surface effects—such as the water level drop over the turbine, or possible hydraulic jumps downstream—are important considerations for array designs. Recommendations for clearance coefficients and turbine spacing (due to wake recovery) should be carefully considered prior to deployment.

Author Contributions: Conceptualization, C.M.N. and M.V.D.; methodology, C.M.N., M.V.D. and L.S.; software, C.M.N. and L.S.; validation, C.M.N. and C.H.; formal analysis, C.M.N., C.H., M.V.D. and L.S.; investigation, C.M.N. and C.H.; resources, C.H.; data curation, C.M.N. and C.H.; writing—original draft preparation, C.M.N.; writing—review and editing, C.H., M.V.D. and L.S.; visualization, C.M.N. and C.H.; supervision, M.V.D. and L.S.; project administration, C.M.N. All authors have read and agreed to the published version of the manuscript.

References

1. Niebuhr, C.M.; van Dijk, M.; Bhagwan, J.N. Development of a design and implementation process for the integration of hy-drokinetic devices into existing infrastructure in South Africa. *Water SA* **2019**, *45*, 434–446. [CrossRef]
2. Riglin, J.D. Design, Manufacture and Prototyping of a Hydrokinetic Turbine Unit for River Application. Master's Thesis, Lehigh University, Bethlehem, PA, USA, 2016.
3. Runge, S. Performance and Technology Readiness of a Freestream Turbine in a Canal Environment. Ph.D. Thesis, Cardiff University, Cardiff, UK, 2018.
4. Kartezhnikova, M.; Ravens, T.M. Hydraulic impacts of hydrokinetic devices. *Renew. Energy* **2014**, *66*, 425–432. [CrossRef]
5. Gunawan, B.; Roberts, J.; Neary, V. Hydrodynamic Effects of Hydrokinetic Turbine Deployment in an Irrigation Canal. In Proceedings of the 3rd Marine Energy Technology Symposium, Washington, DC, USA, 27–29 April 2015; pp. 1–6.
6. Bahaj, A.S.; Myers, L.E.; Rawlinson-Smith, R.I.; Thomson, M. The effect of boundary proximity upon the wake structure of horizontal axis marine current turbines. *J. Offshore Mech. Arct. Eng.* **2011**, *134*, 021104. [CrossRef]
7. Bachant, P.; Wosnik, M. Effects of Reynolds Number on the Energy Conversion and Near-Wake Dynamics of a High Solidity Vertical-Axis Cross-Flow Turbine. *Energies* **2016**, *9*, 73. [CrossRef]
8. Turnock, S.R.; Phillips, A.B.; Banks, J.; Nicholls-Lee, R. Modelling tidal current turbine wakes using a coupled RANS-BEMT approach as a tool for analysing power capture of arrays of turbines. *Ocean Eng.* **2011**, *38*, 1300–1307. [CrossRef]
9. Mycek, P.; Gaurier, B.; Germain, G.; Pinon, G.; Rivoalen, E. Experimental study of the turbulence intensity effects on marine current turbines behaviour. Part II: Two interacting turbines. *Renew. Energy* **2014**, *68*, 876–892. [CrossRef]
10. Hill, C.; Neary, V.S.; Guala, M.; Sotiropoulos, F. Performance and Wake Characterization of a Model Hydrokinetic Turbine: The Reference Model 1 (RM1) Dual Rotor Tidal Energy Converter. *Energies* **2020**, *13*, 5145. [CrossRef]
11. Lalander, E.; Leijon, M. In-stream energy converters in a river—Effects on upstream hydropower station. *Renew. Energy* **2011**, *36*, 399–404. [CrossRef]
12. Myers, L.; Bahaj, A.S. Wake studies of a 1/30th scale horizontal axis marine current turbine. *Ocean Eng.* **2007**, *34*, 758–762. [CrossRef]
13. Adamski, S.J. Numerical Modeling of the Effects of a Free Surface on the Operating Characteristics of Marine Hydrokinetic Turbines. Ph.D. Thesis, University of Washington, Washington, DC, USA, 2013.
14. Henderson, F.M. *Open Channel Flow*; The Mcmillan Company: New York, NY, USA, 1966.
15. Birjandi, A.H.; Bibeau, E.L.; Chatoorgoon, V.; Kumar, A. Power measurement of hydrokinetic turbines with free-surface and blockage effect. *Ocean Eng.* **2013**, *69*, 9–17. [CrossRef]
16. Niebuhr, C.; van Dijk, M.; Neary, V.; Bhagwan, J. A review of hydrokinetic turbines and enhancement techniques for canal installations: Technology, applicability and potential. *Renew. Sustain. Energy Rev.* **2019**, *113*, 109240. [CrossRef]
17. Whelan, J.I.; Graham, J.M.R.; Peiró, J. A free-surface and blockage correction for tidal turbines. *J. Fluid Mech.* **2009**, *624*, 281–291. [CrossRef]
18. Polagye, B.L. *Hydrodynamic Effects of Kinetic Power Extraction by In-Stream Tidal Turbines*; University of Washington: Washington, DC, USA, 2009.
19. Bryden, I.; Grinsted, T.; Melville, G. Assessing the potential of a simple tidal channel to deliver useful energy. *Appl. Ocean Res.* **2004**, *26*, 198–204. [CrossRef]
20. Chanson, H. *Hydraulics of Open Channel Flow*, 2nd ed.; Elsevier Science & Technology: Amsterdam, The Netherlands, 2004.
21. Mańko, R. Ranges of Backwater Curves in Lower Odra. *Civ. Environ. Eng. Rep.* **2018**, *28*, 25–35. [CrossRef]
22. Garrett, C.; Cummins, P. The efficiency of a turbine in a tidal channel. *J. Fluid Mech.* **2007**, *588*, 243–251. [CrossRef]
23. Garrett, C.; Cummins, P. The power potential of tidal currents in channels. *Proc. R. Soc. A Math. Phys. Eng. Sci.* **2005**, *461*, 2563–2572. [CrossRef]
24. Ross, H.; Polagye, B. An experimental assessment of analytical blockage corrections for turbines. *Renew. Energy* **2020**, *152*, 1328–1341. [CrossRef]
25. López, Y.; Contreras, L.; Laín, S. CFD Simulation of a Horizontal Axis Hydrokinetic Turbine. *Renew. Energy Power Qual. J.* **2017**, *1*, 512–517. [CrossRef]
26. Laín, S.; Contreras, L.T.; López, O. A review on computational fluid dynamics modeling and simulation of horizontal axis hydrokinetic turbines. *J. Braz. Soc. Mech. Sci. Eng.* **2019**, *41*, 375. [CrossRef]

27. Adcock, T.A.; Draper, S.; Nishino, T. Tidal power generation—A review of hydrodynamic modelling. *J. Power Energy* **2015**, *229*, 755–771. [CrossRef]

28. Nishino, T.; Willden, R.H. Effects of 3-D channel blockage and turbulent wake mixing on the limit of power extraction by tidal turbines. *Int. J. Heat Fluid Flow* **2012**, *37*, 123–135. [CrossRef]

29. Nishino, T.; Willden, R.H.J. Two-scale dynamics of flow past a partial cross-stream array of tidal turbines. *J. Fluid Mech.* **2013**, *730*, 220–244. [CrossRef]

30. Gotelli, C.; Musa, M.; Guala, M.; Escauriaza, C. Experimental and Numerical Investigation of Wake Interactions of Marine Hydrokinetic Turbines. *Energies* **2019**, *12*, 3188. [CrossRef]

31. Sanderse, B.; van der Pijl, S.P.; Koren, B. Review of computational fluid dynamics for wind turbine wake aerodynamics. *Wind Energy* **2011**, *14*, 799–819. [CrossRef]

32. Whale, J.; Anderson, C.; Bareiss, R.; Wagner, S. An experimental and numerical study of the vortex structure in the wake of a wind turbine. *J. Wind Eng. Ind. Aerodyn.* **2000**, *84*, 1–21. [CrossRef]

33. Pyakurel, P.; Tian, W.; VanZwieten, J.H.; Dhanak, M. Characterization of the mean flow field in the far wake region behind ocean current turbines. *J. Ocean Eng. Mar. Energy* **2017**, *3*, 113–123. [CrossRef]

34. Masters, I.; Chapman, J.C.; Willis, M.R.; Orme, J.A.C. A robust blade element momentum theory model for tidal stream tur-bines including tip and hub loss corrections. *J. Mar. Eng. Technol.* **2014**, *10*, 25–35. [CrossRef]

35. Guo, Q.; Zhou, L.; Wang, Z. Comparison of BEM-CFD and full rotor geometry simulations for the performance and flow field of a marine current turbine. *Renew. Energy* **2015**, *75*, 640–648. [CrossRef]

36. Malki, R.; Masters, I.; Williams, A.J.; Croft, N. The variation in wake structure of a tidal stream turbine with flow velocity. In Proceedings of the MARINE 2011, IV International Conference on Computational Methods in Marine Engineering, Lisbon, Portugal, 28–30 September 2011. [CrossRef]

37. Edmunds, M.; Williams, A.; Masters, I.; Croft, N. An enhanced disk averaged CFD model for the simulation of horizontal axis tidal turbines. *Renew. Energy* **2017**, *101*, 67–81. [CrossRef]

38. Masters, I.; Williams, A.; Croft, T.N.; Togneri, M.; Edmunds, M.; Zangiabadi, E.; Fairley, I.; Karunarathna, H. A Comparison of Numerical Modelling Techniques for Tidal Stream Turbine Analysis. *Energies* **2015**, *8*, 7833–7853. [CrossRef]

39. Masters, I.; Malki, R.; Williams, A.J.; Croft, T.N. The influence of flow acceleration on tidal stream turbine wake dynamics: A numerical study using a coupled BEM–CFD model. *Appl. Math. Model.* **2013**, *37*, 7905–7918. [CrossRef]

40. Niebuhr, C.; Schmidt, S.; van Dijk, M.; Smith, L.; Neary, V. A review of commercial numerical modelling approaches for axial hydrokinetic turbine wake analysis in channel flow. *Renew. Sustain. Energy Rev.* **2022**, *158*, 112151. [CrossRef]

41. Mycek, P.; Gaurier, B.; Germain, G.; Pinon, G.; Rivoalen, E. Experimental study of the turbulence intensity effects on marine current turbines behaviour. Part I: One single turbine. *Renew. Energy* **2014**, *66*, 729–746. [CrossRef]

42. Hill, C.; Neary, V.S.; Gunawan, B.; Guala, M.; Sotiropoulos, F.U.S. *Department of Energy Reference Model Program RM1: Experimental Results*; University of Minnesota: Minneapolis, MN, USA, 2014.

43. Nasef, M.H.; El-Askary, W.A.; AbdEL-hamid, A.A.; Gad, H.E. Evaluation of Savonius rotor performance: Static and dynamic studies. *J. Wind Eng. Ind. Aerodyn.* **2013**, *123*, 1–11. [CrossRef]

44. Franke, J.; Hirsch, C.; Jensen, A.G.; Krus, H.W.; Schatzmann, P.S.; Miles, S.D.; Wisse, J.A.; Wright, N.G. Recommendations on the use of CFD in wind engineering. In Proceedings of the CWE2006 Fourth International Symposium Computational Wind Engineering, Yokohama, Japan, 16–19 July 2006.

45. Malki, R.; Williams, A.; Croft, T.; Togneri, M.; Masters, I. A coupled blade element momentum—Computational fluid dynamics model for evaluating tidal stream turbine performance. *Appl. Math. Model.* **2013**, *37*, 3006–3020. [CrossRef]

46. Bekker, A.; Van Dijk, M.; Niebuhr, C.M. A review of low head hydropower at wastewater treatment works and development of an evaluation framework for South Africa. *Renew. Sustain. Energy Rev.* **2022**, *159*, 112216. [CrossRef]

47. Shen, W.Z.; Mikkelsen, R.; Sørensen, J.N.; Bak, C. Tip loss corrections for wind turbine computations. *Wind Energy* **2005**, *8*, 457–475. [CrossRef]

48. Speziale, C.G.; Sarkar, S.; Gatski, T.B. Modelling the pressure-strain correlation of turbulence: An invariant dynamical systems approach. *J. Fluid. Mech.* **1991**, *227*, 245–272. [CrossRef]

49. Sarkar, S.; Lakshmanan, B. Application of a Reynolds stress turbulence model to the compressible shear layer. *AIAA J.* **1991**, *29*, 743–749. [CrossRef]

50. Roache, P.J. Perspectvie: A method for Uniform Reporting of Grid Refinement Studies. *J. Fluids Eng. Trans. ASME* **1994**, *116*, 405–413. [CrossRef]

51. Silva, P.A.S.F.; De Oliveira, T.F.; Brasil Junior, A.C.P.; Vaz, J.R.P.P.; Oliveira, T.F.D.E.; Junior, A.C.P.B.; Vaz, J.R.P.P. Numerical Study of Wake Characteristics in a Horizontal-Axis Hydrokinetic Turbine. *Ann. Braziian Acad. Sci.* **2016**, *88*, 2441–2456. [CrossRef]

52. Gibson, M.M.; Launder, B.E. Ground effects on pressure fluctuations in the atmospheric boundary layer. *J. Fluid Mech.* **1978**, *86*, 491–511. [CrossRef]

53. Neary, V.S.; Gunawan, B.; Hill, C.; Chamorro, L.P. Near and far field flow disturbances induced by model hydrokinetic tur-bine: ADV and ADP comparison. *Renew. Energy* **2013**, *60*, 1–6. [CrossRef]

54. Yarnell, D. *Bridge Piers as Channel Obstructions*; United States Department of Agriculture: Washington, DC, USA, 1934.

55. Azinfar, H.; Kells, J.A. Backwater Prediction due to the Blockage Caused by a Single, Submerged Spur Dike in an Open Channel. *J. Hydraul. Eng.* **2008**, *134*, 1153–1157. [CrossRef]

56. Martin-Vide, J.; Prio, J. Backwater of arch bridges under free and submerged conditions. *J. Hydraul. Res.* **2005**, *43*, 515–521. [CrossRef]
57. Follett, E.; Schalko, I.; Nepf, H. Momentum and Energy Predict the Backwater Rise Generated by a Large Wood Jam. *Geophys. Res. Lett.* **2020**, *47*, e2020GL089346. [CrossRef]
58. Kocaman, S. Prediction of Backwater Profiles due to Bridges in a Compound Channel Using CFD. *Adv. Mech. Eng.* **2014**, *6*, 905217. [CrossRef]
59. Azinfar, H.; Kells, J.A. Drag force and associated backwater effect due to an open channel spur dike field. *J. Hydraul. Res.* **2011**, *49*, 248–256. [CrossRef]
60. Raju, K.R.; Rana, O.; Asawa, G.; Pillai, A. Rational assessment of blockage effect in channel flow past smooth circular cylinders. *J. Hydraul. Res.* **1983**, *21*, 289–302. [CrossRef]
61. Morandi, B.; Di Felice, F.; Costanzo, M.; Romano, G.; Dhomé, D.; Allo, J. Experimental investigation of the near wake of a horizontal axis tidal current turbine. *Int. J. Mar. Energy* **2016**, *14*, 229–247. [CrossRef]
62. Jeffcoate, P.; Whittaker, T.; Boake, C.; Elsaesser, B. Field tests of multiple 1/10 scale tidal turbines in steady flows. *Renew. Energy* **2016**, *87*, 240–252. [CrossRef]
63. Stallard, T.; Collings, R.; Feng, T.; Whelan, J. Interactions between tidal turbine wakes: Experimental study of a group of three-bladed rotors. *Philos. Trans. R. Soc. A Math. Phys. Eng. Sci.* **2013**, *371*, 20120159. [CrossRef] [PubMed]
64. Lam, W.-H.; Chen, L. Equations used to predict the velocity distribution within a wake from a horizontal-axis tidal-current turbine. *Ocean Eng.* **2014**, *79*, 35–42. [CrossRef]
65. Sandia National Laboritories: Refernce Model Porject (RMP). Available online: https://energy.sandia.gov/programs/renewable-energy/water-power/projects/reference-model-project-rmp/ (accessed on 21 January 2022).

Development of a design and implementation process for the integration of hydrokinetic devices into existing infrastructure in South Africa

CM Niebuhr[1]*, M Van Dijk[1] and JN Bhagwan[2]

[1]Department of Civil Engineering, University of Pretoria, Pretoria, 0001, South Africa
[2]Water Research Commission, Private Bag X03, Gezina 0031, South Africa

ABSTRACT

In South Africa there is currently no notable use of modern small-scale hydrokinetic (HK) energy systems, mainly due to formerly low-cost coal-powered electricity. This renewable energy option makes use of the kinetic energy from flowing water, rather than potential energy, which is more often used in conventional hydropower. Updated refined versions of this technology are now being investigated and manufactured due to the global drive towards reducing carbon emissions and increasing energy efficiency. These modular units allow for installation of HK turbines into existing water infrastructure with very little civil works. The study's objective was to develop a simplified design and implementation process for HK devices within the South African legislative and regulatory environment. Approximately 66% of South Africa's water supply is used by the agricultural sector with more than 6 500 km of canal systems running through many areas which could benefit from alternative energy sources. The recent electricity crisis in the country allowed for problem resolution through funding opportunities and thereby an introduction of an innovative and sustainable technology to provide renewable electricity where otherwise not feasible. A pilot HK project was implemented in an applicable section on the Boegoeberg irrigation canal in the Northern Cape Province and tested for optimum functionality and correct application. This process allowed evolution of a development process for the implementation of HK devices in existing water infrastructure.

Keywords: hydrokinetic turbine, water infrastructure, renewable energy, hydropower, small-scale

INTRODUCTION

Fossil fuels are currently the primary resource for electricity generation in South Africa (SA). However, the availability of renewable energy resources is abundant and holds the potential to assist in solving issues such as reducing greenhouse gas emissions and having larger energy security by diversifying the supply (Kusakana and Vermaak, 2013).

In 2012, Kusakana and Vermaak found approximately 6 000–8 000 potential sites for traditional hydropower installation in SA. The Department of Minerals and Energy (DME) of the Government of SA revealed the country to have a considerable potential for small- and large-scale hydropower generation; however, only a handful of small hydropower developments have been undertaken in the past 30 years (DME, 2003; Koko and Kusakana, 2014). Currently about 3 700 MW of installed hydropower exists in SA although there remains a great lack of knowledge on hydropower and especially hydrokinetic (HK) systems.

Prior to the case study referred to in this paper there was no existing modern HK installation in SA, although the country was previously reported to have a great potential thereof (Kusakana and Vermaak, 2013). SA is a water-scarce country resulting in highly protected water infrastructure. A challenge for implementation of HK systems lies in the ownership of the infrastructure (canals etc.) onto which such systems are installed versus the mandate of the 'owner' in having such systems installed. A general perception exists that hydropower is not fit for installations in SA due to the lack of availability of components, as well as the drawn out regulatory and legislative procedures. It is believed that all these problems have arisen due to lack of knowledge of hydropower systems (due to scarcity of existing systems) and therefore the inability to predict any environmental/social impacts thereof.

Hydropower is also misunderstood and, in many cases, believed to consume or pollute water resources. In the case of HK systems, these can be installed in line with existing infrastructure (or designed to be incorporated with new infrastructure in that instance) and do not require the water to be diverted (as required by most conventional hydropower schemes). Furthermore, the impact of the installation of a HK system into existing infrastructure is novel in SA. The purpose of this paper is to clarify such issues and give a broader understanding of HK installations and the possibilities thereof in SA.

In a report on the assessment of HK turbines in open channel applications prepared by the United States Department of Energy it is stated that 'Hydrokinetic energy from flowing water in open channels has the potential to support local electricity needs with lower regulatory or capital investment rather than impounding water with more conventional means (Gunawan et al., 2017) indicating not only local but international relevance to such studies.

Hydrokinetic applicability to South African canal systems

The demand for energy in SA is increasing with a greatly fossil fuel dependent economy resulting in an unsustainable future. According to environmental statistics SA is among the top 20 countries with the highest level of carbon dioxide emissions, also being the highest emitter of greenhouse gases in Africa (MEAAI, 2011). In 2010 the DME released an Integrated

Resource Plan (IRP) to increase renewable energy sources to 17.8 GW by 2030 (Koko and Kusakana, 2014). This allows a large opportunity for the development of renewable energy, such as biomass, wind, solar and hydropower. Details of the DME targets and evolution of the electrification goals in SA are summarized in Fig. 1.

Hydropower is a trusted technology with significant potential in SA (White, 2011). It is a form of clean renewable energy making use of the available flow or head in water without consuming or polluting the water itself. Often these hydropower systems have long lifespans and high efficiencies with low operating costs (van Vuuren et al., 2011).

Kusakana et al. (2013) investigated the possibility of HK hydropower development for rural and isolated loads in South Africa. The case studies proved that where adequate water resources are available in South Africa, HK power generation could be the best, most cost-effective supply option in relation to wind, photovoltaic and diesel generators (Kusakana and Vermaak, 2013).

A large network of canal systems exist in South Africa, the Department of Water and Sanitation (DWS) asset management database revealed a total of 47 schemes with a network of more than 6 500 km of canals, as shown in Fig. 2. Additional to the HK potential in straight uniform sections on these canal systems, 21 286 structures such as tunnels, syphons, weirs, control gates, chutes and drops exist, which could also hold unexploited HK (and conventional hydropower) potential.

HK energy extraction is a simple process; therefore the cost of energy extraction is low. Due to its modular nature the initial installation cost and deployment time is short as it does not require construction of significant infrastructure. It also allows an easily scalable energy output but limits any decrease in capital cost per kW output (Gaden and Bibeau, 2006). The cost of generation alone, not including the infrastructural cost

itself, may be lower than traditional hydropower forms and more economical when compared to solar power (Kusakana and Vermaak, 2013).

Development process

The development process of a HK installation varies throughout the world, as each country's specific laws and regulatory processes have to be followed. As HK implementation is a new concept in SA, the development remote process is not yet streamlined. An outline of a suggested development process for HK integration into existing water infrastructure was compiled through results from global case studies and the pilot study completed in SA, and is depicted schematically in Fig. 3. Some of the processes are described below by means of reference to the case study.

Step 1: Site-selection and pre-feasibility study

The final HK installation site should be carefully selected, as for the case study described later in this paper. This may be a difficult task when optimal velocities are not available. HK turbines usually require a velocity of around 2–3.5 m/s (based on available turbine operational ranges). Sites at existing narrowed sections (such as flume sections or syphon outlets) are usually more likely to have these velocities readily available; examples of these sites are shown in Table 1. When selecting sites such as these, several issues, such as high damming or interruption of the infrastructure operation (before installation) may occur; therefore, selection of a site with a higher velocity along a uniform section, where only a small fraction of the cross section is utilised for the HK installation, remains the best installation option. The site selection procedure shown in Fig. 4 may be used as a guideline to an optimal site selection process.
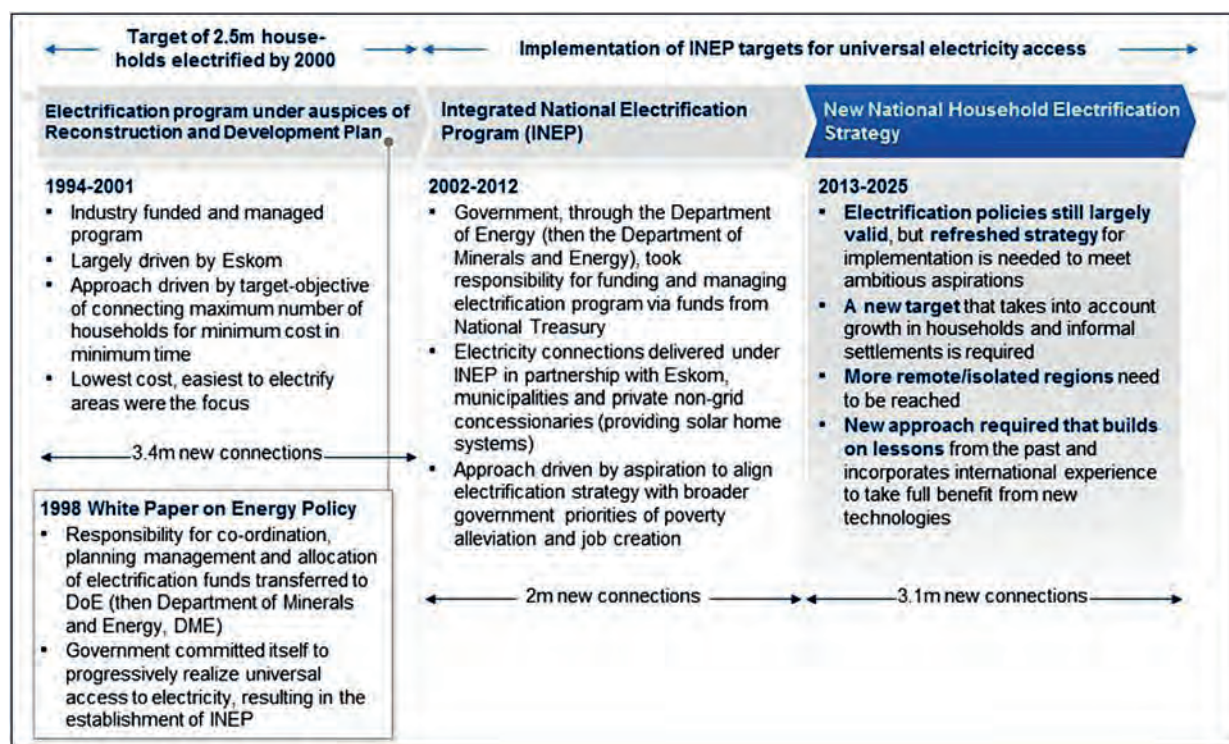

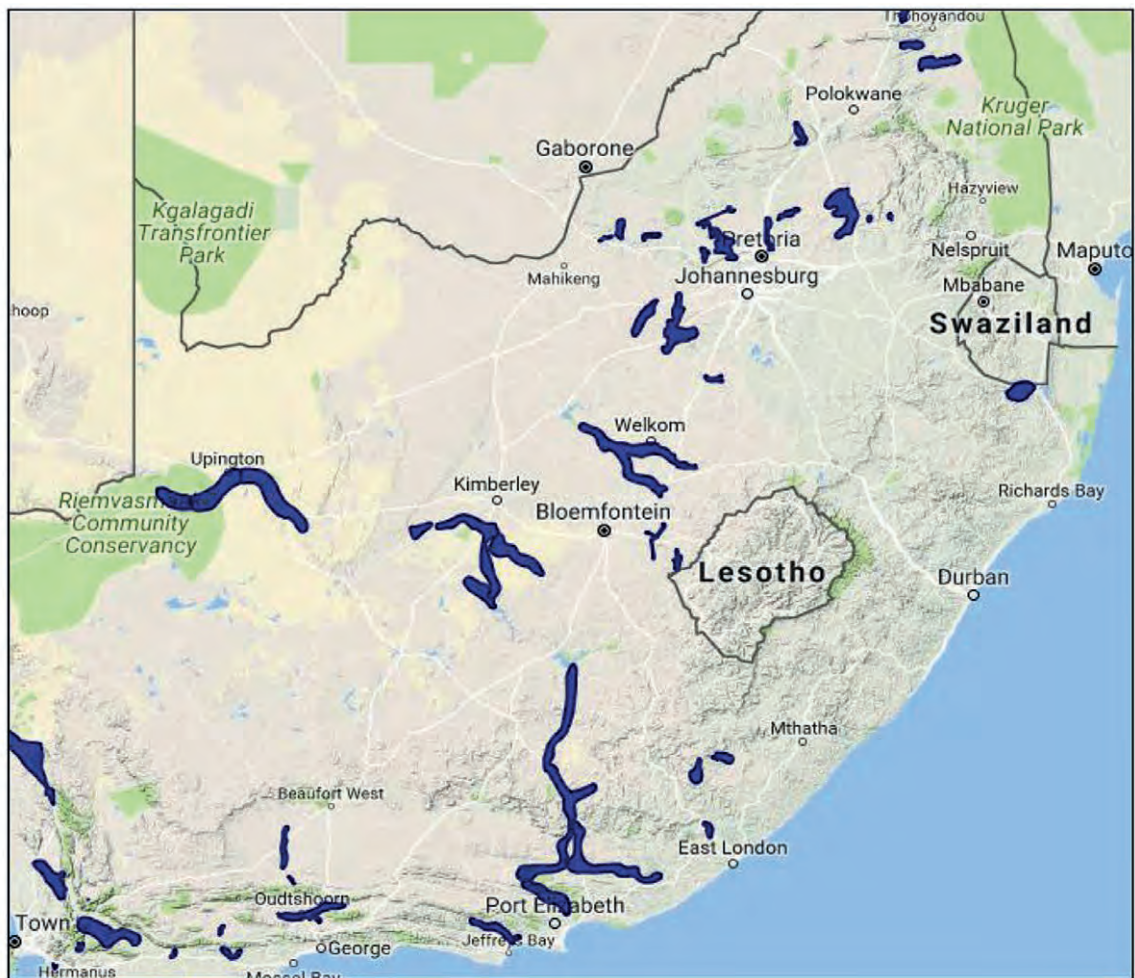**Figure 1.** Evolution of electrification in South Africa (IFC, 2013)

435

Figure 2. Canal schemes in South Africa (DWS, 2015)

Figure 3. Canal HK system development process

Table 1. Sections with higher velocities (DWS, 2016)

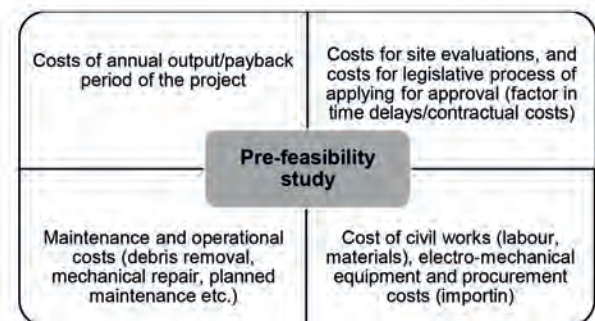| Potential site	Picture
<u>Steep sections</u>: Examples include canal outlets to balancing dams, or sections of higher gradients	
<u>Flume sections</u>: Where a narrowing in the canal occurs, higher velocities may be present	
<u>Siphon/pipe exits</u>: Where siphons are used between canal sections the narrowed section at the exits may be considered as potential sites	
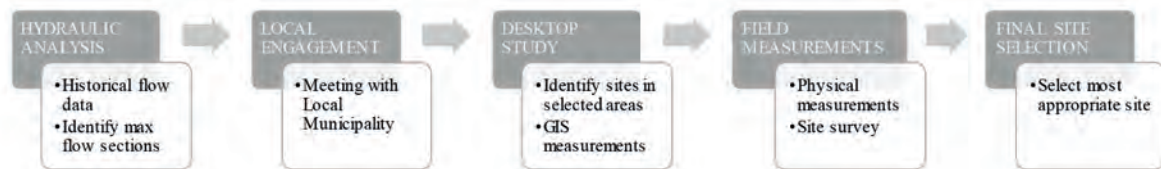
Figure 4. Site selection procedure

In conjunction with site selection, a pre-feasibility study of shortlisted potential sites should be undertaken; this includes:

- Accurate velocity, flow and level measurements
- Identification of electricity use and transmission length
- Identification of connection type and point (grid integration or stand-alone scheme)
- Conceptual design
- Preliminary costing of components for economic evaluation

The pre-feasibility study should be carefully completed, and all costs should be calculated and weighed against the output before final design and implementation of the HK system. The main cost considerations are shown in Fig. 5.

Step 2: Turbine selection

The HK turbine type should be carefully considered before selection. As these devices are not currently readily available in South Africa, high import costs drive up the capital cost. Modular units may be imported, or units may be designed and manufactured locally (where the project owner has a broad knowledge of HK workings). The typical ranges of commonly available turbine units can be seen in Fig. 6.

To suit the design power output the rotor diameters may be adapted. As an indication of the changes experienced in the power curve for a range of rotor diameters, Fig. 7 was included. The exponential behaviour of the curve is emphasized at larger rotor diameters, allowing significantly higher power output when using larger turbines.

Figure 5. Pre-feasibility study cost considerations
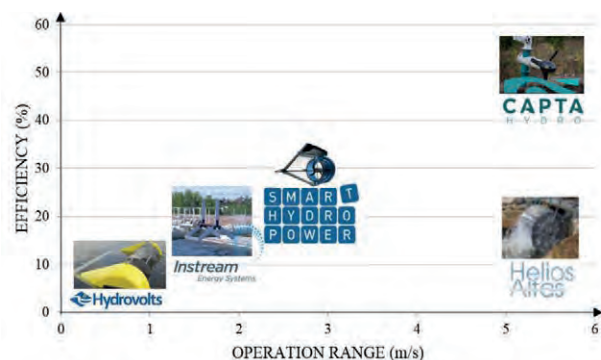
Figure 6. HK turbines (CaptaHydro, 2017)

437
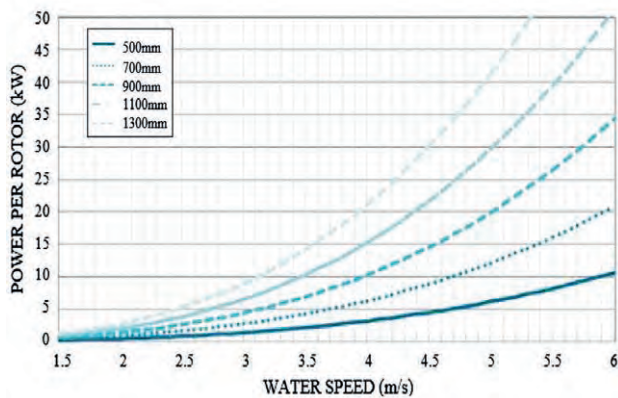
Figure 7. Axial flow rotor diameter comparisons (CaptaHydro, 2017)

Step 3: Grid integration

The control systems for the HK device are designed according to the specified electricity use, which falls within the selected grid integration method:

- Islanded stand-alone method:
  - Control systems including inverters, rectifiers and dump-loads are used to regulate the system
  - This will require the development of a mini grid for the distribution of the power produced
- Grid-connected system:
  - Stand-alone system requiring a grid connection to synchronise frequency
  - Usage of existing transmission lines to feed electricity to the end user (may require additional approvals)

When the grid integration method has been selected the following should be designed or selected as part of the modular turbine unit as supplied by the manufacturer:

- Electric control boards
- Regulation system
- Electric transmission
- Grid connection

Step 4: Legislative assessments and approvals

In each relevant country certain legislative and regulatory requirements may be applicable when installing a HK system in a canal system. The entities which must be considered in a

South African context are listed in Table 2 (it must be noted that this may change as changes in legislation are introduced and the entities involved may vary as the use of electricity and the size of HK system varies). Although specific to SA, similar entities and aspects may be globally representative. Greater detail on these processes can be seen in (Scharfetter and Van Dijk, 2017).

Step 5: Meeting with stakeholders

When all stakeholders have been identified, meetings should be arranged with each relevant entity to obtain the required approvals and if required arrange for agreements to be formalised to utilise the water infrastructure asset.

Due to the large changes in process and legislation as the project owner varies (municipality/ private entity) it must be noted the development process described assumes the municipality as project/asset owners for the purpose of this paper (and this process may vary in other cases).

Step 6: Capital procurement

This phase involves procurement of all equipment required for installation of a complete HK system. This may include (but is not limited to) the following:

- Procurement of materials and equipment required for civil works:
  - Procurement of labourers for site work
  - Anchor block/foundation material
  - Turbine fastening equipment (e.g. anchor cables)
  - Bridge structure, hoisting mechanism
  - Fencing
  - Control room
- Electrical and transmission equipment:
  - Turbine control equipment (regulators, inverters, dump-loads)
  - Transmission lines / grid connectors / mini grid
  - Measuring and monitoring equipment and cabling
- Mechanical equipment:
  - Turbine (blades, generator)
  - Generator
- Spare parts required for maintenance

Step 7: Project implementation and optimisation

During project implementation the considerations shown in Fig. 8 are of importance and must be considered, after which the project can be implemented and tested for correct functioning.

Table 2. Small-scale HK assessment and approval guidelines

Aspect	Entity	Requirement
Water/infrastructure use	Department of Water and Sanitation (DWS)	[If] DWS is the owner of the infrastructure, the user [may] require written permission from DWS to use the infrastructure to anchor the HK turbines for hydropower generation and to provide access to the land
	Water user association (WUA) or Water Board (WB) involved	The project owner may require the statutory body's written permission to non-consumptively make use of the water in the infrastructure, to access and modify the infrastructure and receive acknowledgment and approval for the project
Environmental	Provincial Department of Environmental Affairs (DEA)	Provision of an environmental authorisation should a listed activity according to the National Environmental Management Act be triggered
Electricity	National Energy Regulator (NERSA)	Needs to be informed of the project and depending on the extent of the electricity generation and distribution infrastructure provided, issue licences for these activities
	Eskom	May be consulted if grid-integration, wheeling or feed-in is considered
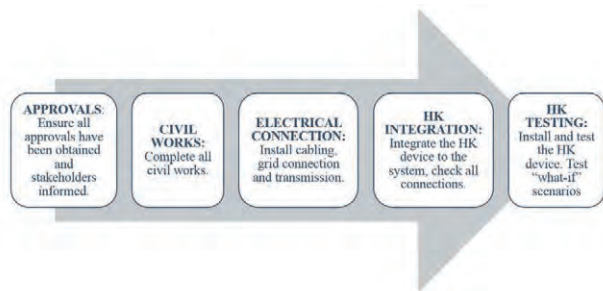
Figure 8. Implementation procedure

During project implementation it may be necessary to optimise the system to obtain a higher output. Some methods of optimisation include:
- Turbine confinement (Shives, 2008)
- Shroud addition (Gaden, 2007)
- Diffuser addition (Gaden, 2007) (Riglin et al., 2014)
- Channel modification (Khan et al., 2008)
- Multiple turbine application (Riglin et al., 2014)

Step 8: Operation and maintenance

The operation and maintenance of the HK installation will govern the lifespan and functioning of the device. The following aspects are of importance for this procedure:
- Training of operation and maintenance staff
- Maintenance plan and schedule of inspections and cleaning
- Issuing maintenance and operating manuals

During the first year of project implementation, additional problems (such as seasonal debris variations) should be evaluated and the relevant mitigation measures put into place. Correct operation and maintenance of the system will result in an efficient system with a long operational life.

Step 9: Monitoring and evaluation

For new technologies such as HK systems in South Africa, monitoring and evaluation of the system over its operational life is an important step to understand system functioning within the South African context. This will result in the construction of more reliable, cost-effective systems in the future once a clearer understanding of the roles of all the variables has been attained.

In addition to this, monitoring the systems will allow risk mitigation by allowing quick response times in blockage or potential canal overflow situations, and will also allow reporting when unplanned maintenance may be required due to observed decreases in system outputs. Some important technical aspects which should be monitored include the following:
- Power output and relevant velocity at specific time intervals
- Damming levels (allowing blockage monitoring)
- For future feasibility studies, monitoring and data collection of the following aspects could be valuable:
- Costs incurred over the operational life (maintenance/operational costs)
- Problems encountered during operational life (blockages/floods/overtopping/theft)

Boegoeberg case study

The first HK installation in SA was designed and implemented through benchmarks highlighted in the developed design and implementation process, which are summarized below. The project was initiated by allocated funding for small-scale hydropower development in the !Kheis Local Municipality (LM) in the Northern Cape Province. This LM has a similar problem to numerous other municipalities throughout the country, this being a lack of revenue due to large sections of the community being unemployed and not able to pay for services.

The Boegoeberg irrigation canal runs adjacent to numerous towns and small settlements in the municipality. Small-scale hydropower schemes along this route could allow a sustainable means of supplementing the income of this municipality and reducing its reliance on Eskom.

Selection of a site in the !Kheis Municipality was based on the following criteria:
i. Technical viability:
- Adequate flow velocity
- Demand for electricity
- Adequate cross section (large enough for turbine and turbulence recovery)
ii. System sustainability:
- Anti-theft/ anti-vandalism
- Identified electricity need
- Community support
- System integration effect on canal functioning (water supply should not be compromised by addition of system)
iii. Site resilience:
- Overflow protection of damming effect
- Accessible to municipal workers in case of emergency (e.g. blockage)
iv. Project specifications:
- A representative canal section of what is available in most areas

The Groblershoop water treatment works (WTW) site lies in the town of Groblershoop in the !Kheis Municipality. This plant supplies water to the majority of the surrounding areas. The WTW pump station is currently partially supplied by a small solar generation plant erected at the WTW facility. The town of Groblershoop lies approximately 38 km downstream of the canal offtake (Boegoeberg Dam). The approximate electricity usage of the pumps at the WTW is 25 kW. The selected site lies on the upper region of the Boegoeberg irrigation canal; the layout of the site can be seen in Fig. 9.

The canal has a rectangular shape with a slightly cambered canal bed, the canal drawings were obtained from the Boegoeberg Irrigation Board in original design drawing format. As shown, the selected section is a combination of two straight

Figure 9. Groblershoop site

sections; this is ideal for installation as there is less turbulence in these sections. The downstream canal section including the bend as well as the typical section parameters can be seen in Fig. 10. Sections further upstream were not considered as these lie at too great a distance from the control room/demand and would result in long transmission cable lengths (and therefore higher costs and increased possibility of vandalism).

A DWS gauging station (D7H17) which has recorded significant amounts of historical flow data lies approximately 63 km upstream of the installation section of the canal. The flow recorded over a ±10-year period can be seen in Fig. 11. The trend indicates an annual average of 40 days of zero flow (during maintenance etc.). The average flow during operational periods was found to be 12.5 m³/s (Fig. 11). A localised flow (due to other offtakes) of around 6.6 m³/s was measured at the selected location for the installation of the HK device through the use of a speedy doppler-type velocity sensor and ultrasonic level sensor. With the flow of 6.6 m³/s, the flow velocity was expected to be 1.1 m/s and measured to be an average of 1.05 m/s (measured by a doppler velocity sensor placed on the canal bed).

The turbine selected for the site is shown in Fig. 12 and is specifically designed by Smart Hydropower Gmbh for canal systems. It is placed directly on the flat canal bed and anchored by steel cables to the sides/bottom of the canal. System specifications can be seen in Table 3. The turbine is equipped with an underwater permanent magnet generator providing AC power to the system. To achieve maximum power output from this specific turbine a flow velocity of 3.1 m/s is required. The output curve of the generator is provided in Fig. 13.

The Groblershoop WTW already had a facility where power could be generated for one of the pumps by means of solar panels which are also grid connected to supply the remaining pumps (however, this was not functioning due to damaged control equipment). This allowed integration of the HK plant with the existing system (and control equipment).

Table 3. Turbine specifications (SHP, 2017)

Output (W)		250–5 000
Dimensions	Length (mm)	2 640
	Width (mm)	1 120
	Height (mm)	1 120
Rotational speed (r/min)		90–230
Weight (kg)		300
Number of rotor blades		3
Rotor diameter (mm)		1 000

Figure 12. Kinetic turbine for deployment in canal (SHP SMART free stream turbine) (SHP, 2017)
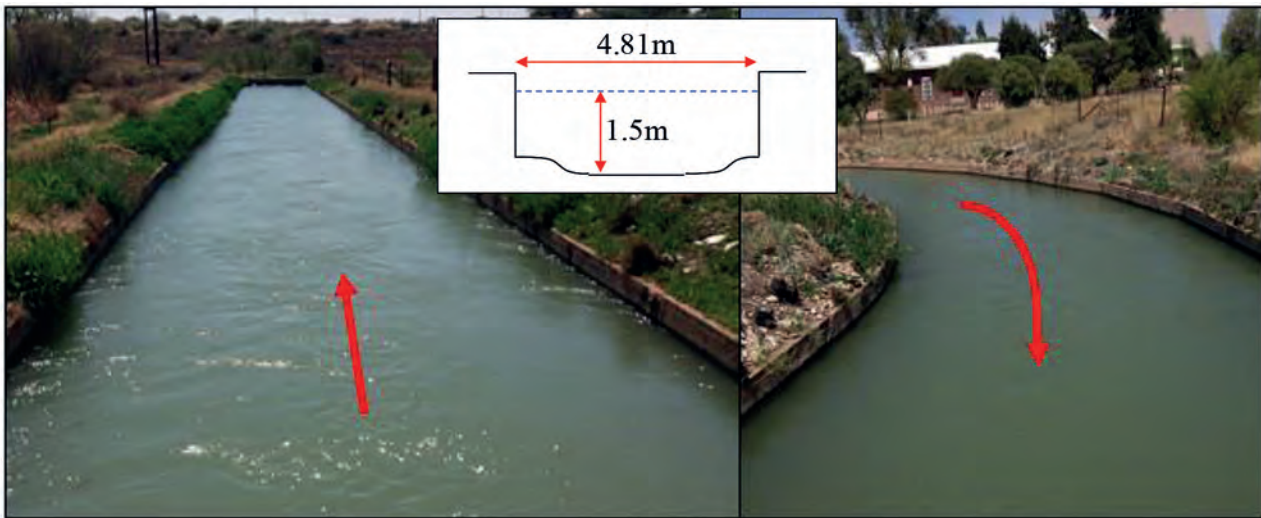
Figure 10. Canal system at the Groblershoop site
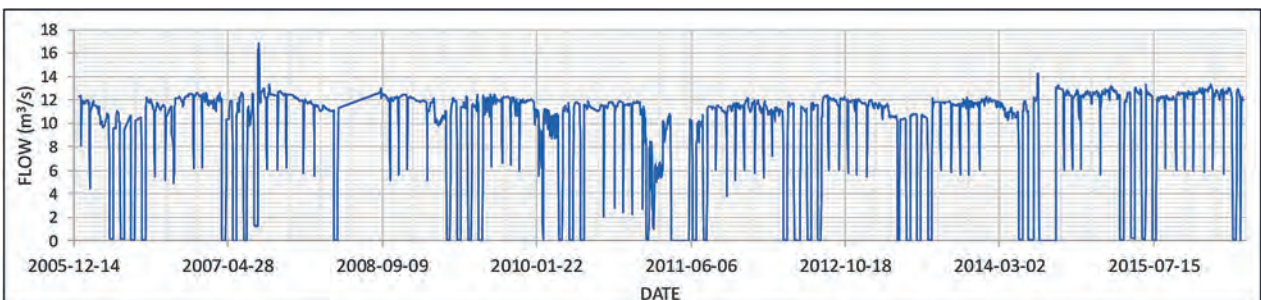
Figure 11. Flowrate in the Boegoeberg Canal Station D7H17 (Dec 2005 to April 2016)

440

Figure 13. Generator capability (SHP, 2017)

The electronic control system is the intelligence of this renewable energy system (Fig. 14). Integrated inside the electrical cabinet is a reverse control (to remove accumulated debris from the blades), optional auxiliary devic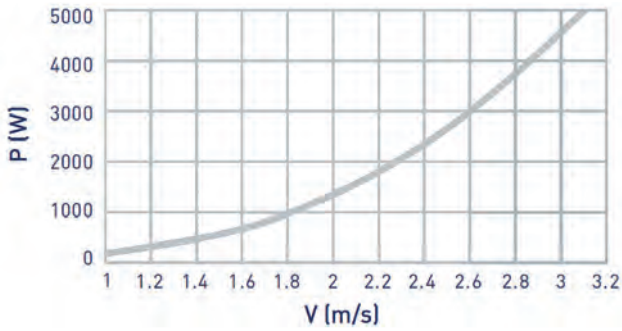es, customizable battery storage interface (it has a built-in battery charger) and integrated monitoring system (monitoring control board). The basic layout of the installation is depicted in Fig. 15.

For hydropower projects developed at local level, the institutional powers, functions, roles and responsibilities of municipalities are of utmost importance. In the context of the four major regulatory requirements necessary to initiate and implement small-scale hydropower projects, namely a Water Use Licence (in terms of the National Water Act (NWA) (RSA, 1998a)), an Environmental Authorisation (in terms of the National Environmental Management Act (NEMA) (RSA, 1998b)), an Electricity Generation Licence and an Electricity Distribution Licence (in terms of the Electricity Regulation Act (ERA) (RSA, 2006)), the DWS (or the regional departmental offices or the catchment management agency, where these are established and have the authority), the provincial office of the Department of Environmental Affairs (DEA) and National Energy Regulator of South Africa (NERSA), would be the primary stakeholders involved in this type of hydropower project, over and above the project initiator.

In the context of local electrification through small-scale hydropower technologies, the DWS is a primary stakeholder. The DWS has the mandate to protect and manage SA's water resources. Furthermore, the DWS owns waterworks across SA such as weirs, irrigation canals and dams which could be utilised to generate electricity (in this case the Boegoeberg irrigation canal). For this study, the project-specific institutional stakeholders are identified in Table 4. The roles of each stakeholder during the project are shown under project specification. The project formed part of the 'Draft policy on sustainable hydropower generation' which allowed a simpler process of approval.

The infrastructure components required for the installation of the HK turbines are listed in three sections, namely, civil components, electro-mechanical components and electrical components:

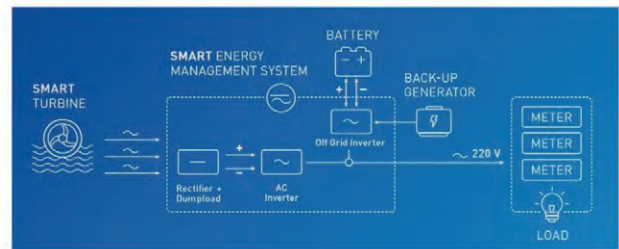i. Electro-mechanical components
- SHP free stream turbine (Equipped with 5 kW underwater generator and rotor)
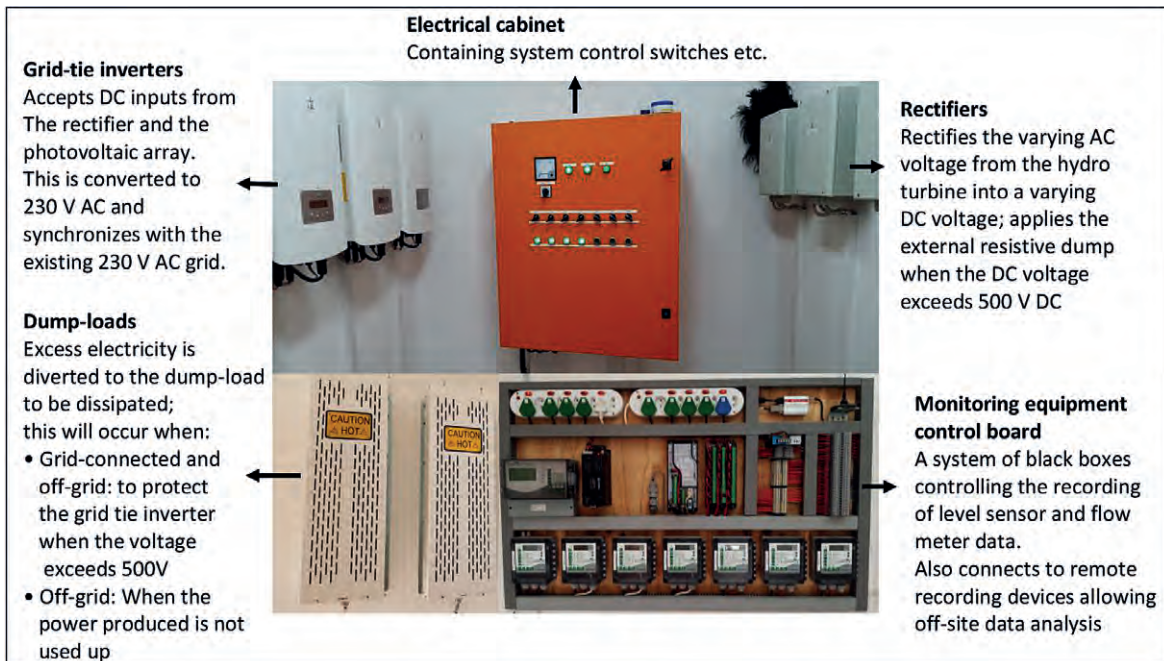
ii. Civil components
- Concrete block foundation for cable hoist
- Turbine lifting system

iii. Electrical components
- Turbine control equipment
- Flow meter
- Level sensors

Figure 15. System layout (SHP, 2017)

Figure 14. Electrical management system components (Control room)

Table 4. Project-specific institutional stakeholders Groblershoop Water Treatment Works

No.	Stakeholder	Role and responsibility	Project specification
1	Department of Science and Technology (DST)	Funder	Funds obtained for the project duration
2	WRC	Implementing Agent for the DST	Reports submitted
3	DWS	Owner of irrigation canal Owner of land on which the irrigation canal is located Custodian of the water resource	A series of meetings set-up to obtain approval Signee on the memorandum of agreement (MoA) between all entities involved to ascertain approval
4	!Kheis LM	Hydropower project owner (asset will be listed onto the LM's Asset Register) All regulatory submissions would be in the name of the !Kheis LM and for the !Kheis LM Operation & maintenance of hydropower generation plants and the electricity transmission infrastructure	A series of meetings were set-up to obtain approval and knowledge of municipal roles and responsibilities concerning the installation Co-signee of MoA
5	Citizens of the !Kheis LM	Beneficiaries of the project's service delivery outcomes	Local labourers were hired and trained to perform maintenance on such an installation Continuous employment to operate and maintain
6	Boegoeberg WUA	Operator of Boegoeberg canal	Meetings were set-up to inform WUA of all construction plans and obtain approval Notified and requested approval during any modification/alteration to canal Co-signee of MoR
7	NERSA	Electricity regulator	No licence required as the electricity produced is for 'own-use' and small scale of generation
8	Eskom	Electricity distributor	No approval/licensing required, no Eskom owned distribution lines used
9	Northern Cape Provincial DEA	Provision of an environmental authorisation should a listed activity according to the NEMA be triggered	No triggers for this authorisation, therefore not required
10	University of Pretoria	Planning and design engineers	Responsible for project implementation

All equipment required for installation was procured together with the completion of civil works (listed above) to allow turbine installation. The velocity in the canal was measured as around 1.2 m/s at the point of installation which provided a lower range of application on the power curve (Fig. 13). This also proved true at the initial testing phase where a maximum output of 228 W was achieved (placing the turbine into the flow area as specified by manufacturer). Due to this optimisation of the section was considered. To achieve a higher velocity through the turbine the option of canal narrowing at the installation points thus creating a venturi effect and speeding up the flow entering the turbine was considered. This was done through the use of steel plates anchored onto a hinge point on the canal wall.

To allow installation of a HK system in SA more information is required on the impacts such devices could have on the canal functioning and water security as a whole. A numerical model using HEC-RAS was developed for both scenarios with and without the narrowing. The findings of such numerical simulations were compared with the constructed test installation from which data could be collected and analysed.

To allow an indication of 'worst case' infrastructural influences, the numerical modelling was used in the testing process identified in 2 phases. Phase 1 included the 'worst case' of full turbine grid blockage which was modelled by an inline structure. The length of the blockage was chosen as 3 m which is the length of the turbine plus an additional 0.75 m allowing for possible debris build up (trees, shrubs etc.)

The maximum damming level was found to be 40 mm just upstream of the turbine, which then returns to normal flow

depth approximately 2.7 km upstream of the installation point. This large backwater effect resulted from the relatively flat canal bed and subcritical flow pattern. The highest damming levels lie within the available freeboard and therefore no overtopping was expected. The damming levels comparing to the 'no turbine' scenario can be seen in Fig. 16.

Phase 2 including narrowing the canal by a total of 1.2 m per side. To model the narrowed width new cross-sections were added to the HEC-RAS model to simulate the new incrementally narrowed section. The blocked turbine was added to the narrowed section, similarly to Phase 1.

Both scenarios at the narrowing of the canal, first, with no installed turbine and, second, with a fully blocked turbine, can be seen in Fig. 17. The maximum damming level of the Phase 2 canal narrowing with a fully blocked turbine grid was found to be around 290 mm just upstream of the blockage and the recovery distance of damming levels was 6.3 km upstream. For the scenario of narrowing alone without the turbine the damming was found to be around 70 mm with a recovery distance of 4.2 km upstream.

During the blocked turbine Phase 2 modelled scenario with the narrowed width, the canal showed overtopping at distances of 440–1 800 m, which lies about 360–1 700 m upstream of the blockage. Consideration was given to heightening of this section when permanent narrowing was considered; however, due to the original canal drawings being used to create the model, and alterations (in terms of heightening the canal wall) having been made since initial construction, it allowed the flexibility for the damming required for the narrowing (without alterations).
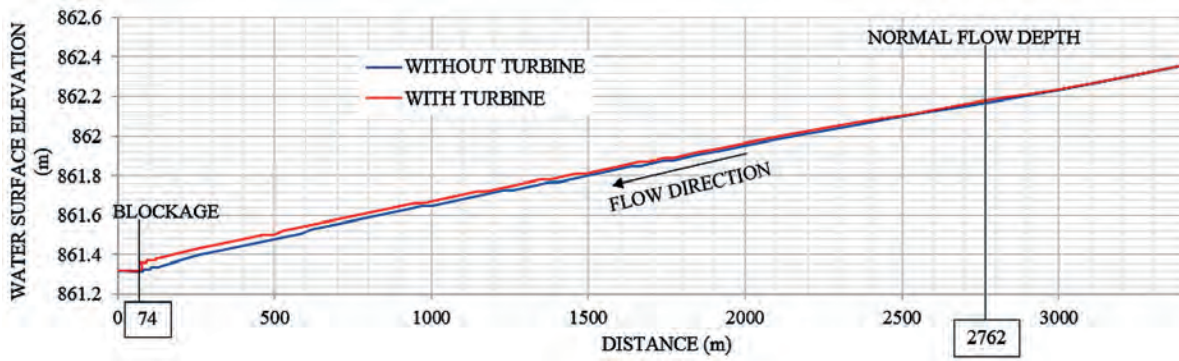
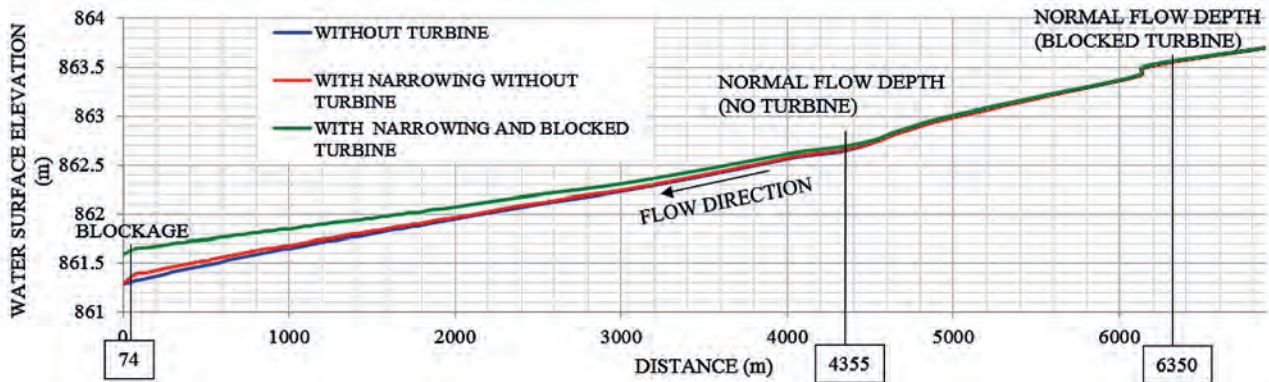**Figure 16.** Phase 1 blockage damming levels

Figure 17. Phase 2 blockage damming levels

The physical testing phase included the construction indicated in Fig. 18. Phase 1 included a single turbine which was temporarily anchored from 8 mm diameter steel cables (lifting capacity of 750 kg) attached to concrete block foundations.

The damming effects of the canal narrowing due to the installation of the HK turbine were measured by means of level sensors at the installation point and a distance upstream (allowing measurement of the upstream effects). The flow velocity was measured at various points by use of a hand-held velocity propeller sensor (wading rod) to allow understanding of the flow characteristics. The results proved a 70% increase in velocity from the canal narrowing with a maximum damming effect of 100 mm (found to be 70 mm with numerical modelling); additional details are shown in Table 5.

For Phase 2 testing the turbine was placed in the flow (within the narrowed flume section) and the water levels,

flow velocity and the impact on water levels further upstream were once again recorded. The freeboard available proved to be sufficient for the damming effects (Table 5). The effects on the canal system were compared to numerical model results and the model was calibrated accordingly. This allowed re-modelling in the numerical model and thus assisted with the design of the final system with greater accuracy.

The final conclusions reached from the correlated physical and numerical testing results can be seen in Table 5.

From the results of the temporary test installation a permanent design was completed. A total of 4 turbines were installed in series along two narrowed sections 45 m apart (2 turbines in each section) with both sections being narrowed to a width of 2.41 m. The final design results in an increased output of 3.9 kW (increased velocity of 2.8 m/s) per turbine and thus a total system production of around 15.6 kW 89% of
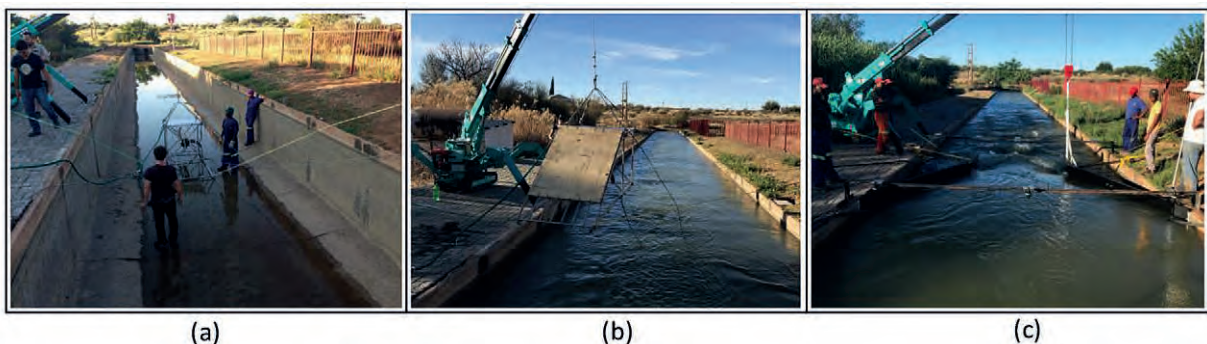

Figure 18. Testing (a) turbine placement testing (b) blocked turbine testing (c) Narrowed section testing

Table 5. Testing results summary

| Scenario		Maximum damming effects	Conclusions reached
Phase 1: Cable anchored turbine	Normal operating turbine	30 mm maximum damming recorded at the point of installation and 50 m further upstream	The turbine proved to have minimal effects on the canal; with no visual or noise disturbances and minimal damming
	Blocked turbine (Fig. 18b)	60 mm maximum damming at the point of installation, reducing to 50 mm within 50 m upstream	If the turbine grid is fully blocked by debris, etc., no interruption of the water supply of the Boegoeberg canal will be experienced (no overtopping etc.)
Phase 2: Canal narrowing with cable anchored turbine	Normal operating turbine	100 mm maximum damming at the point of installation, reducing to 90 mm within 50 m upstream	By narrowing the canal section to obtain optimal output the damming effect remains within the available freeboard; therefore, the final installation should function well with minimal disturbance on the system
	Blocked turbine	140 mm maximum damming at the point of installation, reducing to 100 mm within 50 m upstream	If the turbine grid is fully blocked by debris, etc., no significant interruption of the water supply of the Boegoeberg canal will be felt (no overtopping etc.); improvements can be made to allow flow over narrowing plates or raising of the channel walls in this area

the year (accounting for maintenance and canal dry times). This design can be seen in Fig. 19 and is currently under construction. The design of the system allows simplified removal of each turbine if necessary (in case of blockages) and operational flexibility; the entire system is removable and can be altered and adjusted if necessary.

During the design life of a HK device, efficient functioning is crucial to obtaining design outputs. The energy production is predicted and considered during the preliminary design analysis; this is directly related to the production and therefore profitability/success of the installation. During the operational phase testing, routine maintenance was required due to debris build up (as indicated in Fig. 20). The maintenance strategy that was found to be effective for correct functioning of the installation through its design life involved a single operator hired with the following duties:

- Weekly visual checks and clearing of visible blockages
- Turbine removal and cleaning at 2-week intervals
- Turbine inspection and clearing at all canal shutdown periods, and first day of full flow (as build up occurs during start-up)
- Impromptu response to alarm system linked to level sensors indicating sudden increases in water level and thus unplanned clearing/removal and cleaning as required. During the HK test installation various risks were identified which could impact future developments and result in delays or additional costs:
- Potential of theft and vandalism of the installation during construction, which could result in additional expenditure for fencing and additional security measures
- The test installation site is in close proximity to a school in the town of Groblershoop. In summer temperatures rise above 40°C and children tend to swim in the canal systems (although forbidden); measures had to be taken to prevent
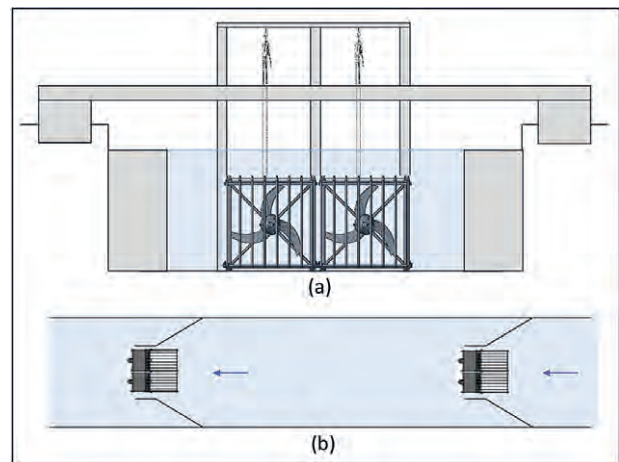
Figure 19. (a) Front view of final design (b) top view of final design with turbines 45 m apart

Figure 20. Debris blockage (a) during maintenance period (b) major debris build up after a 2-week interval (c) turbine removal and cleaning at 2-week interval

swimming in the section (to prevent injury or fatalities from spinning blades) and additional protective casing on the turbine (resulting in additional costs)

- Larger than expected debris, such as deceased livestock floating down the canal, due to livestock and wildlife drinking from the canal (as no barrier exists around the canal) and occasionally falling in. This could potentially result in turbine blockages; therefore, a warning system must be included in the installation to allow for quick removal in such cases.
- The legislation in South Africa is not yet in place to allow entities (municipalities or developers) to utilise DWS infrastructure for hydropower development in any form. This test installation requires special permission and a memorandum of agreement (MoA) between the !Kheis Local Municipality, the Boegoeberg Water User Association (WUA) and the DWS and is a test case for new legislation.
- Due to a lack of specific policy instated in South Africa, which would allow a streamlined process of installation, delays in the process may occur.
- The low velocities in most canal sections result in low efficiency systems due to the exponential behaviour of the power curve; however, as narrower sections or confined sections with a greater flow velocity are selected for installation, additional problems such as complete blockage (due to the turbine covering the majority of the smaller cross section) and large damming effects may occur. Due to this the risk of overflow and thus water loss to the WUA increases and thus the viability of the project decreases (civil works costs increase); it can also result in reluctance of the WUA to agree to the installation.
- Maintenance of the HK system remains a problem in South Africa; municipalities do not have the money and thus not the workforce to complete maintenance of the systems. The debris during short testing periods was evident which could result in large debris build-up over time and with no maintenance this could result in an inefficient system which is prone to blockage stoppages.

SUMMARY AND CONCLUSIONS

South Africa, the country with the second largest installed hydropower capacity in Africa, produces less than 5% of its total electricity demand from hydropower. However, multiple studies have indicated the unexploited potential available (Kusakana and Vermaak, 2013) (Loots et al., 2015). This highlights the lack of and need for innovative hydropower research and installations in Africa. In South Africa, mainly due to a relative scarcity of surface water, there is a prevailing perception that the potential for hydropower development is rather low. The largest percentage (>60%) of water is made available for the agricultural sector, delivered through an extensive water supply network consisting of weirs/intake structures, pipelines, tunnels, siphons, canals, chutes, etc.

Although there is significant HK potential, globally there is little technical literature or validation of successful installations of HK systems. The objective of this study was to address this problem and develop a HK design and implementation process to provide a guideline to HK installations. Literature on small-scale hydropower and specifically HK systems both locally and internationally were reviewed. Although no HK installation had been constructed in South Africa, the potential of these systems in rivers has previously been investigated at a very high level when considering several technologies (Koko and Kusakana,

2014) and a DWS asset management study illustrated the vast network of canals allowing further HK potential in the country.

A pilot project of a HK installation to showcase the installation possibilities was constructed. The working of the device was tested and as a result of the methodology followed during the study the following conclusions have been drawn. These conclusions should be read in the context of the study:

- The modular HK system was installed with all required aspects to operate the system on a permanent basis. This allowed a showcase of the technology in the South African context.
- With the required maintenance met (from debris/blockages) and the correct site selection, HK technology could be used as an additional sustainable renewable energy source in South Africa.
- As the majority of canal systems pose a controlled environment with a constant uniform supply of water (except during short shut-off intervals), with careful site selection and feasibility studies, HK energy systems in canal networks in South Africa can be a feasible alternative energy source. With pilot installations such as these, the way to a streamlined, simplified regulatory and legislative process for the installation of HK systems in South Africa is demonstrated.
- The design, implementation and testing of a HK turbine within the South African environmental context highlighted all important aspects of the design and procedures necessary, thus assisting future installations.
- When designing new canal systems, the potential opportunity to include HK systems should be considered and some design requirements already provided, e.g., designing parts of the canal for faster velocities and higher canal walls in anticipation of damming.

Through the testing and investigation of this modern form of hydropower, a design and implementation process for the integration of HK turbines was formulated, which allows for an improved and streamlined implementation process where uncertainties are reduced.

ACKNOWLEDGEMENTS

REFERENCES

CAPTAHYDRO (2017) Capta SC: For fast flowing canals. URL: http://www.captahydro.com/capta-sc.html (Accessed 9 August 2017).

DME (Department of Minerals and Energy, South Africa) (2003) *White Paper on Renewable Energy*. Department of Minerals and Energy, Pretoria.

DWS (Department of Water and Sanitation, South Africa) (2015) Strategic overview of the water services sector in South Africa. Version 4. Department of Water and Sanitation, Pretoria.

DWS (Department of Water and Sanitation, South Africa) (2016a) Condition Assessment Audit of irrigation scheme infrastructure: Cluster: Central, Scheme: Sand-Vet GWS. Scheme Report. Department of Water and Sanitation, Pretoria.

DWS (Department of Water and Sanitation, South Africa) (2016b) Condition Assessment Audit of irrigation scheme infrastructure: Cluster: Central, Scheme: Orange Riet GWS. Scheme Report. Department of Water and Sanitation. Pretoria.

DWS (Department of Water and Sanitation, South Africa) (2016c) Condition Assessment Audit of irrigation scheme infrastructure: Cluster: Central, Scheme: Hartbeespoort GWS. Scheme Report. Volume 1 (2.4). Department of Water and Sanitation, Pretoria.

GADEN DLF (2007) An investigation of river kinetic turbines: Performance enhancements, turbine modelling techniques and an assessment of turbulence models. MSc thesis, University of Manitoba.

GADEN DLF and BIBEAU EL (2006) Increasing power density of kinetic turbines for cost-effective distributed power generation. University of Manitoba, Manitoba.

GUNAWAN B, NEARY VS, MORTENSEN J and ROBERTS JD (2017) Assessing and testing hydrokinetic turbine performance and effects on open channel hydrodynamics: an irrigation canal case study. U.S Department of Energy, Albuquerque. https://doi.org/10.2172/1367421

HYDRO4AFRICA (2017) hydro4africa.net. URL: http://hydro4africa.net/HP_database/country.php?country=South%20Africa (Accessed 05 April 2017).

IFC (2013) Toward universal energy access: designing a new household electrification strategy for South Africa. International Finance Corporation, South Africa.

KHAN MJ, BHUYAN G, IQBAL J and QUAICOE JE (2008) Hydrokinetic energy conversion systems and assessment of horizontal and vertical axis turbines for river and tidal applications: A technology status review. *Appl. Energ.* **86** 1823–1835. https://doi.org/10.1016/j.apenergy.2009.02.017

KOKO PS and KUSAKANA K (2014) Techno-economic analysis of an off-grid micro-hydrokinetic river system as a remote rural electrification option. Central University of Technology, Free State, South Africa.

KUSAKANA K and VERMAAK HJ (2013) Hydrokinetic power generation for rural electricity supply: Case of South Africa. *Renewable Energ.* **55** 467–473. https://doi.org/10.1016/j.renene.2012.12.051

LOOTS L, VAN DIJK M, BARTA B, VAN VUUREN SJ and

BHAGWAN JN (2015) A review of low head hydropower technologies and applications in a South African context. *Renewable Sustainable Energ. Rev.* **50** 1254–1268. https://doi.org/10.1016/j.rser.2015.05.064

MEAAI (2011) *Energy Report 2011*. Ministry of Economic Affairs, Agriculture and Innovation, The Netherlands.

RSA (Republic of South Africa) (1998a) National Water Act. Act No. 36 of 1998. *Government Gazette* 19182. Government Printer, Cape Town.

RSA (Republic of South Africa) (1998b) National Environmental Management Act. Act No. 107 of 1998. *Government Gazette* 19519. Government Printer, Cape Town.

RSA (Republic of South Africa) (2006) Electricity Regulation Act. Act No. 4 of 2006. *Government Gazette* 28992. Government Printer, Cape Town.

RIGLIN J, SCHLEICHER W and OZTEKIN A (2014) Diffuser optimisation for a micro-hydrokinetic turbine. *ASME International Mechanical Engineering Congress and Exposition*, Montreal, Canada. https://doi.org/10.1115/imece2014-37304

SCHARFETTER B and VAN DIJK M (2017) Legislation governing the implementation of small-scale hydropower projects for rural electrification in South Africa. *J. Energ. South. Afr.* **28** (2) 14–28. https://doi.org/10.17159/2413-3051/2017/v28i2a2005

SHIVES MR (2008) Hydrodynamic modelling, optimisation and performance assessment for ducted and non-ducted tidal turbines. Masters dissertation, Carleton University, Ottawa.

SHP (2017) Smart Hydro Power. URL: https://www.smart-hydro.de/renewable-energy-systems/hydrokinetic-turbines-river-canal/ (Accessed 15 January 2017).

VAN VUUREN SJ, BLERSCH CL and VAN DIJK M (2011) Modelling the feasibility of retrofitting hydropower to existing South African dams. *Water SA* **37** (5) 679–692. https://doi.org/10.4314/wsa.v37i5.5

WHITE J (2011) *Viability of Small-Scale Hydropower in South Africa*. University of Cape Town. Cape town, South Africa. https://doi.org/10.15641/ghi.v2i1.728

Investigating the Hydrokinetic Turbine wake effects as a result of operational parameter variations through validated CFD models

Chantel Niebuhr[*], Marco van Dijk
Department of Civil Engineering, University of Pretoria, South Africa

Christiaan de Wet
Aerotherm Computational Dynamics, South Africa

Summary: Hydrokinetic energy generation devices within water infrastructure are becoming an ever-increasing alternative power source. In these applications the extent and characteristics of the downstream wake are of great importance. The vortex formation and diffusion of the wake has a complex formation and is dependent on numerous factors. Validated Computational Fluid Dynamics (CFD) models provide a detailed insight into these formations. These models allow analysis of the wake behaviour as a result of changes in device operational characteristics which may be helpful to optimise installations, specifically in array applications. To test the applicability of CFD models and further understand the wake vortex formation, the tip speed ratio of a validated turbine model was varied and the changes in the downstream wake analysed.

Introduction

Hydrokinetic (HK) devices placed in canals can have significant water level and hydrodynamic energy loss effects. Comprehension of the flow behaviour in the near and far wake for any specific HK device remains uncertain. The downstream disturbances from a HK turbine are characterised by intense turbulent mixing, helical movements and a complex eddy system defined as the wake [1]. Much of the wake complexity arises from an adverse pressure gradient at the rotor plane. Additionally, a spiral vortex structure is shed outwards from the blade tips producing large eddy structures which last a distance downstream. The eddy size, shape and behaviour vary with changes in impeller rotation rate. This flow behaviour may be identified by vortex shedding and results in non-uniformities in the velocity field [2]. The extent of this behaviour is not well understood or quantifiable as yet. From similar studies on wind turbine wake dissipation, the wake characteristics are defined as velocity deficit downstream and turbulence levels [3]. However, additional parameters such as the vorticity magnitude, determined from the curl and magnitude of the wake velocity vectors, may provide distinct characterisation and visualisation of the flow movement and extent of turbulence present in the wake.

Methods

To allow further understanding of the wake behaviour at different TSRs (tip speed ratios) the RM1 axial flow duo-turbine was simulated in Siemens PLM Simcenter STAR-CCM+ commercial simulation software with a domain size and dimensions similar to the experimental results from the RM1 reference model turbine [4]. The Reynolds Averaged Navier Stokes (RANS) approach was adopted and the K-ω Shear-Stress Transport (SST) model was employed. The SST model has been found to give results for wall-bound flows even in highly separated regions (as typically found in axial turbines) [5, 6]. A polyhedral cell type was used to capture the fine wake dynamics and gradients. A mesh independence study was fulfilled to obtain the final mesh size required. Mesh refinements around the blades and in the turbulent wake region were employed, with care taken to ensure gradual mesh size growth. The finest mesh resulted in a minimum cell size of 3.5 mm.

A 2-part validation study was completed after model convergence, initially the turbine torque was calculated through fluid force moments about the rotational axis and compared to experimental results (Fig. 1). Furthermore, the time-averaged horizontal and vertical velocity profiles were compared to experimental results. The inlet velocity was 1.05 m/s with blade chord length Reynolds number = 3×10^5. To allow further understanding of the wake behaviour and spiral vortex structure downstream of an axial HK device, the rotation rate was varied over 5 TSR's within the operational range (with torque measurement validation with each variation as shown in Fig 1). The vorticity profiles, as well as the vortex structure were recorded.
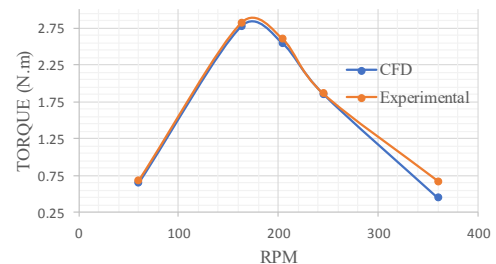

Fig 1.Torque measurement validation

---

[*] Corresponding author.
Email address: Chantel.niebuhr@up.ac.za

Results

The vortex shedding and uneven wake distribution of the turbine operating at lower TSRs are prevalent in the vorticity plot (Fig 2). At higher TSRs, the effect of vortex shedding is minimized with concentrated rotational vortices dissipating uniformly downstream. The vortex shedding effect results in higher flow instabilities in the near wake which may be unfavourable to turbines placed in this zone. However, the turbulence dissipation and velocity deficit are lower at these TSRs. When normalized velocity is displayed, (Fig 2) the flow recovery profile is portrayed and indicates higher velocity changes in the near wake at higher TSRs. Compared to the RM1 experimental analysis, power output from scenario (b) and (d) has similar values to the simulated results with only a 0.03 difference in power co-efficient compared to scenario (c).

Conclusions

The use of validated CFD models allows further understanding and visualisation into wake behaviour and vortex formation. This is specifically relevant in the case of HK conveyance infrastructure installation where the wake dynamics and downstream velocity deficit play a key role. Performing analysis on validated CFD models allows clear visualisation and understanding of the wake behaviour at specific operation parameters (TSR, inflow velocity, etc.) and may allow development of simplified relationships to quantify the wake extent and dissipation rate for any specific installation. Although, quantifying the wake as a function of TSR is a complex task due to the eddy formation and vortex shedding which is more prevalent at lower TSRs.
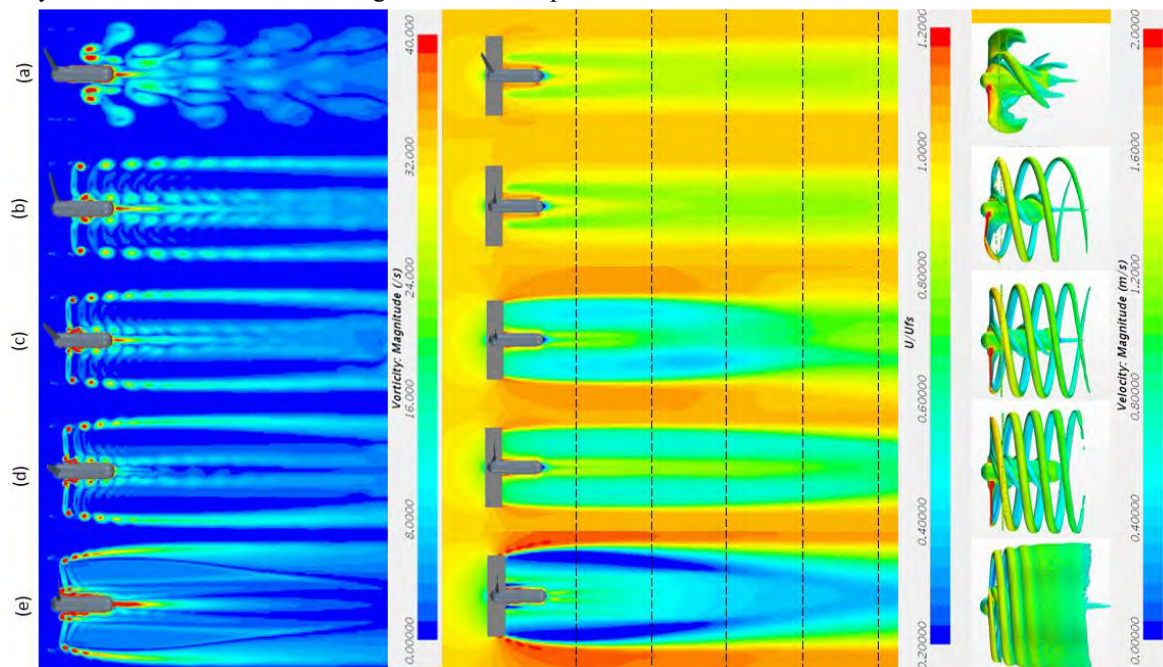

Fig. 2. Vorticity, mean normalized velocity and vortex profiles of a single RM1 turbine with a TSR of (a) 1.5 (b) 4.2 (c) 5.1 (d) 6.2 and (e) 9.1 and Cp (a)0.04 (b)0.45 (c)0.48 (d)0.45 and (e)0.23.

References:

[1] Silva P. A. S. F., Oliveira T. F. D. E., Junior A. C. P. B., Vaz J. R. P. (2016) Numerical Study of Wake Characteristics in a Horizontal-Axis Hydrokinetic Turbine. *Ann Brazilian Acad Sci,* **88**, 2441–2456.

[2] Seyed-aghazadeh B (2015) An experimental investigation of vortex-induced vibration of a rotating circular cylinder in the crossflow direction. *Physics of Fluids.*

[3] Chamorro LP, Porté-agel F (2009) A Wind-Tunnel Investigation of Wind-Turbine Wakes: Boundary-Layer Turbulence Effects. *Boundary-Layer Meteorol* **132**,129–149.

[4] Hill C, Neary VS, Gunawan B, Guala M, Sotiropoulos F (2014) U. S. Department of Energy Reference Model Program RM1: Experimental Results. Minneapolis.

[5] Moshfeghi M, Song YJ, Xie YH (2012) Effects of near-wall grid spacing on SST K-w model using REL Phase VI horizontal axis wind turbine. *J Wind Eng Ind Aerodyn* **107**, 94–105.

[6] Menter FR, Kuntz M, Langtry R (2003) Ten years of industrial experience with the SST turbulence model. *Turbul Heat Mass Transf* **4**, 625–632.

Monitoring operation and maintenance of hydrokinetic schemes through pilot installations in South Africa

C.M. Niebuhr
University of Pretoria
Private bag X20
Hatfield 0028
Pretoria, South Africa

M. van Dijk
University of Pretoria
Private bag X20
Hatfield 0028
Pretoria, South Africa

Intro

Global renewable energy goals together with advances in technology allow a window into new unconventional hydropower applications, specifically in areas where traditional hydropower potential is not readily available. A combination of factors allows testing of hydrokinetic technology in the South African context. Ideally a renewable source should have minimum environmental impact with maximum power output, long term testing of such installations is required to ascertain these variables with confidence. The large network of canal systems and river systems in South Africa and prevalent lack of renewable energy sources provides an opportunity for the installation of small-scale hydrokinetic schemes. Three such installations were undertaken in existing water infrastructure systems in South Africa to test and potentially ascertain the applicability of these systems within inland applications. These installations included two full-scale hydrokinetic inland systems installed in the Northern Cape Province in South Africa as well as a customized hydrokinetic system placed on the outlet works of a scour chamber on the Orange River. These pilot projects were selected to showcase installations which can easily be duplicated at multiple points along riverine and canal systems. Data collection during operation allowed collection of operational and maintenance requirements for such systems as well as overall statistics on pre- and post- commissioning operational parameters in terms of output. A summary of points and lesson learnt within an operational and maintenance assessment is covered in this paper as well as a discussion on the viability of such installations in the long term. Operational issues affecting the normal operation of the water infrastructure system are discussed, as this is a major point of consideration when installing these systems within water supply infrastructure such as irrigation canals. Proven long-term feasibility of these small-scale inland hydrokinetic sites opens possibilities for remote and on-site power production, specifically for water conservation and telemetry in off-grid remote areas and villages in need for electricity. The pilot installations were commissioned in 2018 and are currently being monitored and evaluated by the University of Pretoria's Hydropower Research Group.

1. Background

Small-scale hydrokinetic turbines are a relatively new technology utilising a similar mechanism to the more traditional water wheel concept. These hold the potential to open the market for low to zero head hydropower, meaning they do not require significant potential energy, and rather depend on the kinetic energy of flowing water. In semi-arid countries such as South Africa large amounts of water are conveyed to areas with less rainfall through natural river systems, canals and pipelines, providing a significant potential for these installations if confidence and economic viability can be proven. However one of the main challenges of these systems is the difficulties in estimating the economic viability and system potential due to the lack of operational installations [1]. Additionally many complexities are prevalent in these installations [2] specifically finding ideal sites with the necessary flow velocities to produce the optimum output as well as costs incurred when these are not met (costs per kW).

Small-scale renewable technologies have generally lower environmental influence, especially in the case of hydrokinetic turbines due to the partial extraction of the available energy. For power supply near flowing water, micro-hydro systems such as hydrokinetic schemes have in many cases been estimated to be the most economical and reliable generation option where the potential is available. However, a lack of long-term operational information results in a lack of confidence in these installations and therefore a lack of capital investment. The obvious solution is the need for more tests and pilot installations in various operating conditions, proving the feasibility and requirements of such technology in inland conditions. Specifically indicating what is required during operation and maintenance as well as problems which may be encountered during a typical plant life.

To provide some background to the study this section will cover a short introduction to hydrokinetic energy, literature on maintenance and operation and an overview of the projects undertaken during the study period.

1.1. Hydrokinetic device deployment, operation, and maintenance

Electrification of rural areas consisting of a largely poor population is being carried out in numerous developing or under-developed countries, with monetary help in the form of subsidies and investments coming from more developed countries. Due to the majority of people in these areas not being able to afford electricity supply it is necessary to bring the most cost-effective form of energy to these areas to alleviate poverty.

HK energy extraction is a simplified process therefore the cost of energy extraction is low. Due to its modular nature the initial installation cost and deployment time is short as it does not require significant infrastructure construction. It also allows an easily scalable energy output but limits any decrease in capital cost per kW output [3].

During the operational life of a deployed hydrokinetic device little is known in terms of data on the lifespan on these devices. The obvious causes of maintenance such a debris build up is known, as well as predictive maintenance on machine and electrical parts. Work has been done to reduce the clogging and debris build up [4] as well as laboratory testing on quantifying the effect on power output caused by blockage and the impact on free-surface depths [5] which are important considerations in constrained installations such as those in canals. To further allow prediction of the performance of these device, many experimental (laboratory based) and numerical tests on prototype turbines have been completed [6–8] which work toward allowing an accurate prediction of the turbine performance as well as wake and flow field characteristics. This allows the design of array systems, understanding the inter-effect between devices as well as any losses which may be sustained [9].

In terms of operational life and challenges a number of HK turbines have been installed throughout the world. Many of the application were short term testing procedures which makes an evaluation of long term working of these units difficult to predict, it does however provide example of successful installations in obtaining the design output and practical application. One of the few inland systems was a horizontal axis in the Nile river which was used to pump water [10]. A 6-week installation in the Roza canal was performed by Hydrovolts [11], and a floating barge was installed in a river in Manitoba Canada for less than a year (removed before river icing). Smart Hydropower Gmbh has a few running installations such as the Duofloat installed in Neiva, Colombia which has been in operation for a number of years, however no operational data or published documents have been made available on this [12].

1.2. Hydrokinetic case studies

The University of Pretoria started work on multiple hydrokinetic applications in 2018 with the purpose of the study being twofold. The first objective was to harness and showcase various innovative forms of hydrokinetic technology applicable in free surface flows and the second objective was to assist the overall growth of poor areas and municipalities in South Africa (SA) by providing a sustainable source of electricity. The construction and implementation of sustainable energy sources, in this case hydrokinetic energy generation, has a large untapped potential within water transfer schemes, not only due to its sustainable nature but also its alignment with current legislative goals.

Before the installations described in this study no notable use of modern small-scale hydrokinetic energy systems existed in SA, mainly due to the dependency on low-cost coal-powered electricity. Following detailed site selection procedures and correct turbine selection (based on prototype and numerical modelling studies), three full-scale installations were carried out through the innovative use of existing infrastructure [13,14].

The test installations allowed establishment of a hydrokinetic development process as shown in Fig. 1. These installations were thereafter included as pilot projects under a new policy document under the South Africa Department of Water and Sanitation General notice: *Draft Policy on Sustainable Hydropower Generation*. Thus, allowing policy changes on regulatory and legislative requirements of small-scale hydropower generation subsequently allowing for simpler development processes towards implementation of HK installations.
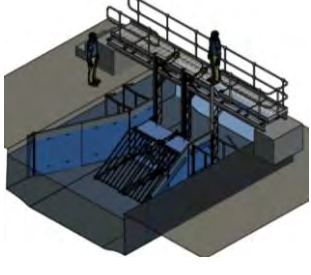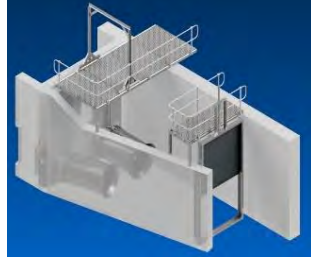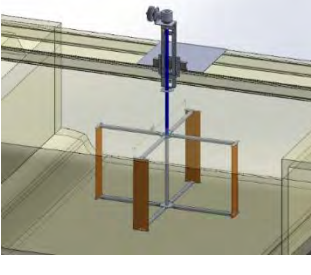
Fig. 1: HK system development process [13]

The chosen installation sites were within the !Kheis Local Municipality (LM) and Joe Gqabi District Municipality's (DM). Since large proportions of these communities are unemployed, and unable to pay for basic services the municipalities have major income shortages and are unable to pay power utilities for rapidly rising electricity costs. To lighten the electricity costs varying configurations of horizontal axis hydrokinetic turbines (HAHT) and vertical axis hydrokinetic turbines (VAHT) were investigated, tested for optimum functionality, and selected for installation. The installations constructed as pilot plants are examples of full-scale installations (summarized in Table 1).

Table 1: Details of the implemented HK installations

	Site 1: Groblershoop HAHT	Site 2: Aliwal Confined HAHT	Site 3: Groblershoop VAHT
Description	Test installation (before optimisation) of a hybrid HAHT plant coupled with a PV system.	A customized installation of HAHT build into a casing utilized as a low-head run-of-river application.	A low-cost locally manufactured VAHT test installation.
Installation infrastructure	Open channel flow, Boegoeberg Irrigation canal	Outlet works Pipe flow, Orange River Weir Scour outlet	Open channel flow, Boegoeberg Irrigation canal
Hydrokinetic turbine type	2 ✖ 2 Vertical axis propeller type turbines Diameter = 1 m	2 ✖ Confined vertical axis propeller type turbines. Diameter = 1 m	1✖ Horizontal axis Darrieus type turbine Diameter = 2 m
Flow characteristics	Channel free flow Flow = 6.6m^3/s Velocity = 1.1 m/s (2.3 m/s in the optimised section)	Riverine weir scour outlet Flow = 6.1 m^3/s Velocity = 3.0 m/s	Channel flume outlet Flow = 6.6 m^3/s Velocity = 1.1 m/s
Projected output	4 ✖ 4 kW (optimised section) 122 880 kWh per annum (not including PV scheme)	2 x 5 kW 79 200 kWh per annum	3 kW 23 040 kWh per annum
Power use	Supply to Groblershoop water treatment works and pump	Supply to Joe Gqabi DM water treatment works and	Supply to Wegdraai water treatment works

	Site 1: Groblershoop HAHT station	Site 2: Aliwal Confined HAHT pump station	Site 3: Groblershoop VAHT
Dates	Project start: 01/2017 Completion: Test installation 01/2018 with further optimisation and performance testing. Current status: Operational	Project start: 02/2018 Completion: Test installation completed 11/2018. Current status: Requires maintenance	Project start: 01/2018. Current status: Final device currently under development, prototype testing and civil works completed.
Final design drawing			
Pilot/ test Installation			

2. Operation and maintenance of pilot installations

Operation and Maintenance integration on small-scale hydropower systems is not only dependant on a clear schedule but an amalgamation of properly trained staff, engineering knowledge and skills as well as proper administration as shown in Fig. 2. The systems put in place to ensure proper and sustainable operation of the plants are summarized in this section.
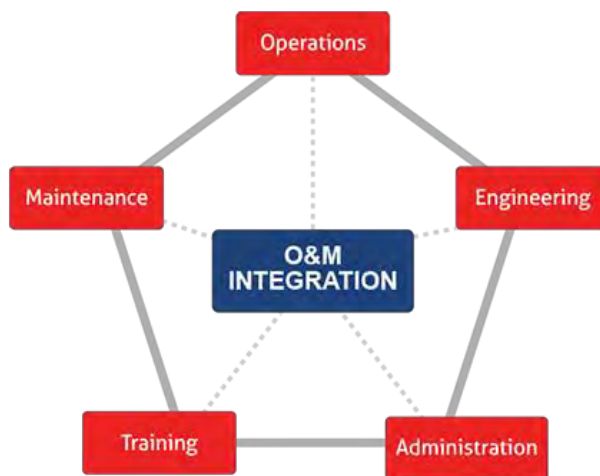

Fig. 2: O&M integration

2.1. Plans

Detailed O&M plans were setup, tested and adjusted during the operational testing period. Most of the equipment cannot be fully assembled or tested at each site, and complex parts may take long periods of time to replace. Maintenance exercised at predetermined time intervals are therefore planned to ensure the following objectives:

- Reliable operation of equipment on a long-term basis through identified periodic inspection/checking of components and subsequent replacement/ rectification of parts, wherever required.
- Maximum availability of equipment with the least number of shutdowns by ensuring that the rate of deterioration of any component does not exceed the life expectancy of the equipment at any stage. Periodic /planned shutdowns should be arranged to avoid long term forced shutdowns.
- Eradication /non-repetition of operational problems by timely analysis of the cause of faults/problems and replacement of short-term solutions by long lasting and permanent ones.

Guidelines for operation of power plant shall have two elements namely the operation of Power Plant and Water operation. For the plant operation the design and nature of the hydrokinetic installation allows the unit to operate efficiently in theory with little to no maintenance, however certain components where debris or other external factors may cause damage to the unit, maintenance and component replacement might be necessary. The maintenance plan was similar for all sites and can be simply described as regular cleaning; Annual measurement of all electronic components (the resistance in the cables, voltage of the batteries); and annual control of all structural components (viewing only).

The technical components of the system such as the generator etc. should need no maintenance. The HAHT has been designed to allow smaller debris to flow through the rotor, and larger debris (>70mm) to be diverted away from the turbine by the protective grid. A large amount of debris can however accumulate on the protection grid and clog the grid. This can block or even damage the rotor blades, therefore visual checks were scheduled in case maintenance is required.

Just like operation of the turbine Generator set or a transformer, efficient water operation forms an important part of hydro systems be it a large storage plant or a small run of river plant. This is even more prominent in irrigation canals (Used in Sites 1 & 3). Water operation means operating the systems in such a manner that efficiency of the plant is maximized.

In addition to planning maintenance and allotting suitable time intervals, on the basis of water supply availability, the following items were noted to require close watch otherwise it may become difficult to adhere to the schedules.

i. Man-power planning and arrangement is most essential as without experienced / skilled staff any maintenance programme may fail.
ii. Planning and arrangement of spares and consumable in advance so that time is not lost in arrangement of a shut down.
iii. The maintenance engineers should have in his possession all the erection and commissioning log sheet documents to establish a record of installed clearances, parameters, alignment results, test characteristics of all the power plant equipment. These may be required at the time of diagnosis of the operational problems as well as defined maintenance purpose.
iv. Log sheets of the previous maintenance exercise carried out on the machines. These may be required to compare with the clearances/settings/characteristics achieved during present maintenance.
v. History registers of various machines duly recorded with all the abnormalities observed on the machine and details of action taken to provide a guideline for future maintenance exercise must be maintained at the power station.
vi. Logging of the performance characteristics of the power plant on daily basis recording all the abnormalities and misbehaviours (if any) of the total plant observed during its generation programme from one maintenance exercise to another.

2.2. Operation and output

Proper measurements of flow and level properties together with power output measurements was crucial to ensure not only efficient operation but the possibility of troubleshooting lower power outputs and system faults. Site 1 can be used as an example where level sensors were placed as various points upstream and downstream of the turbine

installation point allowing detailed reading of damming effects and alarm systems linked to overflow possibilities, signalling possible reactive maintenance requirements. These can be seen in Fig. 3.
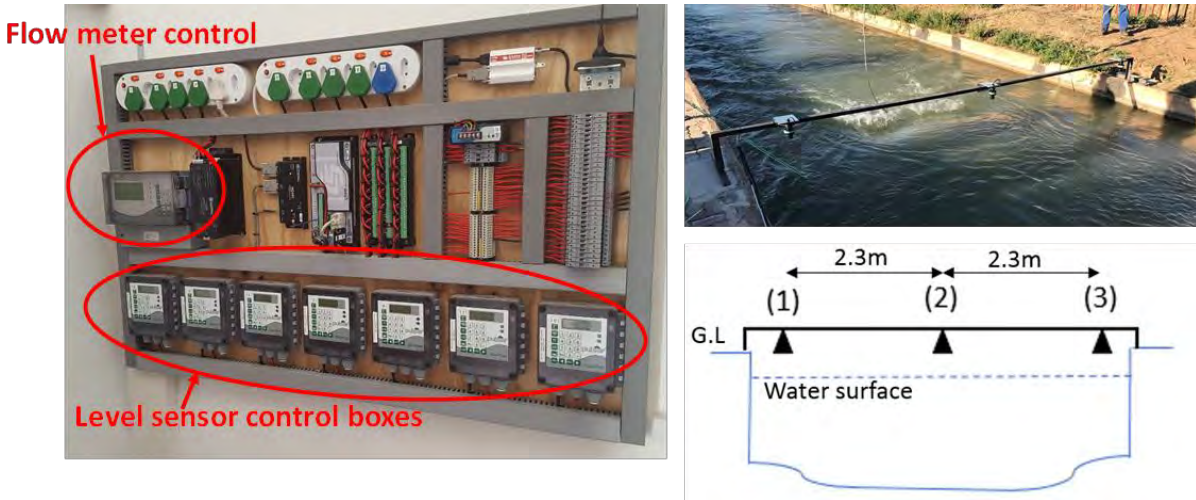

Fig. 3: Measuring equipment

Additional to flow monitoring devices the power output from the schemes were measured through connections to the inverters in the control room. The typical power generation during the week at site 1 (hybrid solar/hydro scheme) can be seen in Fig. 4. With peaks during the daytime hours as a result of the solar scheme with a constant baseload provided from the hydrokinetic scheme (note this is still during the lower output testing phase).
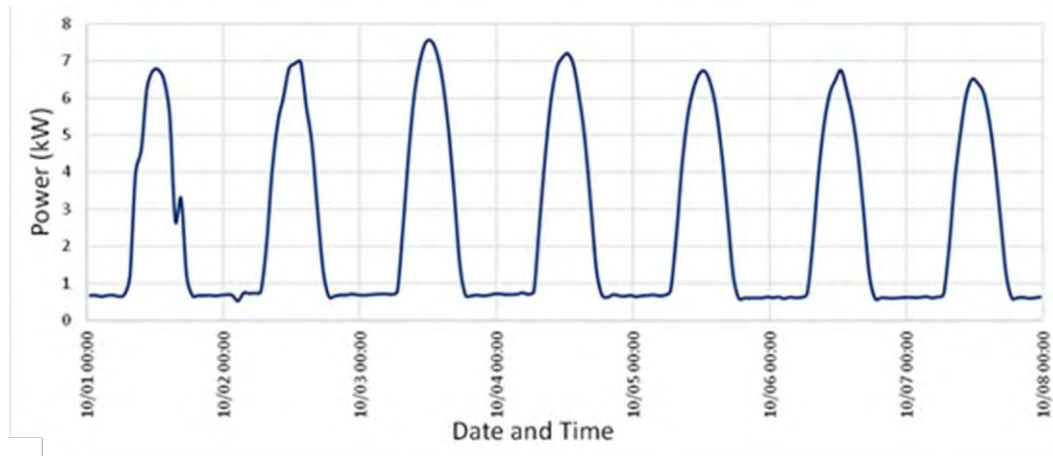

Fig. 4: Power output over a week

2.3. Training and capacity building

The operation of a hydropower station, whether small or large scale, requires not only planned operation and maintenance but also that its staff is trained and well versed with all necessary technical as well as basic trouble shooting knowledge and understand all the different components that make-up O&M. Micro-hydropower plants for rural electrification should be operated and maintained by well-trained operators to ensure a stable supply of electricity. The project offered the opportunity to train the specific municipalities involved. This process of capacity building can be split into three sections:

i. Training workshop
   The themes included in the training material for the workshops to transfer the necessary skills to the local authorities to holistically see the hydropower plant development included:
   1. Features of a hydropower scheme
   2. Hydropower development opportunities
   3. Resource assessment for hydropower development
   4. Status-quo and small hydropower potential in southern Africa
   5. Turbine technologies (Low and high head)
   6. Specific potential in the agricultural sector
   7. Site selection and practical design principles
   8. Construction of small hydropower installations
   9. Case studies of existing pico, micro and mini hydropower installations
   10. Electricity – Grid connection and islanded system
   11. Legislative and regulatory requirements in SA
   12. Feasibility calculations

   Further training of the municipality to enable operation of the small-scale hydropower plants were given on site during the construction and testing phases.
ii. Discussions, meetings, and site visits
   Numerous discussions and visits to the hydropower plant sites ensured that the planning and design thereof was shared with all the stakeholders.
iii. Labourer's training
   During the construction phases of the projects the local labourers were trained and used in developing the hydropower plant sites (Fig. 5). This included acquiring skills such as, brick laying, welding, concrete mixing and casting, steel reinforcement fixing, assembly of the turbine units etc.

Fig. 5: Labourers learning skills and operational training

3. Operational challenges

Experience of running hydropower stations reveals that even after detailed project planning/quality control measures taken at various stages from inception to commissioning, unforeseen problems do occur during the operational phase resulting in forced outages/low generation etc.

During the test installations various problems were encountered which in some cases led to delays in the project, or resulted in additional costs, these include:
   i. In general theft and vandalism of the testing sites during experimental setup construction resulted in large expenses for fencing and additional security to prevent further interference.
   ii. Debris build up and large objects causing blockages and damages to the equipment.
   iii. During the project development, obtaining the approval in the form of a Memorandum of Agreement (MoA) between the Municipalities, the Irrigation Board and the infrastructure owners proved to delay the project significantly as no turbine could be placed without the signing of the document. However, due to the

nature of the project no other legislative and regulatory requirements were necessary, which could pose a delay in future projects of similar nature.

    iv.   For the canal installations the low velocities in most canal sections result in low efficiency systems, however as narrower sections, or confined sections where a greater velocity exists are selected for installation, additional problems such as complete blockage (due to the turbine covering the majority of the smaller cross section) and large damming effects may occur. Due to this the risk of overflow and thus water loss increases and thus the viability of the project decreases (civil works costs increase). It can also result in reluctance of the relevant authority to agree to the installation.

    v.   Maintenance of the system remains a problem in South Africa, municipalities do not have the money and thus not the workforce to complete maintenance of the systems. The debris during short testing periods was evident which could result in large debris build-up over time and with no maintenance this could result in an inefficient system which becomes unsustainable.

More details of specific points are covered in this section.

3.1. Debris build up

A major concern prior to installation of Sites 1 and 2 was the possibility of water supply disturbances affecting downstream irrigation offtakes. Numerical analysis of upstream damming levels (as a result of the flat canal bed slope and subcritical flow conditions) were conducted. Flow effects up to 2 km's upstream with overtopping possibilities were carefully considered and incorporated into the design. Operational testing included prediction analysis; however, some challenges that were not predicted pre-construction arose during the operation phase. In Fig. 6 a few challenges mainly due to excessive debris build up can be seen. The canal was often used as a "dumping ground" therefore large amounts of cut grass, shrubs and small trees were found to block the turbine grids, despite the debris resistant design. This resulted in high damming/backwater levels upstream (in (c)) which also caused overflow at a emergency overflow section 1.7 km upstream.

On one occasion during a testing phase, deceased livestock was washed down the canal. After questioning locals, it was made clear this is a fairly common occurrence due to livestock and wildlife drinking from the canal (as no barrier exists around the canal) and falling in. This could potentially result in turbine blockages; therefore, a warning system must be included to allow for quick response in such cases.

Fig. 6: Site 1 operational challenges due to debris

The effects of debris build up can be seen in a plot indicating the power output from each of the four installed turbines. During the first few hours shown on the Fig. 7 (Hour 1-200) the power output from each turbine is relatively consistent, at hours 200-280 a large amount of debris build up occurred, specifically on the first two turbines in the canal which significantly lowered the power output. A canal shut down, cleaning and maintenance period is then completed, and the higher output is prevalent after cleaning. This indicated the strong effect of debris build up not only on maintenance requirements but monetary power output.
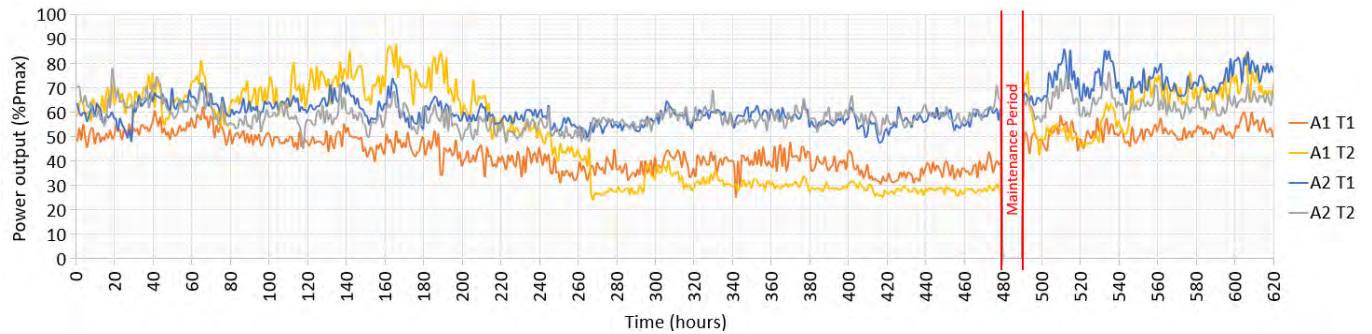
Fig. 7: Power output variation

3.2. Damage to infrastructure

At Site 2 a major concern lay in turbulent inflow, a solution was found in designing an inlet structure consisting of multiple vertical panels forcing a flow approach perpendicular to the blades. This also functioned as a grid protecting the inlet, however during a specific testing phase large rocks fitting within the grid resulted in a blade shearing off the turbine (bolt shear failure) which was found stuck between another blade and the turbine wall shown in Fig. 8. This urged the requirement of smaller screens upstream of the turbine which increases blockages and maintenance requirements.

Fig. 8: Site 2 turbine damage due to large rocks

3.3. Handover and maintenance

Communication and cooperation from the local municipalities and operators (post-handover) was one of the largest problems and primary issues in these installations. The following issues specifically delayed the project and increase the probability of project failure:

i.   Due to a lack of specific policy in-stated in South Africa, which would allow a streamlined process of installation, delays in the process of installation occur (may occur).

ii. The nature of the project in terms of hydropower plants being supplied through grants to the local municipalities resulted in a lack of accountability by the municipalities (including assistance such as providing support, showing interest and performing maintenance.

iii. Labourers who were employed and received the skills/training during the implementation phase were not employed for the operational period.

4. Discussion

Pilot studies and test installations such as these mentioned are necessary to understand the limitations and problems together with additional expenses incurred to allow more confidence in the prediction of costs for future projects. Some important lessons learnt are discussed here.

The process of careful site selection should not be taken lightly, although optimisation can be considered as an alternative, the costs and maintenance requirements are reduced significantly when sites of optimum velocity are used for implementation. The followed should be ensured for selected sites:

i. Velocities should be at the necessary turbine operating point.
ii. Straight flow lines into the turbine are favourable (this may vary depending on the selected turbine; however inflow characteristics should be considered).
iii. In countries such as South Africa, provision for theft and vandalism should be made, and prevention should be ensured (this may incur high costs if the project is in a rural area).
iv. Debris build up and subsequent maintenance requirements should not be underestimated. Sites with less debris (close to outlet works/gridded inlets etc.) are favourable.
v. Where canals are used careful analysis of backwater effects are necessary to prevent water loss. Where freeboard is not provided, civil works may be necessary to prevent overtopping, adding significant costs and additional legislative and regulatory approvals.

Additional to site selection, the purpose of the electricity produced should be carefully considered and it is recommended it be for "own-use" purposes, as this significantly reduces the legislative and regulatory aspects of the implementation. Also, a sustainable structure should be developed for the operation of these units to be implemented on a municipal level.

Additional to physical requirements, technical aspect variations and possibilities must be considered, such as:

i. The turbine itself, as a variation of blade types and orientations which are dependent on: Available velocity; Debris exposure; Available area and geometry of the canal.
ii. The possible influence of the HK turbines on the relevant water infrastructure purpose.
iii. The scale of the project and its possible influence on the infrastructure workings.
iv. The transmission length needed (as this can be high cost if long distances).
v. The electromechanical parts applicability to installation (Generator type and size variations, Power output requirements (e.g. AC or DC output; Grid-tie or stand-alone system.)
vi. The support structure requirements (Space availability; In situ soil strength.)

The technology has been proved to have very little to no environmental impact and an overall strong social impact by educating locals on the technology and more specifically the possibilities of renewable energy. Although the output was lower than initially expected the possibilities of such a system was exhibited. Some techniques proved to function more effectively than others in certain applications (such as lower and higher velocities) and require further testing over a range of applications. The increases in efficiency and limited effect on the supply of water proved these units could potentially be installed with optimisation measures (where required), however the influence not only as the site but on the entire system should be carefully analysed.

With the required maintenance is met and the correct site selected, hydrokinetic technology could be used as an additional sustainable renewable energy source in South Africa. As most canal systems provide a controlled environment with a constant uniform supply of water (except during short shut-off intervals), with careful site selection and feasibility studies, HK energy systems in canal networks in South Africa can be a feasible alternative energy source. With pilot projects such as these, the road to a streamlined, simplified regulatory and legislative process for the installation of HK systems in South Africa is slowly being formed.

5. Conclusions

Success in showcasing the broad potential and possibilities of incorporating HK devices within canals and river systems provides much needed examples of HK potential and demonstrates the applicability in semi-arid countries such as SA where a large network of low-head potential exists in conveyance infrastructure. Localised small-scale HK energy systems allow on-site energy generation without large environment effects or necessity for impoundment or infrastructure alteration. These systems may allow lower-cost installations where needed and may provide local municipalities with a sustainable source of income (and electricity) and thus less reliance on the national grid. Furthermore, these pilot studies introduced HK technologies to SA and provide the basis for further experimental analysis on the reliability and feasibility of hydrokinetic installations. Current studies include a focus on analysis and understanding of the hydrodynamic behaviour in the wake downstream of the HK device, which is an important consideration when installing arrays of these devices.

6. Acknowledgements

References

1. **Santos, I. F. S. dos, Camacho, R. G. R., Tiago Filho, G. L., Botan, A. C. B. & Vinent, B. A.** "Energy potential and economic analysis of hydrokinetic turbines implementation in rivers: An approach using numerical predictions (CFD) and experimental data". *Renew. Energy* 143, 648–662, 2019.
2. **Kirke, B.** "Hydrokinetic and ultra-low head turbines in rivers: A reality check". *Energy Sustain.* Dev. 52, 1–10 (2019).
3. **Gaden, D. L. F. & Bibeau, E. L.** "Increasing Power Density of Kinetic Turbines for Cost-effective Distributed Power Generation". 2006.
4. **Anyi, M. & Kirke, B**. "Tests on a non-clogging hydrokinetic turbine". *Energy Sustain*. Dev. 25, 50–55, 2015.
5. **Birjandi, A. H., Bibeau, E. L., Chatoorgoon, V. & Kumar, A.** "Power measurement of hydrokinetic turbines with free-surface and blockage effect". *Ocean Eng*. 69, 9–17, 2013.
6. **Riglin, J. et al.** "Experimental and numerical characterization of a full-scale portable hydrokinetic turbine prototype for river applications". *Renew. Energy* 99, 772–783. 2016.
7. **Mycek, P., Gaurier, B., Germain, G., Pinon, G. & Rivoalen, E**. "Experimental study of the turbulence intensity effects on marine current turbines behaviour. Part I: One single turbine". *Renew. Energy* 66, 729–746, 2014.
8. **Hill, C., Neary, V. S., Guala, M. & Sotiropoulos, F.** "Performance and Wake Characterization of a Model Hydrokinetic Turbine: The Reference Model 1 (RM1) Dual Rotor Tidal Energy Converter". *Energies* 13, 1–21, 2020.
9. **Stallard, T., Collings, R., Feng, T. & Whelan, J**." Interactions between tidal turbine wakes: Experimental study of a group of three-bladed rotors. Philos". *Trans. R. Soc. A Math. Phys. Eng. Sci*. 371, 2013.
10. **Anyi, M.** "Water Current Energy for a Remote Community: Design and Testing of a Clog-free Horizontal Axis Hydrokinetic Turbine Syste". *PhD Thesis*, University of South Australia, 2013.
11. **Johnson, K., Hart, A., Goerge, L., Yooung, N. & Applegate, M.** Small Hydropower Handbook. (The Colorado Energy Office, 2007).
12. **SHP.** "Decentralized rural electrification projects worldwide", 2021. Available at: https://www.smart-hydro.de/decentralized-rural-electrification-projects-worldwide/. (Accessed: 14th September 2021)
13. **Niebuhr, C. M., van Dijk, M. & Bhagwan, J. N.** "Development of a design and implementation process for the integration of hydrokinetic devices into existing infrastructure in South Africa." *Water SA* 45, 434–446, 2019.
14. **van Rensburg, M. L., van Dijk, M. & Niebuhr, C. M.** "Design and validation of a Darrieus type hydrokinetic turbine for South African irrigation canals experimentally and computational". Hydro 2020.

The Authors

Chantel Monica Niebuhr is a Civil Engineer specialising in Water Resources Engineering, currently completing her Doctoral studies at the University of Pretoria (South Africa). She graduated from the University of Pretoria with a degree in Civil Engineering in 2015, completed her BEng (Hons) degree in 2016 and obtained a MEng degree in Water Resource Engineering in 2018. She is a Researcher for WRC projects and has been working on multiple rural electrification projects using hydropower and more specifically researching and experimenting with newer technologies such as hydrokinetic energy development. She is a lecturer and acts as a private consultant for relevant water projects and small-scale hydropower technology design and installation.

Marco van Dijk is a Professional registered Engineer (PrEng), a Lecturer in the Department of Civil Engineering at the University of Pretoria (South Africa) and a Principal Researcher for WRC research projects. He graduated from the University of Pretoria with a degree in Civil Engineering in 1996, completed his BEng (Hons) degree in 1998. He obtained a MEng degree in Water Resource Engineering in 2003 and he is currently enrolled for a PhD. He has compiled numerous technical reports and journal publications in the field of pipelines, hydropower generation and water distributions systems. He has also presented numerous courses and workshops on network analyses, pipeline engineering and hydropower generation. He is a member of SAICE, SANCOLD and WISA.